



5-2000

## Evaluation of Factors Affecting Earth Pressures on Buried Box Culverts

Michael Zhiqiang Yang  
*University of Tennessee - Knoxville*

Follow this and additional works at: [https://trace.tennessee.edu/utk\\_graddiss](https://trace.tennessee.edu/utk_graddiss)



Part of the [Civil and Environmental Engineering Commons](#)

---

### Recommended Citation

Yang, Michael Zhiqiang, "Evaluation of Factors Affecting Earth Pressures on Buried Box Culverts. " PhD diss., University of Tennessee, 2000.  
[https://trace.tennessee.edu/utk\\_graddiss/2666](https://trace.tennessee.edu/utk_graddiss/2666)

This Dissertation is brought to you for free and open access by the Graduate School at TRACE: Tennessee Research and Creative Exchange. It has been accepted for inclusion in Doctoral Dissertations by an authorized administrator of TRACE: Tennessee Research and Creative Exchange. For more information, please contact [trace@utk.edu](mailto:trace@utk.edu).

To the Graduate Council:

I am submitting herewith a dissertation written by Michael Zhiqiang Yang entitled "Evaluation of Factors Affecting Earth Pressures on Buried Box Culverts." I have examined the final electronic copy of this dissertation for form and content and recommend that it be accepted in partial fulfillment of the requirements for the degree of Doctor of Philosophy, with a major in Civil Engineering.

Eric C. Drumm, Major Professor

We have read this dissertation and recommend its acceptance:

Matthew Mauldon, Richard M. Bennett, Xiaobing Feng

Accepted for the Council:

Carolyn R. Hodges

Vice Provost and Dean of the Graduate School

(Original signatures are on file with official student records.)

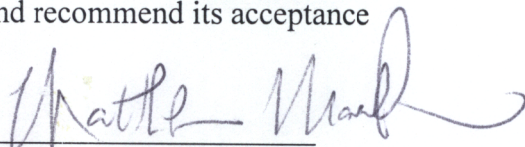
To the Graduate Council:

I am submitting herewith a dissertation written by Michael Zhiqiang Yang entitled "Evaluation of Factors Affecting Earth Pressures on Buried Box Culverts." I have examined the final copy of this dissertation for form and content and recommend that it be accepted in partial fulfillment of the requirements for the degree of Doctor of Philosophy, with a major in Civil Engineering.

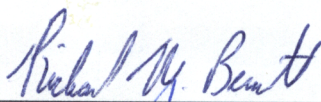


Eric C. Drumm, Major Professor

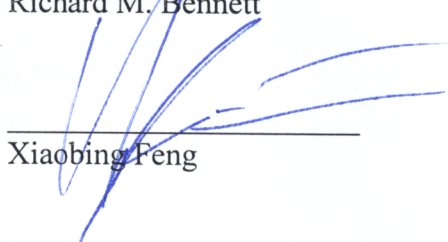
We have read this dissertation  
and recommend its acceptance



Matthew Mauldon

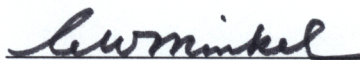


Richard M. Bennett



Xiaobing Feng

Accepted for the Council:



Associate Vice Chancellor and  
Dean of the Graduate School

**EVALUATION OF FACTORS AFFECTING  
EARTH PRESSURES ON BURIED BOX CULVERTS**

A Dissertation  
Presented for the  
Doctor of Philosophy  
Degree  
The University of Tennessee, Knoxville

Michael Zhiqiang Yang  
May 2000



## **DEDICATION**

This dissertation is dedicated to my mother and my father, Suzhen Zhou and Xulong Yang, who gave me the opportunity to dream; to my wife Yongqing Mu, and my daughter Siheng, who help fulfil my dreams; and to my mother-in-law and father-in-law, Yingling Chen and Tongdao Mu, who gave me a great support to let me pursuit my study in the U.S.A.

## **ACKNOWLEDGMENT**

Special thanks is given to my major professor Dr. Eric C. Drumm, who supervised this dissertation. Without his numerous advice, suggestions and critical reviews the whole dissertation, this work would never have been possible. During my four years study, Dr. Drumm spent numerous time improving my technical writing skills. His extraordinary understanding and patience made me feel comfortable in a different environment as an international student.

Sincere gratitude also goes to the members of my dissertation advisory committee, Dr. Matthew Mauldon, Dr. Richard M. Bennett, and Dr. Xiaobing Feng, for their assistance and valuable suggestions during the preparation of this dissertation.

I would also like to express my appreciation for the financial support from the Tennessee Department of Transportation.

I wish to extend my thankfulness to the technical support and help of Mr. Curtis Allin, Mr. Joshua Cole, Dr. Allen Guan, Mr. David Korda, Mr. William Kupsch, Mr. Randy Rainwater, Mr. Gang Zuo.

## **ABSTRACT**

Factors affecting the earth pressures acting on buried box culverts under deep embankments were evaluated by field instrumentation and numerical analyses. Two instrumented cast-in-place concrete culverts were designed and constructed differently. Long term earth pressures under constant embankment height were observed after the completion of construction. Both observed earth pressures and those predicted by numerical analyses were compared with the current AASHTO earth pressure recommendations, as well as the AASHTO design pressures in effect at the time a failed box culvert was designed in the mid 1970s. Field measurements suggested that the previous AASHTO design pressure (1977, 12<sup>th</sup> edition) significantly underestimated both vertical and horizontal earth pressures, whereas the current AASHTO (1996, 16<sup>th</sup> edition) provides more appropriate simplified earth pressures.

Both measured and predicted earth pressures indicated that the level of compactive effort had a significant influence on the earth pressure distribution, especially the horizontal earth pressure acting on the culvert wall.

A parametric finite element study suggested that the stiffness of the gravel backfill beside the culvert, which is dependent on the degree of compaction, had the greatest influence on the magnitude and distribution of earth pressure. An additional parametric study suggested that the modulus of the soil below the culvert also has a significant effect on the horizontal earth pressures.

Dynamic horizontal earth pressures induced by different construction equipment operating close to the structure were also recorded. The measurements suggested that the dynamic strain in the structure in response to the maximum transient loading (about 70 kPa) was small and had negligible effect on the culvert. High residual compaction earth pressures measured after compaction were found to decrease rapidly with time to reach a steady value under constant embankment height.

Analytical evaluation of the culvert orientation with respect to the embankment alignment suggested that the largest horizontal earth pressure acting on the culvert wall occurs when the culvert alignment is perpendicular to the alignment of embankment.

The investigation of factors affecting the earth pressures on cast-in-place box culverts suggested that the design pressures are not only dependent upon the height of the embankment, but the relative stiffness of the surrounding materials is also important.

## Table of Contents

<b>PART I RESEARCH BACKGROUND</b>	<b>1</b>
<b>Chapter 1 Introduction and Scope of Project</b>	<b>2</b>
1.1 Objective	2
1.2 Background	3
1.3 Factors Affecting the Performance of Cast-in-place Concrete Box Culverts	4
1.4 Research Tasks	6
1.4.1 Task 1 - Literature review and preliminary evaluation of earth pressures on box culverts	7
1.4.2 Task 2 - Design and installation of instrumented culvert sections	8
1.4.3 Task 3 - Evaluation of factors affecting the performance of box culverts	9
1.4.3.1 Height of embankment and properties of the backfill.	9
1.4.3.2 Orientation of culvert with respect to alignment of embankment	10
1.4.3.3 Analysis and design procedures for the box culvert concrete structure	10
1.4.3.4 Lateral earth pressures induced during compaction of the backfill	10
1.4.4 Task 4 - Monitoring the earth pressures on box culverts	11
1.5 Format of Dissertation	11
<b>Chapter 2 Literature Review - Earth Pressures on Buried Structures</b>	<b>14</b>
2.1 Earth Pressures on Buried Pipes and the Marston Theory	14
2.1.1 Concept of Soil Arching	14
2.1.2 Classification of Culverts	16
2.1.3 Arching Effects Buried Structures	18
2.1.4 Recommended Earth Pressures on the Box Structures	20
2.2 Earth Pressures on Buried Concrete Culvert-Instrumentation	24
2.3 Earth Pressure Induced by Compaction	43
2.3.1 Compaction Induced Cumulative Residual Pressure	45
2.3.2 Impulse Pressure Induced by Compaction	58
<b>Chapter 3 Characteristics of Instrumented Culverts</b>	<b>72</b>
3.1 Sullivan County	72
3.1.1 Original Sullivan County Culvert	72
3.1.2 New Sullivan Culvert	74
3.2 Greene County	75

3.3 Comparison of the Documented Box Culverts with the Current Study . . . . .	76
<b>Chapter 4 Design and Installation of Instrumented Culvert Sections . . . . .</b>	<b>80</b>
4.1 Concrete Strain Gages . . . . .	80
4.1.1 Electrical Resistance Gages for Static and Dynamic Strain Registration . . . . .	82
4.1.2 Vibrating Wire Strain Gage for Static Strain Registration . . . . .	83
4.2 Earth Pressure Cells . . . . .	87
4.3 Installation of Strain Gages and Pressure Cells . . . . .	90
4.3.1 Installation of concrete Strain Gages . . . . .	90
4.3.2 Stress-Free Strain Gages (Greene County Culvert) . . . . .	92
4.3.2.1 Factors that Influence the Concrete Strain Gage Reading . . . . .	92
4.3.2.2 Installation of Stress Free Strain Gages . . . . .	93
4.3.3 Installation of Pressure Cells . . . . .	96
4.4 Dynamic Loading Measurement . . . . .	97
<b>Chapter 5 Numerical Modeling Considerations for Buried Box Culverts . . . . .</b>	<b>99</b>
5.1 Material Modeling . . . . .	99
5.1.1 Constitutive Model for Backfill Materials . . . . .	99
5.1.2 Constitutive Model for Interface Elements . . . . .	102
5.1.3 Numerical Analysis of Failed Culvert . . . . .	104
5.2 Choice of Element Type . . . . .	106
5.3 Comparison of Different Stress Calculation Methods . . . . .	107
5.4 Simulation of Construction Sequence . . . . .	108
<b>Chapter 6 Data Interpretation - Collection of Fundamental Material Properties and Baseline Data . . . . .</b>	<b>112</b>
6.1 Field Measurements of Fundamental Properties . . . . .	112
6.2 Baseline of Strain Gage Measurements . . . . .	112
6.3 Baseline of Pressure Cell Measurements . . . . .	114
6.4 Laboratory Tests . . . . .	115
6.5 Data Interpretation and Explanation of Subsequent Chapters . . . . .	116
<b>PART II NUMERICAL MODELING OF COMPACTION EFFORTS IN CULVERT INSTALLATION . . . . .</b>	<b>118</b>
<b>Chapter 7 Influence of Compactive Effort on Earth Pressures Around a Box Culvert . . . . .</b>	<b>119</b>
7.1 Abstract . . . . .	119
7.2 Introduction . . . . .	119
7.3 Culvert and Site Description . . . . .	122
7.4 Finite Element Model . . . . .	124

7.5 Results .....	127
7.6 Conclusions .....	132
7.7 Acknowledgments .....	134
7.8 References .....	134

### **PART III FIELD MEASUREMENT OF STATIC EARTH PRESSURES ON BOX CULVERT ..... 136**

#### **Chapter 8 Measurement of Earth Pressures on Concrete Box**

<b>Culverts under Highway Embankments .....</b>	<b>137</b>
8.1 Abstract .....	137
8.2 Introduction .....	137
8.3 Instrumentation Description .....	139
8.4 Measured Vertical Stresses on the Roof .....	142
8.5 Measured Horizontal Stresses on the Walls .....	144
8.6 Discussion .....	147
8.6.1 Comparison of Measurements with AASHTO Recommended Vertical Pressure .....	147
8.6.2 Comparison of Measurements with AASHTO Recommended Lateral Pressure .....	153
8.7 Summary and Conclusions .....	156
8.8 Acknowledgment .....	157
8.9 References .....	157
8.10 Recorded Earth Pressures during Construction and under Service Loads Updated Results since Preparation of Paper .....	159

### **PART IV FIELD MEASUREMENT OF DYNAMIC LATERAL EARTH PRESSURES ON BOX CULVERT ..... 168**

#### **Chapter 9 Measurement and Analysis of Dynamic Pressures**

<b>Induced by Construction Equipment .....</b>	<b>169</b>
9.1 Introduction .....	169
9.1.1 Instrumentation for Dynamic Lateral Pressure Measurement. ...	172
9.1.2 Construction Methods .....	175
9.2 Results From Recorded Dynamic Pressures .....	176
9.2.1 Compaction Equipment Operating Below Culvert Roof .....	176
9.2.2 Dynamic Pressure Induced by Other Construction Equipment ..	184
9.2.3 Compacting Equipment Operating above Culvert Roof .....	187
9.3 Analysis of Dynamic Earth Pressure .....	189
9.3.1 Analytical Solution - Lateral Pressure Increment under a Finite Uniform Load .....	189
9.3.2 Distribution of Dynamic Earth Pressures .....	191
9.4 The Residual Pressure Characterization .....	194
9.4.1 Prediction of Residual Pressure Immediately after Compaction ..	197



9.4.2 Residual Pressure Variation with Time .....	199
9.5 Structural Response of Box Culvert to Dynamic Earth Pressures .....	202
9.6 Summary .....	204
9.7 References: .....	206
 <b>PART V BACK ANALYSIS OF THE FAILED BOX CULVERT IN SULLIVAN COUNTY .....</b>	 <b>208</b>
 <b>Chapter 10 Analysis of Earth Pressures on a Failed Box Culvert .....</b>	 <b>209</b>
10.1 Introduction .....	208
10.2 Analytical Procedure .....	210
10.3 Measured Earth Pressures and Numerical Analysis of Replacement Culvert .....	214
10.3.1 Measured Earth Pressures on Replacement Culvert .....	214
10.3.2 Calibration of Material Properties .....	218
10.3.3 Comparison of Measured Pressures with AASHTO Design Guides .....	218
10.4 Analysis of the Original Failed Culvert .....	221
10.4.1 Analysis Assumptions .....	221
10.4.2 Considerations for Compactive Efforts .....	223
10.4.3 Results and Comparison with AASHTO Design Guides .....	224
10.5 Response of Failed Culvert .....	227
10.5.1 The Internal Forces .....	227
10.5.1.1 Moments and Shear Forces in the Original Culvert Roof .....	228
10.5.1.2 Moments and Shear Forces in the Original Culvert Wall .....	230
10.5.2 Structural Capacities .....	233
10.6 Conclusions .....	238
10.7 References: .....	239
 <b>PART VI ANALYTICAL EVALUATION AND CONCLUSIONS .....</b>	 <b>242</b>
 <b>Chapter 11 The Influence of Highway Alignment on the Soil Pressures Acting on Box Culvert .....</b>	 <b>243</b>
 <b>Chapter 12 Influence of Supporting Layer Stiffness on Lateral Earth Pressure Distribution .....</b>	 <b>248</b>
 <b>Chapter 13 Summaries and Conclusions .....</b>	 <b>258</b>
12.1 Factors Affecting the Earth Pressures .....	258
12.1.1 Height of Embankment .....	258
12.1.2 Compactive Effort .....	260

12.1.3 Subsurface Conditions and Structure Stiffness .....	261
12.1.4 Dynamic Lateral Pressure .....	262
12.1.5 Culvert Orientation with Respect to Embankment Alignment ..	263
12.2 Factors Causing the Failure of Previous Culvert .....	263
<b>References</b> .....	265
<b>Vita</b> .....	272

## List of Figures

<u>Figure</u>	<u>Page</u>
<b>Chapter 1</b>	
Figure 1-1 Photograph of Interior Wall of Failed Concrete Box Culvert, Sullivan County, Tennessee (courtesy of TDOT, 1995) . . . . .	3
Figure 1-2 Photograph of Exterior Wall of Failed Concrete Box Culvert, Sullivan County, Tennessee (courtesy of TDOT, 1995) . . . . .	3
Figure 1-3 Typical Culvert Instrumentation Layout and Numbering Scheme . . . . .	5
Figure 1-4 Site Map of Sullivan County Culvert (N36E31'33.6", W82E12'42") . . . . .	5
Figure 1-5 Site Map of Greene County Culvert (N36E07'55.7", W82E48'39.5") . . . . .	6
Figure 1-6 Schematic of Embankment and Culvert Cross-Section with Typical Sections A and B . . . . .	8
<b>Chapter 2</b>	
Figure 2-1 Various Classes of Culvert Installations (Spangler, 1982) . . . . .	17
Figure 2-2 Classification of Culverts . . . . .	18
Figure 2-3 Systematic Errors in the Measurement of Soil Pressures (Seed et al., 1991) . . . . .	26
Figure 2-4 Instrumentation of Box Culvert (Tadros, 1986) . . . . .	29
Figure 2-5 Comparison of Test and old AASHTO (1973) Results - 1.2 × 1.2 m Box Culvert on Yielding Foundation, Clark County, Kentucky (Tadros, 1986) . . . . .	31
Figure 2-6 Comparison of Test and old AASHTO (1973) Results - 1.5 × 1.5 m Box Culvert on Unyielding Foundation, Clark County, Kentucky (Tadros, 1986) . . . . .	32
Figure 2-7 Recorded Vertical Earth Pressure on the Roof of Box Culvert (Jan Vaslestad et al., 1994) . . . . .	34
Figure 2-8 Measured Horizontal Earth Pressures on the Texas Experimental Culvert (James, 1986) . . . . .	35
Figure 2-9 Layout of Earth Pressure Cells in Nebraska Box Culvert Test (Tadros, et al., 1989) . . . . .	36
Figure 2-10 Measured Soil Pressure Distributions under Permanent Fill at the Completion of Backfilling (Tadros et al., 1989) . . . . .	38
Figure 2 -11 Measured Earth Pressures under Permanent 80 Days after Completion of Backfilling (Tadros, et al., 1986) . . . . .	39

<b><u>Figure</u></b>	<b><u>Page</u></b>
Figure 2-12 Recorded and Predicted Earth Pressures over Model Box Culvert in Sand Fill (Dasgupta and Sengupta, 1991) . . . . .	41
Figure 2-13 Schematic of Dynamic Pressures During a Transient Loading . . . . .	43
Figure 2-14 Experimental Retaining Wall at TRRL, England (Carder, Pocok and Murry, 1977) . . . . .	47
Figure 2-15 Compaction of Sand (Carder et al., 1977) . . . . .	48
Figure 2-16 Compaction of Silty Clay (Carder, et al., 1977) . . . . .	49
Figure 2-17 Compaction of Heavy Clay (Murry, 1988) . . . . .	50
Figure 2-18 Broms' Interpretation of Compaction Induced Lateral Pressure (Ingold, 1979) . . . . .	51
Figure 2-19 Ingold's Interpretation of Compaction Induced Lateral Pressure (Ingold, 1979) . . . . .	52
Figure 2-20 Variation in Total Horizontal Stress in Cohesive Backfills (Clayton and Symons, 1992) . . . . .	53
Figure 2-21 Illustration of Rehnman and Broms' Instrumentation (After Seed and Duncan, 1986) . . . . .	60
Figure 2-22 Stress Increases in Loose Dumped Soil (Section B of Figure 2-21) . . . . .	61
Figure 2-23 Stress Increases in Loosely Dumped Soil (Section A of Figure 2-21) . . . . .	62
Figure 2-24 Stress Increase in Compacted Soil (Section B of Figure 2-21) . . . . .	64
Figure 2-25 Stress Increase in Compacted Soil (Section A of Figure 2-21) . . . . .	65
Figure 2-26 Dynamic Lateral Pressure Increase Induced by Compaction (After Butcher and Marsland, 1989) . . . . .	68
Figure 2-27 Dynamic Lateral Pressure Increase Induced by Vehicle Load in Service (After Butcher and Marsland, 1989) . . . . .	69
 <b>Chapter 3</b>	
Figure 3-1 Photograph of Interior Wall of Failed Concrete Box Culvert, Sullivan County, Tennessee (courtesy of TNDOT, 1995) . . . . .	73
Figure 3-2 Photograph of Exterior Wall of Failed Concrete Box Culvert, Sullivan County, Tennessee (courtesy of TNDOT, 1995) . . . . .	73
Figure 3-3 Definition of Culvert Geometry Terms Used in Table 3-3 . . . . .	79

<b><u>Figure</u></b>	<b><u>Page</u></b>
<b>Chapter 4</b>	
Figure 4-1 EGP-350 Embedment Strain Gage, Measurement Group, Inc . . . . .	82
Figure 4-2 Schematic of Vibrating Wire Gage . . . . .	84
Figure 4-3 Geokon Model VCE-4200 Vibrating Wire Concrete Strain Gage . . . . .	87
Figure 4-4 Geokon Model 4810 Contact Pressure Cell . . . . .	91
Figure 4-5 Schematic of Strain Gage Installation . . . . .	92
Figure 4-6 No-Stress Strain Gage Reading vs. Temperature (Resistance Gage) . . . . .	95
Figure 4-7 No-Stress Strain Gage Reading vs. Temperature (Vibrating Wire Gage) . . .	95
Figure 4-8 Installation of Pressure Cell . . . . .	96
Figure 4-9 Illustration of Pressure Cell Locations in Section A (Greene County, TN) . . . . .	98
<b>Chapter 5</b>	
Figure 5-1 Illustration of Finite Element Meshes for Current Replacement Culvert in Sullivan County . . . . .	100
Figure 5-2 Linear Drucker Prager Model: Yield Surface and Flow Direction in the $p$ - $t$ Plane . . . . .	101
Figure 5-3 Comparison of Measured Earth Pressures with Numerical Prediction of Different Interface Considerations . . . . .	105
Figure 5-4 Illustration of Gauss Point of Different Elements . . . . .	107
Figure 5-5 Predicted Vertical Pressures on Failed Culvert Roof by Different Stress Calculation Methods (Sullivan County, TN) . . . . .	109
Figure 5-6 Predicted Horizontal Pressures on Failed Culvert by Different Stress Calculation Methods (Sullivan County, TN) . . . . .	110
<b>Chapter 6</b>	
<b>Chapter 7</b>	
Figure 7-1 Schematic of Culvert and Pressure Cell Detail (Replacement Culvert, Sullivan Co., TN) . . . . .	123
Figure 7-2 Schematic of Backfill Conditions and Finite Element Mesh (Replacement Culvert, Sullivan Co., TN) . . . . .	125

<b><u>Figure</u></b>	<b><u>Page</u></b>
Figure 7-3 Comparison of Recorded and Predicted Pressure During Back Filling (Replacement Culvert, Sullivan Co., TN) . . . . .	128
Figure 7-4 Comparison of Various Models with Recorded Results at Full Backfill Height (Replacement Culvert, Sullivan Co., TN) . . . . .	131
Figure 7-5 The Influence of Gravel and Side Soil Modulus on the Distribution of Lateral Earth Pressure (Replacement Culvert, Sullivan Co., TN) . . . . .	133

## **Chapter 8**

Figure 8-1 Illustration of Culvert Dimensions and Pressure Cell Location (Greene Co., TN) . . . . .	140
Figure 8-2 Schematic of Embankment and Culvert Cross-Section with Typical Sections A and B (Greene Co., TN) . . . . .	141
Figure 8-3 Installation of Contact Pressure Cell on the Culvert . . . . .	142
Figure 8-4 Recorded Vertical Pressures on the Culvert Roof with Backfill Height above Roof (Greene Co., TN) . . . . .	143
Figure 8-5 Recorded Lateral Pressures on the Culvert Wall with Backfill Height above Cells (Greene Co., TN) . . . . .	145
Figure 8-6 Recorded Lateral Pressures at Bottom of Wall with Backfill above the Cells (Greene Co., TN) . . . . .	146
Figure 8-7 Weighted Average of Recorded Pressures Compared with AASHTO Pressures (Greene Co., TN) . . . . .	149
Figure 8-8 Comparison of the Normalized Vertical Pressures with Normalized AASHTO Pressures . . . . .	151
Figure 8-9 Recorded Lateral Pressures Compared with AASHTO Pressures (Greene Co., TN) . . . . .	154
Figure 8-10 Parametric Study of Earth Pressures under Different Compaction Conditions (Sullivan Co., TN) . . . . .	155
Figure 8-11 Recorded Vertical Pressures on the Culvert Roof during Construction and under Service Load (Greene Co., TN) . . . . .	162
Figure 8-12 Recorded Lateral Pressures on the Culvert Wall during Construction and under Service Load (Greene Co., TN) . . . . .	163

<b><u>Figure</u></b>	<b><u>Page</u></b>
Figure 8-13 Recorded Lateral Pressures at Bottom of Culvert Wall during Construction and under Service Load (Greene Co., TN) .....	164
Figure 8-14 Recorded Vertical Pressures Compared with AASHTO Pressures (Greene Co., TN) .....	166
Figure 8-15 Weighted Pressures Compared with AASHTO Pressures (Greene Co., TN) .....	167
Figure 8-16 Comparison of Measured Earth Pressures on Culvert with AASHTO Pressures (Section A, full embankment height, Greene Co., TN) ..	168
Figure 8-17 Comparison of Measured Earth Pressures on Culvert with AASHTO Pressures (Section B, full embankment height, Greene Co., TN) ..	169

## **Chapter 9**

Figure 9-1 Schematic of Box Culvert with Typical Dimensions of Gravel Backfill Zone .....	171
Figure 9-2 Photograph of Culvert Wall ( Greene Co., TN) Showing Resistance (REP) and Vibrating Wire (PRE) Earth Pressure Cells .....	173
Figure 9-3 Typical Dynamic Pressure Pattern due to Vibratory Roller (recorded interval: 30 seconds) .....	177
Figure 9-4 Dynamic Pressure at Dense Gravel (recording interval: 30 seconds) .....	178
Figure 9-5 Dynamic Pressure Induced by Roller 0.6 m to Wall (recorded interval: 20 seconds) .....	179
Figure 9-6 Dynamic Pressure Distribution along Culvert (recorded interval: 30 seconds) .....	181
Figure 9-7 Dynamic Pressure Distribution along Culvert Wall (recording interval: 60 seconds) .....	183
Figure 9-8 Dynamic Pressures at Different Depths (roller: Ingersoll-Rand SP56, 0.2 m from wall) .....	185
Figure 9-9 Response of Pressure Cells of Loaded Truck Spreading Gravel (recording interval: 30 seconds) .....	186
Figure 9-10 Typical Recorded Dynamic Pressure Pattern When backfill over Culvert Roof .....	188



<b><u>Figure</u></b>	<b><u>Page</u></b>
Figure 9-11 Boussinesq's Elastic Solution for Lateral Earth Pressure Induced by a Vibratory Roller Drum .....	190
Figure 9-12 Total Compaction Pressure Induced by DD130 Double Drum Vibratory Roller .....	192
Figure 9-13 Total Compaction Pressure Induced by SP 56 Single Drum Vibratory Roller .....	193
Figure 9-14 Lateral Impulse Pressure Induced by DD130 Vibratory Roller ( $x_1=0.3$ m) .....	195
Figure 9-15 Lateral Impulse Pressure Induced by SP 56 Vibratory Roller ( $x_1=0.25$ m) .....	196
Figure 9-16 Measured and Predicted Lateral Residual Pressure on Wall (For Backfill Height Below Culvert Roof) .....	200
Figure 9-17 Lateral Residual Pressure Change with Time .....	201
Figure 9-18 Structural Response to the Dynamic Lateral Pressures .....	203

## **Chapter 10**

Figure 10-1 Illustration of Culvert Dimensions .....	210
Figure 10-2 Schematic of Backfill Conditions of Replacement Culvert (Sullivan County, TN) .....	212
Figure 10-3 Observed Vertical Pressures on the Culvert Roof (Replacement Culvert, Sullivan Co., TN) .....	216
Figure 10-4 Observed Lateral Pressures on the Culvert Wall (Replacement Culvert, Sullivan Co., TN) .....	216
Figure 10-5 Temperature Corrected Vertical Pressures (Replacement Culvert, Sullivan Co., TN) .....	217
Figure 10-6 Temperature Corrected Lateral Pressures (Replacement Culvert, Sullivan County, TN) .....	217
Figure 10-7 Comparison of Temperature Corrected Earth Pressures with FEM Analysis and AASHTO Pressures (Replacement Culvert, Sullivan Co., TN) ..	219
Figure 10-8 Assumed Backfill Conditions for Original Culvert and Finite Element Mesh (Sullivan Co., TN) .....	222

<b><u>Figure</u></b>	<b><u>Page</u></b>
Figure 10-9 Comparison of Probable Earth Pressures with AASHTO Pressures (Original Culvert, Sullivan Co., TN) . . . . .	225
Figure 10-10 Culvert Model for Structure Analysis . . . . .	228
Figure 10-11 Calculated Bending Moment in Culvert Roof under Different Pressure Distributions (Original Culvert, Sullivan Co., TN) . . . . .	229
Figure 10-12 Calculated Shears in Culvert Roof under Different Pressure Distributions (Original Culvert, Sullivan Co., TN) . . . . .	231
Figure 10-13 Calculated Bending Moment in Culvert Wall under Different Pressure Distributions (Original Culvert, Sullivan Co., TN) . . . . .	232
Figure 10-14 Calculated Shears in Culvert Wall under Different Pressure Distributions (Original Culvert, Sullivan Co., TN) . . . . .	234
Figure 10-15 Axial Force - Moment Diagram of External Culvert Wall (Original Culvert, Sullivan Co., TN) . . . . .	235
Figure 10-16 Comparison of Probable Shear Forces in the Culvert Wall with ACI Shear Capacity (Original Culvert, Sullivan Co., TN) . . . . .	236
 <b>Chapter 11</b>	
Figure 11-1 Stress at Point in Elastic Half Space . . . . .	243
Figure 11-2 Assumed State of Stress at Point A under the Embankment . . . . .	243
Figure 11-3 State of Stress on Vertical Plane Normal to Embankment Axis . . . . .	245
Figure 11-4 State of Stress on Vertical Plane Skewed with Respect to Embankment Axis ( $\theta > 0$ ) . . . . .	246
 <b>Chapter 12</b>	
Figure 12-1 Measured Horizontal Earth Pressures at Greene County Culvert (Full Embankment Height) . . . . .	250
Figure 12-2 Lateral Pressures at Three Instrumentation Sections with an Embankment Height of 3 m . . . . .	251
Figure 12-3 Finite Element Mesh and Conditions for Parametric Study (Greene County, TN) . . . . .	252

<b><u>Figure</u></b>	<b><u>Page</u></b>
Figure 12-4 Influence of Supporting Layer Moduli on Culvert Earth Pressures (Well Compacted Gravel, Greene County, TN) . . . . .	254
Figure 12-5 Influence of Gravel Compactive Effort on Culvert Earth Pressures (Soft Supporting Layer, Greene County, TN) . . . . .	257

## List of Tables

<u>Table</u>	<u>Page</u>
Table 2-1 AASHTO (1996) Culvert Design Earth Pressures in the Trenched or Untrenched on Yielding Foundation .....	21
Table 2-2 Different Design Earth Pressure on Box Culverts .....	23
Table 2-3 Definition of Horizontal Earth Pressure Components of the Compaction Time History .....	44
Table 2-4 Material Properties of Backfill for TRRL Tests (After Carder et al., 1977 and Murry, 1988) .....	51
Table 2-5 Material Properties in a Large-Scale Test (Rehman and Broms, 1972) .....	52
Table 3-1 The Properties of Backfill and In-situ Soils .....	77
Table 3-2 Compaction Parameters of Backfills .....	77
Table 3-3 Summary of Instrumented Concrete Box Culverts .....	78
Table 4-1 Common Types of Concrete Strain Gages .....	81
Table 4-2 Specifications of the EGP-5-350 Strain Gage .....	83
Table 4-3 Characteristic of VCE-4200 Vibrating Wire Strain Gage .....	86
Table 4-4 Factors Affecting the Earth Pressure Cell Measurement (Modified from Welle and Kulhawy, 1982) .....	89
Table 4-5 Characters of the Contact Earth Pressure Cells .....	90
Table 5-1 Summary of Material Parameters in the Box Culvert Analysis (Replacement Culvert, Sullivan County, TN) .....	103
Table 6-1 Summary of Density Tests .....	113
Table 6-2 Summary of Triaxial Shear Tests .....	116
Table 6-3 Summary of Concrete Compression Tests .....	117
Table 7-1 Summary of Material Parameters, Standard Analysis .....	127
Table 7-2 Parametric Variation of Elastic Modulus of Gravel and Side Soil .....	132
Table 9-1 Details of Resistance Pressure Cells .....	174
Table 9-2 Selected Attributes of Compaction Equipment .....	175
Table 10-1 Comparison of Dimensions of Original and Replacement Culverts .....	210
Table 10-2 Material Properties from the Calibration Analysis of Replacement Culvert .....	220

Table 10-3 Comparison of Measured and Published Values of Elastic Modulus for Gravel . . . . .	224
Table 10-4 Material Properties Used in Analysis of Original Culvert . . . . .	226
Table 12-1 Summary of Material Properties in the Parametric Study . . . . .	253

**The Appendices are stored in the CD-ROM attached at the back**

## **Table of Contents**

<b>Appendix A Sullivan County Data</b> .....	273
Appendix A-1 Dimensions and Details of Culvert Reinforcement for Instrumentation Sections .....	274
Appendix A-2 Instrumentation Scheme - Sullivan County, TN .....	276
Appendix A-3 Chronology of Field Events - Sullivan County Culvert Field Record Results .....	281
Appendix A-4 Selected Recorded Earth Pressure Distributions .....	283
Appendix A-5 Original Vibrating Wire Pressure Cell Records Sullivan County Culvert Site (04/09/96-1/25/00) .....	285
Appendix A-6 Original Vibrating Wire Concrete Strain Gage Records Sullivan County Culvert Site (04/09/96-1/25/00) .....	294
 <b>Appendix B Green County Data</b> .....	 304
Appendix B-1 Dimensions and Details of Culvert Reinforcement for Instrumentation Sections .....	305
Appendix B-2 Instrumentation Scheme - Greene County, TN .....	307
Appendix B-3 Chronology of Field Events - Greene County Culvert Field Record Results .....	314
Appendix B-4 Original Vibrating Wire Pressure Cell Records Greene County Culvert Site (10/31/96-1/25/00) .....	317
Appendix B-5 Original Vibrating Wire Concrete Strain Gage Records Greene County Culvert Site (04/09/96-1/25/00) .....	332
 <b>Appendix C Dynamic Horizontal Earth Pressures Induced by Construction Equipment</b> .....	 358
 <b>Appendix D Triaxial Shear Test Results</b> .....	 371
Appendix D-1 Clayey Shale (Sullivan County, TN) .....	372

Appendix D-2 Gravel (Greene County, TN) .....	391
Appendix D-3 Undisturbed Silty Clay (Greene County, TN) .....	410
Appendix D-4 Clay (Greene County, TN) .....	431
<b>Appendix E Concrete Cylinder Test Data .....</b>	<b>447</b>
Appendix E-1 Sullivan County Culvert Concrete Test .....	448
Appendix E-2 Greene County Culvert Concrete Test .....	457
<b>Appendix F Selected Input Files for Finite Element Analysis</b>	
<b>Using ABAQUS Code .....</b>	<b>463</b>
<b>Appendix G Calibration Sheet for Instrumentation Gages .....</b>	<b>500</b>
<b>Appendix H Earth Pressure Variations under</b>	
<b>Constant Embankment Height .....</b>	<b>533</b>
H1 Abstract .....	533
H2 Introduction .....	534
H3 Examples of Earth Pressures Variation during the	
Long-term Observation .....	534
H3.1 Previous Case Studies .....	534
H3.2 Earth Pressures on A Box Culvert under the	
Constant Embankment Height .....	536
H4 Factors Influence the Earth Pressure Reading with Time .....	537
H5 Contact Pressure Cells Configurations .....	541
H6 Instrumentation on Box Culvert Sites .....	542
H7 Observed Temperature Effects at Different Conditions .....	545
H7.1 Earth Pressure Changes at Zero Load .....	546
H7.2 Earth Pressure Variation under Constant	
Embankment Height .....	550
H8 Earth Pressures acting on the Culvert after	
Temperature Correction .....	556
H9 Summaries and Conclusions .....	561
H10 Acknowledgments .....	563
H11 References .....	563



**PART I**  
**RESEARCH BACKGROUND**

# **Chapter 1**

## **Introduction and Scope of Work**

### **1.1 Objective**

The work described in this dissertation is a part of a research program to evaluate the factors affecting the performance of cast-in-place concrete box culverts, and based on this evaluation, make recommendations regarding design and construction practice. Supported by Tennessee Department of Transportation (TDOT), the scope of this dissertation is the investigation of the factors affecting earth pressures on cast-in-place box culverts.

### **1.2 Background**

A reinforced concrete box culvert in Sullivan County, Tennessee, under approximately 12 meters clayey black shale fill failed shortly after being placed in service in late 1995. The mode of failure suggested that the earth pressures exceeded the capacity of the reinforced concrete walls, Figure 1-1 and Figure 1-2. Uncertainties in the estimation of earth pressures for culvert design have resulted in several changes in the American Association of State Highway and Transportation Officials (AASHTO) guide during the period 1973 - 1996 (AASHTO 12<sup>th</sup> edition to 16<sup>th</sup> edition) with respect to recommended design pressures. To investigate the earth pressures acting on box culverts, an instrumentation project was initiated in March 1996. Pressure cells and strain gages were installed in the new replacement culvert constructed in Sullivan County, TN,



Figure 1-1 Photograph of Interior Wall of Failed Concrete Box Culvert, Sullivan County, Tennessee (courtesy of TDOT, 1995)



Figure 1-2 Photograph of Exterior Wall of Failed Concrete Box Culvert, Sullivan County, Tennessee (courtesy of TDOT, 1995)

(Figure 1-3), which is located as shown in Figure 1-4. The replacement culvert, which was much stiffer than the original culvert, was constructed with reduced compactive effort to limit earth pressures.

To confirm the field recorded earth pressures and structural response in Sullivan County, and to examine the impact of compaction effort on the earth pressures, another culvert in Greene County, Tennessee, was instrumented (Figure 1-5). The Greene County culvert was constructed with typical compactive effort, with about 19 meters of silty clay fill.

### **1.3 Factors Affecting the Performance of Cast-in-place Concrete Box Culverts**

There are a number of factors which may affect the performance of cast-in-place concrete box culverts. The factors identified to be investigated in this study include:

- ! height of embankment and properties of the backfill,
- ! orientation of culvert with respect to the alignment of the embankment,
- ! analysis and design procedures for concrete box culvert structures,
- ! lateral earth pressures induced during compaction of the backfill,
- ! loadings due to construction equipment/placement of haul roads.

The research program described here was designed to focus on these factors. There are other factors, not within the scope of the investigation, that may affect the performance of concrete box culverts. These factors include:

- ! foundation support condition (yielding/unyielding foundation)
- ! expansive minerals in the backfill material
- ! changes in backfill material over time due to weathering, e. g., grain size

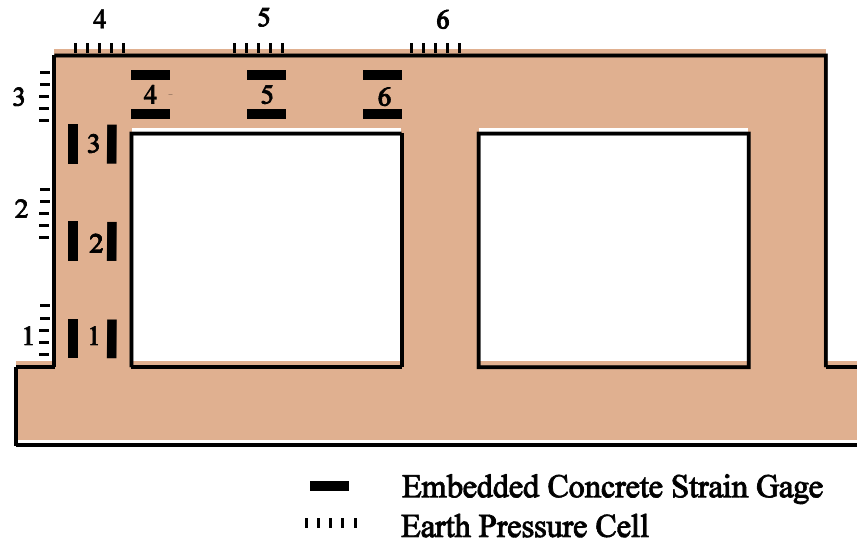


Figure 1-3 Typical Culvert Instrumentation Layout and Numbering Scheme

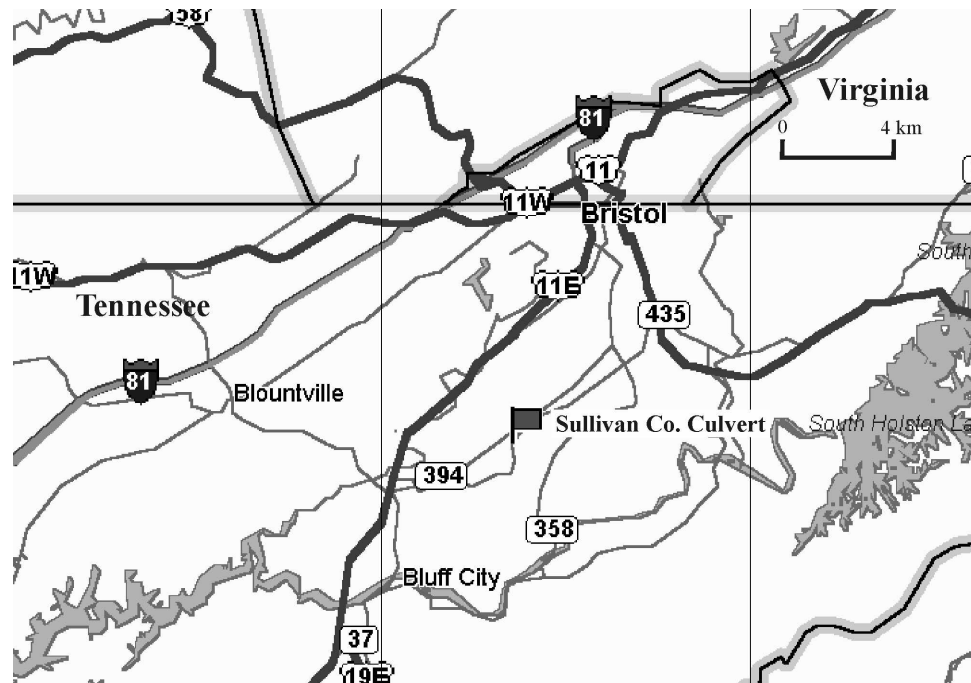


Figure 1-4 Site Map of Sullivan County Culvert  
 (N 36°31'33.6", W 82°12'42")

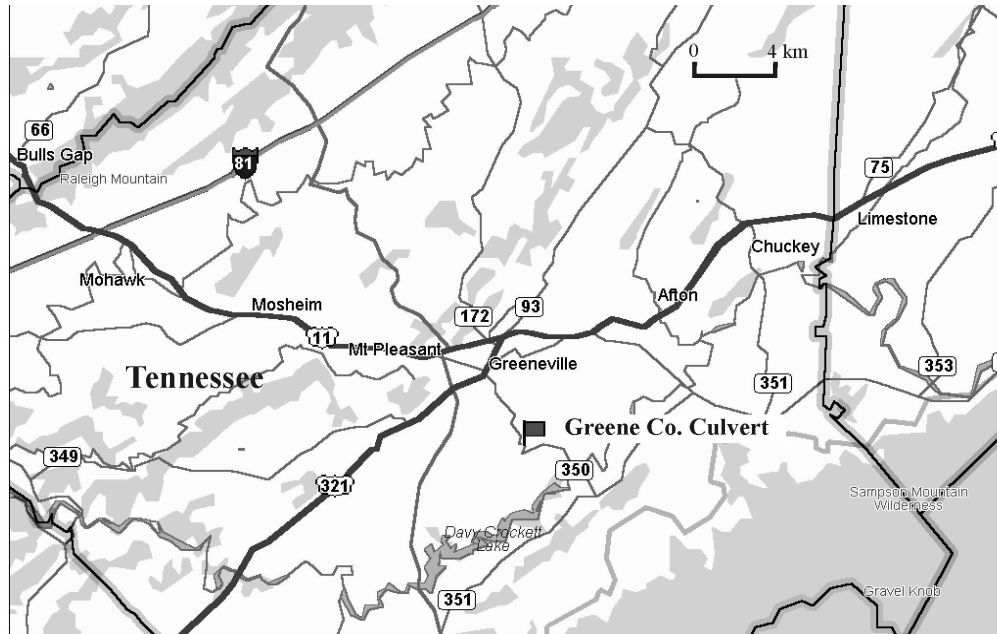


Figure 1-5 Site Map of Greene County Culvert  
(N 36°07'55.7", W 82°48'39.5")

distribution changes.

## 1.4 Research Tasks

Four research tasks were identified:

- ! Task 1 - Literature review and preliminary evaluation of earth pressures on box culverts,
- ! Task 2 - Design and installation of instrumented culvert sections,
- ! Task 3 - Evaluation of factors affecting the performance of box culverts,
- ! Task 4 - Monitoring the earth pressures on box culverts.

Each of these tasks is discussed below.

### 1.4.1 Task 1 - Literature review and preliminary evaluation of earth pressures on box culverts

An analysis of the earth pressures and potential failure modes of a typical box

culvert was necessary prior to the development of a detailed plan for the instrumentation. This analysis included basic calculations of the earth pressures, as well as determination of the load capacity and stiffness of the standard box culvert design. This analysis provided insight into potential failure modes, as well as aided the determination of the number, capacity, and location of the individual instruments.

#### **1.4.2 Task 2 - Design and installation of instrumented culvert sections**

Similar instrumentation schemes were used for both the reconstructed (Sullivan County) and the new (Greene County) box culverts. The general instrumentation scheme for the box culverts is also shown in Figure 1-5. Only one cell of the culvert was instrumented since the loading and response may be assumed to be symmetrical about the culvert centerline.

Two locations (Sections A and B) along the length of each culvert were instrumented. Figure 1-6 depicts the relative location of Sections A and B for the two culverts. Section A is located near the center of the full embankment height, while section B is located such that the overburden height is less than the full height.

Instruments were installed to measure the earth pressures (loading) on the structure, as well as the strain (response) due to these loads. Knowledge of the applied pressures and the resulting strains in the structure can be used to determine the shear forces and bending moments in the concrete. The instrumentation scheme was designed to provide a level of instrument redundancy to account for the anticipated loss of some instruments during construction. In addition, the instrumentation program includes both vibrating



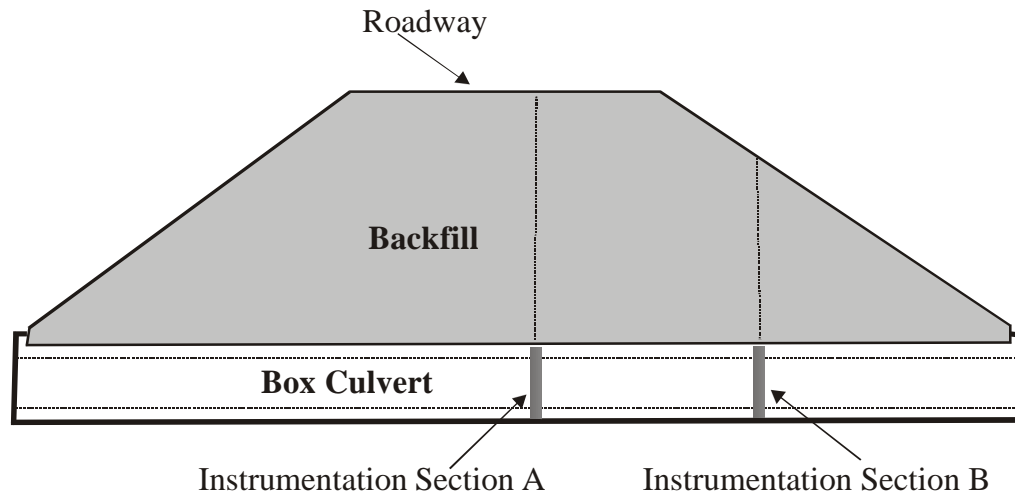


Figure 1-6 Schematic of Embankment and Culvert Cross-Section  
with Typical Sections A and B

wire transducers and resistance gage transducers. Vibrating wire transducers provide excellent long term stability, while the resistance gages provide better response to time varying construction loadings.

Instrumentation for Earth Pressures The instrumentation scheme consists of a system of earth pressure cells along the top and sides of the culvert. Due to arching effects around earth pressure cells, reliable measurements of earth pressure are difficult field to obtain. The results can be improved if the pressure cells are carefully mated to the surface of the structure, and a layer of sand placed between the cell and the backfill material. Six identical vibrating wire pressure cells were placed around one cell of the structure, three on the top and three on the side, as shown in Figure 1-3. In Greene County, additional resistance earth pressure cells were placed in Section A to detect dynamic pressures due to construction loads.

Instrumentation for Concrete Strain Measurements of concrete strain can be obtained with much more reliability than measurements of earth pressure. Strain measurements provide a direct indication of the structural response due to the imposed loads, and can be used to determine the bending moments and shear forces in the concrete. With a knowledge of the structural properties, the strain can be also used to estimate the loads applied to the structure. Two different types of embedded concrete strain gages were used. A series of embedded vibrating wire gages was supplemented with a series of embedded resistance strain gages. The resistance gages provide advantages in terms of lower costs and the ability to measure the time dependent construction loads. However, these gages are a relatively new product and little is known about the long term performance. Therefore, both gage types were used for this important series of measurements.

#### **1.4.3 Task 3 - Evaluation of factors affecting the performance of box culverts**

The following factors were identified as important in terms of the performance of buried box culverts, and were investigated in the research project.

##### **1.4.3.1 Height of embankment and properties of the backfill**

Vertical and lateral earth pressures due to the backfill depend upon the height of the embankment and the unit weight, shear strength, and the modulus of the backfill material. Depending upon the relative stiffness of the structure and backfill, soil-structure interaction effects and arching may occur, resulting in significant changes in the stress distribution around the structure.

#### **1.4.3.2 Orientation of culvert with respect to alignment of embankment**

The orientation of the culvert with respect to the alignment of the embankment may affect the lateral loads acting on the buried structure. This can be evaluated in a qualitative manner by analytical techniques. With field measurements of the earth pressures, these procedures can be evaluated.

#### **1.4.3.3 Analysis and design procedures for the box culvert concrete structure**

The procedures used in the analysis and design of the concrete structure are directly related to the capacity, stiffness and economics of the structure.

#### **1.4.3.4 Lateral earth pressures induced during compaction of the backfill**

Placement and compaction of backfill around and over the box culvert can result in significant stresses. Earth pressures may be reduced by limiting the use of heavy construction equipment until a specified amount of cover soil has been placed. Unfortunately, these limits are often based on judgement and do not consider the weight of the equipment, geometry of the box culvert, nor the properties of the backfill material. Although low compactive effort may reduce the earth pressures, it may result in excessive settlement of the embankment above. Compaction equipment and procedures required to break up shale backfill materials may induce significant lateral loads.

The effects of these factors were investigated through a combination of field measurements and a series of computer analyses. These analyses were conducted on computer models that permit the investigation of a range of factors including the variation of backfill material properties. The results can be used to provide useful guidelines on the range of anticipated loads and the resulting bending moments and shear forces in the box

culverts. This will permit an evaluation of the performance of the culverts due to each of the factors above. This information can then be used to establish guidelines relative to the design and construction practice for buried culverts.

#### **1.4.4 Task 4 - Monitoring the earth pressures on box culverts**

The box culverts were monitored from the time of instrument installation from April 9, 1996 to January 25, 2000. This time period provided a series of background measurements prior to loading, measurements of the loads during construction, and measurements over three years of the service life of the structure.

### **1.5 Format of Dissertation**

The dissertation consists of two portions:

- !      Portion I: Measurements and Analysis** Portion I provides technical details from a literature review of previous concrete box culvert research, a description of the field instrumentation, methods of analysis, parametric studies, and interpretation of results.
- !      Portion II: Field Data and Background Information** Portion II consists of a series of appendices with reduced field data, chronology of field events, and accumulated lab test results.

There are 13 chapters in Portion I: The objective and research tasks are stated in Chapter one. Chapter two is a literature review, in which earth pressure theories are reviewed and previous field instrumentation of reinforced box culverts is described. Chapter 3 summarizes the characteristics of instrumented culverts, both those from this investigation and some from previous investigations. Instrumentation design and

installation considerations are described in Chapter 4. Chapter 5 contains background information on the finite element analysis. An introduction to the data interpretation is included in Chapter 6, along with some general analysis results. Chapter 7 is a paper published in the proceedings of the 9th International Conference of the Association for Computer Methods and Advances in Geomechanics. This paper focused on the impact of reduced compactive efforts on the earth pressures, based on the field data from pressure cells installed in Sullivan County. Chapter 8 is a paper published in the proceedings of the ASTM Symposium on Field Instrumentation for Soil and Rock, and consists of the measurement results of the earth pressures recorded in the Greene County culvert. An addendum section of this chapter provides results obtained since the paper was published. Chapter 9 describes the use of electric resistance pressure cells and strain gages to register the dynamic lateral load induced by construction equipment. Extensive in-situ measurements were made of a wide variety of load impulses induced by different equipment under different conditions. The analysis of the original failed Sullivan County culvert under normal compaction conditions is presented in Chapter 10. The influence of culvert alignment on earth pressures in an embankment is analyzed in Chapter 11. The influence of supporting layer stiffness on the later earth pressure distribution is investigated in Chapter. Chapter 13 contains conclusions and suggestions based on this research.

Portion II consists of a series of appendices as follows:

- ! Appendix A: the structural and instrumentation details of the original and the replacement culvert sections in Sullivan County and the recorded data

from pressure cells. A chronology of the events both during the construction period and during the instrumentation period is also included. The original field recorded data in Sullivan County are also attached in this appendix

- ! Appendix B: the structural details and instrumentation details of the Greene County culvert and the recorded static and dynamic data from pressure cells. A chronology of the events both during the construction period and during the instrumentation period is also included. This appendix also includes the original field recorded data
- ! Appendix C: The dynamic horizontal earth pressures induced by six different construction machines are listed.
- ! Appendix D: Triaxial test result of soil samples collected from two culvert sites.
- ! Appendix E: Test results of concrete cylinders collected from culvert sites.
- ! Appendix F: An input files for ABAQUS finite element analysis of box culverts under deep embankment height is illustrated here.
- ! Appendix G: Calibration sheet of pressure cells provided by the manufacturer
- ! Appendix H: Temperature correction method for earth pressure readings under constant embankment height.

These appendices are contained electronically in a CD-ROM in Adobe Acrobat PDF format. The CD-ROM is attached in the back of this dissertation.

## **Chapter 2**

### **Literature Review - Earth Pressures on Buried Structures**

#### **2.1 Earth Pressures on Buried Pipes and the Marston Theory**

Cast-in-place concrete box culverts are often used as conduits for water from one side of a highway embankment to another. Although this is a rather simple role, the loads applied to these structures during construction and the subsequent service life can be complex. These structures must resist substantial vertical and lateral earth pressures, and are often subject to significant loadings during construction of the embankment. Due to soil-structure interaction effects, the state of stress around the structure depends upon the stiffness of both the backfill material and the structure. In spite of the complex state of stress around these structures, simple routine design procedures must be used for these structures due to the large number that are placed in service. Current design methods distinguish between “rigid” culverts, which are structurally stiff with respect to the surrounding soil and “flexible” culverts.

##### **2.1.1 Concept of Soil Arching**

The loads exerted on buried structures were first studied by Anson Marston, on relatively small size pipe culverts. The Marston theory (Spangler, 1982), mainly focused on the reduction of vertical loads on circular pipe culverts by placing the culvert into a trench. The basic concept of the theory is that the load due to the weight of the soil prism

above a buried structure (mainly small diameter pipe) is modified by arching action. Part of the soil weight is transferred to the adjacent side soils with the result that in some cases the vertical pressure on the pipe may be less than that due to the weight of the overburden.

The arching effects are dependent upon the relative movement of soil near the structure, and can be divided into positive and negative arching effects. Positive arching effect decreases the vertical pressure exerted on the structure whereas negative arching effect increases the vertical pressure.

In the case of a culvert installed in a trench, the backfill material is more compressible than the adjacent soil and has a tendency to consolidate and settle downward. This tendency, combined with the culvert deformation and settlement of the culvert into the bedding soil, causes the backfill immediately above the culvert to move downward relative to the existing trench soil at the side. The relative downward movements within the trench mobilize upward shearing stresses along the sides and create an arching action that partially supports the soil column weight above the structure. From the definition of the mechanism of positive arching by Marston (Spangler, 1982), it is clear that positive arching involves two phases: a reduction of the earth pressure on the yielding part of the soil-structure system and an increase in the earth pressures on the adjacent nonyielding areas. It is noted that the increase in pressure on the adjacent nonyielding areas is equal to or larger than the reduction in pressure on the yielding part. Similarly, in soil-culvert systems, the increase of vertical earth pressure above the culvert can result in a decrease of the vertical load in a zone adjacent to the culvert, which, in



turn, may reduce horizontal earth pressures on the side of the culvert.

### **2.1.2 Classification of Culverts**

For the purpose of vertical load characterization, culverts can be divided into different classes. According to the structural stiffness, the culverts are classified as rigid culverts or flexible culverts. Based on the construction and environmental conditions which may influence the loads, culvert installation may be classified as trench conditions or embankment conditions. Embankment conditions are further subdivided into the positive projecting embankment condition and the negative projecting embankment condition.

A trench condition is defined as an installation in a relatively narrow trench dug in passive or undisturbed soil which is then covered with earth backfill (Figure 2-1-(a)). Most utility pipes are installed this way. A positive projecting embankment is where the top of the culvert is above the natural ground and is then covered with an embankment, as shown in Figure 2-1-(b). Railway and highway culverts are frequently installed in this manner. A negative projecting embankment condition is when the pipe is installed in a relatively narrow and shallow trench with its top at an elevation below the natural ground surface and is then covered with an embankment (Figure 2-1-(c)). In construction of small size railway and highway culverts, this is a very advantageous installation since it can produce a lower vertical load at a given embankment height than would be the case for a positive projecting condition. With respect to the reduction in vertical earth pressure, this method of installation is more effective if the trench between the culvert and the natural ground surface is backfilled with highly compressible material. The imperfect trench

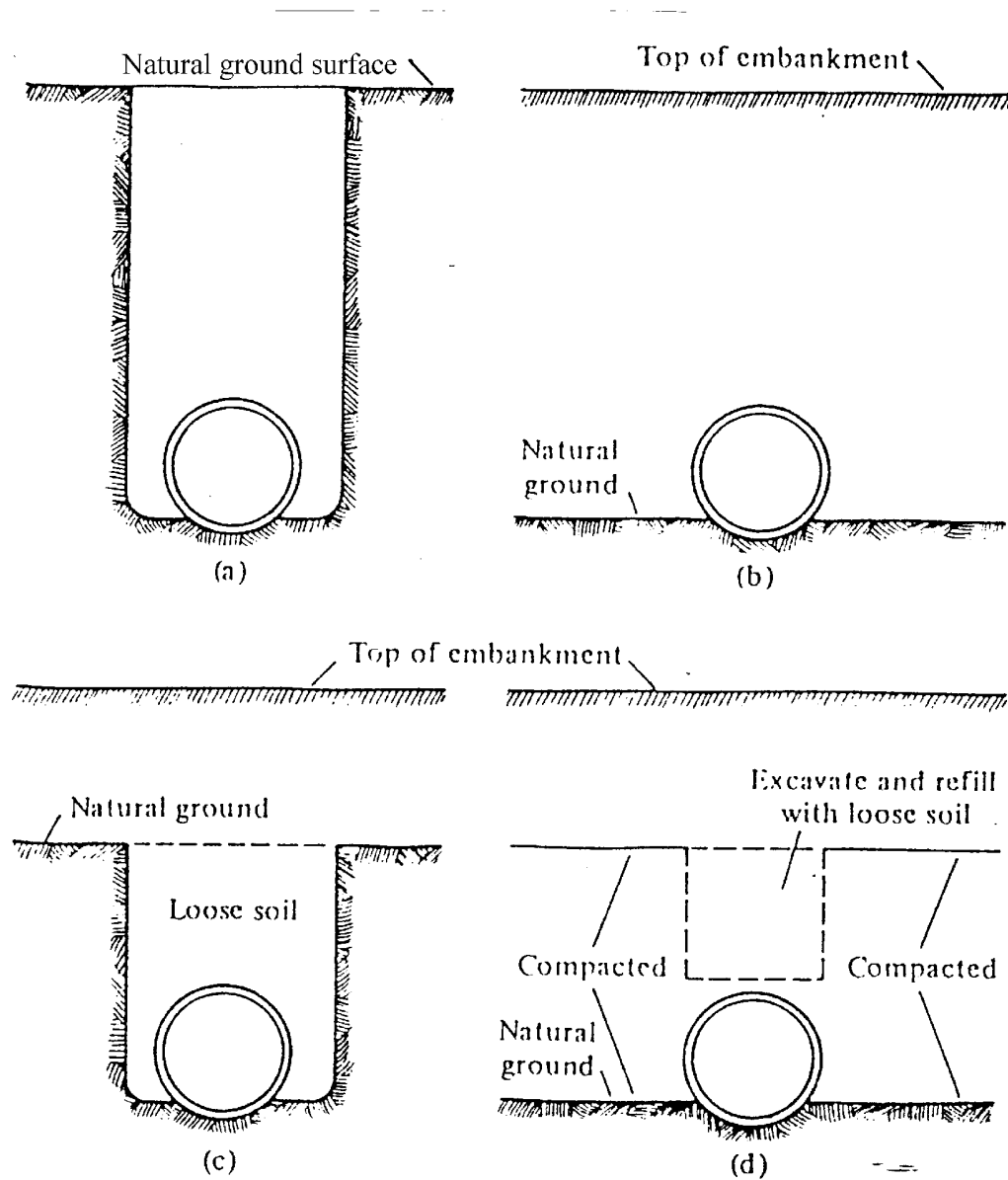


Figure 2-1 Various classes of culvert installations

- (a) Trench condition
- (b) Positive projection embankment condition
- (c) Negative projection embankment condition
- (d) Imperfect trench condition (Spangler, 1982)

condition, sometimes called the induced trench condition, and is a special mixed case (Figure 2-1-(d)). The culvert is placed on the natural ground, backfill in the area immediately above the culvert is replaced by an extremely compressible material to some height and then covered with normally compacted materials. This installation can also greatly reduce the vertical load exerted on the culvert. These installation types are used in the current AASHTO design guideline (AASHTO, 1996) to distinguish different soil-structure interaction effects. A summary of the classification of culverts is shown in Figure 2-2.

### 2.1.3 Arching Effects on Buried Structures

The installation conditions can have a significant effect on the earth pressures acting on buried structures. In a long-term full-scale field instrumentation project in Norway (Vaslestad et al. 1994), a 1.6 m diameter circular concrete culvert was constructed with the imperfect trench condition (the compressible material was expanded

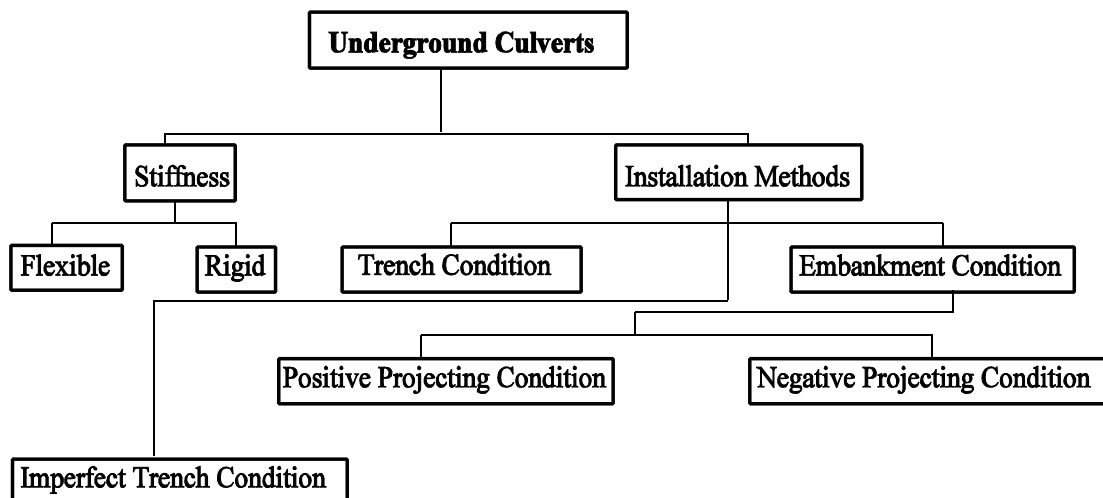


Figure 2-2 Classification of Culverts

polystyrene foam) with 14 m embankment height. Vertical earth pressure directly above the culvert was only 25% of that due to the soil prism weight. Horizontal earth pressure at the mid elevation of the culvert, however, was 73% of that due to the soil column weight above that elevation. In the same research, the vertical pressure above a box culvert with 10-m backfill height but with 0.5-m of expanded polystyrene foam placed immediately above the culvert was 50% of the pressure due to the weight of the soil prism above. However, the vertical pressure above an identical box culvert under the same embankment height without the foam, and with normally compacted backfill, was about 120% of that due to the soil prism weight. These examples indicate that installation methods and culvert shape can strongly influence the magnitude and distribution of earth pressures on rigid culverts.

The magnitudes of the loads exerted on culverts depend on arching effects, which are the result of relative deformation of the backfill in a certain zone above the culverts. This deformation is related to both the soil and the structural stiffness. In the case of flexible culverts, culvert deformation results in arching effects which reduce the vertical loading regardless of the installation method. Typically, the vertical earth pressure on flexible culverts is less than that due to the weight of the soil above the culvert. For rigid culvert installation, arching effects can also be achieved by introducing compressible material into the backfill. In the case of positive projecting embankments, arching results in vertical earth pressures that are greater than that due to the weight of soil above the culvert. Thus, according to the Marston theory, the vertical earth pressures on culverts are a function of the installation method, the soil and structural stiffness, the geometry of the

structure, and the boundary condition with the natural ground. It is worth noting that even for flexible culverts, a load reduction is achieved as differential settlements transfer loads to the surrounding soil adjacent to the structure.

#### **2.1.4 Recommended Earth Pressures on the Box Structures**

Marston Theory (Spangler, 1982) for earth pressures on buried pipes defines an equal settlement plane, which is a horizontal plane in the embankment. Above this plane the soil elements at the same elevation settle equally. Below this plane, the interior soil prisms immediately above the culvert settles relative to the adjacent exterior soil. A plane of equal settlement develops because a part of the vertical pressure in the exterior prisms is transferred by shearing to the interior prism, or vice versa. According to the Marston Theory, the load reduction installation techniques may not be used if strict settlement control is required. Also, installation methods employing loosely compacted backfills should not be employed in embankments which serve as a water barrier, since the loosely placed backfill may encourage channeling of the seepage water through the embankment.

The impact of foundation stiffness is not considered by Marston theory, although structural distress of rigid pipes below high embankments over soft soil has been observed (Heger and Selig, 1994). In the current AASHTO design guidelines (AASHTO, 16<sup>th</sup> edition, 1996), the earth pressures over yielding foundations are given, but no design earth pressures are defined in the case of unyielding foundations. Current AASHTO standards define the earth pressures on both trenched and untrenched culverts on yielding foundations in terms of the equivalent fluid pressure in Table 2-1.

Table 2-1 AASHTO (1996) Culvert Design Earth Pressures in the Trench or Untrenched on Yielding Foundation

Culvert Type	Equivalent Unit Weight for Vertical Earth Pressure (kN/m <sup>3</sup> )		Equivalent Unit Weight for Horizontal Earth Pressure (kN/m <sup>3</sup> )	
	Max. Pressure	Min. Pressure	Max. Pressure	Min. Pressure
Rigid Culverts Except for Concrete Box Structures	18.8	18.8	18.8	4.7
Reinforced Concrete Box Structures	18.8	18.8	9.4	4.7
Flexible Culverts	18.8	N/A	18.8	N/A

Note: the minimum equivalent fluid pressures in the table are used to check the moments in the culvert under the load combinations.

From Table 2-1, it is clear that the current design guidelines distinguish between rigid culverts and flexible culverts, and even between concrete box culverts and other types of rigid culverts.

Due to the relatively large size of reinforced concrete box culverts, it is unlikely that they would be installed in trench condition. Only the positive projecting embankment condition, in which the culvert is placed on existing level ground, is discussed here. In the previous editions of the AASHTO design code for reinforced concrete box culverts (AASHTO, 12th edition 1977), the specifications allowed the use of soil pressures of 0.7 of due to an equivalent fluid unit weight of 18.8 kN/m<sup>3</sup> and horizontal soil pressure due to a unit weight of 4.7 kN/m<sup>3</sup> (0.25 times of assumed equivalent fluid unit weight for vertical pressure). For checking positive moments in the culvert top and bottom slabs, AASHTO allowed the horizontal soil pressure to be reduced by 50 percent. A nationwide survey of state DOTs (Tadros, 1986) indicated that the 0.7

reduction factor applied to vertical soil pressure in the AASHTO service load method was not likely intended to account for the effect of soil arching. Rather, the purpose of the 0.7 factor was probably to reflect an increase in the allowable stress under the dead load, as compared with that allowed under a live load. In its 14<sup>th</sup> edition, AASHTO (1987) increased recommended soil pressures on box culvert: load reduction factor was removed from the vertical earth pressure prediction, and the horizontal soil pressure had doubled to 9.4 kN/m<sup>3</sup>. Later, a modification coefficient  $F_e$  (called the soil-structure interaction factor and based on the Marston theory) was introduced in AASHTO's 15<sup>th</sup> edition (1992) of vertical pressure prediction. This modification coefficient is a function of culvert width and overburden height, for use in yielding foundation box culvert design:

$$F_e = 1 + 0.20 \frac{H}{B_c} \quad (2-1)$$

where H is the embankment height above the culvert and  $B_c$  is the width of the box culvert. This factor need not be taken greater than 1.15 for installations with compacted fill at the sides of the box section, and not greater than 1.40 for installations with uncompacted fills at the sides of box section. However for lateral loads, AASHTO (1996) defined maximum and minimum horizontal earth pressures given by the unit weights of 9.4 kN/m<sup>3</sup> and 4.7 kN/m<sup>3</sup>, respectively. Considering that the vertical load defined in the AASHTO (6.2.1) due to an equivalent unit weight of 18.8 kN/m<sup>3</sup>, this results in maximum and minimum load factors of 0.5 and 0.25 applied to the unit weight for lateral pressures.

For the design of railroad culverts (AREA, 1996), the vertical pressure is taken as an equivalent fluid pressure (unit weight of 18.8 kN/m<sup>3</sup>) without a soil-structure

interaction correction. Horizontal soil pressures have maximum and minimum earth pressure coefficients of 1.0 and 0.33, respectively, in a maximum and minimum horizontal earth pressures of  $18.8 \text{ kN/m}^3$ , and  $6.2 \text{ kN/m}^3$ , respectively. Compared with the design earth pressures in current AASHTO, the AREA vertical loads are smaller since they are not corrected by the soil-structure interaction factors. The horizontal earth pressure specified by AREA, however, is greater than that recommended in AASHTO. It is worth noting that the maximum embankment height considered by AREA in the dead load computation is 10 meters. One possible interpretation of the larger lateral earth pressures used in the AREA method is consideration of the extra horizontal earth pressure induced by compaction equipment during construction of the embankment. Design earth pressures recommended by AASHTO and AREA for reinforced concrete box culverts under positive projecting embankment conditions are summarized in Table 2-2.

Table 2-2 Different Design Earth Pressures on Box Culverts

Design Guide	Equivalent Fluid Unit Weight for Vertical Earth Pressures ( $\text{kN/m}^3$ )		Equivalent Fluid Unit Weight for Lateral Earth Pressure ( $\text{kN/m}^3$ )	
	Maximum	Minimum	Maximum	Minimum
Old AASHTO (1977)	13.2	13.2	4.7	2.4
Current AASHTO (1996)	18.8*	18.8*	9.4	4.7
AREA (1996)	18.8	18.8	18.8	6.2

\* subject to the correction by  $F_e$

Recommended values for the lateral thrust on basement walls and similar vertical structures below grade are provided in ASCE (1995) “Minimum Design Loads for Buildings and Other Structures.” The load magnitude depends upon the soil type and the



structure stiffness. For cohesionless backfill material, the pressure on a relatively flexible structure is about  $5.5 \text{ kN/m}^3$  of equivalent fluid pressure, and  $9.43 \text{ kN/m}^3$  on a relatively rigid structure. In the case of silty soil backfill, the lateral pressure equals to  $13.4 \text{ kN/m}^3$  of equivalent fluid pressure for flexible structures and  $15.7 \text{ kN/m}^3$  for rigid structures. These design pressures are given for the specified soils for moist conditions at their optimum densities above the ground water line.

Overall, significant differences occur among the different guidelines, with respect to both the vertical and horizontal earth pressures. This may reflect the uncertain nature of earth pressures on soil-box culvert systems. Further research on the behavior of large size box culverts under relatively high overburden depths is especially needed.

## **2.2 Earth Pressures on Buried Concrete Culvert - Instrumentation**

While there has been significant research of earth pressures on flexible metal and circular concrete culverts (Davis and Bacher, 1972; Selig et al., 1982; Duncan and Seed, 1986), limited research has been conducted on concrete box culverts. Soil arching effects are more significant with circular culverts. Since metal and concrete circular culverts are typically more flexible than concrete box culverts, the results from investigations of circular culverts are of limited value for the study of rigid concrete box culverts.

Spangler and Handy (1982) provide a good discussion of the loads on buried culverts. They suggest an alternative to the normal compaction backfill method, known as the imperfect trench technique. In the imperfect trench technique, the normally compacted backfills immediately above the culvert is replaced by an extremely compressible material (such as baled straw, leaves, compressible soil, expanded polystyrene and other foams or

cellular materials) to some height and then covered with normally compacted fill again (Figure 2-1 (d)). This installation method results in soil arching and directs the vertical loading away from the culvert and onto the side soil. Although this may reduce the vertical pressures on the culvert, large settlements in the area above the culvert may also be induced, and the horizontal soil pressure around the structure is increased due to the transfer of vertical pressures to the side soil. This method is not appropriate when the size of the culvert is relatively large and strict settlement or permeability control is required. For the current study, only instrumented culverts installed without the imperfect trench condition are discussed.

Culvert installation routinely involves the placement and compaction of backfill material in layers or lifts. Compaction of soil is accomplished by means of one or more passes by compaction equipment operating on the surface of the most recently placed layer of the fill. These repeated passes result in a process of repeated application and removal of a traveling, transient surface load. This process introduces stresses within the backfill, both during and after completion of compaction. Compaction-induced soil pressure and the resulting structural stresses and deformations can be of concern in the design and analysis of the culvert system.

A large number of laboratory and field studies of compaction-induced stress and deformations have been performed during the past 50 years. Unfortunately, much of the data currently available pertaining to compaction-induced soil pressure measurements is of limited value, since earth pressures are so difficult to measure. Proper installation of the pressure cells is of primary importance in full-scale instrumentation. Stress

measurements in soil fall into two basic categories: (1) measurements within the soil mass and (2) measurements at the face of structure elements. Attempts to measure total stress within a soil mass are plagued by errors resulting from poor conformance, because both the presence of the cell and the installation method generally creates a significant change in the free-field stress. Measurements of pressure against a structure, however, are not affected by most of the errors associated with measurements within a soil mass, and it is possible to measure soil stress at the face of a structure element with greater accuracy than within a soil mass. These measurements are subject to systematic errors, however (Seed et al., 1991).

Seed et al. (1991) illustrated the two most common types of systematic soil pressure measurement system errors (Figure 2-3). An earth pressure measurement cell which protrudes from a wall face is typically much less compressible than the soil it replaces. The protruding cell thus represents a rigid inclusion, and attracts more than its share of the soil pressure, resulting in an over-registration of pressure, Figure 2-3 (a). When the

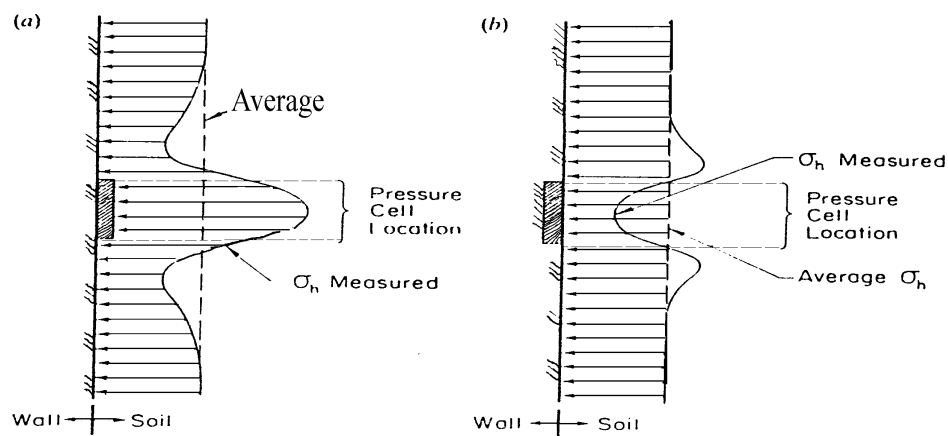


Figure 2-3 Systematic Errors in the Measurement of Soil Pressures  
(Seed et al., 1991)

(a) Over-registration of soil pressure (b) Under-registration of soil pressure

earth pressure cell is inset into the wall with its face flush with the wall face, a second problem can arise. Most soil pressure cells require some small deflection of the face in order to register some pressure. Unfortunately, very small pressure cell face deflections are sufficient to cause soil arching, which results in under-registration of soil pressures, Figure 2-3 (b). Seed et al. (1991) indicated that the best technique for avoiding these problems is to employ a very stiff (essentially non-displacement) type of pressure cell inset into the wall with its face flush with the wall face.

Full scale field test data on a reinforced concrete double-cell box culvert were reported by Tadros et al. (1989). Their focus was to reveal the role of live loads on the behavior of the culvert under shallow fill and investigate the soil-structure interaction effects. Rigid box culvert tests (Girdler, 1974; Jan Vaslestad, 1994) under deep fills were instrumented, but the culverts were relatively small and installed with the imperfect trench conditions. Since a higher backfill height is needed to create the arching zone (both positive and negative arching), only those culverts test results with normally compacted backfill are reviewed herein.

The Kentucky Department of Transportation constructed and instrumented two single cell culverts in 1974 (Girdler, 1975), and another in 1980 (Tadros, 1986). The culverts were constructed with normal compactive effort and the sizes (inside dimensions) ranged from 1.2×1.2 m to 1.8×1.8 m. Overburden thickness varied from 9 to 24 meters. These were perhaps the earliest instrumented reinforced concrete box culverts built under highway embankment service loads. Located in Clark County, Kentucky, the 1.2×1.2 m box culvert was designed for yielding foundation conditions, with 24 meters of

overburden height. In the yielding foundation, the bedrock is undercut, and backfilled prior to construction of the base slab with a specified thickness of material (usually crushed rock or coarse sand) which is relatively compressible compared with the stiffness of the bed rock. The excavation of site soil was about 1.2 m deep and 5 m wide. Bedrock and soil encountered at foundation level were undercut, and about 30 cm of crushed gravel was placed to the foundation line. After construction of the culvert, the original soil was used as backfill along the sides of the structure, and as a 3-meter thick layer of fill on the top of the box. The remaining fill was placed in 6-meter layers of shot limestone rock alternating with 1.3-meter layers of soil. The embankment soil, classified as MH, contained 43% clay, 40% silt and 17% sand. Ten Carlson soil pressure cells were installed, two each in the side walls, the top and the bottom slab, plus two at the foundation bedrock, as shown in Figure 2-4. The two cells at the bedrock were located 0.6 m from each side of the base slab. Five settlement gages were installed, and the three that were operative were located over the center of the culvert at heights of 0.6 m, 10 m and 14 m above the top slab. Two piezometers were also installed in the embankment to measure the pore pressure.

The other box culvert in Clark County, Kentucky, (Girdler, 1975), had inner dimensions of 1.5×1.2 m (height and width, respectively) and a backfill height of 11.5 m. This culvert was designed for the unyielding foundation condition. The instrumentation and excavation scheme were identical to the previous (Tadros, 1986) box culvert except that an unyielding foundation condition was used. In the unyielding foundation condition, only a thin layer of crushed rock or coarse is placed on the bedrock to level the



foundation. The backfill material below a height of 5.8 m was the site soil, which was classified as ML-CL and contained 31% clay, 31% silt and 38% sand. The remaining fill was shot limestone rock.

Soil pressure readings on both culverts were taken over a period of more than 2000 days, and pressure-time curves show that earth pressures increased approximately in proportion to fill height. During the period between the completion of fill and last reported measurements, vertical soil pressures on both culverts increased about 25%. Relative to the pressures due to the soil column above, the measured soil pressures on the top of the culverts were greater by factors of 1.5 and 2 for the yielding and unyielding foundations, respectively. The horizontal pressure records, however, remained constant during the observation time. The average measured lateral pressures were 50% greater than that predicted by the applicable AASHTO (12<sup>th</sup> edition, 1977) guide for yielding foundation and 2 times greater than that predicted for the unyielding foundation. The maximum and minimum pressure readings from the individual cells varied considerably during 2000 days of observation time. Figure 2-5 and Figure 2-6 show the soil pressures observed at the last reporting date, which were the maximum pressures reported. Comparison of the maximum soil pressure with those suggested by the applicable AASHTO (1977) Standard Specifications for Highway Bridges indicates that the AASHTO (1977) were too low.

Measured settlements were consistent with those expected for the foundations at the two sites, but the gages at mid-depth registered larger settlements than either the gage below (nearest the top slab) or above (nearest the ground surface). The piezometer

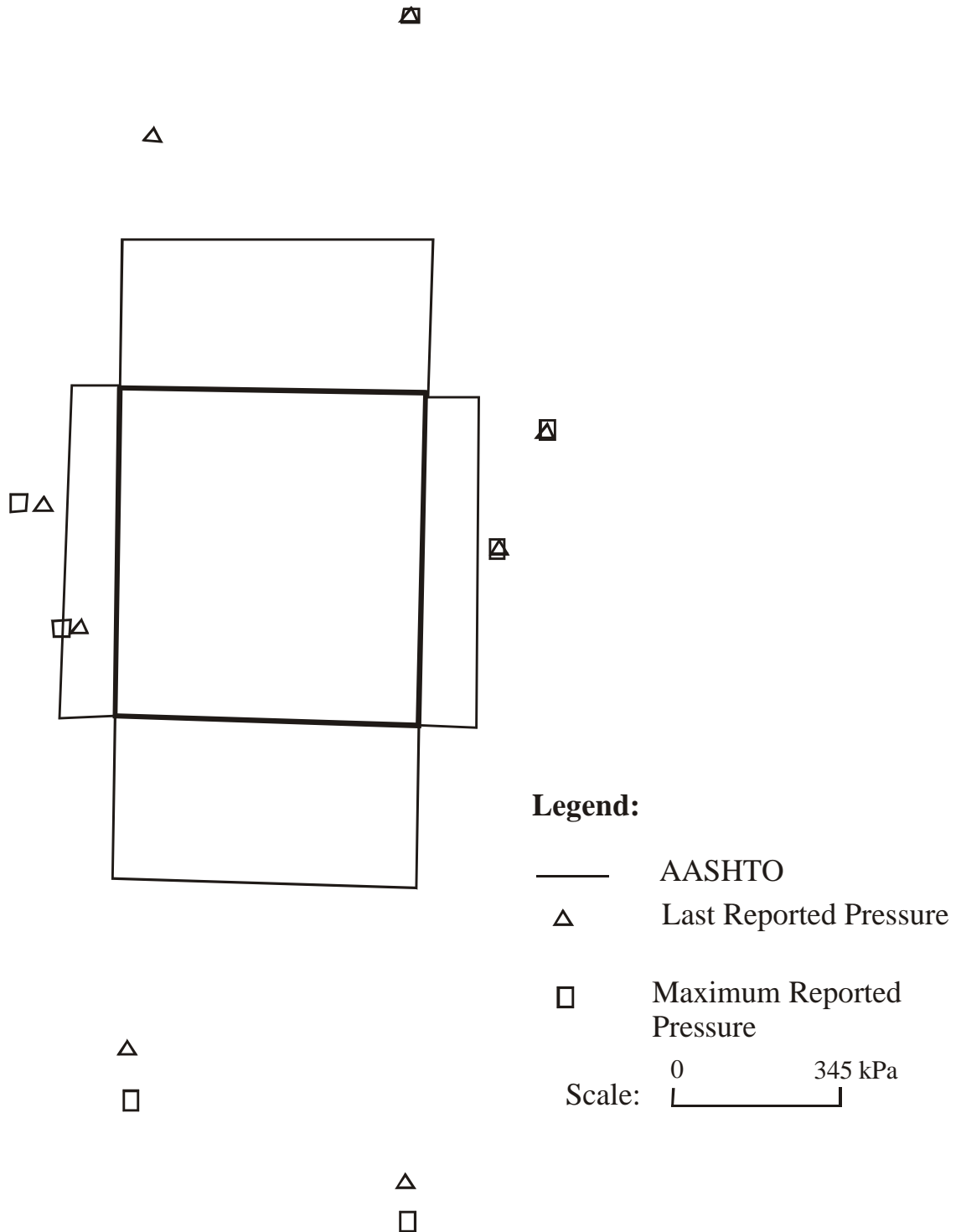


Figure 2-5 Comparison of test and old AASHTO (1973) Results:  
 $1.2 \times 1.2$  m box culvert on yielding foundation  
 (Clark County, KY; Tadros, 1986)



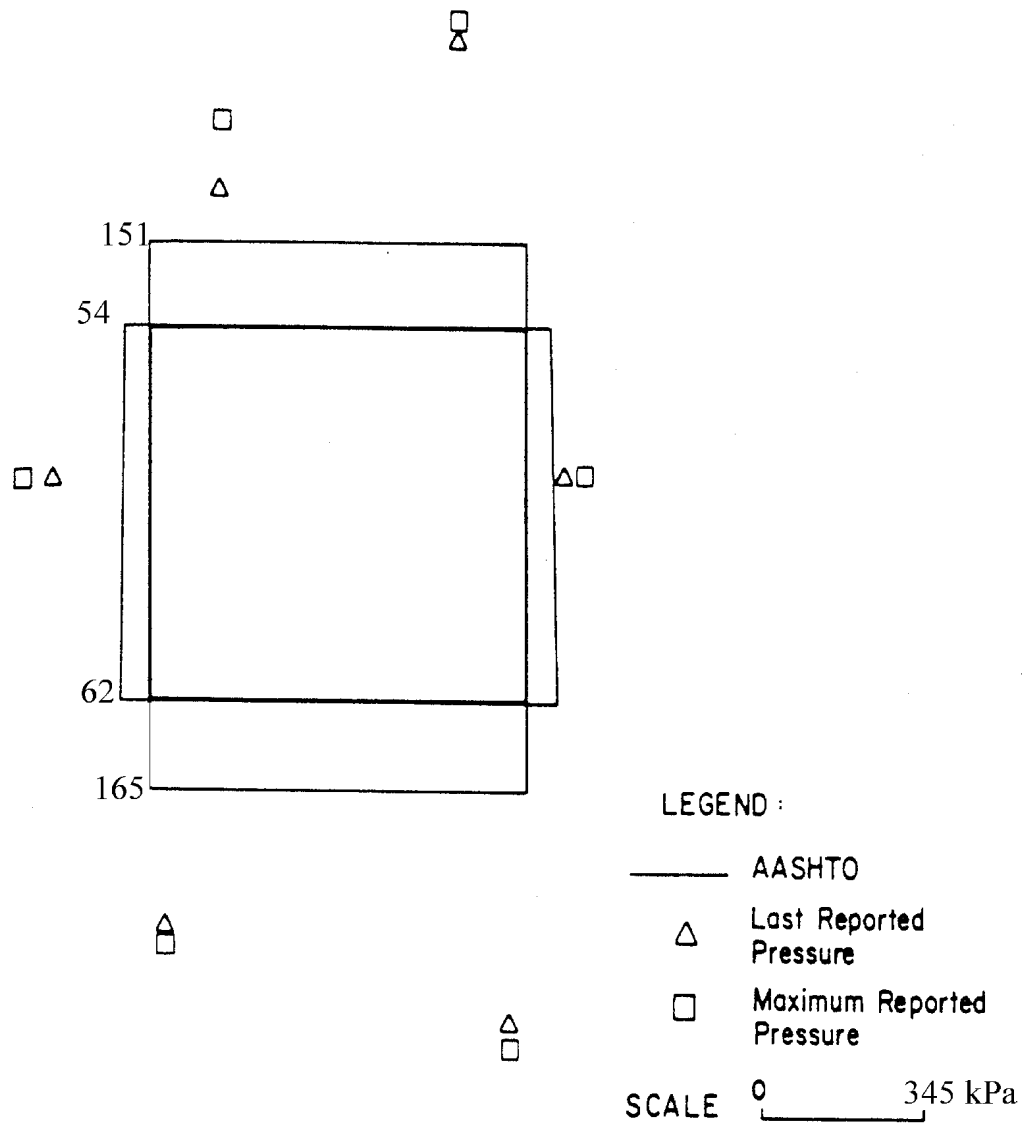


Figure 2-6 Comparison of Test and Old Aashto Results:  
1.5×1.5 M Box Culvert on Unyielding Foundation  
(Clark County, KY; Tadros, 1986)

readings indicated no pore-water pressure in the embankment, due to the good drainage characteristics of the shot limestone rock fills. These test results were widely cited by other researchers (Katona et al. 1981; James et al. 1985; Tadros, 1986), and the well known box culvert design program CANDE (Culvert ANalysis and Design) (Katona, 1981) was examined by these results. It is worth noting that all three culverts were placed in bedrock trenches with a depth about equal to the culvert height, and the stiffness of the bedrock was much higher than that of the backfill materials. Since these two culverts were installed in the negative projecting condition with compacted backfills on the top, instead of the positive projecting embankment condition, the magnitude and distribution of earth pressures on these culverts may not be the same as those if the culverts had been constructed on level ground.

In a full-scale test on a single cell cast-in-place concrete box culvert in Norway (Jan Vaslestad et al. 1994), a 2.55 m high by 2.0 m wide culvert was constructed under an embankment in a valley. The subsoil consisted of overconsolidated silty clay with a moisture content of 25 to 30%, undrained strength of 35 to 70 kPa, and bulk density of 20 kN/m<sup>3</sup>. The overburden height above the culvert was 9.8 meters. One Gloetzl type hydraulic earth pressure cell was placed on the center of the top slab. At the completion of the fill, the measured actual earth pressure on the top slab was 1.24 times the pressure due to the overburden. In the two and half years of monitoring after completion of the backfilling, the highest recorded vertical earth pressure was immediately after completion of the embankment. The pressure slightly decreased with time (Figure 2-7).

The Texas Transportation Institute and Texas State Department of Highways and

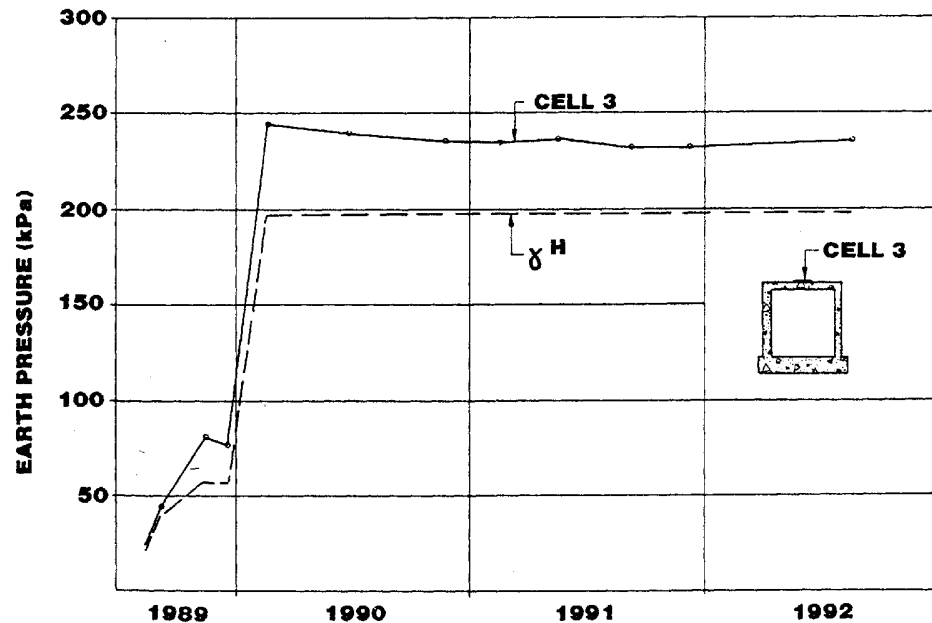


Figure 2-7 Recorded Vertical Earth Pressure on the Roof of Box Culvert  
(Jan Vaslestad et al., 1994)

Public Transportation (James et al., 1986) monitored a heavily instrumented 2.4×2.4 m experimental box culvert. The subsoils in the test site were sedimentary deposits from an ancient river, consisting of thin layers of gravel, medium sands and silts, interlain by thicker layers of fine clayey sand. The average wet density of the soil was 19.8 kN/m<sup>3</sup>. The excavated soil was used as backfill material up to 2.4 m above the top of the culvert. Twenty pressure cells of three kinds, were installed on the culvert, four on each side and twelve on the top. Six rebar strain gages were also installed. The backfilling was completed by a crawler tractor, which was reported to be an appropriate compaction device for the coarse-grain soils. The loose soil was spread in lifts approximately 10 cm thick, and conventional compaction criteria were used to control the degree of compaction. The registered vertical pressures on the top of the culvert were 20% larger

than recommended by the current AASHTO (1996) guides. The horizontal pressure data was scattered, but the maximum horizontal pressures, were recorded in the middle of the wall (Figure 2-8 ), and the average pressures were greater than the value of predicted by the AASHTO (1996) guide.

Tadros et al. (1989) instrumented a double cell culvert (4.3 m high and 8.1 m wide). The final backfill height was 3.7 m. The instrumentation consisted of 28 vibrating-wire earth pressure cells, 14 on the top, 4 on each side and 6 in the bottom slab (Figure 2-9). Supplementing the earth pressure cells were 6 vibrating-wire piezometers (2 in the bottom and 2 on each side) to measure hydrostatic boundary pressures, and 40 vibrating-wire strain gauges mounted on rebars to allow the determination of the moments and thrusts in the structure. The backfill material consisted of excavated glacial till (LL=44,

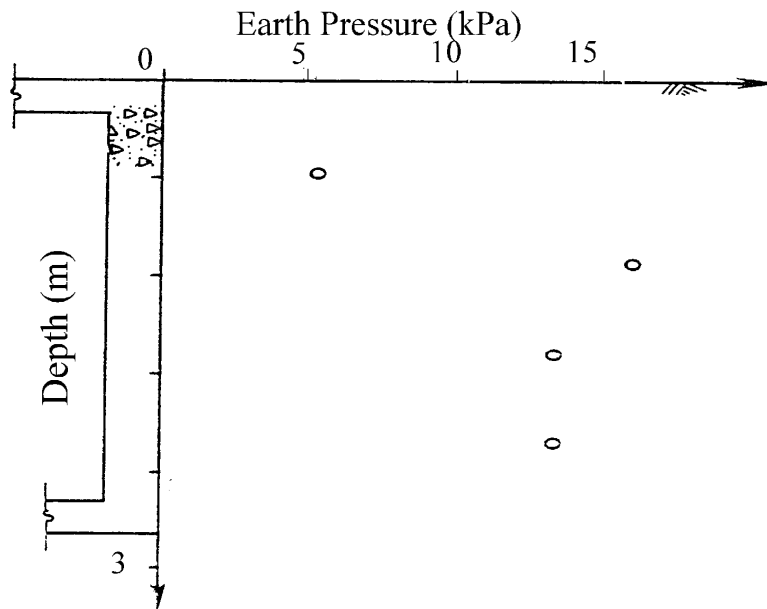


Figure 2-8 Measured Horizontal Earth Pressures on the Texas Experimental Culvert (James, 1986)

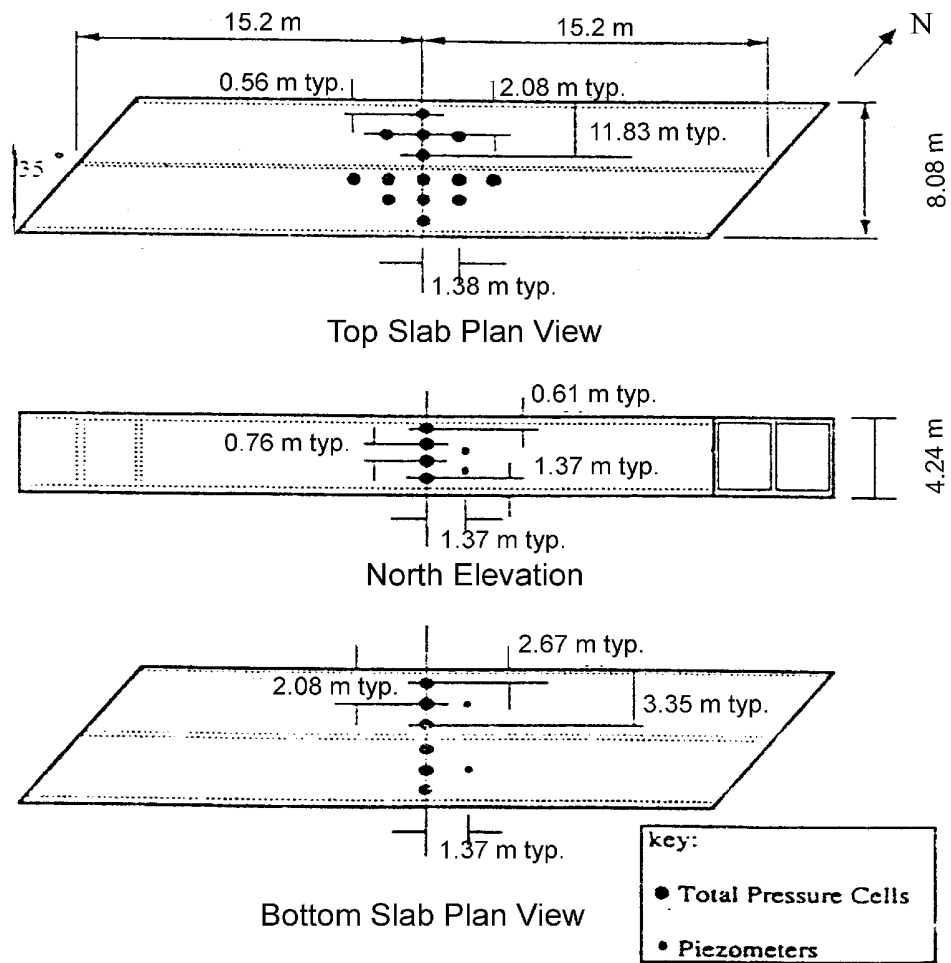


Figure 2-9 Layout of Earth Pressure Cells in Nebraska Box Culvert Test  
(Tadros et al., 1989)

PI=20) and silty clay loess (LL=37, PI=14), with average wet density of  $19.3 \text{ kN/m}^3$ . The backfill soil was placed in 20 cm loose lifts with a minimum of two passes by a vibrating pad foot roller (Bomag BW 124PD). Conventional compaction control was followed and the moisture content of soil was adjusted so that satisfactory compaction could be obtained. Figures 2-10 and 2-11 show pressure cell readings for various fill heights and compare the soil load predicted by the AASHTO (1987, 14<sup>th</sup> edition) specification, which the vertical pressure was predicted by an equivalent fluid pressure of  $18.8 \text{ kN/m}^3$  without soil structure interaction correction. At the completion of backfilling, measured vertical and horizontal pressures were greater than predicted by the AASHTO (1987, 14<sup>th</sup> edition) guideline. With the passing of time, vertical pressures on the top slab decreased slightly, but the maximum vertical pressures remained at the corners of the culvert where the structural stiffness was the greatest. The horizontal pressure on the wall in Figure 2-10 decreased significantly, with average pressures even lower than those predicted by AASHTO (1987). The maximum horizontal pressures at both the completion of backfilling and 80 days after completion were approximately in the middle elevation of the culvert wall. This finding is consistent with work of James et al. (1986) and the work of Jan Vaslestad et al. (1994).

Penman et al. (1975) measured vertical pressures in the rock fill of the 53 m high Winscar dam adjacent to the crown of a rigid reinforced concrete culvert. The recorded pressure above the approximately elliptical shaped (4.6 m wide 4.9 m high) culvert was two times the pressure due to the weight of the soil prism. The authors used the finite element method to support their findings. It should be noted that for their numerical

Fill Height: 2.60 m  
Date of Reading: 4/18/1988

Key:

● Measured

--- Current AASHTO

70 kPa

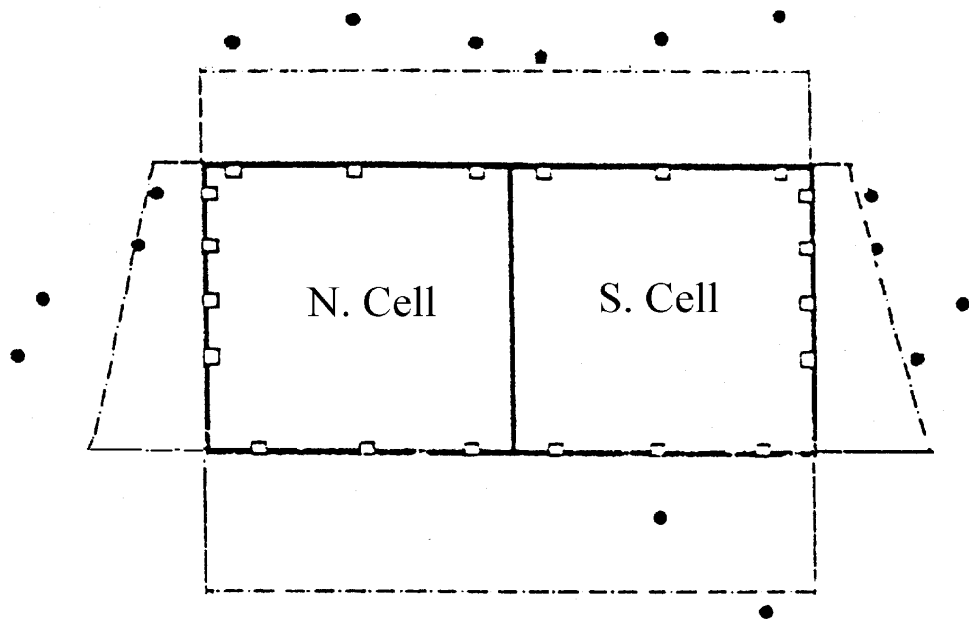


Figure 2-10 Measured Soil Pressure Distributions under Permanent Fill at the Completion of Backfilling (Tadros et al., 1989)

Fill Height: 2.60 m  
Date of Reading: 7/7/1988

Key:  
● Measured  
--- Current AASHTO  
70 kPa

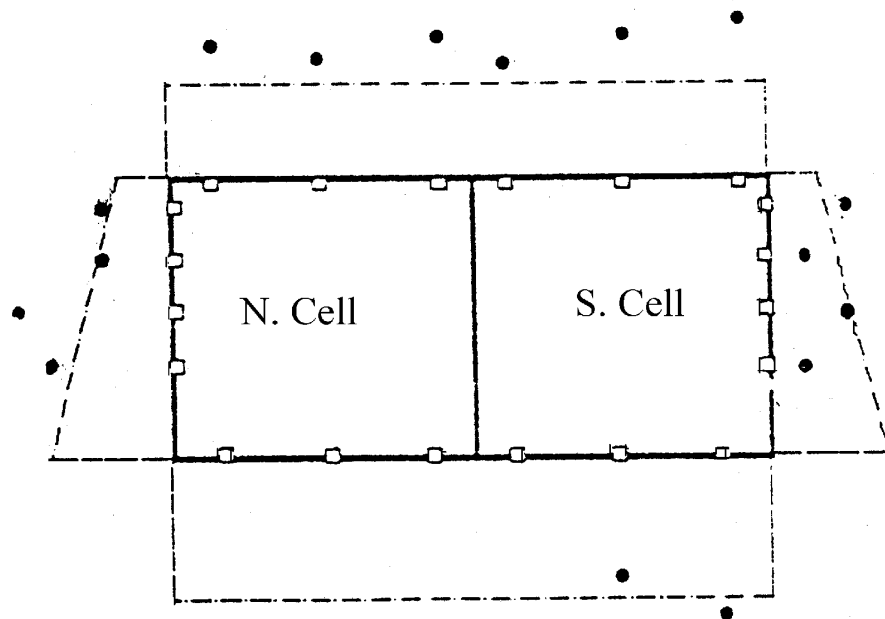


Figure 2-11 Measured Earth Pressures under Permanent Fill 80 Days after Completion of Backfilling (Tadros et al.,1986)



analysis, the elastic modulus of the coarse backfill materials was obtained from large diameter (1 m) oedometer tests. The measured and FEM vertical pressure was about two times that due to the soil prism above the crown of the culvert, which corresponded with results reported for another dam by Trollope et al. (1963).

Model tests can provide well-controlled boundary conditions for the measurement of earth pressures. Dasgupta and Sengupta (1991) instrumented a large-scale model reinforced box culvert (1.3×1.3 m) in sand. An area 7 m wide and 10 m long was excavated to a depth of 2.4 m below ground level. A concrete model culvert was placed in the excavated area, then, the space between the model and trench was filled with dry sand with dry density of 15.77 kN/m<sup>3</sup> and internal friction angle of 30°. The backfill was compacted manually by a wooden tamper. The top slab of the model culvert was 2.4 m below the surface of the sand fill. Twelve pressure cells (deflecting diaphragm type) were installed in the central section of the model with three each on the top and the bottom slab, one cell in the center of the wall on one side and five on the other side. Forty concrete strain gages were also mounted in the structure in two sections with twenty gages in each. Symmetry of the earth pressure distribution was assumed due to the symmetry of the structure and boundary conditions. The finite element method was used to predict the pressures surrounding the model culvert, and the results of the measured and predicted pressures are shown in Figure 2-12. From the results, both the vertical and horizontal pressures deviated from the straight line distribution assumed in the AASHTO specification. The calculated vertical stress due to the weight of the sand above the model culvert was 37.8 kPa, but the average vertical earth pressure was 63 kPa, about 1.7 times

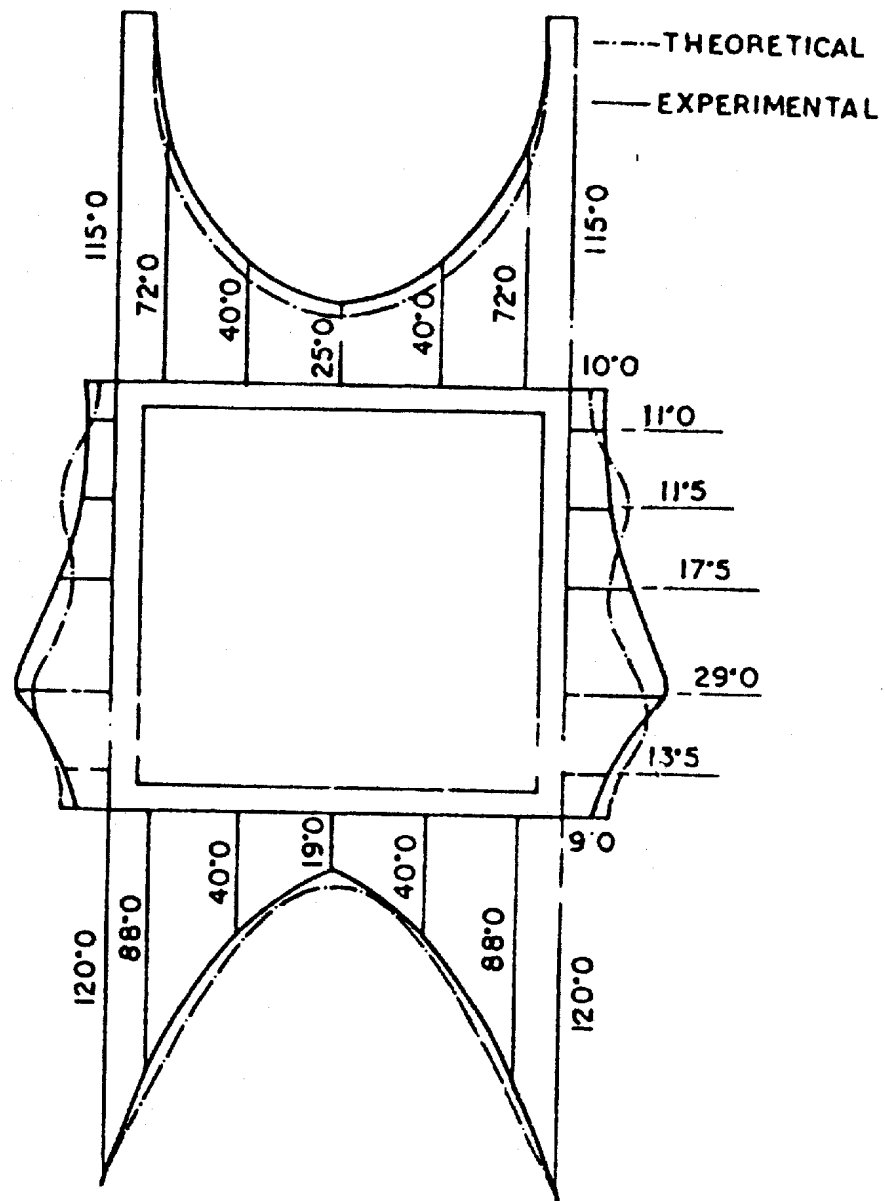


Figure 2-12 Recorded and Predicted Earth Pressures over Model Box Culvert in Sand Fill (Dasgupta and Sengupta, 1991)

that due to the weight of the soil prism. The maximum to minimum vertical pressure ratio was greater than 4. As observed by others, the maximum vertical pressure was over the corners, and the maximum horizontal pressure was located in the middle of the wall. The measured horizontal pressure was almost one half that predicted by the current AASHTO (1996).

Although the behavior of box culverts under different supporting conditions has not been documented, the impact of foundation stiffness on the pressures acting on other types of structures has been investigated. Heger and Selig (1994) reported two case histories of severe distress to large diameter circular concrete culverts under about 18 m of embankment. The culverts were placed on a firm foundation, but there was a thin layer of soft clay adjacent to the firm bedding or pipe in each installation. Both culverts failed in diagonal and radial tension before they reached their final embankment height. A soil-structure interaction analysis showed the presence of the soft soil was one of the main factors causing the distress. It was suggested that the failure of the culvert could be prevented if the soft clay within at least one culvert diameter was removed and replaced with well compacted granular soils. Moore (1991) studied the effect of foundation stiffness on the horizontal earth pressure on a retaining wall with cohesionless backfill. The earth pressure was found to vary from active pressure conditions in a soft foundation situation, to close to the  $K_0$  pressure for a very stiff foundation. Kellogg (1993) investigated the vertical soil loads on buried structures, considering the shape of the trench and slope and concluded that the vertical loads were more dependent on the excavation geometry or boundary conditions than on soil strength parameters.

## 2.3 Earth Pressure Induced by Compaction

When construction equipment is close to a retaining wall or buried structure, there is a horizontal pressure increment on the structure surface corresponding to this transient load. After removal of the equipment, the pressure acting on the structure will decrease. Due to the densification of the surrounding soil, the horizontal pressure on the structure may not be totally reduced to the magnitude that existed before loading. Figure 2-13 is a schematic of the horizontal pressure variation with time. Different components of the compaction time history are defined. Detailed definitions are provided in Table 2-3. For convenience in the discussion of the compaction process, an abbreviation is given for each component in the table.

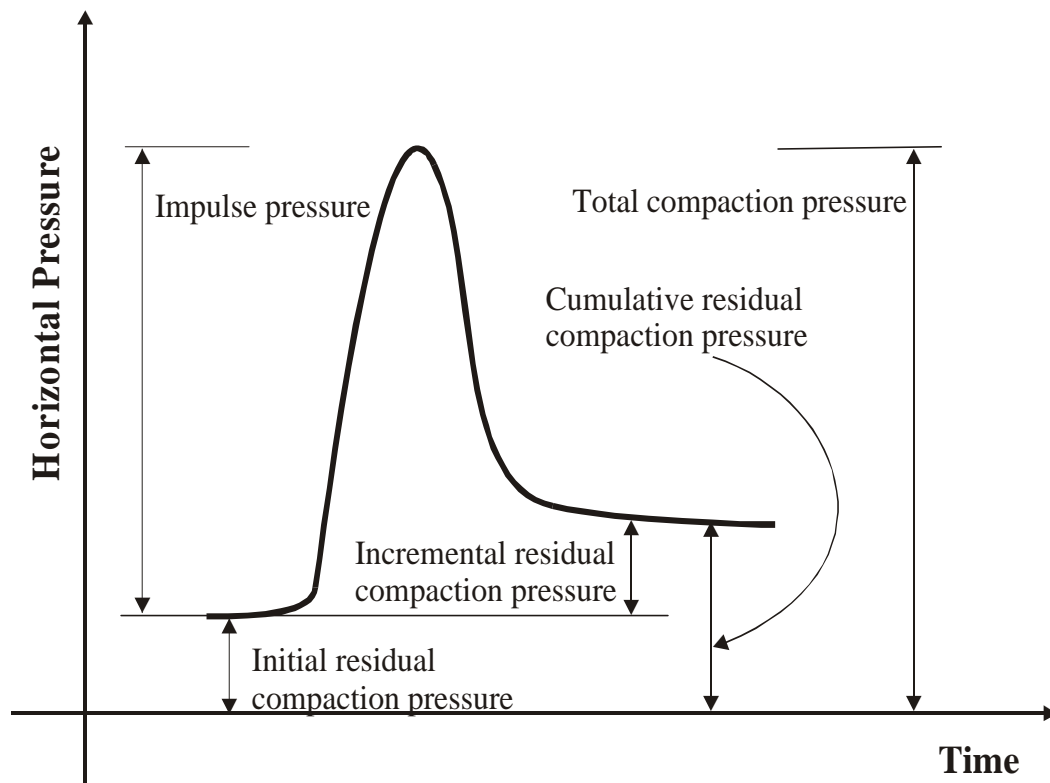


Figure 2-13 Schematic of Dynamic Pressures during a Transient Loading

Table 2-3 Definition of Horizontal Earth Pressure Components  
of the Compaction Time History

Compaction Component in Figure 2-13	Abbreviation	Definition and Comment
Impulse Pressure	Impulse Pressure	The maximum earth pressure increment in response to the compaction. It is a measure of current transient (dynamic) loading intensity. Due to the technical difficulty measuring this process, it is rarely recorded.
Initial Residual Compaction Pressure	Initial Pressure	The static compaction induced earth pressure prior to the arrival of the equipment. It is the result of previous historical loading and unloading events.
Incremental Residual Compaction Pressure	Incremental Pressure	The static earth pressure difference between the pressures before and after the arrival of compaction equipment. It is an indication of soil compaction or densification and reflects the static pressure “locked-in” the soil after the removal of compaction equipment. The incremental pressure is expected to be very small or zero after several passes of the equipment when the compaction process is completed (for the applied compaction energy).
Cumulative Residual Compaction Pressure	Residual Pressure	The final earth pressure after compaction consisting of the initial pressure and the incremental pressure. Residual pressure reflects the overall compaction efforts of the earth pressure against the structure wall. This compaction related earth pressure component has been extensively discussed in the literature on earth pressures acting on retaining structures.
Total Compaction Pressure	Total Pressure	The maximum transient pressure applied to the structure due to the compaction equipment. It is an overall compaction induced earth pressure and consists of the initial pressure (historical compaction induced pressure) and the impulse pressure (current compaction induced transient pressure). Since a significant impulse pressure may be generated during a compaction pass, the structure may be damaged during the compaction operation.

Short term static loads exhibit a pressure-time response similar to Figure 2-13, except for the time scale.

The discussion of compaction induced earth pressure can be divided into two parts: a) the behavior of the cumulative residual compaction pressure (residual pressure) which results from the compaction process, and b) the characteristics of the impulse pressure.

The residual compaction pressure has been extensively investigated in the previous instrumented retaining structures (Broms and Ingleson, 1971; Carder et al., 1977; Ingold, 1979; Seed and Duncan, 1983; Duncan et al., 1991; Clayton, 1992; Filz and Duncan, 1996), but due to the technical difficulties related to the measurement of dynamic pressure, few published results on this transient impulse pressure have been published.

### **2.3.1 Compaction Induced Cumulative Residual Compaction Pressure**

Whereas classical earth pressure theory does not consider the construction process by which the soil and box culvert are brought together, in practice the culvert installation routinely involves the placement and compaction of backfill material in layers or lifts. Compaction of soil is accomplished by means of one or more passes by compaction equipment operating on the surface of the most recently placed layer of fill. These repeated passes represent a process of repeated application and removal of a traveling, transient surface load. This process introduces stress within the backfill, both during and after completion of compaction. Compaction-induced residual pressure and/or the resulting structural stresses and deformations can be of serious concern in the design and analysis of the culvert system. Although there has been limited research on the lateral pressure exerted on large culverts, at lower backfill height the soil pressures are similar to

those acting on rigid retaining walls. The pressures on retaining walls have been extensively investigated and can be used to interpret the box culvert behavior under increasing backfill height.

Sehn and Duncan (1990) reviewed previous investigations of residual pressure induced by compaction, and reported several reasons for the difficulties associated with compaction induced earth pressure measurement: (1) Earth pressure cells sometimes give erroneous readings, depending on their stiffness and how they are installed. (2) Compaction-induced earth pressures vary rapidly with depth, resulting in misinterpretation if elevations are not measured with sufficient accuracy. (3) There appears to be large inherent variability in earth pressures, resulting in possible erroneous evaluations if too few measurements are made. (4) Small wall movements can change earth pressures significantly, requiring walls to be very stiff and mounted on unyielding supports to measure earth pressures that are not influenced by wall movements.

The pilot-scale retaining wall facility at TRRL (Transport and Road Research Laboratory, Crowthorne, England) has enabled studies to be made of the pressures produced by the compaction of backfill using full-size equipment (Carder et al. 1977; Symons and Murray, 1988; Clayton et al. 1991). Using this facility, experimental work can be carried out under more closely controlled conditions than those present in many field situations, reducing the influence of the above errors.

The experimental retaining wall at TRRL was comprised of both movable and rigid retaining walls. A cross section of the structure is shown in Figure 2-14. The movable wall consisted of three 2 m tall articulated steel panels. The jacking system mounted on

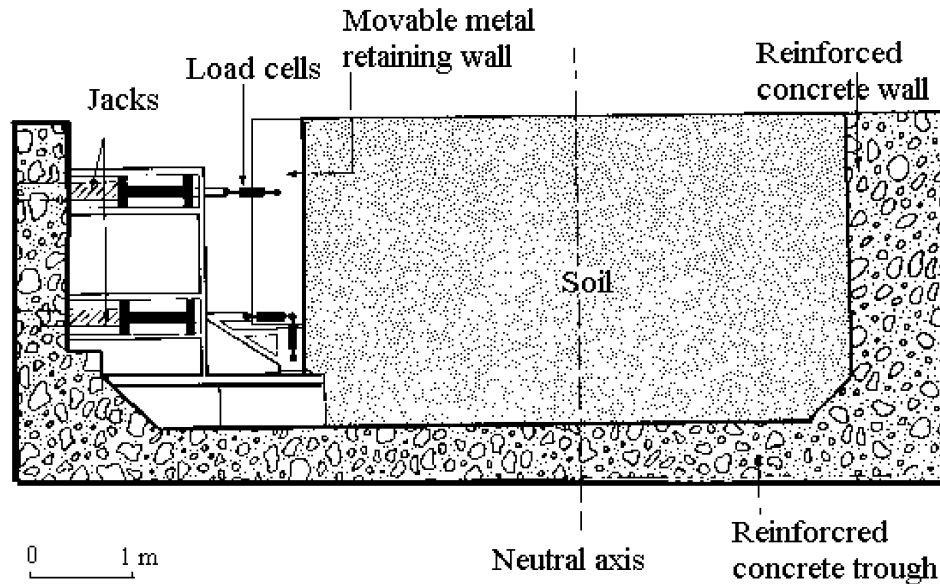


Figure 2-14 Experimental Retaining Wall at TRRL, England  
(Carder, Pocock, and Murray, 1977)

the metal wall permitted large translational and rotational movement with a displacement accuracy of better than 0.1 mm. Earth pressures on the faces of both walls were measured by using flush mounted pressure cells of three types: hydraulic, pneumatic, and stiff strain gaged diaphragm. Pressure distributions measured by arrays of each cell type on the face of the movable wall were calibrated with the known total lateral force exerted on the wall by jacks and measured by means of load cells. The resulting earth pressure measurements were of unusually high reliability.

Three pilot test-scale tests have been carried out at TRRL (Carder, et al., 1977; Clayton, et al., 1991) with different soil types: clean sand, silty clay, and high plasticity expansive London clay. Table 2-4 provides a summary of some of the properties of the soil tested. The soils were compacted to meet the specified water content and unit weight.



Table 2-4 Material Properties of Backfill for TRRL Tests  
(After Carder et al., 1977 and Murray, 1988)

Soil Tested	plastic limit (PL)	liquid limit (LL)	moisture content (%)	bulk unit weight (kN/m <sup>3</sup> )	compacted layer thickness (mm)	cohesion C (kPa)	friction angle $\phi$ (E)	compaction machine	passes compacted
Washed Sand	—	—	10.5	19.6	150	0	39	1300 kN vibrating roller	6
Silty Clay	17	43	18.5	19.6	125	25*	13*	3250 kN smooth-wheeled roller	6
Heavy Clay	29	78	28.5	17.9	120	125*	19*	7000 kN self-propelled vibrating roller	8-16

note: \* unconsolidated undrained triaxial shear test result construction with silty

The measured lateral pressures on both walls are shown in Figure 2-15 through Figure 2-17 (after Carder et al., 1977). The studies showed that the lateral pressures on both flexible (movable) metal walls and rigid concrete walls were substantially greater than the at-rest pressure ( $K_0$  line), which was calculated for zero pore pressure in the fill. The heavy clay had the greatest average lateral pressures and the washed sand the smallest. The results also showed that pressures on the rigid wall were higher than on the movable wall. In contrast with the behavior of the sand fill, pressures recorded in the clay samples began to decrease after completion of filling. Four months after the clay fill was placed, the measured distribution of total lateral pressure on both walls was close to the  $K_0$  pressure. In the two clay backfill materials, piezometers were mounted to measure the pore pressure near the wall. The sample with intermediate plasticity showed that on completion of compaction of the backfill, measured water pressure close to the movable

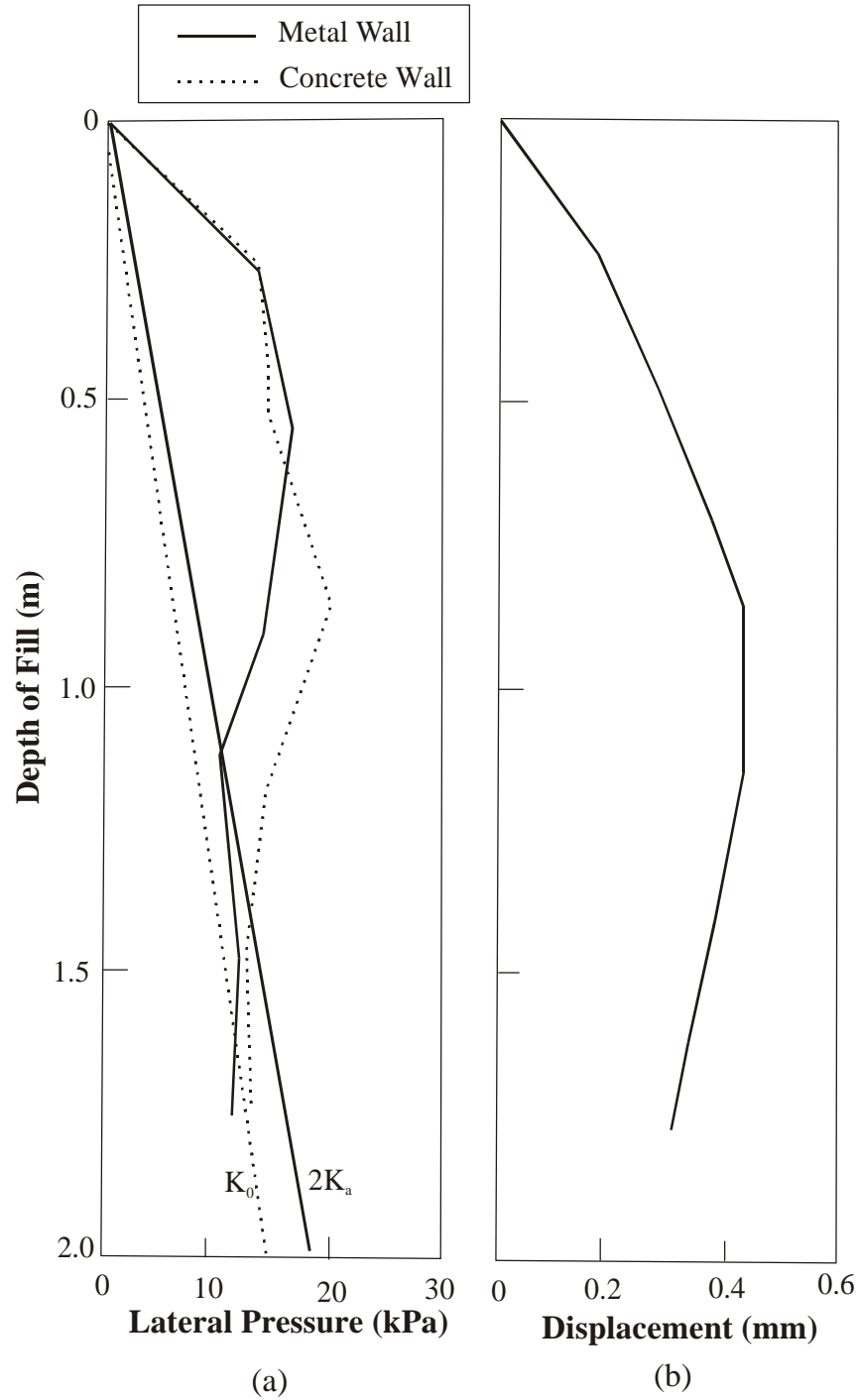


Figure 2-15 Compaction of Sand: (a) comparison of earth pressures on the moveable metal and rigid concrete walls; (b) total displacement of metal wall at each level from the initial stage when the soil was first compacted at that level until completion of backfilling (Carder et al., 1977)

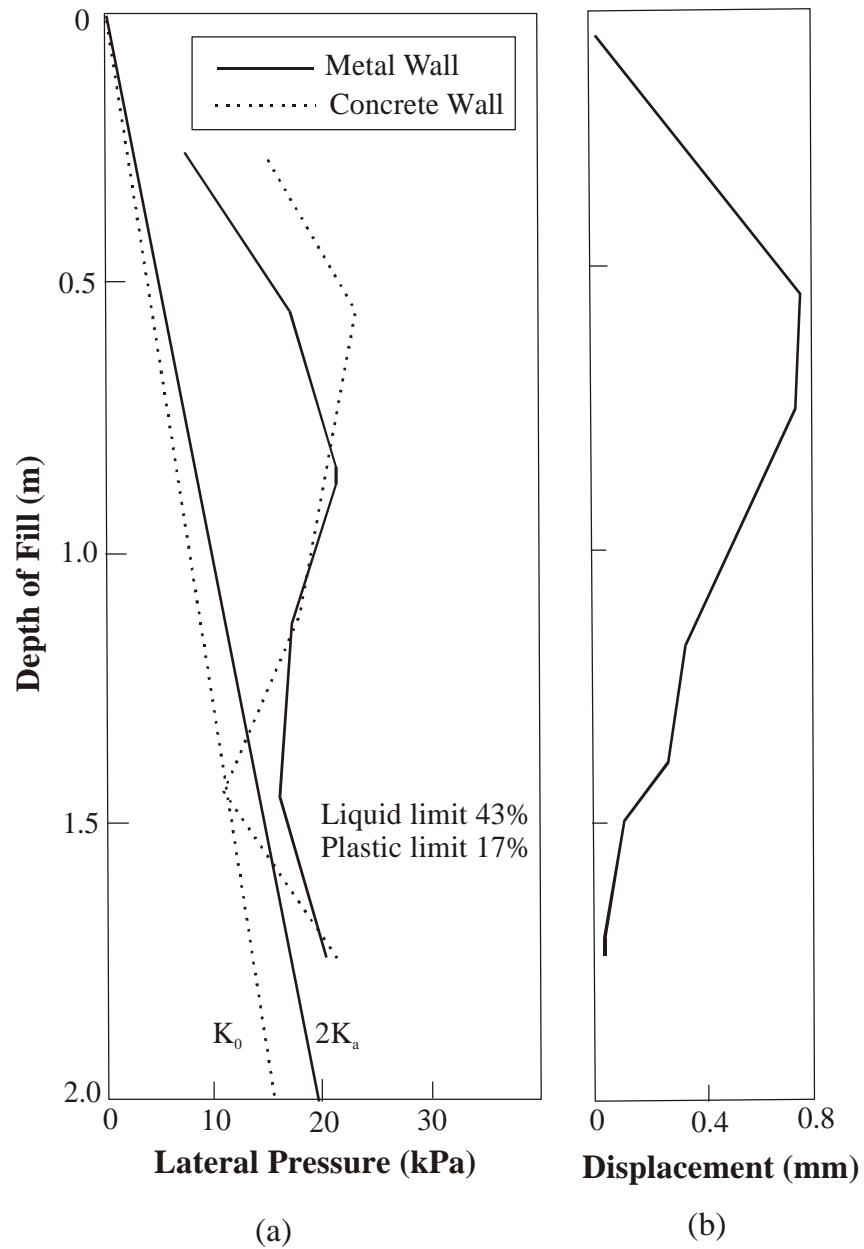


Figure 2-16 Compaction of Silty Clay: (a) comparison of earth pressures on the moveable metal and rigid concrete walls; (b) total displacement of metal wall at each level from stage when the soil was first compacted at that level until completion of backfilling (Carder et al., 1977)

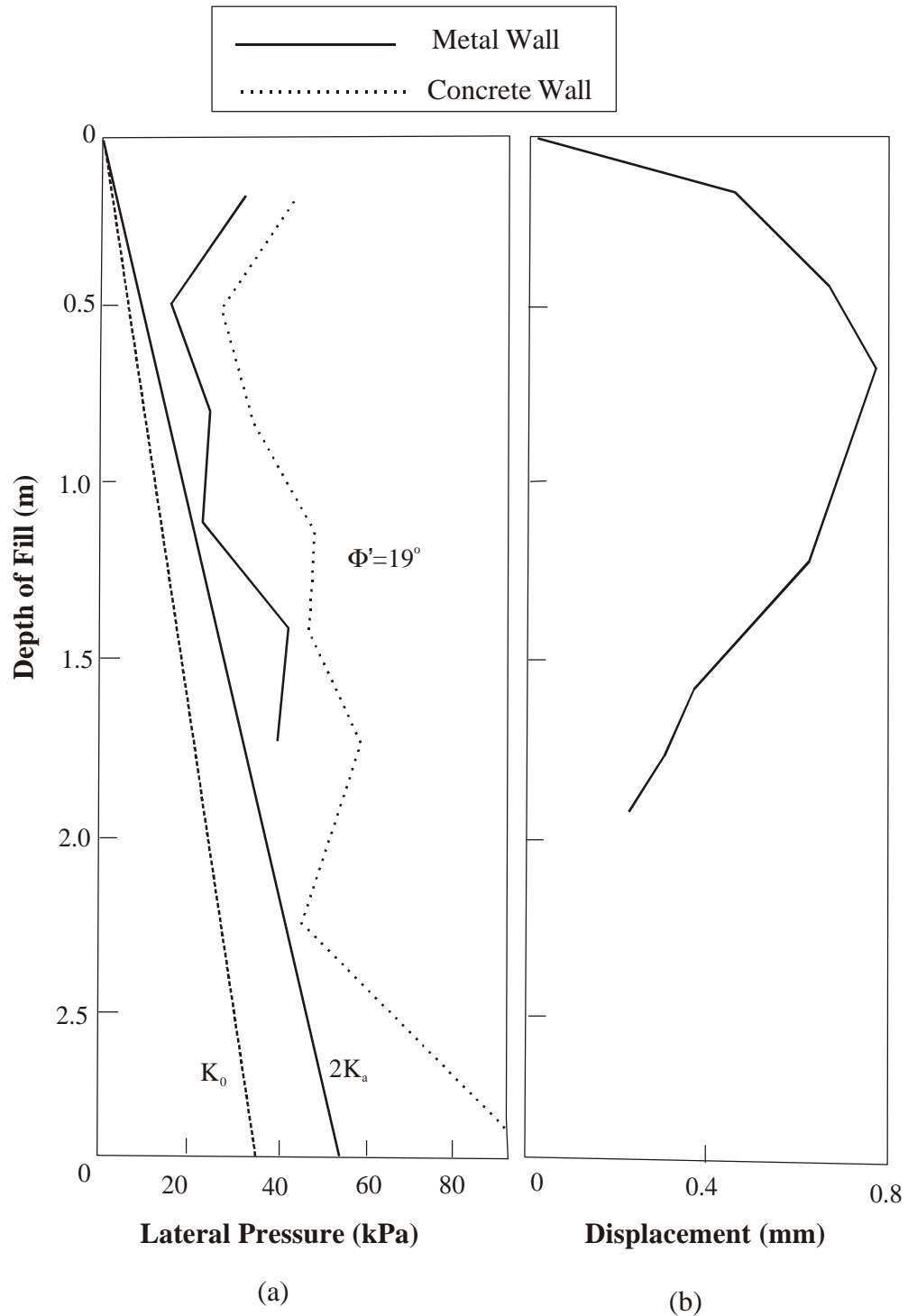


Figure 2-17 Compaction of Heavy Clay: (a) comparison of earth pressures on the moveable metal and rigid concrete walls; (b) total displacement of metal wall at each level from stage when the soil was first compacted at that level until completion of backfilling (Murray, 1988)

wall was negative both near the fill surface and close to the toe of the wall. Positive pore water pressures were recorded at middle depths, and there was no significant change of the pore pressure with time. In the heavy clay test, the average pore pressure was zero at the end of filling, but decreased to -7.2 kPa over 4 months of “relaxation” time. The authors (Clayton et al., 1991) believed this reduction in pore pressure was consistent with the average decrease in total lateral stress on the wall recorded by the pressure cells. After relaxation, additional water was introduced by sand drains to release the suction in the heavy clay and to study the swelling potential. The results showed that the fill gradually developed pressures even greater than the passive pressures calculated using conventional, triaxial compression values of  $\phi'$ .

Broms (1971) proposed an semi-empirical analytical procedure to predict the compaction induced residual pressure in cohesionless fill based on the stress paths imposed on the soil during the passage of a roller at the surface. This procedure, which was limited to consideration of placement and compaction of horizontal layers of soil adjacent to a non-deflecting vertical wall, provided fairly good agreement with field test data. Figure 2-18 shows the proposed lateral pressures for a roller at the surface of a free-draining granular fill located above the water table. Assuming that the soil has been placed uniformly, the thrust on a smooth wall depends on wall stiffness and can be related to the earth pressure at rest (line 3) or active earth pressure (line 1) as shown in Figure 2-18. Curve 2 in the figure represents the combination of horizontal stress due to both the soil self weight and the roller. The application of the roller at the surface of the fill leads

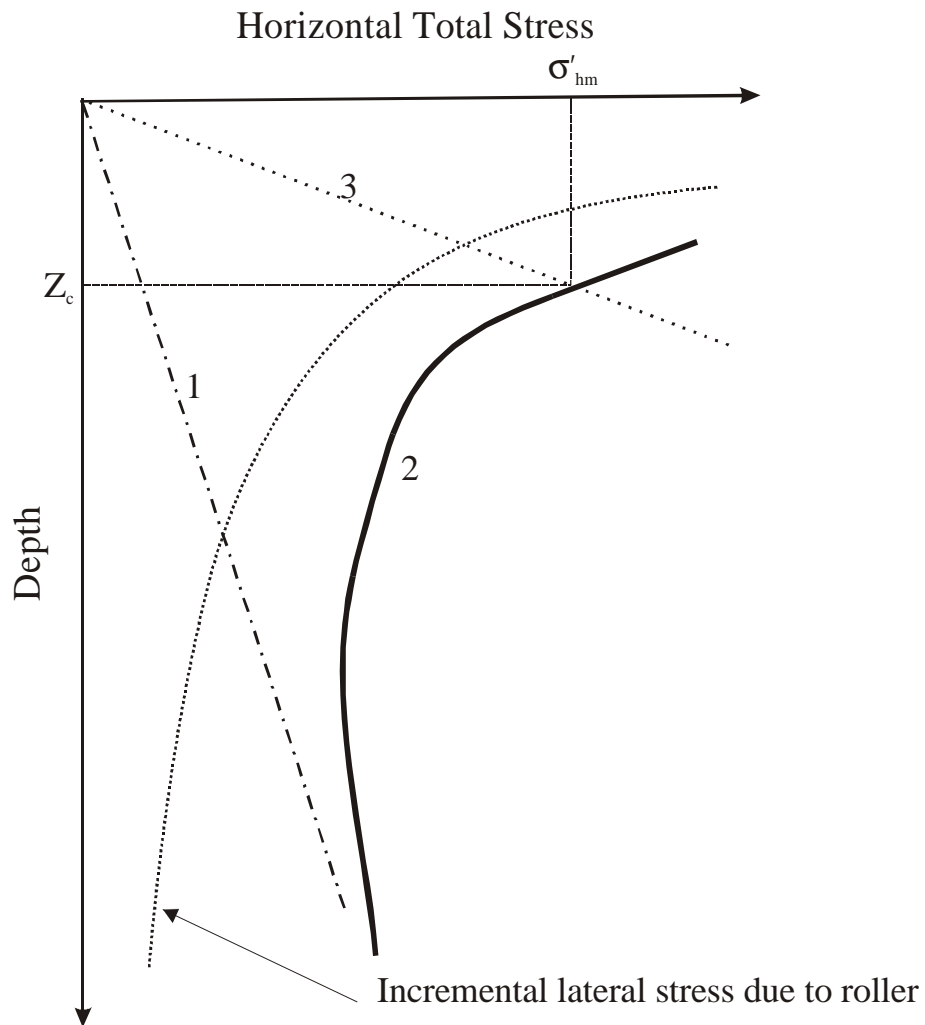


Figure 2-18 Broms' Interpretation of Compaction Induced Residual Pressure: Curve 2 represents the combination of horizontal stress due to both soil self weight and the roller. The application of roller on the fill leads to an increase in both the vertical and the horizontal pressures in the soil, with significant stress increase at shallow depths below the roller. (Ingold, 1979)

to an increase in both vertical and horizontal pressures in the soil, with significant stress increase at shallow depth below the roller. Curve 2 can be described by:

$$s'_{hl} = 2pK_a / p z \quad (2-2)$$

where  $s'_{hl}$  is the lateral stress,  $p$  is the roller pressure/unit width, (which should be doubled for a vibrating roller),  $K_a$  is the active earth pressure coefficient and  $z$  is the depth in question from surface.

Once the roller has been removed, the simplifying assumption is made that the full horizontal stress (curve 2 ) is retained in the fill below a critical depth  $z_c$ , which is related to the at-rest earth pressure. Above this level, the stresses will relax, yielding a pressure distribution corresponding to the unloading or  $K_0$  line (line 3) with residual horizontal stresses assumed to equal to  $s'_v / K_0$  for a rigid wall and  $s'_v / K_a$  for a flexible wall.

In practice, the fill is placed and compacted from the bottom of the wall.

Summation of the residual stress distributions within each layer as the height of the fill increases leads to an expected residual pressure distribution shown in Figure 2-19 (Ingold, 1979). Two critical heights are noted in Figure 2-19 at points  $Z_c$  and  $h_c$ . When the depth considered is between  $z_c$  and  $h_c$ , the lateral earth pressure on the wall will be independent of the backfill strength properties for granular fills and equal to  $s'_{hm}$ , which is the combination of compaction induced residual pressure and the self weight induced lateral earth pressure. Since the self weight induced lateral earth pressure increases with depth and the combination is constant between  $z_c$  and  $h_c$ , the compaction induced residual pressure decreases with depth. When the depth considered is beyond  $h_c$ , the lateral

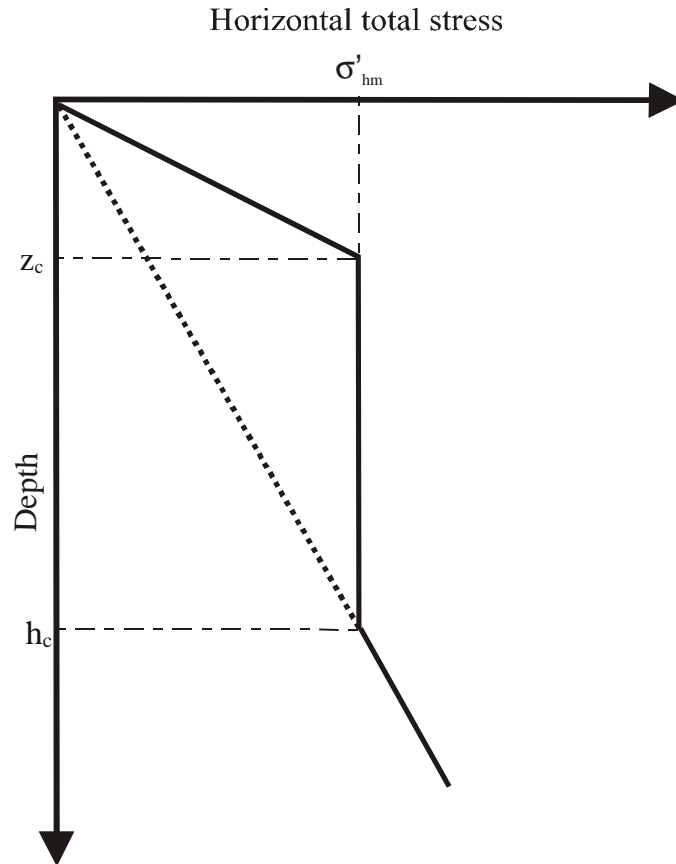


Figure 2-19 Ingold's Interpretation of Compaction Induced Residual Pressure (Ingold, 1979)

pressure can be described by the  $K_0$  line or  $K_a$  line according to the stiffness of the retaining wall. For a smooth rigid wall the depths  $z_c$  and  $h_c$  are estimated as:

$$z_c = K_0 \sqrt{2 p / \rho g} \quad (2-3)$$

$$h_c = (1 / K_0) \sqrt{2 p / \rho g} \quad (2-4)$$

$$s'_{hm} = \sqrt{2 p g / \rho} \quad (2-5)$$

where  $\rho$  is the bulk density of the fill and  $p$  is contact line load of compacting roller.

For granular fills, the critical depth is a function of the construction equipment and density.



Duncan and Seed (1986) reviewed the principle of Broms' loading-unloading model, and proposed a hysteretic model for the stresses generated by multiple cycles of loading and unloading. This model was adapted to incremental analytical methods for the evaluation of peak and residual earth pressures resulting from the placement and compaction of fill. It involved tracking the hysteretic changes in stresses through each single lift in the placement. This complex model was based on the assumption that the noncompaction-induced stresses result from essentially  $K_0$  conditions, and could only be used to consider the placement of horizontal lifts either in the free field or adjacent to vertical non-deflecting walls. Duncan and Seed (1986) used the general hysteretic model and developed a finite element program to predict effects of a wider range of compaction conditions. This theory was verified by the field measurement of different conditions. To avoid the cumbersome calculations, a simplified chart (Duncan et al., 1991) was developed. The magnitude of the residual pressure was found to be governed by the type of construction equipment and the method of placement. The Duncan and Seed model (1986) did not consider the role of the pore water pressure in the cohesive soil, due to the extreme difficulty of tracking the variation of pore pressure under the hysteretic loading-unloading, and due to the unsaturated conditions likely to exist during the backfilling process.

From the results of the TRRL clay fill pilot test result, Clayton and Symons (1991, 1992) suggested that the assumption of a drained condition (zero pore water pressure) usually adopted with granular fill was not valid with cohesive fill. They suggested that for the long term behavior of clay fill with relatively rigid walls, at least three overlapping

stages need to be considered: compaction, relaxation, and pore-pressure equilibration.

This phenomenon is illustrated in Figure 2-20.

From the start of construction at point 0 to point 1 in Figure 2-20, the soil is compacted and will induce significantly higher than  $K_0$  lateral pressure. From the limited test results, it was concluded (Clayton et al., 1991, Symons and Murray, 1988) that the residual pressure was a function of the compacted undrained shear strength of the clay fill. If the clay is placed relatively dry, a relaxation in the lateral stress after completion of back filling was observed (segment 1 - 2 in Figure 2-20). This stage occurs due to equilibration of pore pressures in the compacted clay fill with those at its boundary.

If positive excess pore pressures exist after compaction, then the clay will

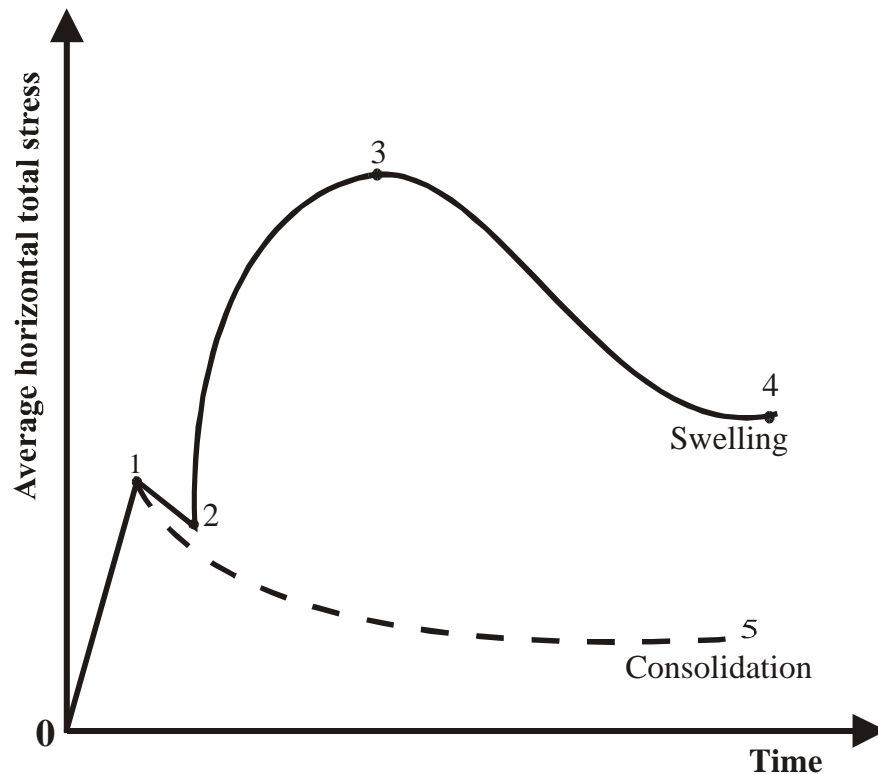


Figure 2-20 Variation in Total Horizontal Stress in Cohesive Backfills (Clayton and Symons, 1992)

consolidate and the lateral stress will reduce with time (segment 1-5 in Figure 2-20).

Under these conditions, the residual pressure will be maximum on completion of the backfilling. If after the construction negative excessive pore pressure remains in the clay, the ingress of water into the soil mass will release the soil suction and swelling will take place (segments 2-3-4 in Figure 2-20). The potential for swell within a clay fill depends on its plasticity, placement moisture content, and density, as well as the stresses imposed on it during construction and the long-term equilibrium pore-water pressure.

### **2.3.2 Impulse Pressure Induced by Compaction**

The distribution of transient lateral pressure acting against a vertical wall due to a surcharge was first reported by Spangler (1938), who concluded that the magnitude of the pressure could be approximated by doubling the Boussinesq's elastic solution for lateral stress induced by an infinite line load. The same conclusion was supported by Smolczyk and Hilmer (1979) through a model test and finite element analysis. In Duncan and Seed's (1986) hysteretic model, the lateral pressure is calculated directly from doubling the Boussinesq's elastic solution for a finite distributed load. The Boussinesq horizontal stresses against the wall induced by a finite uniform distributed load can be obtained by integrating the point load along the roller load along its drum width.

According to the definition of the pressure component defined in Figure 2-13 and Table 2-3, this "transient lateral pressure" is the same as the impulse pressure. In order to be consistent with the previous definition, the lateral earth pressure induced by the surcharge load is called impulse pressure.

Field measurements also suggested that the impulse pressure on vertical planes perpendicular to the roller path are significantly higher than those on planes parallel to the roller path. To consider the maximum impulse pressures induced by compaction parallel to the wall, the transient loading from a drum roller can be modeled as a line load of finite length perpendicular to the wall and moving parallel to it.

A series of large-scale tests reported by Rehnman and Broms (1972) were focused on measuring the effect of compaction on lateral pressures in cohesionless soils. Different impulse and incremental pressures were measured in loosely dumped and compacted soils due to the addition and removal of wheel loaders. The tests were conducted on a braced, reinforced concrete wall which was instrumented with 12 Glotzl hydraulic pressure cells with their faces flush with the concrete, as shown in Figure 2-21. The concentrated load was applied to the completed surface of the backfill by positioning a Michigan 175A-series front loader with its scoop filled so that its front wheel represented a pair of 73.6 kN loads. There was no vibratory action involved in the tests. Two types of backfill were used for these tests: gravelly sand and silty sand. Testing procedures involved the application and removal of wheel loads in both loosely dumped backfill and in backfill that was placed and compacted in layers. For the compacted cases, the silty sand was placed in 40 cm lifts whereas the gravelly sand was placed in 20 cm lifts, and compacted by four passes with either a 140 or 400 kg vibratory plate (a small compaction machine compared with current conventional equipment in practice). The properties of the two sands in the different states are listed in Table 2-5

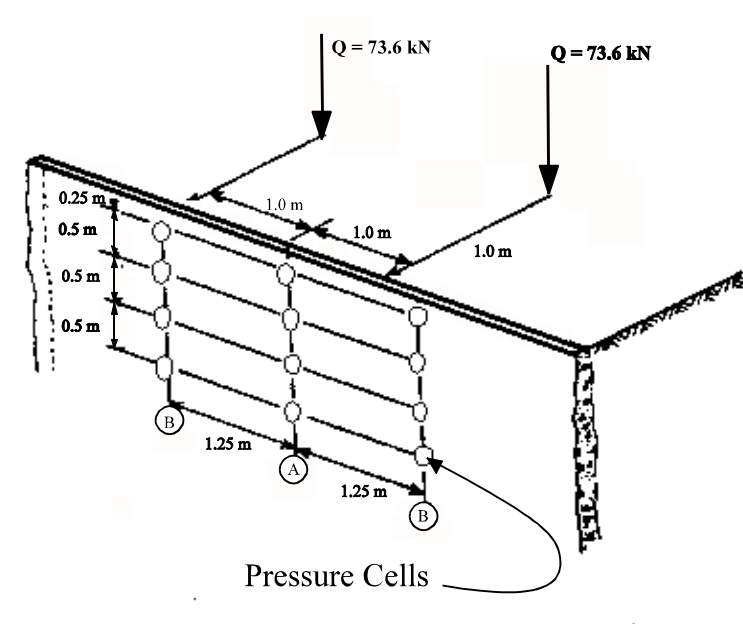


Figure 2-21 Illustration of Rehnman and Broms' Instrumentation (After Seed and Duncan, 1983)

Table 2-5 Material Properties in a Large-Scale Test (Rehnman and Broms, 1972)

Soil Properties	Gravelly Sand (GS) Back Fill		Silty Sand (SS) Backfill	
	Loosely Dumped	Compacted	Loosely Dumped	Compacted
$n'$ (degrees)	34	42	32	37
$\gamma$ (kN/m <sup>3</sup> )	17.1	19.8	14.7	18.1

The impulse pressures measured for the two loosely dumped soils are illustrated in Figures 2-22 (Section B of Figure 2-21) and 2-23 (Section A of Figure 2-21). These pressures were compared with different multiples of the Boussinesq solution (for distributed or line load) with Poisson's ratio = 0.4. The results suggest that the impulse pressure (the difference between the total pressure and the initial pressure before loading) induced by the wheel loader were bounded by one and three times the Boussinesq elastic results. In the two loose dumped soils, there was no previous compaction involved, so the

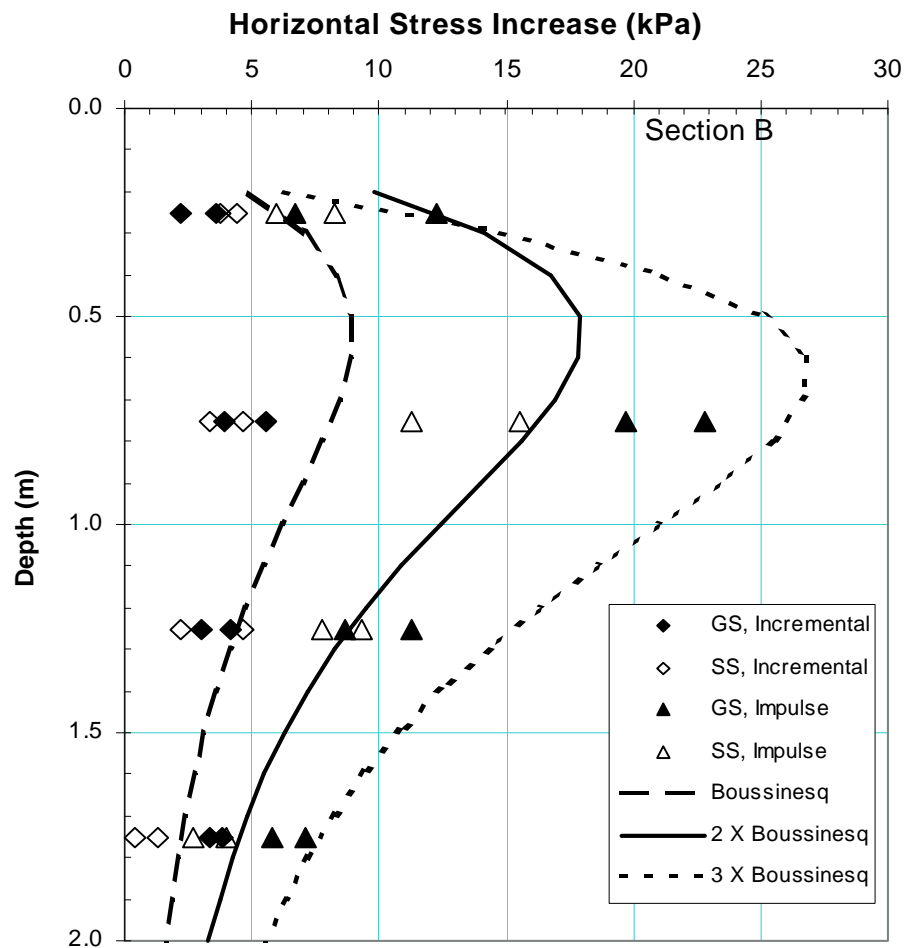


Figure 2-22 Measured Earth Pressures in Loosely Dumped Soil  
(Section B of Figure 2-21, Rehman and Broms, (1972))

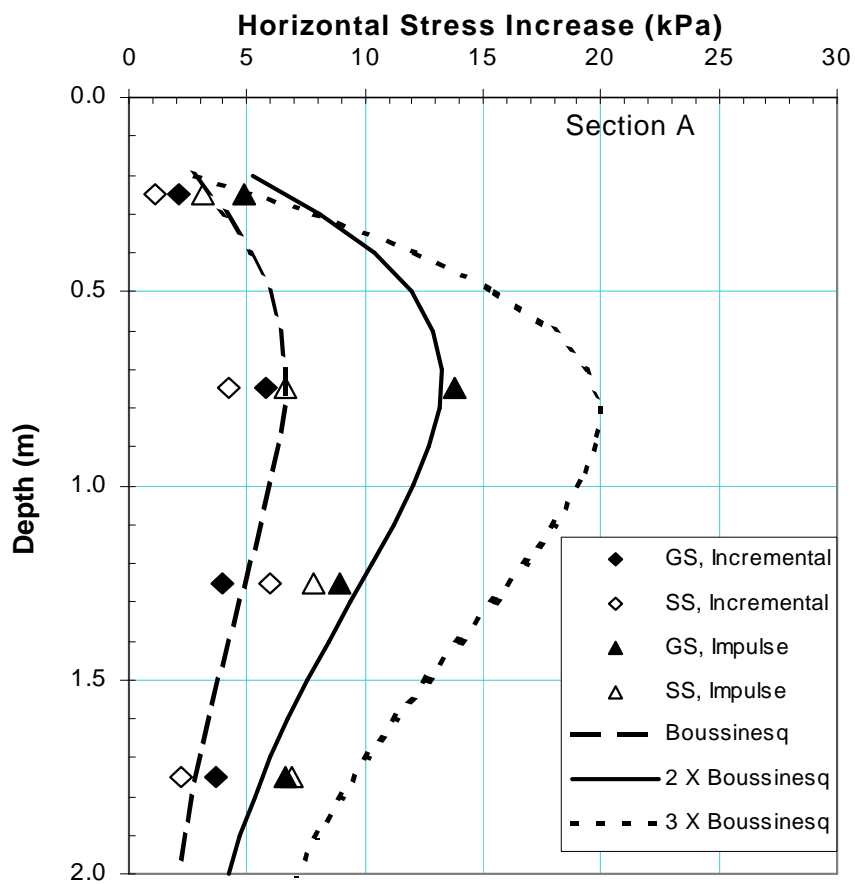


Figure 2-23 Measured Earth Pressures in Loosely Dumped Soil (Section A of Figure 2-21, Rehman and Broms, (1972))

initial pressure, which reflected the historical compaction effect, was zero. Therefore, the impulse pressure equaled the total pressure and the incremental pressure equaled residual pressure. The results suggested that the impulse pressure or total pressure could be roughly expressed by two times the Boussinesq pressure. The incremental pressure or residual pressure after removal of the load, was generally bounded by the Boussinesq elastic solution. The magnitude of the “locked in” residual pressure after the removal of a surface load was in the range of 40% to 80% of the impulse or total pressure.

When the soil backfill was placed in thin layers and well compacted, both the impulse and the incremental pressure were smaller than when loosely dumped. The results are illustrated in Figures 2-24 and 2-25. Since the compacted soil experienced loading and unloading cycles during the compaction, it had higher stiffness and lower compressibility than the loosely dumped soil. Thus, when it was subjected to surcharge loading, it exhibited more elastic properties and had smaller “locked in” incremental pressures after the removal of the surcharge load. Although the incremental pressure due to the surcharge load was small in a single loading-reloading cycle in the well compacted soils, residual pressure could accumulate to a considerable amount after a routine compaction procedure (Rehman and Broms, 1972; Carder et. al, 1977, Seed and Duncan, 1983; Filz and Duncan, 1996). While the impulse and incremental pressures measured in the compacted soil were smaller than those in the loosely compacted soil, the residual or final pressures were greater. Usually, a higher recorded residual pressure was reported near the ground surface. This compaction induced residual pressure even contributed to the failure of earth retaining structures (Seed and Duncan, 1983; Filz and



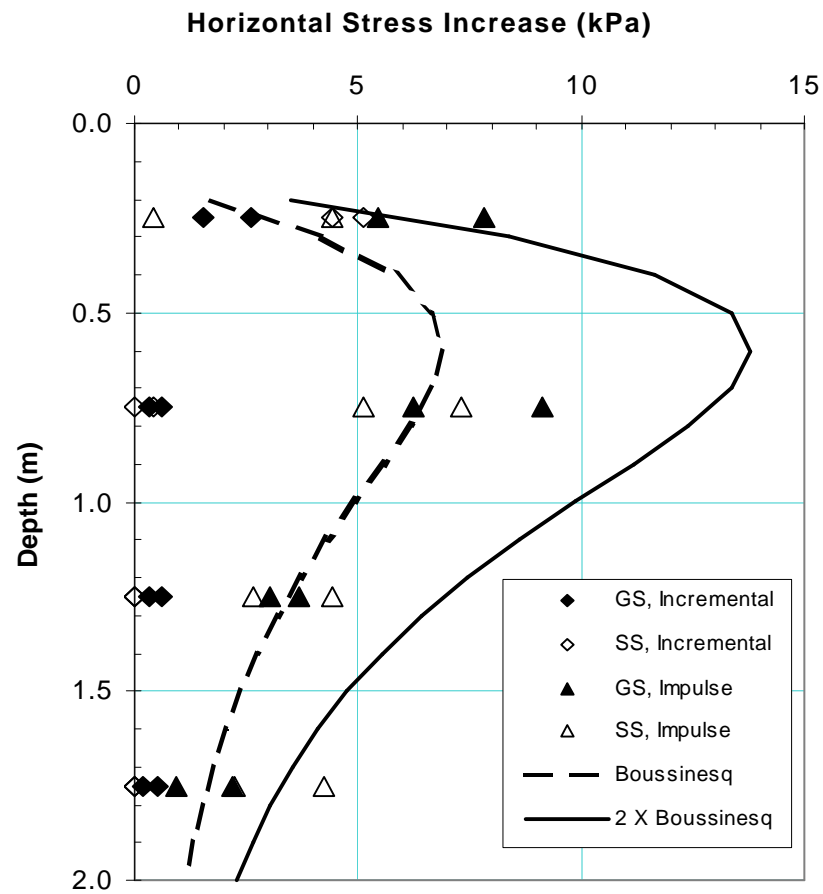


Figure 2-24 Measured Earth Pressures in Compacted Soil  
(Section B in Figure 2-21, Rehman and Broms, (1972))

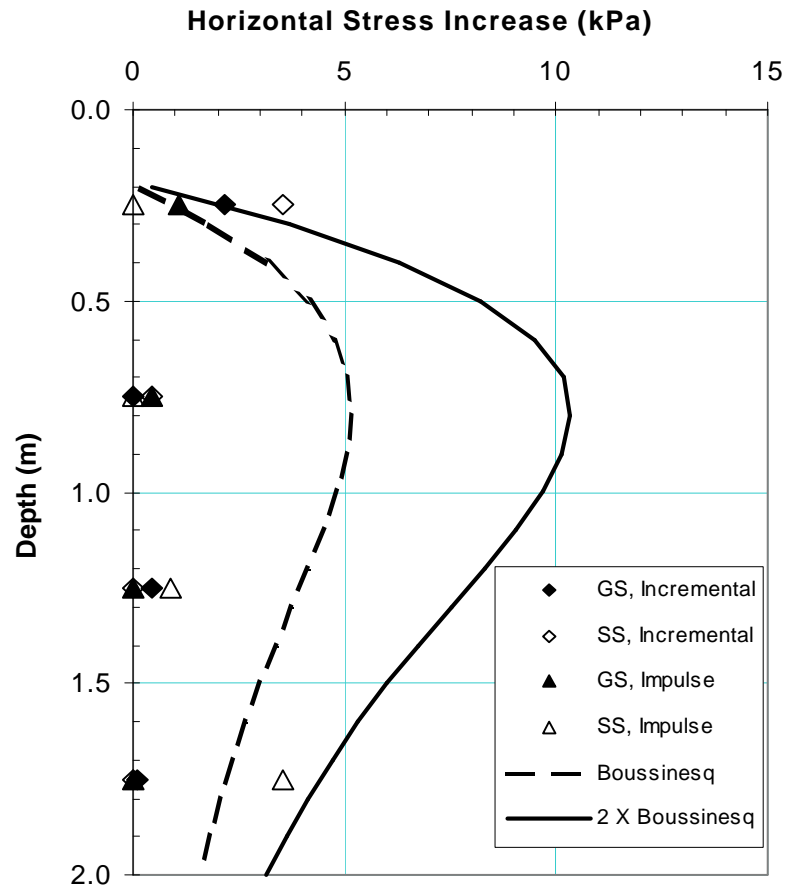


Figure 2-25 Measured Earth Pressures in Compacted Soil  
(Section A of Figure 2-21, Rehman and Broms, (1972))

Duncan, 1996). It is worth noting that the impulse pressures recorded in Rehnman and Broms' instrumentation had no vibrating components. Therefore, the earth pressure recorded was only the pseudo-dynamic impulse pressure induced by the wheel pressures of a loader.

The dynamic effects of a vibratory roller include the dynamic vibrating force during the compaction. Ingold (1979) used an equivalent static force, which was two to three times the roller drum weight, to approximate the dynamic force during vibratory compaction. A procedure for estimating the dynamic compactor force for a vibratory roller was also developed by Yoo and Selig (1979). The displacement of the drum was suggested to be the key factor which affected the dynamic force in a vibrating roller. Duncan et al. (1991) used the combination of static weight of the roller and the centrifugal force given by manufactures in their analysis, or three times of the static weight of the drum when the dynamic force was not available.

As part of a research program to study lateral earth pressures on retaining walls, Filz and Brandon (1994) compared the dynamic compaction force measured from direct instrumentation and from the embedded earth pressure cell responses. The comparisons were conducted in the laboratory at a small scale. The experimental facility at Virginia Tech is similar in principle to the TRRL wall but equipped with more advanced measuring systems (Sehn and Duncan, 1990; Filz and Brandon, 1994; Filz and Duncan, 1996). Of 17 pressure cells mounted on the walls, three types of pressures cells are used: Gloetzl cells (11), Carlson cells (4), and Geonor cells(2). They concluded that the earth pressures might be influenced by the soil type, soil water content, compaction equipment

and the installation method of pressure cells. The pressure beneath the base of the compactor could also influence the embedded pressure cell readings. Compaction forces estimated from the pressure cells were very scattered.

It is difficult to estimate the compaction induced lateral impulse pressure because the modern vibratory roller is designed to have a wide range of centrifugal forces to meet different field conditions. For example, the Ingersoll-Rand DD-130 double drum roller has 8 different forces ranging from 71.2 kN to 160 kN. Unless the exact dynamic force during compaction is known, it is difficult to obtain a reasonable approximation of the actual impulse pressure.

A few researchers actually measured the impulse pressures during the experimental construction. Kohls et al. (1989) installed small size pressure cells (Kulite type semiconducting silicone cells, 55 mm in external diameter) to measure the vertical earth pressure induced by the vehicle load. The pressure cells were located near a pipeline under a pavement. Different shapes of stress waves were recorded. Filz and Brandon (1993) used the same type of pressure cell to evaluate the effectiveness of lightweight compaction equipment. Due to the large aspect ratio (ratio of the cell thickness to cell diameter), both studies concluded that a special calibration was needed.

Using field instrumentation of lateral pressures on reinforced concrete bridge abutments in Britain (Butcher and Marsland, 1989), the dynamic total pressures induced by a vibrating roller during construction and vehicle loads in service were recorded. The height of the instrumented abutment was about 11.4 m. The grain size of the granular fill material ranged from 0.06 mm to 60 mm with an average of 2 mm (sandy gravel), with

effective angles of friction ranging from 40E to 50E. Gravels were placed in 15 cm thick layers, and were compacted by 2 passes of a double drum roller (Bomag BW200). The roller had a dead weight of 70 kN and a centrifugal force of 314 kN when vibrating at the design frequency. The pneumatic displacement pressure cell used to record the dynamic earth pressure was 138 mm in diameter and 11 mm thick. The cell was 2.8 m below the surface and the horizontal distance from roller edge to the pressure cell ranged from 0.5 to 4 m.

The recorded dynamic earth pressure pattern indicated a significant drop in the load as the machine approached the pressure cell position, with impulse pressures generated as the roller passed the cell, and an incremental pressure remaining as the machine moved away. The recorded dynamic pressure pattern is illustrated in Figure 2-26. Only the dynamic total lateral earth pressure by the vibrating roller at one point induced was

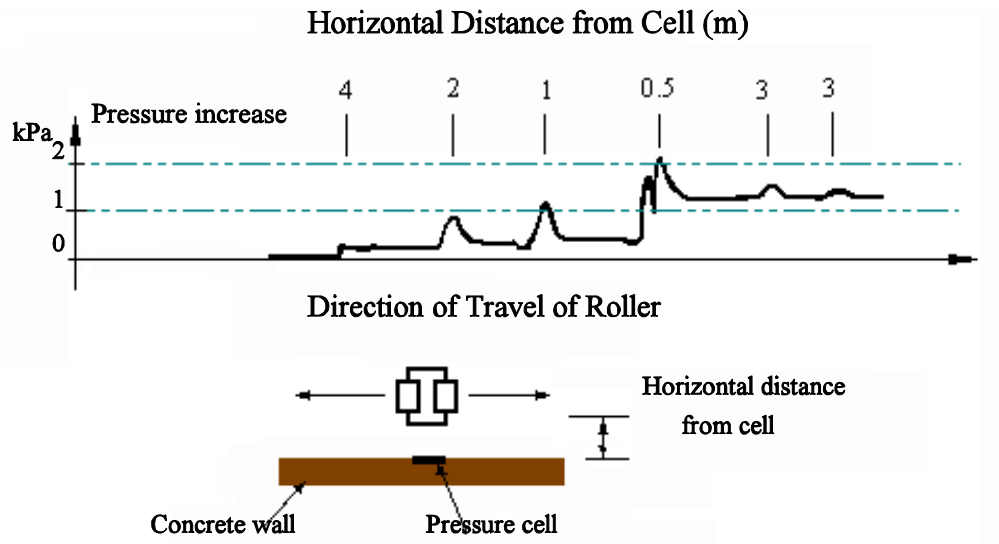


Figure 2-26 Dynamic Lateral Pressure Increase Induced by Compaction  
(After Butcher and Marsland, 1989)

reported. Higher impulse pressures were recorded when the roller was closer to the wall. The highest recorded impulse pressure was about 2 kPa when the roller was 0.5 m from the wall. About 1 kPa of maximum incremental pressure was also recorded after the a roller passed 0.5 m from the wall.

Butcher and Marsland (1989) also installed pressure cells below the pavement. Figure 2-27 illustrates the dynamic impulse pressure increase of a cell 3.5 m below the pavement. The load was induced by a moving vehicle. Since the soil was presumably well compacted before paving, there was not significant incremental pressure produced after the removal of the surface moving load.

Clayton and Symons (1992) summarized the previous TRRL lateral earth pressure instrumentation results and concluded that the cumulative residual compaction pressure

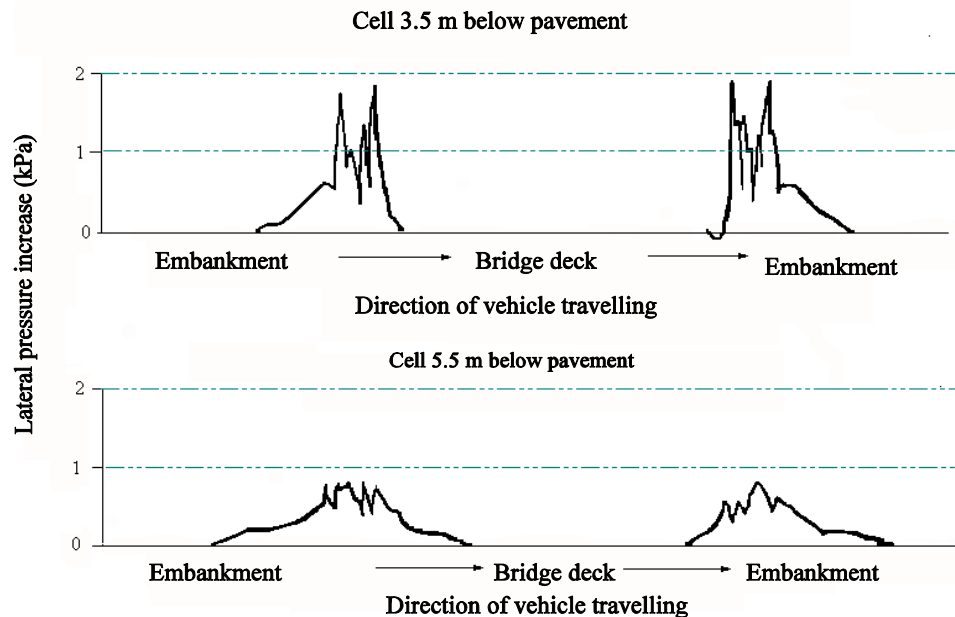


Figure 2-27 Dynamic Lateral Pressure Increase Induced by Vehicle Load in Service (After Butcher and Marsland, 1989)

acting on the retaining wall after the removal of compaction equipment may change within a short time due to stress relaxation (as indicated in Figure 2-20). In a field record, Sowers et al. (1957) observed lateral earth pressure in sandy silty clay of the order of 100 - 150 kPa, which declined by about 30% during the first 24 hours after compaction.

Although compaction induced residual pressures are dependent on many factors, including the type of compaction equipment, the stiffness of the adjacent structure, the soil placement method, and the properties of the fill material, general conclusions can be drawn from the previous research results of field and pilot tests:

1. Compaction of soil provide significant increases in residual pressures which remain after compaction. In clay backfill, the pressure may vary with time. At shallow depths, the available overburden pressure is insufficient to prevent failure and the cumulative residual compaction pressure may be limited. A high percentage of the impulse pressure induced during compaction may remain as incremental pressure. In high plasticity clay fills, lateral earth pressures, including residual pressure, greater than the passive pressure have been recorded.
2. The depth to which compaction increases the incremental pressures appears to be governed by the construction equipment and the structural stiffness of the adjacent structure. This depth generally does not exceed 3 to 4 m, but depths as great as 15 m were recorded with very heavy compaction equipment.

3.       Compaction induced residual pressures are unlikely to exceed 20-30 kPa.  
  
          Furthermore, a small displacement of the structure away from the soil  
  
(active case) can greatly reduce the magnitude of the lateral earth  
  
pressures.
4.       Due to the restraints in the measurement of the direct dynamic impulse  
  
pressure, no data on the pressures throughout the entire compaction  
  
process been published. The impact of total pressure on structures remains  
  
uncertain.



## **Chapter 3**

### **Characteristics of Instrumented Culverts**

As described in Chapter 1, two concrete box culverts were instrumented. The first culvert located in Sullivan County, TN, replaced a previous culvert that had failed. The second culvert was a new culvert constructed in Greene County, TN.

#### **3.1 Sullivan County**

##### **3.1.1 Original Sullivan County Culvert**

The original culvert was a double-cell cast-in-place reinforced concrete structure on SR394 in Sullivan County, TN. Each cell was 2.44 m in high and 4.57 m wide. The thickness of the top and bottom slabs were 0.32 m, and the side and the middle walls were 0.25 m thick. The culvert was 126 m long and oriented at about a 60E skew angle with respect the alignment of the highway. The overburden height was about 12 m above the roof of the culvert. The original culvert failed shortly after being placed in service (figures 3-1 and 3-2). TDOT post-failure mapping showed two horizontal cracks throughout the east external wall. The cracks divided the wall approximately into three parts. The middle part of the damaged wall had moved inward with about a 20cm offset. On the roof, two main cracks approximately 10 m long were found on the opposite side of the damaged cell in the area of full overburden height, oriented about 15E with the



Figure 3-1 Photograph of Interior Wall of Failed Concrete Box Culvert, Sullivan County, Tennessee (courtesy of TDOT, 1995)



Figure 3-2 Photograph of Exterior Wall of Failed Box Culvert, Sullivan County, Tennessee (courtesy of TDOT, 1995)

culvert alignment. Several minor cracks were found near the center of the roof along the culvert alignment. The minor cracks mainly were found in the areas with less than full overburden height.

Post-failure borings showed that the bottom slab of the culvert was supported by about 3 m of firm shaley clay, over about 2.1 m of very firm, weathered shale over hard fresh shale. Limestone gravel was used as fill surrounding the culvert with about 0.6 m placed above the roof. Above the gravel, the backfill consisted of clayey weathered shale from a nearby cut slope. The coarse material included particles to 500 mm or larger, but most were smaller than 100 mm. The grain size distribution curves can be found in the Appendix. The clay size material had a liquid limit of 35, and a plastic limit of 24. Compaction followed the conventional quality control guideline of 95% of standard Proctor density. Nuclear density test data suggested wet density values ranging from 20.0 kN/m<sup>3</sup> to 24.1 kN/m<sup>3</sup>, with an average density of 21.9 kN/m<sup>3</sup>. The average moisture content was 7.5 percent, with the data ranging between 4.4 and 10.1 percent. The laboratory (TDOT internal report, 1995) direct shear test results on the backfill material excavated from the site had cohesion values varying from 7.6 kPa to 36.4 kPa, and friction angles ranging between 31E and 33E.

### **3.1.2 New Sullivan Culvert**

The new culvert was designed to be much stiffer than the original, with the top and bottom slab 0.76 m in thickness. A 0.18 m thick prefabricated prestressed concrete roof panel was used as a supporting form for the top slab concrete. The side walls were 0.61 m thick and the middle wall was 0.46 m thick. Detailed drawings of the both the original

and replacement culverts are provided in the Appendix. To avoid excessive lateral pressure during construction, compaction equipment was not used to compact the fill within 2 m of the culvert, and the thickness of each loose lift of the clayey shale backfill material was maintained at 300 to 400 mm. This was expected to minimize the vertical and lateral earth pressures by achieving a lower degree of compaction. In-situ density tests with the sand replacement method (ASTM D 4914-89) performed on the normally compacted layers yielded an average density of  $21.1 \text{ kN/m}^3$ . Samples of the fill material (10 cm in diameter) were taken for triaxial testing. Details are in the Appendix.

### **3.2 Greene County**

The Greene County culvert, on SR350, is a double-cell cast-in-place concrete box 99 m long, with typical inside cell dimensions of 3.0 high and 2.44 m wide. The thickness of the middle wall is 0.28 m, while the thickness of the side walls, and the top and bottom slabs vary according to the change in the overburden height. Typically, the culvert has 0.78 m thick top and bottom slabs and 0.41 m thick side walls. The 18 cm thick prestressed prefabricated concrete panels were used to support the fresh concrete, eliminating the need for formwork.

Although subsurface boring data at this site were not available, subsurface conditions at this culvert were estimated from observations of the shallow excavation trench. The culvert overlays silty clay with shallow outcrops of limestone rock. Immediately below the culvert, a 30 cm thick layer of well graded crushed gravel was used to level the ground and adjust for the thickness change of the bottom slab.

The culvert was backfilled with gravel to a height of 0.6 m above the top of the culvert roof. Then the silty clay from a nearby cut area was used for backfill. The final elevation of the pavement is about 19 m above the culvert roof with the embankment slope of 1 vertical :2 horizontal. Some properties of the backfill material and the in-situ soils are listed in Tables 3-1 and 3-2.

As stated previously, the magnitude of the lateral pressures on the culvert wall is dependent upon the construction equipment, the distance from the edge of the roller to the wall, and the number of passes by the compaction equipment. The loose gravel was dumped by trucks and spread by a dozer and grader into lifts 10 to 15 cm thick. Ingersoll-Rand SP56 single drum and DD-130 double drum vibratory rollers were used to compact the gravel with 4-6 compaction passes. For the compaction of the clayey layers above the gravel, self-propelled single-drum sheep foot rollers (Ingersoll-Rand SP 150, 814F, 824G) were used. Conventional compaction practice specifying 95% of standard Proctor optimum density was used.

### **3.3 Comparison of the Documented Box Culverts with the Current Study**

The earth pressures acting on the roof and walls of box culverts are expected to depend upon embankment height and the dimensions of the culvert. A summary of the culvert dimensions and the recorded vertical and horizontal earth pressures from the published literature and the Tennessee sites is presented in Table 3-3. Vertical and horizontal earth pressures determined by the current AASHTO design guideline are also shown. The rigidity of the roof and wall can be described by the slenderness ratio, defined as  $L/t$  where  $L$  is the span length of the roof of one cell or wall and  $t$  is the thickness of

Table 3-1 Properties of Backfill and In-situ Soils

	Wet Density (kN/m <sup>3</sup> )	Moisture Content (%)	Plastic Limit PL(%)	Liquid Limit LL(%)	Void Ratio <i>e</i>	Cohesion <i>c</i> (kPa)	Friction Angle $\phi$ (deg)
In-situ Soil	19.0	21.9	15.7	26.5	0.69	36	29
Gravel	22.8	8.5	!	!	0.26	54	43
Backfill	20.0	16.8	21	45	0.56	22	27

Note: the density of the Gravel is tested in-situ by sand replacement method (ASTM D 4914-89) the values of the backfill are averaged.

Table 3-2 Compaction Parameters of Backfills

Sample No.	Name	Plastic Limit (%)	Liquid Limit (%)	Maximum Unit Weight (kN/m <sup>3</sup> )	Optimum Moisture Content (%)	Maximum Dry Unit Weight (kN/m <sup>3</sup> )
1	silty clay	16	28	19.0	18	16.1
2	clay	20	43	18.9	21	15.6
3	expansive clay	20	50	17.0	36.5	12.5

the roof or wall. The relative embankment height, defined by the ratio of embankment height  $H$  to culvert width  $B$ , is also shown. These quantities are shown in Figure 3-3.

Although the pressures summarized in Table 3-3 cover a wide range, and the culvert installation conditions were very different, several conclusions can be drawn:

- ! For low  $H/B$  values, typically less than one, recorded vertical pressure was approximately equal to the AASHTO pressure (the density of the backfill soils in these references was similar to the AASHTO assumed value). The recorded lateral pressures were generally greater than AASHTO and  $K_0$  pressure.
- ! For high  $H/B$  values, recorded vertical pressures were greater than the AASHTO

Table 3-3 Summary of Instrumented Concrete Box Culverts

Culvert Size (m) (B×h)	Roof Slenderness Ratio (L/t)	Wall Slenderness Ratio (L/t)	Relative Embankment Height H/B	AASHTO $\sigma_v$ (kPa)	Recorded $\sigma_v$ (kPa)	$\sigma_v/\sigma_{vAASHTO}$	AASHTO $\sigma_h$ (kPa)	Recorded $\sigma_h$ (kPa)	$\sigma_h/\sigma_{hAASHTO}$	Reference	Comments
1.7×1.7 Single	5.8	5.8	13.5	443	690	1.56	272	173	0.63	Tadros et al, 1986	Embedded in in-situ firm clay trench under yielding foundation
2.0×1.7 Single	7.0	7.0	5.63	217	423	1.95	136	169	1.24	Tadros et al, 1986	Embedded in bedrock trench under unyielding foundation
2.0×2.55 Single	5.67	5.67	4.90	185	244	1.32	-	-	-	Vaslestad et al, 1994	Installed from level ground under yielding foundation.
1.3×1.3 Single	17.0	17.0	1.78	45	68	1.51	28	18	0.65	Dasgupta et al, 1991	Large Scale model test in sand.
2.8×2.8 Single	14.5	14.5	0.87	46	35	0.76	12*	16*	1.34	James, 1986	Installed from level ground under yielding foundation.
8.1×4.25 Double	12.4	15.5	0.45	69	72	1.043	54	70	1.30	Tadros, 1989	Installed from level ground under yielding foundation.
9.9×2.77 Double	15.2	8.52	1.29	241	N/A	N/A	160	N/A	N/A	TDOT Sul. Co. Original	Installed from level ground under yielding foundation.
9.9×3.66 Double	5.46	3.49	1.18	265	277	1.04	153**	85.7**	0.56	TDOT Sul. Co. Replaced	Installed in bottom of excavated slope 2 H:1V, and overlaid on the original bottom slab.
7.01×4.0 Double	3.87	9.47	2.67	409	554	1.58	236**	156**	0.66	TDOT Greene Co.	Installed from level ground under yielding foundation.

**Note:** The vertical AASHTO load is based on assumed soil unit weight of 18.84 kN/m<sup>3</sup>. The lateral load is 0.6 times the equivalent fluid pressure of the same height.

For the lateral pressure, the value at the middle height of the wall is given.

For the vertical pressure, the recorded value is the average if values from more than two pressures were reported on the roof.

The recorded pressures at TDOT culverts were the average of all recorded pressures after the construction work

B: the total width of the culvert.

h: height of the culvert.

L: the center length of the roof (wall). For the double-cell culverts, the span of one cell.

t: the thickness of the roof (wall)

H: the final embankment height above the roof of the culvert.

\*: the values were taken when the side fills reach the roof of the culvert.

\*\*: calculated at the middle of wall.

pressure, and the lateral pressures were generally less than those prescribed by AASHTO.

! The influence of the foundation condition is important. A comparison with unyielding foundation cases (Tadros, 1986) suggests that for the unyielding condition, the vertical pressure was almost two times that predicted by current AASHTO pressures, and the lateral pressure was greater than predicted. For the yielding foundation condition, lateral pressures were generally less than the current AASHTO value.

Details of the recorded vertical and horizontal earth pressures will be provided in

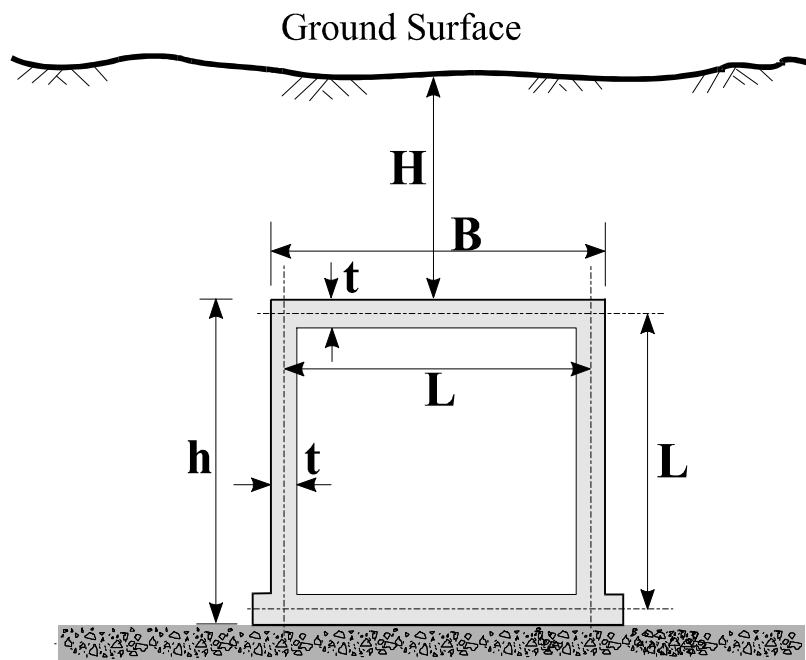


Figure 3-3 Definition of Culvert Geometry Terms  
Used in Table 3-3

subsequent chapters, and discussed in terms of the rigidity of the box culvert.



## **Chapter 4**

### **Design and Installation of Instrumented Culvert Sections**

Embedded concrete strain gages were attached to the culvert rebar prior to pouring the concrete. After the concrete forms were removed, earth pressure cells were installed on the exterior of the culverts. This chapter describes the instruments used and the installation procedures.

#### **4.1 Concrete Strain Gages**

Concrete strain gages are often used to measure strain in the concrete during construction and service life of a structure. Several types of strain gages are available from numerous manufactures (Rourke and Cording, 1975; Abramson and Green, 1984; Dunnicliff, 1988; McRae and Simmonds, 1991; Benmkorane et al, 1995). Dunnicliff (1988) described strain gages in great detail, as well as their uses. Typically, the concrete strain gages fall into two categories: surface-mounted strain gages, which are used for measurements on the concrete surface, and embedment strain gages, which measure strain in the concrete. Table 4-1 lists the common types of concrete strain gages. For the box culverts described here, two different types of embedment strain gages were chosen, electrical resistance gages and vibrating wire gages.

Table 4-1 Common Types of Concrete Strain Gages

Category	Type of Instrument	Remarks
<b>Surface-Mounted Strain Gages</b>	Mechanical Strain Gages: (Portable dial indicator, Scratch and Multiple telltales)	Simple and inexpensive. Require access to structure and care to read. Scratch can record large dynamic strain but currently rarely used.
	Vibrating Wire	Remote readout lead wire effects minimal, factory water proofing; arc welded or bolted version is reusable. Limited range and cannot be used for high frequency dynamic strains; special design features required to minimize zero drift.
	Electrical Resistance (weldable and bonded foil)	Remote readout, suitable for monitoring dynamic strains. Low electrical output, lead wire effects; possible errors owing to moisture, temperature and electrical connections; installation of bonded gages requires great skill and experience.
<b>Embedment Strain Gages</b>	Multiple Telltales	Simple and inexpensive. Require access to the structure; low accuracy.
	Vibrating Wire (Type similar to the arc welded surfaces mounted gage and sister bar type)	Lead wire effects minimal; no conformance problem; reliable; readout can be automated; high accuracy. Cannot be used to measure high frequency dynamic strains; often attached to a “dummy” or sister bar which must be small relative to the size of structure member; special design features required to minimize zero drift.
	Electrical Resistance Gages (Bonded foil or weldable resistance gage; Unbonded resistance; Mustran cell; Plastic encased gage; Eaton Corporation gage; Measurement Group Corporation gage)	Robust and low cost; suitable for dynamic strain but unbonded resistance gage can record frequencies only up to about 25 Hz. Low electrical output; lead wire effects; possible errors owing to moisture, temperature, and electrical connections; lower accuracy compared to the vibrating wire gages; lower reliability for long time performance.

Note: Modified from Dunnicliff (1988)

#### 4.1.1 Electrical Resistance Gages for Static and Dynamic Strain Registration

The embedment electrical resistance strain gages used for the culvert instrumentation were EGP-5-350 type manufactured by Measurement Group (Figure 4-1). These gages are specially designed for measuring mechanical strains inside concrete structures. The sensing grid is constructed of a nickel-chromium alloy (similar to Karma alloy) cast into a proprietary/cement composite material to ensure maximum strain sensitivity. The resulting assembly is designed for strain measurement after being embedded in concrete. The gage has an active gage length of 100 mm for averaging strains in aggregate materials. A rugged 130-mm outer body of proprietary polymer concrete prevents mechanical damage during pouring, and provides protection from moisture and corrosive attack. The grid is self-temperature-compensated to minimize thermal output when installed in concrete structures. Each gage incorporates a heavy-duty 3-m cable with 22-AWG (0.643-mm in diameter) lead wires. A three-wire construction to the sensing grid helps minimize temperature effects in the instrumentation leads. Some information related to the performance of the gage is listed in Table 4-2.



Figure 4-1 EGP-5-350 Embedment Strain Gage,  
Measurement Group, Inc

Table 4-2 Specifications of the EGP-5-350 strain gage

Character	Description
Sensing Grid	Nickel-chromium alloy on polyimide backing; 100 mm nominal active gage length.
Grid Resistance	350 ohms, $\pm 0.8\%$ at room temperature (24 EC).
Gage Factor	$2.061 \pm 0.8\%$ at 24 EC.
Strain Range	5000 $\mu\epsilon$ at 24 EC.
Temperature Range	Nominal usage range -5 EC to 50 EC.
Self-Temperature Compensation	Best temperature compensation is -5 EC to 50 EC with bridge voltage set at 10 volts or less (15 volts maximum)
Leadwire System	Three 3-m leads of 22-AWG (0.63-mm dia.) Stranded, thinned copper with PVC insulation. Each leadwire has a nominal resistance of 0.056 O/m, which is not included in gage resistance.
Outer Body	Proprietary polymer concrete. 130×17×10 mm nominal.

#### 4.1.2 Vibrating Wire Strain Gage for Static Strain Registration

Since the introduction of vibrating wire strain gages in 1930s (McRae and Simmonds, 1991), they have been used in a wide range of civil engineering applications, such as the measurement of load, earth pressure, pore-water pressure, liquid level, movement, and inclination. A vibrating-wire gage essentially consists of a length of steel wire which is constrained at each end by clamps and tensioned so that it is free to vibrate at its natural frequency. The steel wire is excited magnetically by an electrical coil (illustrated in Figure 4-2). Either this coil or a second coil is used to measure the frequency of vibration. In order to compensate for temperature effects, a thermistor is included in the gage to measure the real-time temperature.

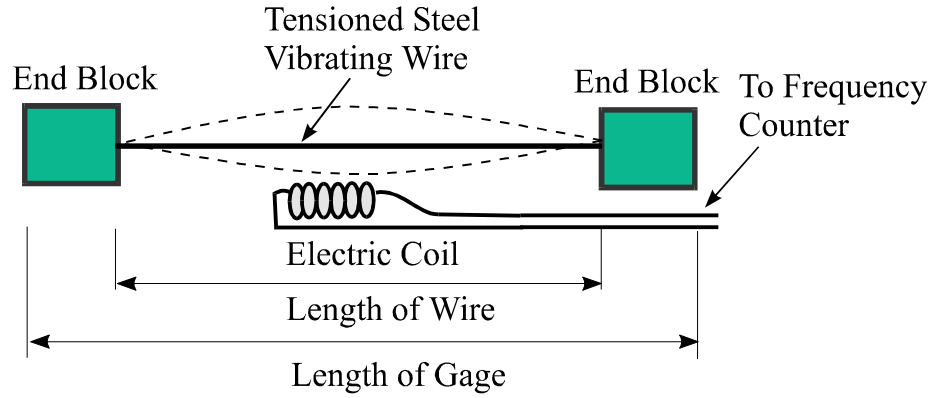


Figure 4-2 Schematic of Vibrating Wire Gage

When there is a relative movement between the two end clamps, the natural frequency of the steel wire is changed. The wire can therefore be used as a strain gage by plucking the wire, measuring the natural frequency and relating the frequency change to strain.

There are two types of wire plucking and reading methods (Dunnicliff, 1988; McRae and Simmonds, 1991; Benmokrane et al., 1995): the pluck and read method and the continuous-excitation method. The former oscillates at adjustable intervals by a direct-current plucking pulse, then the frequency of the tensioned steel wire oscillation is picked up by the same magnetic coil. The continuous-excitation type uses two electromagnets, one for continuously exciting the wire, and the other for continuously picking up the induced vibration so that this type of gage can be used measure low-frequency dynamic loads.

The frequency of a vibrating wire in terms of wire stress (Dunnicliff, 1988) is

$$f = \frac{1}{2L} \sqrt{\frac{s}{r}} \quad (4-1)$$

Where  $f$  = natural frequency of wire (Hz)

$L$  = length of wire (m)

$s$  = stress in wire (Pa)

$\rho$  = density of the wire material (kg/m<sup>3</sup>)

Equation 4-1 can be written in terms of wire strain:

$$f = \frac{1}{2L} \sqrt{\frac{Ee}{\rho}} \quad (4-2)$$

Where  $E$  = modulus of elasticity of the wire (Pa)

$e$  = strain in the wire

Thus,

$$e = \frac{4L^2 f^2 \rho}{E} = K_1 f^2 \quad (4-3)$$

Where

$$K_1 = \frac{4L^2 \rho}{E} \text{ is constant for a definite gage.}$$

Since the deformation of wire must equal the deformation of the body of the gage:

$$eL = e_b L_b \quad (4-4)$$

Where  $e_b$  = strain of the gage body

$L_b$  = length of the gage body

The strain reading

$$e_b = \frac{Le}{L_b} = \frac{LK_1 f^2}{L_b} = K_2 f^2 \quad (4-5)$$

where

$$K_2 = \frac{LK_1}{L_b} = \frac{4L^3 \rho}{L_b E} \text{ is a gage factor which is constant for a definite strain gage.}$$

Taking into account the fact that the gage is always installed under initial tension, equation (4-4) can be written:

$$\Delta e = K_2 (f^2 - f_0^2) \quad (4-6)$$

Where  $\Delta e$  = strain change measured by the gage;  $f_0$  = initial frequency value.

The use of frequency as the output signal (rather than the magnitude of a resistance or voltage as used in resistance gages) minimizes undesirable effects associated with long

lead wires, contact resistance or leakage to ground. Very long cable lengths are acceptable without distortion of the measurement results.

The vibrating wire concrete strain gage used for the culvert instrumentation is a product of Geokon Inc. Model VCE-4200. Its characteristics are listed in Table 4-3.

Table 4-3 Characteristic of VCE-4200 Vibrating Wire Strain Gage

<b>Character</b>	<b>Descriptions</b>
Working Mechanism	Plucking and reading
Active Gage Length	153 mm
Maximum Strain Range	3000 $\mu\epsilon$
Sensitivity	1.0 $\mu\epsilon$
Temperature Range	-20 - 80 EC
Coil Resistance	150 ohms
Typical Frequency Datum	800 Hz
Dimensions	153 mm long and two flanges at the ends are 19mm in dia.

The measured frequency in this type of gage is automatically converted into the strain reading in the built-in microprocessor in the Model GK-403 readout box. One of the advantages of this type of gage is that if the strain reading cannot be measured, the frequency reading may be recorded and then converted manually to strain. Because the frequency is measured over an interval of time, vibrating wire gages are not applicable for the measurement of dynamic loads induced by construction equipment. The VCE-4200 strain gage is shown in Figure 4-3.



Figure 4-3 Geokon Model VCE-4200  
Vibrating Wire Concrete Strain Gage

## 4.2 Earth Pressure Cells

Earth pressure cells were used to measure the contact pressures on the walls and roof of the culvert. Pressure measurements are especially useful when combined with the strain data from strain gages embedded in the box culvert structure. The pressure cells register the stress input into the structure, whereas the strain gages in the concrete reflect the response of the structure. Thus the behavior of the box culvert under the embankment can be observed under known loads.

The behavior of earth pressure cells under different geotechnical conditions and materials has been extensively investigated during the past 50 years (Lazebnik, 1998), and different types of earth pressure cells were developed for special instrumentation purposes. Generally, there are two types of embedment earth pressure cells: hydraulic cells and diaphragm cells (Hannon and Jackura, 1984; Dunnicliff, 1988; Lazebnik, 1998). The hydraulic type of cell consists of two circular plates welded together around their periphery. The intervening cavity between the plates is filled with a de-aired liquid, and a length of high-pressure steel tubing connects the cavity to a nearby pressure transducer. The total stress acting outside of the cell is then sensed by the internal liquid.



The diaphragm cell consists of a stiff circular membrane, which is fully supported by an integral stiff edge ring. External soil pressure will make the diaphragm deform, and this deformation is sensed by a transducer bonded directly on the interior surface of the cell. Dunnicliff (1988) gives a comprehensive evaluation of the advantages and limitations of a wide variety of earth pressures cells.

As discussed in Chapter 2, the inclusion of the pressure cell into the soil mass usually distorts the stress state of the natural soil due to the significant stiffness difference between the cell and the surrounding soil. Furthermore, the heterogenous nature of the soil mass itself makes the stress state in the soil complex and unpredictable. Hence, measurement of pressures in the soil becomes extremely difficult. Some factors which affect the cell performance as summarized by Weller and Kulhawy (1982) are listed in Table 4-4. Table 4-4 indicates that the selection of adequate cells for the specific project is critical to the success of the pressure measurement. Other than the cell information, the influence of the cell placement procedure and the environment temperature are also factors that can affect the cell stress registration.

To investigate the earth pressure acting on buried box culverts, hydraulic cells specifically designed for monitoring pressures acting on a structure were selected. In this type of cell, one of the plates is thick and designed to bear against the external surface of the structure in order to prevent flexure of the cell. Two types of readout systems were chosen: 1) Vibrating wire strain gage cells (Geokon Model 4810 contact pressure cell), which are good for long term performance; 2) electric resistance gage cells (Geokon Model 3650), which are ideal for the registration of dynamic pressure induced by

Table 4-4 Factors Affecting the Earth Pressure Cell Measurement

Factor	Description	Recommended Control Method
Aspect Ratio (ratio of cell thickness $t$ to diameter $D$ )	Cell thickness alters stress field around cell.	Use relatively thin cell; $t/D < 0.2$
Soil/cell stiffness ratio $S$ (ratio of soil stiffness to cell stiffness)	At low values of $S$ , small changes of soil stiffness do not cause significant changes in cell registration. At high values of $S$ , changes in soil stiffness cause nonlinear registration.	Design cell for high stiffness and use correction factors
Size of cell	Very small cells subject to scale effects and placement errors. Very large cells difficult to install and subject to nonuniform bedding.	Use intermediate size of cell; typically 230-300 mm diameter
Deflection of active face (arching)	Excessive deflection changes stress distribution over cell.	Design cell for low deflection: a diaphragm diameter/diaphragm deflection at center $> 2000 - 5000$ .
Eccentric, nonuniform, and point loads	Soil grain size too large for cell size used. Nonuniform bedding causes nonuniform loading.	Increase active diameter of cell. Take great care to maximize uniformity of bedding.
Lateral stress rotation	Presence of cell in soil causes lateral stress to act normal to the cell.	Use correction factors
Stress-strain behavior of soil	Cell measurements influenced by confining conditions.	Calibrate cell under near-usage conditions
Placement effects	Nonuniform conditions in the vicinity of the cell can cause erroneous response.	Use reproducible placement procedures for calibration and field installations
Proximity of structures and other stress cells	Interactions of stress fields near instruments and structures causes errors.	Use adequate spacing
Placement stresses	Over-stressing during soil compaction may permanently damage cell	Check cell and transducer design for yield strength
Temperature	Temperature change causes change of cell reading	Design cell for minimum sensitivity to temperature; if significant temperature change is likely, measure temperature and apply temperature correction factor determined during calibration.
Dynamic stress measurement	Response time, natural frequency, and inertia of cell cause errors	Use resistance or semiconductor strain gages, stiff cells and dynamic calibration.

Note: Modified from Dunncliff (1988)

construction equipment. The resistance pressure cells were only installed at the Greene County culvert site. These two types of pressure cells differed only in the type of transducer used to record the internal fluid pressure. The plate designs were identical. Figure 4-4 illustrates the schematic of the vibrating wire pressure cell. Characteristics of the pressure cells are listed in Table 4-5.

Table 4-5 Characters of the Contact Earth Pressure Cells

<b>Character</b>	<b>Geokon Model 4810</b>	<b>Geokon Model 3660</b>
Transducer Type	Vibrating wire	Electric resistance strain gage
Cell Dimensions	230 mm in dia.(D) and 6mm in thickness (t). Aspect Ratio: D/t = 38	230mm in dia. and 6mm in thickness. Aspect Ratio: D/t = 38
Typical Range	170 kPa in Sullivan County culvert and wall of Greene County culvert; 340 kPa in the culvert roof of Greene County.	Typically 350 kPa and installed on the wall of Greene County
Excitation Voltage	5 volts square wave	10 volts
Transducer Housing Dimension	25.4mm in dia. and 153 mm in length	50mm in dia. and 153 mm in length

### 4.3 Installation of Strain Gages and Pressure Cells

#### 4.3.1 Installation of concrete Strain Gages

Before pouring the concrete, concrete strain gages were installed by tying the gages to the rebar with plastic cable ties. The gages were cushioned with tyrofoam blocks at the two ends of the gages to separate the gage body from the rebar. The styrofoam blocks served as shock absorbers, minimizing the possible high frequency oscillation generated by the concrete vibrator during the placement of concrete. This can also protect the gage

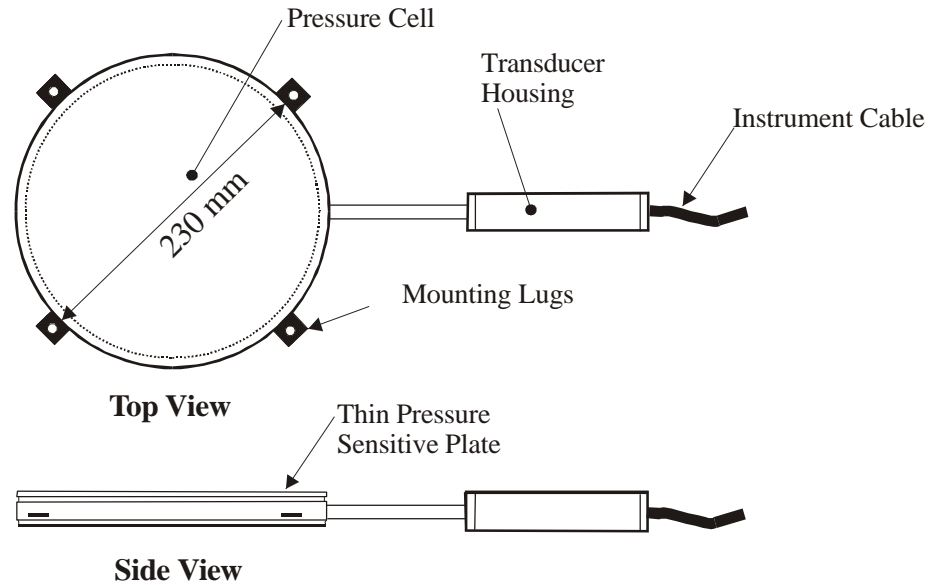


Figure 4-4 Geokon Model 4810 Contact Pressure Cell

from damage which may result from movement of the reinforcing gage. It is assumed that there is no relative slip between the concrete and the gage provided the concrete is not cracked. When the structural member is under tension, micro-cracks may be present in the concrete, so that the recorded strain reflects the average deformation over the length of the gage. On the bottom of the culvert roof slab, a 150 mm thick prestressed pre-cast concrete panel was used, so that reinforcing rebars were not available to mount the gage. A “dummy” rebar of the same diameter as the top reinforcing bars was suspended about 25 mm above the concrete panel and used to mount the strain gages. A schematic of gage installation is shown in Figure 4-5.

The gages were mounted to the reinforcing rebar so that the concrete deformation could be recorded by the strain along the active length of the gage. The gage length of 140 mm is long enough to cross several interfaces between the aggregate and the cement, which are the locations where micro-cracks would be likely to develop first.

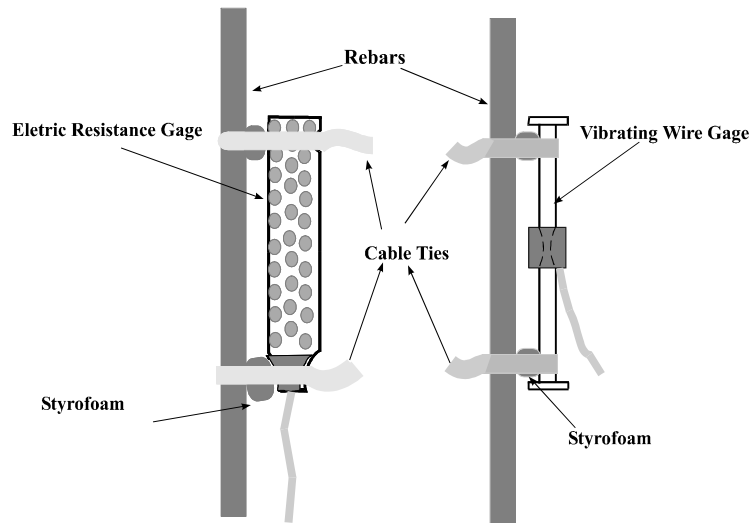


Figure 4-5 Schematic of Strain Gage Installation

In order to measure the bending moments in the box culvert, the gages were installed in pairs at one particular location to register the tensile and compressive deformations. The electric resistance gage and vibrating wire gages were installed on nearby bars to compare the structural deformation at the same location. The position of the gages was recorded so that it was possible to convert the recorded structural strain into moments and axial forces.

#### **4.3.2 Stress-Free Strain Gages (Greene County Culvert)**

##### **4.3.2.1 Factors that Influence the Concrete Strain Gage Reading**

Strain in concrete can result from several factors other than stress change. These factors include creep (strain under constant stress), shrinkage and swelling (moisture content change) in concrete, and temperature. The strain gage does not distinguish the types of strain. The stress change induced by the strain difference may likely be distorted by these factors if the influence of these factors cannot be determined.

Creep and shrinkage are influenced by the mix design of the concrete as well as the

stress level (Dunnicliff, 1988). The effect of creep and shrinkage becomes significant when the stress is greater than about 60% of the ultimate strength of concrete. For the instrumented culverts it is unlikely that the stress level of the structure would cause significant creep. According to ACI (1993), the effects of creep and shrinkage can be corrected by using averaged empirical data that relate to the environmental and mix parameters. Temperature can cause a real stress change, as well as a change in the strain gage reading without a change in the stress.

#### **4.3.2.2 Installation of Stress Free Strain Gages**

Although both the electric resistance and vibrating wire strain gages have a self-temperature-compensation mechanism, the gages would still likely undergo some temperature induced stress free readings. In order to correct for the temperature affects, a stress free gage procedure was used in the Greene County culvert. This procedure involved installation of resistance and vibrating wire gages within a 150-mm dia. cylinder of the same concrete as the culvert structure. The cylinder was placed in the bottom of the culvert wall and isolated from the surrounding concrete by an approximately 30-mm thick layer of Styrofoam so that the gages in the cylinder would not be subject to the external stress by the backfill. The stress free gages would likely experience the same temperature as the gages mounted to the reinforcing steel, but without stress. Hence, the stress free gages reflected all the factors except the stress. Both the resistance and vibrating types had one gage installed as the stress free gage. The stress free gages were read at the same time with the other gages, and the change of strain was used to correct the active gage readings.

The strain reading results from the stress free gages over a period of nearly 500 days are plotted in Figure 4-6 and Figure 4-7. The temperature recorded by the thermistor in the vibrating wire stress free gage is also plotted in order to compare the effect of temperature change. From these two figures, it is clear that during the placement of concrete, the strain reading recorded by two types of gages likely underwent a drastic change due to the setting and curing effects of concrete. These effects included high temperature gradient, swelling and shrinking between gage and the cement slurry.

Except for the readings during the concrete placement, the highest recorded temperature by the gage in the summer was 22.3 EC, and the lowest temperature was 4.3 EC in the winter. The maximum difference of the strain reading registered by the electric resistance gage was about 100 micro-strain, which corresponds to 4000 kPa uniform axial stress. The readings had a similar fluctuation as the temperature change. This suggests that the temperature may cause fairly large changes in strain reading as recorded by the resistance gage. In the vibrating wire gage, however, the registered stress free reading difference is less variable, but still significant (the maximum difference is 50 micro-strain). In general, the readings after 200 days are more constant in both gages, with a slight tendency to increase over time. This may be due to the significant temperature gradient between the inside and the outside of the culvert had great impact on the reading when the outside surface of the culvert was exposed to the air. However, when the culvert was covered by soil, factors other than temperature contributed more to the changes of the readings.

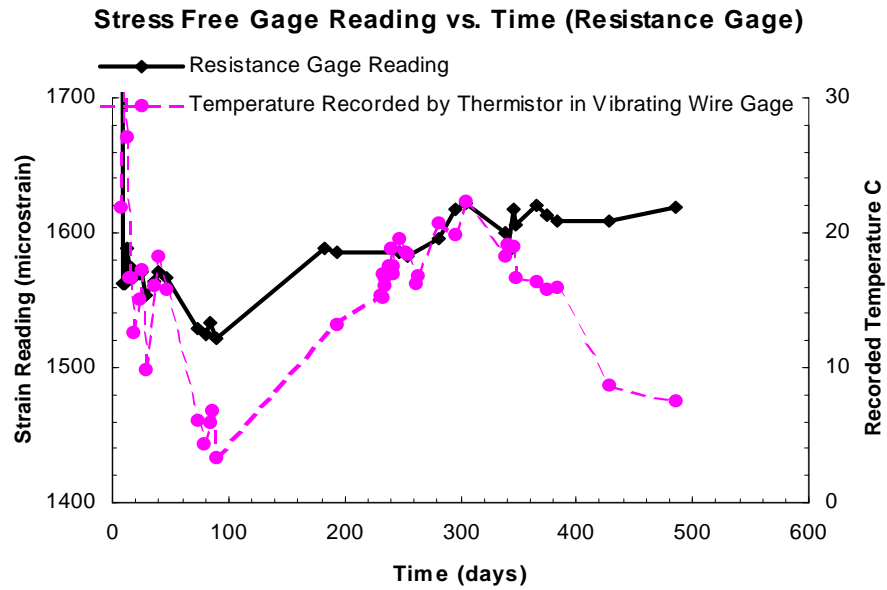


Figure 4-6 Stress Free Resistance Strain Gage Reading vs. Temperature

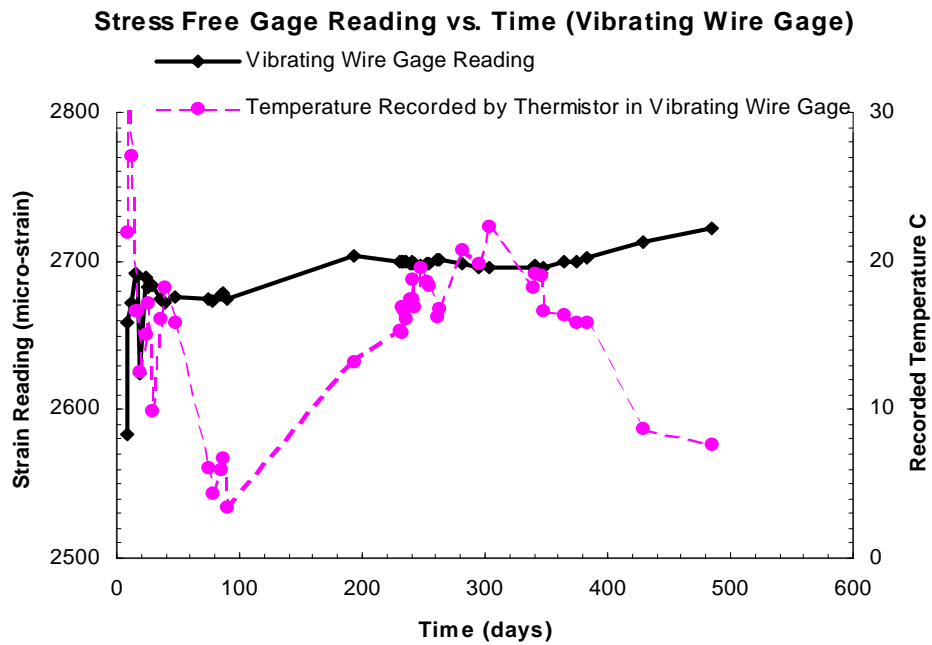


Figure 4-7 Stress Free Vibrating Wire Strain Gage Reading vs. Temperature



Because of the significant change in the stress free gages readings, it is likely inappropriate to use the active concrete strain gage readings directly in the strain-stress conversion. Recorded strain values should be adequately corrected in order to obtain reasonable stress and internal force results.

#### **4.3.3 Installation of Pressure Cells**

The cell was first fixed to the culvert wall and roof with concrete anchors through 4 mounting lugs around the edge of the plate, and a quick setting high strength grout pad was used to assure uniform contact between the plate and concrete. Medium sand was used to cover the cell and transducer housing to protect the cell from possible point loads or other stress distortions induced by large size particles in the crushed gravel. A geosynthetic cover was attached to the concrete with adhesive to separate the gravel and the sand (Figure 4-8). A total of 30 pressure cells, 24 vibrating wire and 6 resistance pressure cells, were installed at the two culvert sites.

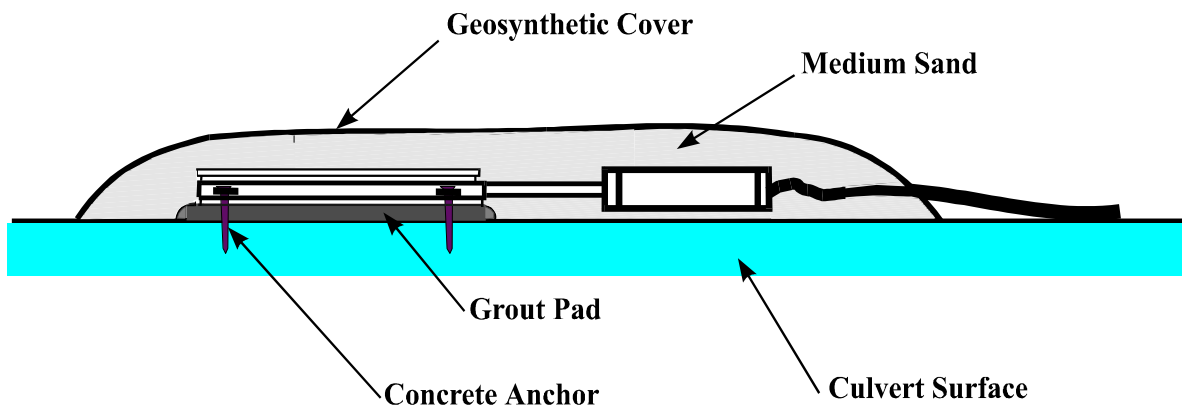


Figure 4-8 Installation of Pressure Cell

#### **4.4 Dynamic Loading Measurement**

The dynamic earth pressures induced by construction equipment were measured by resistance gage earth pressure cells on the Greene County culvert. The structural response due to these impulsive lateral pressures was measured by the embedded resistance concrete strain gages. Six Geo-Kon resistance strain gage pressure cells were installed in instrumentation Section A to record the dynamic lateral earth pressure. They were aligned vertically and were located 1.40 m horizontally from the alignment of the static vibrating wire pressure cells (Figure 4-9). Both the size and the pressure sensing mechanism were the same as the vibrating wire pressure cells, and an identical installation method was used. Resistance strain gage transducers were chosen to record the dynamic pressures because the vibrating wire transducers are not well suited to high frequency pressure variations.

In order to determine the structural response due to the dynamic lateral load, embedded resistance concrete strain gages were attached to the inside and outside rebar in the concrete wall to coincide with the vibrating wire strain gage locations. The dynamic strain signals from the resistance pressure cells were recorded by an OPTIM MEGADAC 3415 data acquisition system, which was connected to an on-site computer. Due to the large amount of data collected (30 channels), the acquisition rate was 10 samples per second. The output from the computer was verified using a strain gage readout box before recording the dynamic lateral pressure induced by the construction equipment.

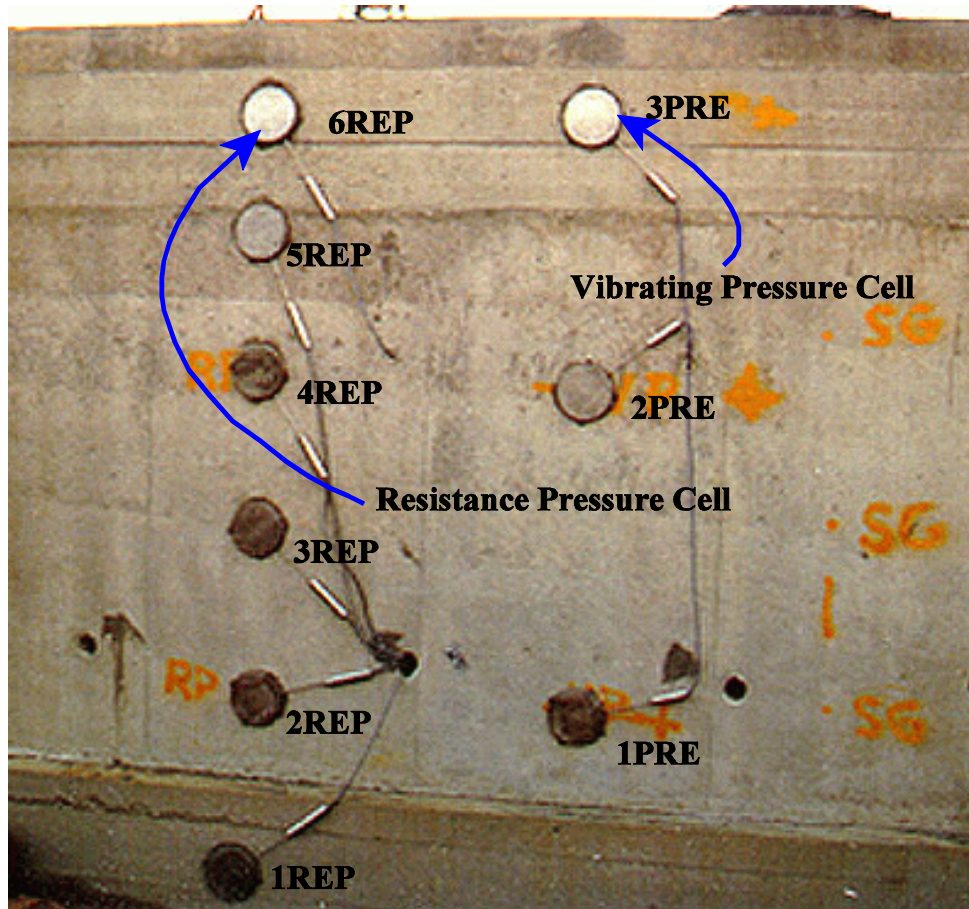


Figure 4-9 Illustration of Pressure Cell Locations  
in Section A (Greeneville Culvert , TN)  
**REP = resistance gage, PRE = vibrating wire gage**

## **Chapter 5**

### **Numerical Modeling Considerations for Buried Box Culverts**

As stated previously, the earth pressures on box culverts may be affected by many factors, e. g. soil conditions surrounding the structure, relative stiffness of the box culvert and soil, compaction forces induced by construction equipment, construction sequence, and even the initial geometry of the ground surface. To evaluate these effects, the general purpose commercial finite element code ABAQUS (HKS, 5.7, 1997) was used.

The stress conditions around the culvert were idealized as plane strain so that the culvert system was characterized with 2-D plane strain elements. A typical mesh for the final stage of the replacement culvert analysis in Sullivan County is shown in Figure 5-1. A similar mesh was used for the Greene County culvert, except that the culvert was constructed on nearly flat ground without the excavation and existing slope. Additional discussion of the meshes accompanies the discussion of the analysis results, in Chapters 7 and 10.

#### **5.1 Material Modeling**

##### **5.1.1 Constitutive Model for Backfill Materials**

The elastic plastic Drucker-Prager model (HKS, 1998) was used in the analysis to represent the gravel around the culvert, the clayey shale backfill and the existing soil

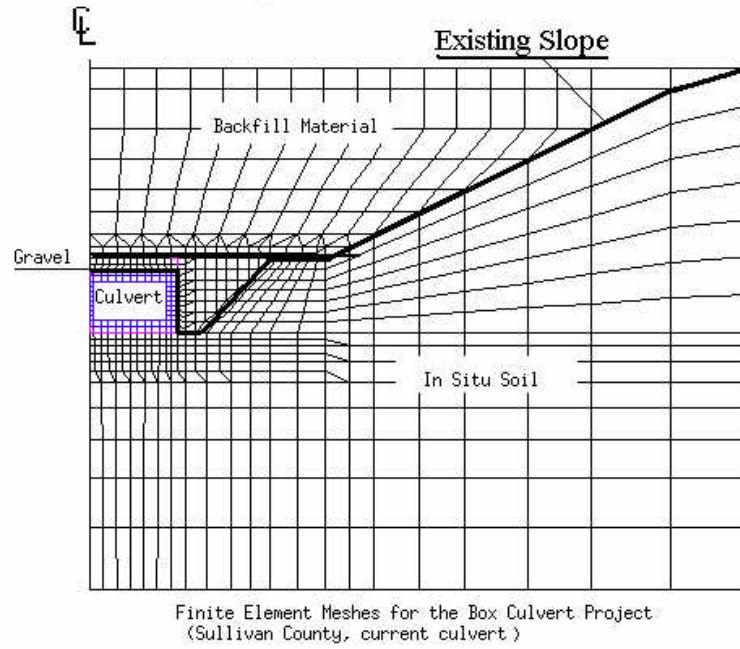


Figure 5-1 Illustration of Finite Element Mesh for Replacement Culvert in Sullivan Co.

slope beside the culvert. The linear Drucker-Prager yield criterion (graphically depicted in Figure 5-2) is:

$$F = t - p \tan \beta - d = 0 \quad (1)$$

Where  $t$  and  $p$  are stress invariants of the stress matrix  $\mathbf{s}$ :

$$p = -\frac{1}{3} \text{trace}(\mathbf{s}) \quad (2)$$

$$t = \frac{1}{2} q \left[ 1 + \frac{1}{K} - \left( 1 - \frac{1}{K} \right) \left( \frac{r}{q} \right)^3 \right] \quad (3)$$

The parameter  $\beta$  is the slope of the linear yield surface in the  $p$ - $t$  plane (Figure 5-2);  $d$  is the hardening parameter and  $K$  is a material parameter, the ratio of the yield stress in triaxial tension to the yield stress in triaxial compression. This parameter controls the dependence of the yield surface on the value of the intermediate principal stress. To

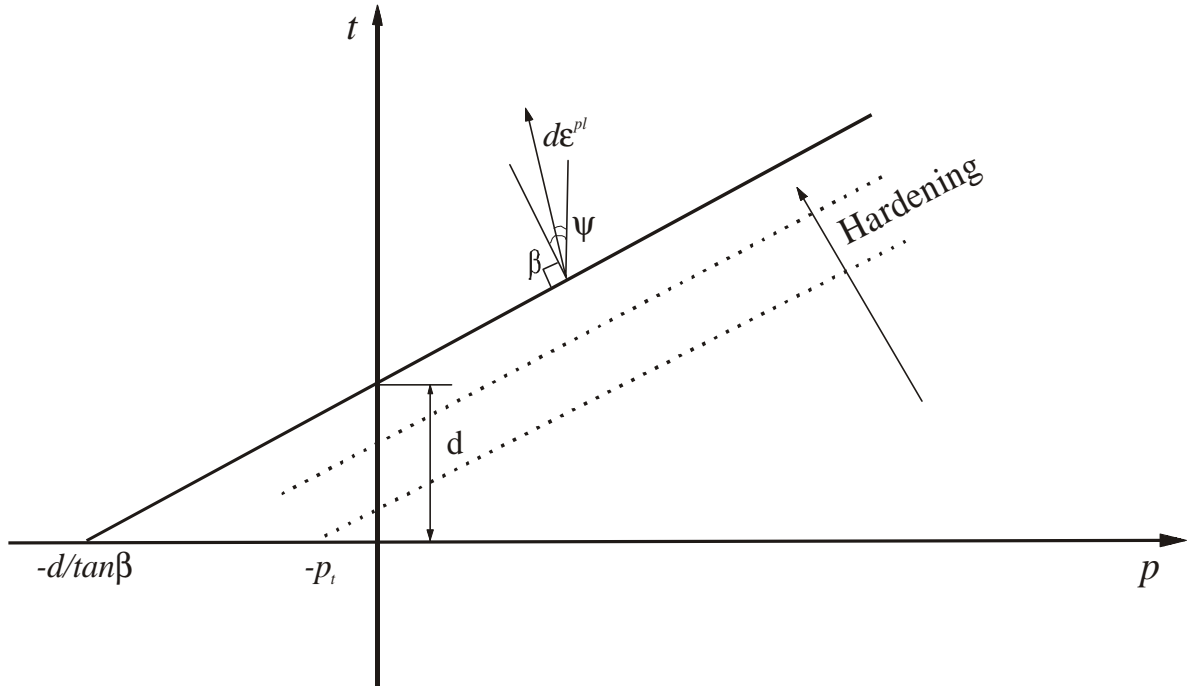


Figure 5-2 Linear Drucker-Prager Model:  
Yielding Surface and Flow Direction in  $p$ - $t$  Plane

simplify the problem,  $K$  was selected as 1.0, thus the yield stress in triaxial tension and compression are the same, and the yield surface is the von Mises circle in the deviatoric principal stress plane (the  $\pi$  plane). The Mises equivalent stress is :

$$q = \sqrt{\frac{3}{2}(\mathbf{s}:\mathbf{s})} \quad (4)$$

and

$$t = q \quad (5)$$

where  $\mathbf{s}$  is the deviatoric stress tensor .

In the Drucker-Prager elastic plastic model, yielding occurs when the stress state satisfies Equation (1) such that  $F = 0$ . When the material yields, the yield function translates. Hardening parameter  $d$ , which is related the material cohesion, describes the growth of the yield surface as the plastic strain accumulate. An isotropic plastic strain rate-independent hardening model is used in this model:

$$d = (1 - \frac{1}{3} \tan \beta) \mathbf{s}_c \quad (6)$$

where  $s_c$  is the uniaxial compression yield stress. Stress states below yielding are assumed to behave in a linear elastic manner.

A nonassociated flow rule was used in the analysis, which means that a function other than the yield function (equation 1) is used as the plastic flow potential  $G$  to define the direction of the incremental plastic strain  $de^{pl}$ . The plastic potential function  $G$  is used:

$$G = t - p \tan \psi \quad (7)$$

where  $\psi$  is defined as dilatancy angle. It is the angle between the direction of plastic strain and the vertical line in the  $p$ - $t$  plane. Usually  $\psi < \beta$ , as illustrated in Figure 5-2. If  $\psi = 0$ , the inelastic deformation has no volumetric component, and if  $\psi > 0$ , the material is dilatant. Nonassociated flow implies that the material stiffness matrix is not symmetric, therefore, the unsymmetric matrix storage and equation solution scheme was used in the ABAQUS analysis procedure.

An isotropic linear elastic model was used to represent the behavior of the concrete, the firm clay underneath the culvert and the bedrock. The basic parameters used in the modeling of the replacement Sullivan County culvert behavior are represented in Table 5-1. Similar properties were used for the Greene County culvert, and a discussion of these material parameters is included in the description of the various analyses.

### 5.1.2 Constitutive Model for Interface Elements

To simulate the contact between the outer surface of the culvert and the soil backfill, interface or contact elements were used. In the culvert problem, inclusion of the contact element is critical to the pattern of the earth pressure, especially the horizontal

Table 5-1 Summary of Material Parameters in the Box Culvert Analysis  
(Replacement Culvert, Sullivan County, TN)

Material Description	Cohesion c (kPa) Yield Stress ( $s_c$ , in ABAQUS)	Friction Angle $\phi$ (deg) ( $\beta$ , in ABAQUS)	Dilatancy Angle $\psi$ (deg)	Elastic Modulus E (kPa)	Poisson's Ratio $\mu$	Source and Reference
Gravel #57 stone	33 (66.1)	38.5 (46.1)	20	1.58E4	0.27	Shear strength from Law Engineering (1990), modulus from Penman (1975)
Side soil near gravel and existing excavated slope	32 (63.8)	20 (30.3)	15	1.58E4	0.32	Measured shear strength, modulus from Penman (1975)
Loose fill above culvert	25 (46.2)	7 (11.9)	0	6.5E3	0.32	Estimated shear strength, Poisson's ratio from Bowles(1988).
Normal fill away from culvert	32 (63.8)	20 (30.3)	15	1.58E4	0.32	Measured shear strength from TDOT (1995), modulus from Penman (1975)
Firm residual clay and weathered shale	NA			6.5E4	0.30	Bowles(1988)
Fresh shale	NA			1.12E6	0.25	Goodman(1989)
Concrete	NA			4.06E7	0.18	Modulus from lab test

pressure distribution. The CONTACT PAIR option in ABAQUS was used to model the behavior at the soil and culvert interface. A strict “master-slave” contact formulation was used to define the interaction between the two surfaces, in which the slave nodes are constrained not to penetrate into the master surface. However, the nodes of the master surface can, in principle, penetrate into the slave surface. The basic form of the Coulomb model was used to characterize friction in the interface. In this model, two contacting surfaces can carry shear stress up to a certain magnitude before they start sliding relative



to one another. The critical shear stress,  $t_{crit}$ , at which sliding of the surface starts is a function of the contact normal pressure,  $p$ , between the surfaces, with  $t_{crit} = \mu p$ , where  $\mu$  = coefficient of friction. By definition, the contact pair algorithm can only transfer compression pressures throughout the interface. The coefficient of friction  $\mu$  was assumed to be 2/3 of the tangent of the angle of internal friction of the surrounding soil.

Figure 5-3 compares the field measured earth pressures with those obtained from the numerical analysis. Numerical results are shown for three cases: zero interface friction (perfectly smooth), interface friction equal to that of the well graded gravel, and no interface behavior (no slip between backfill and concrete). As expected, in the region over the culvert roof where little relative slip expected, the results from all three analyses are nearly identical, and good agreement with the field measurements is obtained. However, because slip would be expected along the upper portion of the culvert wall, the vertical stress distribution over the edge of the roof is somewhat dependent upon the interface friction. Higher vertical earth pressures were measured in this area, and correspond to the increased rigidity of the culvert wall. Without the interface slip, the zone of maximum vertical stress is shifted slightly outside the region immediately above the culvert. The predicted distribution of lateral earth pressures on the culvert wall were somewhat dependent upon the interface friction, with the pressures slightly greater at the bottom when no interface is included.

### **5.1.3 Numerical Analysis of Failed Culvert**

One of the principal assumptions in the analysis of the culverts is that the compactive effort can be represented by assigning appropriate elastic moduli to the soil

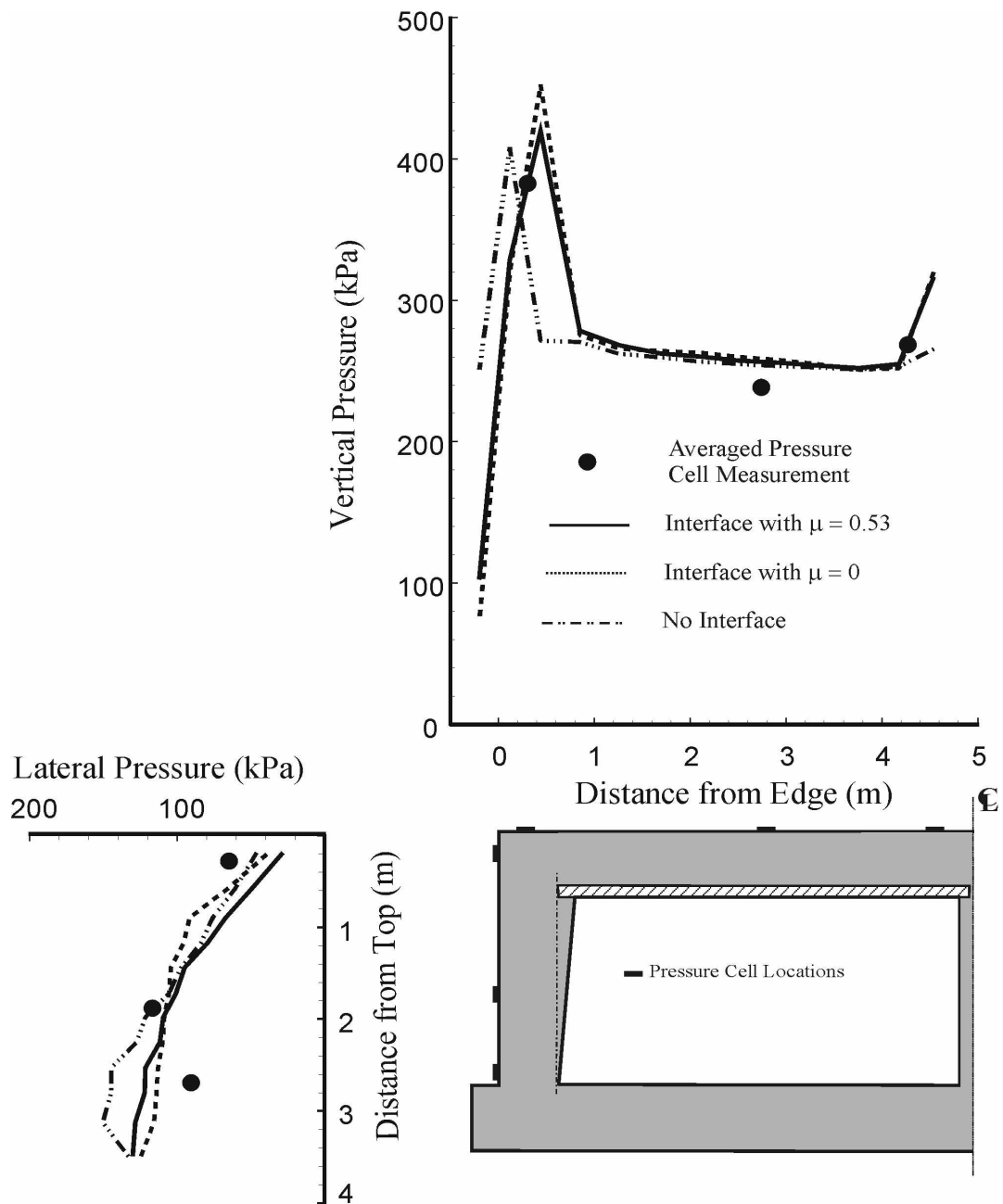


Figure 5-3 Comparison of Measured Earth Pressures with Numerical Prediction of Different Interface Considerations

layers in. According to the construction specifications, a reduced compaction effort was utilized in the replacement culvert in Sullivan County. The numerical model can be calibrated by tuning some of the estimated parameters to fit the field record results, and the influence of other factors such as stiffness of the subsoil under the culvert can then be revealed by parametric study. Furthermore, the information from the results of the current culvert in Sullivan County can be used to back analyze the failure mechanism of the original culvert, which was assumed to be constructed under normal compactive effort.

## **5.2 Choice of Element Type**

The symmetry was assumed along the centerline of the box culvert, so that only half of the culvert was considered in the numerical analysis. The meshes utilize three different kinds of first order plane strain elements: two quadrilateral elements (CPE4, CPE4I) and a triangular element (CPE3). All three of the elements assume a linear variation of strain between nodes. Generally, the soil was discretized with the regular displacement element CPE4, and CPE3 was used to fit the mesh size changes of CPE4 elements. Since a significant bending moment was expected within the culvert structure and the regular CPE4 element may distort the bending behavior due to an artificially high stiffness, the deformation incompatible mode element CPE4I was used to discretize the culvert. The incompatible deformation modes add an extra internal degree of freedom to the element, so that, the so-called parasitic shear stresses, which are observed in regular CPE4 elements if they are loaded in bending, are eliminated.

### 5.3 Comparison of Different Stress Calculation Methods

In the conventional displacement based finite element analysis scheme, the stresses are determined from the computed strains, multiplying the strain vector by the stiffness matrix. The calculated strains and stresses are determined at the Gauss integration points of each element. Figure 5-4 illustrates the location and numbering of the Gauss points for the elements used in this analysis. Stresses at other locations in an element are extrapolated from the Gauss points, with some loss in precision. In the current analyses, the first order element type is used in all analyses, so that a linear variation of strain and stress within the element is assumed. The stress at a particular node is obtained by the

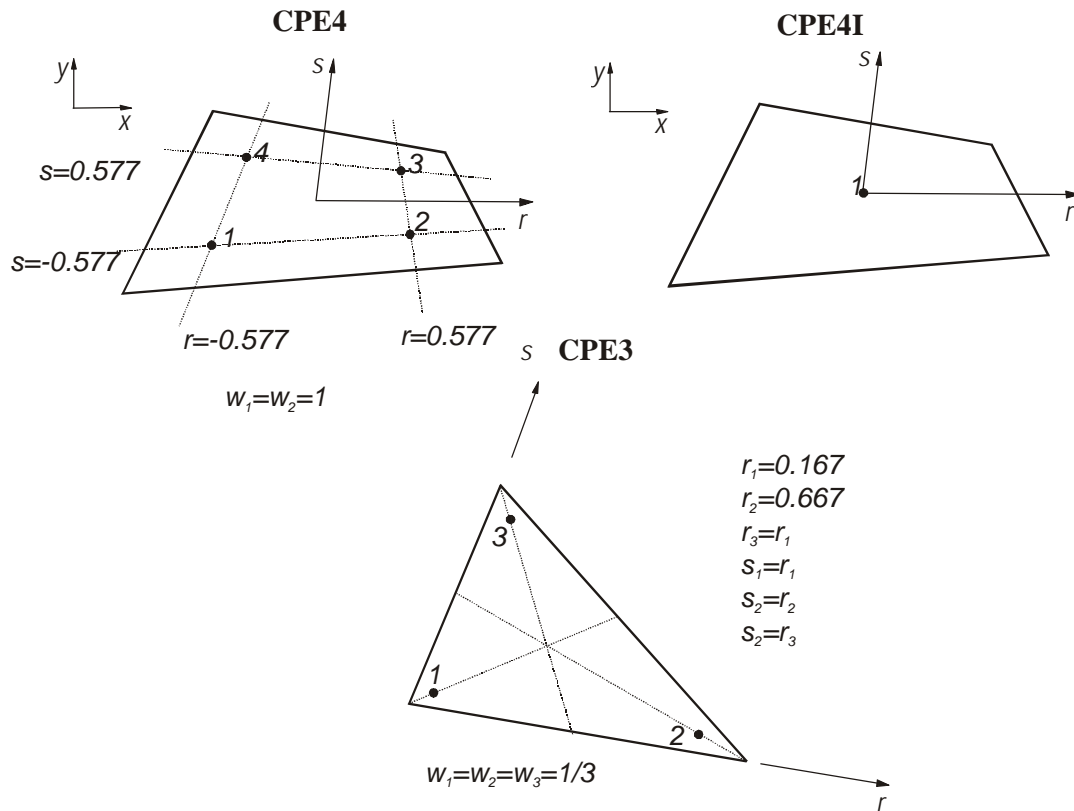


Figure 5-4 Illustration of Gauss Point of Different Element Types

average of the stresses at the Gauss points from the adjacent elements connected to that node.

Slight differences in the result may be obtained depending upon where the stresses are calculated. Figures 5-5 and 5-6 compare the earth pressures on the culvert surface from a typical analysis. Three stress calculation methods are compared: 1) the average normal stress from two integration points in the soil element adjacent to the structure; 2) the average normal stress calculated at a node; and 3) the contact normal pressure directly output from the contact element nodes. Along most of the roof, Figure 5-5 all three measures yield essentially the same result. A greater discrepancy between the average stress at the nodes and the stress at the integration point is found at the corners of the structure, where a high stress gradient exists and a zone of plastic strain is located.

Compared with the normal stress on the roof, difference between normal stresses on the wall, computed by the three methods is greater (Figure 5-6). The differences are only about 25-50 kPa (Scale is different in two figures). This is may be because of a larger relative movement at the interface of the soil and the wall. The focus of the current numerical investigations is on the normal pressure on the culvert structure. In the results discussed here, the replaced normal pressures are the normal pressure output by the contact element.

#### **5.4 Simulation of Construction Sequence**

Highway embankment construction is carried out by placing and compacting the backfill material layer by layer. In the nonlinear numerical analysis, an incremental loading technique was used. This involved simulating the overall construction as a series

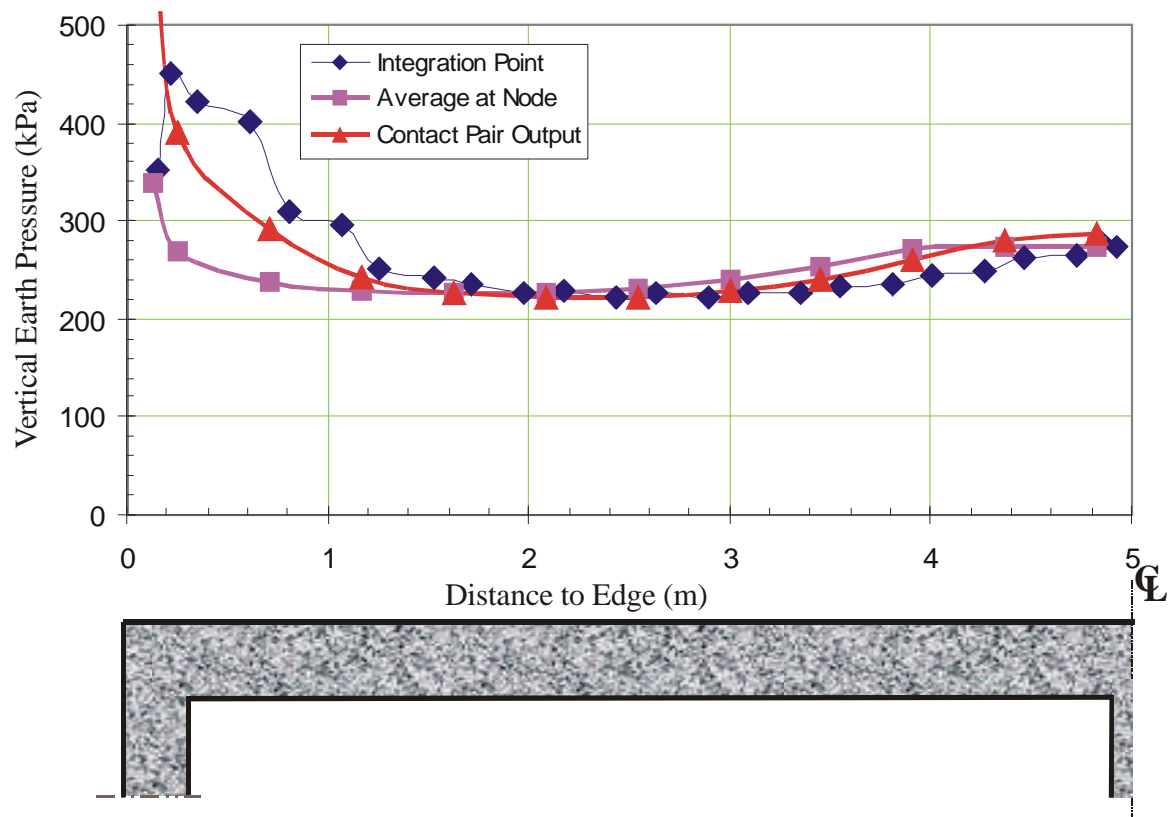


Figure 5-5 Predicted Vertical Pressures of Failed Culvert Roof by Different Stress Calculation Methods (Sullivan County, TN)

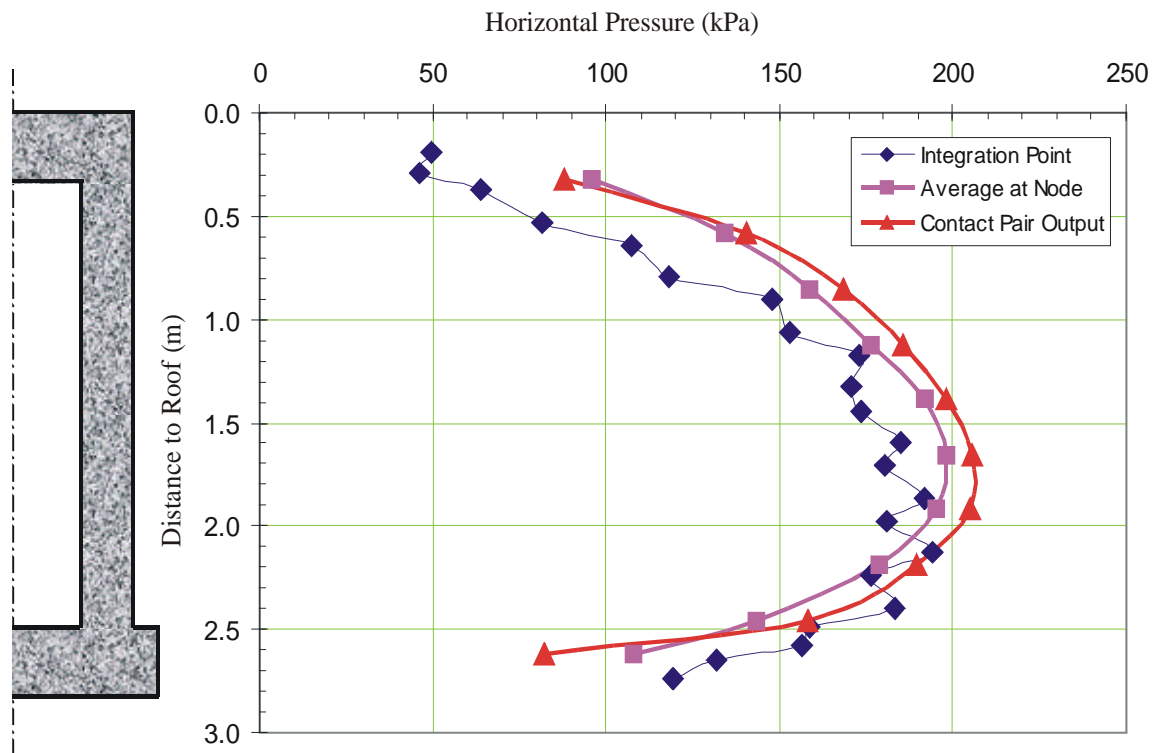


Figure 5-6 Predicted Horizontal Earth Pressure on Failed Culvert Wall by Different Stress Calculation Methods (Sullivan County, TN)

of steps. In each step, a layer of elements was added to the mesh. The final embankment height was achieved by adding ten layers of backfill, which should be sufficient according to the suggestions of Duncan (1996).

This incremental loading technique was achieved in AQAQUS by using the MODEL CHANGE command. All elements needed in the analysis were previously generated, and the elements to be used in the incremental steps were removed before turning on the gravity load. After the reference state satisfied the stress equilibrium, the meshes representing the backfill layers were added to the analysis. Results from the numerical analysis are provided and discussed in subsequent chapters.



## **Chapter 6**

### **Data Interpretation - Collection of Fundamental Material Properties and Baseline Data**

Prior to the measurement of earth pressures and the culvert response, fundamental material properties for the culvert and backfill were determined. In addition, baseline values for the measured quantities were obtained such that changes due to earth pressures could be determined.

#### **6.1 Field Measurement of Fundamental Material Properties**

The density of the backfill material directly affects the earth pressures and is important input to the numerical analysis. In-situ densities of the clayey shale backfill material in Sullivan County site and the limestone gravel in Greene County site were measured by the sand replacement method (ASTM D4914-89). At the Greene County culvert a fine-grained soil was placed above the limestone gravel backfill. The densities of the fine-grain fill and gravel were measured by a nuclear density gage operated by the representative from TDOT. For comparison, the density of the fine grained soil was also measured by the drive tube method. The test results are summarized in Table 6-1.

#### **6.2 Baseline of Strain Gage Measurements**

A total of 38 resistance concrete strain gages and 49 vibrating strain gages were installed at the two culvert sites in East Tennessee. The concrete strain gages were placed

Table 6-1 Summary of Density Tests

Material	Location	Test Method	Number of Tests	Average Density (kN/m <sup>3</sup> )	Note
Clayey Shale	Sullivan Co.	Sand Replacement	4	21.1	Performed at about 8.0 m and 10.0 above the culvert roof.
Gravel	Greene Co.	Sand Replacement	3	22.8	Performed at the culvert side with elevations about 0.5, 1.5 m and 3.0 above the bottom slab. Nuclear density gage: 22.8 kN/m <sup>3</sup> .
Fine-Grained Soil	Greene Co.	Tube Sample	14	18.8	Primarily performed at elevations below 12.0 m above the culvert roof. Nuclear density gage: 18.7 kN/m <sup>3</sup> .

in pairs at each location in order to measure bending moments in the wall and roof.

Strain in the concrete is measured by the concrete gages in terms of microstrains (strain reading  $\times 10^{-6}$ ). The strain at any time is the difference between the current reading and the datum or baseline reading. Theoretically, the datum reading should be the reading taken at the time the concrete in the instrumented section has cured and all shrinkage has stopped, yet before the backfill soil or any load have been placed on the culvert.

Unfortunately, at the Sullivan County site, the construction schedule did not permit the collection of much baseline strain data, and the data of April 3, 1996 immediately prior to the placement of backfill, was selected as a baseline. At the Greene County culvert site, there was about eight months between the completion of concrete work and the start of backfilling operations. During this period, a large amount of data was taken, facilitating the selection of the datum or baseline readings. Since a difference in temperature between

the inside and the outside of the culvert structure can cause temperature related strain, the datum reading at the Greene County culvert site was selected as the reading when temperatures recorded in the vibrating wire strain gages in the inside and outside locations had similar values. Based on this, the datum in Greene County was taken as the average of three readings taken on October 28, 31 and November 8, 1996. Furthermore, in order to reduce the influence of factors other than stress on the strain reading, both resistance and vibrating wire “stress free” strain gages were installed in the Greene County site to assist in the determination of the baseline or datum strain.

The resistance strain gages demonstrated a good performance in response to the dynamic earth pressures induced by the construction equipment at Greene County, but the readings were subject to long term drift and the influence of environmental factors. Data from both sites suggest that resistance concrete strain gages are not suitable for long term measurements. Strains obtained from the vibrating wire gage were used to analyze the long term static structural response, with the resistance gages only used for the dynamic strains.

### **6.3 Baseline Pressure Cell Measurements**

A total of 24 hydraulic type vibrating wire contact pressure cells were installed in the four sections of the two culvert sites, with 6 cells in each section. To record the construction equipment induced dynamic earth pressure, 6 additional hydraulic type resistance strain gage contact pressure cells were installed on the culvert wall near Section A at the Greene County site (Figure 4-9). Baseline data were obtained for each cell prior to placement of backfill.

Backfill placement at the Sullivan County site was from April 8, to May 8, 1996, and the backfill operation in Greene County site was from December 9, 1996 to October 24, 1998. The last readings at each of the two sites were taken on January 25, 2000. A large amount of data was recorded during construction of the embankments. During construction, the embankment height at each instrumentation section was measured. To observe the long term performance of the culverts under constant embankment height, readings were continued after completion of the construction work. By the time the last readings were taken in January 2000, there were about 42 months of data with constant embankment height at the Sullivan County site and 15 months of data at the Greene County site. The details of the recorded data can be found in Appendix A and B.

#### **6.4 Laboratory Tests**

Soil samples from both sites were collected to conduct laboratory tests to measure the soil properties needed in the numerical analyses. For the triaxial shear testing, both 50 mm and 100 mm diameter samples were prepared. Coarse materials such as the clayey shale and the limestone gravel were tested with the 100 mm diameter samples. All the samples were tested under saturated conditions, and a back pressure saturation technique was used to assure a high degree of saturation. Table 6-2 summarizes the triaxial shear test results.

The modulus of elasticity of the concrete was obtained from cylinder compression tests. The concrete cylinders were prepared at the construction sites and cured in the University of Tennessee laboratory curing room till the time of testing. A total of 14

Table 6-2 Summary of Triaxial Shear Test

Material	Location	Sample Status	Number of Tests	Test Method	Strength	
					Cohesion c (kPa)	Friction Angle (degree)
Clayey Shale	Sullivan Co.	Remolded	3	Consolidated Drained	2	22
Clayey Shale	Sullivan Co.	Remolded	2	Consolidated, Undrained with pore pressure measurement	NA	
Gravel	Greene Co.	Remolded	5	Consolidated, Drained	54	43
Clay (Backfill)	Greene Co.	Undisturbed	4	Consolidated, Undrained with pore pressure measurement	22	27
Silty Clay	Greene Co.	Undisturbed	2	Isotropic compression	NA	
Silty Clay Supporting Material	Greene Co.	Undisturbed	4	Consolidated Drained	36	29

samples were tested. Table 6-3 summarizes the test results. The modulus of elasticity reported is the 40% chord modulus.

## 6.5 Data Interpretation and Explanation of Subsequent Chapters

Field recorded earth pressures were compared with the current AASHTO design pressure recommendations (15<sup>th</sup> edition, 1996)) and the AASHTO design guide (12<sup>th</sup> edition, 1977) used for the design of the failed Sullivan County culvert. Analyses of the measured earth pressures on the replacement culvert in Sullivan County and the new culvert in Greene County are presented in Chapter 7 and Chapter 8, respectively. When granular material near a culvert is compacted, the construction equipment may induce

Table 6-3 Summary of Concrete Compression Test Results

Culvert Location	Number of Samples	Mean Compressive Strength (MPa)	Mean Elastic Modulus (GPa)	Elastic Modulus Used in the Numerical Analysis (GPa)
Sullivan County	8	31.6	37.8	40.0
Greene County	6	33.1	37.8	40.0

dynamic earth pressures which have a significant impact on the culvert structure. The transient earth pressure and concrete strain data from the Greene County Culvert are analyzed in Chapter 9. The empirical methods used to estimate the peak impulse pressure and the residual earth pressure after the removal of construction equipment were developed based on the field measurement results. Appendix C presents the typical recorded maximum lateral earth pressures induced by different types of construction equipments. Chapter 10 describes the analysis of the original Sullivan County culvert that failed. This analysis is based on a numerical model developed from the results of the instrumented replacement culvert. The structural response of the failed culvert under various types of earth pressures was also analyzed. Chapter 11 discusses the effect of embankment/highway alignment relative to culvert orientation on the earth pressure. A summary and conclusions are provided in Chapter 12.

**PART II**

**NUMERICAL MODELING OF COMPACTIVE EFFORTS IN**

**CULVERT INSTALLATION**

This Part is a paper published in the proceedings of the 9<sup>th</sup> International Conference on Computer Methods and Advances in Geomechanics, Wuhan, China, Nov., 2-7, 1997.

Authors: Michael Zhiqiang Yang, Eric C. Drumm, Richard M. Bennett and  
Matthew Mauldon

## **Chapter 7**

### **Influence of Compactive Effort on Earth Pressures Around a Box Culvert**

#### **7.1 Abstract**

A cast-in-place concrete box culvert, overlain with about 12 meters of backfill, was instrumented to measure the vertical and horizontal earth pressures during both the construction and the service life. To reduce the pressures on the culvert, compaction equipment was prohibited from working within 2 meters of the culvert. This resulted in a zone of low density material around the culvert. To evaluate the effects of this low density material on the vertical and lateral earth pressures, a series of finite element analyses was conducted. The results from a standard analysis based on the actual as-built material properties produced horizontal and vertical pressure distributions that compared well with the measured pressures. Both the measured and predicted vertical pressures were 1.5 to 1.8 times those obtained from the AASHTO recommended pressures, but the horizontal pressures were 0.7 times the AASHTO pressures. A parametric study of the effect of backfill compaction, as manifested in backfill modulus, found that the vertical pressures were not significantly affected by compaction. However, the distribution of lateral pressure was significantly affected, with high density backfill resulting in larger pressures at the bottom of the wall.

#### **7.2 Introduction**



Cast-in-place concrete box culverts are often used as conduits for water from one side of a highway embankment to another. Although this is a rather simple role, the loadings applied to these structures during construction and the subsequent service life can be complex. These structures must resist substantial vertical and lateral earth pressures, and are often subject to significant loadings during construction of the embankment. Due to soil-structure interaction effects, the state of stress around the structure depends upon the stiffness of both the backfill material and the structure. In spite of the complex state of stress around these structures, simple routine design procedures must be used for these structures due to the large number that are placed in service.

While there has been much investigation on flexible metal and circular concrete culverts (Davis and Bacher, 1972; Selig et al. 1982; Duncan and Seed, 1986), limited research has been conducted on concrete box culverts. Circular concrete or metal culverts experience more significant soil arching effects than box culverts, and the soil pressure on the sides tends to provide lateral support. In addition, metal and concrete circular culverts are normally more flexible than concrete box culverts. The results from investigations of circular culverts are of limited value for the study of rigid concrete box culverts.

Spangler and Handy (1982) provide a good discussion of the loads on buried conduits. They suggest an alternative to the normal compaction backfill method, known as the imperfect trench technique. In the imperfect trench technique, an extremely compressible material is placed immediately above the culvert to some height and

covered with normally compacted fill. This installation method creates soil arching effects and directs the vertical loading away from the culvert and on to the side soil. Although this may result in large settlement in the area above the culvert and is not appropriate when strict settlement control is required, the loads on the culvert are often reduced.

The Kentucky Department of Transportation constructed and instrumented three single cell culverts in 1974 (Tadros, 1986). The culverts were constructed with normal compaction methods (without imperfect trench conditions), and with overburden thickness ranging from 9 to 24 meters. Measured soil pressures on the top of the culverts were 1.5 to 2 times the pressure due to the soil column above, and the pressure increased about 25% more during the 2000 days after fill completion. The lateral pressure records remained constant after construction. Penman et al. (1975) recorded the vertical pressures in the soil surrounding a rigid concrete culvert under 53 m of rock fill, and found the pressure was about two times that due to the column of overburden directly above it. Penman et al. (1975) obtained good predictions of vertical stress above the culvert, using an elastic soil model with the elastic soil modulus determined by a large scale, one dimensional compression test. Similar findings were reported from a large-scale model test on a square box culvert (1.2×1.2 m inner dimensions) embedded in a 7 m wide, 10 m long and 7 m deep sand trough (Dasgupta and Sengupta, 1991). They showed that the soil pressure distribution on the top of the box and the sides differed significantly from the uniform fluid pressure assumption often used in design. Greater than  $K_0$  state lateral pressures were recorded in field tests done by Tadros et al. (1989) on a double cell cast-

in-place concrete box culvert with 3.35×3.5 m inner dimension with 3.5 meters silty clay backfill, and in a single cell culvert reported by James et al. (1986) with 2.4×2.4 m inner dimension with 2.4 meters of clay backfill.

In the present study, a cast-in-place concrete box culvert was placed in service under about 12 meters of backfill. To reduce the earth pressures on the culvert, low compactive effort was used on the gravel and soil within about 2 m of the culvert. The structure was instrumented to measure earth pressures, both during the construction and during the service life. In this paper, the measured response is compared with that predicted from finite element analysis, which considered the soil-concrete interface response and staged construction. The effect of the low density backfill was investigated through a parametric study in which the backfill modulus was varied.

### **7.3 Culvert and Site Description**

The instrumented culvert was a double-cell, cast-in-place reinforced concrete structure, located in northeast Tennessee. The culvert was 150 m long and was oriented at about a 60° skew angle with respect to the alignment of the highway. The subsurface investigation showed that the bottom slab of the culvert was supported by about 3 m of firm shaley clay, and underneath the clay layer was 2.1 m of very firm weathered shale over hard fresh shale. Limestone gravel was used to surround the culvert with a thickness of 2 m on the side and 0.6 m at the top of the culvert. Above the gravel, the backfill consisted of clayey weathered shale from a nearby cut slope. The weathered shale material contained particles with diameters over 500 mm, but most particles were smaller than 100 mm. The clay size material had a liquid limit of 35 and a plastic limit of 24.

Each cell of the culvert was 2.13 m in height and 4.13 m in width, with 0.76 m thick top and bottom slabs and 0.61 m thick side walls. To avoid excessive lateral pressures during construction, compaction equipment was not used to compact the fill within 2 m of the culvert, and the thickness of each loose lift of the clayey shale backfill material was maintained at 300 to 400 mm. This was expected to minimize the lateral earth pressure by achieving a lower degree of compaction, and can be considered to reflect the imperfect trench condition as described by Spangler and Handy (1982).

The instrumentation consisted of pressure cells on the concrete structure surface. The general instrumentation scheme is illustrated in Figure 7-1. Only one cell of the culvert was instrumented assuming the loading and the response was symmetrical about

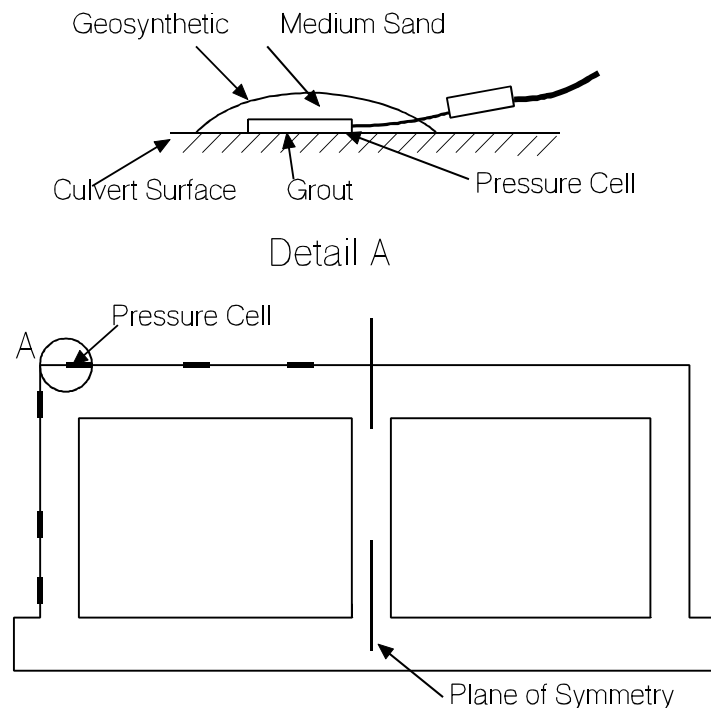


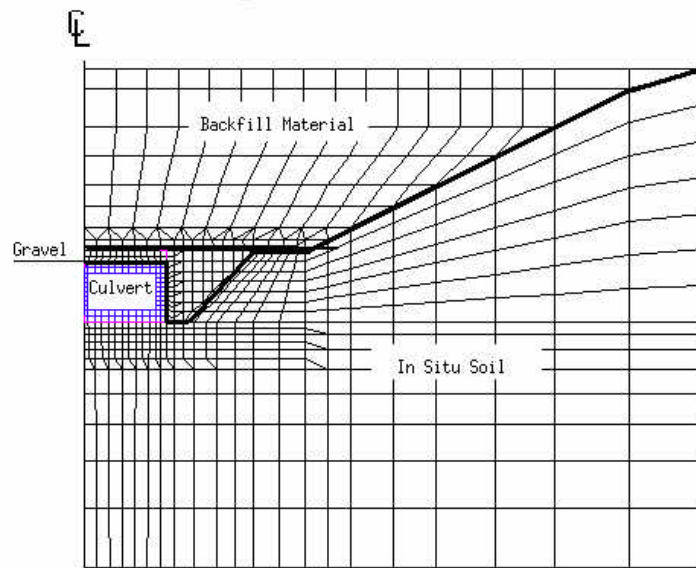
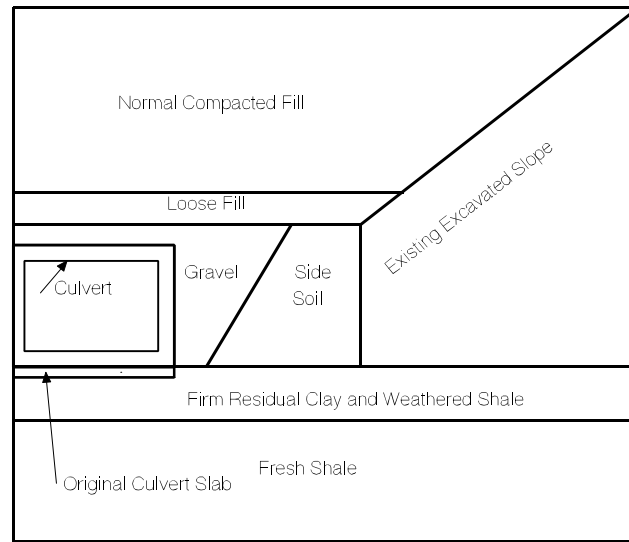
Figure 7-1 Schematic of Culvert and Pressure Cell Detail

the culvert centerline. The instrumented culvert section was located under the edge of the full embankment height (11.74 m).

Six identical Geokon 4810 vibrating wire pressure cells with 180 kPa capacity were placed around one cell of the structure, three on the top and three on the side. These cells are designed for measuring earth pressures on structures. The cell consists of two plates, where one of them is thick and designed to bear against the external surface of the structure in a way that will prevent flexure of the cell, and the other is thin and reacts to the soil pressure. To minimize the arching around the cells, medium sand was placed around the pressure cells and then covered by a layer of geosynthetic fabric. Arching around pressure cells is assumed to be the primary factor of recording errors (Dunnicliff, 1988). The vibrating wire transducers were chosen because of their excellent long term stability (McRae and Simmonds, 1991).

#### **7.4 Finite Element Model**

The general purpose commercial finite element code ABAQUS Version 5.5 (Hibbitt, Karlsson & Sorensen, Inc. 1995) was used to model the behavior of the culvert under the backfill loads. Figure 7-2 shows a schematic of the culvert with the various backfill materials, and the plane strain linear element mesh that was utilized to analyze the section. Advantage was taken of the symmetry of the culvert and loading. The new culvert was constructed directly on the 0.32 m thick bottom slab of a previous culvert. The concrete, and the underlying firm clay and shale were represented in the model by linear elastic models.



Finite Element Meshes for the Box Culvert Project  
(Sullivan County, current culvert)

Figure 7-2 Schematic of Backfill Conditions  
and Finite Element Mesh

A non-associative Drucker-Prager elasto-plastic model with linear yield criteria was chosen for the gravel surrounding the culvert, the backfill material, and the existing excavated slope. The interface between the structure and the surrounding was represented by contact pair surfaces (Hibbit, Karlsson & Sorensen, Inc. 1995), which allow sliding and loss of contact during the loading. The tangent friction angle of the concrete-gravel interface was assumed to be two thirds the tangent of the friction angle of the gravel.

The modulus of concrete was obtained from lab tests on 15 cm  $\times$  30 cm cylinders. Since the elastic modulus of soil is dependent on the void ratio (Hicher, 1996), it is therefore dependent on the relative density and the compactive effort. Thus a change in degree of compaction in the backfill zone was assumed to be represented by a variation of elastic modulus in the analysis.

The modulus of the back fill material was estimated based on in-situ density tests performed on the fill by the sand replacement method (ASTM D 4914-89), and published results from large scale oedometer tests (1 m in diameter and 0.5 m in height) of material with similar grain size and distribution (Penman et al. 1975). It was assumed that the modulus of the crushed lime stone gravel was equal to that of the backfill, although it would typically be greater than that of the clayey shale backfill. Since the heavy compactor was not permitted near the culvert, a lower elastic modulus was assumed to simulate the reduced compactive effort. For the same reason, a lower elastic modulus and strength was used for the side backfill soil near the culvert, and the dilatancy angle,  $\psi$ , was reduced. The resulting material properties represent the best estimate of actual field conditions, and are termed “Standard” analysis in this paper. The material properties are

Table 7-1 Summary of Material Parameters, Standard Analysis

Material Description Figure 2	Cohesion c (kPa)	Friction Angle $\phi$ (deg)	Dilatancy Angle $\psi$ (deg)	Elastic Modulus E (kPa)	Poisson's Ratio $\mu$	Source and Reference
Gravel	33	38.5	20	1.58E4	0.27	Shear strength from Law Engineering (1990), modulus from Penman (1975)
Side soil near gravel and existing excavated slope	32	20	15	1.58E4	0.32	Measured shear strength modulus from Penman (1975)
Loose fill above culvert	25	17	0	6.5E3	0.32	Estimated shear strength Poisson's ratio from Bowles(1988).
Normal fill away from culvert	32	20	15	1.58E4	0.32	Measured shear strength from TDOT (1995), modulus from Penman (1975)
Firm residual clay and weathered shale	NA			6.5E4	0.30	Bowles(1988)
Fresh shale	NA			1.12E6	0.25	Goodman(1989)
Concrete	NA			4.06E7	0.18	Modulus from lab test

summarized in Table 7-1.

After the initial stresses in the excavated slope and weathered shaled were computed, an incremental analysis technique was used to represent the sequential embankment construction. Each layer involved the addition of extra elements to the mesh, and the gravity load was assigned to the new elements. A total of eight incremental steps were applied to simulate the full backfill height. This is consistent with the recommendations by Duncan (1996), where six to ten increments were suggested as adequate to achieve reasonable accuracy.

## 7.5 Results

The recorded pressures on the top and the side of the culvert at different back filling heights are compared with the results from the Standard analysis in Figure 7-3. The



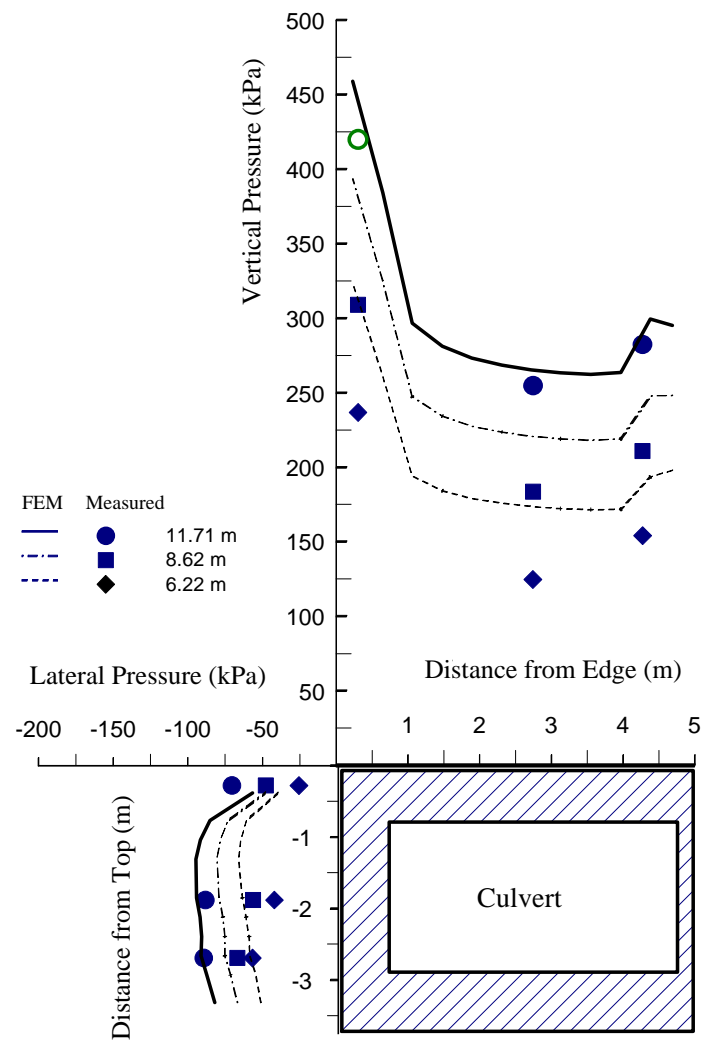


Figure 7-3 Comparison of Recorded and Predicted Pressure during Back Filling

pressure cell near the edge of the culvert roof failed when the pressure exceeded twice the working pressure of 180 kPa. Therefore the final pressure at this location was estimated based on the pressure increases at the other two locations and is shown by the open circle in Figure 7-3. The incremental analysis provided a reasonable reproduction of the measured pressures as a function of back fill height. Both the measured and predicted stress were larger over the walls of the culvert than over the center. This is consistent with the results by James et al. (1986) and Tadros et al. (1989) for culverts with lower backfill height, and also with the large-scale test results reported by Dasgupta and Sengupta (1991). The maximum recorded and predicted vertical pressures are on the outside corner of the roof where the structure has the largest stiffness. These pressures correspond to 1.5-1.8 times the stress due to the overburden soil column.

It is also possible to compare the recorded and the predicted results with the current design loads recommended by the American Association of State Highway and Transportation Officials (AASHTO, 1992). The AASHTO recommended pressure is based on an equivalent fluid pressure, with a unit weight of 18.84 kN/m<sup>3</sup> for vertical pressure and 11.3 kN/m<sup>3</sup> for lateral pressure. The AASHTO loadings are compared with the results from the Standard analysis in Figure 7-4. These AASHTO vertical pressures can be corrected for soil-structure interaction effects by the Marston-Spangler theory (Spangler and Handy, 1982) using the soil-structure interaction factor  $F_{e1}$ :

$$F_{e1}=1+0.20(H/B_c) \quad (1)$$

where the  $B_c$  is the width of the culvert and  $H$  is the overburden height on top of the culvert. The recommended value for the correction factor  $F_{e1}$  is less than 1.15 for

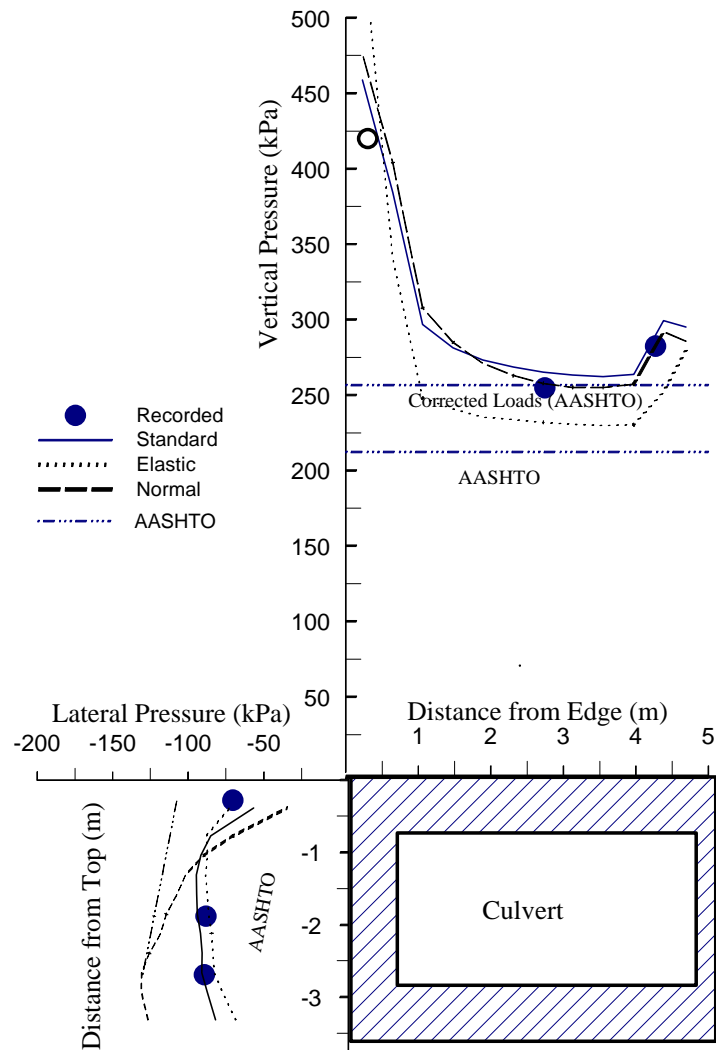


Figure 7-4 Comparison of Various Models with Recorded Results at Full Backfill Height

installations with compacted fill at the sides of the box section, and less than 1.4 for installations with uncompacted fill at the sides of the box section. For the culvert in this study  $F_{el} = 1.20$ , and the resulting pressure is shown as the corrected AASHTO pressure in Figure 7-4. For the culvert investigated here, both the AASHTO and corrected AASHTO design pressures underestimated the vertical pressures, but overestimated the lateral pressure.

A parametric study was conducted to investigate the influence of modeling assumptions and the effect of decreased compactive effort on the predicted soil pressures. For purposes of comparison, the models and properties described above are considered the “Standard” analysis. An “Elastic” analysis was performed, in which only linear elastic material models were used, and all materials had the same elastic modulus as in the Standard analysis. A “Normal Compaction” analysis was also performed, which was identical to the “Standard” except the modulus for the loose backfill and the gravel was increased to  $E = 1.58E4$  kPa, and  $E = 3.2E4$  kPa, respectively. It was found that the yielding occurred only in the gravel layer near the edge of the culvert roof with the full backfill height of about 12 m. This explains the difference in the normal contact pressures obtained by the elastic analysis and the plastic analysis. The results for the final backfill height are compared with the measurements in Figure 7-4.

Figure 7-4 suggests that for the culvert and backfill properties investigated, the level of compaction adjacent to the culvert had little effect on the vertical pressures. Neglecting the yielding in the gravel (Elastic analysis) over the culvert walls resulted in lower predicted vertical stress, but had little effect on the horizontal stresses. The lateral

pressure, however, was dramatically influenced by the modulus or level of compaction of the fill material near the side walls. A higher level of compaction resulted in greater pressure at the bottom of the culvert wall.

An additional parametric study was performed to determine the effect of large variations in the modulus on the lateral pressures. The modulus of the gravel and the side soil was varied as shown in Table 7-2 from the 1.58E4 KPa value used in the “Standard” analysis, and the results are shown in Figure 7-5. High modulus backfill materials result in very large pressures near the bottom of the culvert wall. This can have significant impact on the shear forces and bending moments that the culvert must resist. The results of the analysis suggest that although the resultant force due to the lateral pressure may not vary much with compaction effort, the distribution or location of the resultant may change significantly.

Table 7-2 Parametric Variation of Elastic Modulus of Gravel and Side Soil

Name of Analysis	Modulus of Gravel	Modulus of Side Soil
Dense gravel	2.5 times the 1.58E4 kPa	1.58E4 kPa
Very Dense gravel	5 times the 1.58E4 kPa	1.58E4 kPa
Loose Side Soil	1.58E4 kPa	0.5 times the 1.58E4 kPa
Dense Side Soil	1.58E4 kPa	2 times the 1.58E4 kPa

## 7.6 Conclusions

The horizontal and vertical pressures obtained from the “Standard” finite Element analysis were consistent with the recorded data. The AASHTO (1992) recommendations under-estimate the vertical pressure at the corner of the culvert roof, where the structure has the larger stiffness. In this area of the culvert, both recorded and predicted pressures

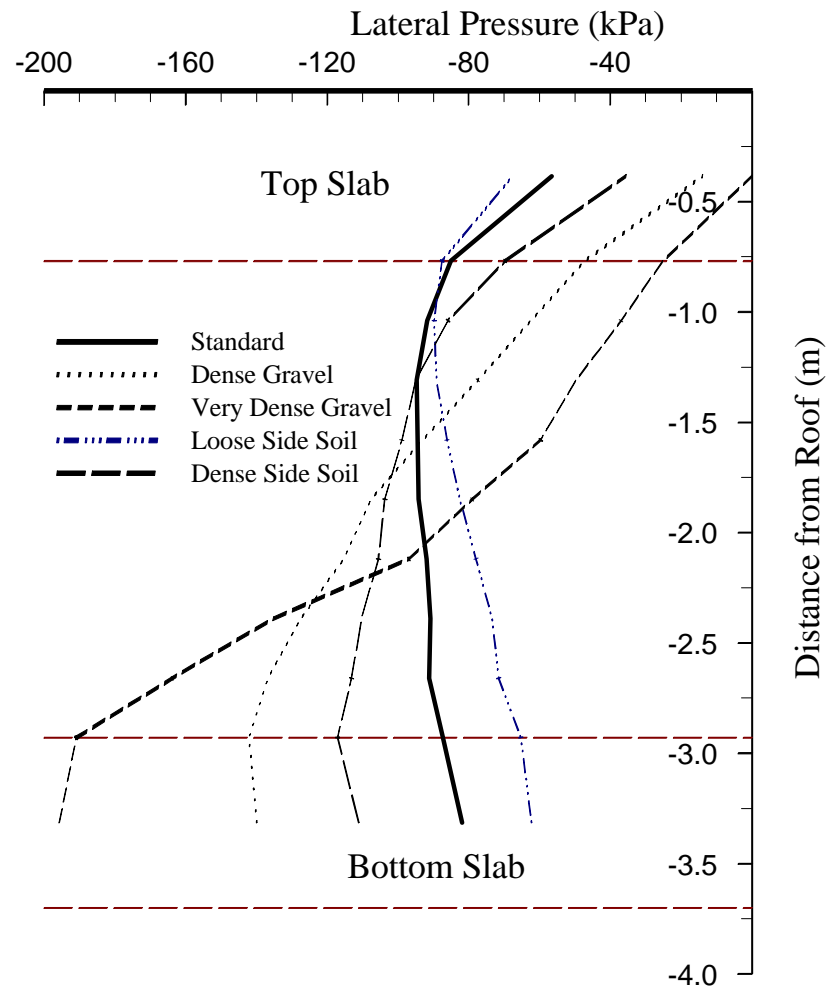


Figure 7-5 The Influence of Gravel and Side Soil Modulus on the Distribution of Lateral Earth Pressure

are 1.5 to 1.8 times higher than the AASHTO design value. This is consistent with the published results reported by others. On the other hand, the calculated and predicted lateral earth pressures on the wall of the culvert were 0.7 times that obtained from the straight line fluid pressure distribution assumption suggested by AASHTO (1992).

The results of a parametric study to investigate the effects of backfill modulus or compactive effort suggest that the vertical earth pressures are not significantly affected by placing low density (modulus) backfill around the culvert. However, the lateral pressure distribution is affected by backfill modulus, with very high modulus values resulting in large pressures at the bottom of the wall.

## **7.7 Acknowledgments**

This investigation was supported by the Tennessee Department of Transportation, contract #CUT123RES1085. This support, and the input from Billy R. Burke, Structures Division, and William D. Trolinger, Division of Materials and Tests, is appreciated.

## **7.8 References**

- Bowles, J. E. (1988). *Foundation Analysis And Design*. McGraw-Hill, New York.
- Dasgupta, A. and Sengupta, B. (1991). "Large-scale model test on square box culvert backfilled with sand." *J. Geotech. Engrg. Div.*, ASCE, 117(1), 156-161.
- Davis, R. E. and Bacher, R. C. (1972). "Concrete arch culvert behavior-phase 2." *J. Soil Mech. Founda. Div.* ASCE, 98(11), 2329-2350.
- Duncan, J. M. (1996). "State of the art, limit equilibrium and finite-element analysis of slopes." *J. Geotech. Engrg. Div.*, ASCE, 122(7), 577-596.
- Dunnicliff, J. (1988). *Geotechnical instrumentation for monitoring field performance*. John Wiley and Sons, New York.
- Goodman, R. E. (1989). *Introduction to Rock Mechanics*. John Wiley and Sons, New York.
- Hibbitt, Karlsson & Sorensen, Inc. (1995) *ABAQUS/Standard User's Manual*. Vol. 1, Vol. 2. Ver. 5.5.
- Hicher, P. Y. (1996). "Elastic properties of soils." *J. Geotech. Engrg. Div.*, ASCE, 122(8), 641-648.

- James, R. W., Brown, D. E., Bartoskewitz, R. E. and Cole, H. M. (1986). "Earth pressures on reinforced concrete box culvert" *Research Report 294-2F*, Texas Trans. Ins., The Texas A&M Univ. Sys. College Station.
- Law Engineering (1990) *Report Triaxial Tests on #57 Stone*, Knoxville, TN.
- McRae, J. B. and Simmonds, T. (1991). "Long-term stability of vibrating wire instruments: one manufacturer's perspective." *Field Measurements in Geomechanics*, Balkema, Rotterdam. 283-293.
- Penman, A. D. M., Charles, J. A., Nash, J. K. and Humphreys, J. D. (1975). "Performance of culvert under Winscar Dam." *Geotechnique*, 25(4), 713-730.
- Selig, E. T., McVay, M. C. and C. S. Chang. (1982) "Finite element modeling of buried concrete pipe installations." *Trans. Res. Record* 878, 17-23.
- Spangler, M. G. and Handy, R. L. (1982). *Soil Engineering*. 4th edition, Harper & Row, New York.
- Standard specifications for highway bridges*. (1992). 15th Ed., The American Association of State Highway and Transp. Officials (AASHTO), Washington, D. C.
- Tadros, M. K. (1986). "Cost-effective concrete box culvert design." *Project No. HRP83-3*, Engineering Research Center, Univ. Nebraska, Lincoln.
- Tadros, M. K., Benak, J. V., Abdel-Karim, A. M. and Bexten, K. A. (1989). "Field testing of a concrete box culvert." *Trans. Res. Record* 1231, 49-55.
- TDOT. (1995). "*Intenal report: shear strength of Sullivan County culvert backfill material*"



**PART III**  
**FIELD MEASUREMENT OF STATIC EARTH PRESSURES**  
**ON BOX CULVERT**

This part is a paper published in the proceedings of the ASTM symposium on field instrumentations for soil and rocks, Atlanta, Georgia, May, 1998

Authors: Michael Zhiqiang Yang, Eric C. Drumm, Richard M. Bennett and Matthew Mauldon.

The data collected after the preparation of this paper are updated and attached at the end of this part.

## **Chapter 8**

### **Measurement of Earth Pressures on Concrete Box Culverts under Highway Embankments**

#### **8.1 Abstract**

To obtain a better understanding of the stresses acting on cast-in-place concrete box culverts, and to investigate the conditions which resulted in a culvert failure under about 12 meters of backfill, two sections of a new culvert were instrumented. The measured earth pressure distribution was found to depend upon the height of the embankment over the culvert. For low embankment heights (less than one-half the culvert width), the average measured vertical earth pressures, weighted by tributary length, were about 30% greater than the recommended AASHTO pressures. The measured lateral pressures were slightly greater than the AASHTO pressures. As the embankment height increased, the measured weighted average vertical stress exceeded the AASHTO pressures by about 20%. Lateral pressures which exceeded the vertical pressures were recorded at the bottom of the culvert walls, and small lateral pressures were recorded on the upper locations of the wall. The high lateral pressures at the base of the wall are consistent with the results from finite element analyses with high density (modulus) backfill material placed around the culvert.

#### **8.2 Introduction**

Cast-in-place concrete box culverts are commonly incorporated into highway

embankments. To simplify the design of these structures, the earth pressures are usually taken as a function of the equivalent fluid stress due to the overburden. Although the structural response may depend upon the stress level, there is no distinction made between low overburden heights and high overburden heights. The actual loadings experienced by the structures can be complex, and may change during construction and the subsequent service life. Soil-structure interaction effects result in a state of stress around the structure that is dependent upon the stiffness of both the backfill materials and the structure.

Small size circular culverts have been instrumented and studied over the past 60 years (Davis and Bacher, 1968; Corotis and Krizek, 1977; Davis and Semans, 1982). Because circular culverts have equal rigidity and strength in the horizontal and vertical directions, culvert installation methods were developed to reduce the vertical pressures acting on the culvert. These methods divert the vertical stresses from the culvert to the adjacent soil and result in an increase of the lateral pressures on the culvert sides (Spangler and Handy, 1982; Vaslestad, et al., 1994). For culverts built on level ground, the “imperfect trench” (Spangler and Handy, 1982) condition installation method may be used. This method involves spreading a specified thickness of compressible material such as baled straw or plastic foam immediately above the culvert followed by compaction with normal backfill reducing the vertical earth pressures acting on the culverts. A comparison between this method and normal compaction on two instrumented (2.0 m height and 2.55 m width) concrete box culverts under a 10 m silty clay embankment height showed that the imperfect trench method resulted in a significant vertical load

reduction (Vaslestad et al. 1994). The earth pressure immediately above the box culvert installed with the imperfect trench condition was 62% of the pressure due to the weight of the soil column above the culvert. The earth pressure on the culvert roof under normally compacted backfill was 125% of pressure due to the soil weight. However, field measurements (Yang et al., 1997) of pressures on an instrumented double cell concrete box culvert (3.66 m in height and 9.91 m in width) under about 12 m backfill height, indicated that the vertical earth pressure was not reduced by placing 2 m loose fill soil around the culvert roof. The average measured vertical pressure was 124% of the soil prism pressure (actual backfill unit weight of  $22 \text{ kN/m}^3$ ) above the culvert and 145% of the current AASHTO recommended pressure (recommended unit weight of  $18 \text{ kN/m}^3$ ). Furthermore, the induced differential settlement due to the loose fill may cause damage to the pavement at the top of the embankment.

Field test data on box culverts with normally compacted backfill are limited. The reported instrumented culverts have been either small size culverts with a width less than 3 m (Russ, 1975; James et al., 1986; Vaslestad et al., 1994) or large size culverts with relatively low backfill heights (Tadros et al., 1989). The suitability of the current AASHTO recommended design pressures for these culverts was examined by monitoring the pressures on an instrumented culvert throughout the backfilling process.

### **8.3 Instrumentation Description**

The instrumented box culvert was 99 m long and 3.9 m high by 7.0 m wide. It was a double cell culvert, constructed of cast-in-place reinforced concrete. Typically, the top and bottom slabs were 0.78 m thick and the side walls were 0.41 m thick, although the

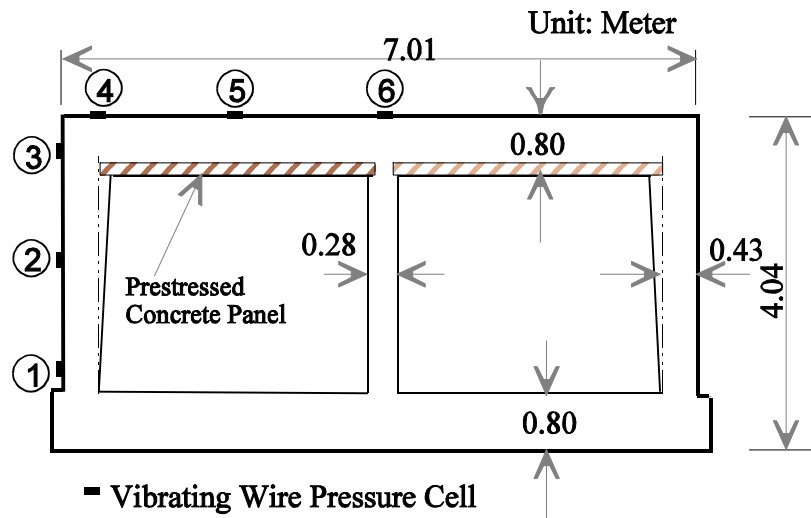


Figure 8-1 Illustration of Culvert Dimensions and Pressure Cell Location

dimensions varied along the length of the culvert with the change of the overburden embankment height. The culvert's typical dimensions under the full embankment height are illustrated in Figure 8-1. The culvert was constructed on relatively level ground at the bottom of a broad valley. The site soil was a soft silty residual clay with shallow outcrops of limestone rock. About 0.6 m of well graded crushed gravel was spread immediately below the culvert in order to level the foundation and adjust for the variable thickness of the bottom slab along the length. Well graded crushed stone was backfilled to a height of 0.6 m above the culvert roof to provide drained conditions for the culvert, then the culvert was backfilled with silty clay, and high plasticity clay with occasional limestone boulders of 0.35m or smaller diameter.

To monitor the earth pressures during the construction, 12 vibrating wire hydraulic type soil contact pressure cells were installed in two separate sections. Upon completion of the embankment, section A would be under about 19 meters of fill, and section B

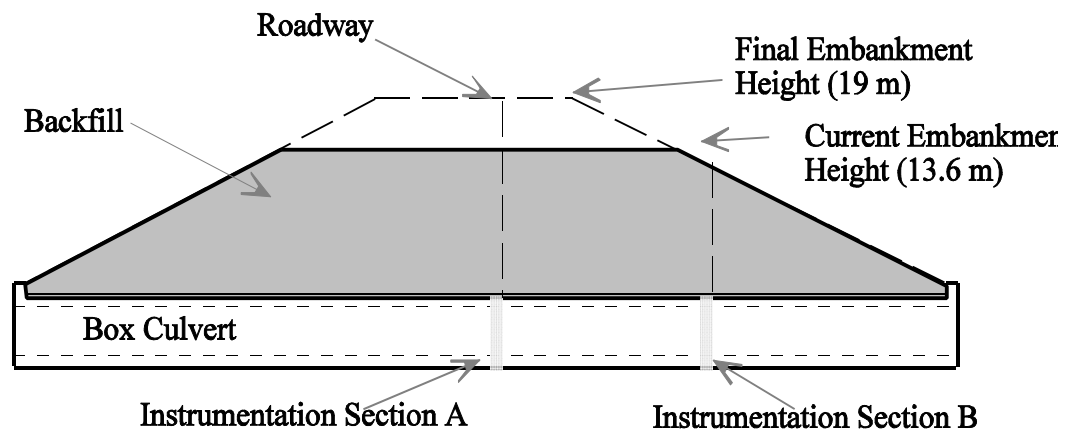


Figure 8-2 Schematic of Embankment and Culvert Cross-Section with Typical Sections A and B

would be under 11.7 meters. The relative locations of instrumented sections are shown in Figure 8-2. The slope of the embankment was 1:2. Each instrumented section consisted of 6 pressure cells with 3 cells mounted on the surface of the culvert wall and 3 on the roof. The location and pressure gage numbering scheme are shown in Figure 8-1. The pressure cell (Geokon model 4810) consists of two 230 mm diameter circular plates welded together around their periphery. One of the plates is thicker and designed to bear against the external surface of the structure in order to prevent flexure of the cell. The total thickness of the cell is 6 mm, and the aspect ratio (cell diameter over plate thickness) is 38. This “intermediate” cell size is appropriate for the measurement of soil pressure as suggested by Weller and Kulhawy (1982). Two different cell capacities were chosen: 345 kPa on the roof and 172 kPa on the culvert wall. The cells are capable of operating at up to twice the rated capacity, but the accuracy decreases.

The cell was first fixed to the culvert wall and roof with concrete anchors through 4 mounting lugs around the edge of the plate, and a quick setting high strength grout pad

was used to assure uniform contact between the plate and concrete. Medium sand was used to cover the cell and transducer housing to protect the cell from possible point loads or other stress distortions induced by the large size particles in the crushed gravel. A geosynthetic cover was attached to the concrete with adhesive to separate the gravel and the sand. This installation is illustrated in Figure 8-3. The backfill was placed with conventional compaction control criteria, with the dry density greater than 95% maximum dry density determined by standard Proctor compaction. The unit weight of the backfill gravel was measured in-situ by the sand replacement method (ASTM D 4914-89) and the average was found to be  $22.0 \text{ kN/m}^3$ . The unit weights of the silty clay and high plasticity clay were determined by the drive tube method and the average value for both materials was determined to be about  $18.0 \text{ kN/m}^3$ .

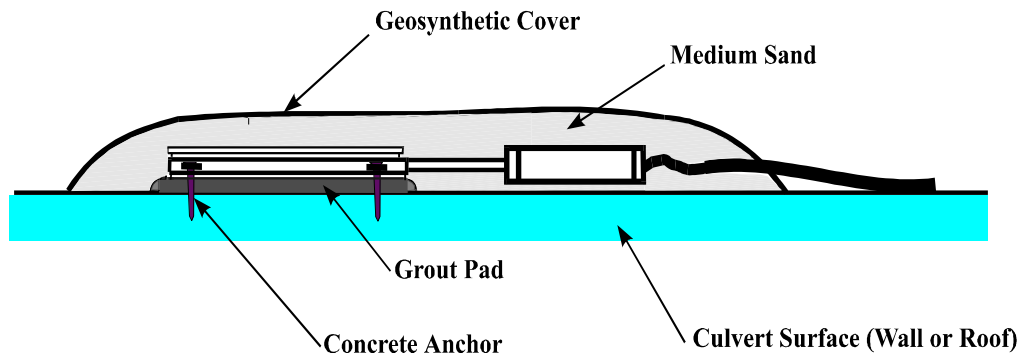


Figure 8-3 Installation of Contact Pressure Cell on the Culvert

#### 8. 4 Measured Vertical Stresses on the Roof

The pressure changes during placement of the first 13.6 meters of backfill on the culvert roof were recorded with respect to the backfill height. The recorded vertical pressures and the surveyed backfill height above the cell are shown in Figure 8-4. The

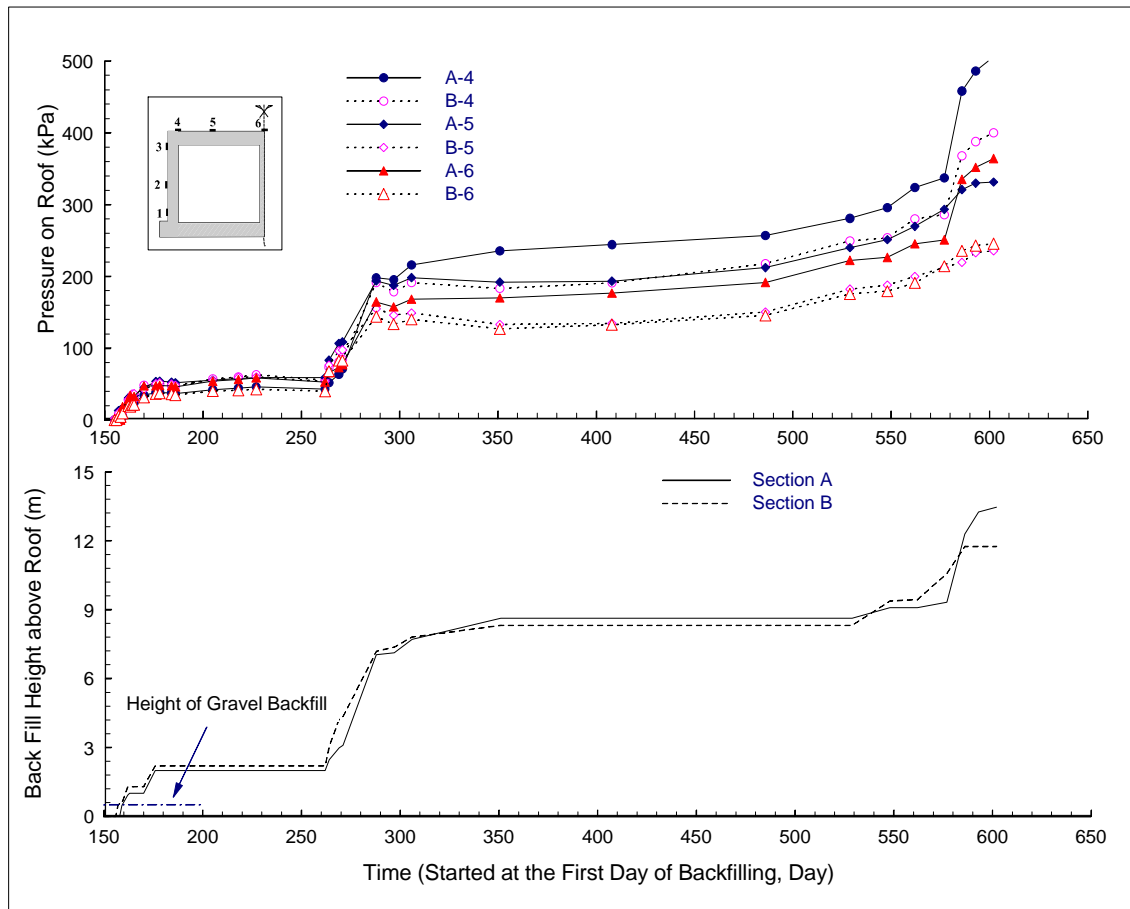


Figure 8-4 Recorded Vertical Pressures on the Culvert Roof  
with Backfill Height above Roof  
(Greene County, TN)



data were collected over about 600 days (20 months), during which there were two periods of about 3 months each when no construction took place. Figure 8-4 indicates that the variation in backfill height in both instrumentation sections A and B are similar until about day 580, when section B (under the slope) reached the final embankment height. Up to about 2 m backfill depth, the recorded pressures are similar in sections A and B, and the measured pressures were nearly uniform across the roof. When the backfill height reached about 6 meters, the pressures were found to vary significantly across the roof. The highest recorded pressures were on the culvert corner (gage 4), which corresponds to the location of greatest structural stiffness. This is consistent with results from previous instrumented culverts (Tadros et al., 1989; Yang et al., 1997). The large deviation of vertical pressures may reflect the influence of soil-structure interaction effects, which become more significant as the structural deflections increase with increasing embankment height. At backfill heights greater than about 6 m, the vertical pressures measured at section B are less than those at section A. This is likely a result of the position of section B close to the embankment slope.

### **8. 5 Measured Horizontal Stresses on the Walls**

The recorded lateral pressures on the culvert wall (Figure 8-5 and Figure 8-6) show an increase with backfill height similar to the vertical pressures on the roof. However, the cells at the bottom of the wall (Figure 8-6) registered pressures exceeding the vertical pressures, whereas the upper cells recorded relatively low lateral pressure. The influence of compaction equipment on the lateral pressure can be identified as the recorded stress peaks in Figure 8-5 during the 155-170th day, corresponding to the time when the gravel

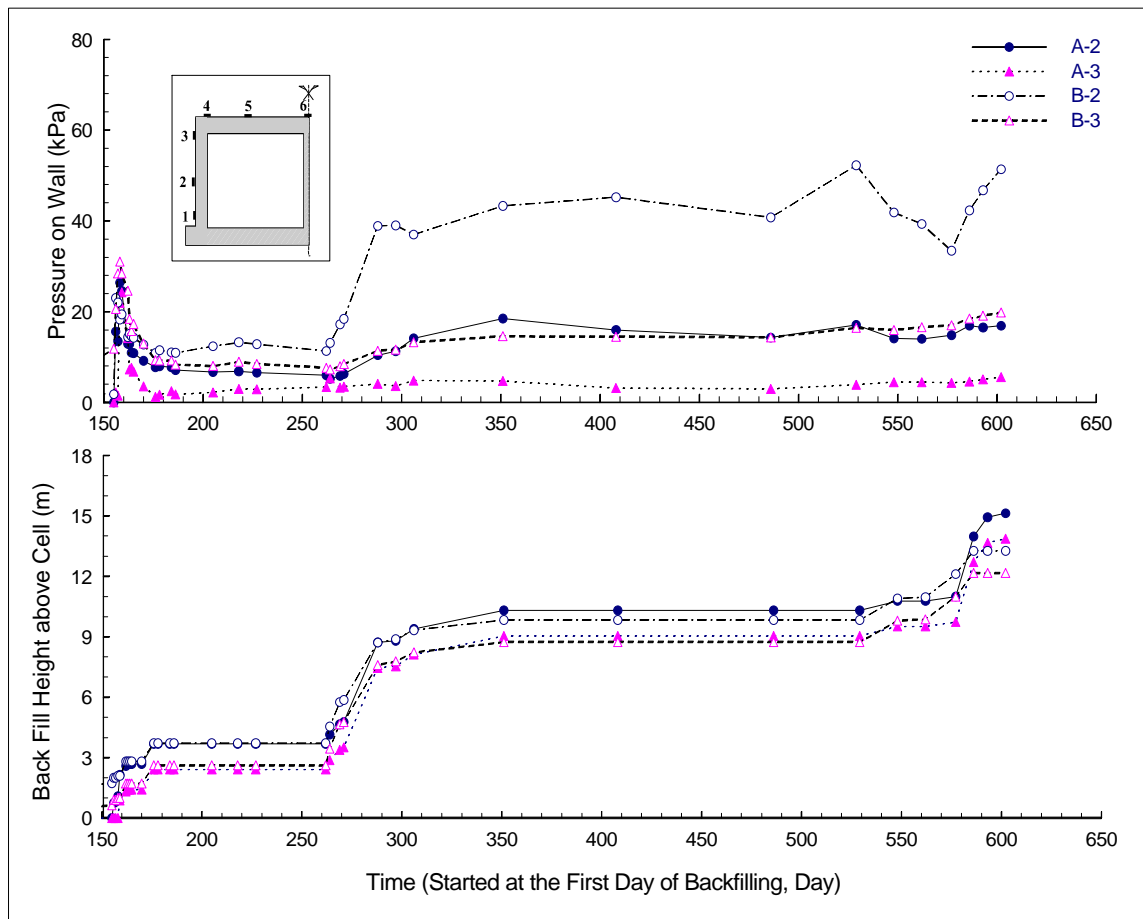


Figure 8-5 Recorded Lateral Pressures on the Culvert Wall  
with Backfill Height above Cells  
(Greene County, TN)

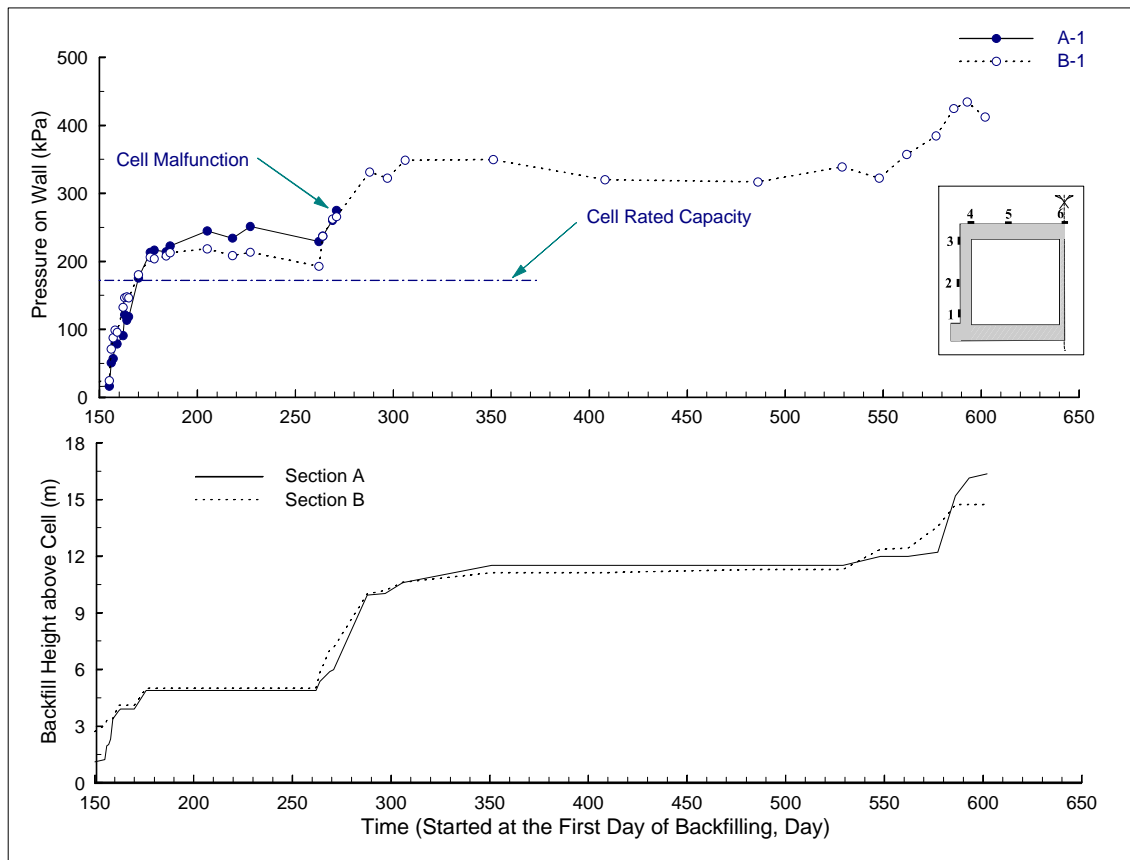


Figure 8-6 Recorded Lateral Pressures at Bottom of Wall  
with Backfill above the Cells  
(Greene County, TN)

was placed around the culvert. This is followed by a period of stress relaxation with residual stresses differing at sections A and B. This relaxation does not appear to occur in the lower portion of the wall (Figure 8-6), where the overburden stress is greater. The added lateral pressure contributed by the additional thickness of overburden is negligible with respect to the short term increase caused by compaction. As the backfill height was increased above the culvert roof (about day 155), the upper cells in both sections recorded a decrease in lateral pressure, whereas the pressure cell reading at the bottom of the wall kept increasing and exceeded the vertical pressure. The high horizontal pressures were observed at both section A and section B, and were larger than the manufacturer's rated capacity for the pressure cells.

## 8.6 Discussion

### 8.6.1 Comparison of Measurements with AASHTO Recommended Vertical Pressure

The instrumentation results were compared with the AASHTO (1996) recommended design pressures. The AASHTO recommended pressure is an equivalent uniform fluid pressure that will give approximately the same internal forces (moments and shears) that are generated by the actual pressure distribution. The AASHTO vertical pressure for the embankment condition is the embankment height times an assumed unit weight of  $18.8 \text{ kN/m}^3$ . To account for soil-structure interaction effects, AASHTO suggests that this pressure be increased by a dimensionless correction factor or soil-structure interaction coefficient,  $F_{el}$

$$F_{el} = 1 + 0.20 \frac{H}{B} \leq F_{el, \max} \quad \text{where} \quad F_{el, \max} = \begin{cases} 1.15 & \text{for well - compacted side soil} \\ 1.40 & \text{for uncompacted side soil} \end{cases} \quad (1)$$

and  $H$  is the embankment height above the box culvert and  $B$  is the width of the box culvert. For well-compacted fills at the sides of the culvert,  $F_{el}$  should not be taken greater than 1.15, and for uncompacted fills at the sides of the culvert, it should not be exceed 1.40.

The AASHTO recommended vertical pressure  $s_v$  used in design is then:

$$s_v = F_{el} gH \quad (2)$$

The AASHTO soil-structure interaction coefficient (Equation 1) increases linearly with backfill height,  $H$ . For the current instrumented culvert ( $B = 7$  m) with well-compacted fill, the limiting value of 1.15 is reached at a backfill height of 5.3 m.

The results presented in Figure 8-4 suggest that the vertical pressure distribution on the roof is not uniform and thus cannot directly be compared to AASHTO design pressures. An equivalent uniform pressure can be calculated by assigning a tributary length to each cell and obtaining a weighted average. Based on the predicted distribution of vertical pressure from a finite element analysis, a tributary length was assigned to each pressure cell and the equivalent uniform pressure determined. The tributary width for cells 4 and 6 at the culvert corner and at the centerline was taken as  $0.2b$  and tributary width at cell 5 in the middle of the span was  $0.6b$ , where  $b$  is the span of one cell. Figure 8-7 compares the weighted average vertical pressures with both the uncorrected ( $F_{el}=1$ ) and the corrected AASHTO pressures. The weighted average vertical earth pressures were generally greater than the AASHTO design pressures, even at the lower backfill heights ( $H/B < 0.5$ ). Figure 8-7 shows that the soil pressure recommended by AASHTO is less than the tributary-weighted average pressure observed at the site.

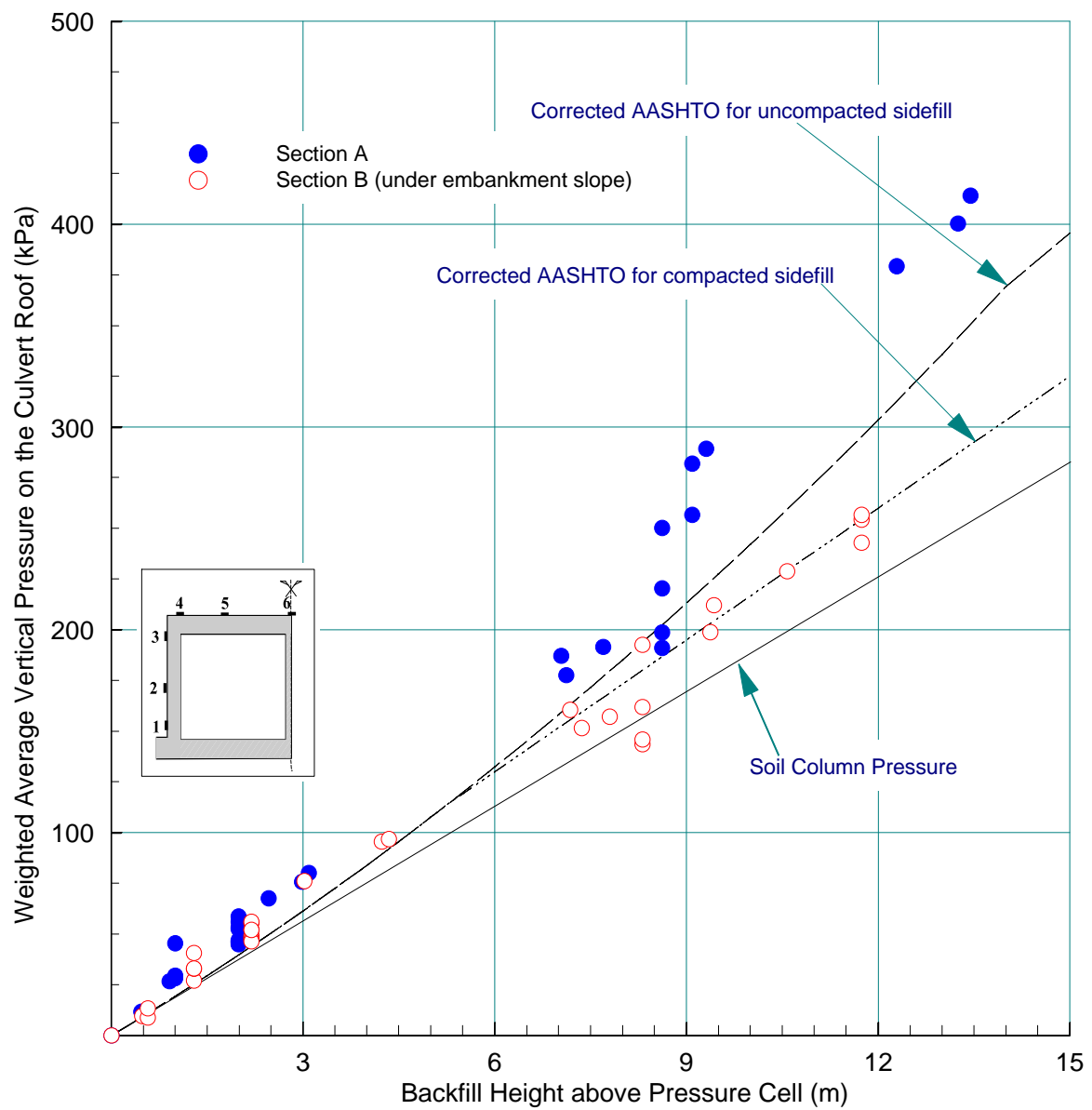


Figure 8-7 Weighted Average of Recorded Pressures  
Compared with AASHTO Pressures  
(Greene County, TN)

The measured soil-structure interaction coefficient (the measured ratio between the recorded vertical pressure and the calculated overburden pressure,  $\gamma H$ ), can be compared to the coefficient  $F_{el}$  recommended by AASHTO (Eq. 1). Although the AASHTO coefficient is intended to produce an equivalent uniform pressure, it is instructive to compare the coefficient  $F_{el}$  determined from individual pressure cells with the AASHTO values. Figure 8-8 compares the coefficients from the instrumented culvert with the AASHTO coefficients. Of 96 recorded pressure data from the instrumented culvert with backfill height less than 3.5 m ( $H/B < 0.5$ ), the range of the recorded soil-structure interaction coefficient  $F_{el}$  is from 0.73 to 1.85. The average value is 1.30 with a standard deviation of 0.34. The highest recorded  $F_{el}$  values were readings taken immediately after compaction of the backfill.

Also shown in Figure 8-8 are the soil-structure interaction coefficients calculated from an instrumented culvert in Nebraska reported by Tadros (1989). This was a double cell concrete box structure 8.1 m wide and about 4.3 m high. The permanent backfill height was 2.6 m, but it was temporarily backfilled to a height of 3.7 m for several days. Compacted silty clay was used as fill adjacent to the culvert. This culvert was under a low embankment height ( $H/B < 0.5$ ), with a maximum  $H/B$  value of 0.47, and a corresponding  $F_{el} = 1.06$ . As noted in Figure 8-8, the majority of the measured coefficients from the Nebraska culvert also exceed the AASHTO design coefficient. Of 30 recorded vertical pressures from 6 locations on the roof at backfill heights of 1.1, 2.4, 2.6, and 3.7 m, the recorded  $F_{el}$  ranged from 0.94 to 2.07. The mean value was 1.36 with a standard deviation of 0.26. Some of the cells recorded slightly less than the soil column pressure

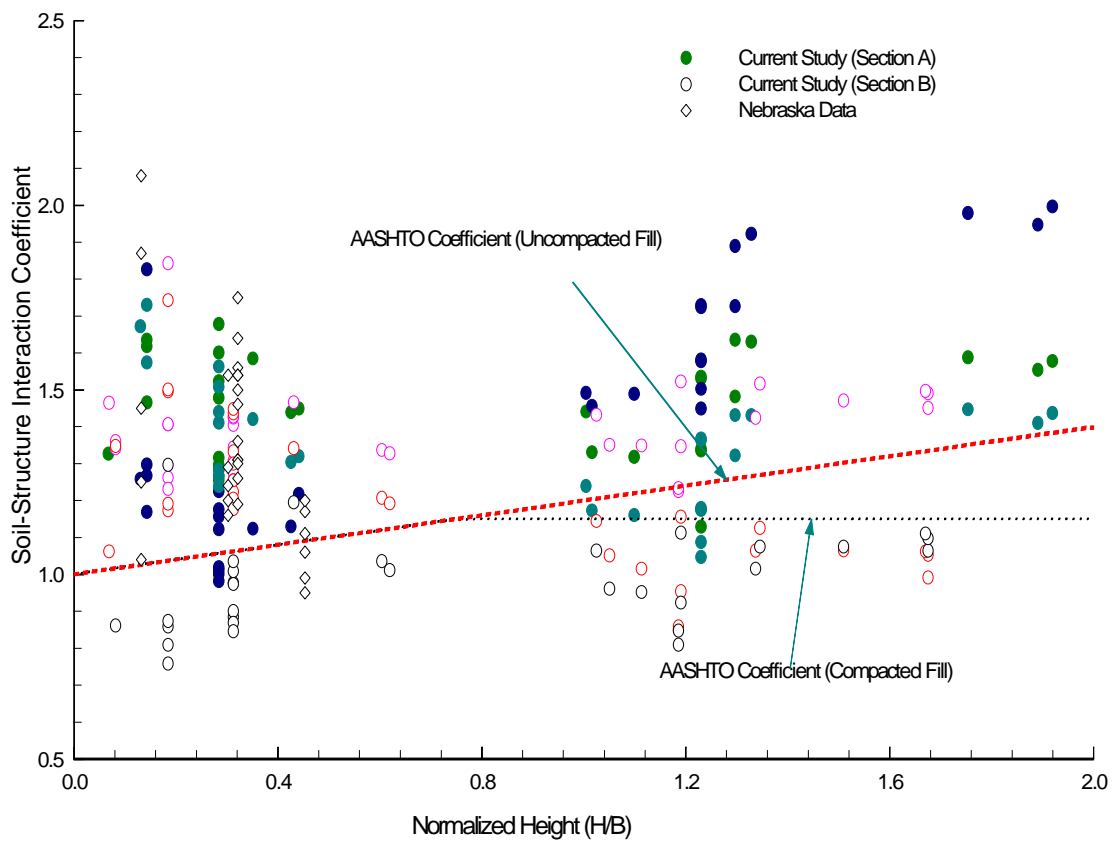


Figure 8-8 Comparison of the Normalized Vertical Pressures with Normalized AASHTO Pressures



?H, when the fill height reached the maximum height of 3.7 m.

Although the materials adjacent to the two culverts were different, the vertical pressures on the roofs under low backfill height were similar. When the embankment height was less than 0.5B, the average recorded vertical pressures were greater than the AASHTO recommended vertical pressure by approximately 30%.

In the current study, when the embankment height exceeded 4 m ( $H/B > 0.5$ ), some of the recorded soil-interaction coefficients are lower than the AASHTO  $F_{el}$  values. Of 90 recorded pressure data points, the range of the recorded soil-structure interaction coefficients was from 0.8 to 2.0, with a mean value of 1.31 and a standard deviation of 0.27. This suggests that 90% of the measured pressure data were greater than the soil column pressure. The average recorded soil-structure interaction coefficient was still greater than the recommended AASHTO soil-structural interaction coefficient by about 33%.

For any given backfill height, the mean of the weighted average pressures (using the assumed tributary widths of 0.2b for the pressure recorded at cells 4 and 6, and 0.6b for the pressure recorded at cell 5) is greater than AASHTO design pressure. For low embankment heights ( $H/B < 0.5$ ), the mean value is greater than the current AASHTO design pressure by 31%. For high embankment heights ( $H/B > 0.5$ ), the mean value is greater by 19%. The AASHTO upper limit of  $F_{el} = 1.15$  does not seem justified based on these measurements.

In Figure 8-8, all of the recorded soil-structure interaction coefficient values less than 1.0 from the current study are at locations in section B, which are close to the edge

of the slope (Figure 8-2). Lower vertical pressures recorded in this section may be attributed to the lower lateral constraint compared with that in section A.

### **8.6.2 Comparison of Measurements with AASHTO Recommended Lateral Pressure**

The current AASHTO (1996) recommended lateral pressure is obtained by the embankment height multiplied by an equivalent liquid unit weight. For the maximum lateral pressure, this equivalent unit weight is  $9.4 \text{ kN/m}^3$ , and for the minimum pressure, the equivalent unit weight is  $4.7 \text{ kN/m}^3$ . Based on the unit weight of  $18.8 \text{ kN/m}^3$  used for the vertical pressure, this corresponds to lateral earth pressure coefficients of 0.5 and 0.25, respectively. Figure 8-9 compares the recorded lateral pressures at different fill heights with the AASHTO recommended pressures. The bottom cells (Number 1) recorded larger than vertical pressure and the intermediate and upper cells (Numbers 2 and 3) recorded pressures below the AASHTO minimum pressure. This was observed at both instrumented sections A and B.

Very high lateral earth pressures were observed for some combinations of backfill modulus during a parametric study using the finite element method (Yang et al., 1997). It was assumed that the backfill modulus was proportional to compaction energy, and lateral pressures against a 9.9 m high, 3.7 m wide double cell culvert under 11.7 m fill were investigated. For a range of modulus values, both the distribution and the magnitude of the lateral pressure were found to depend strongly on the modulus of backfill. As shown in Figure 8-10 (Yang et al., 1997), very large lateral pressures at the bottom of culvert walls were obtained with the very dense gravel (high modulus) surrounding the culvert. The elastic modulus of the very dense gravel was 74 MPa, or 5 times the modulus of

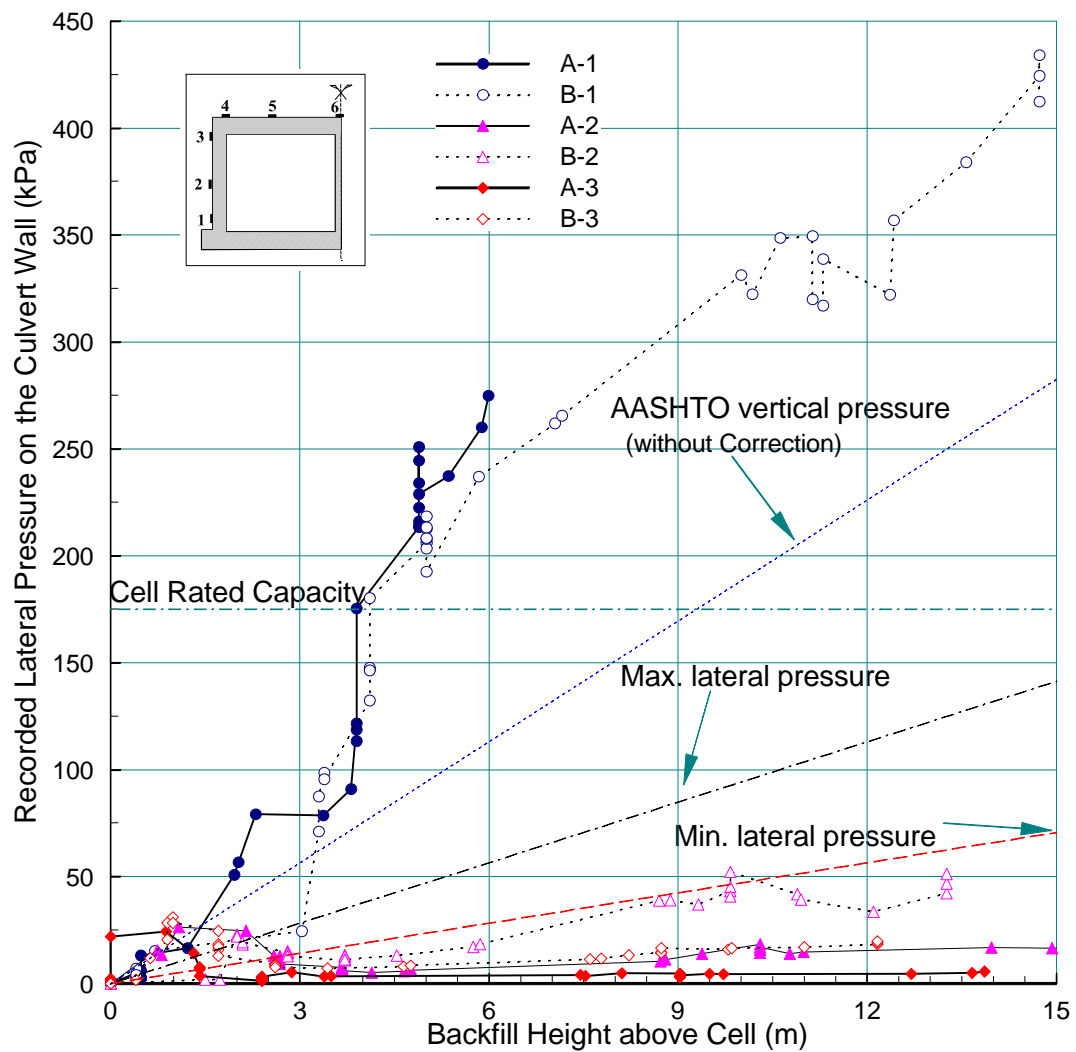


Figure 8-9 Recorded Lateral Pressures Compared with AASHTO Pressures (Greene County, TN)

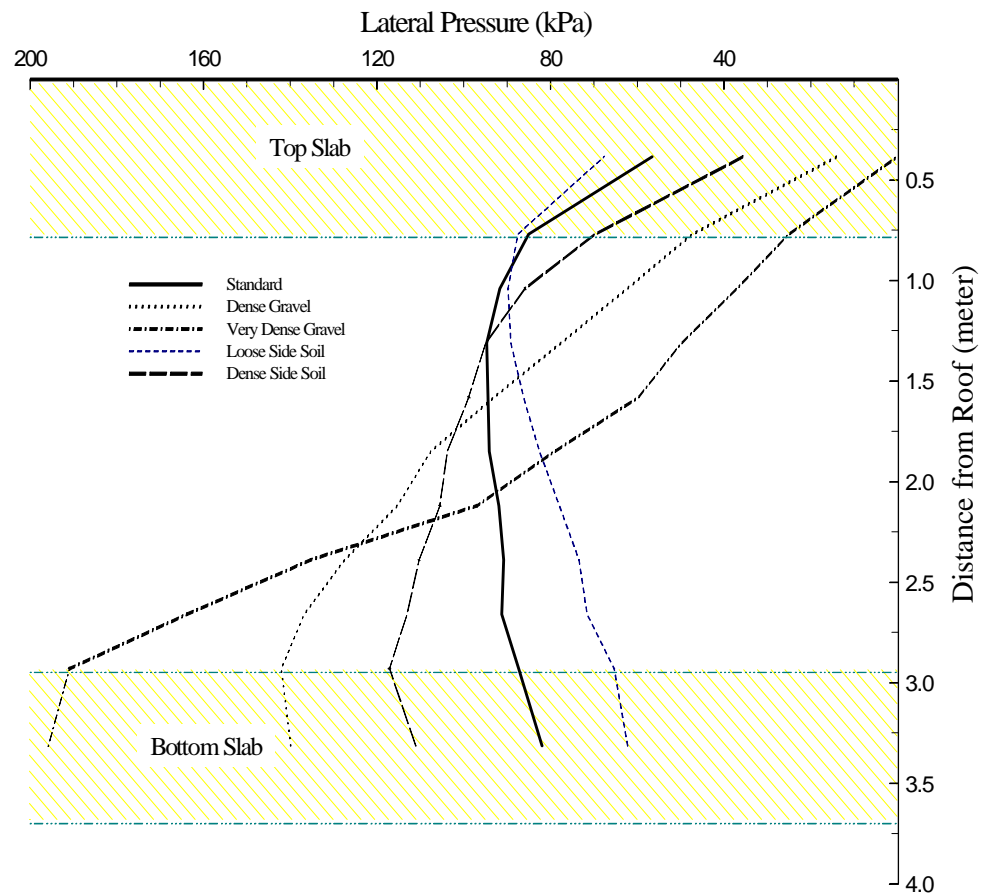


Figure 8-10 Parametric Study of Earth Pressures under Different Compaction Conditions (Yang et al., 1997)

gravel in the “standard analysis” which used a value of 14.8 MPa (Penman et al., 1975). These analytical results suggest that high lateral pressures may be induced at the bottom of the culvert wall when the backfill is well compacted. These high lateral pressures may result in significant shear forces in the bottom of the culvert wall.

## **8.7 Summary and Conclusions**

Pressure measurements on an instrumented culvert during backfill construction provided a record of the change in vertical and lateral pressure with increasing embankment heights. The pressure acting on two different sections along the culvert changed in a similar manner as the height of the embankment increased. At lower backfill height ( $H/B < 0.5$ ), the vertical pressures acting on the roof are consistent with the results of other instrumented culverts of similar size. Based on the results from a numerical analysis on a similar box culvert, the tributary width of pressure cells at different locations can be determined and then a weighted average vertical pressure can be obtained. The recorded weighted average vertical pressures are about 30% greater than the recommended AASHTO pressure at low backfill heights. At high backfill heights ( $H/B > 0.5$ ) the weighted average vertical pressures exceed the AASHTO recommendation by about 20%. Although there are no other reported test results for box culverts at high values of  $H/B$ , consistent measurements were obtained at two different instrumented sections along the box culvert.

The lateral pressures acting on the culvert wall vary in a complex manner with the increase of backfill height. At low values of  $H/B$ , the AASHTO recommended pressures were found to slightly underestimate the actual lateral pressure on the culvert. At higher

$H/B$  ratios, or  $H/B > 0.5$ , the recorded lateral pressure became very large at the base of the wall, exceeding the vertical pressure. The pressure at the top and mid-height of the wall experienced some relaxation after compaction, and thereafter remained below the AASHTO recommendation. The high lateral pressure at the base of the wall was consistent with results from finite element analyses reported previously, in which high modulus, a well compacted gravel backfill was found to result in large lateral pressures at the base of the culvert wall.

The reported field measurements of earth pressures on large concrete culverts suggest that the current AASHTO recommended pressure does not reflect field observations. Furthermore, the current soil-structure interaction coefficient may not account for important features such as the effect of backfill compaction effort.

## **8.8 Acknowledgment**

This investigation was supported by the Tennessee Department of Transportation, contract #CUT123RES1085. This support, and the input from William D. Trolinger, Division of Materials and Tests, and Billy R. Burke, Structures Division, are appreciated.

## **8.9 References**

- Corotis, R. B. and Krizek, R. J., "Analysis and Measurement of Soil Behavior Around Buried Concrete Pipe," *Concrete Pipe and the Soil-Structure System*, ASTM STP 630, 1977, pp. 91-104.
- Davis, R. E. and Bacher, A. E., "California's Culvert Research Program-Description, Current Status, and Observed Peripheral Pressures," *Highway Research Record* 249, 1968, pp. 14-23.
- Davis, R. E. and Semans, F. M., "Rigid Pipe Proof Testing under Excess Overfills with Varying Backfill Parameters," *Transportation Research Record* 878, 1982, pp. 60-82.
- James, R. W., Brown, D. E., Bartoskewitz, R. E. and Cole, H. M. "Earth Pressures on Reinforced Concrete Box Culvert" *Research Report 294-2F*, Texas Trans. Ins., The Texas A&M Univ. Sys. College Station, 1986.

Penman, A. D. M., Charles, J. A., Nash, J. K. and Humphreys, J. D. "Performance of Culvert under Winscar Dam," *Geotechnique*, Vol. 25, No. 4, 1975, pp. 713-730.

Russ, R. L., "Loads on Box Culverts under High Embankments: Positive Projection, without Imperfect Trench," *Research Report No. 431*, Division of Research, Department of Transportation, Lexington, KY., 1975.

Spangler, M. G. and Handy, R. L., "*Soil Engineering*" 4th edition, Harper & Row, New York, 1982.

Tadros, M. K., Benak, J. V., Abdel-Karim, A. M. and Bexten, K. A., "Field Testing of a Concrete Box Culvert," *Transportation Research Record 1231*, 1989, pp. 49-55.

Vaslestad, J., Johansen, T. H. and Holm, W., "Load Reduction on Rigid Culverts Beneath High Fills: Long-Term Behavior," *Transportation Research Record 1415*, 1994, pp. 58-68.

Weller, W. A., Jr., and Kulhawy, F. H., "Factors Affecting Stress Cell Measurements," *Journal of Geotechnical Engineering Division*, ASCE, Vol. 108, No. 12, 1982, pp. 442-449.

Yang, M. Z., Drumm, E. C., Bennett, R. M. and Mauldon, M., "Influence of Compactive Effort on Earth Pressure on a Box Culvert," *Proceedings, 9th International Conference of the Association for Computer Methods and Advances in Geomechanics*, Wuhan, China, 1997, pp. 2021-2026.

*Standard Specifications for Highway Bridges*. 16th Ed., The American Association of State Highway and Transp. Officials (AASHTO), Washington, D. C. 1996.

## **8.10 Recorded Earth Pressures during Construction and under Service Loads - Updated Results since Preparation of Paper**

Figures 8-11 to 8-13 present the recorded earth pressures acting on the culvert during construction period and under the service load. These are updated versions of Figure 8-4 to Figure 8-6. Seasonal pressure variations were observed at cells on the culvert roof (Figure 8-11) under constant final embankment height (18.9 m for Section A, and 11.7 m for Section B). The recorded sharp pressure increase at about May 1997 in Figure 8-12 reflects the response due to compaction efforts during the backfilling of gravel. This compaction induced pressure later decreased to a low level in a very short time. The lateral pressure acting on the bottom of wall was also found to be very large, with similar values recorded by the two cells at different sections of the culvert(Figure 8-13). The measured pressures at the bottom exceeded the capacity of gage, and one of these two ultimately ceased to provide data.

The recorded pressures were compared with AASHTO design guides (Figures 8-14 to 8-17). The vertical pressure in Section A was observed to be in general greater than current AASHTO pressure (15<sup>th</sup> version, 1996). Since the contribution of the pressure measured at different locations have different effects on the internal forces of the culvert, the weighted average pressure, as defined previously, was also compared with the design load (Figure 8-15). This figure suggests that the recorded average vertical pressure in Section A is greater than the pressure recommended by the current AASHTO design



guide. The measured pressure in Section B, which was located under the north side of embankment slope, was found to be close to the design pressure. However, the presence of the slope reduces the vertical stress.

The recorded vertical and horizontal earth pressures acting on the culvert under a constant embankment height are summarized in Figures 8-16 and 8-17 for Section A and B, respectively. Significant vertical pressure variations were recorded after the completion of construction on October 24, 1998. The lateral pressure distribution on the culvert wall was found to be significantly different from that measured on the Sullivan County replacement culvert. Very large pressures at the bottom were found with three cells (two vibrating wire cells and one resistance gage cell). Observed lateral pressures were very different from the recommended AASHTO design value. The lateral pressures are described in more detail in Chapter 12.

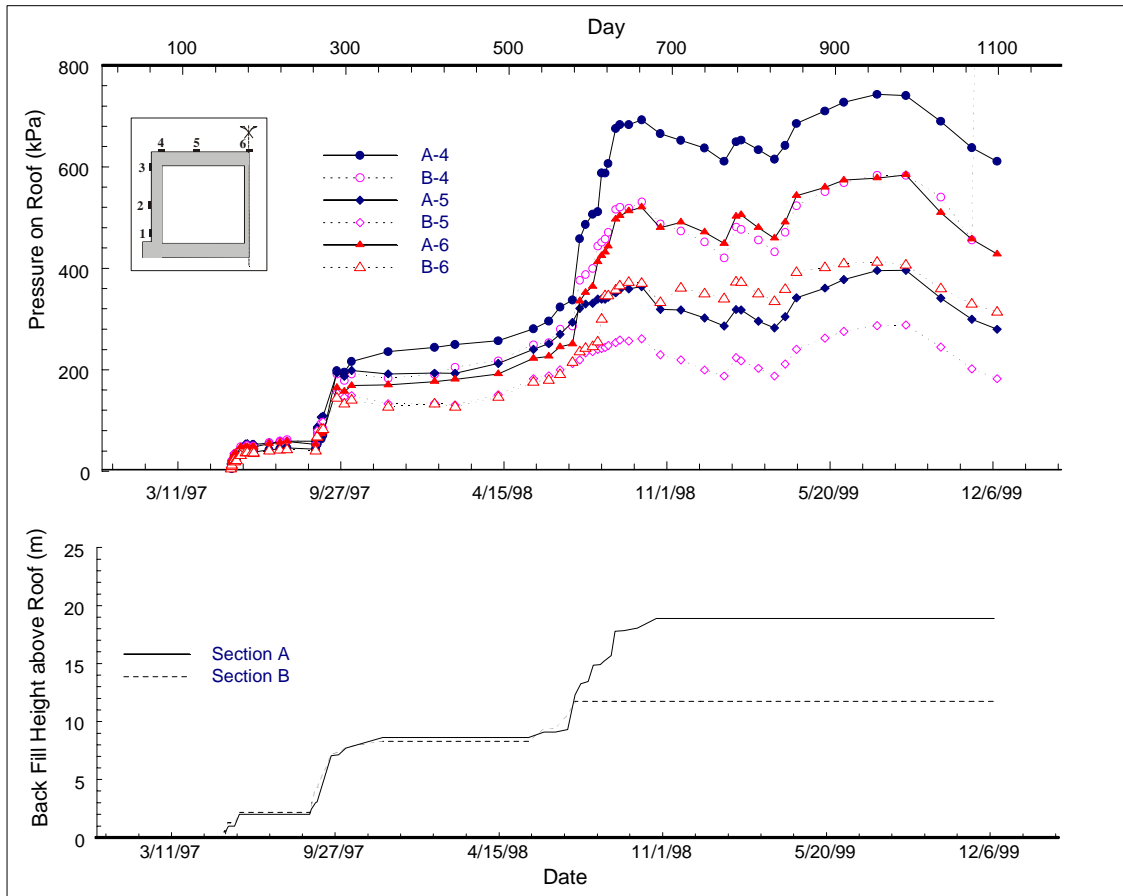


Figure 8-11 Recorded Vertical Pressures on the Culvert Roof During Construction and under Service Load to Jan., 2000 (Greene Co., TN. Start Date: 12/08/96)

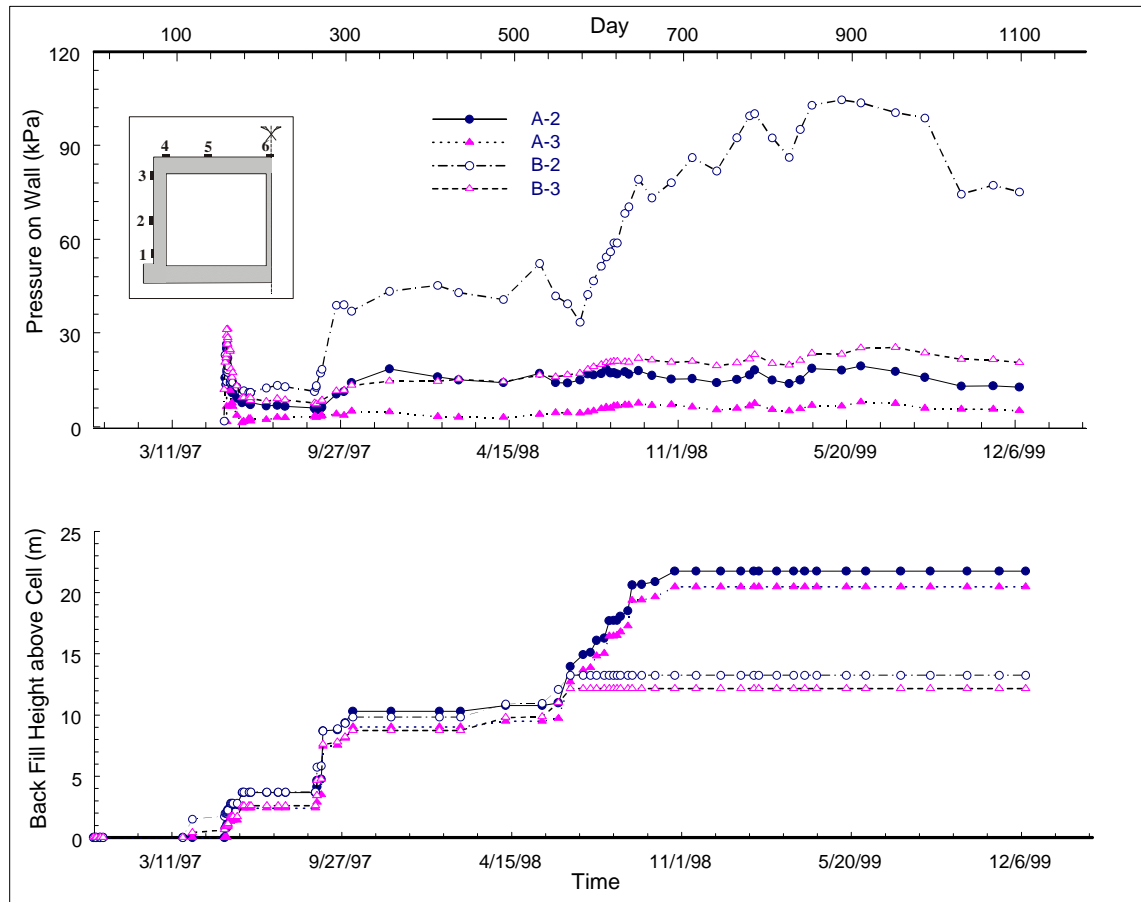


Figure 8-12 Recorded Lateral Pressures on the Culvert Wall during Construction and under Service Load to Jan., 2000 (Greene Co. TN. Start Date: 12/08/96)

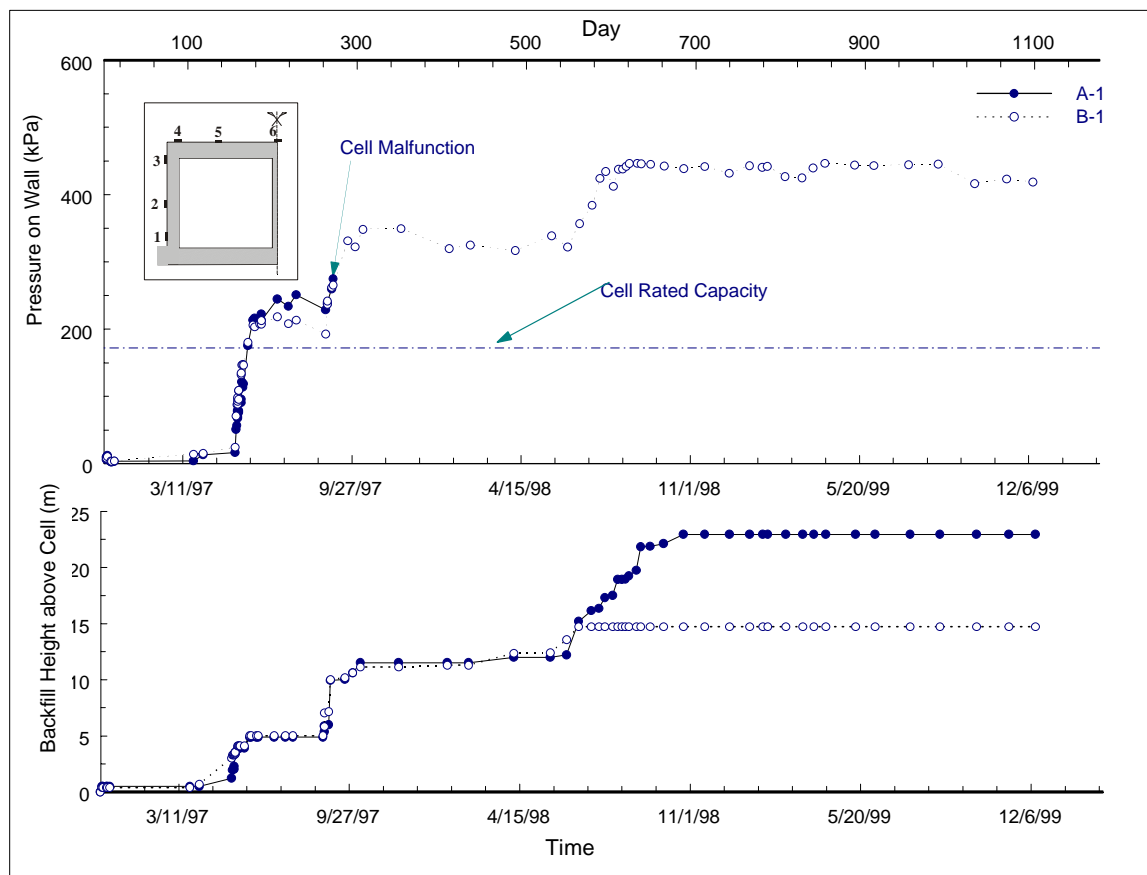


Figure 8-13 Recorded Lateral Pressures at Bottom of Culvert Wall during and Construction and under Service Load to Jan., 2000 (Greene Co., TN. Start Date: 12/08/96)

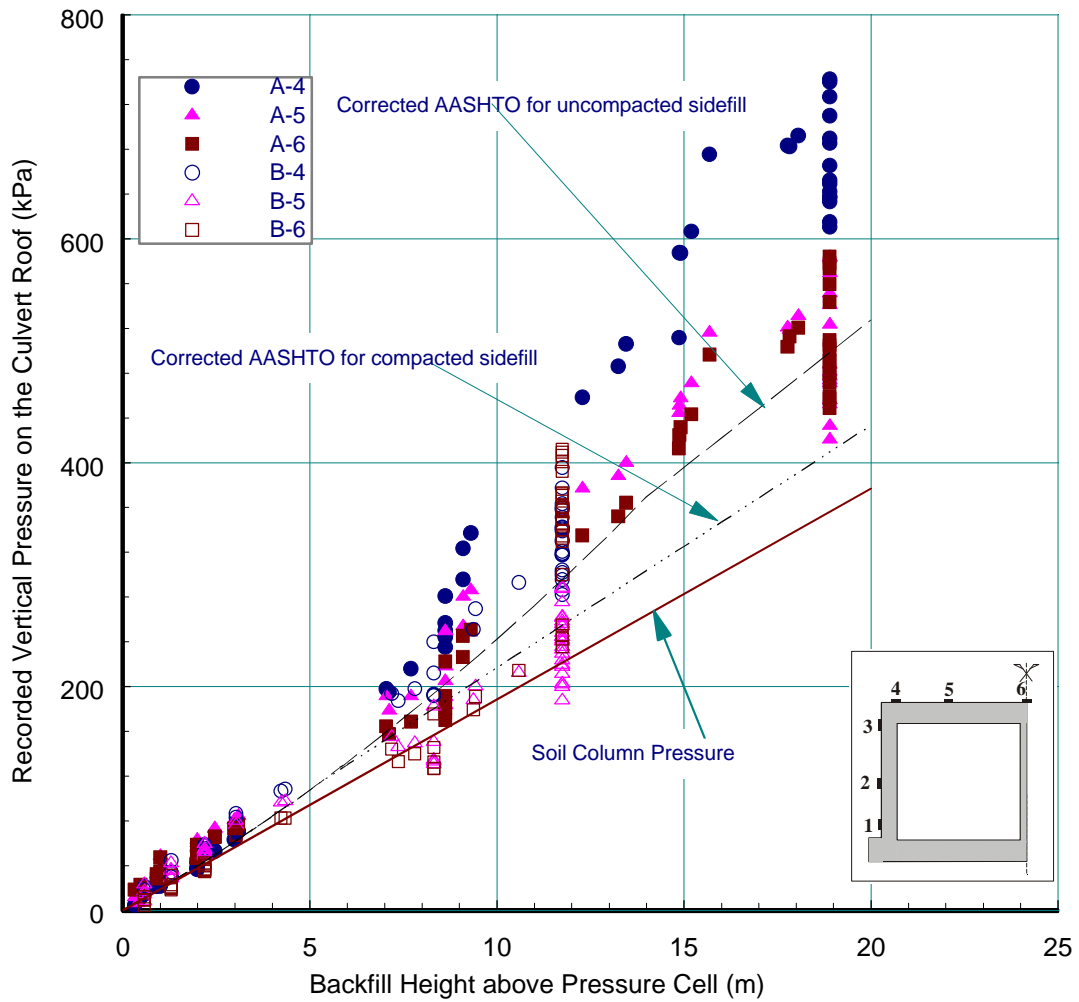


Figure 8-14 Recorded Vertical Pressures Compared with AASHTO Pressures (Greene County, TN)

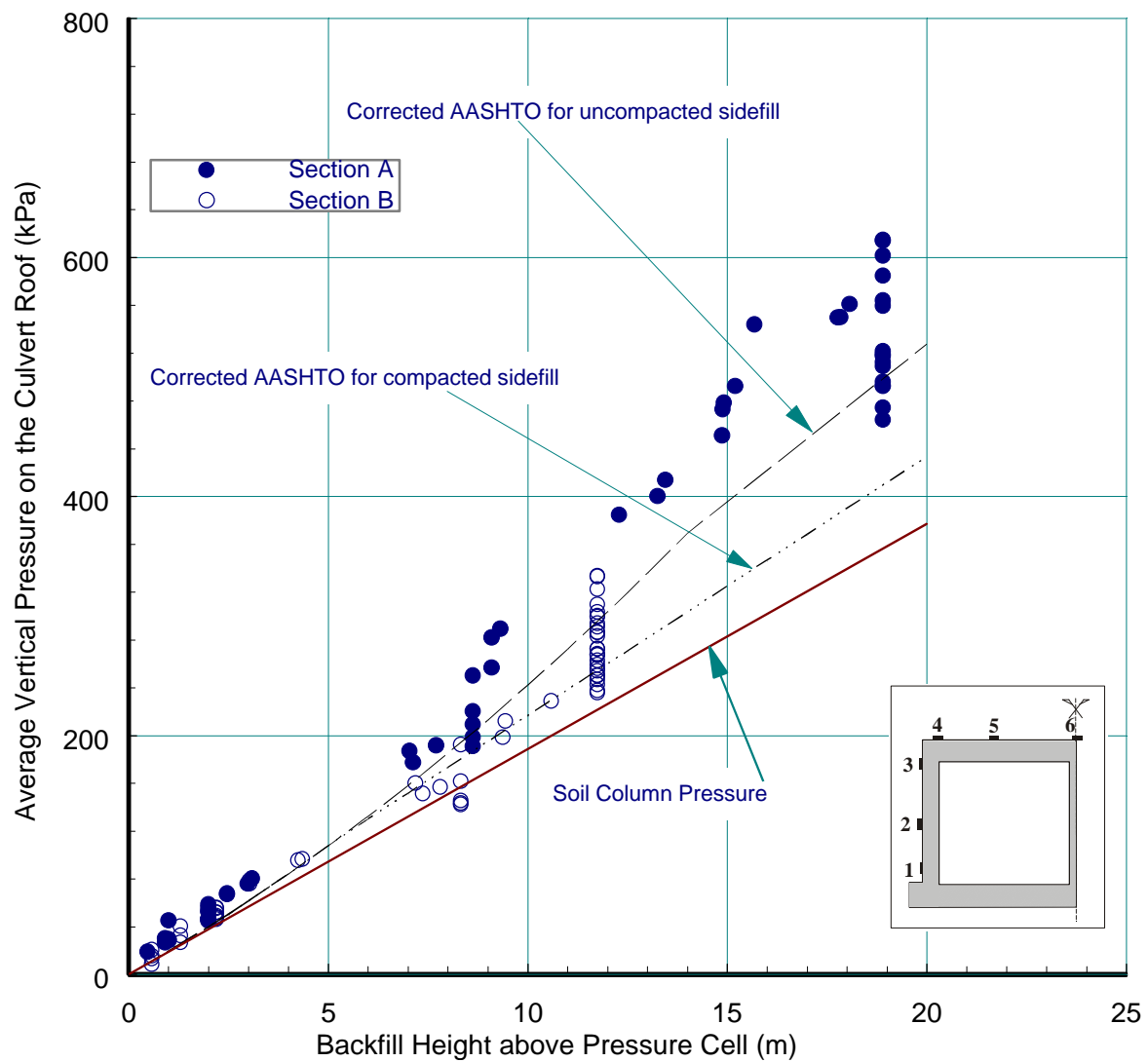


Figure 8-15 Weighted Average Vertical Pressures Compared with AASHTO Pressures (Greene County, TN)

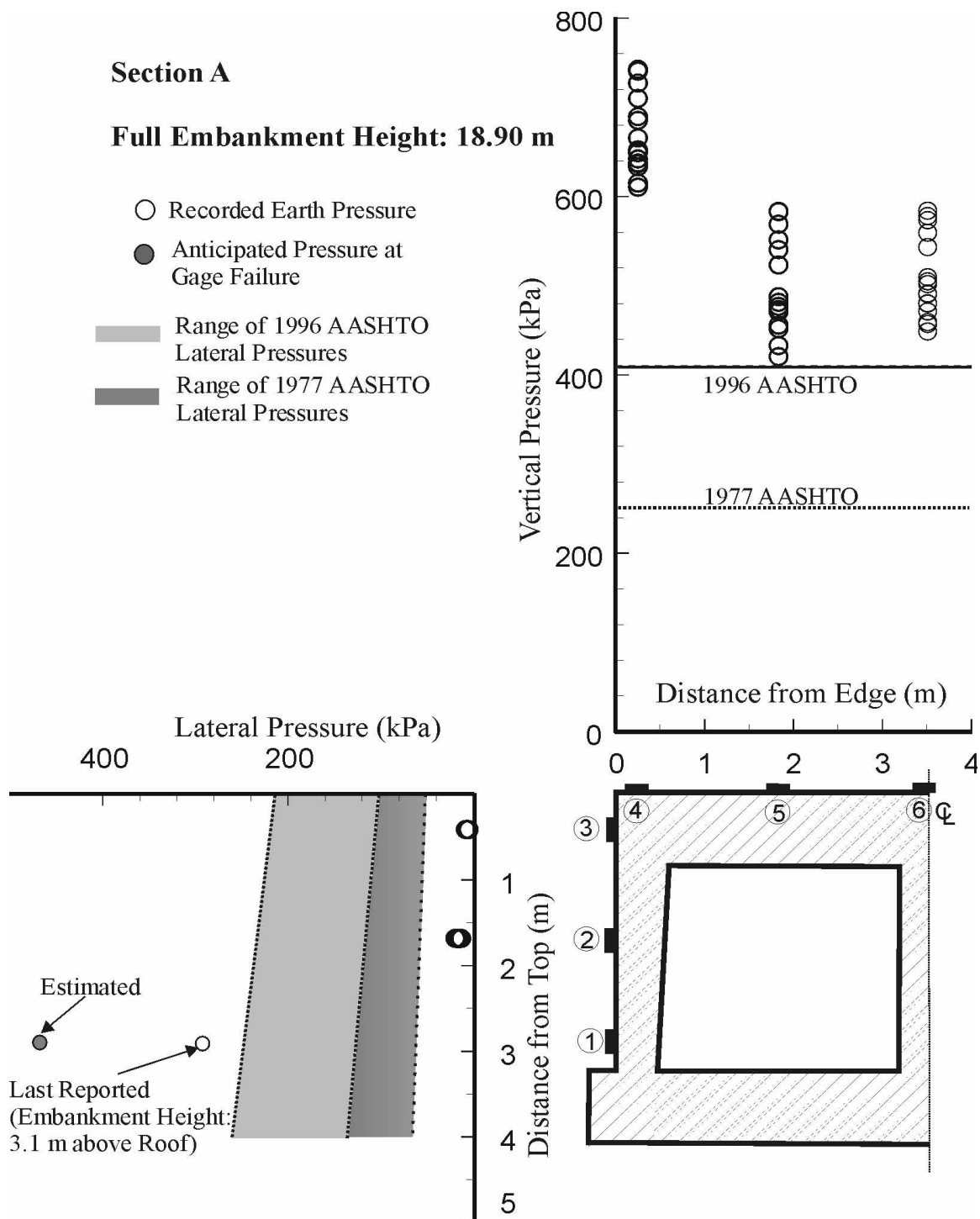


Figure 8-16 Comparison of Measured Earth Pressures on Culvert with AASHTO Pressures (Section A, full embankment height, Greene County, TN)

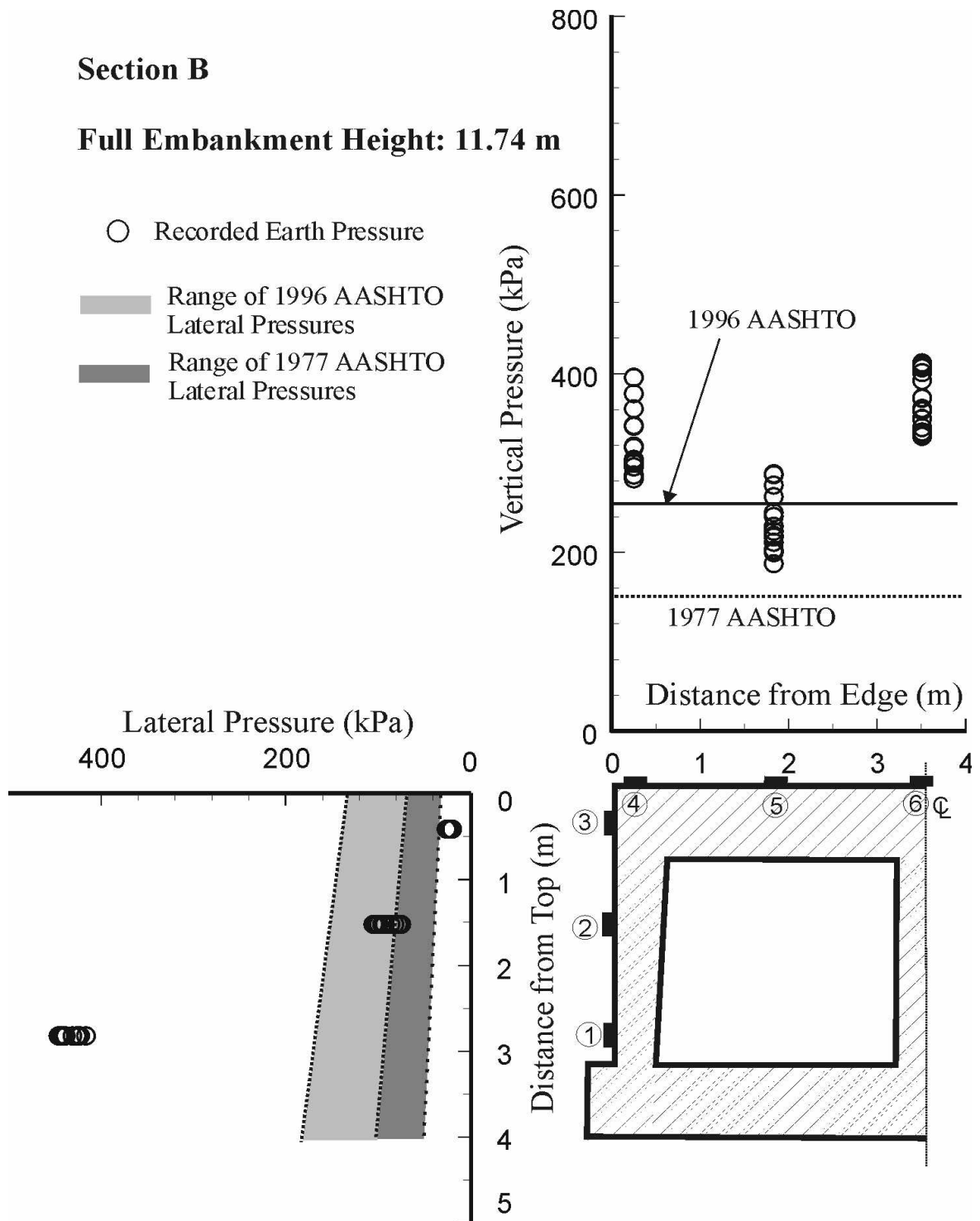


Figure 8-17 Comparison of Measured Earth Pressures on Culvert with AASHTO Pressures (Section B, full embankment height, Greene County, TN)



**PART IV**

**FIELD MEASUREMENT OF DYNAMIC LATERAL**

**EARTH PRESSURES ON BOX CULVERT**

## **Chapter 9**

### **Measurement and Analysis of Dynamic Pressures Induced by Construction Equipment**

#### **9.1 Introduction**

The lateral pressures induced by construction equipment can impact the performance of retaining walls and buried structures. The design of these structures is usually based on the long term or static earth pressures, but short term dynamic loadings may also be significant. The magnitude of the peak pressure as well as the duration and attenuation characteristics of the transient construction pressures may affect the magnitude and distribution of the residual static earth pressures. Although the residual static lateral pressure exerted on structures after compaction has been studied extensively (Rehman and Broms, 1972; Ingold, 1979; Seed, 1986), limited data exists on the dynamic impulse pressures induced during construction (Butcher and Marsland, 1989; Filz and Brandon, 1994). Filz and Brandon (1994) utilized small (semiconductor silicone cells, 55 mm external diameter) pressure cells to evaluate the effectiveness of light weight compaction equipment under the laboratory condition.

As indicated in Chapter 2, Section 2.3 (Figure 2-13 and Table 2-3), different components of the compaction time history are defined to describe the compaction induced earth pressures at various time stages. The abbreviated pressure components will be used throughout this chapter.

Residual pressure is the earth pressure that remains after the attenuation of the dynamic or impulse pressure. Residual pressure has been extensively investigated by other researchers (Rehman and Broms, 1972; Carder, et al., 1977; Ingold, 1979; Duncan and Seed, 1986; Duncan and Seed, 1991; Filz and Brandon, 1993). In order to estimate the residual compaction pressure, Duncan and Seed (1986) developed a computer based hysteretic model to track changes in stress during the loading and unloading cycles. Later, they simplified the model and developed hand calculation charts (Duncan and Seed, 1991) to evaluate residual compaction pressure due to different construction equipment.

Butcher and Marsland (1989) briefly reported the dynamic lateral earth pressures on an instrumented bridge abutment induced by construction vehicles and by the subsequent service loading. The published results were cells from located far (3 m) from the dynamic sources, and therefore limited conclusions could be drawn for the effect of construction equipment when it is close to the structure.

In conventional construction practice, granular materials are spread near the structure and compacted in thin layers. Horizontal pressure acting on the structure is a results from repeated loading and unloading during compaction. Typical pressure changes with time during the compaction were illustrated in Figure 2-14. Various compaction induced pressures were also defined in Chapter 2. These pressures are: impulse pressure, initial residual compaction pressure, incremental residual compaction pressure, cumulative residual compaction pressure, and total compaction pressure. In this chapter, cumulative residual compaction pressure is abbreviated as residual pressure.

As with the measurement of static earth pressure, recorded dynamic pressure can be influenced by many factors. In addition to factors influencing static pressure readings such as cell size, aspect ratio (ratio of cell thickness to diameter), and soil/cell stiffness ratio, dynamic pressure measurements can be affected by cell response time, differences between cell and soil density, and differences between cell and soil impedance. According to Weller and Kulhawy (1982), the use of large size rigid resistance earth pressure cells can overcome some of these problems, and fairly good results can be obtained.

The box culvert in Greene County, TN (Figure 9-1), was instrumented to measure construction induced horizontal dynamic earth pressures. The objectives of this instrumentation program were:

- Record actual dynamic pressures on the culvert during a typical backfill compaction practice using different types of compaction equipment close to the

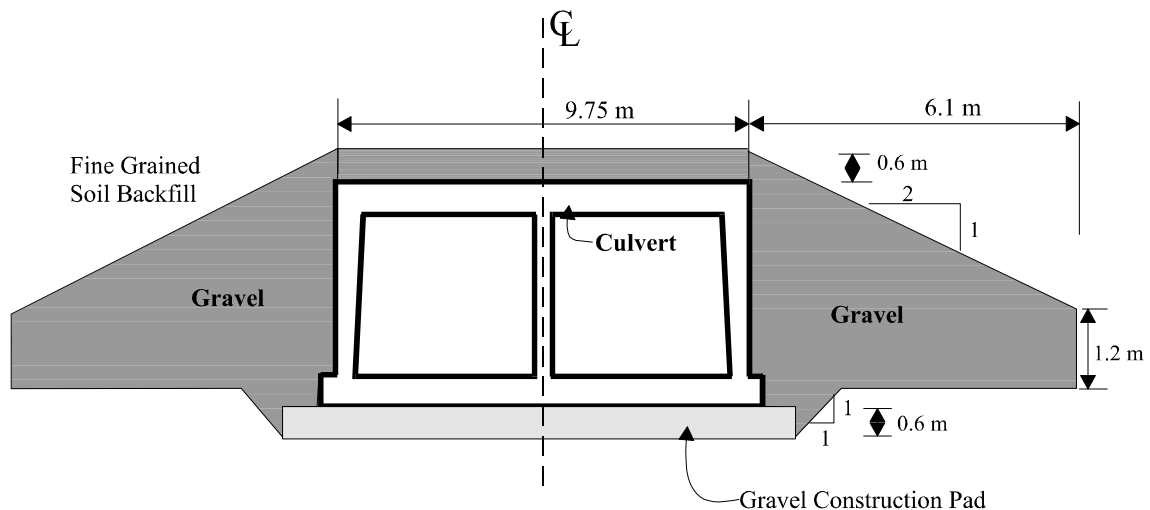


Figure 9-1 Schematic of Box Culvert with Typical Dimensions of Gravel Backfill Zone (Not to Scale)

structure.

- Compare the construction induced dynamic pressures with the maximum static earth pressures, and provide guidance for future culvert design.
- Develop a simple and rational method to estimate the lateral impulse pressure and the lateral residual pressure induced by typical compaction equipment.
- Investigate the response of the culvert to impulse pressures.
- Obtain a better understanding of the time variation characteristics of lateral residual pressures.

### **9. 1.1 Instrumentation for Dynamic Lateral Pressure Measurement.**

Six GeoKon resistance strain gage pressure cells were installed in instrumentation Section A (under the maximum embankment height of 18.9 m) to record the dynamic lateral earth pressures during construction. They were aligned vertically and were located about 1.40 m horizontally from the column of vibrating wire pressure cells used for recording the static pressures (Figure 9-2). The size and the earth pressure sensing mechanisms were the same as the vibrating wire pressure cells, and an identical installation method was used (Chapter 8). Resistance strain gage transducers were chosen to record the dynamic pressures because the vibrating wire transducers are not well suited to high frequency pressure variations.

In order to determine the structural response due to the dynamic load, resistance concrete strain gages were embedded in both the internal and external sides of the concrete wall and roof coinciding with the vibrating wire pressure cell locations.

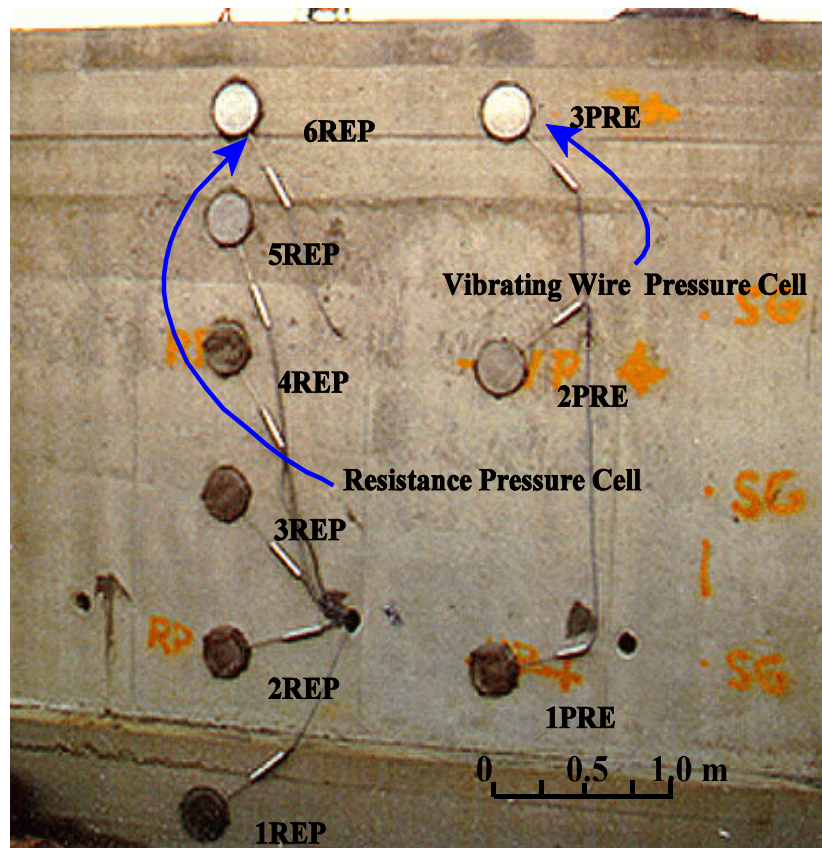


Figure 9 - 2 Photograph of Culvert Wall (Greene Co., TN)  
Showing Resistance (REP) and Vibrating Wire (PRE)  
Earth Pressure Cells

The dynamic strain signals from the resistance pressure cells and concrete strain gages were recorded by an OPTIM MEGADAC 3415 data acquisition system, which was connected to an on-site computer. Due to the large amount of data collected (30 channels), an acquisition rate of 10 samples per second was chosen.

Before the compaction work began, a baseline or initial reading was obtained for each pressure cell and strain gage. The actual lateral pressure (both static and dynamic) was obtained by subtracting the baseline from each measurement. The output from the computer was verified using a strain gage readout box before recording the dynamic lateral pressure induced by the construction equipment. The capacities and locations of the resistance pressure cells are listed in Table 9-1, and the cell installation scheme is shown in Figure 9.2.

The soil conditions and strength parameters for the gravel, the undisturbed soil underneath the culvert, and the clay soil backfill near the culvert, can be found in Chapter 3.

Table 9-1 Details of Resistance Pressure Cells

<b>Cell No.</b>	<b>Model</b>	<b>Capacity (kPa)</b>	<b>Gage Factor</b>	<b>Distance from Bottom of Culvert (m)</b>
<b>1REP</b>	LM/2345-01	345	5.058	0.42
<b>2REP</b>	LM/2345-01	345	5.440	1.14
<b>3REP</b>	LM/2345-23	207	9.078	1.85
<b>4REP</b>	LM/2345-23	207	7.607	2.51
<b>5REP</b>	LM/2345-01	345	5.532	3.12
<b>6REP</b>	LM/2345-01	345	2.751	3.63

### 9.1.2 Construction Methods

Gravel was spread by dump truck in about 0.15 layers beside the culvert wall. The loose gravel was first leveled by a dozer and then graded with a power grader. Typically, the leveled gravel was compacted by a vibrating roller making 4 passes. The closest distance between the roller drum edge and the wall was about 0.15 m. Some attributes of the compaction equipment are shown in Table 9-2 with details provided in the Appendix.

Table 9-2 Selected Attributes of Compaction Equipment

Model	Ingersoll-Rand SP-56	Ingersoll-Rand DD130	Caterpillar 815F
Type	Single Drum, Vibrating	Double Drum, Vibrating	Sheep's-foot, Self-propelled
Target Material	Gravel	Gravel	Clayey Soil
Operation Weight (kg)	8,900	12,300	20,900
Drum Weight (kg)	5,350	6,720 (front)	NA
Drum width (m)	2.14	2.14	3.76
Drum Base (m)	3.43	3.23	NA
Frequency (Hz)	0 to 30.4	41.7	0
Centrifugal Force (kN)	186.8	71.2 to 160	NA

Completion of the gravel around the culvert was performed in two stages. The first stage lasted from Dec. 8 to 11, 1996. During this stage, a double drum vibrating roller (Ingersoll-Rand DD130) was used to compact the gravel. The final gravel surface was 1.50 m above the culvert bottom at the end of this stage. At this point construction was delayed until spring of the following year.



Construction was resumed on May 13, 1997. Gravel was placed to a level 0.6 m above the culvert roof. The roller used in this stage was a single drum wheel vibrating roller (Ingersoll-Rand SP56). Above this level, a fine grained backfill material was used for the remainder of the embankment. The fine grained backfill material was compacted with a sheep's-foot, self-propelled roller (Caterpillar 815F).

## **9.2 Results From Recorded Dynamic Pressures**

As indicated previously, gravel was placed around the culvert and compacted with vibrating rollers. After the gravel reached an elevation of 0.6 m above the roof, fine grained soil was spread by dozers and compacted by a kneading roller. Significantly different dynamic lateral pressure patterns were recorded with different construction equipment. The measured earth pressures are therefore discussed for conditions below and above the culvert roof.

### **9.2.1 Compaction Equipment Operating Below Culvert Roof**

Figures 9-3 to 9-5 illustrate the typical dynamic response of pressure cells when a vibratory roller (Ingersoll-Rand DD130) compacts the same layer of gravel during the third and fourth compaction passes. The time history of pressure at two different depths (1REP and 2REP) is shown in each figure. A significant stiffness increase was expected in the gravel after each compaction pass. When the roller passed by the instrumented section, two peak dynamic pressures were generated in response to each of the two roller drums. In Figure 9-3, the second impulse pressure with the greater magnitude and the higher frequency content at about 58 seconds reflects the response from the active (vibrating) front drum (the roller was operating in reverse). The impulse pressure

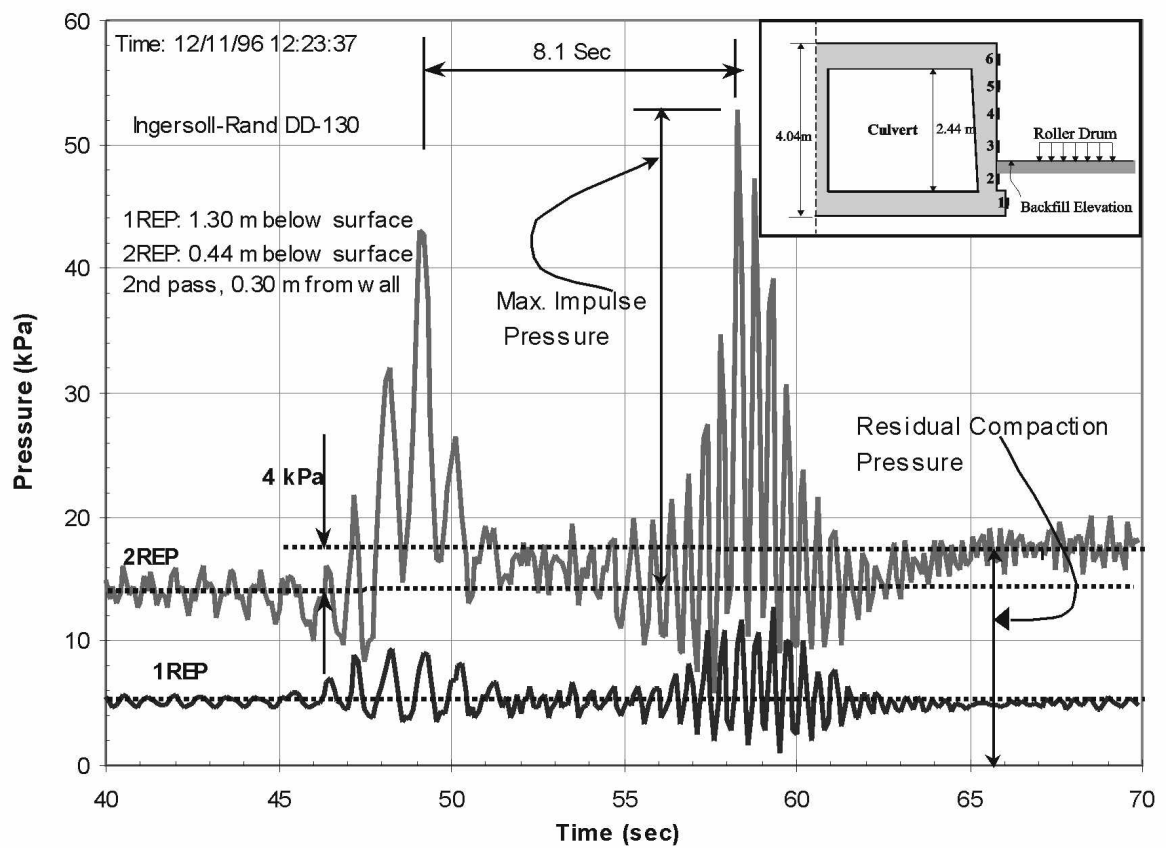


Figure 9-3 Typical Dynamic Pressure Pattern due to Vibratory Roller - Second Pass  
(recording interval: 30 seconds)

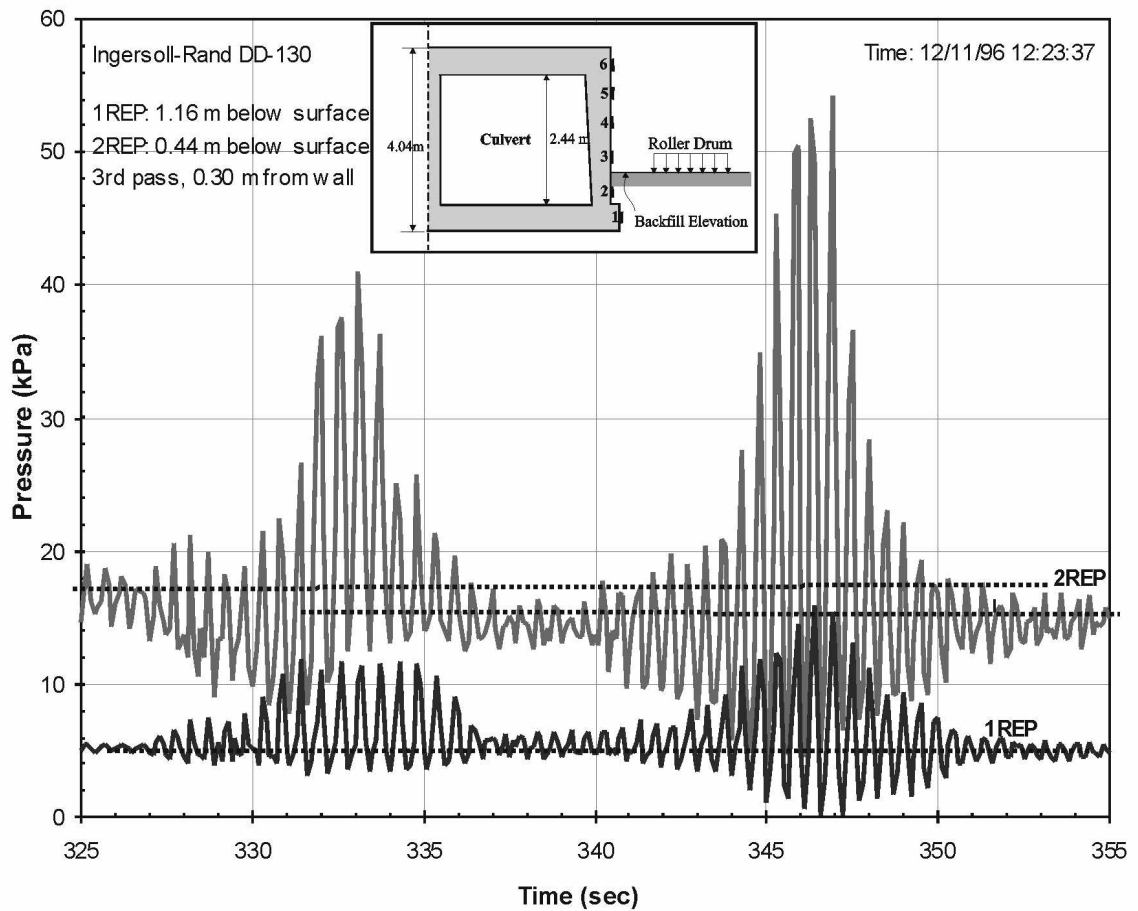


Figure 9-4 Typical Dynamic Pattern due to Vibratory Roller - Third Pass  
(recording interval: 30 seconds)

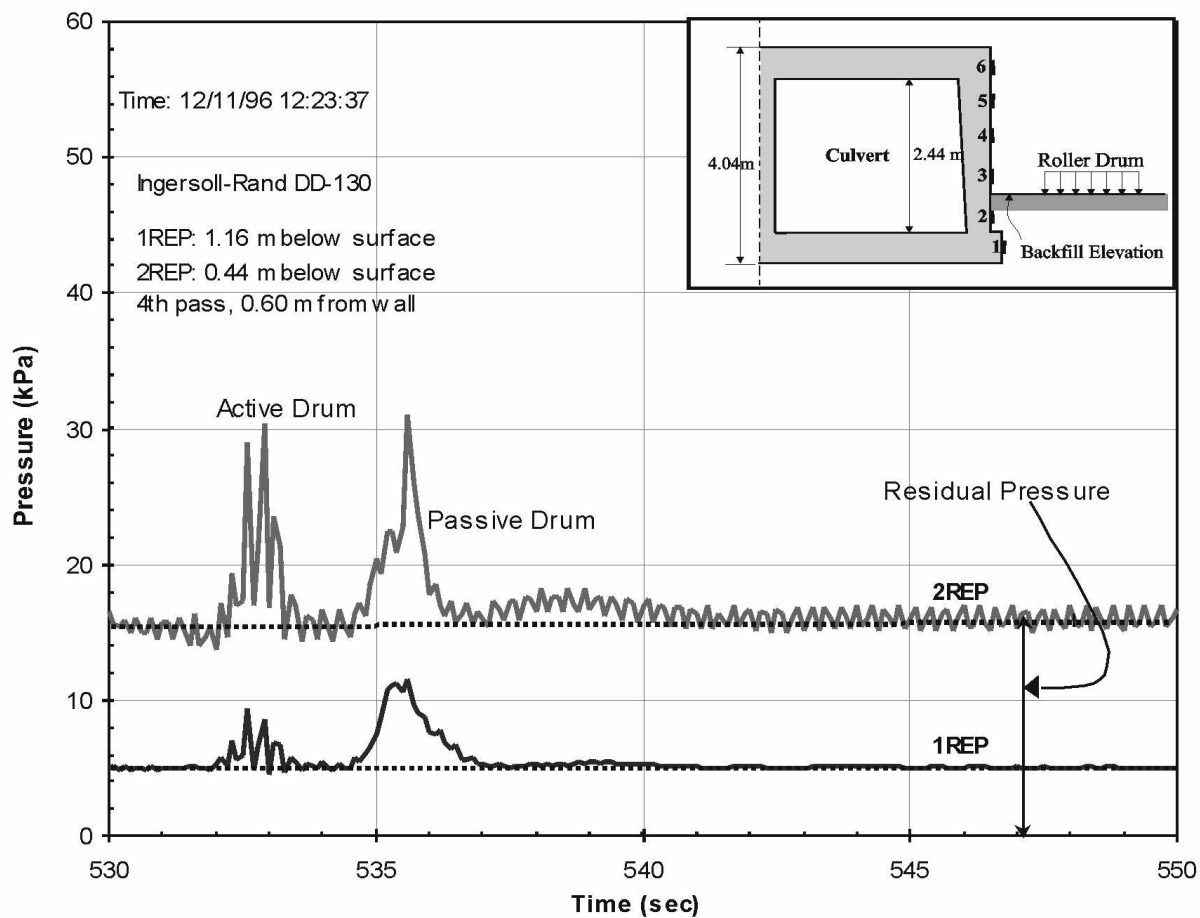


Figure 9-5 Typical Dynamic Pressure Pattern due to Vibratory Roller - Fourth Pass  
(recording interval: 20 seconds)

generated by the passive (non-vibrating) rear drum, which had a similar static contact pressure, was slightly lower than that induced by the active front drum. The impulse pressure induced by the passive drum had lower frequency content at this pass. Both the initial residual compaction pressure before the approach of the equipment, and impulse pressure due to the roller are smaller in gage 1REP, which was about 0.7 meters deeper than gage 2REP. The maximum impulse pressure recorded in cell 2REP was about 39 kPa. The incremental residual compaction pressure or the increase in pressure due to compaction, recorded by 2REP after the pass of the roller was about 4 kPa. That is, about 10% of the maximum impulse pressure was “locked” into the gravel increasing the residual compaction pressure. But, the results in Figure 9-6 suggest that if the cell was too close the ground surface there was no increase in the residual pressure recorded, when the roller was very close to the wall (cell 6REP, 0.06 m below surface, first pass). Cells deeper in the gravel (1REP) indicated no increase in residual compaction pressure after the pass of a roller.

Figure 9-4 illustrates the dynamic response of the same gravel under the 3rd compaction pass with the roller drum at the same distance from the wall. While the response of the active drum was similar to the previous pass and the peak total compaction pressures were identical, the pressure induced by the passive drum was found to be greater in both cells. This additional pass of the roller did not increase the residual pressure; instead, a slight residual pressure decrease was recorded by the upper cell (2REP).

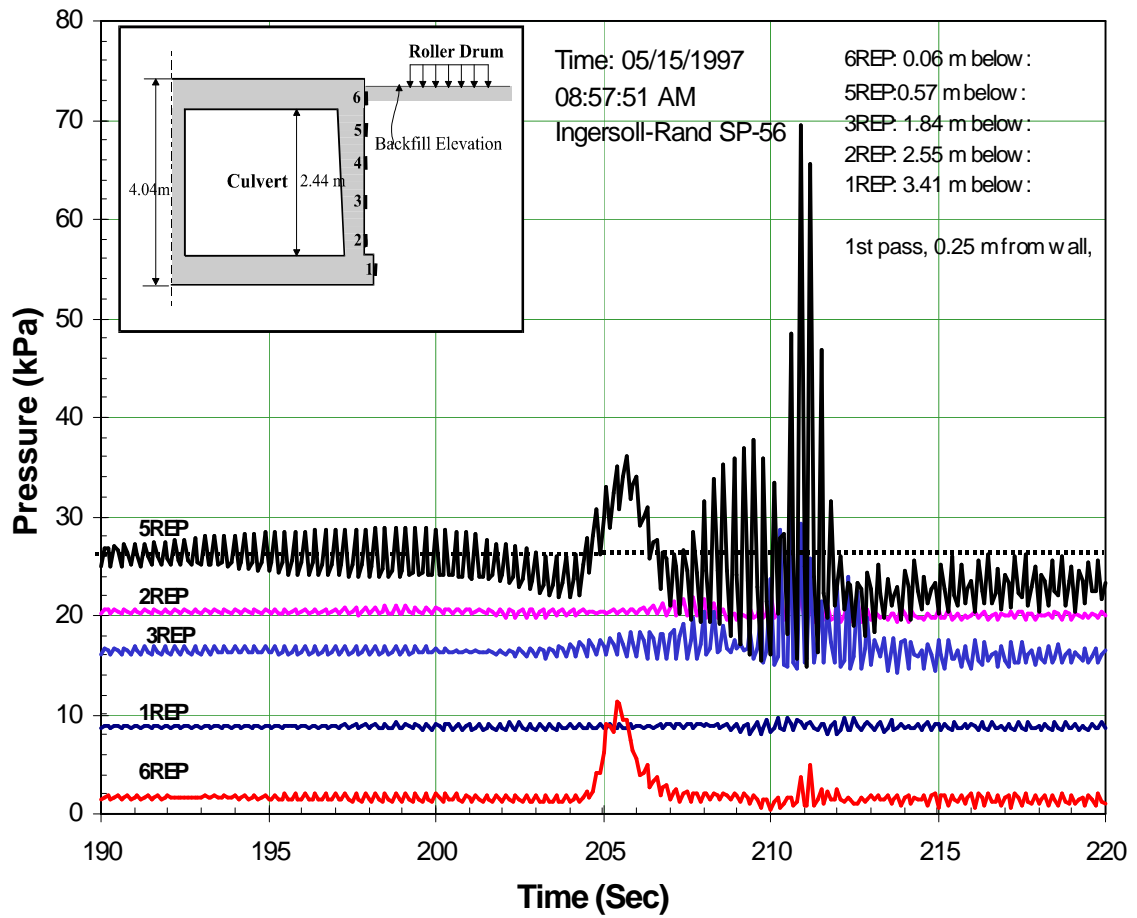


Figure 9-6 Dynamic Pressure Distribution along Culvert Wall  
(recording interval: 30 seconds)

The magnitude of the impulse pressure at shallow depths was sensitive to the distance from the edge of the roller drum to the wall. A slight change of roller distance to the wall can produce a significant difference in the pressure pattern. This is evident in Figure 9-5, which shows the pressure patterns induced by a roller passing 0.6 m from the wall (4<sup>th</sup> pass) on the same layer of gravel depicted in Figures 9-3 and 9-4. Although the roller is only 0.3 m farther away from the wall, the recorded impulse pressure in cell 2REP is about half that shown in Figures 9.3 and 9.4. The pressures recorded in the deeper cell (1REP) were also smaller than the previous passes, but the pressure change was not as significant as the cell at shallow depth (2REP). It was found that the impulse pressure was not significant (magnitude less than 15 kPa) when the roller edge was more than 1 meter away from the culvert wall. It is also found that at depths greater than 1 meter below the ground surface the residual pressure would not change after the compaction process.

Figures 9-6 and 9-7 illustrate the response of pressure cells at different depths. The compaction is applied by the Ingersoll-Rand SP56 with a vibratory steel drum and a passive rubber tire. The location of both the maximum impulse pressure and the maximum residual pressure are at shallow depths, but are not recorded by the cells which were the closest to the ground surface. Due to the difference in wheel weight and nature of the steel drum vibration, the rubber tire and the steel drum have different influence depths. From Figure 9-7, cell 3REP, which was 2 m below the gravel surface, did not detect the impulse pressure induced by the rubber tire. The induced pressures from the rubber tire were clearly recorded by cells at shallower locations (5REP, 6REP).

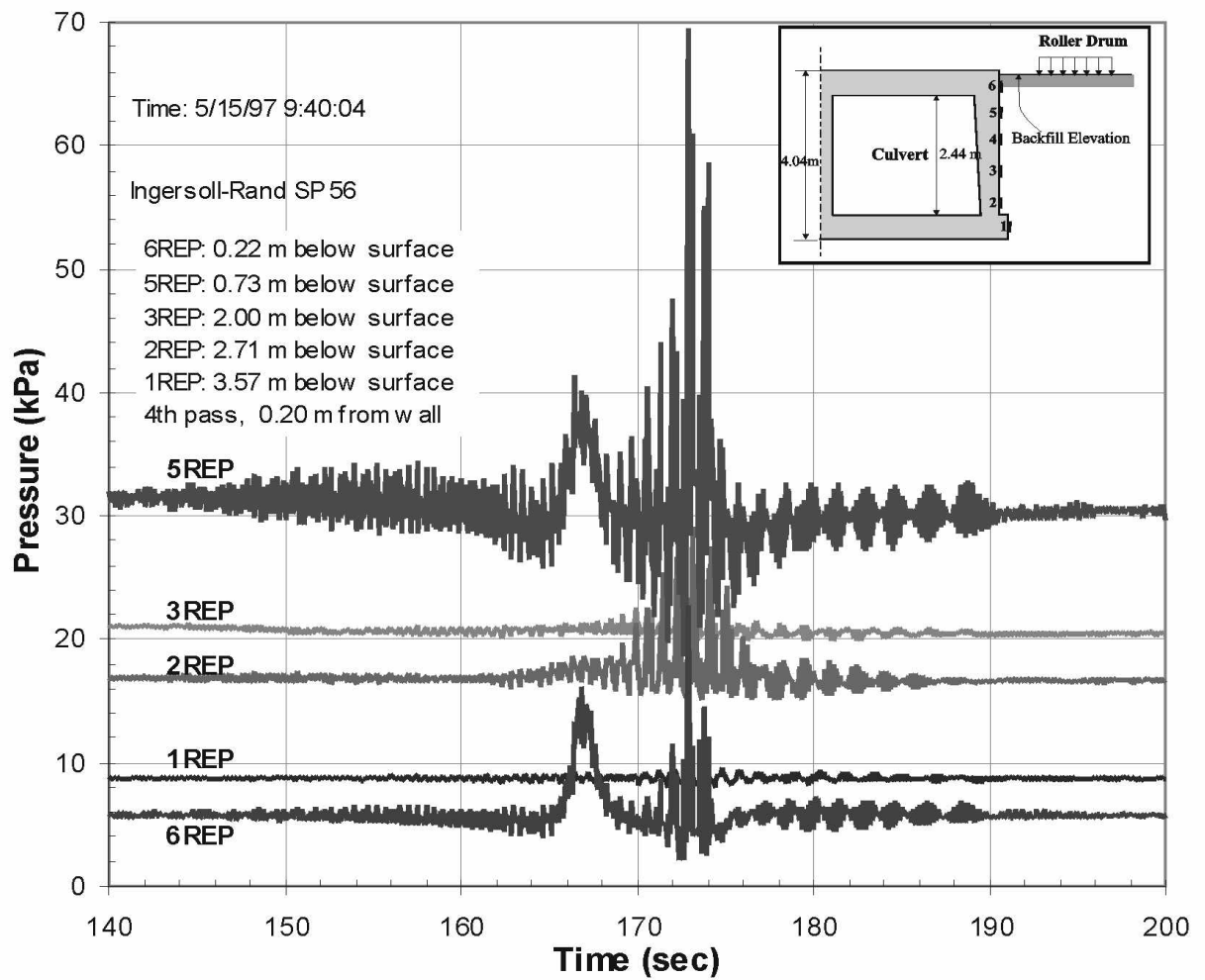


Figure 9-7 Dynamic Pressure Distribution along Culvert Wall  
 (recording interval: 60 seconds)



Therefore, the influence depth of the rubber tire was less than about 2 meters. Similarly, the influence depth of steel drum (active drum) can be estimated to be about 3.5 m.

When the surface of the backfill was below the culvert roof, the largest recorded impulse pressure recorded was 42.7 kPa, corresponding to a pressure cell 0.57 m below the gravel surface (Figure 9-6, cell 5REP, 1st pass). The maximum residual pressure recorded in the study was 31.6 kPa, which was recorded by a cell 0.73 m below the surface (Figure 9-7, cell 5REP, 4th pass). Both maximum pressures were generated by a single drum roller (Ingersoll-Rand SP56) with its drum edge a distance of 0.25 m from the culvert wall.

Figure 9-8 is a summary of the peak compaction induced pressures at different depths as recorded in Figure 9-7. From the pressure distribution relationship, it appears that both the maximum residual pressure and the maximum total compaction pressure were close to the ground surface. Although the peak total compaction pressure was as high as 70 kPa, the duration time is very short (less than 0.1 second). The structural response under this transient load will be analyzed later.

### **9.2.2 Dynamic Pressure Induced by Other Construction Equipment**

A significant pressure response was recorded by a loaded dump truck with its wheel about 0.3 m from the instrumented wall (Figure 9-9). The maximum total pressure induced by this truck was about 60 kPa. Compared with the vibratory roller in Figure 9.7, the influence depth of the truck induced lateral pressure is slightly shallower or about 2.0 m. Significant incremental pressures were also recorded by two shallow cells (5REP, 6REP).

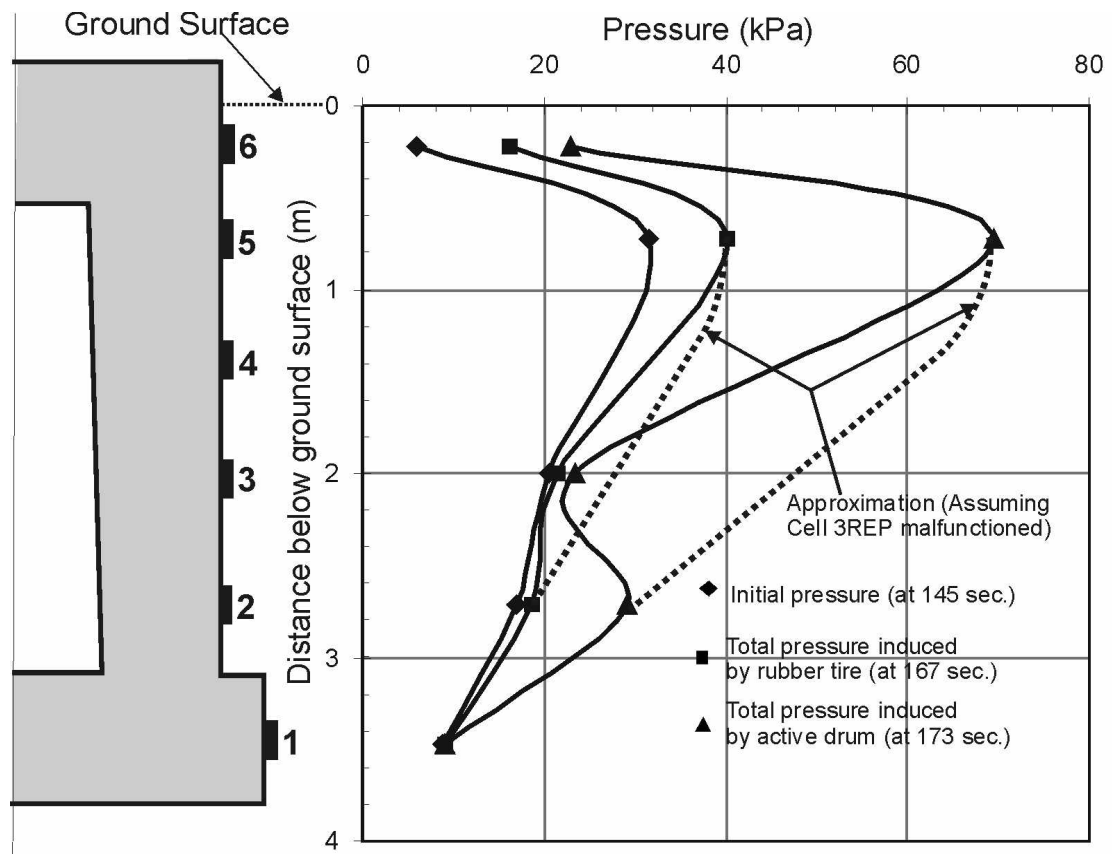


Figure 9-8 Dynamic Pressures at Different Depths

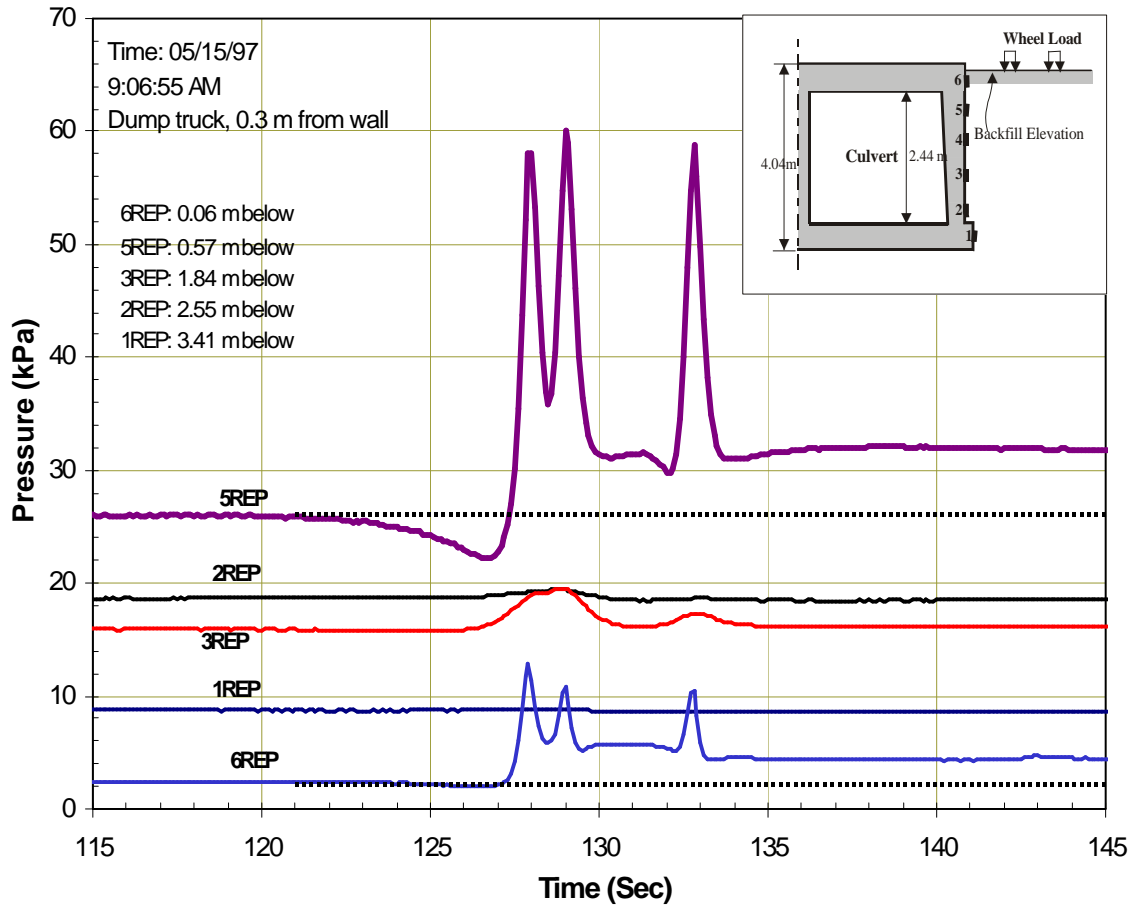


Figure 9-9 Response of Pressure Cells of Loaded Truck Spreading Gravel  
(recording interval: 30 seconds)

The instrumentation also recorded the dynamic pressure induced by other construction vehicles such as an all-drive scraper, a bulldozer, a motor grader, and a small plate compactor. With the exception of the loaded dump truck, the dynamic pressures from these pieces of construction equipment were negligible. Detailed dynamic pressures generated by different machines are listed in Appendix.

### **9.2.3 Compacting Equipment Operating above Culvert Roof**

After the gravel was filled and compacted to a level 0.6 m above the culvert roof, a fine grained clayey soil backfill was spread and compacted by a Caterpillar 815F kneading compactor. This machine was a self-propelled sheep's foot roller designed to impart static kneading action to fine grained soils. Figure 9-10 illustrates a typical dynamic lateral pressure time history from this compaction device. Both the shape and the magnitude of the dynamic lateral pressures induced by the kneading compactor were significantly different from those generated by the vibrating rollers used to compact the gravel. When the roller passed over the instrumented section (at about 5-10 seconds in Figure 9-10), the maximum impulsive pressure was about 9 kPa (cell 6PRE). Cell 5REP, at a slightly greater depth, recorded a smaller impulsive pressure but was left with a decrease in total pressure. This suggests that the compaction above may result in a redistribution of stress or actual unloading of some of the compaction induced stresses. Figure 9-10 suggests that the impulse pressures induced by the sheep's foot roller are small compared with those produced by vibrating rollers.

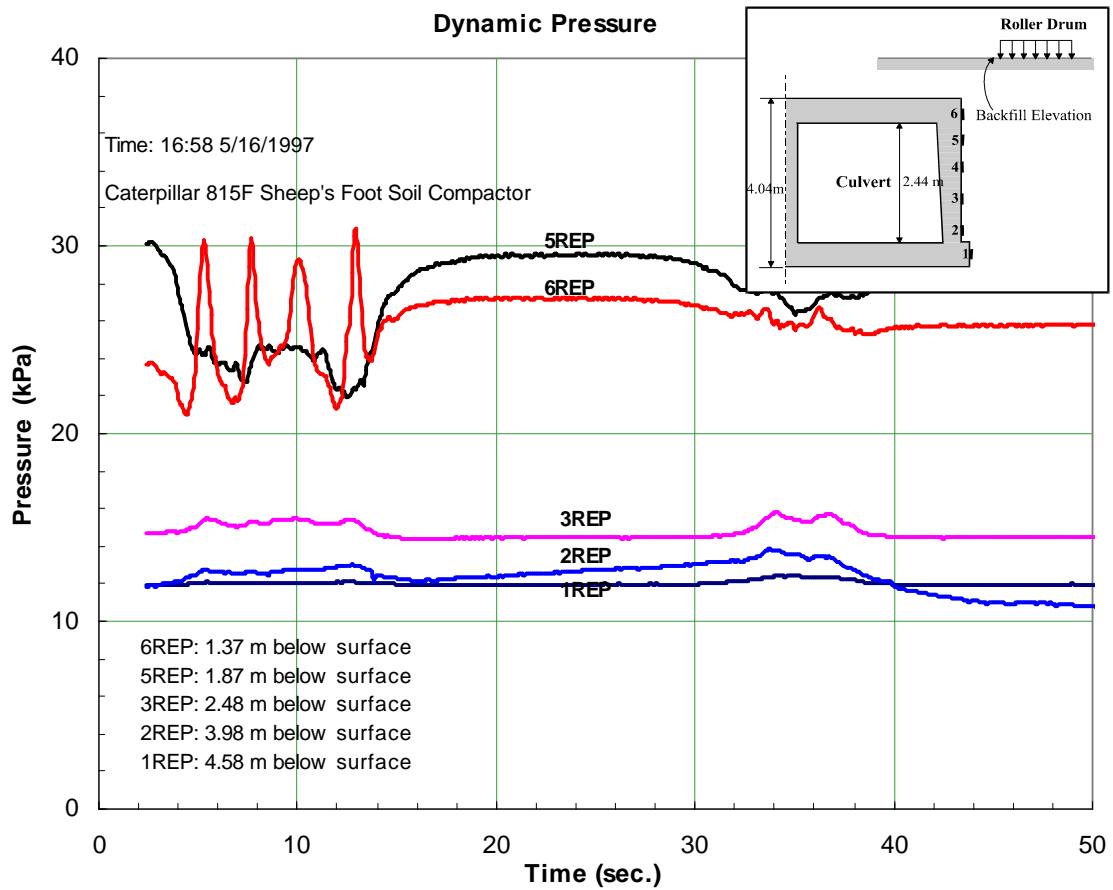


Figure 9-10 Typical Recorded Dynamic Pressure Pattern  
When Backfill over Culvert Roof

### 9.3 Analysis of Dynamic Earth Pressure

#### 9.3.1 Analytical Solution - Lateral Pressure Increment under a Finite Uniform Load

The distribution of lateral pressure acting against a vertical wall due to a static surface surcharge was first reported by Spangler (1938), who concluded that the magnitude of the pressure can be approximated by doubling the Boussinesq's elastic solution for lateral stress induced by an infinite linear load. A similar conclusion was supported by Smolczyk and Hilmer (1979) through a model test and a finite element analysis. Seed and Duncan (1986) proposed a hysteretic model, in which the lateral pressure is calculated directly by doubling the Boussinesq elastic analysis under a finite distributed load. The Boussinesq horizontal pressures induced by a finite uniform distributed load can be obtained by integrating the linear distribution of a roller load along its drum width, as explained in the following paragraph.

In the Boussinesq solution, loading by a compactor roller drum is modeled as a uniform load of finite length perpendicular to the wall. The pressure from the rubber tires of a roller can also be approximated as a uniformly distributed load. To estimate the peak response, the dynamic centrifugal force from the vibrating compactor can be replaced by an equivalent static force. The face of the wall is assumed to be parallel to the  $z$ -axis (Figure 9-11), and the surface on which the load is applied is parallel to the  $x$ -axis. The Boussinesq point load solution was integrated (Duncan and Seed, 1986) to obtain the horizontal pressure increase,  $\Delta s_x$ , in the free field away from the wall, for points within the vertical plane that include the line load. The impulse pressure increase,  $\Delta s_h$ , acting

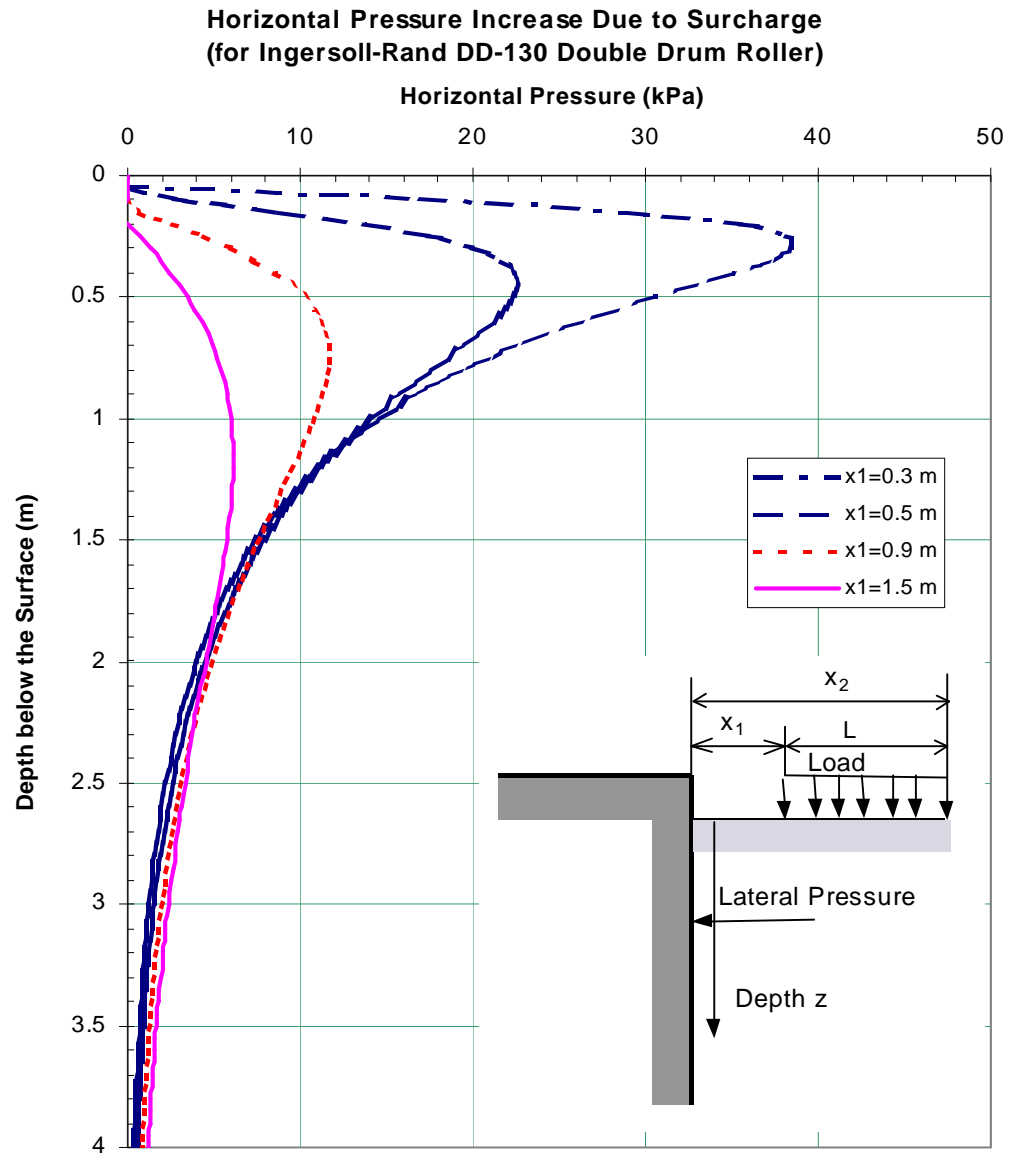


Figure 9-11 Boussinesq's Elastic Solution for Lateral Earth Pressure  
Induced by a Vibratory Roller Drum

against a nondeflecting wall was computed by doubling  $\sigma_x$  for the free field to take into account stress reflection at the wall. The closed form solution for  $\sigma_h$  is as follows (Seed and Duncan, 1983):

$$\Delta \sigma_h = 2\Delta \sigma_x = \frac{p}{pz} \left( \frac{1}{\left[1 + \left(\frac{z}{x_2}\right)^2\right]^{\frac{3}{2}}} - \frac{1-2\mu}{\left[1 + \left(\frac{z}{x_2}\right)^2\right]^{\frac{1}{2}} + \frac{z}{x_2}} - \frac{1}{\left[1 + \left(\frac{z}{x_1}\right)^2\right]^{\frac{3}{2}}} + \frac{1-2\mu}{\left[1 + \left(\frac{z}{x_1}\right)^2\right]^{\frac{1}{2}} + \frac{z}{x_1}} \right) \quad (2)$$

in which  $x_1$  and  $x_2$  = the distances from the wall to the near and far sides of the drum path, respectively (Figure 9-11), and  $\mu$  is Poisson's ratio. The distributed line load  $p=W/(x_2-x_1)$  is applied over the length of the roller,  $L=x_2-x_1$ , where  $W$  = the effective weight of the compactor. When this expression is used for a vibrating roller, the effective weight equals the static weight plus the dynamic centrifugal force. Table 9-2 summarizes the variables used for the Ingersoll-Rand DD130 and SP56 vibratory compactors.

Figure 9-11 illustrates the peak impulse pressure computed by Equation (2) for an Ingersoll-Rand DD130 roller for different distances from the wall. In Equation (2), the only unknown parameter is Poisson's ratio of the gravel. An estimated value of 0.35 was used in calculations in Figure 9-11. It is clear that for depths less than about 1.5 m, the lateral pressures are sensitive to the distance from the roller edge to the wall.

### 9.3.2 Distribution of Dynamic Earth Pressures

As illustrated previously, when a vibratory roller is close to a rigid wall, the magnitude of dynamic pressure might be significant. The recorded total compaction pressures induced by vibratory rollers at different depths are shown in Figures 9-12 and



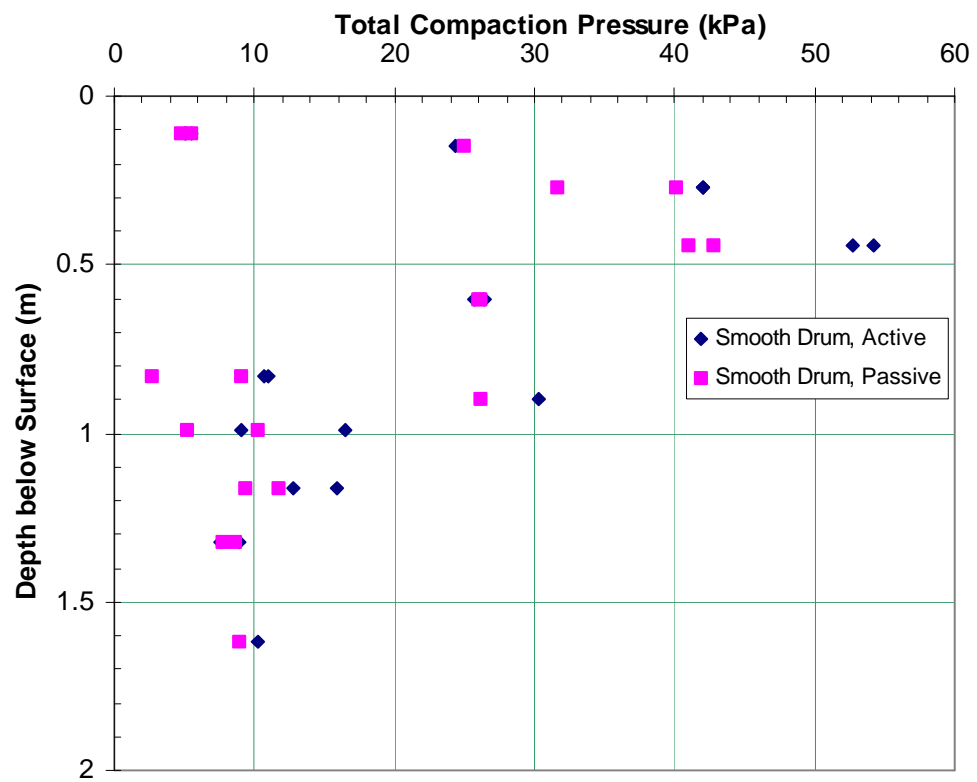


Figure 9-12 Total Compaction Pressure Induced  
by DD130 Double Drum Vibratory Roller

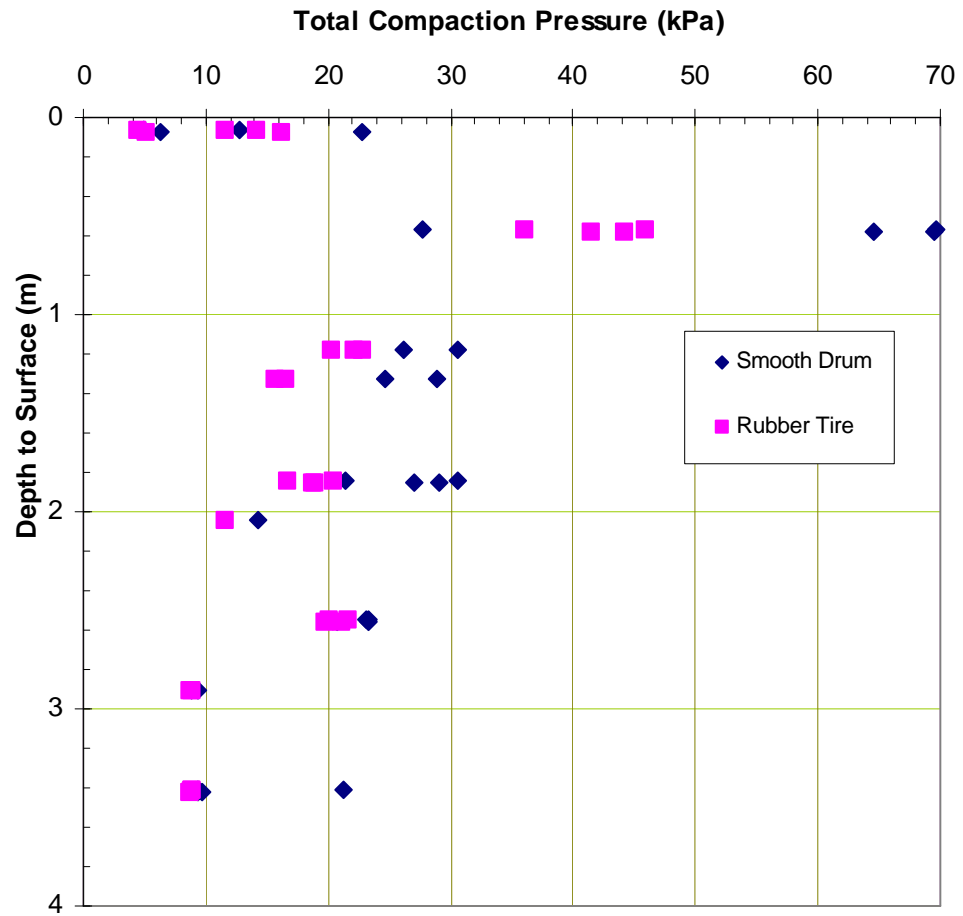


Figure 9-13 Total Compaction Pressure Induced  
by SP-56 Single Drum Vibratory Roller

9-13. The pressures in the figures are peak values taken from the pressure time history recorded by pressure cells. The recorded data indicate that the total compaction pressure attenuates rapidly with depth. A maximum impulse pressure of 70 kPa was recorded at the cell about 0.6 m below the ground, it decreased to about 22 kPa at a depth of 3.4m.

The impulse pressure, which reflects the response of soil under the current compaction pass, can be obtained from the difference between the total compaction pressure and initial residual compaction pressure. The maximum impulse pressures induced by the DD130 and SP-56 vibratory rollers are illustrated in Figures 9-14 and 9-15, respectively. The recorded pressures are compared with the Boussinesq lateral pressure distribution (dotted line) (Equation 2), and twice the Boussinesq pressure (solid line). Impulse pressures induced by the rubber tire wheel and rear drum (passive) were smaller due to the absence of the dynamic forces.

Figures 9-12 through 9-15 suggest that both the total pressure and impulse pressure are significant only at a shallow depth, and they decrease rapidly with depth. The results suggest that twice the Boussinesq's elastic solution provides a good approximation for the upper bound of the impulse pressure due to the active drums (drums which generate centrifugal force) during compaction.

#### **9.4 Residual Pressure Characterization**

The field instrumentation recorded significant differences in the lateral earth pressure distribution when the backfill was at or below the culvert roof and when the backfill was greatly above the roof. Since the instrumented culvert was designed to resist pressures under about 19 m embankment height, the rigidity of the structure was high.

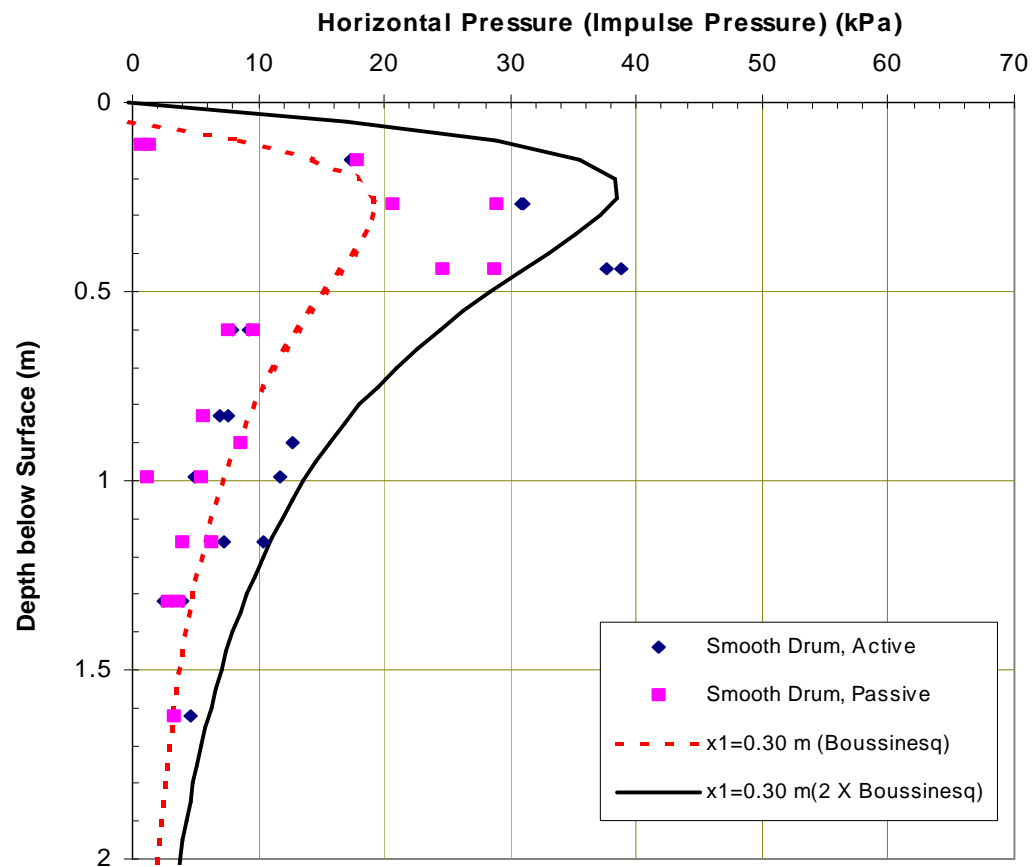


Figure 9-14 Lateral Impulse Pressure Induced by DD130 Vibratory Roller ( $x_1=0.3$  m)

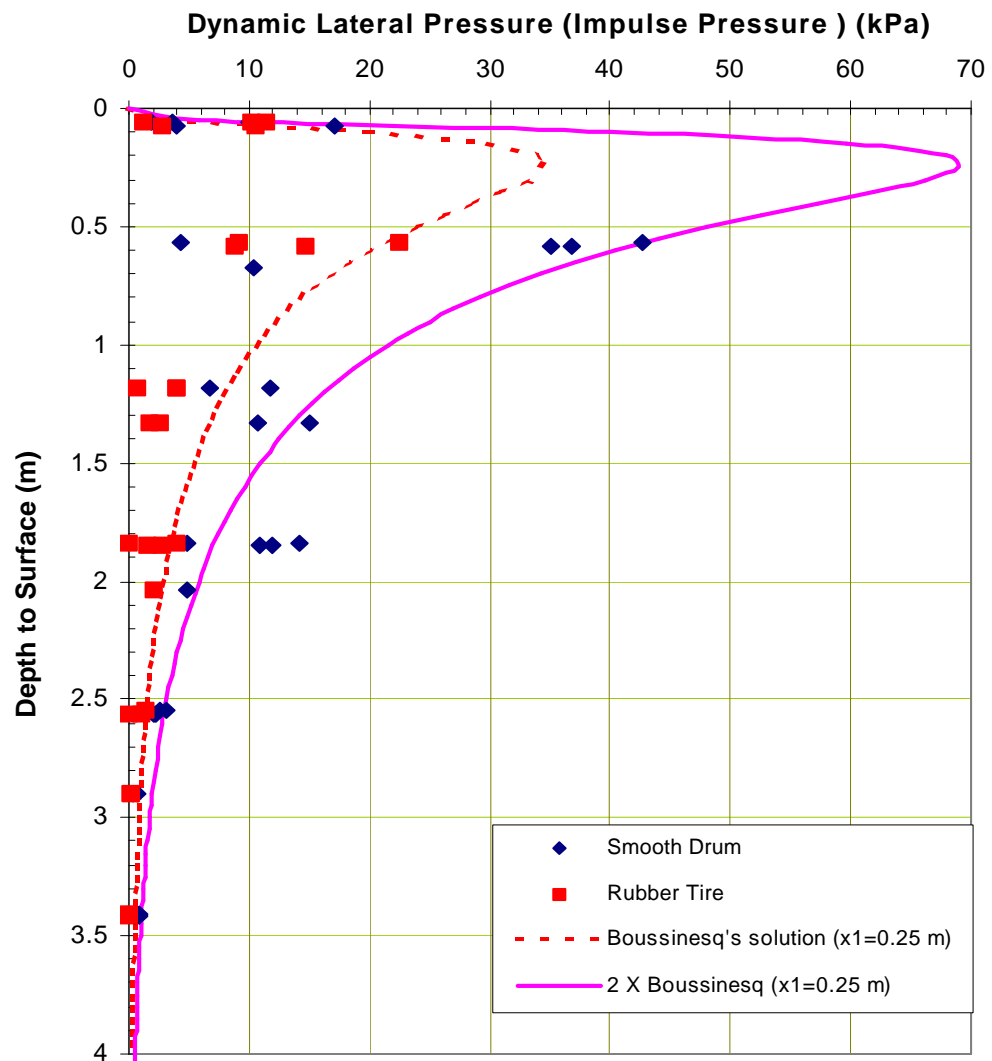


Figure 9-15 Lateral Impulse Pressure Induced by SP-56 Vibratory Roller ( $x_1=0.25$  m)

The lateral pressure under low embankment height (backfill height below or near the culvert roof) could be characterized as the residual pressure acting on a non-deflecting wall. Thus, the resulting lateral earth pressure distribution on the culvert wall can be compared with published results on the residual pressures on rigid retaining walls (Carder et al., 1977; Ingold 1979; Duncan and Seed, 1986).

As the backfill height was raised significantly above the culvert roof, the earth pressure acting on the buried culvert was more affected by soil-structure interaction result. The discussion of the residual compaction pressure is therefore limited to the low embankment height condition.

#### **9.4.1 Prediction of Residual Pressure Immediately after Compaction**

As previously indicated, the distribution of lateral pressure obtained by doubling the Boussinesq elastic solution can be used as an upper bound to the impulse lateral pressure acting on a nondeflecting wall due to compaction equipment. If the backfill material behaved in an ideally elastic manner, after the equipment passed by, the lateral pressure would return to that which existed prior to the compaction pass. In an approximate sense this is what was observed after several passes of the equipment and the material is fully compacted. Prior to full compaction, the material behaves inelastically, and a portion of this dynamic pressure is “locked in” to the soil lift. This locked in stress corresponds to the incremental residual compaction pressure (incremental pressure) in Figure 9-3. The magnitude of the locked in stress decreases with subsequent passes until compaction is complete (for a given energy level) and the material becomes nearly elastic. Therefore, the magnitude of residual horizontal pressure  $\sigma_h$  at a certain depth after

compaction is an accumulation of all previous incremental residual compaction pressures.

Assuming that noncompacted lateral stress can be represented by  $K_0$  condition, adding the effect of soil self-weight, or geostatic stress, the total lateral pressure,  $\mathbf{s}_h^{total}$ , immediately after full compaction can be expressed by the following equation:

$$\mathbf{s}_h^{total} = K_0 \mathbf{g}z + \Delta \mathbf{s}_h'' \quad (3)$$

where,  $K_0$  = coefficient of earth pressure at rest,  $\gamma$  is unit weight of backfill,  $z$  is the soil depth to be considered, and  $\mathbf{s}_h''$  is the compaction induced horizontal residual pressure.

However, the recorded maximum incremental pressure after one pass of compaction was only 10%, and this magnitude decreased with number of passes. Because the initial residual compaction pressures were also observed to be subject to a “stress relaxation” process, the lateral earth pressure decreased with time. Thus the recorded maximum residual pressure always occurred at shallow depth near the backfill surface (Figure 9-16). The recorded residual pressures were not likely to exceed the maximum impulse pressure induced by the roller. From the previous analysis, the impulse pressure,  $\mathbf{s}_h$  (Equation (2)), was concluded to be an upper bound of the accumulated previous initial residual compaction pressures  $\mathbf{s}_h''$ . So, substituting the approximate relationship  $K_0 = (1 - \sin \mathbf{j}')$  (Lambe and Whitman, 1979), the maximum lateral earth pressure immediately after the compaction can be estimated as:

$$\mathbf{s}_h^{total} = (1 - \sin \mathbf{j}') \mathbf{g}z + \Delta \mathbf{s}_h \quad (4)$$

Since soil near the ground surface exhibits highly inelastic behavior during compaction, the elastic based Equation (4) is not appropriate at shallow depths. Based on

the measured data, at shallow depths, an approximate expression can be used to predict the residual pressures:

$$s_h^{total} = K_1 s_z = \frac{s_z}{\sqrt{K_0}} = \frac{gz}{\sqrt{(1 - \sin j')}} \quad (5)$$

Equation (5) is compared with the measured residual pressure in Figure 9-16, which suggests that the recorded lateral residual pressure close to the surface is bounded by a straight line  $K_1$ . The use of a similar straight line to describe the measured earth pressures on rigid retaining walls was reported by others (Rehman and Broms, 1972; Carder et al., 1977). Equation (5) also suggests that the residual pressure near the ground surface may be independent of type and size of compaction equipment employed. The pressure difference between this line and the twice the Boussinesq pressure reflects the energy that is spent in the compaction process and that lost through vibration damping.

Equations (4) and (5) provide a reasonable approximation to the residual pressure remaining after the completion of compaction. The residual pressure exists at a shallow depth below the backfill surface. As the depth increases, total lateral pressure asymptotically approaches the  $K_0$  pressure.

#### 9.4.2 Residual Pressure Variation with Time

Field observations of the residual pressures have indicated the pressure relaxes over time. The relaxation of measured residual pressures is illustrated in Figure 9-17, for conditions with the backfill height 0.97 m above the culvert roof. During the period shown, there was no additional soil placed or compaction performed. Soon after the passage of compaction equipment (Caterpillar 815F) at time 12:55, the cell at the top registered the maximum lateral pressure of about 48 kPa whereas the bottom cell had the



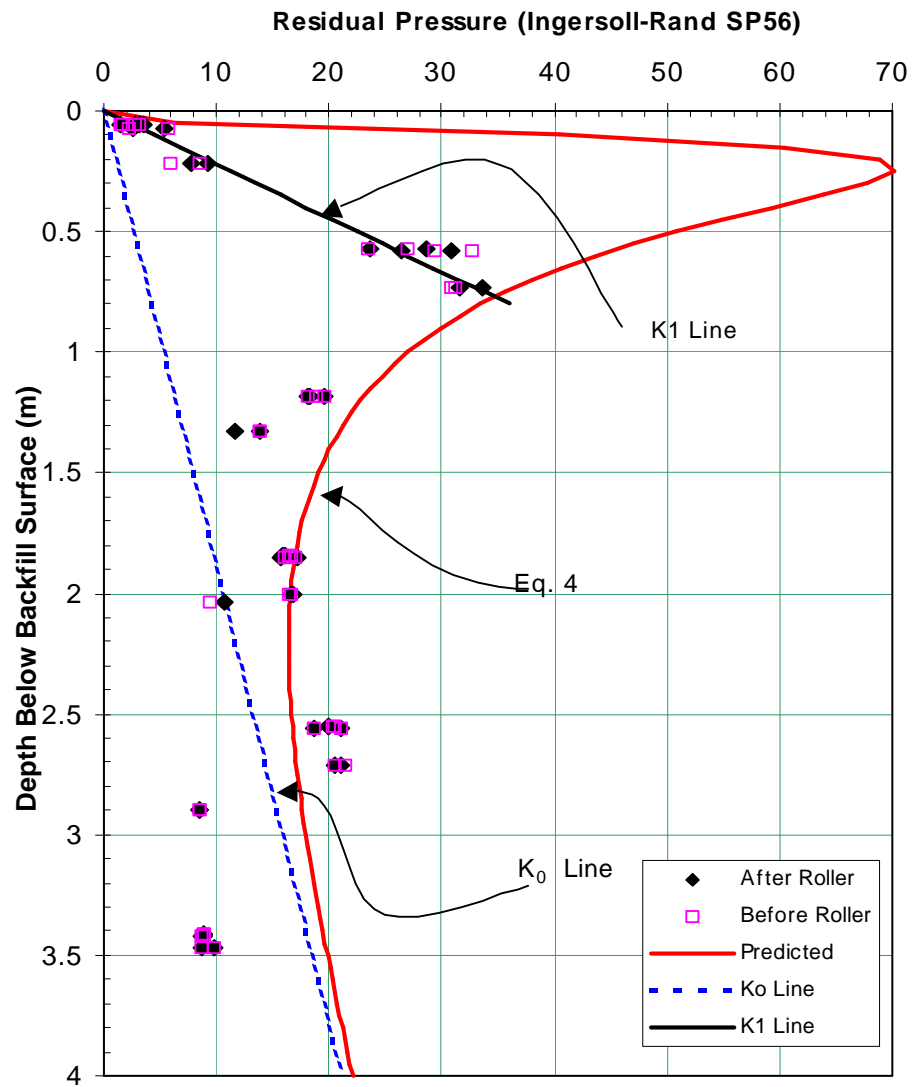


Figure 9-16 Measured and Predicted Lateral Residual Pressure on Wall  
(For Backfill Below Culvert Roof)

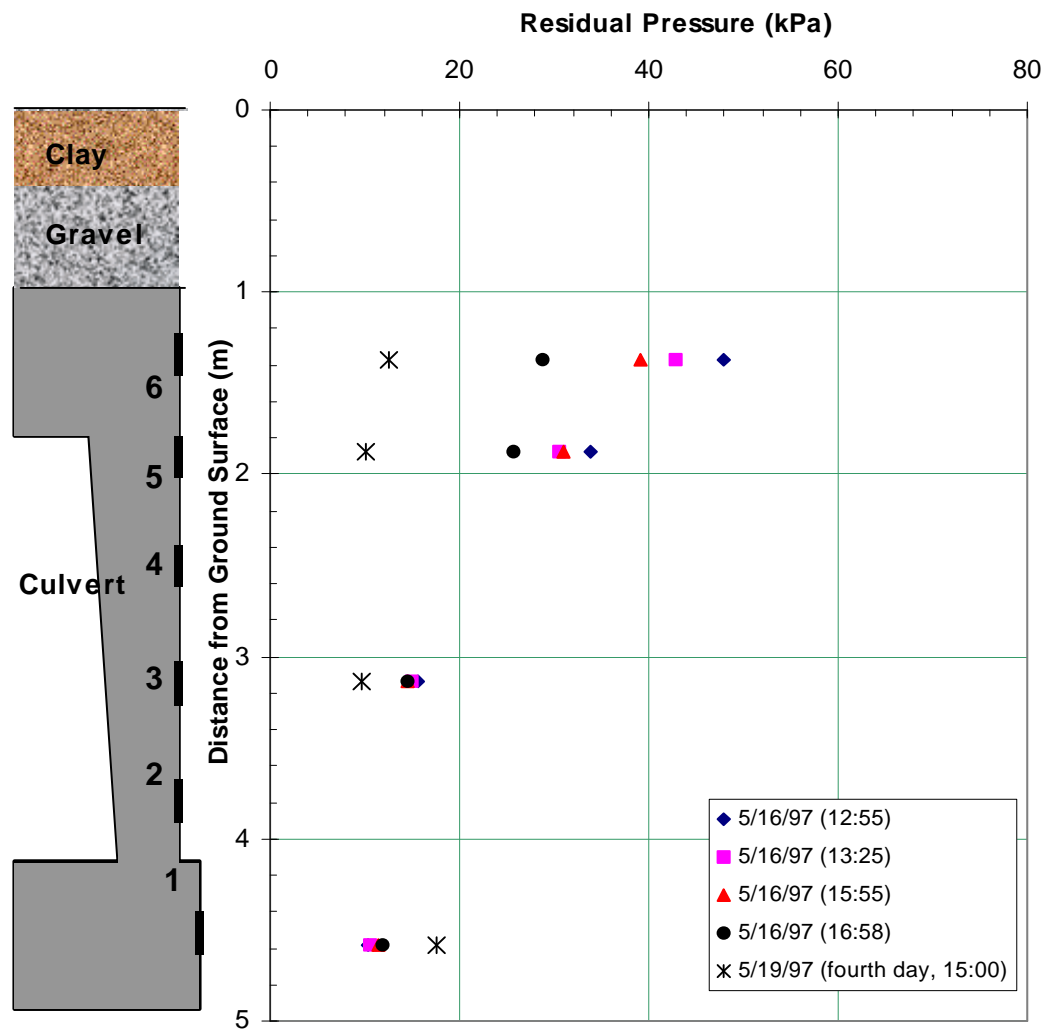


Figure 9-17 Lateral Residual Pressure Change with Time

minimum. Four hours later (time 16:58), the pressure at the top had decreased to about 30 kPa, with little change at the bottom. Although the impulse pressure during compaction was not available, the recorded residual lateral pressures at various times within a 4 hour period suggests that the major stress relaxation was limited to the soil zone close to the surface. Within the first 4 hours, the lateral pressure registered by a cell 1.37 m below the surface decreased 40% from the “initial” value, and pressure recorded by a cell 1.87 m below decreased 24%. The change of pressure in the two deeper cell was negligible. The lateral earth pressure distribution on the culvert wall 75 hours after the “initial” recordings is also plotted in Figure 9-17 illustrating a further decrease in pressure. There was little decrease observed after 75 hours.

The time effect on the residual pressure indicates that the maximum residual pressure predicted by Equations (4) and (5) will decrease to a lower value of “steady” state lateral earth pressure within a short time (several days) after the compaction. The “steady” state compaction was investigated by others (Duncan and Seed, 1986).

### **9.5 Structural Response of Box Culvert to Dynamic Earth Pressures**

The structural response of the culvert wall due to the dynamic earth pressures can be evaluated from measurements of the strain in both the external and internal sides of the culvert. In instrumentation Section A, which was the location of the resistance pressure cells (Figure 9-2) used to measure the dynamic pressure, six resistance concrete strain gages were embedded in the concrete in pairs at three different elevations. The change in the bending moment and in the axial forces can be calculated from these strain gages.

A typical time history of the dynamic concrete strain due to the dynamic lateral pressure is illustrated in Figure 9-18 ((a), (b), (c)), when the backfill elevation was about

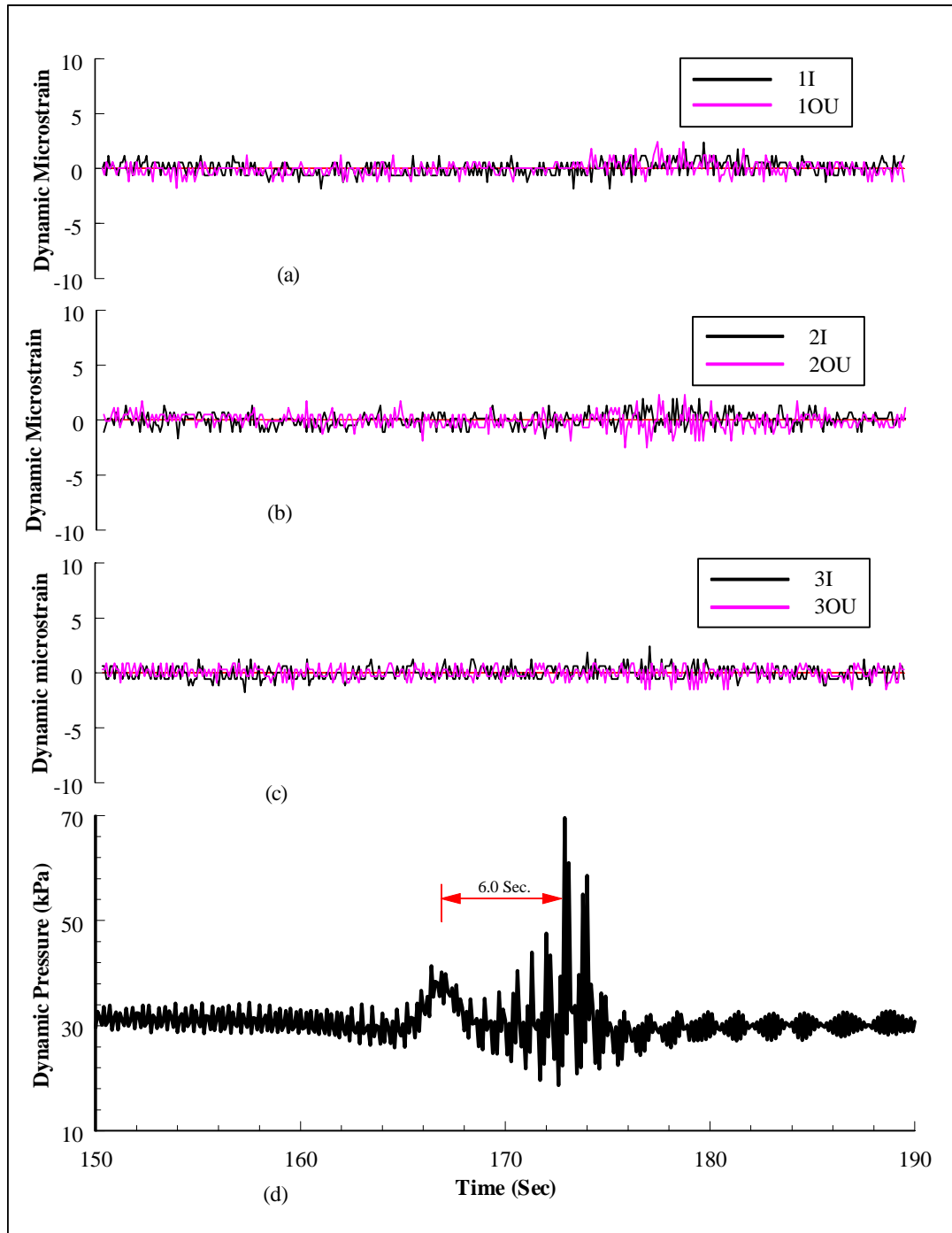


Figure 9-18 Structural Response to the Dynamic Lateral Pressures  
 (a) Concrete strain on the inside and outside of the wall at position 1  
 (b) Concrete strain on the inside and outside of the wall at position 2  
 (c) Concrete strain on the inside and outside of the wall at position 3  
 (d) Dynamic pressure in gage 5 at a depth 0.73 m below backfill surface  
 And roller 0.3 m from the wall

0.20 m below the culvert roof and the roller was 0.3 m from the wall. At the time of the recording, pressure cell (5REP), which was 0.73 m below the backfill surface, registered the maximum dynamic lateral pressure of about 70 kPa (Figure 9-18 (d)). The response of the strain gages to the dynamic pressure was very small. The maximum recorded concrete strain change took place in the gages installed at the middle of wall (Gages 2I, 2OU), but this change was less than  $\pm 5$  microstrains. These strain changes can hardly be distinguished from background noise (the resolution of concrete strain gages is about 1 microstrain). Since the magnitude of strain in concrete at cracking is about 153 microstrain, these strain changes due to the vibrating roller were negligible (less than 5% of cracking strain). Therefore, the vibrating roller operating near the culvert wall is not likely to cause cracks in the concrete. The structural response to the maximum dynamic lateral pressure suggests the culvert capacity is sufficient to resist the short duration lateral dynamic pressure without damage. This culvert was designed for a high embankment, and consequently was able to resist the dynamic construction loads. A culvert designed for only one or two meters of fill may not perform as well during the compaction process.

## **9.6 Summary**

From the results of the dynamic field instrumentation and the analysis of compaction pressures, the following conclusions can be drawn:

1. The influence of construction equipment on the magnitude of dynamic lateral earth pressure depends upon the stage of embankment height. When the backfill height is below or near the culvert roof, a vibrating roller close

to the culvert wall produces large impulse pressures as well as large residual pressures. When the backfill height was significantly (1.0 m higher) over the culvert roof, the induced dynamic pressures were small.

- Significant dynamic lateral earth pressures may be built up on a nondeflecting wall during construction when the compaction equipment is close to the culvert structure. Although different vehicles produce a vast range of dynamic pressure patterns, vibrating rollers induced the largest dynamic impulse pressure and had the greatest effective depth.
- When the backfill was near or below the culvert roof, the largest recorded total dynamic lateral pressure was about 70 kPa in a shallow zone below the surface. This dynamic lateral pressure is a function of construction equipment, distance of equipment to wall, and soil properties. As suggested by Duncan and Seed (1983), it was found that the distance from equipment to wall was critical for the lateral pressure at shallow depths. Doubling of the Boussinesq elastic solution, in which a finite uniformly distributed load acts on an infinite half space, can be used to approximate the impulse lateral pressure. The recorded maximum impulse pressure was about 40 kPa.
- The lateral earth pressure after the removal of the roller can be approximated by a straight line  $K_1$  (equation (5)), and a combination of the  $K_0$  pressure and modified induced residual pressure (equation (4)). The  $K_0$  line is an asymptotic line for compaction induced lateral pressure. For the instrumented culvert wall the recorded maximum residual pressure was 35 kPa. The residual pressure decreases

with time, especially in the period immediately after compaction.

- Based on the measurements from the embedded concrete strain gages, the impulse pressures from vibrating compaction do not induce destructive response of the culvert. This is likely because the impulsive pressures are of relative short duration and very localized.
- In the current investigation, the instrumented culvert was designed for about 19 meters of embankment height, therefore, the impact of compaction induced dynamic lateral earth pressure was small. The response of flexible culvert designed for low embankment height to the dynamic lateral pressure may be large.
- When the backfill was above the culvert roof, construction equipment produced much smaller dynamic lateral pressure. This may also be attributed to the kneading static compaction roller that was used to densify the fine grained soil.

## 9.7 References

- Butcher, A. P., and Marsland A., (1989), "Measurements of Lateral Earth Pressures on Bridge Abutments," *Geotechnical Instrumentation in Practice - Purpose, Performance and Interpretation*, Proceedings of the Geotechnical Instrumentation in Civil Engineering Projects Conference. Nottingham, Britain, April 3-5, 1989, 341-356.
- Clayton, C. R. I., and Symons, I. F., (1992), "The Pressure of Compacted fill on Retaining Walls," *Geotechnique*, Vol. 42, No. 1, 127-130.
- Carder, D. R., Pocock, R. G., and Murray, R. T., (1977), "Experimental Retaining Wall Facility - Lateral Stress Measurement with Sand Backfill," *Laboratory Report 766*. Transport and Road Research Laboratory, Crowthorne, Berkshire, United Kingdom.
- Duncan, J. M., and Seed, R. B., (1986), "Compaction Induced Earth Pressures under  $K_0$  Conditions," *J. of Geotech. Engr. Div.*, ASCE, 112 (1), 1-22.
- Duncan, J. M., and Seed, R. B., (1991), "Estimation Earth Pressures Due To Compaction," *J. of Geotech. Engr. Div.*, ASCE, 117 (12), 1833-1847.
- Filz, G. M., and Duncan. J. M. (1996), "Earth Pressure Due to Compaction: Comparison of Theory with Laboratory and Field Behavior," *Trans. Res. Rec. No. 1526*, 28-37.

- Filz, G. M., and Brandon, T. L., (1993), "Compactor Force and Energy Measurements," *Geotechnical Testing Journal*, GTJODJ, 16(4), Dec., 442-449.
- Filz, G. M., and Brandon, T. L., (1993), "Static and Dynamic Measurements Using Embedded Earth Pressure Cells," *Trans. Res. Rec.*, No. 1432, 86-95.
- Ingold, T. S., (1979), "The Effects of Compaction on Retaining Walls," *Geotechnique*, Vol 29, No. 3, 265-283.
- Kohl, K. M., New, B. M., and O'Rourke, T. D., (1989) "Stress Cell Measurements for the Investigation of Soil-Pipeline Interactions during Vehicular loading," *Geotechnical Instrumentation in Practice - Purpose, Performance and Interpretation*, Proceedings of the Geotechnical Instrumentation in Civil Engineering Projects Conference. Nottingham, Britain, April 3-5, 1989, 717-733.
- Lambe, T. W. and Whitman, R. V. (1979), *Soil Mechanics, SI Version*, John Wiley & Sons.
- Rehman, S. E., and Broms, B. B., (1972), "Lateral Pressures on Basement Wall - Results from Full-Scale Tests," Proceedings, 5<sup>th</sup> European Conference on Soil Mechanics and Foundation Engineering, Vol. 1, 1972, 189-197.
- Seed, R. B., and Duncan, J. M., "Soil-Structure Interaction Effects of Compaction Induced Stresses and Deflections," *Geotechnical Engineering Research Report* No. UCB/GT/83-06, University of California, Berkeley, CA, 1983.
- Smolczyk, U. and Hilmer, K. (1979), "Horizontal Pressure Increment by Surcharge Load," *Proceedings of Design Parameters in Geotechnical Engineering*, British Geotechnical Society, London, Vol. 2, 131-139.
- Weller, K. A., Jr., and Kulhawy, F. H. (1982). "Factors affecting stress cell measurements." *J. of Geotech. Engrg. Div.*, ASCE, 118(12) 442-449.



**PART V**

**BACK ANALYSIS OF THE FAILED BOX CULVERT**

**IN SULLIVAN COUNTY, TN**

## Chapter 10

### Analysis of Earth Pressures on a Failed Box Culvert

#### 10.1 Introduction

A cast-in-place reinforced concrete box culvert (double cell, each cell  $4.6 \text{ m} \times 2.1 \text{ m}$  inside dimensions) under approximately 13 meters clayey shale fill failed shortly after being placed in service (Chapter 3). Conventional compaction procedures were followed in the installation of the culvert, which was built on level ground under the positive projection condition (Spangler and Handy, 1982). A replacement culvert was designed such that it was much stiffer and could resist much higher earth pressures. The new culvert was built directly on the floor of the previous failed culvert. A schematic of a typical double cell box culvert is shown in Figure 10-1, and the dimensions of the two culverts are compared in Table 10-1. It is suggested that while the two culverts have similar dimensions, the replacement culvert is much more rigid as expressed in terms of the slenderness ratio of the roof,  $L_R/t_1$ , and wall,  $L_w/t_3$ , where  $L_R$  and  $L_w$  are the span lengths of the roof and wall, respectively, and  $t_1$ ,  $t_3$ , are the respective thicknesses (Figure 10-1).

To obtain a better understanding of the stresses acting on cast-in-place concrete box culverts under deep fills, and to investigate the conditions which resulted in the culvert failure, two sections of the replacement culvert were instrumented with pressure cells to

Table 10-1 Comparison of Dimensions of Original and Replacement Culverts

Culvert	External Dimensions (m)		Internal Dimensions (m)		Thickness (m)			Slenderness Ratio	
	Height $t_h$	Width B	Span $L_R$	Height $L_W$	Slab $t_1$	Internal Wall $t_2$	External Wall $t_3$	Roof $L_R/t_1$	Wall $L_W/t_3$
Original	2.77	9.91	4.57	2.13	0.32	0.25	0.25	14.28	8.52
Replacement	3.66	9.91	4.15	2.13	0.76	0.46	0.61	5.46	3.49

record earth pressures during construction as well as under service loads. Measurements from the instruments on the replacement culvert were used to develop a computer model to estimate the stresses acting on the failed original culvert.

## 10.2 Analytical Procedure

Since only a limited amount of data on the material properties was available from the original culvert system, the following three-step analytical procedure was used to predict the performance of the failed culvert based on an analysis of the instrumented

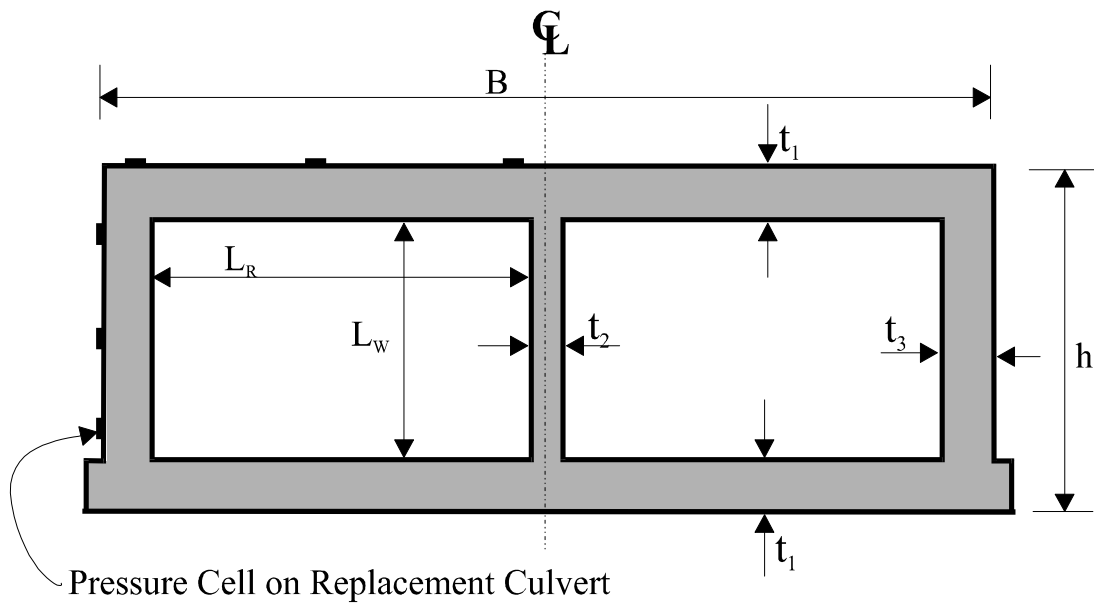


Figure 10-1 Illustration of Culvert Dimensions

replacement culvert. (1) Analysis of the replacement culvert based on “calibrated” parameters obtained from a back prediction of field measurement results. (2) Analysis of the original culvert using calibrated parameters to estimate the probable earth pressures. (3) Comparison of the structural capacity of the failed culvert to these probable earth pressures, in terms of axial force and bending moments.

In the first step, a finite element model was developed to analyze the replacement culvert. The material parameters used in the model were “tuned” or “calibrated” until the numerical results reasonably matched the earth pressures from more than three years of instrumentation measurements. Because of the failure of the original culvert, special reduced compactive effort was used when placing the backfill around the replacement box culvert. Limestone gravel was placed with very low compactive effort in the bottom of an existing “V” shape cut excavated into the embankment surrounding the original culvert (Figure 10-2). A 2 m thick layer of loose clayey shale fill was spread immediately above the gravel. Above the loose fill, the backfill material was compacted in the conventional manner and placed to a final embankment elevation of about 12 meters above the culvert roof. In the numerical simulation, the reduced compactive effort was represented by a reduced elastic modulus for the backfill gravel surrounding the structure. This approximation of reduced compaction effort in elastic modulus is supported by the literature (Hicher, 1996). Laboratory test results on the surrounding gravel have also shown that the elastic modulus under conventional compaction efforts would likely have a higher value than the value used in the analysis (see Appendices). The approximate material boundary between the firm residual clay and the fresh shale was obtained by a

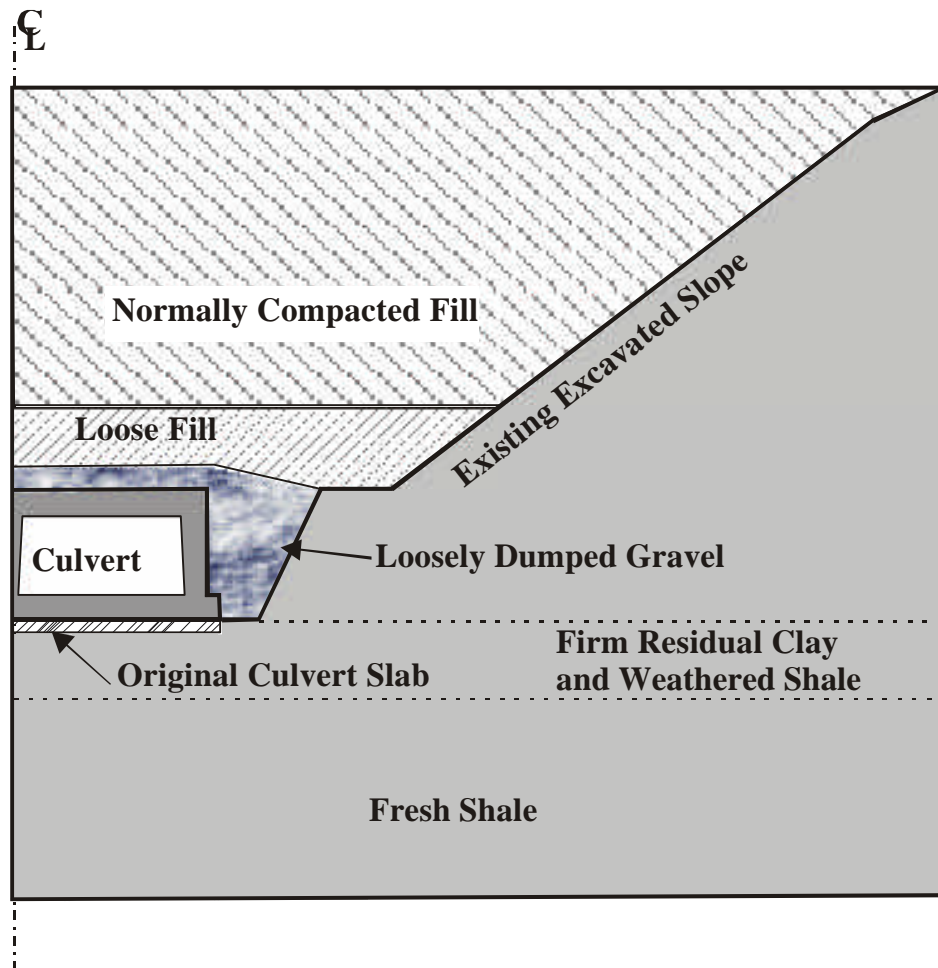


Figure 10-2 Schematic of Backfill Conditions of Replacement Culvert  
(Sullivan County, TN)

post failure subsurface boring (TDOT, 1995). The shape of the existing slope was estimated based on observation during the construction. The general purpose commercial finite element code ABAQUS was used to model the replacement culvert, and details of the numerical analysis can be found in Chapter 7. The material properties were tuned in the numerical model until the “best fit” with field measurement results was achieved.

In the second step, calibrated material properties from the first step were used to analyze the failed culvert. However, the failed culvert was installed with conventional compaction practice, in which normal compactive effort was utilized in the gravel backfill operation. In the first step, the elastic modulus of gravel was found to be a critical factor affecting the magnitude of the horizontal earth pressures, which suggests that horizontal earth pressures are dependent upon the culvert installation method. Since it was impossible to determine the stiffness of gravel surrounding the original failed culvert, the probable range of gravel modulus was estimated, based on the laboratory tests on a representative gravel material. Therefore, during this step, probable earth pressures acting on the failed culvert could be obtained corresponding to various gravel modulus values. These earth pressures were also compared with the current as well as the previous AASHTO (12<sup>th</sup> edition, 1977) design guides.

Finally, in the third step, the structural response of the failed culvert under the probable earth pressures, expressed in terms of the internal axial forces, bending moments and shear forces, were compared with the structural capacity.

### **10.3 Measured Earth Pressures and Numerical Analysis of Replacement Culvert**

As illustrated in Figure 10-1, six identical Geokon model 4810 vibrating wire contact pressure cells with 180 kPa capacity were placed around one cell of the replacement culvert, three on the top and three on the side. Two sections under different embankment heights were instrumented.

#### **10.3.1 Measured Earth Pressures on Replacement Culvert**

Vibrating wire transducers used in the earth pressure cells have been reported to provide good performance for long term instrumentation (McRae and Simmons, 1991; Benmokrane, et al., 1995). According to the manufacturer (Flynn, 1999), the vibrating wire pressure cell has a linear pressure to output relationship for up to two times its rated capacity. The principles behind vibrating wire transducers can be found in detail in Chapter 4.

Although the hydraulic pressure cells were covered with gravel, they were installed on the concrete surface, and were subject to temperature variations which might affect the pressure readings. The temperature correction coefficient provided by the manufacturer is applied only to the pressure transducer (vibrating steel wire). Seasonal pressure changes of hydraulic pressure cell results have been reported elsewhere (Coyle and Bartoskwtz, 1976; Smolczyk et al., 1977; Felio and Bauer, 1984; Dunnicliff, 1988), both with vibrating wire and non-vibrating wire transducers. No correction method has been suggested to account for the effect of temperature on the fluid-filled pressure sensing element of the gages.

Field measurement of earth pressures under constant embankment height was used to correct the measured pressures for temperature fluctuations. The earth pressure measurement results for the roof and walls are shown in Figures 10-3 and 10-4, respectively. The average temperatures measured inside the pressure cells are also plotted in the same figures. During more than three years of monitoring, a strong seasonal pressure fluctuation was observed in all pressure cells. The recorded maximum difference in temperature was 12 EC, and a maximum measured variation of vertical earth pressure was 105 kPa, or 34% of the measured average pressure on the same cell. 71 kPa of variation in the horizontal pressure cells was recorded which was 64% of the mean value.

The measured pressures were corrected with respect to the temperatures at the first measurement under full embankment height (May 8, 1996). The datum temperature recorded at that time was approximately 15 EC. Details of the temperature correction technique can be found in the Appendix: "Temperature Effects on the Earth Pressure Measurement." The temperature corrected results are shown in Figures 10-5 and 10-6.

Seasonal pressure fluctuations were greatly reduced after applying the temperature correction. However, some periodic variation still exists, especially in the lateral earth pressures. The maximum variation of vertical pressure was reduced to 59 kPa (Cell 5BPPE), which was 24% of the average corrected pressure. A 50 kPa (Cell 2APPE) maximum pressure variation was found in the horizontal pressure acting on the wall. A better temperature correlation relationship was found for both the vertical and horizontal pressures recorded after about 9 months from completion of construction.



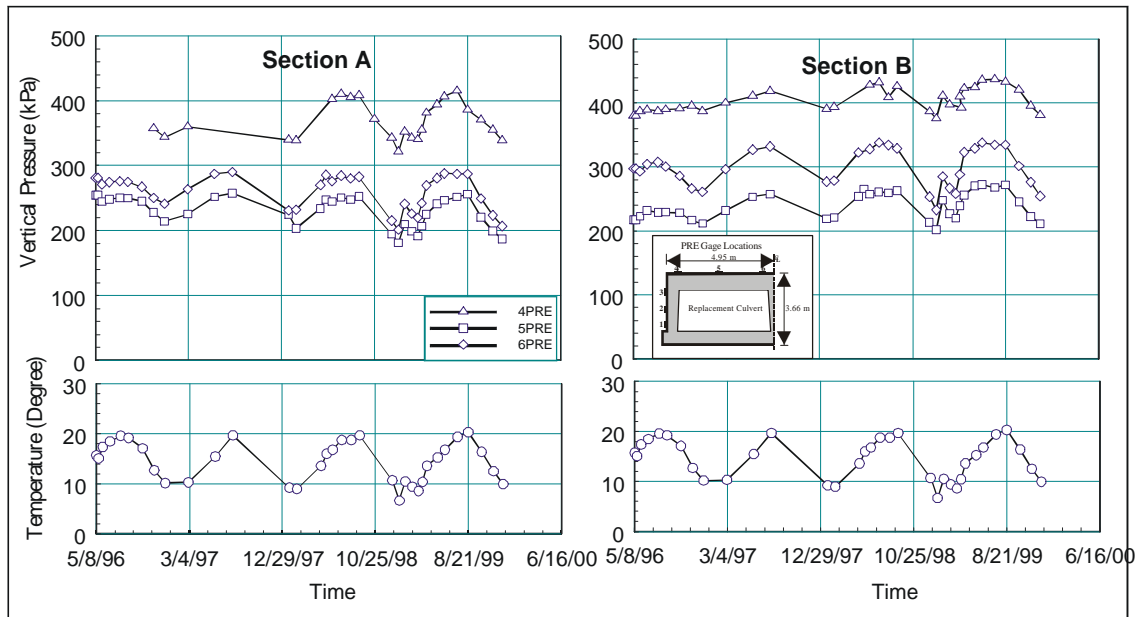


Figure 10-3 Observed Vertical Pressures on the Culvert Roof  
(Replacement Culvert, Sullivan County, TN)

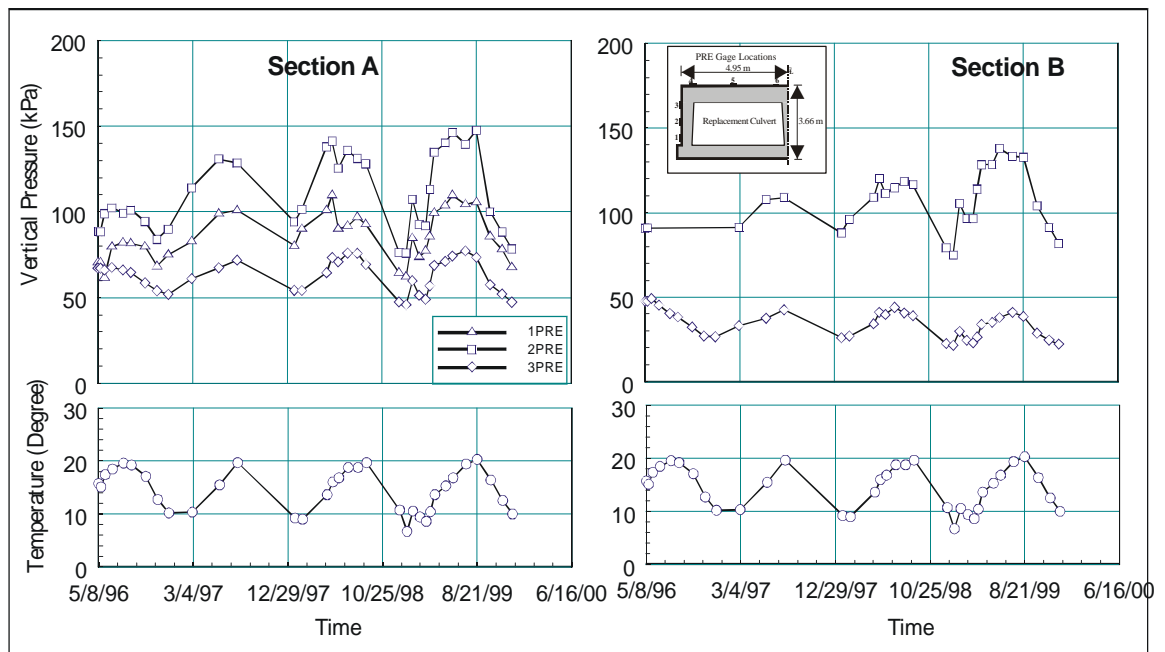


Figure 10-4 Observed Lateral Pressures on the Culvert Wall  
(Replacement Culvert, Sullivan County, TN)

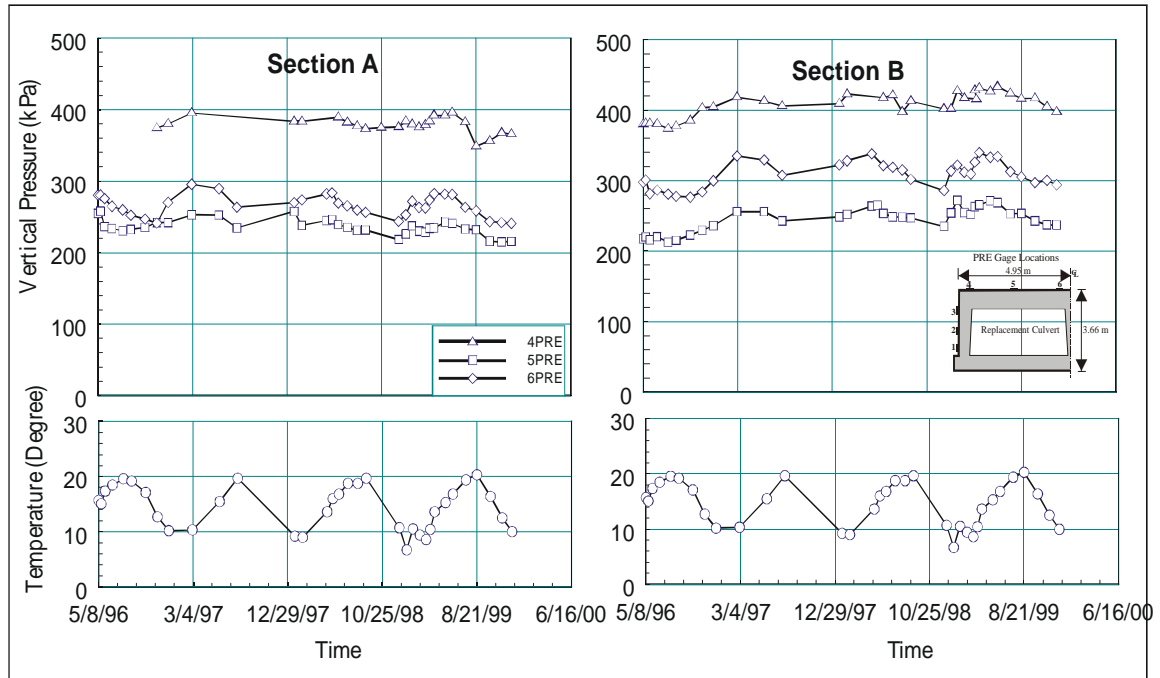


Figure 10-5 Temperature Corrected Vertical Pressures  
(Replacement Culvert, Sullivan County, TN)

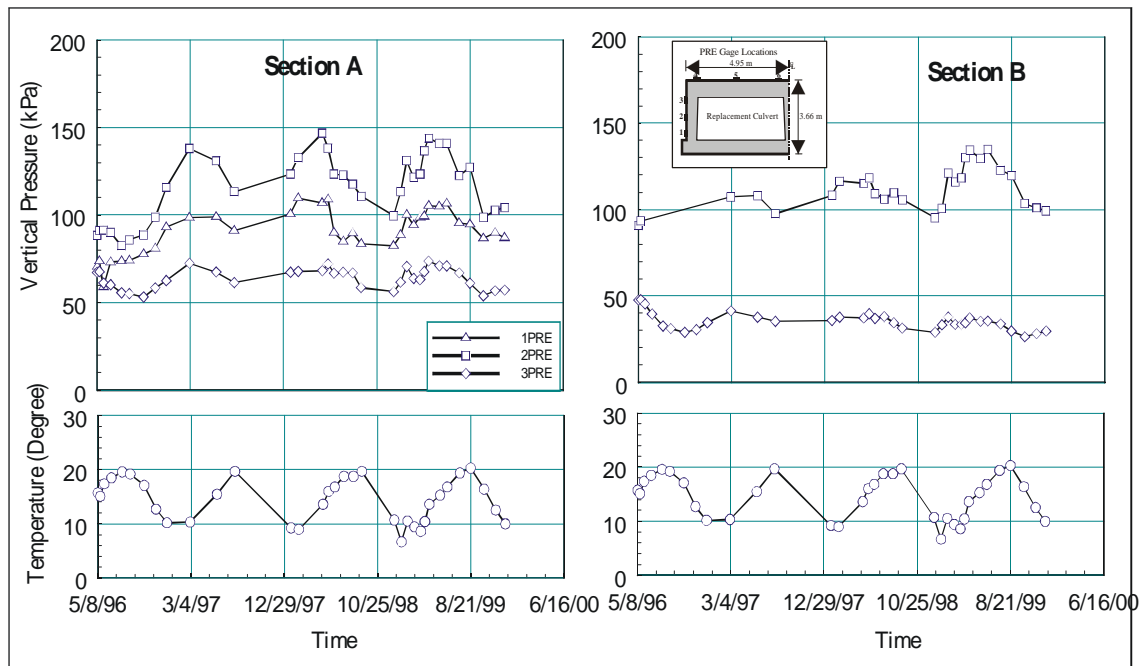


Figure 10-6 Temperature Corrected Lateral Pressures  
(Replacement Culvert, Sullivan County, TN)

### **10.3.2 Calibration of Material Properties**

The temperature corrected field pressure data were used to “calibrate” the numerical model input for the application of earth pressures on the replacement culvert. The reduced compactive effort in the surrounding gravel and 2 meters of clayey shale above was simulated by assigning a low elastic modulus. With limited soil property data available, some of the parameters had to be estimated based on engineering judgement. After carefully comparing the pressure results from the numerical analyses with the corrected field average pressures, the “best fit” material properties were determined as listed in Table 10-2. A comparison of predicted earth pressures and the range of measured earth pressures is illustrated in Figure 10-7.

The numerical analysis indicated two small zones of yielding, plastic deformation under the service loading. These zones were small and located near the culvert corners and center. It is suggested that the earth pressure distribution around the box culvert is not sensitive to the backfill soil strength. The modulus of the material immediately surrounding the culvert, however, was critical to the magnitude of earth pressures.

### **10.3.3 Comparison of the Measured Pressures with AASHTO Design Guides**

The predicted and measured earth pressures can be compared with the AASHTO recommended earth pressures (Figure 10-7). Since the numerical results were obtained by calibration of the model to the field measurements, the predicted and measured earth pressures are expected to be fairly close. To simplify the culvert design, AASHTO recommends a uniform earth pressure distribution. For design loads to be reasonable, the simplified pressure distribution should result in a structural response similar to that

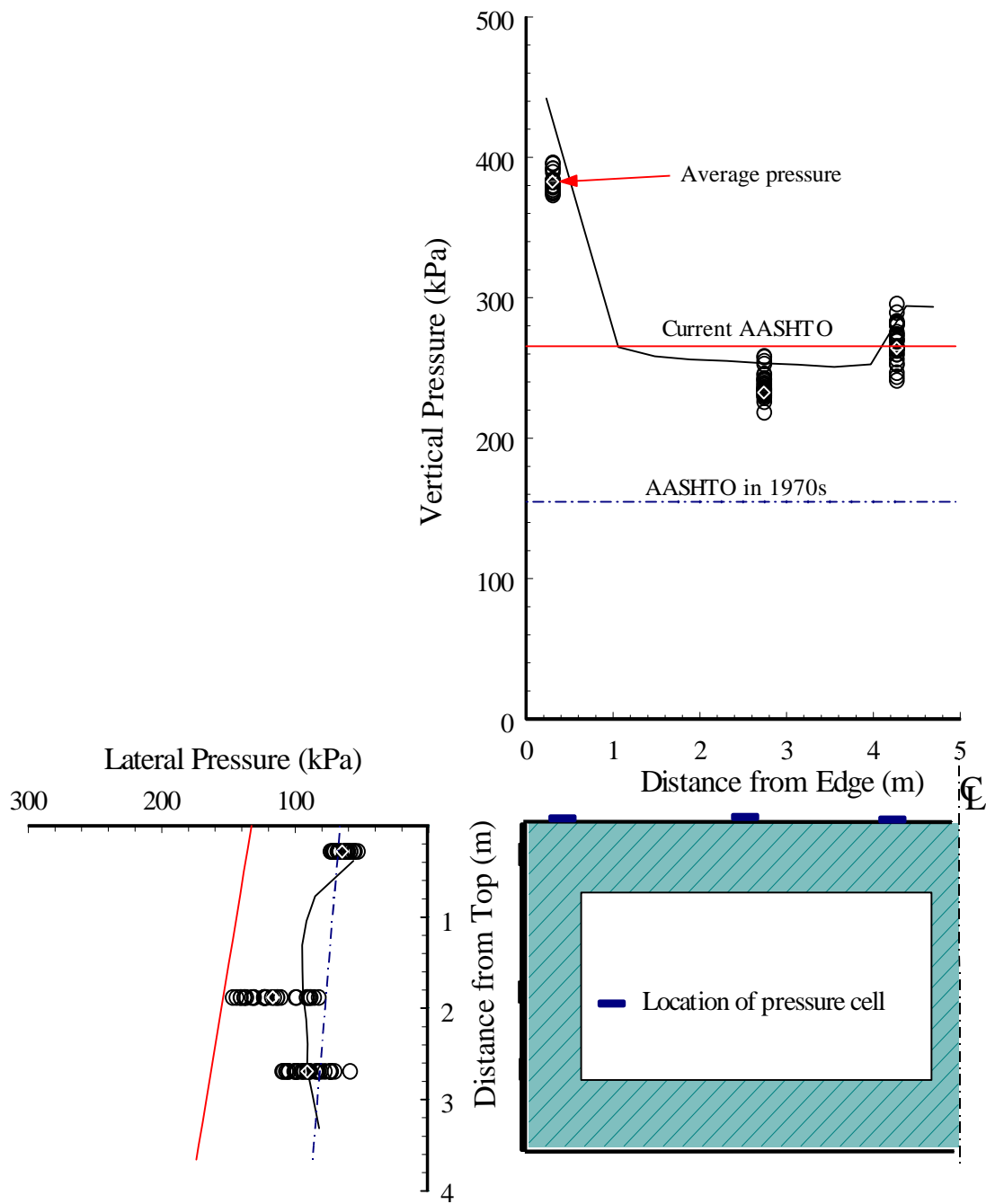


Figure 10-7 Comparison of Temperature Corrected Earth Pressures with FEM Analysis Results (Replacement Culvert, Sullivan County, TN)

Table 10-2 Material Properties from the Calibration Analysis of Replacement Culvert

Material Description Figure 10-2	Cohesion c (kPa)	Friction Angle $\phi$ (deg)	Dilatancy Angle $\psi$ (deg)	Elastic Modulus E (MPa)	Poisson's Ratio $\mu$	Source and Reference
Low density gravel	33	38.5	20	16	0.27	Shear strength from Law Engineering (1990), “tuned” modulus from measured pressure results.
Side soil near gravel and existing excavated slope	32	20	15	16	0.32	Direct shear tested strength, modulus from Penman (1975)
Loose fill above culvert	25	17	0	6.5	0.32	Estimated shear strength, “tuned” modulus from measured pressure results Poisson's ratio from Bowles(1988).
Normal fill away from culvert	32	20	15	16	0.32	Measured shear strength from TDOT (1995), modulus from Penman (1975)
Firm residual clay and weathered shale	Linear Elastic			65	0.30	Bowles(1988)
Fresh shale	Linear Elastic			112	0.25	Goodman(1989)
Concrete	Linear Elastic			4000	0.18	Modulus from lab test

produced by the actual pressure distributions.

Although the vertical pressure at the upper culvert corners was significantly higher than the AASHTO pressure, the current AASHTO (16<sup>th</sup> edition, 1996) vertical pressure is a good approximation at other locations of the culvert roof. The high measured pressure at the corner makes only a small contribution to the bending moment in the roof, and bending often governs the design. Measured horizontal earth pressure fell into a zone bounded by current AASHTO maximum and minimum pressure recommendations. It is suggested that the current AASHTO design pressures are a good representation of actual vertical and horizontal pressure acting on the culvert under conditions with reduced compactive effort.

Also shown in Figure 10-7 is the AASHTO recommended pressure distribution in effect at the time the culvert was designed (12<sup>th</sup> edition, 1977). The older guidelines were found to significantly underestimate both vertical and horizontal actual pressure for the replacement culvert under reduced compactive effort. It is worthy note that AASHTO recommended design pressures increased significantly from when the culvert was designed, and the time failure took place.

#### **10.4 Analysis of the Original Failed Culvert**

Although the original culvert was designed and constructed differently from the replacement culvert, probable earth pressures acting on the failed culvert could be rationally estimated based on the calibrated material properties from analysis of the replacement culvert. Axial forces and bending moments resulting from the probable earth pressures can then be compared with the capacity of the original culvert.

##### **10.4.1 Analysis Assumptions**

The following basic assumptions were made in evaluating the original culvert:

- Based on the site conditions, the original culvert rested on a level ground surface, and conventional compaction practice was utilized during the backfill installation. Therefore, the gravel and the clayey shale backfill materials were subjected to a normal compaction effort.
- The boundary conditions and material properties below the ground surface were identical to those used in the analysis of the replacement culvert . An illustration of the backfill conditions and the finite element mesh for the original culvert are shown in Figure 10-8. It was assumed that the original culvert was constructed on

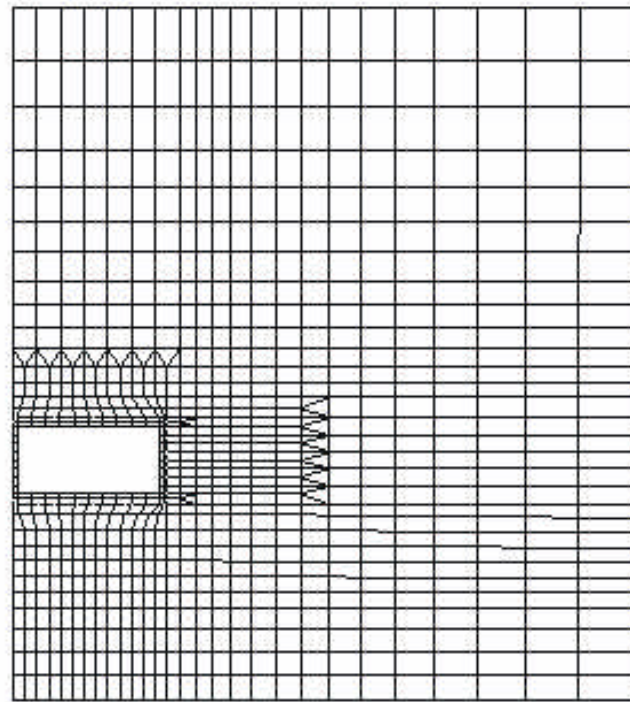
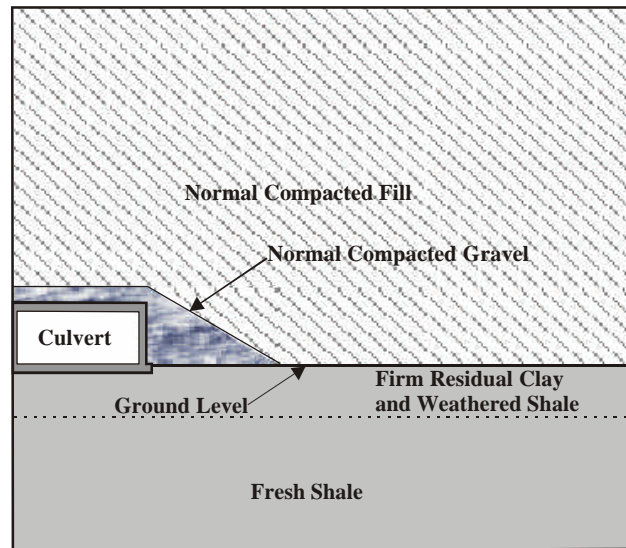


Figure 10-8 Assumed Backfill Conditions for Original Culvert and Finite Element Mesh (Original Culvert, Sullivan County, TN)

level ground, since the excavated slope in Figure 9-2 would not have been present.

- The normally compacted clayey shale shared the same strength and stiffness values as the material in the replacement culvert (“Normal Fill away from Culvert”, Table 10-2).

#### **10.4.2 Considerations for Compactive Efforts**

Since the horizontal earth pressure was highly dependent upon the compactive effort, and the modulus of gravel for failed culvert was unavailable, various probable earth pressures were obtained by inputting different values for the gravel modulus in the analysis. The various gravel modulus values represent different levels of compactive effort (Hicher, 1996).

Guidance on the selection of the magnitude of the gravel modulus was obtained from laboratory tests on samples from the Greene County culvert project. Representative 100 mm diameter gravel samples were prepared for triaxial tests. The gravel samples used in the laboratory tests were prepared at a similar dry density as measured in the field by the sand replacement method (ASTM D 4914-89). Table 10-3 summarizes the elastic modulus of the gravel and compares the measured values with those from the literature.

The nonlinear stress-strain response of the gravel can be approximated as a linear elastic material with an elastic modulus between the secant modulus  $E_s$  and initial modulus  $E_i$ . This range of modulus values is about 30 to 80 MPa, or approximately 2 to 5 times that of the modulus of the normal compacted clayey shale. To investigate the effect of gravel modulus on the culvert, several values of elastic modulus were used in the numerical analysis: 16, 32, 80 and 160 MPa. The material properties used in the analysis



Table 10-3 Comparison of Measured and Published Values of Elastic Modulus of Gravel

Confining Pressure (kPa)	Initial Modulus $E_i$ based on hyperbolic model (MPa)	Secant Modulus at Half of Failure Stress $E_s$ (MPa) (Lambe and Whitman, 1979)	Unloading-Reloading Slope in Triaxial Test (MPa) (Appendix)	Possible Range from Other Sources (MPa)
69	56	37	NA	56~105 (Lambe and Whitman, 1979)
103	63	44	137	
137	67	33	NA	69~172 (Das, 1999)
275	77	47	NA	

of original box culvert are listed in Table 10-4.

#### 10.4.3 Results and Comparison with AASHTO Design Guides

Earth pressures due to the different values of gravel modulus are illustrated in Figure 10-9. Although a wide range of moduli were used to reflect different compactive efforts, the vertical earth pressures on the culvert roof did not change significantly.

The current AASHTO design load underestimated the vertical pressures at the corner and the center of the culvert (middle wall), but it slightly overestimated the pressure at the central span (center of each cell). All of the predicted vertical pressures are significantly greater than the pressure recommended by the previous AASHTO design guide (12<sup>th</sup> edition, 1977).

The magnitude of the lateral earth pressure was influenced significantly by the modulus of the gravel around the culvert. The numerical analysis yielded parabolic horizontal pressure distributions for all cases, with the maximum earth pressure located at the middle of wall (Figure 10-9). It is apparent that the probable earth pressures were significantly greater than the early AASHTO recommended design loads in effect when

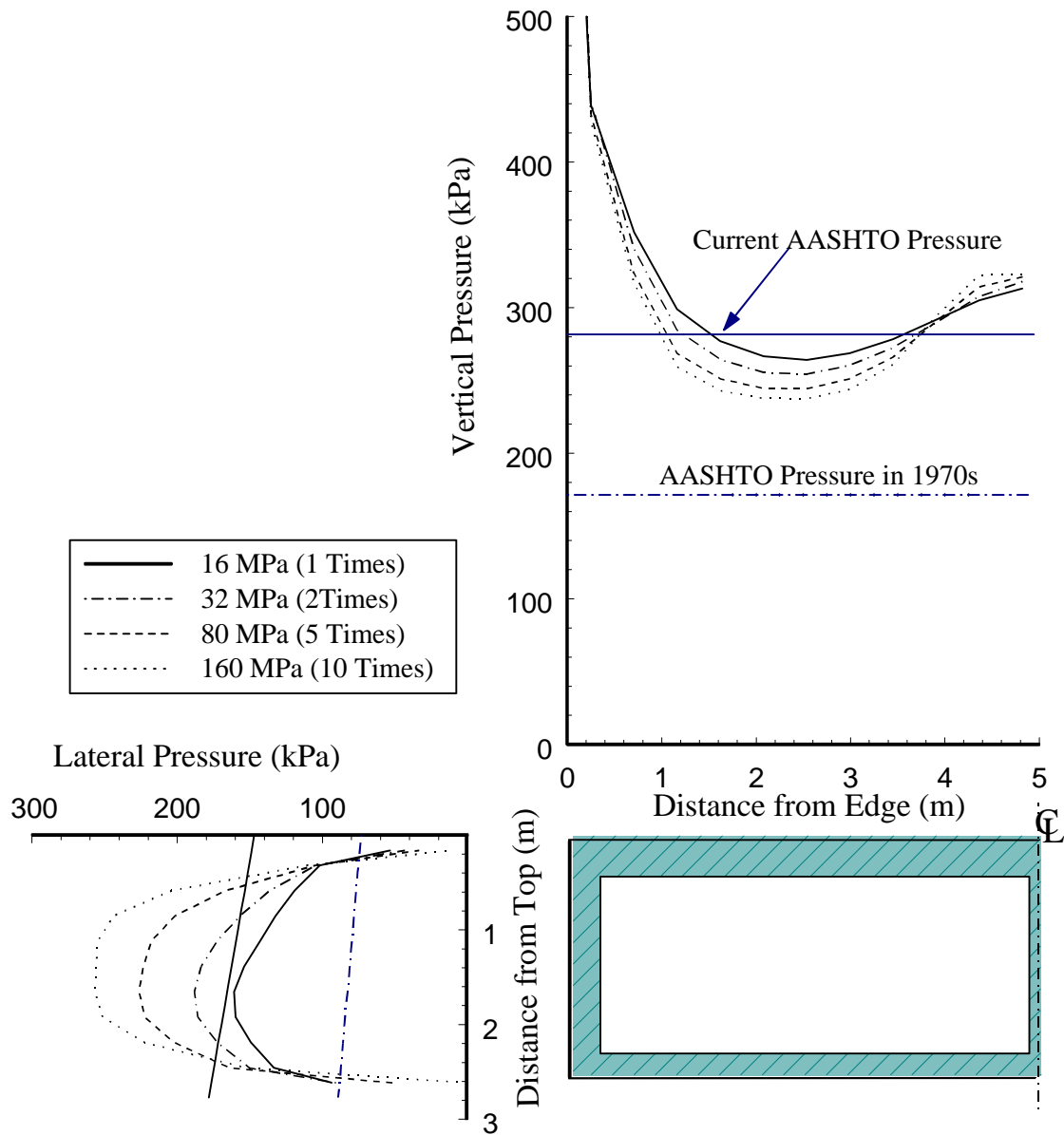


Figure 10-9 Comparison of Effect of Gravel Backfill Modulus on Earth Pressures (Original Culvert, Sullivan County, TN)

Table 10-4 Material Properties Used in Analysis of Original Culvert

Material Description (Figure 10-8)	Cohesion c (kPa)	Friction Angle $\phi$ (deg)	Dilatancy Angle $\psi$ (deg)	Elastic Modulus E (MPa)	Poisson's Ratio $\mu$	Source and Reference
Gravel	33	38.5	20	16, 32, 80, 160	0.27	Shear strength from Law Engineering (1990), lab tested modulus
Normal backfill	32	20	15	16	0.32	Direct shear test for strength from TDOT (1995), modulus from Penman (1975)
Firm residual clay and weathered shale	Linear Elastic			65	0.30	Bowles(1988)
Fresh shale	Linear Elastic			112	0.25	Goodman(1989)
Concrete	Linear Elastic			40,000	0.18	Modulus from lab test

the culvert was designed. Figure 10-9 also suggests that the current AASHTO (16<sup>th</sup> version, 1996) guidelines may not properly predict the lateral earth pressure distribution, especially at high values of gravel modulus. The current AASHTO pressure reasonably approximated the horizontal pressure with the 32 MPa gravel modulus, but it significantly underestimated the horizontal pressure with the stiffer gravel of 160 MPa modulus.

A comparison of Figures 10-7 and 10-9 suggests that based on both the analytical and measured results, the low compaction effort successfully reduced the lateral earth pressure acting on the wall. The vertical pressure reduction on the culvert roof, however, is minimal.

Since the structural rigidities of the two culverts are different (the difference can be represented by slenderness ratios shown in Table 10-1), the responses for the same gravel stiffness (gravel modulus = 16 MPa) should be different. This is observed by comparing

the numerical analysis results in Figure 10-7 and Figure 10-9. This difference in response under similar backfill heights is due to soil-structure interaction effects. Many laboratory experiments and field measurements (Handy, 1985; Bhatia and Baker, 1989; Ono and Yamaha, 1993; Lazeknik, 1997, Yang et al., 1997) have shown parabolic, trapezoidal or linear distributions of lateral earth pressure on retaining structures and box culverts. Soil-structure interaction occurs because the earth pressures acting on the structure depend upon the stiffness of the structure, and the stiffness of the soil depends upon the earth pressures. For buried structures, structural flexibility leads to greater horizontal pressure magnitudes. As a result, some flexible circular culverts may undergo horizontal pressures as high as the equivalent vertical pressure (AASHTO, 16<sup>th</sup> edition, 1996). It has been suggested (Handy, 1985) that the horizontal pressure distribution is also dependent on the characteristics of the soil structure interface or contact properties.

## **10.5 Response of Failed Culvert**

The structural response of the failed culvert under various earth pressures can be evaluated by comparing the corresponding internal forces with the structural capacity. The structural analysis code Visual Analysis was used to determine the internal forces due to the earth pressures obtained from the finite element analysis and AASHTO design guides.

### **10.5.1 The Internal Forces**

The box culvert was idealized as a box frame in plane strain condition. Linear elastic behavior for the concrete material was assumed. Although a vertical shear force along the culvert wall was found in the numerical analysis, it was neglected in the

determination of the internal force. The structural analysis model with various external pressures is illustrated schematically in Figure 10-10.

Three types of external pressure distributions were applied to the model: (1) the probable earth pressures obtained from numerical analyses, (2) the previous AASHTO (12<sup>th</sup> edition, 1977) pressures, and (3) the recent AASHTO (16<sup>th</sup> edition, 1996) pressures. The corresponding moments and shear forces in the original culvert roof and wall are shown in Figures 10-11 to 10-14.

#### 10.5.1.1 Moments and Shear Forces in the Original Culvert Roof

For all assumed external load distribution cases, the maximum moments and shears were found at the center of the structure. This coincides with the location where the

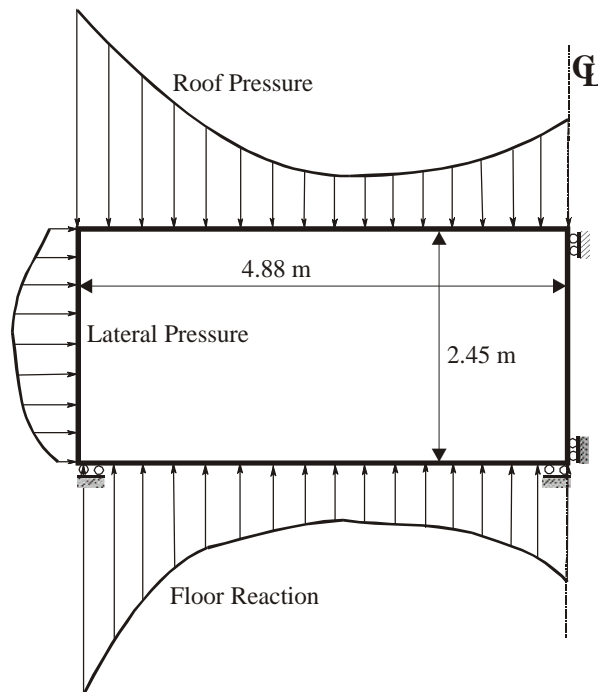


Figure 10-10 Culvert Model for Structure Analysis

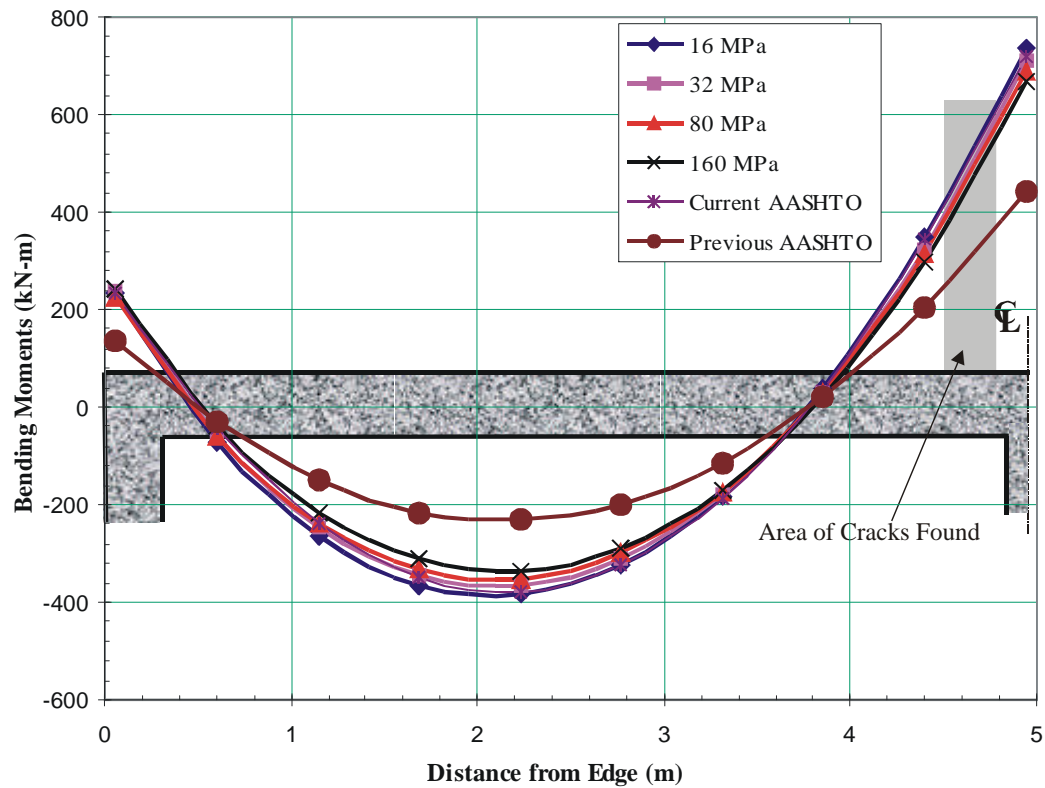


Figure 10-11 Calculated Bending Moment in Culvert Roof under Different Pressure Distributions (Original Culvert, Sullivan County, TN)

resistance concrete strain gage abruptly failed and the vibrating wire strain gages registered a significantly large tension strain.

The distribution of bending moments on the roof (Figure 10-11) indicates that the stiffer gravel induced a small moments in the mid span. Although the current AASHTO design load simplifies vertical load as uniformly distributed, the corresponding bending moments are still a good approximation of the moments induced by pressure distributions from the complex numerical analyses. The bending moments induced by previous AASHTO design load are significantly smaller than those corresponding to probable pressures and pressures recommended by current AASHTO design guide on the culvert roof.

The shear diagram on the roof (Figure 10-12) indicates that the previous AASHTO design pressure could lead to a significant underestimation of the shear force. The shear forces correspond to other earth pressure distributions were very close.

#### **10.5.1.2 Moments and Shear Forces in the Original Culvert Wall**

A parabolic distribution of bending moment was obtained under the different external earth pressures (Figure 10-13), with larger moments at the two ends of the wall. As expected, the gravel modulus had a significant effect on the bending moments in the culvert wall. Larger horizontal pressures yielded a smaller magnitude moment. The distribution of bending moment on the wall suggested that the primary bending moment acting on the wall was the moment transferred from the roof and the floor. The high horizontal earth pressure on the wall could reduce the overall bending moment on the middle of the wall. Therefore, the worst possible combination is high vertical pressure

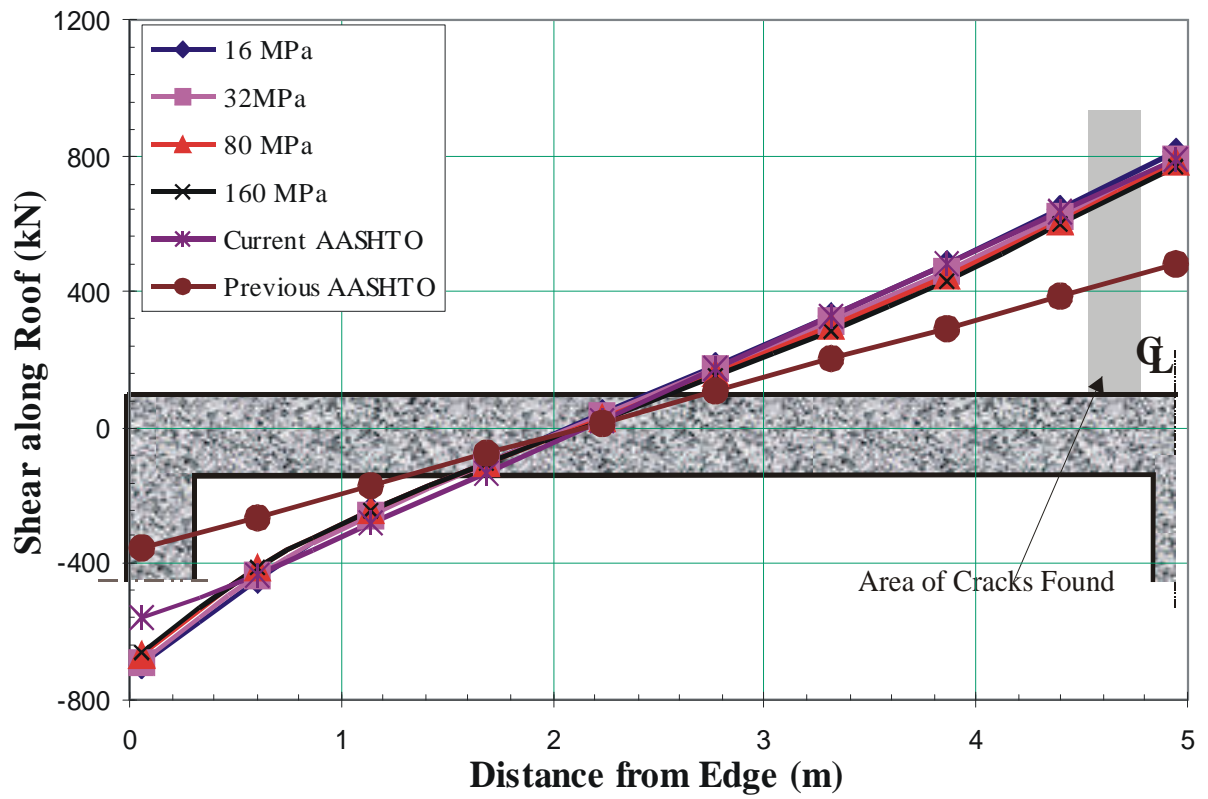


Figure 10-12 Calculated Shears on Culvert Roof Under Different Pressure Distributions (Original Culvert, Sullivan County, TN)



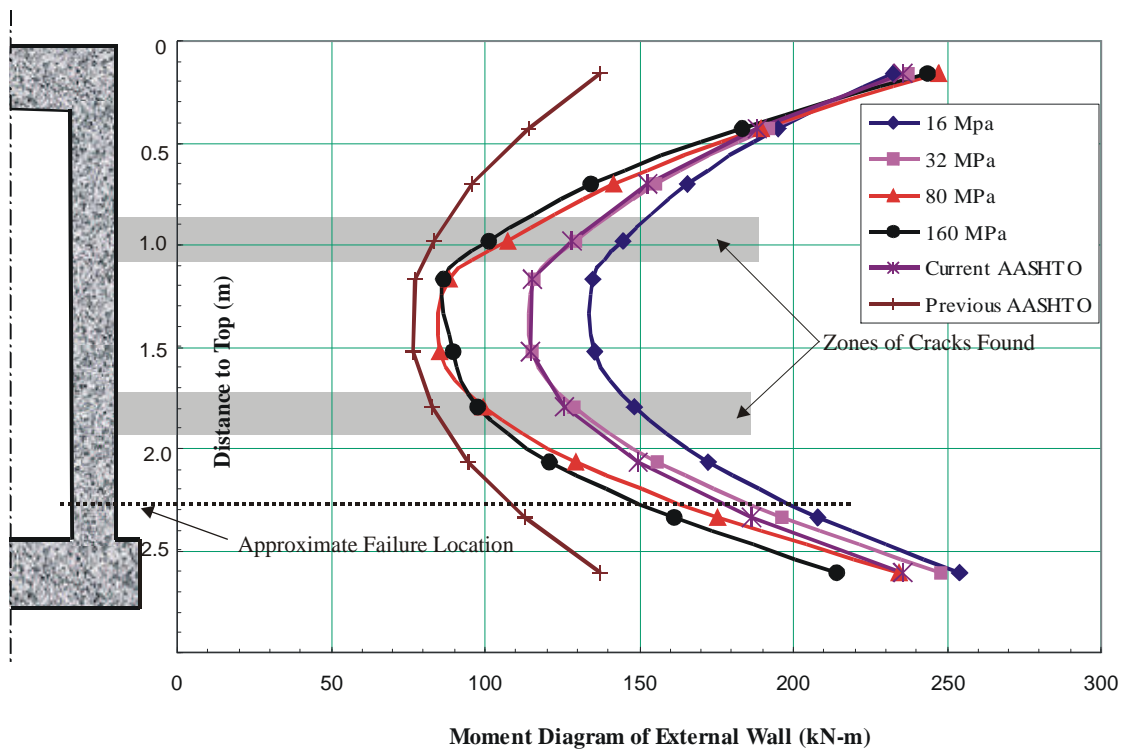


Figure 10-13 Calculated Bending Moments on Culvert Wall under Different Pressure Distributions (Original Culvert, Sullivan County, TN)

and low horizontal pressure, which is the condition that results when reduced compactive effort is utilized in the structural backfill installation. From Figure 10-9, the horizontal pressure corresponding to a reduced compactive effort (16 MPa of modulus) was greater than the minimum current AASHTO design load. So that, although there was a great variation of horizontal pressure induced by different compactive efforts, the current AASHTO design recommendation was still a good approximation of actual earth pressure from this point of view. Previous AASHTO design loads, however, considerably underestimated both the bending moment and the shear in the wall.

For the convenience of comparison, the approximate failure location and areas, where moderate cracks were found after post-failure examination, were also plotted on the wall in Figure 10-14. It is apparent that the failure location has fairly larger moments and shears (Figure 10-14) than those of where the cracks were found. Uncracked middle wall had lower moments and shears in magnitude.

### **10.5.2 Structural Capacities**

From the design of the as-built original culvert, the flexural and shear capacities of the structure could be obtained (Figures 10-15 and 10-16). The figures represent the section at the wall where the original culvert failed. In the capacity calculations, a standard concrete compressive strength of 20.7 MPa (3 ksi) was assumed.

The flexural capacity of the original culvert wall was represented in terms of axial force and bending moment interaction diagram, Figure 10-15. Each point in this figure indicates the combination of bending moment and axial compression force under different external earth pressures. Three different levels of capacities are also illustrated

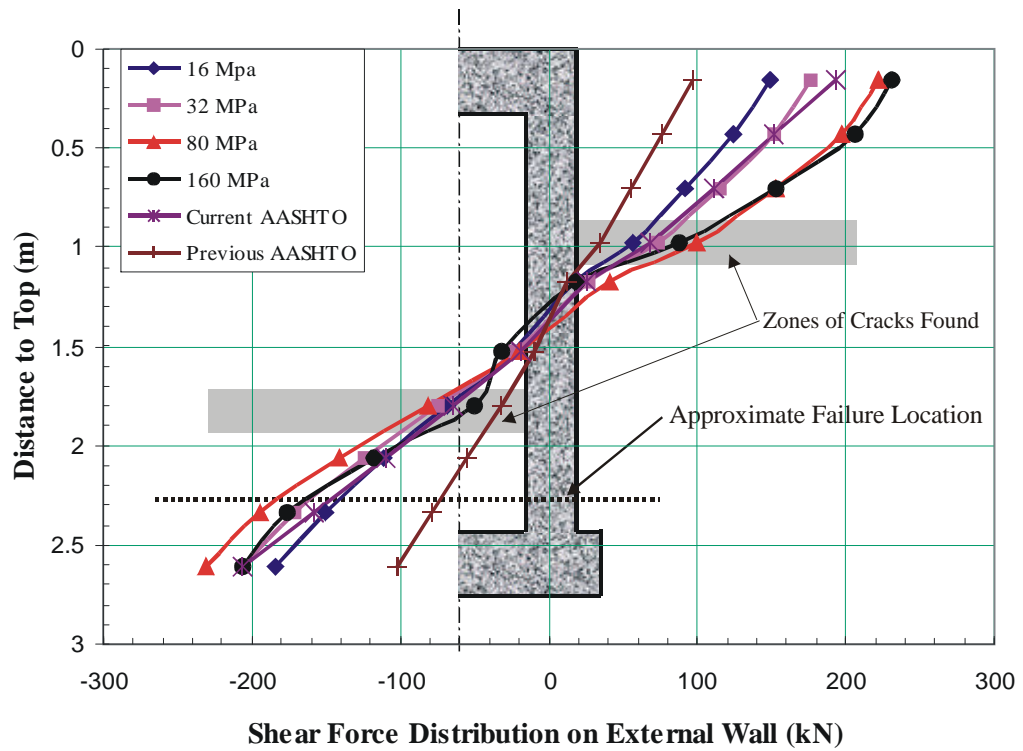


Figure 10-14 Calculated Shears on Culvert Wall under Different Pressure Distributions (Original Culvert, Sullivan County, TN)

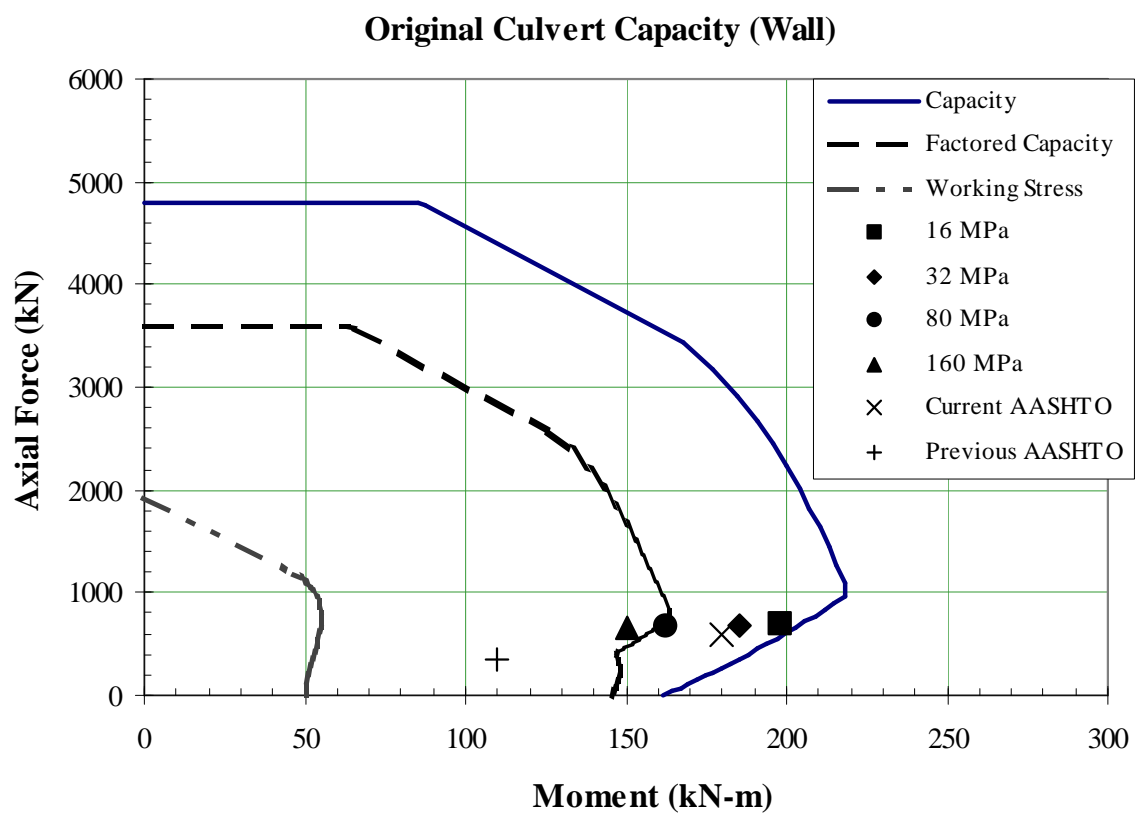


Figure 10-15 Axial Force - Moment Diagram of External Wall  
(Original Culvert, Sullivan County, TN)

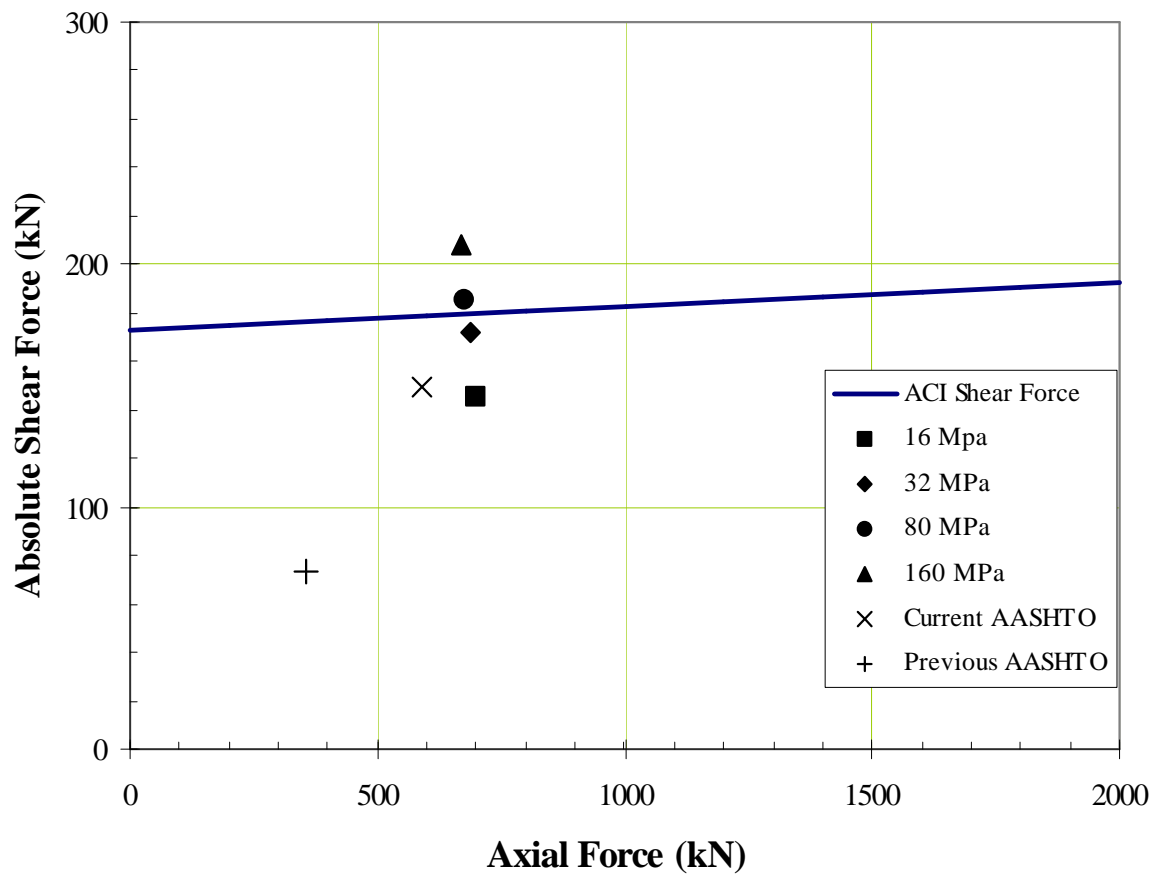


Figure 10-16 Axial Force - Shear Force Diagram of External Wall  
(Original Culvert, Sullivan County, TN)

in Figure 10-15: working stress, factored capacity and ultimate capacity. To ensure the culvert wall works functionally, the moment and internal force due to the external earth pressures should at least fall inside the area bounded by the factored capacity. At the location where the original culvert wall failed, the moments and the axial forces induced by normal compactive effort (represented by 32 and 80 MPa modulus) exceeded the factored capacity. A reduced compactive effort (16 MPa gravel modulus) even resulted in an unsafe structural response, and the point on the capacity diagram was very close to the ultimate capacity. Figure 10-15 also suggests that if the previous AASHTO design load had correctly represented the actual external earth pressures, the structure would have performed functionally. From the moment diagram in the culvert wall, an under estimation of actual vertical pressure on the roof by using previous AASHTO design guide resulted in a much smaller moment magnitude in the two ends of the wall. So that the moment induced by the probable earth pressures in the wall is close to its structural capacity.

The shear capacity recommended by AASHTO design guide does not consider the influence of axial force, which is conservative. The shear capacity in Figure 10-16 was obtained by ACI code. The current AASHTO design load and various probable earth pressures induced significantly higher shear forces than that of the previous AASHTO recommendation. The compactive effort had a considerably large influence on shear force at the bottom of the wall. The highly compacted gravel (modulus of 80 and 160 MPa) could result in a shear force at the bottom of the wall exceeding the shear capacity. The

normal compactive efforts also generated shear forces close to the capacity of the as built original culvert wall.

Comparing the current AASHTO (15<sup>th</sup> version, 1996) with the previous version (1977), the recommended lateral earth pressure was doubled while the vertical pressure was increased by 65% percent. From the analysis results, it is suggested that the original culvert was most likely under earth pressures which were significantly greater than the previous AASHTO design loads. The induced bending moments and shears force were close to their ultimate capacities. Therefore, the original culvert likely failed by a combination of flexural and shear failure. Figures 10-15 and 10-16 suggest that while the current AASHTO design load appropriately represented the earth pressures in terms of response in the axial force and the bending moments, it might underestimate the shear force at the bottom of the wall induced by excessive compactive effort.

## **10.6 Conclusions**

The probable earth pressure distributions on the culverts and their effect on the structural capacities, can be evaluated by a numerical analysis, in which the material properties are “calibrated” to reflect measured pressures.

Both the magnitude and the distribution of the earth pressures on the box culvert are the result of soil-structural interaction. Numerical analysis results indicated that the culvert backfill installation method had a significant influence on the earth pressures acting on the culvert. The magnitude of horizontal pressure was found to have a significant dependence on the compactive effort.

Both the field measurements and the numerical analysis results suggested that the previous AASHTO design load significantly underestimated the earth pressures. The current AAHSTO design load, however, appropriately approximated the earth pressure in terms of the axial load and bending moment, but might underestimate the shear force at the bottom of the culvert wall. Excessive compactive efforts may induce a large shear force.

The reduced compactive effort used in the installation of the replacement culvert successfully limited the horizontal earth pressure acting on the culvert wall. No significant vertical earth pressure reduction was found as the result of this technique. The numerical analysis indicated that the primary bending moment on the wall was induced by the vertical pressures on the culvert roof and the bottom slab. Large horizontal pressures could reduce the magnitude of moment on the wall.

The structural response analysis suggested that both the bending moment and the shear force at the location where the wall failed were close to the ultimate capacity, therefore, the culvert was likely under a combination of a excessive flexural and a shear stress.

## **10.7 References:**

- Bhatia, S. K. and Bakeer, R. M. (1989). "Use of the finite element method in modeling a static earth pressure problem." *Inter. J. for Ana. Methods in Geomechanics*, 13(2), 207-213.
- Benmokrane, B., Chekired, M., Xu, H. and Ballivy, G. (1995). "Monitoring behavior of grouted anchors using vibrating-wire gages." *J. Geotech. Engrg. Div.*, ASCE, 121(6), 466-475.



- Coyle, H. M and Bartoskwtz, R. E., (1976), "Earth pressure on precast panel retaining wall," *J. of Geotech. Engrg. Div.*, ASCE, 102(5), 441-456.
- Das, B. M., (1999), *Principles of Foundation Engineering*, Fourth Edition, Brooks/Cole Publishing Company.
- Felio, G. Y. and Bauer, G. E., (1984). "Monitoring and performance of bridge abutment," *Proceedings of International Conference on Case Histories in Geotechnical Engineering*. St. Louis, MO, 235-239.
- Flynn, John (1999) "Response of vibrating wire earth pressure cells at pressures exceeding stated capacity." Geokon Incorporated, Personal Communication with E. C. Drumm, 7-26-99.
- Handy, R. L. (1985). "The arch in soil arching" *J. Geotech. Engrg. Div.*, ASCE, 111(3), 302-318.
- Heger, F. J. and Selig, E. T., (1995). "Rigid pipe distress in high embankments over soft soil strata," *Transportation Research Record*, 1431, 46-52.
- Hicher, P. Y. (1996). "Elastic properties of soils." *J. Geotech. Engrg. Div.*, ASCE, 122(8), 641-648.
- Lambe, T. W. and Whitman, R. V. (1979), *Soil Mechanics, SI Version*, John Wiley & Sons.
- Lazebnik, G. E., (1997) "*Monitoring of soil-structure interaction - Instruments for measuring soil pressures.*" Chapman & Hall, New York.
- McRae, J. B. and Simmonds, T. (1991). "Long-term stability of vibrating wire instruments: one manufacturer's perspective." *Field Measurements in Geomechanics*, Balkema, Rotterdam. 283-293.
- Ono, K. and Yamada, M. "Analysis of the arching action in granular mass." *Geotechnique*, 43(1), 105-120.
- Smoltczyk, U. Hilmer, K., and Schuppener, B. (1977). "Earth pressure variations due to temperature change," *Proceedings of the Ninth International Conference on Soil Mechanics and Foundation Engineering*. Vol. 2, 725-733.
- Spangler, M. G. and Handy, R. L. (1982). *Soil Engineering*. 4<sup>th</sup> edition, Harper & Row, New York.
- Standard specifications for highway bridges*. (1977). 12th Ed., The American Association of State Highway and Transp. Officials (AASHTO), Washington, D. C.
- Standard specifications for highway bridges*. (1996). 16th Ed., The American Association of State Highway and Transp. Officials (AASHTO), Washington, D. C.
- Yang, M. Z., Drumm, E.C., Bennett, R. M and Mauldon, M. (1997). "Influence of compactive effort on earth pressures around a box culvert," *Proceedings of the Ninth*

International Conference on Computer Methods and Advances in Geomechanics,  
Wuhan, China, Nov. 2-7, 2021-2026.

**PART VI**

**ANALYTICAL EVALUATION AND CONCLUSIONS**

## Chapter 11

### The Influence of Highway Alignment on the Soil Pressures Acting on the Box Culvert

The highway alignment with respect to the orientation of the culvert can affect the horizontal pressures acting on the culvert wall. This effect can be evaluated analytically.

For an element at depth  $h$  from the ground surface in a homogenous elastic half space

Figure 11-1, its stress state can be determined as:

$$\{\mathbf{s}\} = \begin{pmatrix} \mathbf{s}_x & \mathbf{t}_{xy} & \mathbf{t}_{xz} \\ \mathbf{t}_{yx} & \mathbf{s}_y & \mathbf{t}_{yz} \\ \mathbf{t}_{zx} & \mathbf{t}_{zy} & \mathbf{s}_z \end{pmatrix} = \begin{pmatrix} K_0 \gamma h & 0 & 0 \\ 0 & K_0 \gamma h & 0 \\ 0 & 0 & \gamma h \end{pmatrix} = \begin{pmatrix} \mathbf{s}_2 & 0 & 0 \\ 0 & \mathbf{s}_3 & 0 \\ 0 & 0 & \mathbf{s}_1 \end{pmatrix} \quad (1)$$

where  $\gamma$  is the unit weight of soil,  $K_0$  is the lateral earth pressure coefficient at rest

$K_0 = \frac{\mu}{1 - \mu} < 1$ , where  $\mu$  is Poisson's ratio, and  $s_1$ ,  $s_2$  and  $s_3$  are the three principal stresses.

The principal directions correspond with the local element coordinate system.

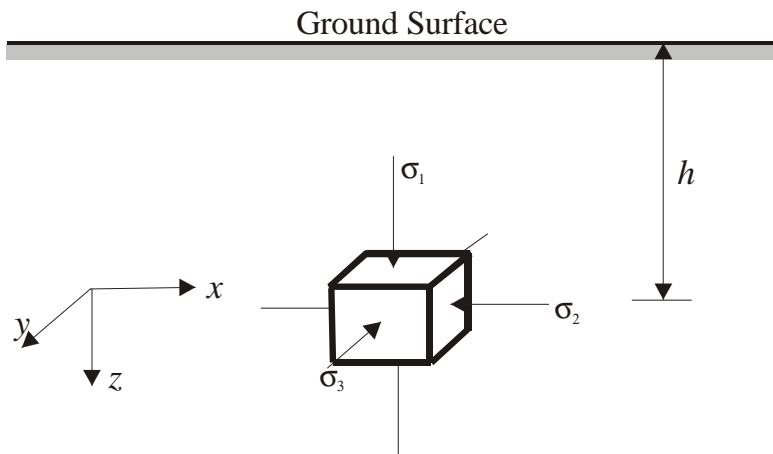


Figure 11-1 Stress at Point in Elastic Half Space

The stress state for an element at depth  $h$  below an infinite embankment surface is more complex (Figure 11-2). The  $y$  and  $z$  directions are no longer principal directions because of the presence of shear stress in the  $yz$  plane. Since the embankment is assumed to be infinite (plane strain) in the  $x$  direction, there is no deformation in the  $x$  direction so that there is no shear stress in the  $xy$  and  $xz$  planes ( $t_{xy} = t_{yx} = t_{xz} = t_{zx} = 0$ ). Since deformation in  $y$  and  $z$  directions are allowed, we have the following relationship:

$$\{s\} = \begin{pmatrix} s_x & t_{xy} & t_{xz} \\ t_{yx} & s_y & t_{yz} \\ t_{zx} & t_{zy} & s_z \end{pmatrix} = \begin{pmatrix} s_x & 0 & 0 \\ 0 & s_y & t_{yz} \\ 0 & t_{zy} & s_z \end{pmatrix} = \begin{pmatrix} s_2 & 0 & 0 \\ 0 & s_y & t_{yz} \\ 0 & t_{zy} & s_z \end{pmatrix} \quad (2)$$

which indicates that the  $x$  axis is one principal direction and the other two directions are perpendicular.

Consider a box culvert under an embankment with its alignment perpendicular to that of the embankment. To simplify the discussion, the stresses induced by soil-structure interaction are neglected. The embankment has two slopes are at each side, as shown in

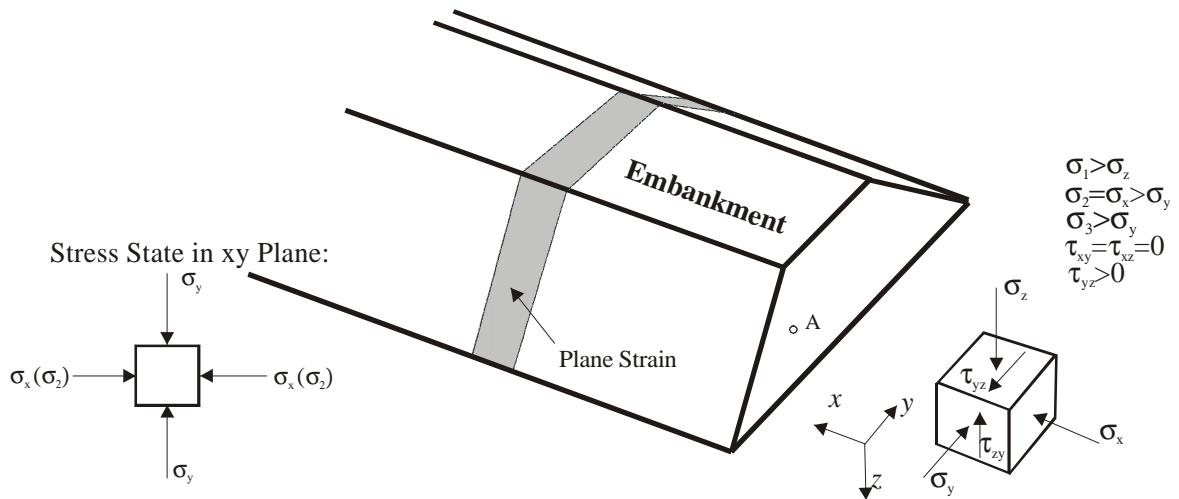


Figure 11-2 Assumed State of Stress at Point A under the Embankment

Figure 11-3. Since the embankment has been assumed to be infinite in the  $x$  direction, the stress state at any point inside the embankment can be described by equations (2), and the stress state in the horizontal plane is as illustrated in Figure 11-3.

Assuming a second identical box culvert is buried in a similar embankment with a skew angle  $\theta$  from  $x$  axis, as shown in Figure 11-4. The stresses acting on the culvert wall can be obtained by rotating the stress axis within the horizontal plane. Under these conditions, the stress components  $s_z$  is unchanged and  $t_{mz}$  is less than, but approximately equal to  $t_{yz}$ . The stresses acting on the skewed culvert wall can be written:

$$\{s_{mm}\} = \begin{pmatrix} s_n & t_n & 0 \\ t_n & s_m & t_{yz} \\ 0 & t_{yz} & s_z \end{pmatrix} \quad (3)$$

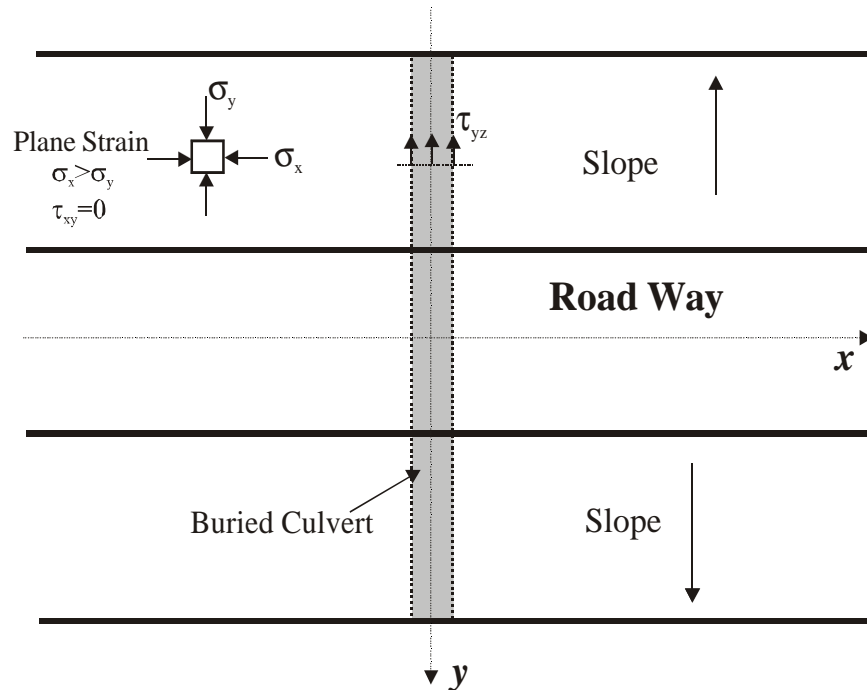


Figure 11-3 State of Stress on Vertical Plane  
Normal to Embankment Axis

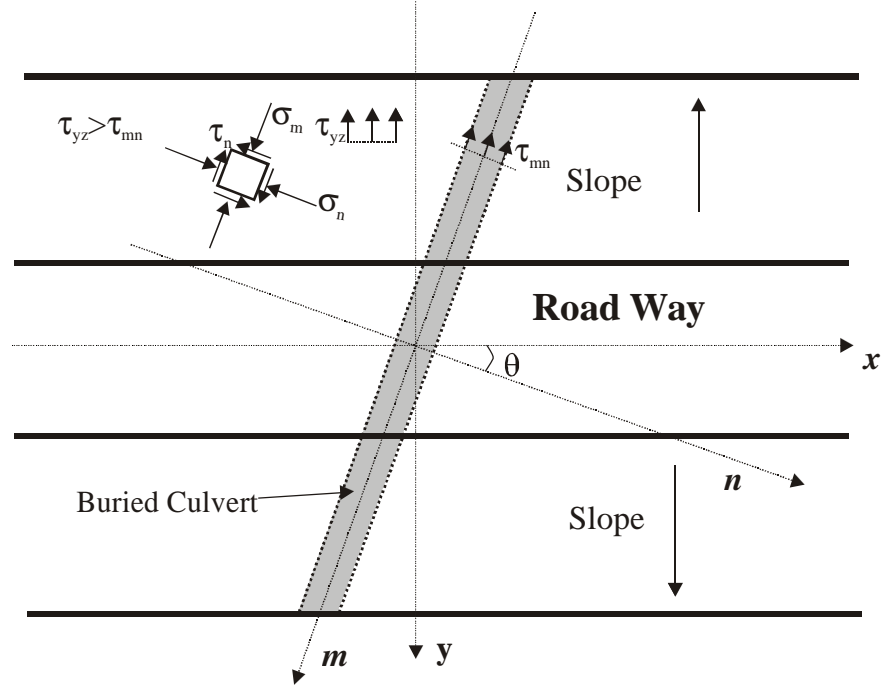


Figure 11-4 State of Stress on Plane Skewed with Respect to Embankment Axis ( $\theta > 0$ )

where  $s_n$  is the normal stress in the plane of the culvert wall, or the horizontal earth pressure on the wall,  $t_{nm} = t_{mn}$  is the horizontal shear stress along the alignment of wall, and  $s_m$  is the normal stress perpendicular to the direction of culvert wall.

Let a positive number  $C$  represents the difference between  $s_x$  and  $s_y$ :

$$\begin{aligned} C &= s_x - s_y > 0 \\ s_x &= C + s_y \end{aligned} \quad (4)$$

Then:

$$\begin{aligned} s_n &= s_x \cos^2 q + s_y \sin^2 q = (C + s_y) \cos^2 q + s_y \sin^2 q \\ s_n &= C \cos^2 q + s_y (\cos^2 q + \sin^2 q) = C \cos^2 q + s_y \\ s_n &\leq C + s_y = s_x \\ t_n &= \cos q \sin q (s_x - s_y) = \frac{1}{2} C \sin(2q) \geq 0 \end{aligned} \quad (5)$$

This suggests that the lateral normal stress acting on the wall of a skew culvert is less than that acting on a culvert with a skew angle  $\theta=0$ . When a box culvert is constructed in an embankment with a skew angle,  $\theta>0$ , a horizontal shear stress  $t_{nm}$  along the culvert will be induced. Since the shear stiffness along the culvert alignment is very large, the induced shear stress can be neglected in the design. Therefore, the analyses conducted in previous chapters assuming  $\theta=0$  represents the worst stress condition for a buried box culvert in a two side sloped embankment with an arbitrary skew angle.



## **Chapter 12**

### **Influence of Supporting Layer Stiffness on Lateral Earth Pressure Distribution**

The parametric studies conducted in Chapters 7 and 10 were based on the subsurface conditions at the Sullivan County culvert, which had a 3 meter thick supporting layer of firm shaley clay over weathered shale bedrock. Results from these parametric studies indicated that the compactive effort applied to the backfill had a significant influence on the horizontal earth pressures acting on the wall. Vertical pressures were not significantly affected by the compactive effort. Reduced compactive effort on the backfill layers immediately above the roof of a stiff culvert (such as that used in the instrumentation of the replacement culvert, Sullivan County, TN) resulted in a relatively low horizontal earth pressure (Figure 7-4). The compactive effort applied to the gravel beside the culvert walls was shown to affect the lateral earth pressure distribution (Figure 7-5). Well-compacted gravel could result in a large earth pressure on bottom of culvert wall, and small pressure on the top (Figure 7-5, Dense Side Soil). Under the expected conditions of a firm supporting layer and normally compacted backfill around a relatively flexible culvert (Original Culvert, Sullivan County, TN), the resultant lateral pressures induced by different gravel compactive efforts had a parabolic distribution with

a maximum near the middle height of the wall (Figure 10-9). Well-compacted gravel induced a large earth pressure at the middle of culvert wall.

As in indicated previously (Chapters 3 and 8), the culvert in Greene County, TN had a lower structural stiffness than the replacement culvert in Sullivan County and was constructed with conventional backfill practice (well-compacted backfill). The measured horizontal earth pressures indicated small horizontal pressures at the upper part of the culvert wall and a very large pressure near the bottom of the wall (Figure 12.1). Although this earth pressure distribution was not expected, it was confirmed by three independent measurements, two at Sections A (vibrating wire and resistance gage pressure cells) and one at Section B (vibrating wire pressure cells). These results are shown in Figure 12-2 for an embankment height of about 3 m, at which time the gage at Section A position 1 (1APRE) was still operating..

To investigate the impact of stiffness of the supporting layer on earth pressures against the culvert, a finite element (ABAQUS 5.8) parametric study was conducted based on the configuration of the Greene County culvert site. The subsurface conditions and laboratory test results were described in Chapter 3. Figure 12-3 illustrates the finite element mesh and designates the various materials. The full box culvert, both boxes, was modeled. The thickness of the supporting layer underneath the culvert was about 1.0 meter (based on a site visit result before construction). The material properties of the concrete and soils are provided in Table 12-1.

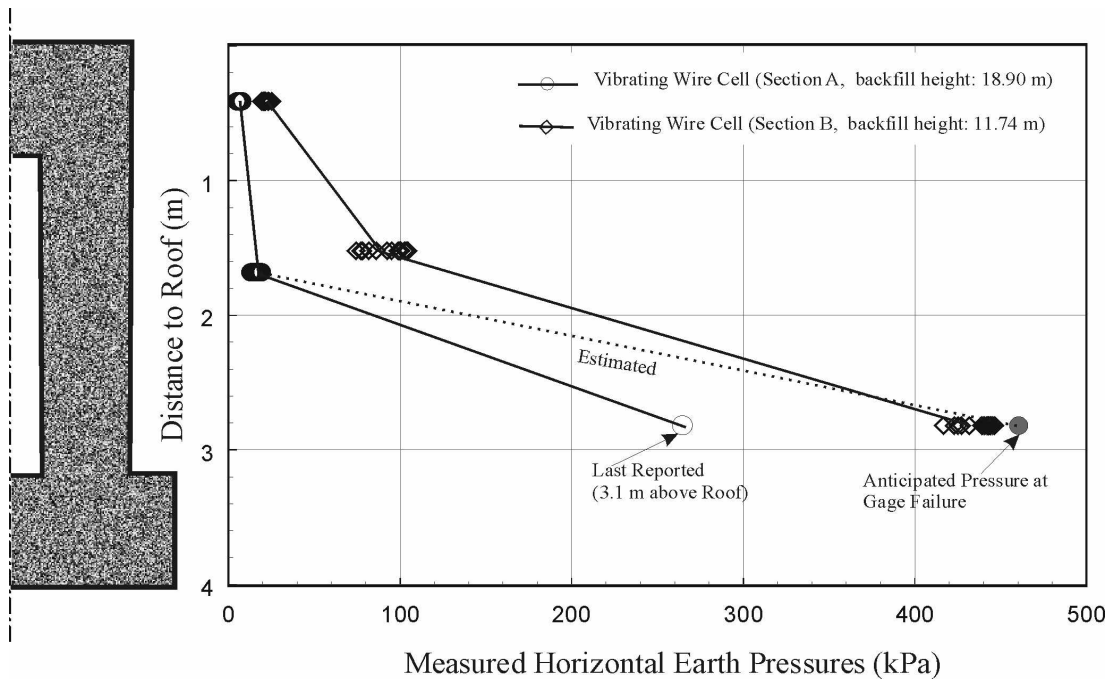


Figure 12-1 Measured Horizontal Earth Pressures at Greene County Culvert (Full Embankment Height)

Due to the rapid increase in embankment height, no readings were obtained in Gage No.1 (1APRE) after an embankment height of 3.1 m. The recorded pressure at this time was 274 kPa, or 1.6 times the manufacturer's stated capacity. These gages are designed to provide output (with reduced accuracy) up to about two times the design pressure. This would suggest that the earth pressure at gage No. 1 is at least 470 kPa (which is about the maximum pressure that can provide an output signal and is similar to the maximum horizontal pressure registered at Section B)

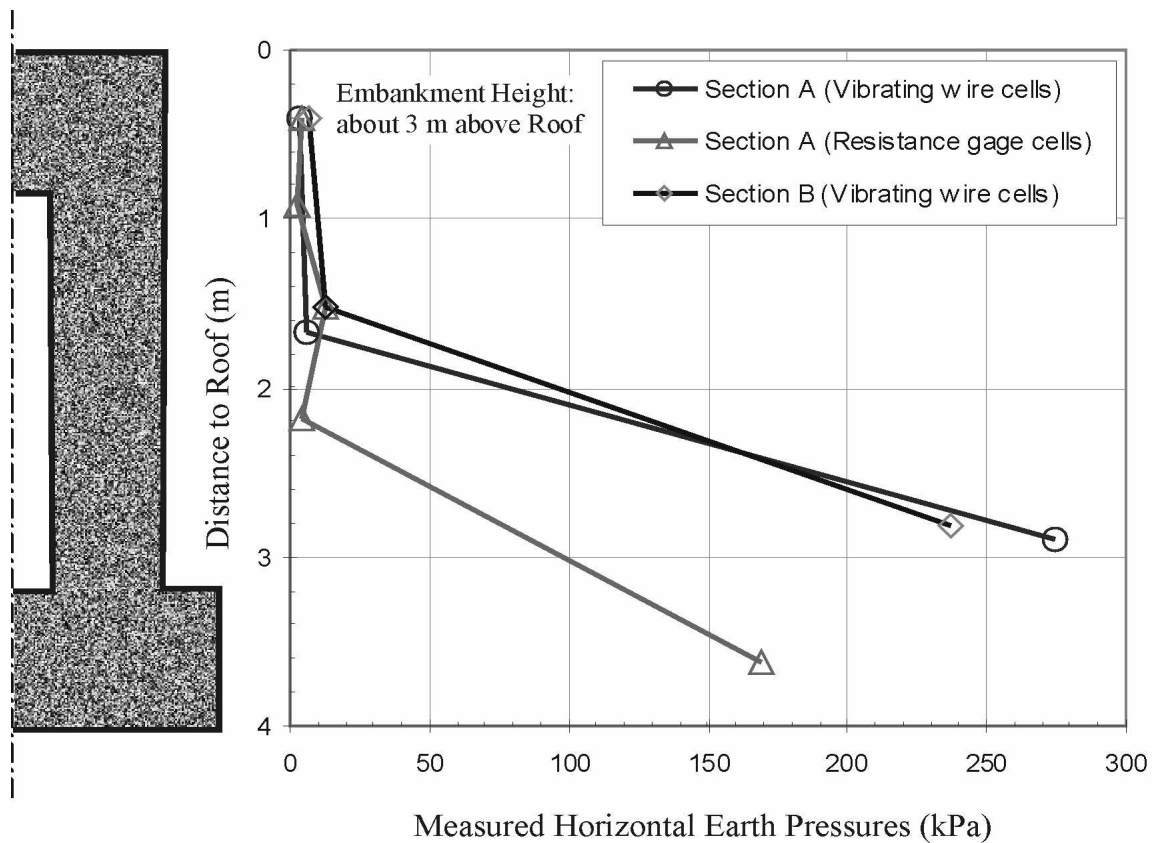


Figure 12-2 Lateral Pressures Measured at Three Instrumentation Sections with an Embankment Height of 3 m

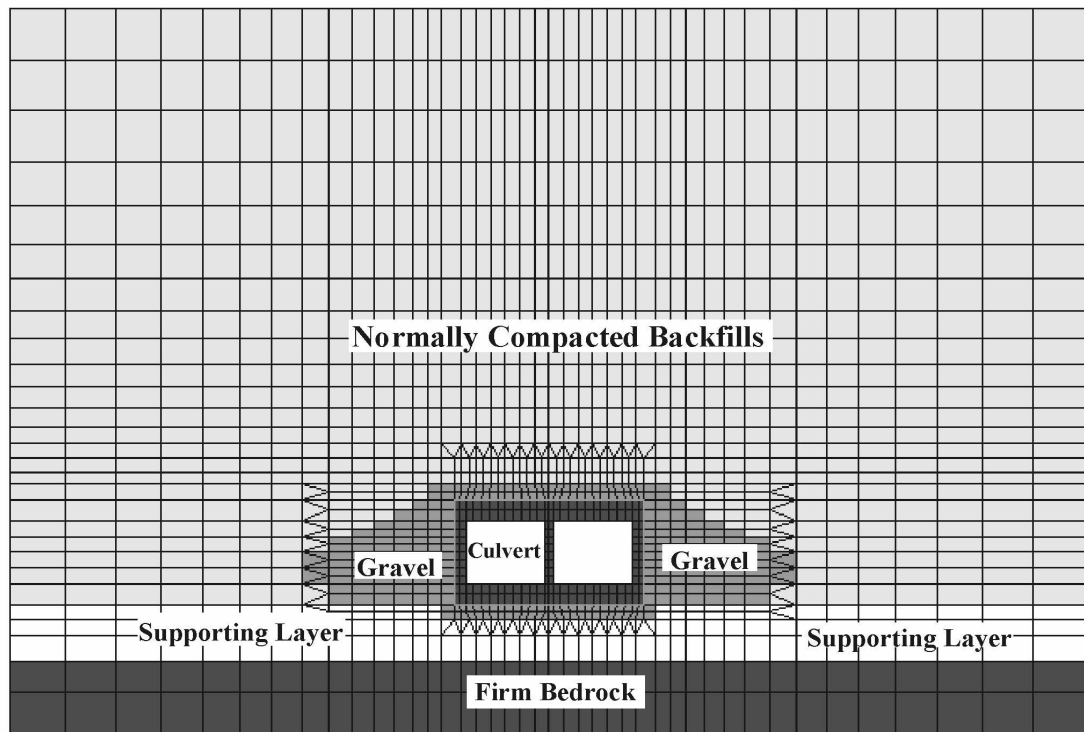


Figure 12-3 Finite Element Mesh and Conditions for Parametric Study  
(Greene County, TN)

Table 12-1 Summary of Material Properties in the Parametric Study

Material Description Figure 12-3	Cohesion c (kPa)	Friction Angle f (deg)	Dilatancy Angle ? (deg)	Elastic Modulus E (MPa)	Poisson's Ratio $\mu$	Source and Reference
Supporting Layer	29	30	0	1, 2, 8, 80	0.35	Measured shear strength, Modulus of 6 to 10 MPa from CD test result
Gravel	70	30	20	16, 32, 80	0.27	Measured shear strength, Modulus of 56 to 77 MPa from CD test result
Normally compacted backfill	32	20	15	16	0.32	Measured shear strength modulus from Penman (1975)
Bedrock	NA			1.12E6	0.25	Goodman(1989)
Concrete	NA			4.06E7	0.18	Modulus from lab test

Triaxial shear test results performed on gravel samples with the same unit weight as that measured in the field suggested an elastic modulus of 80 MPa. This was assumed to represent the well compacted gravel. Gravel with values of 16 and 32 MPa represent lower compactive efforts. The elastic modulus for the supporting layer, which was assumed to vary from 1 to 80 MPa, represents a wide range of soil stiffness, from very soft (1MPa) to very stiff (80 MPa). The normally compacted backfill was modeled with constant modulus of 16 MPa, as in the previous numerical analyses.

Figure 12-4 illustrate the influence of supporting layer modulus on the earth pressures acting on the culvert. Under the conditions of well-compacted gravel at the culvert sides, vertical pressures obtained from a wide range of supporting layer moduli are about the same, however, both the magnitude and distribution of lateral earth pressure are significantly different. A thin layer of soft clay (low modulus) results in very high

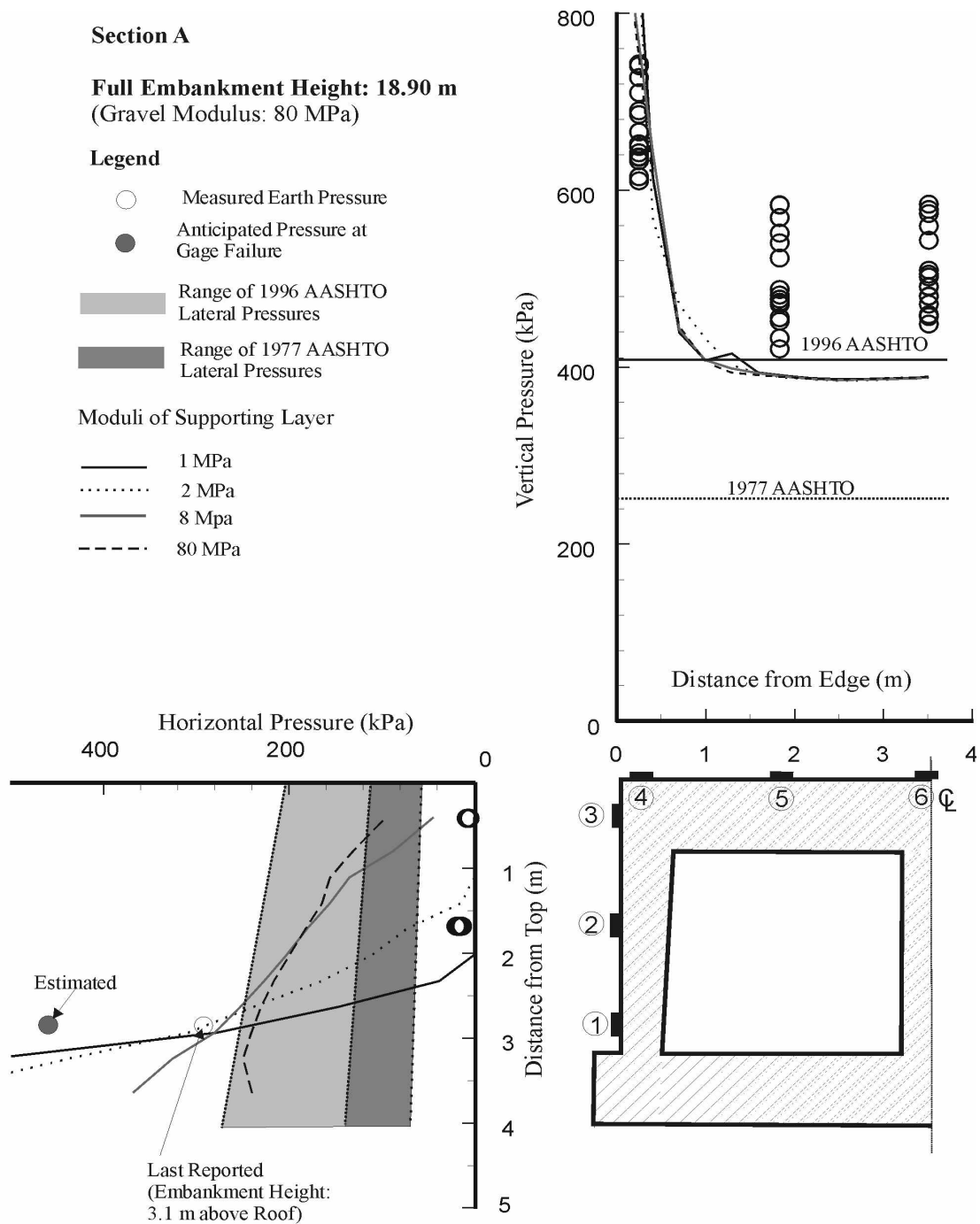


Figure 12-4 Influence of Supporting Layer Moduli on Culvert Earth Pressures  
(Well Compacted Gravel, Greene County, TN)

pressures at the bottom of the wall, similar to the earth pressure distribution measured at the Greene County culvert. A firm supporting layer results in a lateral earth pressure distribution similar to that recommended by the current AASHTO (16<sup>th</sup> edition, 1996) guidelines.

Figure 12-5 demonstrates the influence of compactive efforts of the gravel on the earth pressures for the case with a soft supporting layer underneath the culvert (the modulus of supporting layer is 2 MPa). The three gravel different compactive efforts result in different horizontal pressure distribution patterns, but in all cases high pressures exist at the bottom of the wall. Consistent with the results of the parametric study of gravel modulus with a firm supporting layer (Figure 7-5), the compactive effort of the gravel has a significant influence on horizontal earth pressures acting on the culvert wall.

The results suggest that the horizontal earth pressures acting on the culvert depend significantly on the modulus of the backfill adjacent to the culvert, and the modulus of the soft supporting layer. A soft supporting layer can lead to an earth pressure distribution with very high pressures at the bottom of the wall, and low pressures at the top. This pressure distribution would provide small bending moments than the current AASHTO (16<sup>th</sup> edition, 1996) minimum horizontal pressure, which would be an unfavorable load combination for culvert wall design. According to the parametric study, if the soft supporting layer underneath the culvert can be removed and replaced by an engineered granular material, this undesirable horizontal earth pressure distribution can be eliminated. In a similar study of the earth pressure on concrete pipe (Heger and Selig,



1994), low modulus (soft material) of the supporting layer was shown the reason of the structural distress.

### Section A

**Full Embankment Height: 18.90 m**  
(Supporting Layer Modulus: 2 MPa)

#### Legend

- Measured Earth Pressure
- Anticipated Pressure at Gage Failure
- Range of 1996 AASHTO Lateral Pressures
- Range of 1977 AASHTO Lateral Pressures
- Moduli of Gravel:
  - 16 MPa
  - ..... 32 MPa
  - 80 MPa

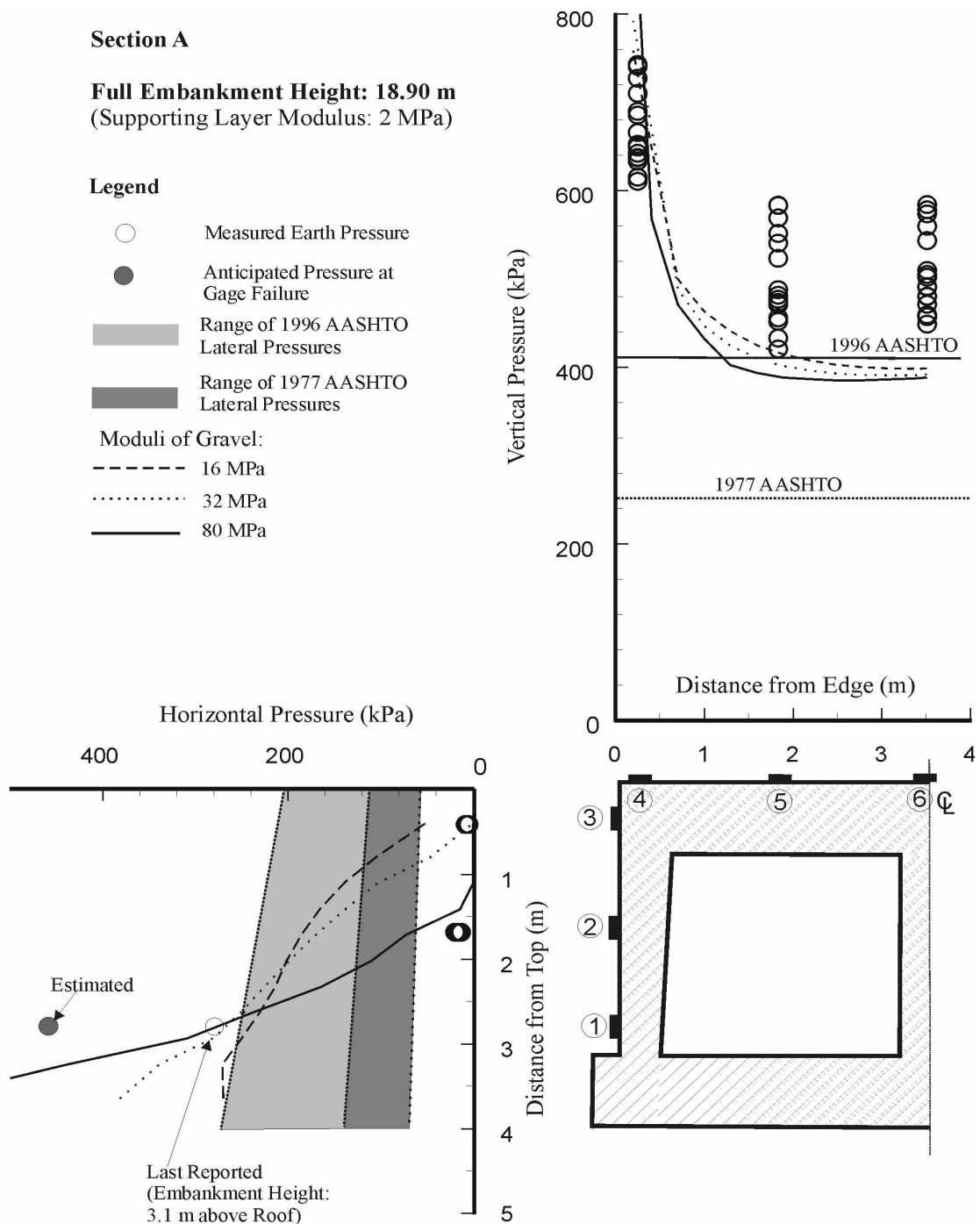


Figure 12-5 Influence of Gravel Compactive Effort on Culvert Earth Pressures  
(Soft Supporting Layer, Greene County, TN)

## **Chapter 13**

### **Summary and Conclusions**

The factors affecting the earth pressures acting on buried box culverts were evaluated by field instrumentation and numerical analyses on two box culverts. Long term earth pressures under constant embankment heights were observed after the completion of construction. Both the observed earth pressures and those predicted by numerical analyses were compared with the current AASHTO earth pressure recommendations (16<sup>th</sup> edition, 1996), as well as the AASHTO design guide pressures in effect at the time (12<sup>th</sup> edition, 1977) the failed box culvert was designed.

#### **12.1 Factors Affecting the Earth Pressures**

Five factors which may affect the earth pressures of buried culverts were evaluated. Conclusions relative to each of these are summarized below.

##### **12.1.1 Height of Embankment**

The embankment height largely affected vertical earth pressure distribution on the culvert roof. The literature review suggested that previous field instrumentation of rigid box culverts were either small size, single cell box culverts under deep fill, in which the objective focused on the vertical load reduction under the imperfect trench condition, or larger size box culverts under low embankment height (less than 4.0 m), which

concentrated on the impact of live load on the structural performance of the culvert. The two box culverts instrumented in this study were under deep backfill (11.7 m and 18.9 m), and reflect conditions unlike others in the literature.

The vertical earth pressure acting on the culvert roof can be divided into two stages: low embankment height stage ( $H/B < 0.5$ , where  $H$  is the backfill height above the roof and  $B$  is the width of the culvert), and high embankment height stage. Significant differences were found between these two stages.

At low embankment height, the instrumentation results indicated that the recorded vertical earth pressures on the roof were consistent with the results of other instrumented culverts of similar size. The current AASHTO vertical design pressure was slightly lower than the mean measured value. The measured pressures at different locations on the roof were relatively uniform. The measured lateral pressures were greater than the current AASHTO recommended lateral pressure.

At high embankment height ( $H/B > 0.5$ ), the vertical pressures measured at the center of the roof span were smaller than those at the edges and above the center wall. This was observed at all four instrumented sections, two culverts with two instrumentation sections each. The measured horizontal pressures varied greatly at the two culvert sites. This was attributed to compaction effects and different subsurface conditions at two sites.

The long term recorded vertical pressures at the two sites under the constant embankment heights (Figures 8-16, 8-17, and 10-7) were similar in distribution. Higher pressures were recorded above the stiff walls. The current AASHTO vertical pressure

recommendation closely predicted the earth pressure at the center of the roof, and under estimated the pressures at the two ends of the span. The structural response analyses (Chapter 10) suggested that the contribution of high earth pressures to the bending moment in the culvert roof is not significant. Earth pressures were found to contribute the bending moments in the wall, however.

### **12.1.2 Compactive Effort**

Both the instrumentation results and the numerical analysis indicated that the level of compactive effort had a significant influence on the earth pressure distribution, especially the horizontal earth pressure acting on the culvert wall.

The replacement culvert in Sullivan County was installed with a reduced compactive effort. The recorded horizontal earth pressures (Figure 10-7) fell into a zone defined by the current AASHTO recommended maximum and minimum horizontal pressures. The instrumented culvert in Greene County was backfilled with conventional construction practice, in which the gravel and clay backfill materials were spread in thin lifts and compacted to their optimum density. The recorded lateral pressures (figures 8-16 and 8-17) acting on the culvert wall were significantly different from the result in Sullivan County culvert. A very large pressure was observed at the base of culvert wall, and small pressures were recorded at the middle and upper cells on the wall. This pressure distribution was observed at both instrumentation sections of the Greene County culvert. The recorded horizontal pressure distribution was very different from that in the AASHTO recommendations.

The numerical model to analyze the culvert was calibrated using the field measurement results and used material properties measured in-situ and in the laboratory, and properties from the literature. The parametric studies (Figures 7-5 and 10-10) suggested that both the magnitude and the distribution of the horizontal earth pressure depend up on the stiffness of the gravel beside the culvert wall. Over compaction of the gravel beside the culvert would result in a large horizontal earth pressure with a distribution (Figure 7-5) similar to the recorded horizontal pressures in Greene County culvert.

The numerical analysis suggested that lower compactive efforts in the gravel beside the culvert would result in a higher vertical earth pressure on the roof (Figure 10-10), and parametric studies (Chapter 7) suggested that placing 2 m of loose fill immediately above the replacement culvert (imperfect trench condition) only slightly reduced the vertical earth pressures on the culvert wall. The parametric studies investigated a wide range of gravel modulus values reflecting different compactive effort, and the corresponding vertical pressure on the culvert roof did not exhibit a significant variation compared to the horizontal pressure on the culvert wall.

### **12.1.3 Subsurface Conditions and Structure Stiffness**

Subsurface conditions and the structural stiffness have a significant impact on the horizontal pressures on the culvert wall. The stiffness of the subsurface materials supporting the culvert can affect the pressure distribution on the culvert. This can be illustrated by comparing the predicted horizontal pressure distributions in the failed and replacement culverts in Sullivan County (figures 7-4 and 10-10). The replacement culvert

was constructed in a pre-existing V-shaped valley and was constructed directly on the bottom slab of the failed culvert, whereas the previous culvert was installed on a leveled ground. Both the magnitude and the distribution of horizontal pressures induced by normal compactive efforts were significantly different.

The recorded earth pressures corresponding to the backfill height in Greene County culvert (figures 8-11 to 8-13) also illustrated a change in vertical earth pressure with respect to the relative structural stiffness. With the increase of embankment height, higher vertical pressures were recorded near the structural corners and centers where the structures had higher stiffness. The recorded vertical pressures were similar under deep embankment heights in the two culverts, and the measurements were also consistent with the results from the numerical analysis (Figure 7-4) and the previous model tests (Figure 2-12).

#### **12.1.4 Dynamic Lateral Pressure**

The field instrumentation at the Greene County culvert recorded dynamic horizontal earth pressures induced by different types of construction equipment. The largest construction induced dynamic horizontal pressure was recorded when the gravel was below the culvert roof. When the backfill elevation was above the culvert roof, the static sheep's-foot roller was used to compact the fine grain backfill material. The corresponding dynamic earth pressure from this equipment was not significant.

When the backfill height was below the culvert roof, the results indicated that the vibratory compaction roller, compared to other conventional construction equipment, induced the largest dynamic horizontal earth pressure. The recorded maximum impulsive

lateral pressure was about 70 kPa (1.5 ksf, Figure 9-7) when the roller was at the closest possible distance to the instrumented wall. The corresponding maximum dynamic strain was less than 10 microstrains (Figure 9-18). Compared with the concrete cracking strain of 153 microstrains, the dynamic lateral earth pressure should not cause any detrimental effects on the culvert in Greene County, which was designed for an embankment height of 18.9 meters. The recorded lateral dynamic earth pressure decreased rapidly with depth below the ground surface and with horizontal distance away from the culvert wall. The impulse pressure can be estimated by doubling the Bousinesq's lateral earth pressure solution in an elastic half space. Based on the field measurement result, the residual lateral earth pressure immediately after the removal of construction equipment can be estimated by simple equations (Equations 3 through 5 in Chapter 9).

#### **12.1.5 Culvert Orientation with Respect to Embankment Alignment**

The analytical evaluation of the culvert orientation with respect to the embankment alignment suggested that the horizontal pressures acting on the culvert wall vary with skew angle  $\theta$ . The analysis indicated that the largest horizontal earth pressure acting on the culvert wall is when the culvert alignment is perpendicular to the alignment of embankment, or  $\theta = 0$ . This was the assumption in each of the analyses here.

#### **12.2 Factors Causing the Failure of Previous Culvert**

Both the numerical and field instrumentation results (figures 8-16, 8-17 and 10-7) indicated that the previous AASHTO earth pressure recommendations (12<sup>th</sup> edition, 197) in place at the time the culvert was designed significantly underestimate the vertical pressure on the culvert roof. An analysis was performed to estimate the probable earth



pressures on the original failed culvert based on the field instrumentation results. The structural response of the original failed culvert under different types of earth pressures were also analyzed (Chapter 10). The results suggested that both the bending moments and the shear forces in the failed culvert wall were near capacity.

## **REFERENCES**

## References

- Abramson, L. W. and Green, G. E., (1984). "Reliability of strain gauges and load cells for geotechnical engineering applications." *Trans. Res. Record 1004*, 13-19.
- Benmokrane, B., Chekired, M., Xu, H. and Ballivy, G. (1995). "Monitoring behavior of grouted anchors using vibrating-wire gages." *J. Geotech. Engrg. Div.*, ASCE, 121(6), 466-475.
- Bhatia, S. K. and Bakeer, R. M. (1989). "Use of the finite element method in modeling a static earth pressure problem." *Inter. J. for Ana. Methods in Geomechanics*, 13(2), 207-213.
- Bowles, J. E. (1988). *Foundation Analysis and Design*. McGraw-Hill, New York.
- Broms B., and Ingleson, I. (1971). "Earth pressures against abutment of rigid frame bridge." *Geotechnique*, Vol. 21, No. 1, 15-28.
- Butcher, A. P., and Marsland A., (1989), "Measurements of lateral earth pressures on bridge abutments," *Geotechnical Instrumentation in Practice - Purpose, Performance and Interpretation*, Proceedings of the Geotechnical Instrumentation in Civil Engineering Projects Conference. Nottingham, Britain, April 3-5, 1989, 341-356.
- Carder, D. R., Pocock, R. G., and Murray, R. T. (1977). "Experimental retaining wall facility \_ Lateral stress measurement with sand backfill." *Transport and Road Research Laboratory Report No. LR 766*, Crowthorne, England.
- Clayton, C. R. I. (1989). "Discussion on conventional retaining walls: pilot and full-scale studies." *Proc. Instn. Civ. Engrs*, Part I, 86, 980-986.
- Clayton, C. R. I. and Symons, I. F. (1992). "The pressure of compacted fill on retaining walls" *Geotechnique*, 42(1), 127-130.
- Clayton, C. R. I, Symons, I. F., and Hiedra-Cobo, J. C. (1991). "The pressure of clay backfill against structures" *Can. Geotech. J.* 28 (1), 282-297.
- Coyle, H. M and Bartoskwtz, R. E., (1976), "Earth pressure on precast panel retaining wall," *J. of Geotech. Engrg. Div.*, ASCE, 102(5), 441-456.
- Corotis, R. B. and Krizek, R. J., "Analysis and measurement of soil behavior around buried

- concrete pipe,” *Concrete Pipe and the Soil-Structure System*, ASTM STP 630, 1977, pp. 91-104.
- Dasgupta, A. and Sengupta, B. (1991). “Large-scale model test on square box culvert backfilled with sand.” *J. Geotech. Engrg. Div.*, ASCE, 117(1), 156-161.
- Davis, R. E. and Bacher, R. C. (1972). “Concrete arch culvert behavior-phase 2.” *J. Soil Mech. Founda. Div.* ASCE, 98(11), 2329-2350.
- Design and construction of Reinforced concrete box culverts* (1996), American Railway Engineering Association, Vol. 97, Bulletin 758, 625-639.
- Duncan, J. M. (1996). “State of the art, limit equilibrium and finite-element analysis of slopes.” *J. Geotech. Engrg. Div.*, ASCE, 122(7), 577-596.
- Duncan, J. M. and Seed, R. B. (1986). “Compaction-induced earth pressures under  $K_0$ -conditions” *J. Geotech. Engrg. Div.* ASCE, 112(1), 1-22.
- Duncan, J. M., Williams, G. W., Sehn, A. L., and Seed, R. B. (1991). “Estimation earth pressures due to compaction.” *J. Geotech. Engrg. Div.* ASCE, 117(12), 1833-1847.
- Dunnicliff, J. (1988). *Geotechnical instrumentation for monitoring field performance*. John Wiley and Sons, New York.
- Felio, G. Y. and Bauer, G. E., (1984), “Monitoring and performance of bridge abutment,” *Proceedings of International Conference on Case Histories in Geotechnical Engineering*. St. Louis, MO, 235-239.
- Filz, G. M., and Brandon, T. L., (1993), “Compactor force and energy measurements,” *Geotechnical Testing Journal*, GTJODJ, 16(4), Dec., 442-449.
- Filz, G. M. and Brandon, T. L. (1994). “Static and dynamic measurements using embedded earth pressure cells” *Trans. Res. Record* 1432, 86-95.
- Filz, G. M. and Duncan, J. M. (1996). “Earth pressure due to compaction: comparison of theory with laboratory and field behavior.” *Trans. Res. Record* 1532, 28-37.
- Filz, G. M. and Duncan, J. M. (1997). “Vertical shear loads on nonmoving walls. I: theory.” *J. Geotech. Engrg. Div.*, ASCE, 123 (9), 856-862.
- Flynn, John (1999). "Response of vibrating wire earth pressure cells at pressures exceeding stated capacity" Geokon Incorporated, Personal Communication by E.C.Drumm,

7-26-99.

- Girdler, H. F., (1974). "Loads on box culverts under high embankments." *Research Report No. 386*, Kentucky Department of Transportation.
- Goodman, R. E. (1989). *Introduction to Rock Mechanics*. John Wiley and Sons, New York.
- Handy, R. L. (1985). "The arch in soil arching" *J. Geotech. Engrg. Div.*, ASCE, 111(3), 302-318.
- Heger, F. J. and Selig, E.T. (1994). "Rigid pipe distress in high embankments over soft soil strata" *Trans. Res. Record 1431*, 46-52.
- Hibbitt, Karlsson & Sorensen, Inc. (1995) *ABAQUS/Standard User's Manual*. Vol. 1, Vol. 2. Ver. 5.5.
- Hibbitt, Karlsson & Sorensen, Inc. (1998) *ABAQUS/Standard User's Manual*. Vol. 1, Vol. 2. Ver. 5.7.
- Hicher, P. Y. (1996). "Elastic properties of soils." *J. Geotech. Engrg. Div.*, ASCE, 122(8), 641-648.
- Ingold, T. S. (1979). "The effects of compaction on retaining walls" *Geotechnique*, 29(3), 265-283.
- James, R. W., Brown, D. E., Bartoskewitz, R. E. and Cole, H. M. (1986). "Earth pressures on reinforced concrete box culvert" *Research Report 294-2F*, Texas Trans. Ins., The Texas A&M Univ. Sys. College Station.
- Katona, M. G., Vittes, P. D., Lee, C. H., and Ho, H. T. (1981). "CANDE—1980: box culverts and soil models." *Report No. FHWA/RD-80/172*, Federal Highway Admin., Washington D. C.
- Kellogg, C. G., (1993). "Vertical earth Loads on buried engineered works" *J. Geotech. Engrg. Div.*, ASCE, 119(3), 487-507.
- Kohl, K. M., New, B. M., and O'Rourke, T. D., (1989) "Stress cell measurements for the investigation of soil-pipeline interactions during vehicular loading," *Geotechnical Instrumentation in Practice - Purpose, Performance and Interpretation*, Proceedings of the Geotechnical Instrumentation in Civil Engineering Projects Conference. Nottingham, Britain, April 3-5, 1989, 717-733.

- Law Engineering (1990) *Report Triaxial Tests on #57 Stone*, Knoxville, TN.
- Lambe, T. W. and Whitman, R. V. (1979), *Soil Mechanics, SI Version*, John Wiley & Sons.
- Lazebnik, G. E., (1997) “*Monitoring of soil-structure interaction - Instruments for measuring soil pressures.*” Chapman & Hall, New York.
- McRae, J. B. and Simmonds, T. (1991). “Long-term stability of vibrating wire instruments: one manufacturer’s perspective.” *Field Measurements in Geomechanics*, Balkema, Rotterdam. 283-293.
- Minimum design loads for buildings and other structures*, (ANSI/ASCE 7-95, 1995). American Society of Civil Engineers, New York.
- Mirza, S.A., Hatzinikolas, M., and MacGregor, J.G. (1979). "Statistical descriptions of strength of concrete." *Journal of the Structural Division, ASCE*, 105(ST6), 1021-1037.
- Moore, P. J., (1991). “Evaluation of earth pressures on walls.” *Proceedings of Geotechnical Aspects of Embankments, Excavations and Buried Structures*, Balkema, Rotterdam, 247-260.
- Ono, K. and Yamada, M. “Analysis of the arching action in granular mass” *Geotechnique*, 43(1), 105-120.
- Penman, A. D. M., Charles, J. A., Nash, J. K. and Humphreys, J. D. (1975). “Performance of culvert under Winscar Dam.” *Geotechnique*, 25(4), 713-730.
- Rehman, S. E., and Broms, B. B., (1972), “Lateral pressures on basement wall - results from full-scale tests,” *Proceedings, 5<sup>th</sup> European Conference on Soil Mechanics and Foundation Engineering*, Vol. 1., 189-197.
- Seed, R. B., and Duncan, J. M., (1983). “Soil-structure interaction effects of compaction induced stresses and deflections,” *Geotechnical Engineering Research Report No. UCB/GT/83-06*, University of California, Berkeley, CA.
- Seed, R. B. and Duncan, J. M., and Ou, C. Y., (1991). “Finite element analysis of compaction problems.” *Advanced Geotechnical Analysis- Development in Soil Mechanics and Foundation Engineering-4*, Ed. Banerjee, P. K. and Butterfield, R. Elsevier Applied Science.
- Sehn, A. L., Duncan, J. M. (1990). “Instrumentation for measuring earth pressures due to

- compaction” *Trans. Res. Record* 1277, 44-52.
- Selig, E. T., McVay, M. C. and C. S. Chang. (1982) “Finite element modeling of buried concrete pipe installations.” *Trans. Res. Record* 878, 17-23.
- Smoltczyk, U. and Hilmer, K. (1979), “Horizontal pressure increment by surcharge load,” *Proceedings of Design Parameters in Geotechnical Engineering*, British Geotechnical Society, London, Vol. 2, 131-139.
- Smoltczyk, U. Hilmer, K., and Schuppener, B. (1977). “Earth pressure variations due to temperature change,” *Proceedings of the Ninth International Conference on Soil Mechanics and Foundation Engineering*. Vol. 2, 725-733.
- Sowers, G. F., Robb, A. D., Mullis, C. H. and Glenn, A. J. (1957). “The residual lateral pressures produced by compacting soils.” *Proc. 4<sup>th</sup> Intl. Conf. On Soil Mech. And Found. Engrg.*, London, 1957.
- Spangler, M. G. (1938). “Lateral pressures on Retaining walls caused by superimposed loads.” *Proc. Highway Research Board*, Part II, England.
- Spangler, M. G. and Handy, R. L. (1982). *Soil Engineering*. 4th edition, Harper & Row, New York.
- Standard specifications for highway bridges. (1987). 14th Ed., The American Association of State Highway and Transp. Officials (AASHTO), Washington, D. C.
- Standard specifications for highway bridges. (1977). 12th Ed., The American Association of State Highway and Transp. Officials (AASHTO), Washington, D. C.
- Standard specifications for highway bridges. (1996). 16th Ed., The American Association of State Highway and Transp. Officials (AASHTO), Washington, D. C.
- Symons, I. F. and Murray, R. T. (1988). “Conventional retaining walls: pilot and full-scale studies.” *Proc. Instn. Civ. Engrs*, Part I, 84(10), 980-986.
- Tadros, M. K. (1986). “Cost-effective concrete box culvert design.” *Project No. HRP83-3*, Engineering Research Center, Univ. Nebraska, Lincoln.
- Tadros, M. K., Benak, J. V., Abdel-Karim, A. M. and Bexten, K. A. (1989). “Field testing of a concrete box culvert.” *Trans. Res. Record* 1231, 49-55.

- TDOT. (1995). "Internal report: shear strength of Sullivan County culvert backfill material"
- Trollope, D. H., Speedie, M. C. E. and Lee, I. K. (1963). "Pressure measurements on Tullaroop dam culvert." *Proc. 4th Australia-New Zealand Conf. Soil Mech. Fdn Engng*, 81-92.
- Tuner, A. K. and Schuster, R. L. (1996) "Landslides investigation and mitigation" *Trans. Res. Record special report 247*, National Academy Press, Washington, D. C.
- Vaslestad, J., Johansen, T. H. and Holm, W. (1994). "Load reduction on rigid culverts beneath high fills: long-term behavior" *Trans. Res. Record 1415*, 58-68.
- Weller, K. A., Jr., and Kulhawy, F. H. (1982). "Factors affecting stress cell measurements." *J. of Geotech. Engrg. Div.*, ASCE, 118(12) 442-449.
- Yang, M. Z., Drumm, E.C., Bennett, R. M and Mauldon, M. (1997), "Influence of compactive effort on earth pressures around a box culvert," Proceedings of the Ninth International Conference on Computer Methods and Advances in Geomechanics, Wuhan, China, Nov. 2-7, 2021-2026.
- Yoo, T-S., and Selig, E. T., (1979). "Dynamics of vibratory-roller compaction." *Journal of the Geotechnical Engineering Division*, ASCE, Vol. 105, No. 10, 1211-1231.



## **VITA**

Michael Zhiqiang Yang was born on October 31th, 1965 in Sichuan, China. He graduated from Huazhong University of Science and Technology, Wuhan China, in July, 1986 with a Bachelor's of Science Degree in Civil Engineering. In October, 1989, he received his Master of Science Degree in Civil Engineering with concentration in Geotechnical Engineering from Wuhan Institute of Rock and Soil Mechanics (IRSM), Chinese Academic of Sciences. He was a research engineer, senior research engineer in IRSM from 1989 to 1996. In February, 1996, he came to the United States and worked as graduate research assistant for the Civil and Environmental Department at the University of Tennessee. He received his Doctor of Philosophy Degree in Civil Engineering with concentration in Geotechnical Engineering in May, 2000.

**Evaluation f Factors Affecting  
Earth Pressures on Buried Box Culverts**

**Part Two**

**Appendices**

A Dissertation  
Presented for the  
Doctor of Philosophy  
Degree  
The University of Tennessee

Michael Zhiqiang Yang

May 2000

## **Table of Contents**

<b>Appendix A Sullivan County Data</b> .....	273
Appendix A-1 Dimensions and Details of Culvert Reinforcement for Instrumentation Sections .....	274
Appendix A-2 Instrumentation Scheme - Sullivan County, TN .....	276
Appendix A-3 Chronology of Field Events - Sullivan County Culvert Field Record Results .....	281
Appendix A-4 Selected Recorded Earth Pressure Distributions .....	283
Appendix A-5 Original Vibrating Wire Pressure Cell Records Sullivan County Culvert Site (04/09/96-1/25/00) .....	285
Appendix A-6 Original Vibrating Wire Concrete Strain Gage Records Sullivan County Culvert Site (04/09/96-1/25/00) .....	294
<b>Appendix B Green County Data</b> .....	304
Appendix B-1 Dimensions and Details of Culvert Reinforcement for Instrumentation Sections .....	305
Appendix B-2 Instrumentation Scheme - Greene County, TN .....	307
Appendix B-3 Chronology of Field Events - Greene County Culvert Field Record Results .....	314
Appendix B-4 Original Vibrating Wire Pressure Cell Records Greene County Culvert Site (10/31/96-1/25/00) .....	317
Appendix B-5 Original Vibrating Wire Concrete Strain Gage Records Greene County Culvert Site (04/09/96-1/25/00) .....	332
<b>Appendix C Dynamic Horizontal Earth Pressures Induced by Construction Equipment</b> .....	358
<b>Appendix D Triaxial Shear Test Results</b> .....	371
Appendix D-1 Clayey Shale (Sullivan County, TN) .....	372
Appendix D-2 Gravel (Greene County, TN) .....	391
Appendix D-3 Undisturbed Silty Clay (Greene County, TN) .....	410
Appendix D-4 Clay (Greene County, TN) .....	431
<b>Appendix E Concrete Cylinder Test Data</b> .....	447
Appendix E-1 Sullivan County Culvert Concrete Test .....	448
Appendix E-2 Greene County Culvert Concrete Test .....	457
<b>Appendix F Selected Input Files for Finite Element Analysis Using ABAQUS Code</b> .....	463
<b>Appendix G Calibration Sheet for Instrumentation Gages</b> .....	500

<b>Appendix H Earth Pressure Variations under</b>	
<b>Constant Embankment Height</b> .....	533
H1 Abstract .....	533
H2 Introduction .....	534
H3 Examples of Earth Pressures Variation during the	
Long-term Observation .....	534
H3.1 Previous Case Studies .....	534
H3.2 Earth Pressures on A Box Culvert under the	
Constant Embankment Height .....	536
H4 Factors Influence the Earth Pressure Reading with Time .....	537
H5 Contact Pressure Cells Configurations .....	541
H6 Instrumentation on Box Culvert Sites .....	542
H7 Observed Temperature Effects at Different Conditions .....	545
H7.1 Earth Pressure Changes at Zero Load .....	546
H7.2 Earth Pressure Variation under Constant	
Embankment Height .....	550
H8 Earth Pressures acting on the Culvert after	
Temperature Correction .....	556
H9 Summaries and Conclusions .....	561
H10 Acknowledgments .....	563
H11 References .....	563

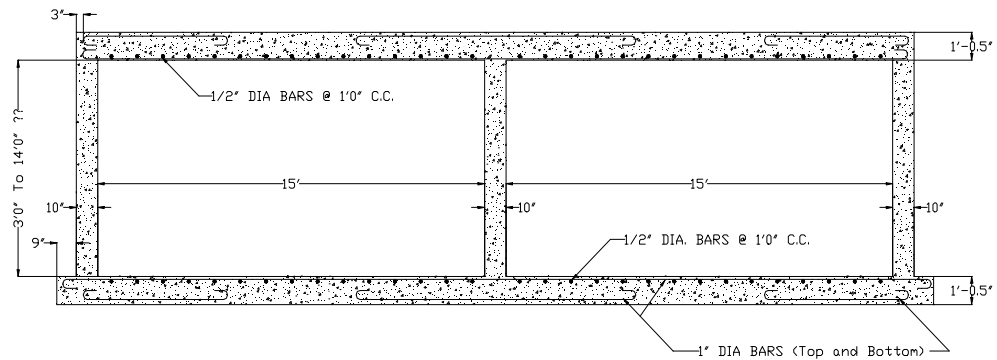
**APPENDIX A**

**SULLIVAN COUNTY DATA**

## Appendix A-1

### Dimensions and Details of Original and Replacement Culvert

Note: the height of original culvert is 7'



Units: feet, inches

REINFORCED DETAIL - ORIGINAL	THE UNIVERSITY OF TENNESSEE	
SULLIVAN COUNTY CULVERT	Date: 24-June-96	Drawn By: William G. Kupsch

Figure A-1 Reinforcing Detail for Original Culvert  
(Sullivan County, TN)

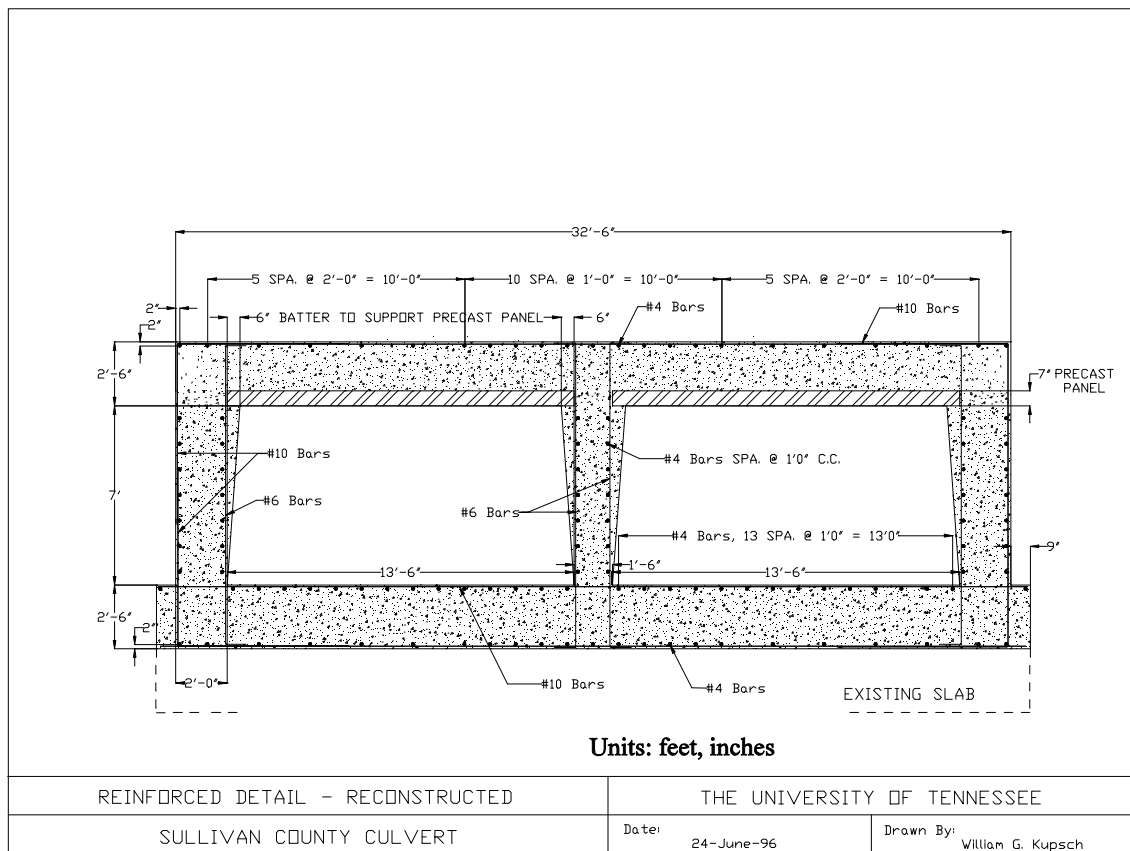


Figure A-2 Reinforcing Detail for Replacement Culvert  
(Sullivan County, TN)

## Appendix A-2

### Instrumentation Scheme - Sullivan County, TN

Table A-1 Instrumentation Scheme - Sullivan County

Instrument Type	Location/Transducer	A or B Position ( indicates Section along culvert where instrument was installed)					
		1	2	3	4	5	6
Embedded Concrete Strain Gages	Inside / Resistance Gages	B	B	B	A B	A B	A B
	Outside / Resistance Gages	A B	B	B	A B	A B	A B
	Inside / Vibrating Wire Gages	B	B	B	A B	A B	A B
	Outside / Vibrating Wire Gages	B	B	B	A B	A B	A B
Earth Pressure Cells	Vibrating Wire Gages	A B	A B	A B	A B	A B	A B



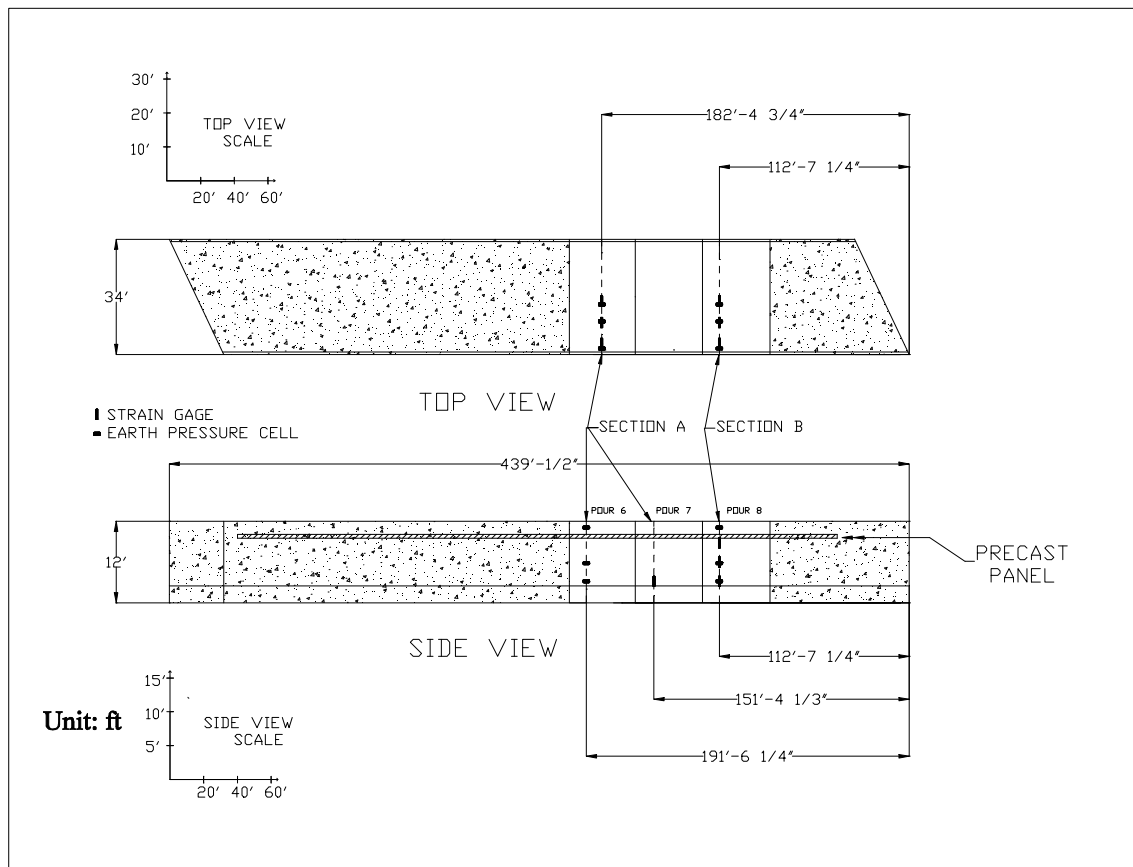


Figure A-3 Location of Instrumentation Sections(Sullivan County, TN)

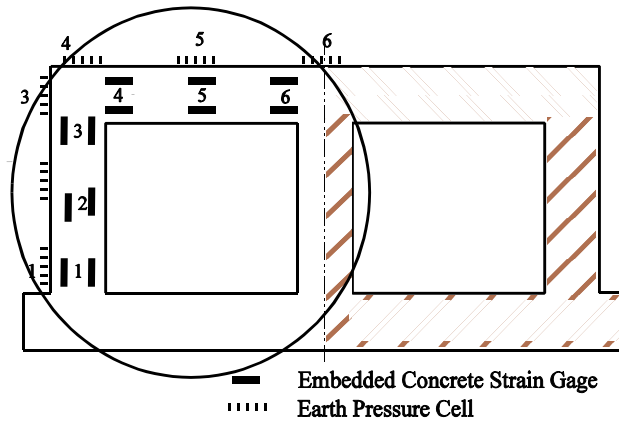


Figure A-4 Sullivan Co. Culvert Instrumentation Plan

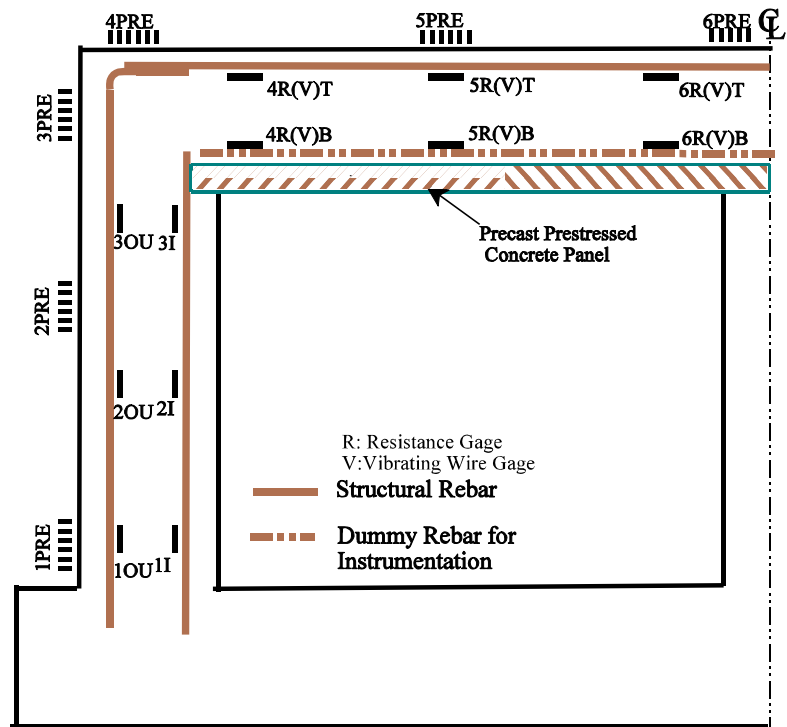


Figure A-5 Detailed Illustration of Sullivan Co. Culvert Instrumentation

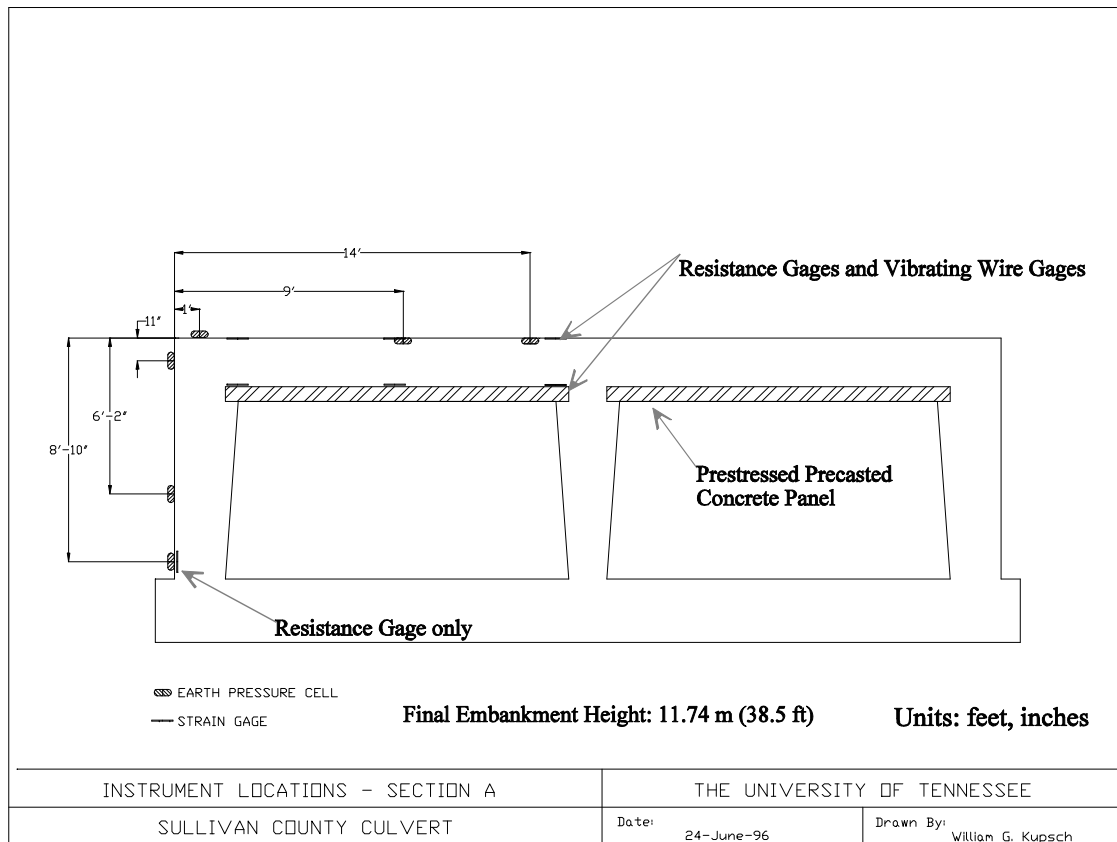
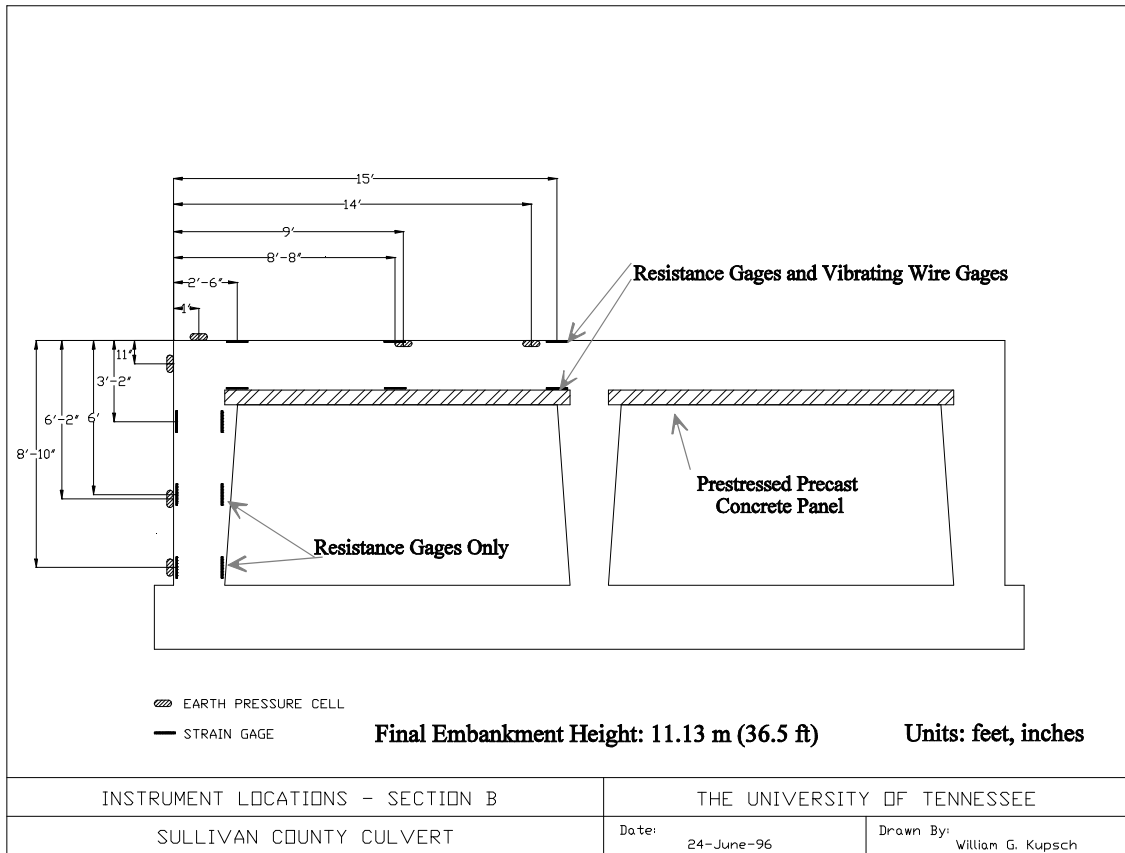


Figure A-6 Instrumentation Detail of Section A in Replacement Culvert  
(Sullivan County, TN)



Appendix A-7 Instrumentation Detail of Section B in Replacement Culvert  
(Sullivan County, TN)

## Appendix A-3

### Chronology of Field Events - Sullivan County Culvert Field Record Results

The Sullivan Co. culvert replaced a previous culvert that had been removed. The new culvert was constructed with “reduced compaction effort” which should not be considered as typical construction practice. Table 1 lists some major events during the construction instrumentation and data collection.

Table 1 the major events during the construction of the embankment and after

Date	Event
04/03/96	Pouring the concrete at the roof of Section B, the strain gage readings in section B were recorded before the pouring of the concrete. Section A had previously poured.
04/08/96	The initial reading of vibrating gages were taken, some of the gages failed to response possibly due to the hardening of concrete.
04/09/96	Installation of the pressure cell on the surface of culvert, initial readings took after the cells on the wall were covered by loosely dumped gravel. No strain gage readings.
04/15/96	Readings recorded when there was loosely dumped gravel piled at Section A, (Triangular shape in cross section, the bottom length was about 4.0m and the height was 2.5m. There was no additional gravel put at the Section B. For the cells on the roof, A4PRE was covered by gravel, the rest of them had no loads on them (both Section A and Section B). The reading was assumed as the datum.
04/23/96	The estimated backfill height in Section A was 20 ft and 18 ft in Section B.
04/26/96	The estimated backfill height in Section A was 28ft and 23 ft in Section B.
04/30/96	The estimated backfill height in Section A was 32 ft and 28 ft in Section B.
05/08/96	Completion of construction the final backfill height of Section A is 38.5 ft, and Section B is 34.0 ft. Gage 6RT in Section A was no reading, the vibrating wire gage 6VT registered very large strain. This may due to the presence of the crack near that area.
05/29/ 96	Readings took after a heavy thunderstorm. The pressure recorded by two pressure cells in Section B (1PRE and 2PRE), abruptly drop to the very small even negative.
01/25/00	Last Reading Taken.

Notes on the recording of the instrumentation in Sullivan County:

Generally 1, 2, 3 are in the wall and 4, 5, 6 are on the roof of the culvert. As illustrated in the Figure 1, detailed location of these gages and the dimension of the culvert are shown elsewhere.

Vibrating Pressure Cell:

A4PRE : No. 4 pressure cell in Section A

Concrete Strain Gage:

B2I : No. 2 resistance gage in the inside side of the culvert in Section B. OU means outside side of the culvert.

A4VT: No. 4 vibrating wire gage in the top of culvert roof in Section A.

B6RB: No. 6 resistance gage in the bottom of culvert roof in Section B.

## Appendix A-4

### Selected Recorded Earth Pressure Distributions

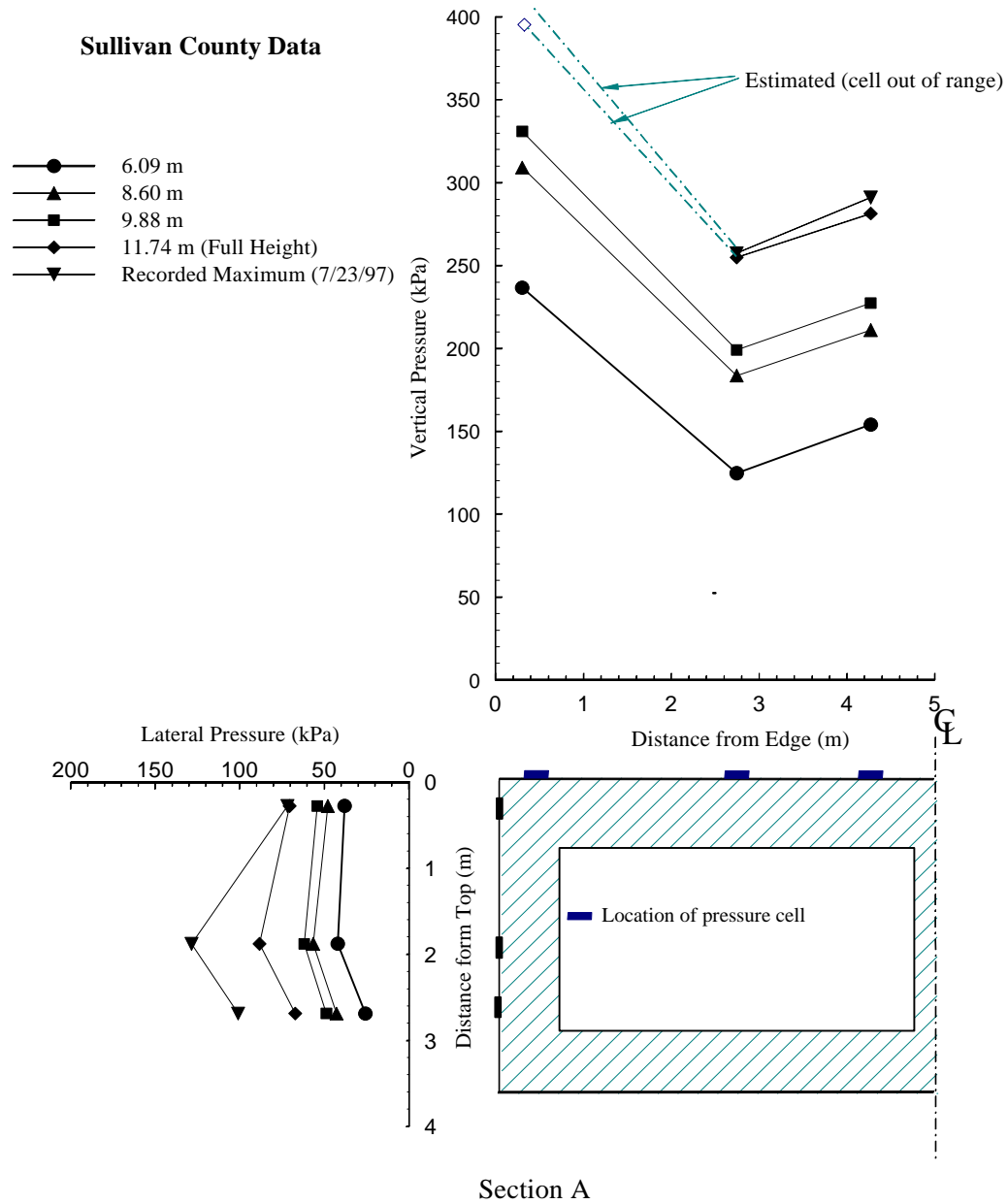


Figure A-8 Recorded Pressures in Section A at Different Fill Heights

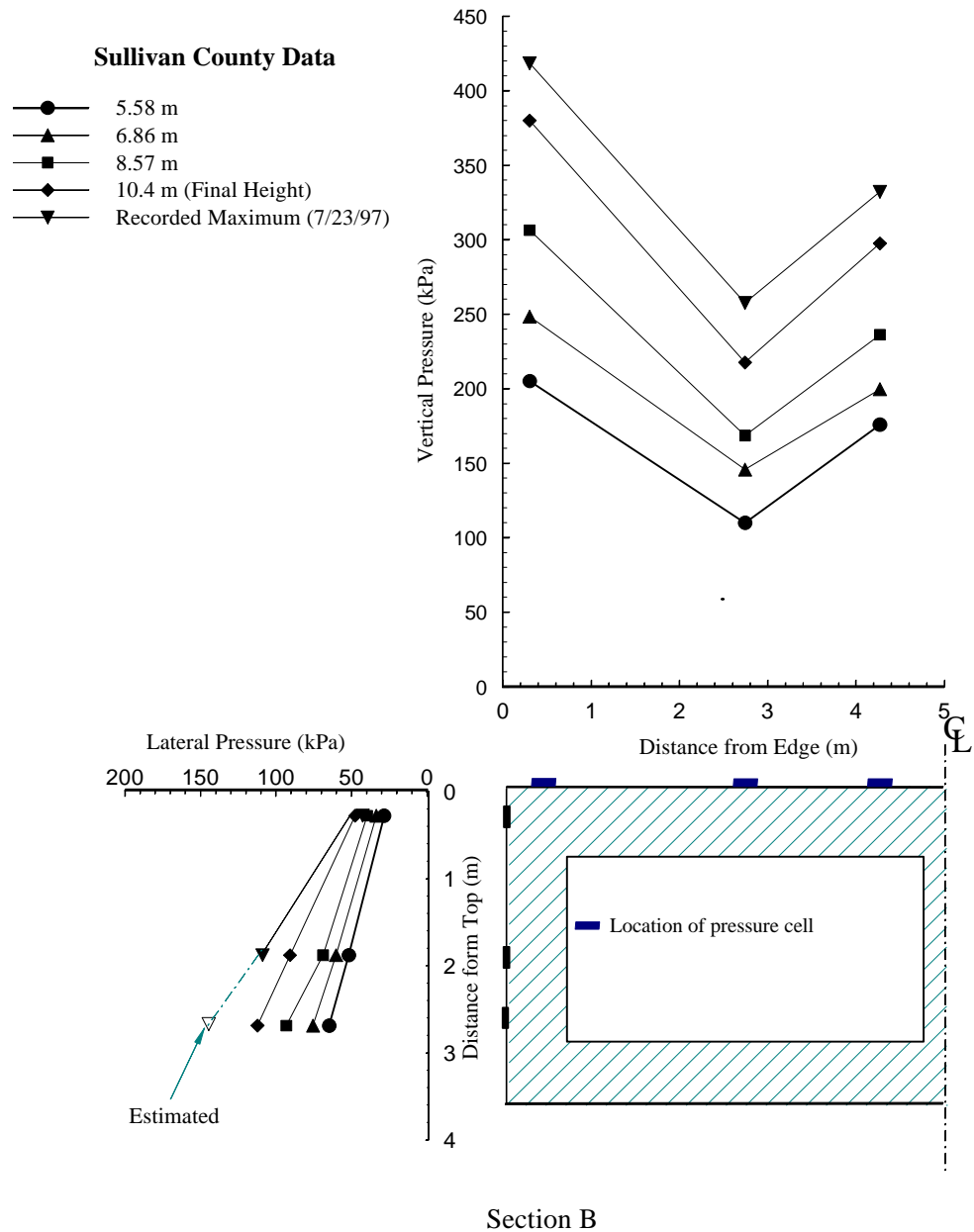


Figure A-9 Recorded Pressures in Section B at Different Fill Heights



## **Appendix A-5**

### **Original Vibrating Wire Pressure Cell Records**

#### **Sullivan County Culvert Site**

**(04/09/1996-1/25/00)**

	1PREA 34674			2PREA 34668			3PREA 34670		
	Factor K	Factor C		Factor K	Factor C		Factor K	Factor C	
	-0.000670	0.006531		-0.008080	0.006546		-0.018560	0.006683	
	Temperature	Reading	Pressure (kPa)	Temperature	Reading	Pressure (kPa)	Temperature	Reading	Pressure (kPa)
Initial Reading 4/9/96	10.2	10482.3	NA	10.2	10861.4	NA	10.2	9551.7	NA
4/15/96	11.4	10297.5	8.3	10.2	10777.5	3.8	10.6	9515.7	1.7
4/18/96	11.5	9931.2	24.8	11.1	10223.1	28.9	11.6	9320.4	10.8
4/23/96	13.5	9637.7	38.0	13.1	9925.7	42.4	13.1	8986.7	26.4
4/26/96	13.6	9418.5	47.9	13.3	9605.1	56.9	13.3	8614.4	43.6
4/30/96	14.2	9279.4	54.1	14.1	9484.6	62.4	13.8	8479.0	49.9
5/8/96	15.9	8915.5	70.5	15.5	8897.2	88.9	15.1	8080.8	68.4
5/16/96	14.6	8887.9	71.8	14.8	8860.8	90.6	14.9	8127.8	66.2
5/29/96	17.0	9111.1	61.7	17.3	8660.6	99.7	17.1	8098.5	67.8
06/21/96	18.5	8712.1	79.7	18.5	8583.0	103.3	18.1	8064.4	69.5
07/26/96	19.3	8658.0	82.1	19.6	8649.9	100.3	19.4	8093.3	68.4
8/20/96	18.9	8668.8	81.6	19.2	8609.7	102.1	19.0	8126.8	66.8
10/4/96	16.7	8709.5	79.8	16.9	8762.5	95.1	17.3	8260.5	60.4
11/11/96	10.8	8966.0	68.3	11.9	8999.0	84.2	13.3	8370.7	54.8
12/16/96	8.6	8815.8	75.1	9.2	8870.5	89.8	10.7	8423.6	52.0
3/1/97	9.6	8640.4	82.9	9.7	8335.9	114.0	10.4	8225.9	61.1
5/27/97	15.9	8284.5	98.9	15.5	7955.3	131.5	15.1	8073.9	68.7
7/23/97	19.9	8239.6	100.9	19.9	8001.1	129.6	19.4	7967.4	74.2
1/20/98	7.7	8699.6	80.3	8.4	8778.4	93.9	9.7	8376.7	54.1
2/14/98	8.1	8481.2	90.1	9.5	8610.8	101.5	9.5	8375.4	54.1
5/3/98	13.4	8242.5	100.8	13.4	7797.2	138.5	13.5	8144.9	65.2
5/21/98	16.2	8044.6	109.7	16.1	7728.4	141.7	15.6	7945.1	74.7
6/9/98	16	8479.1	90.2	16.6	8074.4	126.1	16.7	7998.7	72.4
7/8/98	16	8479.1	90.2	16.6	8074.4	126.1	16.7	7998.7	72.4
8/8/98	18.8	8330.5	96.9	19	7945.5	132.1	18.7	7884.4	77.9
9/4/98	19.6	8420.5	92.8	19.7	8012.9	129.1	19.5	8022.7	71.6
10/24/98	12.7	8945	69.2	14	8984.4	84.9	15.2	8411.6	53.2
12/18/98	8.6	9051.8	64.4	9.8	9173.3	76.2	11.5	8517	47.8
1/10/99	5.2	9101.7	62.2	6.4	9186.8	75.4	8.6	8561.3	45.4
1/30/99	9.7	8600.5	84.7	9.7	8483.9	107.3	10.6	8255	59.8
2/21/99	7.6	8843.5	73.8	8.5	8812.8	92.4	10	8436.7	51.4
3/13/99	7.2	8767	77.3	7.8	8832.4	91.4	9.3	8490.6	48.8
3/26/99	9.6	8580.2	85.7	9.8	8354.4	113.1	10.6	8318.2	56.9
4/9/99	13.8	8270.6	99.6	13.3	7870.3	135.2	13.1	8050.4	69.5
5/14/99	15.5	8174.8	103.9	15.3	7751.6	140.6	15.1	7994.4	72.4
6/6/99	17.1	8045.7	109.7	16.8	7610.3	147.1	16.5	7919.7	76.0
7/17/99	19.5	8162.2	104.4	19.6	7758.9	140.6	19.4	7848.2	79.7
8/21/99	20.4	8132.6	105.8	20.5	7577.3	148.8	20.2	7930.1	76.0
10/3/99	15.5	8578.4	85.7	15.8	8642.5	100.5	16.6	8285.2	59.2
11/10/99	11.2	8745.5	78.2	12.0	8904.2	88.4	13.1	8415.8	52.7
12/11/99	8.1	8979.3	67.7	9.2	9125.3	78.4	11.0	8523.3	47.29
1/25/00	4.3	9079.6	63.2	5.8	9348.9	68.5	8.2	8668.7	40.94

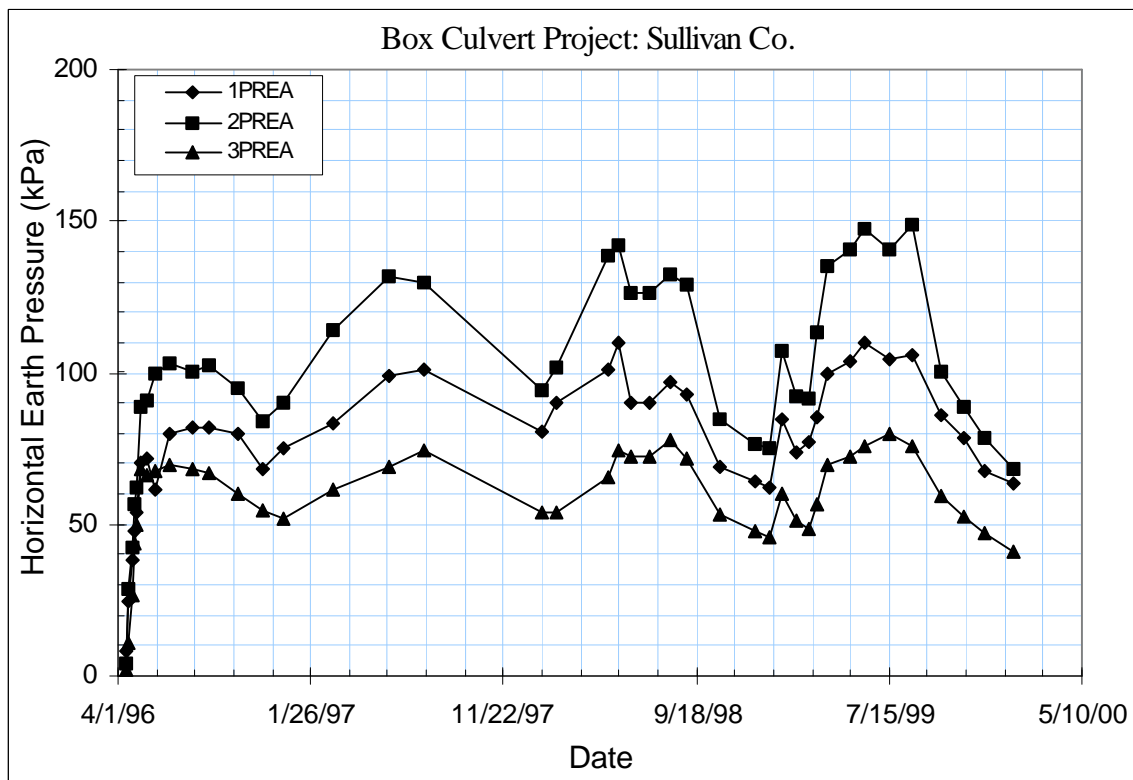


Figure A-10 Recorded Horizontal Pressures (Section A, Sullivan County, TN)

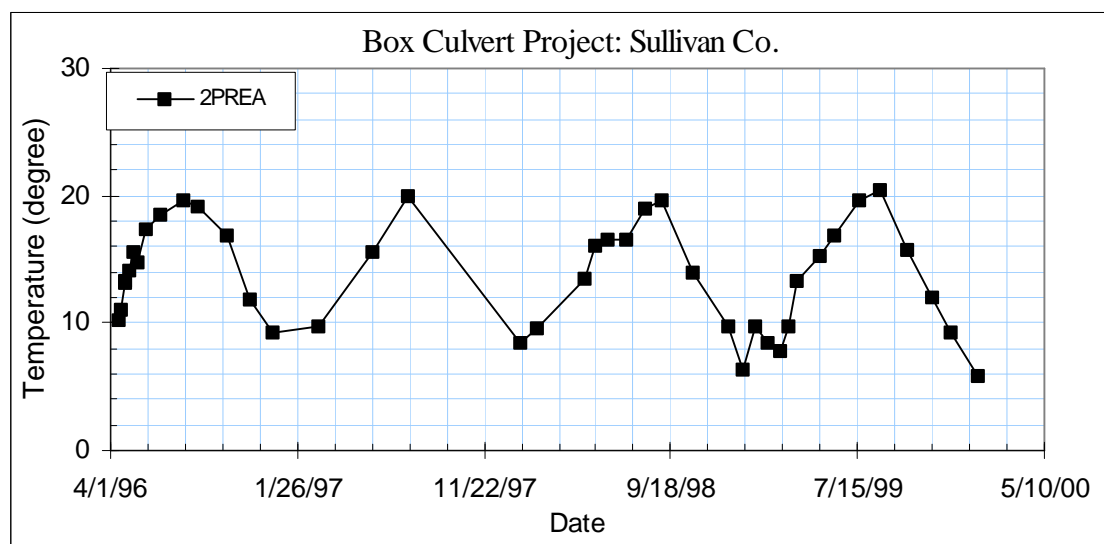


Figure A-11 Recorded Temperature at Cell 2PREA (Sullivan County, TN)

	4PREA 34678			5PREA 34679			6PREA 34673		
	Factor K	Factor C		Factor K	Factor C		Factor K	Factor C	
	-0.014270	0.006607		-0.006950	0.006752		-0.016750	0.006514	
	Temperature	Reading	Pressure (kPa)	Temperature	Reading	Pressure (kPa)	Temperature	Reading	Pressure (kPa)
Initial Reading 4/9/96	5.6	9829.1	NA	7.2	10429.7	NA	6.7	10679.2	NA
4/15/96	12.8	9445.7	16.8	14.6	10270.0	7.8	14.0	10500.8	8.9
4/18/96	13.0	7301.9	114.4	14.7	9115.8	61.5	14.8	8794.2	85.6
4/23/96	13.5	4604.9	237.2	14.6	7744.4	125.4	14.6	7229.7	155.8
4/26/96	13.8	3016.9	309.5	14.4	6479.4	184.3	14.5	5962.7	212.7
4/30/96	14.2	2537.1	331.3	14.6	6147.5	199.7	14.7	5598.4	229.1
5/8/96	15.1	2537.1	331.3	15.7	4946.4	255.7	15.8	4395.5	283.3
5/16/96	15.2	1228.4	390.9	15.1	5214.9	243.2	15.0	4452.9	280.6
5/29/96	17.1	1228.9	390.7	17.3	5158.5	245.9	17.3	4613.6	273.7
06/21/96			NA	18.4	5083.7	249.4	18.2	4529.6	277.5
07/26/96			NA	19.4	5039.7	251.5	19.3	4508.3	278.6
8/20/96			NA	18.9	5050.2	251.0	19.0	4521.8	278.0
10/4/96			NA	17.5	5154.3	246.1	17.2	4697.8	269.9
11/11/96	13.9	1970.9	357.2	13.1	5532.2	228.3	13.1	5086.2	251.9
12/16/96	11.7	2262.9	344.1	10.6	5823.3	214.6	11.1	5300.4	242.1
3/1/97	11.2	1907.9	360.3	10.6	5590	225.5	10.6	4803.2	264.4
5/27/97			NA	15.6	5003.8	253.0	15.4	4253.9	289.6
7/23/97			NA	19.9	4888	258.6	19.9	4182.4	293.3
1/20/98	11	2356	339.9	9.5	5608.6	224.6	9.5	5533.5	231.4
2/14/98	10.1	2384.9	338.7	9.3	6054.6	203.8	9.2	5501.3	232.8
5/3/98			NA	13.7	5393.4	234.8	13.8	4645.6	271.8
5/21/98			NA	16.1	5090.1	249.0	16.1	4288.4	288.1
6/9/98	17.7	959.286	402.9	16.7	5164.2	245.6	16.8	4508.5	278.3
7/8/98	18.7	780.68	410.9	18.6	5026.8	252.1	18.7	4314.4	287.3
8/8/98	18.3	897.1	405.7	18.8	5093.7	249.0	18.9	4417.5	282.6
9/4/98	19.5	834.33	408.4	19.6	4988.1	253.9	19.9	4351.4	285.7
10/24/98	15.6	1640.7	372.0	15	5713.8	219.9	15	5364.3	239.7
12/18/98	11.3	2272.3	343.7	11.3	6246.9	194.9	11.2	5870.4	216.5
1/10/99	9.1	2754.8	321.9	7.5	6532.4	181.5	7.5	6191.9	201.6
1/30/99	11.4	2078.2	352.5	10.6	5919.6	210.1	10.8	5304.3	241.9
2/21/99	10.7	2283.4	343.2	9.9	6161.4	198.8	9.8	5638.8	226.7
3/13/99	9.9	2343.2	340.6	8.9	6306.3	192.0	8.9	5783.3	220.1
3/26/99	11.2	2013.9	184.0	10.7	5982.7	207.2	10.7	5277.2	243.1
4/9/99	13.6	1436.9	381.5	13.9	5593	225.5	13.7	4657.5	271.3
5/14/99	15.3	1092.1	397.1	15.5	5231.3	242.4	15.5	4411	282.5
6/6/99	16.5	866.7	407.2	16.8	5123.4	247.5	16.7	4245.8	290.1
7/17/99	19.1	677.5	415.6	19.2	5006.1	253.1	19.5	4242.6	290.6
8/21/99	20	710.54	414.0	20.2	4913.5	257.4	20.3	4248	290.4
10/3/99	16.9	1330.5	386.0	16.6	5674.9	221.8	16.7	5097	251.9
11/10/99	13.4	2006.9	355.6	12.7	6145.3	199.7	12.7	5690.2	224.8
12/11/99	11.4	2377.6	338.9	10.3	6408.5	187.1	10.3	6062.3	207.0
1/25/00	8.7	2895.0	315.58	7.2	6673.8	174.9	7.2	6407.3	191.81

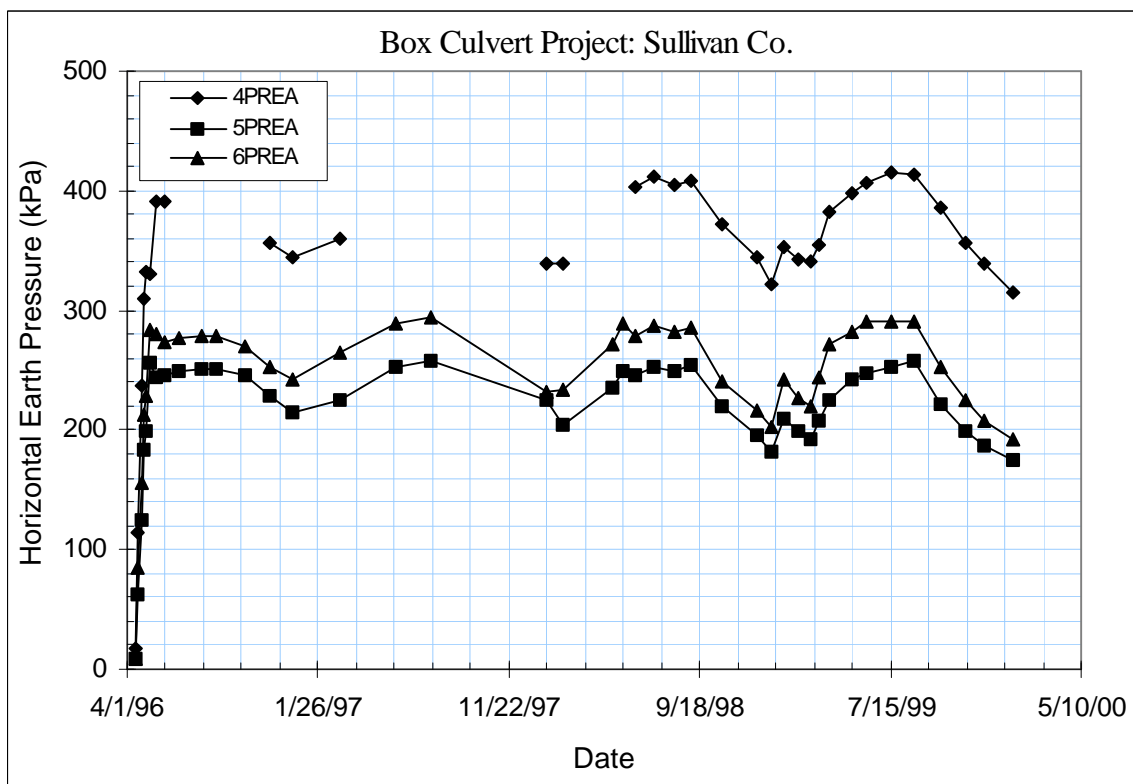


Figure A-12 Recorded Vertical Pressures (Section A, Sullivan County, TN)

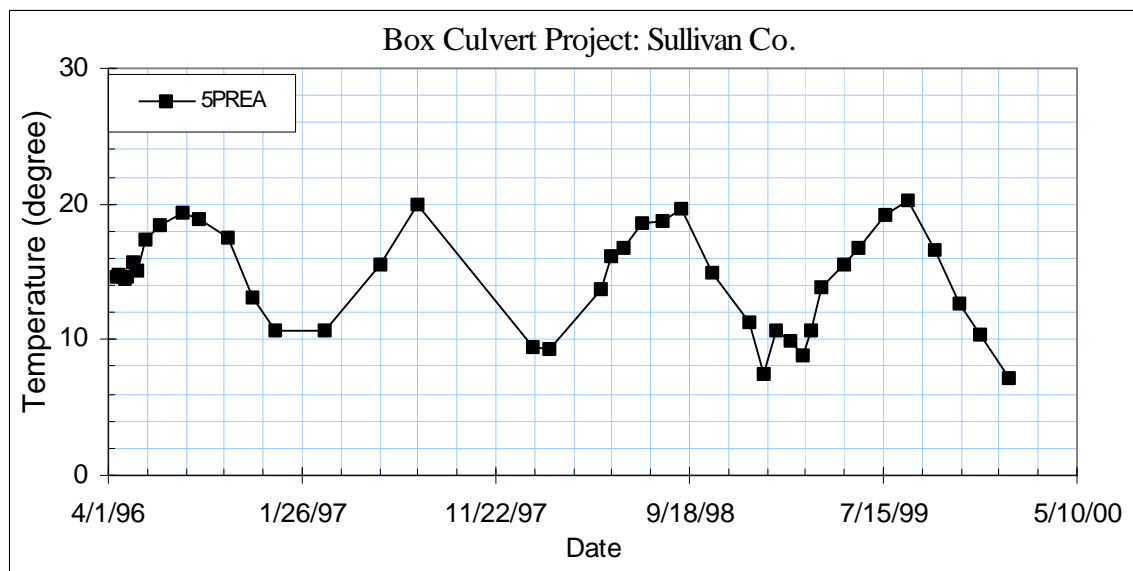


Figure A-13 Recorded Temperature at Cell 5PREA (Sullivan County, TN)

	1PREB 34671			2PREB 34672			3PREB 34675		
	Factor K	Factor C		Factor K	Factor C		Factor K	Factor C	
	-0.014630	0.006462		-0.018990	0.006837		-0.017110	0.006929	
	Temperature	Reading	Pressure (kPa)	Temperature	Reading	Pressure (kPa)	Temperature	Reading	Pressure (kPa)
Initial Reading 4/9/96	8.8	10450.7	NA	3.3	10639.7	NA	4.0	10664.0	NA
4/15/96	10.9	9930.5	23.0	10.1	10411.1	11.7	10.7	10595.6	4.1
4/18/96	11.3	9571.4	38.9	10.9	9982.3	32.0	11.5	10454.6	10.9
4/23/96	13.5	8982.2	65.0	13.0	9513.1	54.4	12.9	10046.2	30.6
4/26/96	13.6	8743.0	75.6	13.2	9331.9	62.9	13.3	9938.6	35.8
4/30/96	14.3	8348.1	93.1	14.1	9148.6	71.7	14.0	9805.9	42.2
5/8/96	16.0	7914.3	112.3	15.7	8680.2	94.0	15.5	9637.9	50.4
5/16/96	14.6	7858.5	114.9	14.7	8640.6	95.7	15.3	9680.4	48.3
5/29/96	17.1	10540.7	-4.8	17.5	10061.4	29.1	17.7	9600.5	52.4
06/21/96	18.5	10460.3	-1.4	18.7	9590.5	51.5	18.7	9681.2	48.7
07/26/96	19.3	10396.8	1.3	19.9	9359.9	62.5	19.9	9779.8	44.1
8/20/96	19.0	10364.8	2.8	19.3	9207.6	69.6	19.5	9824.4	41.9
10/4/96	16.7	10338.0	4.2	16.9	9166.8	71.2	17.3	9954.2	35.5
11/11/96	10.6	10381.2	2.9	11.7	9228.4	67.6	13.5	10075.3	29.2
12/16/96	8.6	10501.4	-2.2	9.2	9041.7	76.1	10.9	10088.8	28.3
3/1/97	9.6	10470.2	-0.9	9.8	8684	93.0	10.7	9951.4	34.8
5/27/97	15.9	10545.6	-4.9	15.6	8318.6	111.0	15.4	9851.5	40.2
7/23/97	19.9	10536.7	-5.0	19.9	8281.5	113.3	19.7	9732.3	46.4
1/20/98	7.7	10568.4	-5.1	8.2	8759.2	89.3	9.9	10103.6	27.5
2/14/98	8.2	10542.9	-4.0	8.2	8587.1	97.4	9.6	10084.7	28.3
5/3/98	13.5	10547.1	-4.8	13.4	8298.2	111.7	13.7	9923.7	36.5
5/21/98	16.2	10516.7	-3.7	16.3	8058.4	123.4	16.2	9774.6	43.9
6/9/98	16.1	10529.1	-4.2	16.5	8240	114.9	17	9800.6	42.8
7/8/98	18.8	10514.9	-3.9	18.9	8162.9	118.8	18.9	9706.7	47.5
8/8/98	18.9	10498.7	-3.2	19	8080.6	122.7	19	9784	43.8
9/4/98	19.6	10515.3	-4.0	19.7	8122.7	120.8	19.8	9809.5	42.7
10/24/98	13	10516.3	-3.3	13.8	8846.4	85.9	15.5	10083.2	29.1
12/18/98	8.6	10548	-4.3	9.7	8941.9	80.9	11.7	10172.9	24.4
1/10/99	5	10535.6	-3.4	6.2	9039.8	75.8	8.7	10202.4	22.6
1/30/99	9.7	10488.3	-1.8	9.8	8387.6	107.0	10.9	10024.6	31.4
2/21/99	7.6	10529.9	-3.4	8.4	8581.6	97.7	10.3	10134.7	26.0
3/13/99	7.1	10531.1	-3.4	7.6	8579.6	97.7	9.4	10169.3	24.3
3/26/99	9.5	10512.1	-2.8	9.7	8206.7	115.5	10.8	10094.3	28.0
4/9/99	13.8	10528.2	-4.0	13.5	7886.4	131.1	13.5	9930.5	36.2
5/14/99	15.5	10486.3	-2.3	15.3	7787.1	136.0	15.3	9898.5	37.9
6/6/99	17.2	10458.2	-1.2	16.9	7674	141.6	16.8	9838.9	40.9
7/17/99	19.5	10479.5	-2.4	19.6	7765.7	137.6	19.6	9764.2	44.8
8/21/99	20.4	10485.5	-2.7	20.5	7775.8	137.3	20.5	9817.2	42.4
10/3/99	15.4	10501.5	-2.9	15.9	8396.4	107.4	16.8	10032.7	31.7
11/10/99	11.3	10506.1	-2.7	12.1	8677.9	93.6	13.4	10126	26.8
12/11/99	8.1	10515.3	-2.81	9.2	8892.3	81.6	11.2	10181.1	22.2
1/25/00	4.1	10562.6	-4.51	5.6	9262.6	74.1	8.4	10260.0	18.8

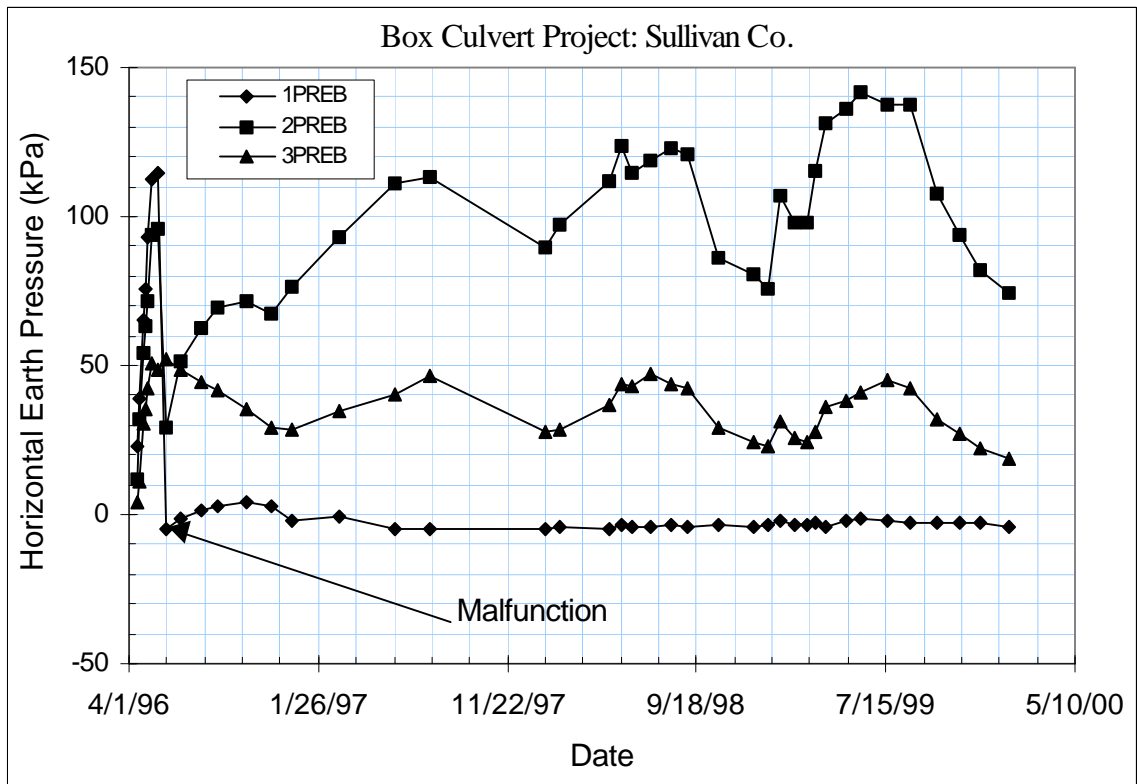


Figure A-14 Recorded Horizontal Pressures (Section B, Sullivan County, TN)

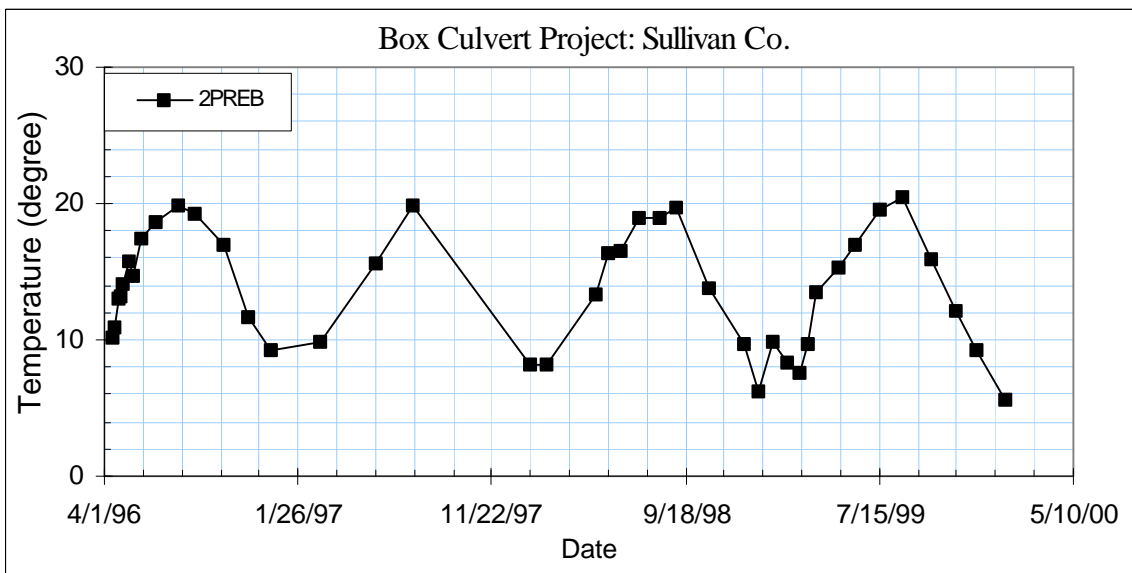


Figure A-15 Recorded Temperature at Cell 2PREB (Sullivan County, TN)

	4PREB 34676			5PREB 34669			6PREB 34677		
	Factor K	Factor C		Factor K	Factor C		Factor K	Factor C	
	-0.018300	0.006588		-0.023910	0.006456		-0.001390	0.006739	
	Temperature	Reading	Pressure (kPa)	Temperature	Reading	Pressure (kPa)	Temperature	Reading	Pressure (kPa)
Initial Reading 4/9/96	5.9	10799.4	NA	7.5	10664.7	NA	6.6	10213.4	NA
4/15/96	12.3	10424.8	16.2	19.0	10647.6	2.7	18.7	10190.6	1.2
4/18/96	11.8	8869.8	86.9	12.9	9337.1	60.0	13.0	7842.3	110.2
4/23/96	13.0	6263.3	205.2	14.0	8170.8	112.1	13.9	6817.0	157.9
4/26/96	13.4	5310.6	248.4	14.2	7366.1	147.9	14.1	5914.6	199.8
4/30/96	13.9	4034.4	306.3	14.7	6850.3	171.0	14.4	5103.4	237.5
5/8/96	15.7	2406.2	380.0	16.2	5745.3	220.4	16.0	3809.2	297.7
5/16/96	15.3	2305.8	384.6	15.6	5751.9	220.0	15.5	3819.4	297.2
5/29/96	17.3	2245.5	387.1	17.9	5611.8	226.6	17.7	3906.1	293.2
06/21/96	18.1	2193.4	389.4	18.8	5418.7	235.4	18.6	3664.3	304.4
07/26/96	19.4	2233.3	387.4	19.9	5483.0	232.7	19.9	3602.1	307.3
8/20/96	19.1	2184.5	389.7	19.5	5470.6	233.2	19.3	3753.6	300.3
10/4/96	17.2	2164.1	390.8	17.5	5502.6	231.4	17.4	4055.6	286.2
11/11/96	13.7	2062.9	395.9	13.2	5775.4	218.6	13.3	4490.5	266.0
12/16/96	11.2	2256.0	387.4	10.5	5898.3	212.7	10.3	4590.8	261.3
3/1/97	10.9	1975.7	400.2	10.6	5439.2	233.1	10.3	3835.7	296.4
5/27/97	15.2	1735.7	410.5	15.8	4943.9	256.0	15.6	3181.1	326.8
7/23/97	19.1	1551.9	418.4	19.9	4833.2	261.6	19.6	3065	332.3
1/20/98	10.7	2191.7	390.4	9.3	5740.8	219.5	9.3	4254.7	276.9
2/14/98	9.8	2130.4	393.3	9	5696.1	221.4	8.8	4212.2	278.9
5/3/98	13.6	Failed	NA	13.8	4945.1	255.6	13.6	3280.2	322.2
5/21/98	15.2	Failed	NA	16.3	4666.6	268.5	16	Failed	NA
6/9/98	17.1	1342.91	428.1	17.1	4851.1	260.4	17	3158.6	327.9
7/8/98	18.5	1261.36	431.7	19.1	4760.3	264.7	18.8	2940.2	338.1
8/8/98	18.7	1775.2	408.3	18.8	4800.4	262.9	18.8	3020.1	334.4
9/4/98	19.3	1384.24	426.0	20	4705.8	267.3	20	3133.5	329.1
10/24/98	15.5	1824.3	406.5	15	5444.9	233.6	15.1	4275.9	276.0
12/18/98	11.9	2264.7	386.9	11.1	5860.9	214.4	11.1	4770.2	253.0
1/10/99	8.7	2521	375.7	4	6141.9	200.8	4	5215.4	232.2
1/30/99	11.2	1741.8	410.8	10.5	5085.9	248.8	10.5	4087.1	284.7
2/21/99	10.5	2030.2	397.8	9.7	5565.3	227.4	9.4	4468	267.0
3/13/99	9.6	2147.5	392.5	8.8	5714.2	220.6	8.4	4655.9	258.2
3/26/99	11	1754.5	410.2	10.6	5281.3	240.1	10.4	4015.7	288.0
4/9/99	13.5	1463.8	423.1	14	4890.5	258.1	13.5	3266	322.9
5/14/99	15.3	1419.8	424.9	15.8	4567.4	272.8	15.4	3135.7	329.0
6/6/99	16.5	1167.3	436.2	17.1	4507.5	275.7	16.6	2938.2	338.1
7/17/99	19.2	1147.6	436.7	19.6	4612.4	271.4	19.3	3000.8	335.3
8/21/99	20.1	1235.3	432.7	20.6	4503.7	276.4	20.3	3013.3	334.7
10/3/99	16.8	1505.6	420.8	16.8	5115.4	248.6	16.7	3719.9	301.8
11/10/99	13.3	2067.5	395.7	12.8	5644.4	224.3	12.5	4267.7	276.3
12/11/99	10.2	2398.3	380.9	11.3	5908.2	211.3	10.1	4744.6	254.1
1/25/00	6.8	2738.4	365.8	8.5	6128.0	202.1	6.6	5317.0	227.51



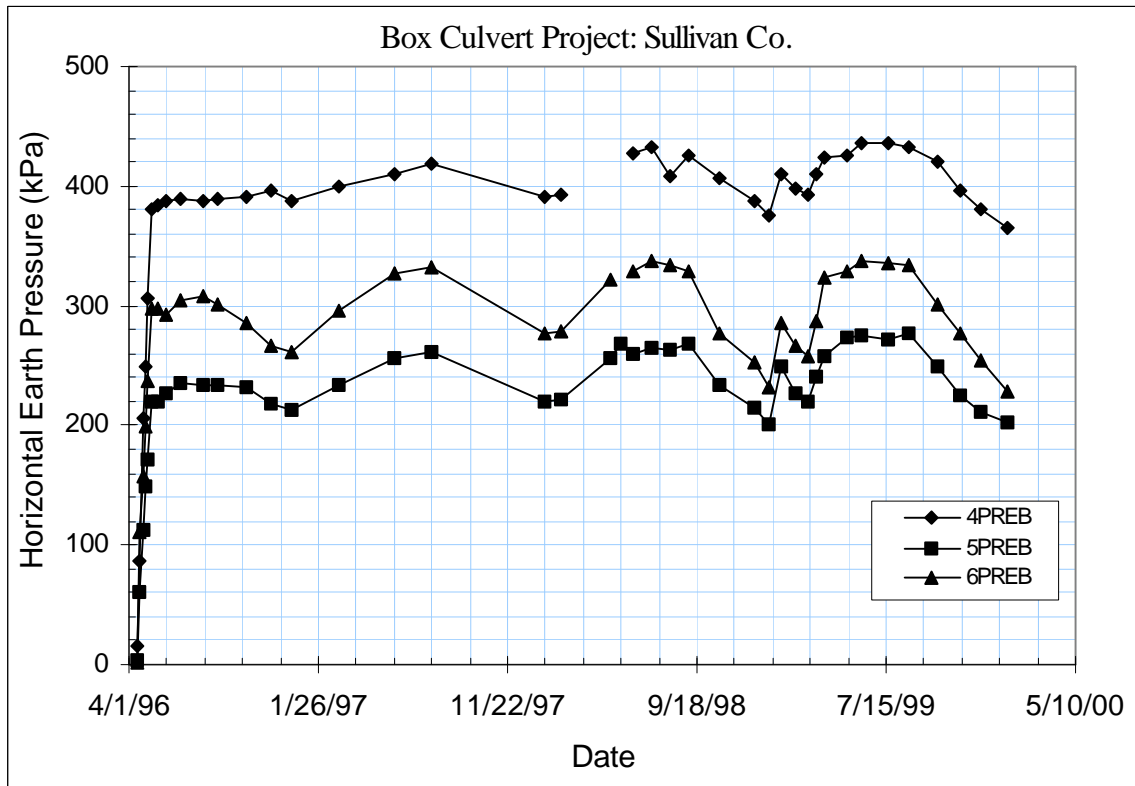


Figure A-16 Recorded Vertical Pressures (Section B, Sullivan County, TN)

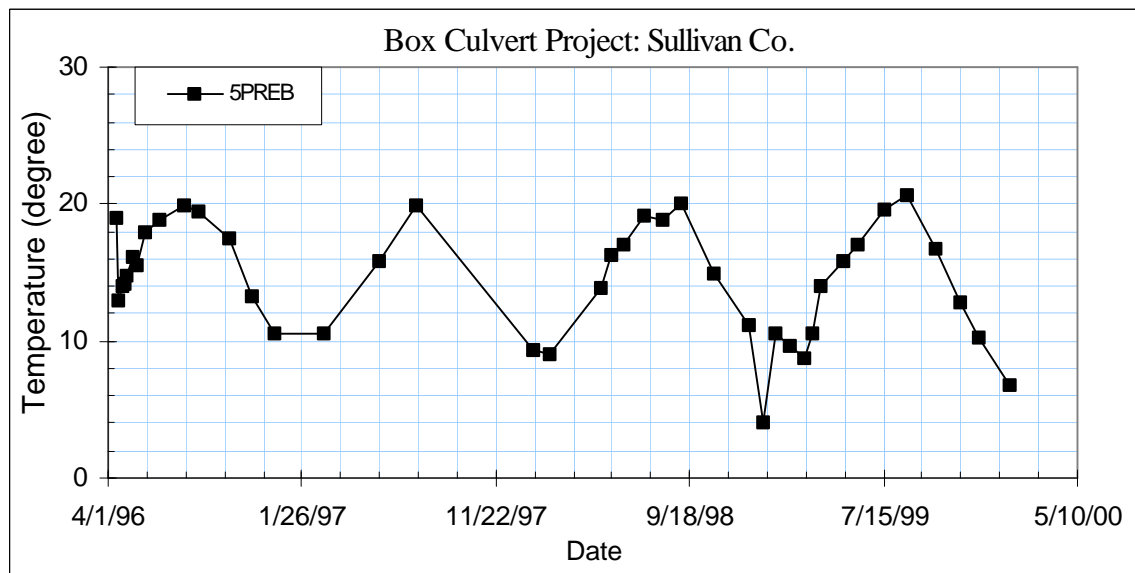


Figure A-17 Recorded Temperature at Cell 5PREB (Sullivan County, TN)

**Appendix A-6**

**Original Vibrating Wire Concrete Strain Gage Records**

**Sullivan County Culvert Site**

**(4/9/1996-1/25/2000)**

Sullivan County Culvert Concrete Strain Gages								
Date	4VTA		4VBA		5VTA		5VBA	
	Temperature	Reading	Temperature	Reading	Temperature	Reading	Temperature	Reading
4/9/96	27.7	2309.2	30.2	2545.8	25.6	2362.5	29.5	2579.1
4/15/96	12.7	2337.7	12.6	2634.8	14.8	2384.8	15.1	2670.1
4/18/96	13.1	2327.9	11.8	2629.7	14.5	2356.3	11.1	2676.7
4/23/96	13.9	2306.2	15.0	2624.9	14.6	2329.2	15.5	2682.3
4/26/96	14.1	2286.5	14.6	2640.5	14.5	2295.5	14.1	2693.4
4/30/96	14.5	2275.1	15.2	2638.9	14.7	2282.8	15.9	2689.1
5/8/96	15.6	2341.8	16.0	2629.2	15.8	2249.4	16.4	2691.0
5/16/96	16.0	2394.9	16.1	2629.8	16.1	2242.3	16.9	2691.0
5/29/96	17.3	2400.4	17.7	2609.7	17.4	2213.7	17.9	2679.6
6/21/96	18.3	2392.9	18.9	2590.0	18.4	2197.8	19.3	2665.6
7/26/96	19.4	2385.5	19.4	2574.3	19.4	2180.3	19.5	2668.7
8/20/96	19.3	2383.4	19.4	2564.8	19.0	2177.0	19.7	2647.7
10/4/96	17.2	2386.1	16.6	2562.5	17.1	2169.3	16.8	2638.7
11/11/96	13.2	2417.2	11.1	2576.8	12.8	2173.7	11.0	2649.2
12/16/96	10.8	2457.4	9.3	2581.5	10.4	2184.4	9.4	2650.5
3/1/97	10.9	2527.5	10.6	2567.4	10.6	2184.8	10.9	2634.2
5/27/97	15.5	2526.2	16	2549.2	15.8	2163.5	16.5	2604.4
7/23/97	19.5	2523.3	20	2543.4	19.6	2150.4	20.4	2601.4
1/20/98	9.9	2612.7	8.4	2567.1	9.2	2169.4	8.4	2628.3
2/14/98	9.6	2614.7	8.7	2565.4	9	2170.9	8.6	2622.8
5/3/98	13.8	2617.3	13.5	2550.4	13.7	2159.5	13.5	2600
5/21/98	16	2615	16.8	2539.2	16.4	2157.6	17.4	2589
6/9/98	16.8	2614.85	16.4	2545.6	16.6	2152.4	16.4	2600.1
7/8/98	18.7	2614	19.1	2539.1	18.8	2151.5	19.4	2593.4
9/4/98	19.7	2612.7	19.5	2544.9	18.5	2148.2	19.7	2592.9
10/24/98	15.1	2629.1	13.1	2562	14.6	2148.7	12.8	2609.4
12/18/98	11.5	2651.7	9.8	2563.7	10.8	2157.2	9.5	2613
1/10/99	8.3	2691.5	6.5	2572.4	7.3	2169.2	6.5	2621.4
1/31/99	11.1	2682.5	10.3	2558.2	10.7	2162.6	10.3	2606
2/21/99	10.1	2689.1	8.4	2565.5	9.5	2162.2	8.1	2613
3/13/99	9.3	2697.3	8	2566	8.7	2165.3	7.7	2611.3
3/26/99	10.9	2692.5	9.7	2560.6	10.5	2160.2	9.7	2605.4
4/9/99	13.7	2686	14.4	2544.2	14	2160.2	14.9	2556.8
5/14/99	15.5	2679.4	15.5	2541.9	15.7	2152	16	2580.1
6/6/99	16.8	2679.4	17.2	2538	17	2151.7	17.7	2577
7/17/99	19.4	2674.1	19.7	2534.5	19.4	2146.8	19.9	2576.8
8/21/99	20.3	2672.3	20.3	2537	20.3	2142.8	20.5	2577
10/3/99	16.7	2689.9	15.6	2550.4	16.5	2147.5	15.5	2592.2
11/10/99	13.1	2709.1	13	2556.4	12.1	2597.8	11.6	2579.7
12/11/99	9.0	2723.9	8.1	2567.9	8.4	2160.7	6.5	2592.6
1/25/00	7.9	2751.2	5.6	2573.1	6.8	2164.9	5.2	2612.0

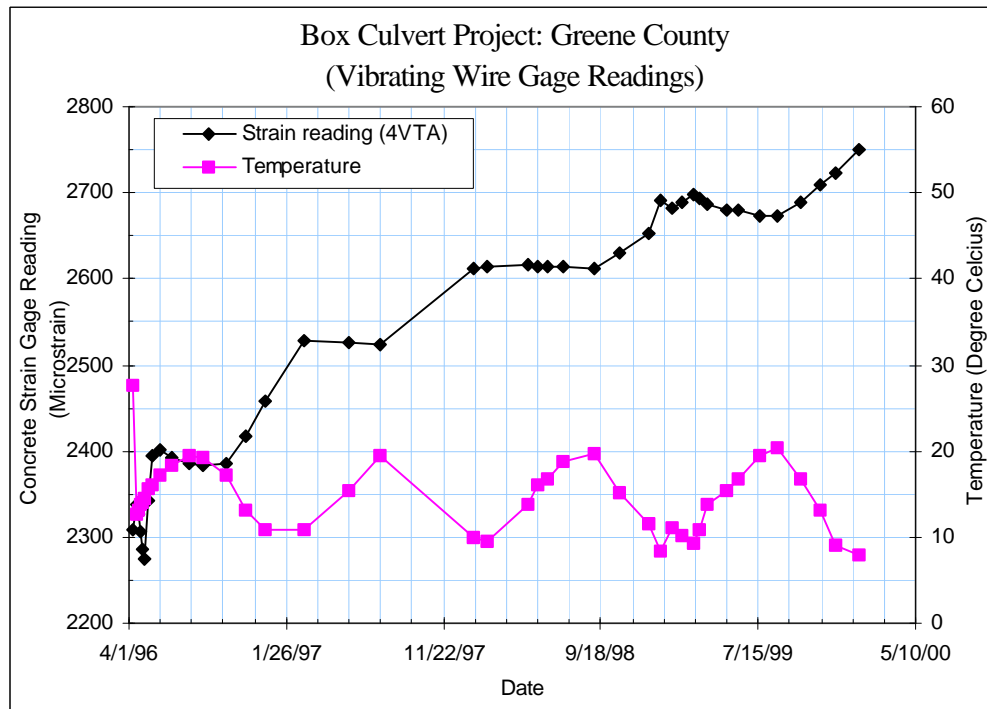


Figure A-18 Recorded Strain Reading and Temperature at 4VTA  
(Sullivan County, TN)

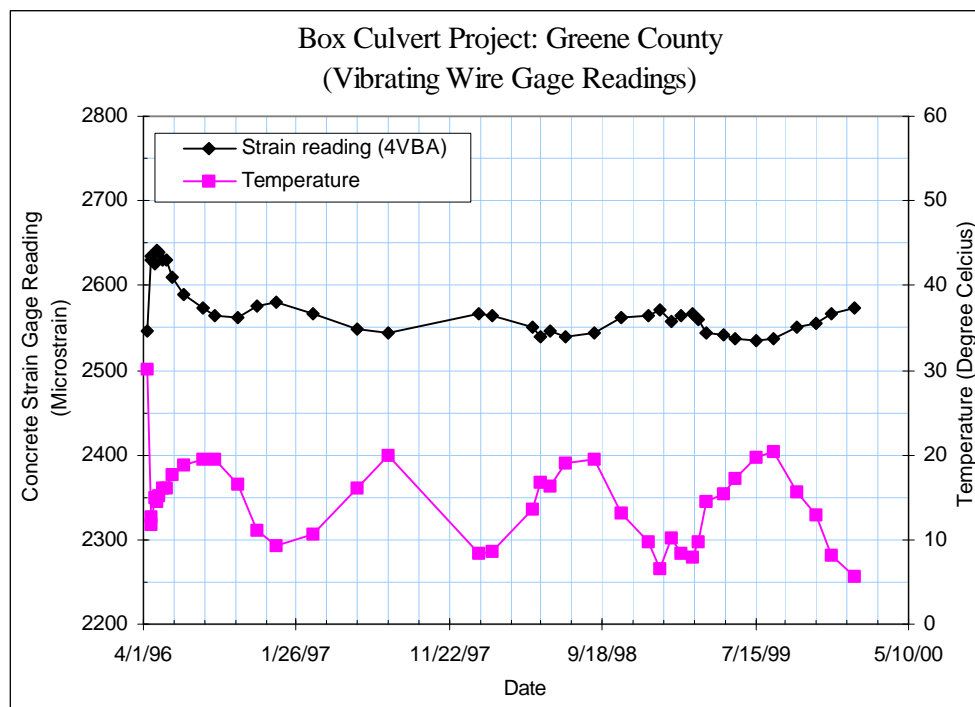


Figure A-19 Recorded Strain Reading and Temperature at 4VBA  
(Sullivan County, TN)

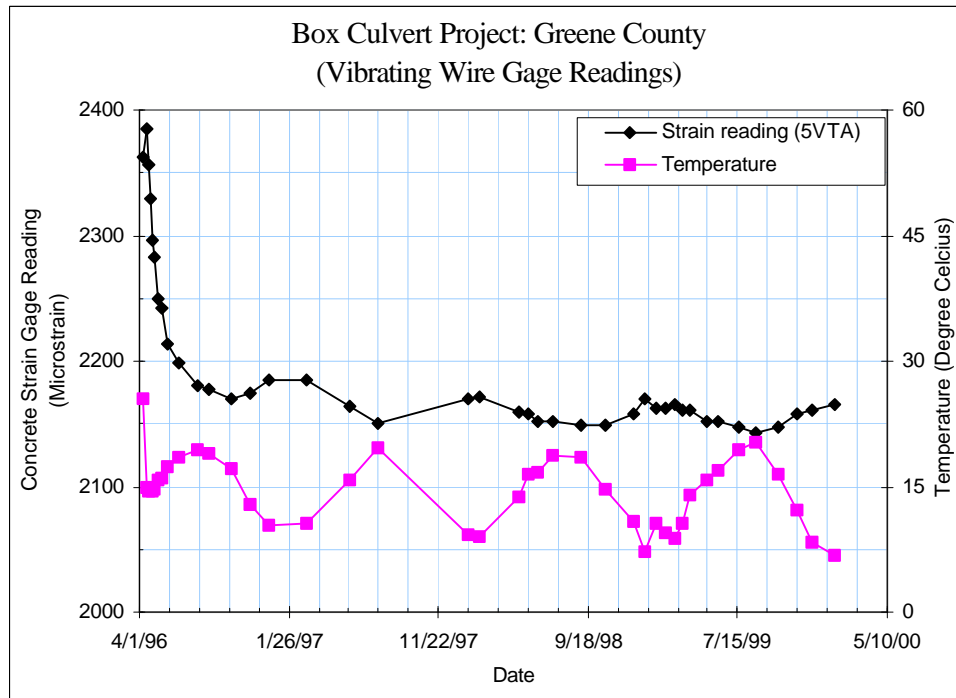


Figure A-20 Recorded Strain Reading and Temperature at 5VTA  
(Sullivan County, TN)

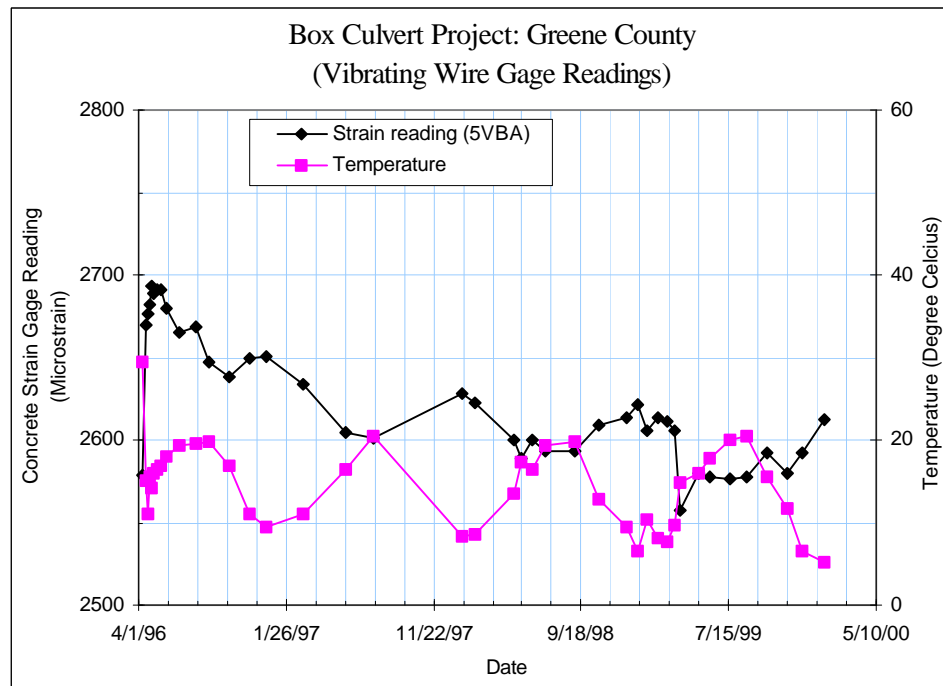


Figure A-21 Recorded Strain Reading and Temperature at 5VBA  
(Sullivan County, TN)

Greene County Culvert Concrete Strain Gages								
Date	6VTA		6VBA		4VTB		4VBB	
	Temperature	Reading	Temperature	Reading	Temperature	Reading	Temperature	Reading
4/9/96	28.8	2429.7	31.5	2630.5	12.8	2646.3	12.6	2702.6
4/15/96	15.5	2471.5	14.4	2711.8	12.8	2646.3	12.6	2702.6
4/18/96	15.2	2494.6	14.2	2692.8	12.3	2648.7	12.2	2695.5
4/23/96	15.1	2544.7	15.7	2654.6	13.7	2628.6	14.6	2691.4
4/26/96	15.0	2592.6	15.2	2722.3	14.0	2614.1	14.4	2697.3
4/30/96	15.1	2814.7	15.8	2739.5	14.7	2597.7	15.1	2697.3
5/8/96	16.3	3373.0	16.6	2809.2	16.0	2816.3	16.1	2692.6
5/16/96	16.1	3408.0	16.7	2810.3	15.6	2853.2	16.0	2700.2
5/29/96	17.9	3384.1	18.1	3043.8	18.0	2856.6	18.0	2679.4
6/21/96	18.9	3394.3	19.4	3034.9	18.9	2849.1	19.2	2663.5
7/26/96	19.9	3388.3	19.8	3027.2	20.0	2834.5	19.6	2650.1
8/20/96	19.5	3389.6	19.6	3013.0	19.6	2824.2	19.7	2639.5
10/4/96	17.3	3364.4	16.7	2994.4	17.7	2826.0	16.8	2639.8
11/11/96	13.0	3344.3	10.8	2984.5	13.5	2877.9	11.2	2667.6
12/16/96	10.2	3368.6	8.7	2985.7	11.1	2906.0	9.4	2673.2
3/1/97	10.5	3372.1	10.4	2956.9	11.0	2994.7	10.7	2654.7
5/27/97	15.7	3343.2	16.2	2915.6	15.8	3001.5	16	2669.0
7/23/97	19.9	3349.6	20.4	2911.9	19.6	2994.7	20.1	2659.7
1/20/98	9.2	3340	7.9	2922.2	10	3089.4	8.5	2714.3
2/14/98	9	3342.4	8.2	2917	9.7	3091.8	8.6	2712.2
5/3/98	13.8	3328.4	13.5	2894.4	13.9	3096.8	13.4	2719.2
5/21/98	16.4	3342.5	17.2	2886.5	16.2	3091.8	16.9	2703.9
6/9/98	17	3329.9	16.7	2893	17	3088.6	16.5	2701.5
7/8/98	19.1	3351.5	19.5	2891.6	19	3086.3	19.4	2701.2
9/4/98	19.9	3339.4	19.6	2887.2	20	3083.6	19.8	2710.8
10/24/98	14.9	3314.3	12.8	2894.9	15.3	3104.5	13.4	2741.1
12/18/98	10.8	3327.2	9.1	2897.9	11.7	3131.4	9.9	2751.6
1/10/99	6.7	3338.9	5.2	2905.7	8.3	3185.6	6.2	2792.8
1/31/99	10.5	3339.8	9.9	2888.8	11.2	3175.9	10.1	2776.2
2/21/99	9.3	3331	7.7	2894.9	10.2	3181.4	8.4	2788.8
3/13/99	8.4	3336.7	7.1	2893.3	9.3	3193.5	7.8	2792.8
3/26/99	10.4	3331.3	9.3	2884.9	10.9	3185.3	9.6	2789.3
4/9/99	13.7	3347.5	14.4	2870.6	13.9	3181.7	14.5	2763.5
5/14/99	15.5	3329.3	15.7	2863.1	15.7	3175.4	15.6	2764
6/6/99	16.8	3331.8	17.2	2859.7	17	3175.1	17.2	2761.3
7/17/99	19.7	3337.9	19.8	2831.2	19.6	3169	19.8	2755.1
8/21/99	20.6	3335.4	20.5	2862.2	20.6	3163.4	20.5	2757.3
10/3/99	16.6	3327.5	14.8	2874.1	16.8	3178.6	15.7	2777.7
11/10/99	12.4	3338.9	12.6	2857.5	13.3	3202.6	12.3	2772.2
12/11/99	8.2	3331.6	7.6	2875.2	8.9	3213.0	7.3	2819.2
1/25/00	6.5	3329.3	4.4	2896.1	7.9	3252.0	5.3	2844.0

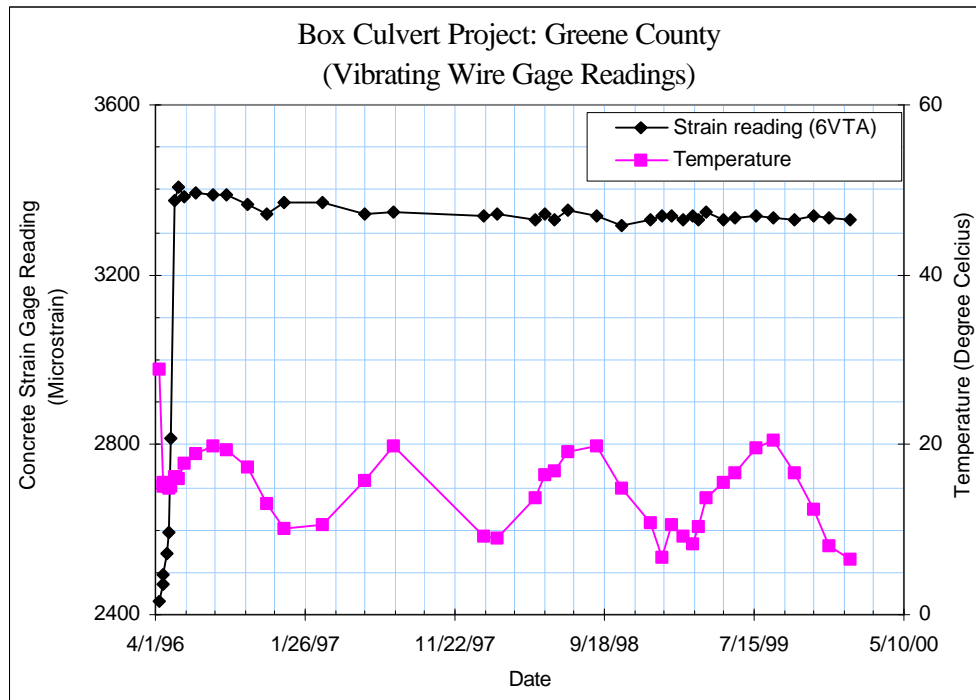


Figure A-22 Recorded Strain Reading and Temperature at 6VTA  
(Sullivan County, TN)

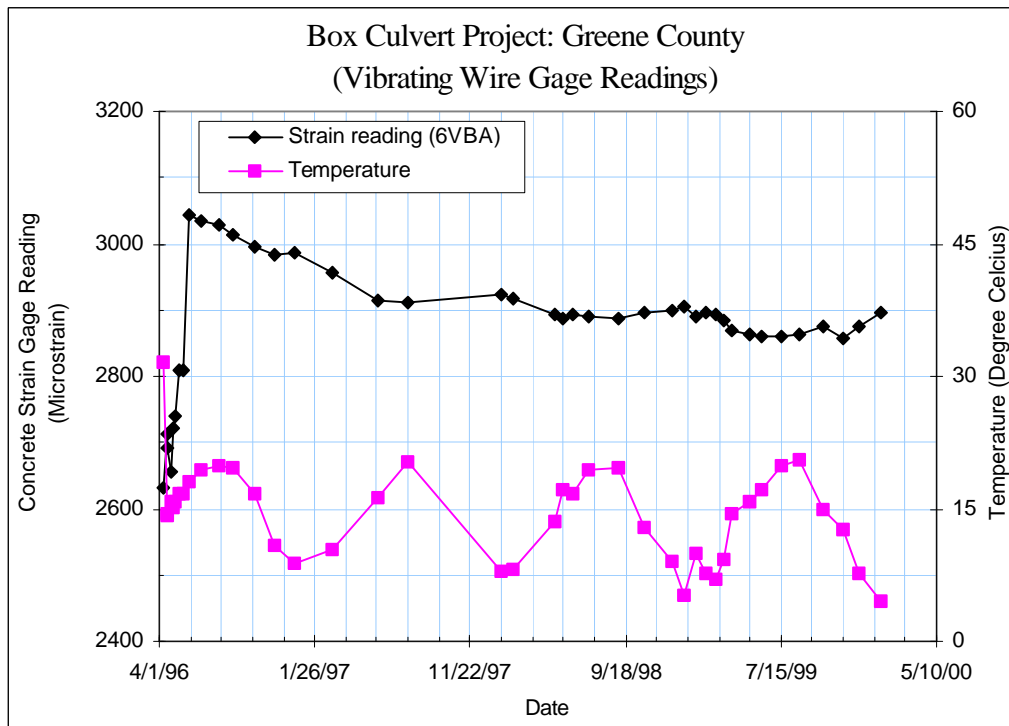


Figure A-23 Recorded Strain Reading and Temperature at 6VBA  
(Sullivan County, TN)

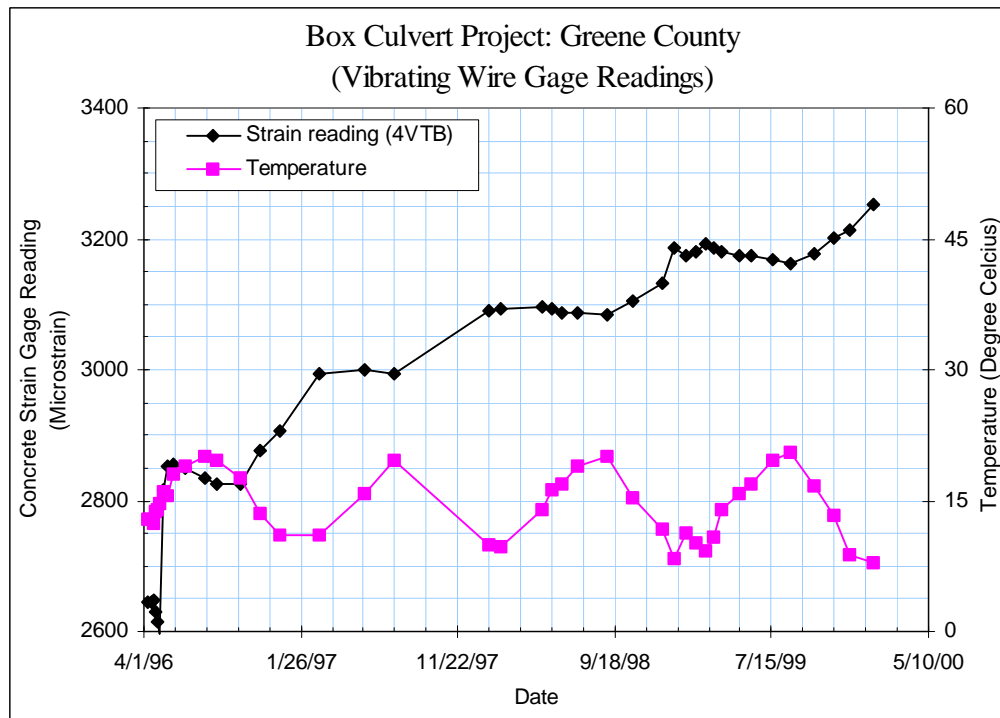


Figure A-24 Recorded Strain Reading and Temperature at 4VTB  
(Sullivan County, TN)

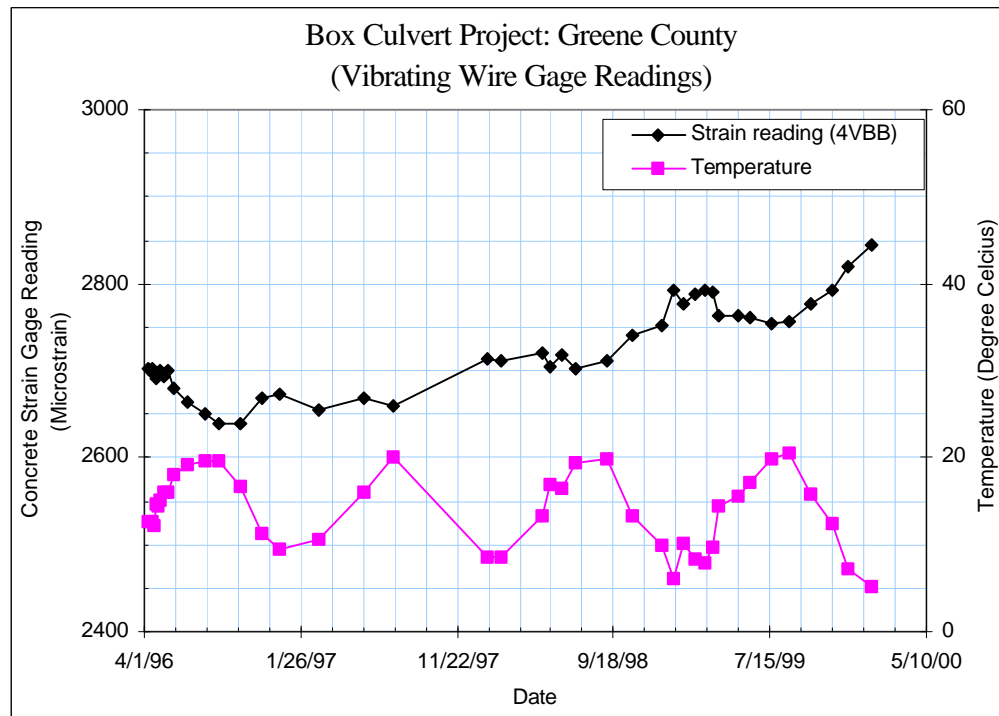


Figure A-25 Recorded Strain Reading and Temperature at 4VBB  
(Sullivan County, TN)



Greene County Culvert Concrete Strain Gages								
Date	5VTB		5VBB		6VTB		6VBB	
	Temperature	Reading	Temperature	Reading	Temperature	Reading	Temperature	Reading
4/9/96	16.5	2414.3	15.9	2605.2	16.0	2477.4	15.8	2467.4
4/15/96	16.5	2414.3	15.9	2605.2	16.0	2477.4	15.8	2467.4
4/18/96	12.7	2412.4	13.1	2619.1	13.0	2518.3	13.1	2456.3
4/23/96	13.9	2384.9	15.6	2617.2	14.1	2544.7	15.4	2431.8
4/26/96	14.1	2372.3	14.2	2614.8	14.2	2561.0	15.0	2427.0
4/30/96	14.7	2356.7	16.1	2621.6	14.7	2583.5	15.8	2414.2
5/8/96	16.1	2326.1	16.9	2623.8	16.1	2571.1	16.7	2463.5
5/16/96	15.8	2318.2	16.4	2628.7	16.3	2575.1	16.6	2463.8
5/29/96	17.7	2298.5	18.0	2679.4	17.9	2572.8	18.4	2451.8
6/21/96	19.6	2281.3	18.8	2591.5	18.8	2568.6	19.6	2433.0
7/26/96	19.7	2254.8	19.8	2633.1	19.9	2541.5	20.0	2419.9
8/20/96	17.1	2230.8	20.0	2560.1	19.4	2538.9	19.8	2404.3
10/4/96	17.1	2230.8	17.1	2557.0	17.2	2521.1	16.9	2402.4
11/11/96	12.6	2233.8	11.0	2574.5	12.8	2519.9	10.8	2418.6
12/16/96	10.1	2243.8	9.5	2576.1	9.9	2542.5	8.8	2417.0
3/1/97	10.4	2249.7	10.9	2561.9	10.4	2562.6	10.1	2397.3
5/27/97	15.8	2231.0	16.7	2528.0	15.5	2547.3	16.3	2372.1
7/23/97	19.7	2219.9	20.7	2525.1	19.7	2551.7	20.5	2363.9
1/20/98	8.8	2234.2	8.4	2553.1	8.8	2545.3	7.9	2377.3
2/14/98	8.7	2235.3	8.6	2547.9	8.5	2546.7	8.1	2373
5/3/98	13.5	2222.5	13.8	2524.7	13.6	2538.7	13.5	2357.1
5/21/98	17.6	2220.8	17.6	2514	17.6	2551.8	16.1	2346.6
6/9/98	16.3	2213.9	16.5	2513.6				
7/8/98	18.7	2213.1	19.7	2520.4	18.9	2554.9	19.6	2347.5
9/4/98	19.8	2206	20	2518.5	19.9	2545.1	20	2346.2
10/24/98	14.5	2207.2	13.1	2532.4	14.7	2542.4	13	2361.4
12/18/98	10.6	2216.9	9.6	2536.3	10.7	2527.3	9.3	2363.3
1/10/99	6.7	2231.6	5.8	2544.9	6.3	2544.5	5.1	2370.1
1/31/99	10.5	2222.8	10.4	2528.6	10.3	2544.2	10	2351.7
2/21/99	9.2	2222.7	8.4	2535	9	2537.1	7.8	2361.3
3/13/99	8.3	2226.5	7.7	2536.6	8	2540.9	7.1	2361.2
3/26/99	10.2	2220.6	9.7	2528.3	10.1	2537.1	9.3	2354.3
4/9/99	13.9	2219.3	15.3	2511.7	13.6	2555.6	14.6	2336.9
5/14/99	15.6	2217.3	16.2	2503.1	15.3	2540.3	15.6	2330.4
6/6/99	17	2210.9	18	2500.1	17	2544	17.4	2331.4
7/17/99	19.5	2204.3	20.2	2500.5	19.4	2547.3	19.9	2327.6
8/21/99	20.4	2198.3	20.9	2499.7	20.4	2543.2	20.7	2327.6
10/3/99	16.4	2202.2	15.9	2513.3	16.5	2533.7	15.6	2337
11/10/99	12.4	2213.7	12.5	2518.6	12.3	2544.1	11.6	2340
12/11/99	6.9	2220.9	7.2	2531.9	7.6	2540.1	7.1	2350.0
1/25/00	4.7	2233.3	5.4	2544.2	60.	2635.0	4.3	2361.5

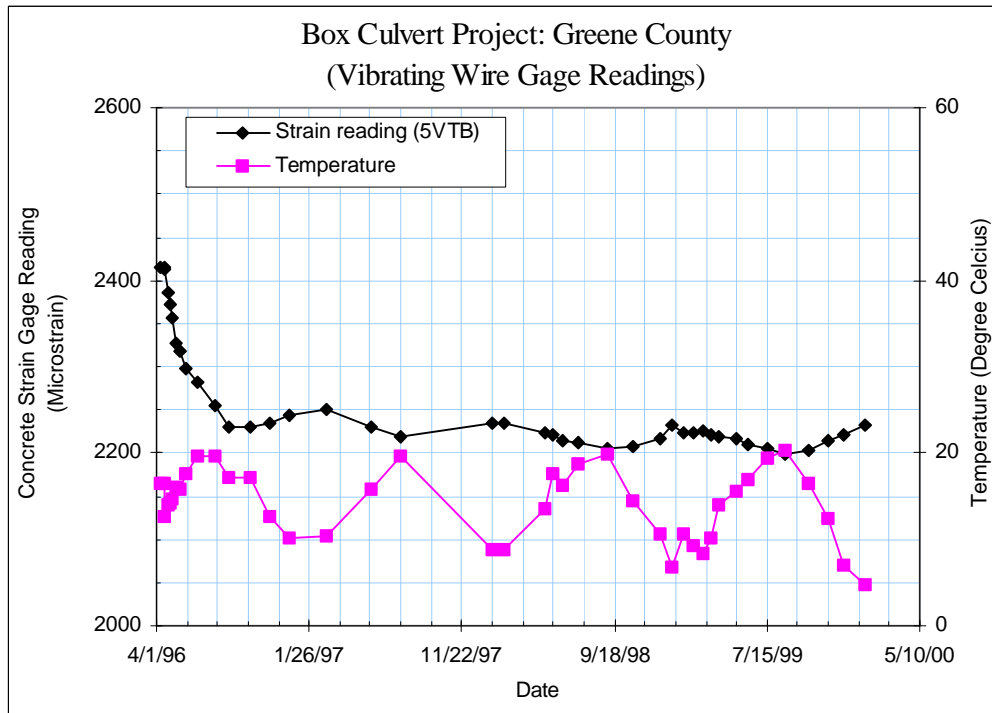


Figure A-26 Recorded Strain Reading and Temperature at 5VTB  
(Sullivan County, TN)

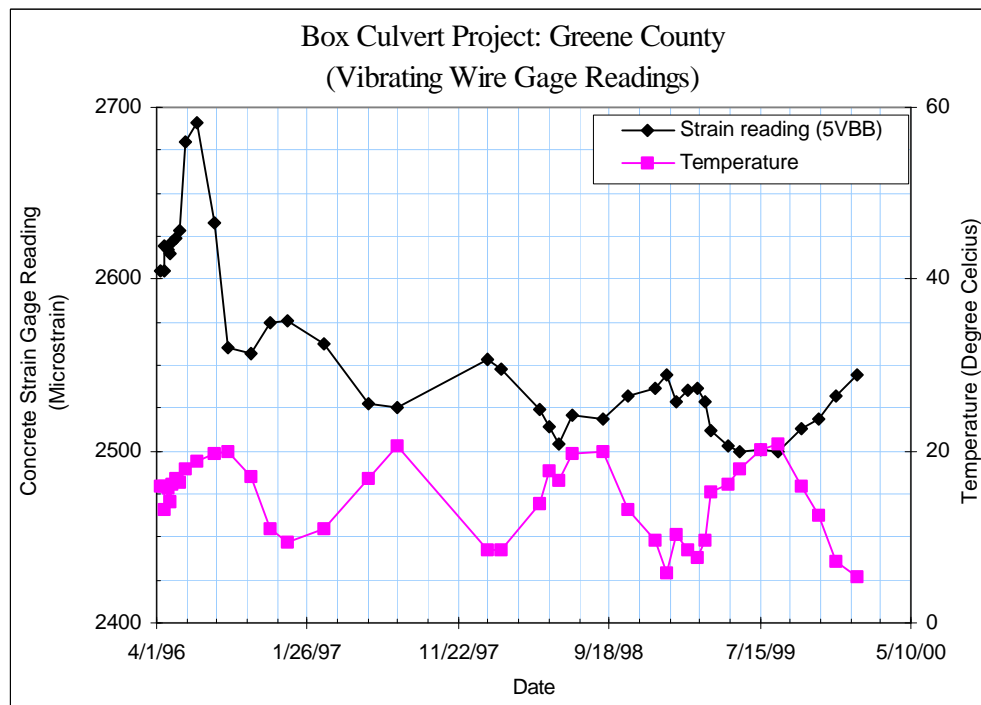


Figure A-27 Recorded Strain Reading and Temperature at 5VBB  
(Sullivan County, TN)

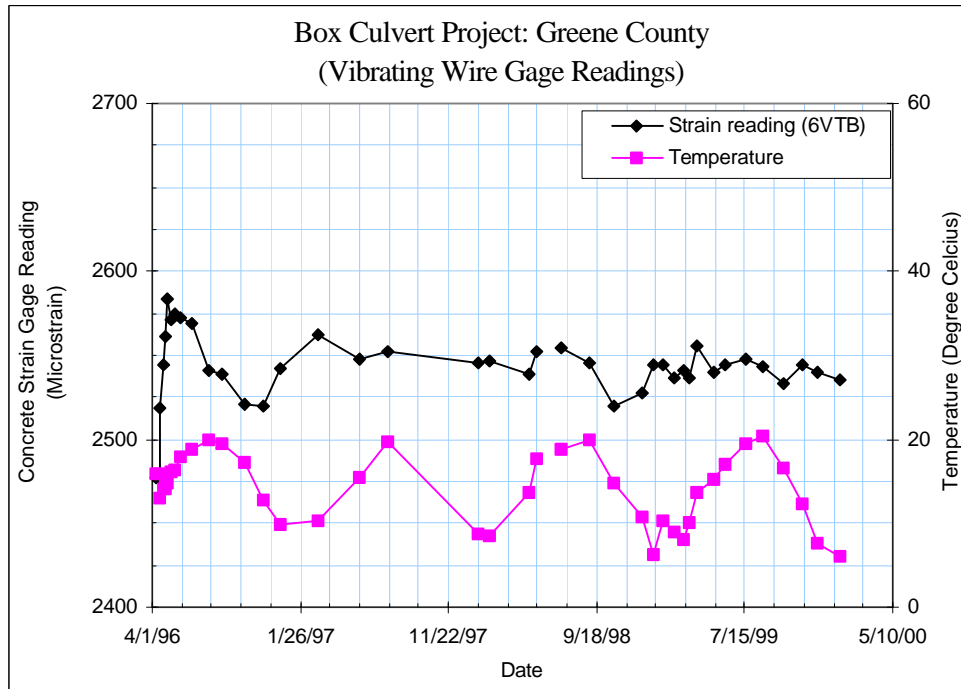


Figure A-28 Recorded Strain Reading and Temperature at 6VTB  
(Sullivan County, TN)

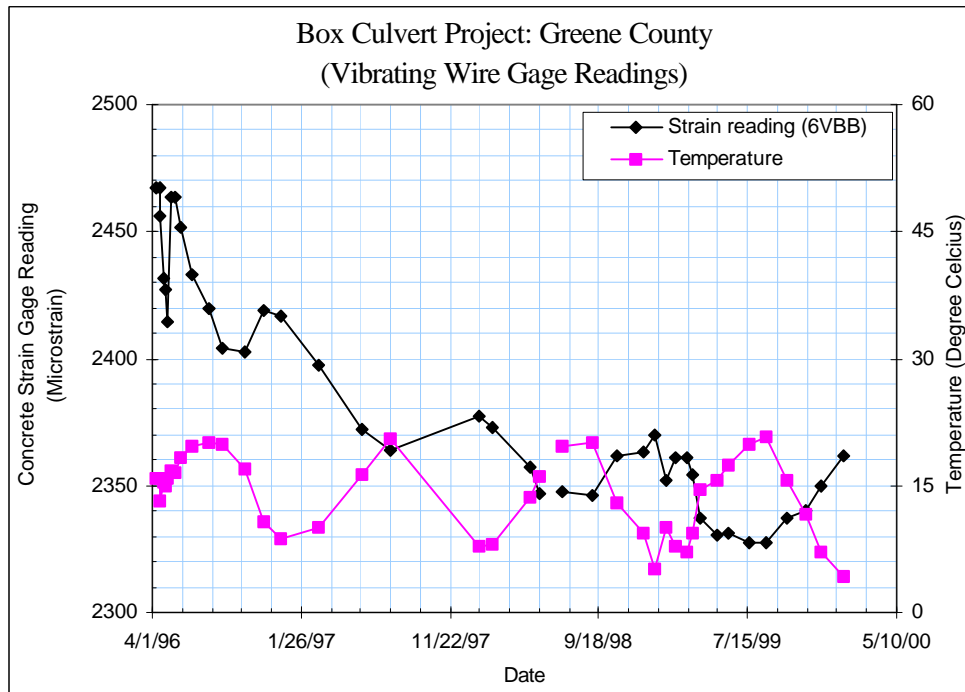


Figure A-29 Recorded Strain Reading and Temperature at 6VBB  
(Sullivan County, TN)

**APPENDIX B**

**GREENE COUNTY DATA**

## Appendix B-1

### Dimensions and Details of Culvert Reinforcement for Instrumented Sections

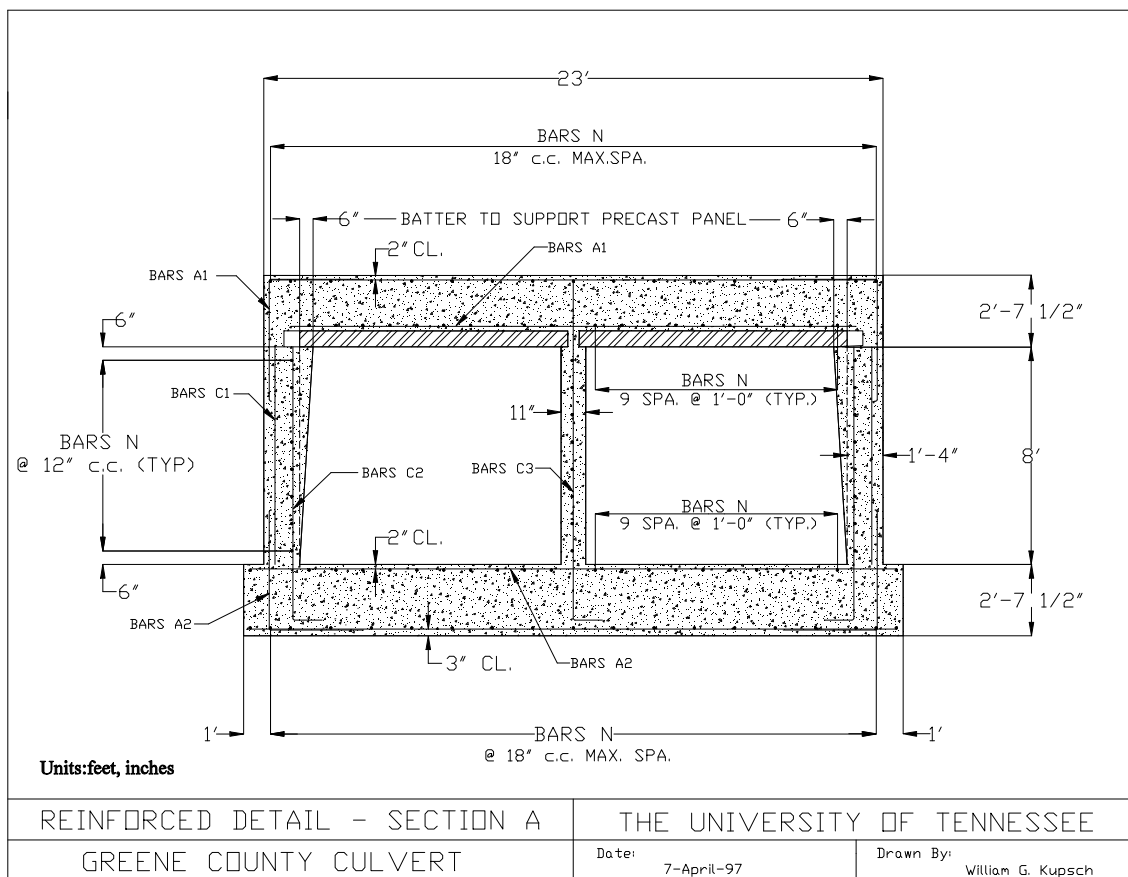


Figure B-1 Reinforced Detail of Culvert in Greene County, TN  
(Section A)



## Appendix B-2

### Instrumentation Scheme-Greene County, TN

Table B-1 Instrumentation Scheme

Instrument Type	Location/Transducer	A or B Position (indicates Section along culvert where instrument was installed)					
		1	2	3	4	5	6
Embedded Concrete Strain Gages	Inside / Resistance Gages	A B	A B	A B	A B	A B	A B
	Outside / Resistance Gages	A B	A B	A B	A B	A B	A B
	Inside / Vibrating Wire Gages	A B	A B	A B	A B	A B	A B
	Outside / Vibrating Wire Gages	A B	A B	A B	A B	A B	A B
Earth Pressure Cells	Resistance Gages*	A	A	A	A	A	A
	Vibrating Wire Gages	A B	A B	A B	A B	A B	A B

Note: The resistance pressure cells were installed on the wall.

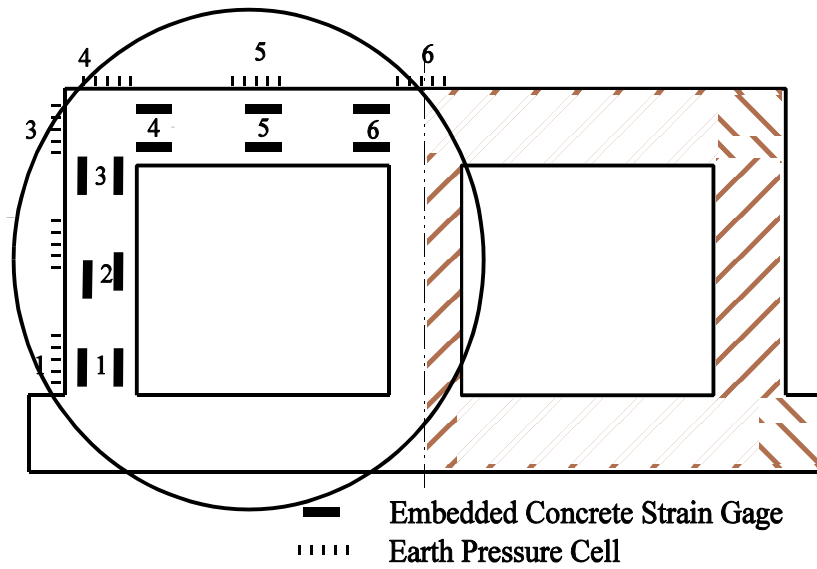


Figure B-3 Greene County Culvert Instrumentation Plan

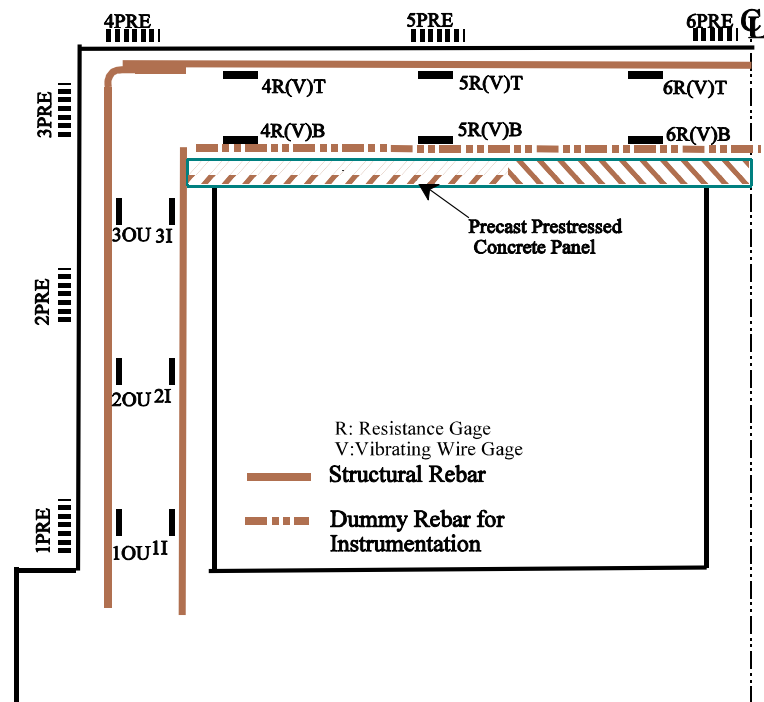


Figure B-4 Detailed Illustration of Greene Co. Culvert Instrumentation for Static Cells



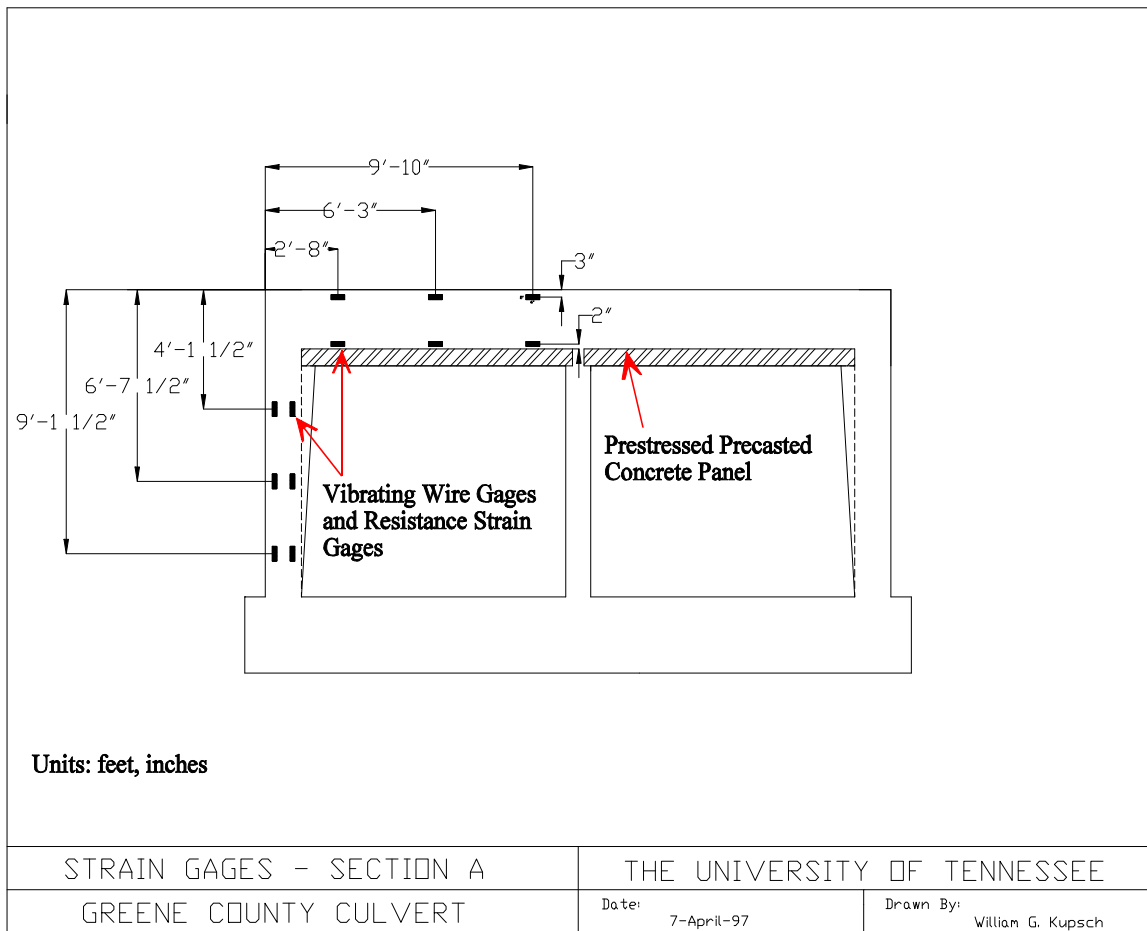


Figure B-5 Location of Strain Gages in Greene County Culvert, TN  
(Section A)

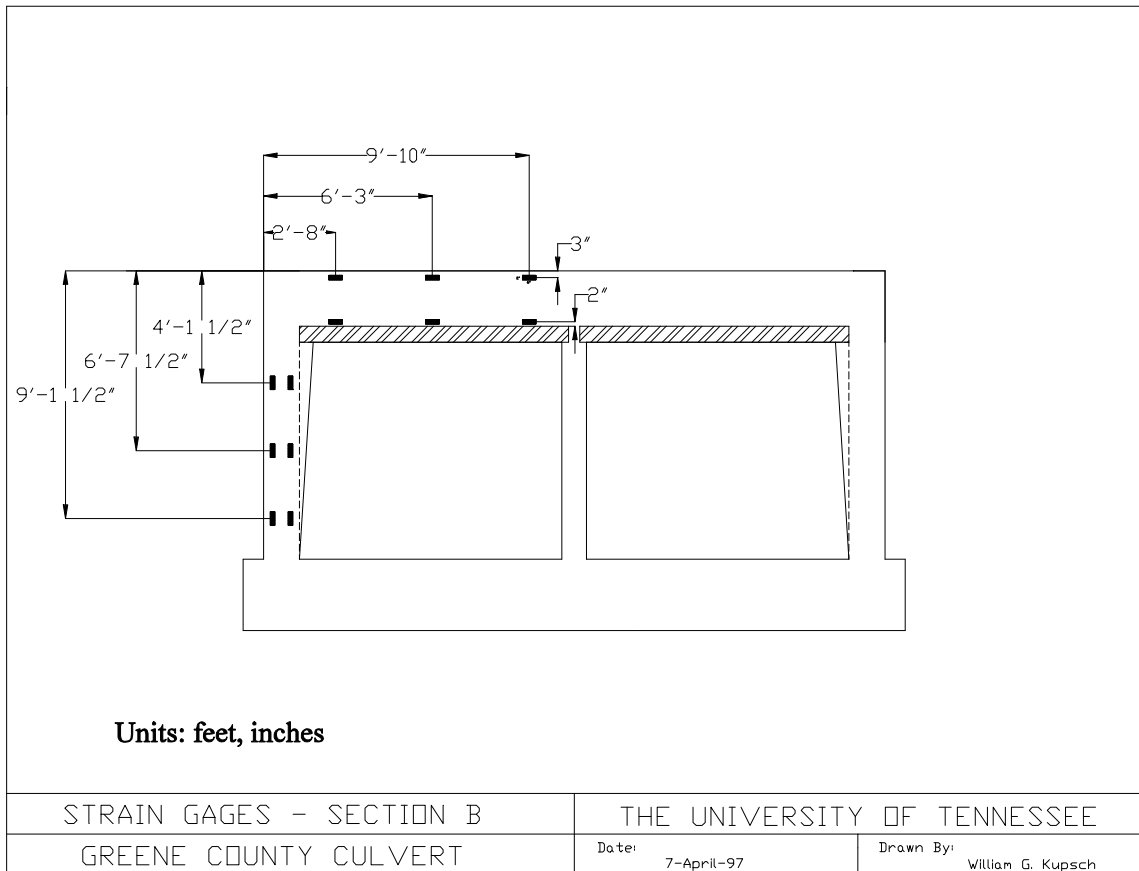


Figure B-6 Location of Strains Gages in Greene County Culvert, TN  
(Section B)

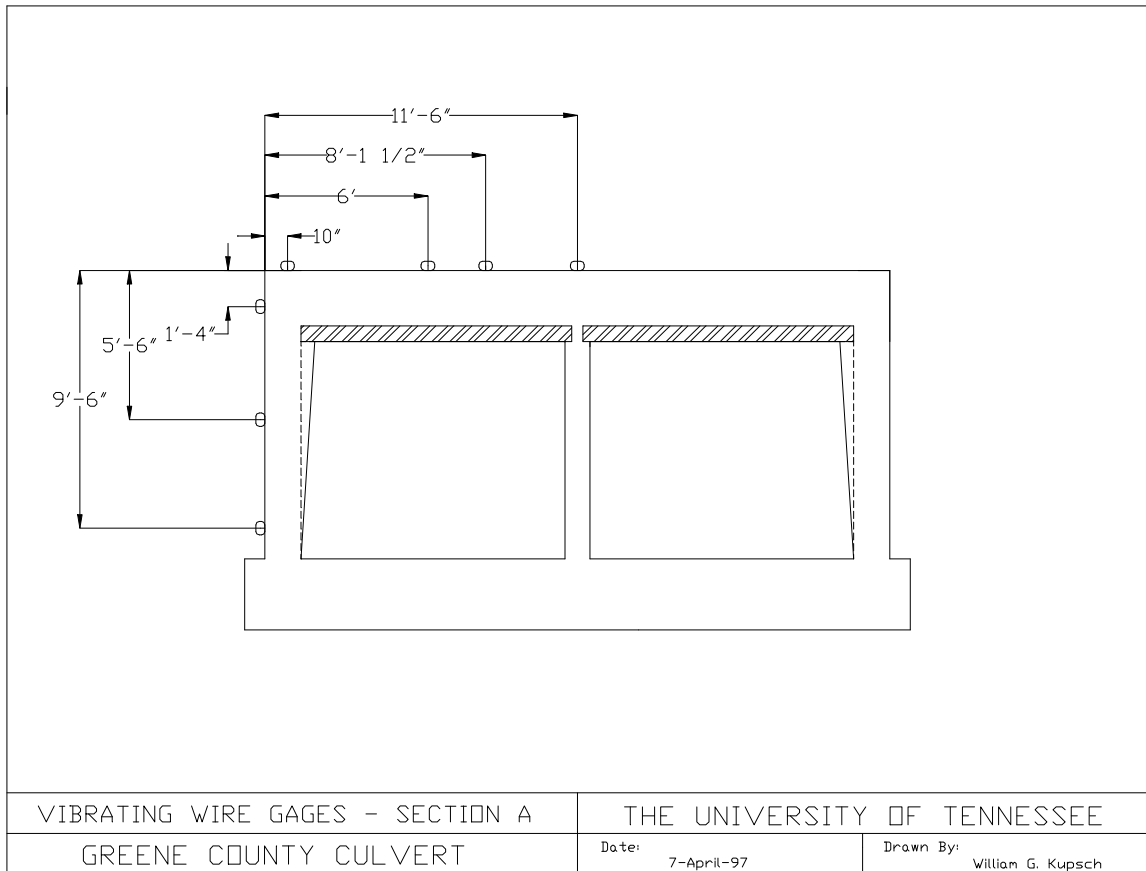


Figure B-7 Location of Pressures Cells in Greene County Culvert, TN  
(Section A)

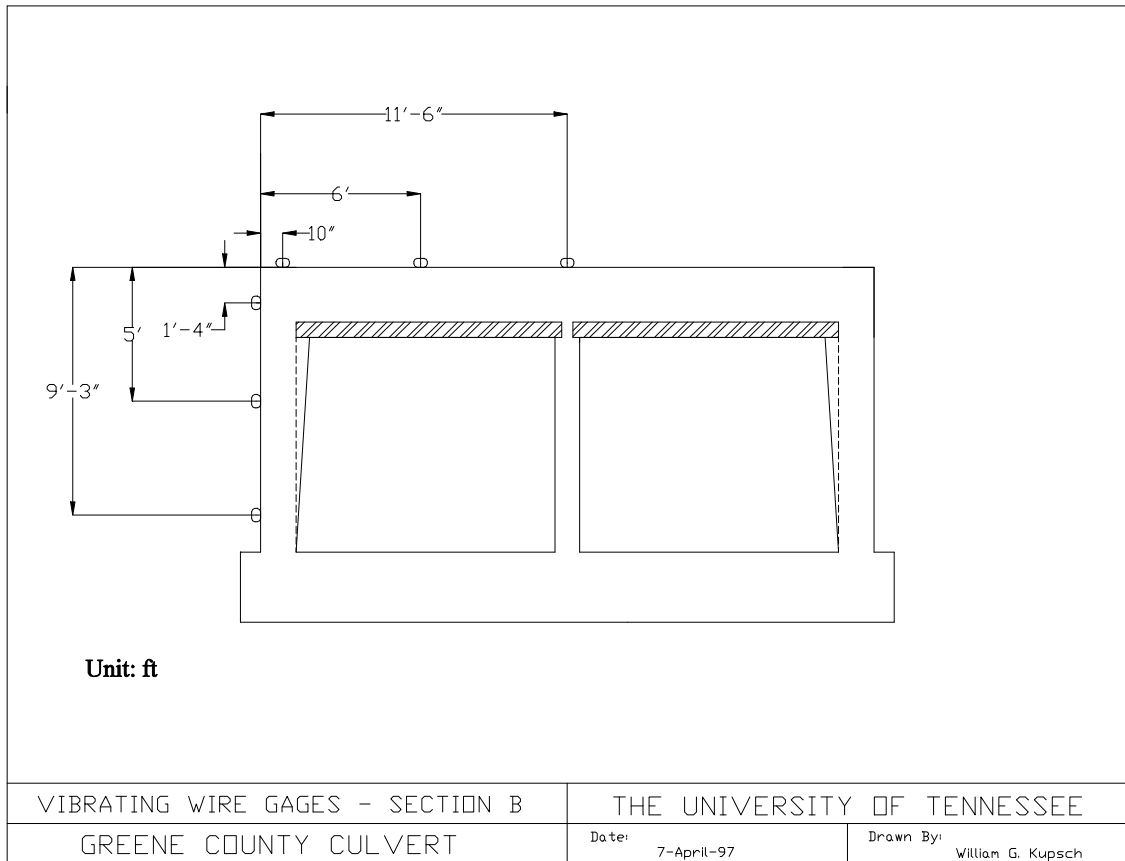
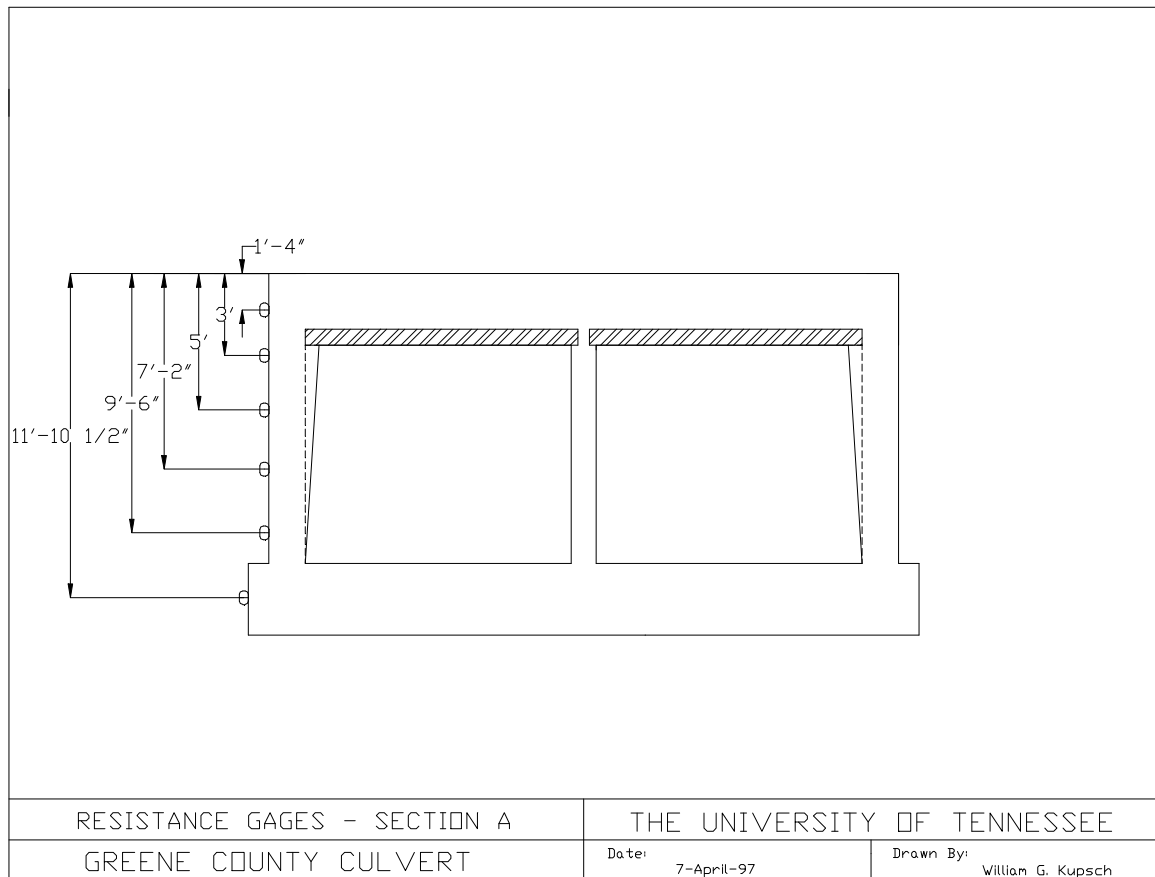


Figure B-8 Location of Vibrating Pressure Cells in  
Greene County Culvert, TN (Section B)



**Figure B-9 Location of Resistance Pressure Cells  
(Dynamic Earth Pressure Measurement, Greene County, TN, Section A Only)**

## Appendix B-3

### Chronology of Field Events- Greene County Culvert Field Record Results

The culvert in Greene County was constructed with backfilling procedures considered to be typical construction practice. The major events during the construction are shown in Table 2. The final embankment height is 18.90 m in Section A and 11.74 m in Section B.

Table B-2. Major Events of the Instrumentation Work in Greene Co. Culvert

Date	Event
8/14/96	In-door the initial (pre-installation) readings of the pressure cells and strain gages
9/23/96	Installed the concrete strain gages in the wall of section A, readings taken before pouring the concrete.
9/25/96	Recorded readings 1 hour after the pouring of concrete in wall of Section A. Significant reading changes in resistance strain gages.
10/1/96	Installed the concrete strain gages in the wall of section B and the stress free gages in the bottom of Section B (both resistance gages and vibrating wire gages). Reading taken before pouring the concrete.
10/3/96	Recorded readings during the pouring of concrete in wall of Section B. Significant reading changes in resistance strain gages.
10/6/96	Installed the gages in the roof of Section A, reading taken before the pouring of the concrete.
10/10/96	Recorded readings 1 hour after the pouring of concrete in roof of Section A.
10/15/96	Placement of the precast prestress panel on the roof in Section B, Sunny, warm, the influence of the differential temperature between the in-side and out-side wall can be found.
10/21/96	Recorded readings during the pouring of concrete in roof of Section B.
10/30/96	Installed the 12 vibrating pressure cells and 6 resistance pressure cells (to register the dynamic loading induced by the construction equipment). Initial readings of the pressure cells taken.
12/5/96	Started backfilling with thin layers of gravel (waste stone) on both sides of the culvert. The wires of resistance pressure cell 2REP and 3REP severely damaged by construction machine. 2REP could not be recovered.

Date	Event
12/8/96- 12/12/96	Backfilled the waste stone till elevation: 1.95 m below the roof (Section A), 2.10 below the roof (Section B). Temperature was slightly above the freezing. Both dynamic and static readings taken. The several sets of dynamic pressure data taken on 12/11 with different construction equipment at different elevations.
12/15/96	Tried to repair 3REP. Readings taken the next day. Stress relaxation can be found.
5/12/97	Resumed the backfilling work, and another vibrating pressure cell 7PRE was installed on the roof of Section A between 5PRE and 6PRE.
5/13/97- 6/2/97	Backfilled the culvert with waste stone and silty clay to the elevation of 1.99 m above the roof in Section A and 2.18 m above the roof in Section B. Dynamic pressure also recorded.
7/1/97	Reading taken after heavy rain. No new backfill.
7/14/97	Reading taken in hot weather (32°C). No new backfills.
7/23/97	Precise surveying the elevation of each section. No new backfills.
8/27/97	Restarted the backfill work. Dynamic horizontal earth pressure recorded on August 28 and 29, and the pressure found to be very small.
9/22/97	Backfilled with clayey material to 7 meters above the roof, clay with expansive potential material was utilized. New Compaction criterion was used. The optimum dry density was about 12.5 kN/m <sup>3</sup> , and the wet density was 17 kN/m <sup>3</sup> . The dry density was fairly smaller than the previous criterion of 14 kN/m <sup>3</sup> for silty clay. Pressure cell at bottom of Section A failed due to excessive loading (last recorded pressure: 275 kPa, the capacity: 172 kPa).
10/1/97	Backfill work stopped after heavy rain.
10/10/97	Thin layer of limestone boulders were moved to the backfill site from the hill slope-cutting site. The survey backfill height was 8.5 meters above the culvert roof.
11/24/97	Reading taken after long rain, Section A 8.61 m and Section B 8.31 m above the roof. The construction work stopped till June 9, 1998. During this time, took several readings, and the recorded vertical pressures slightly increased with time.
6/9/98	New fills put on the culvert. First work since Oct. 1, 1997.
6/23/98	Backfill height: Section A: 9.09 m; Section B: 9.37 m above the culvert roof. Deep mud (40 cm in the center of culvert, where Section A located).
7/8/98	The overburden height: Section A: 9.09 m; Section B: 9.43 m above the roof.

<b>Date</b>	<b>Event</b>
7/17/98	Section A: 12.3 m; Section B: 11.7 m (achieved full height).
7/24/98	Backfill height: Section A: 13.25 m above the roof.
8/2/98	Heavy flood between July 24 and August 2, the scaffold (about 1.1 m above the floor) and stool were washed away. Straws retained at the wire fence near the culvert inlet side about 1.2 meters. One piece of the concrete separated from the panel was taken to the lab for inspection. Backfill height: Section A: 13.45 m above the roof.
8/8/98	Backfill height: Section A: 14.57 m above the roof.
10/18/98	The construction work completed.
1/25/2000	Last field reading recorded.



**Appendix B-4**

**Original Vibrating Wire Pressure Cell Records**

**Greene County Culvert Site**

**(10/31/1996-1/25/2000)**

		1PREA 36353			2PREA 37156			3PREA 36356		
		Factor K	Factor C		Factor K	Factor C		Factor K	Factor C	
		0.00896	0.00721		-0.01648	0.00665		0.003724	0.007194	
		Temp	Reading	Pressure (kPa)	Temp	Reading	Pressure (kPa)	Temp	Reading	Pressure (kPa)
Initial Reading	Height above roof (m)	23.9	10503.1	NA	22	10341.5	NA	24.2	9487.4	NA
10/31/96	0	19.5	10565.4	-0.1	21.3	10404	-0.6	21.8	9480.9	0.4
11/4/96	0			-0.1						
11/8/96	0	12.1	10582.2	-0.2	13.7	10463.5	-0.6	13.9	9505.3	-0.6
11/13/96	0	4.9	10555.0	-0.2	3.9	10473.1	-0.6	5.1	9479.5	0.1
12/5/96	0	4.9	10555.0	-0.2	7	10507.5	-0.6	7.2	9506.4	-0.5
12/9/96	0	4.0	10566.3	-0.2	4.6	10486.7	-0.6	3.9	9482.5	0.8
12/11/96	0	7.4	10439.0	2.2	12.7	10499.4	-0.7	15.8	9531.3	-0.3
12/11/96	0	8.6	10362.3	5.9						
12/11/96	0	8.3	10319.7	9.8						
12/12/96	0	8.2	10420.5	11.9						
12/16/96	0	6.9	10507.4	2.5	4.5	10495.7	-1.1	4.8	9490.7	0.3
12/17/96	0	6.8	10510.6	2.3	7.4	10501.4	-1.7	7.4	9506.1	-0.5
12/20/96	0	3.9	10498.2	3.4	-1.7	10504.2	-0.8	-2	9479.7	1.1
3/24/97	0									
4/4/97	0	12.8	10301.9	13.1	25.4	10411.3	-0.4	27.1	9453.7	1.6
5/12/97	0	15.4	10235.4	16.5	27.3	10419.4	-0.2	26.1	9455	1.6
5/13/97	0	16.5	9546.6	50.8	19	10095.7	15.6	17.6	9442.3	2.4
5/14/97	0	16.3	9426.6	56.8	16.7	10147.6	13.5	16	9455.2	1.8
5/15/97	0	16.6	9206.5	67.8	16.8	9971.3	21.6	16.5	9453.4	1.6
5/15/97	0	16.6	9165.4	69.8	16.8	9967.4	21.7	16.6	9355.2	6.5
5/15/97	0	16.7	9014.5	77.31	16.7	9896.4	25.0	17.1	9068.1	20.7
5/15/97	0	16.6	8979.9	79.0	16.7	9865.7	26.4	17.1	9043.3	21.9
5/16/97	0.32	16.6	9034.4	76.3	16.8	9905.1	24.6	17.9	8997	24.3
5/16/97	0.4			72.6			22.0	17.6	8857.1	31.2
5/16/97	0.47	16.2	8987.2	78.6	16.5	10036.3	18.6	17.6	8993.7	24.4
5/19/97	0.91	17.0	8742.2	90.9	16.9	10159.7	12.9	17.1	9187.1	14.8
5/19/97	0.91	17.0	8644.1	95.7	17.1	10176.5	12.1	17.1	9250.9	11.6
5/20/97	1	18.2	8125.1	121.6	17.7	10159.7	12.8	17.6	9339.6	7.3
5/21/97	1	17.7	8289.6	113.4	17.7	10199.3	11.0	17.7	9332.7	7.6
5/22/97	1	17.4	8182.8	118.7	17.2	10203.5	10.9	17.6	9355.5	6.5
5/27/97	1	18.7	7045.2	175.3	18.4	10237.1	9.2	18.4	9414.8	3.6
6/2/97	1.99	18.0	6278.2	213.4	18	10270.3	7.7	18.2	9461.3	1.2
6/4/97	1.99	18.1	6224.3	216.1	18	10264.8	8.0	18.3	9452.1	1.7
6/10/97	1.99	16.7	6263.2	214.1	17.2	10271.3	7.7	17.8	9436.7	2.4
6/12/97	1.99	17.0	6094.9	222.5	17.5	10284.8	7.1	17.9	9451.1	1.7
6/19/97	1.99	1.7	6263.2	213.2	17.2	10271.3	7.7	17.8	9436.7	2.4
7/1/97	1.99	20.6	5655.4	244.5	20	10287	6.7	20.1	9442.3	2.2
7/14/97	1.99	19.9	5865.1	234.1	20.7	10281.8	6.9	21	9427.7	3.0
7/23/97	1.99	21.8	5527.9	251.0	21.5	10286.6	6.6	21.8	9429.8	2.9
8/27/97	1.99	19.0	5969.1	228.8	20.4	10301.3	6.0	21.3	9420.4	3.3
8/29/97	2.46	19.5	5799.1	237.3	20.8	10317.4	5.2	21.1	9427.2	3.0
8/29/97	2.46	19.6	5744.8	240.0	20.8	10316	5.3	21.4	9428.4	3.0

	1PREA 36353			2PREA 37156			3PREA 36356		
	Factor K	Factor C		Factor K	Factor C		Factor K	Factor C	
	0.00896	0.00721		-0.01648	0.00665		0.003724	0.007194	
	Temp	Reading	Pressure (kPa)	Temp	Reading	Pressure (kPa)	Temp	Reading	Pressure (kPa)
10/1/97	7.12			18.5	10191.5	11.3	18.1	9413.5	3.6
10/10/97	7.7			17.9	10131.3	14.1	18.7	9389.9	5.0
11/24/97	8.62			11.1	10052.9	18.5	12.3	9389	4.7
1/20/98	8.62			9.8	10110.3	16.0	11	9419.1	3.1
2/14/98	8.62					15.0			3.0
4/8/98	8.62			11.8	10145.5	14.1	12.3	9423	3.0
5/21/98	8.62			17.4	10067.9	17.1	16.9	9406.9	3.9
6/9/98	9.09			17.3	10132.9	14.1	17.6	9395.9	4.5
6/23/98	9.09			19.7	10128.8	14.0	19.1	9396.6	4.5
7/8/98	9.31			19.7	10109.8	14.9	19.4	9400.2	4.3
7/17/98	12.29			19.8	10065.2	16.9	19.5	9394.3	4.6
7/24/98	13.25			20	10071.4	16.6	19.7	9385.3	5.0
8/2/98	13.45			19.6	10062.5	17.0	19.3	9371.6	5.7
8/8/98	14.87			19.2	10034	18.4	19.2	9361	6.2
8/13/98	14.88			19.4	10059.4	17.2	19.3	9367.9	5.9
8/17/98	14.91			19.7	10057.7	17.3	19.5	9354.7	6.6
8/21/98	15.2			19.4	10067.2	16.9	19.5	9351.2	6.7
8/30/98	15.68			19.8	10050.8	17.6	19.6	9348.6	6.9
9/4/98	17.77			19	10069	16.8	19	9347.2	6.9
9/15/98	17.83			18.8	10045	17.9	18.6	9335.1	7.5
10/1/98	18.06			18.9	10079.3	16.4	19.2	9350.4	6.8
10/24/98	18.9			13.4	10117.1	15.2	14.8	9344	7.0
11/18/98	18.9			12.7	10115.4	15.4	13.6	9356	6.3
12/17/98	18.9			9.8	10150.4	14.1	11.1	9376.2	5.3
1/10/99	18.9			7.3	10135	15.1	8.5	9365.3	5.8
1/25/99	18.9			10.5	10095	16.6	11	9350.2	6.6
1/31/99	18.9			10.3	10060.1	18.2	10.8	9333	7.4
2/21/99	18.9			8.2	10136.6	14.9	9.4	9372.6	5.4
3/13/99	18.9			6.5	10166.4	13.8	7.9	9379.3	5.0
3/26/99	18.9			8.6	10133.4	15.0	9.6	9366.2	5.7
4/9/99	18.9			13	10046	18.6	12.8	9347.2	6.8
5/14/99	18.9			14.6	10052.1	18.1	14.6	9353.2	6.5
6/6/99	18.9			16.5	10018.6	19.4	16.2	9325.7	7.9
7/17/99	18.9			19.3	10048.3	17.7	19	9338.3	7.4
8/21/99	18.9			20.1	10088.5	15.8	20	9368.1	5.9
10/3/99	18.9			15.6	10159.8	13.0	16.4	9372.4	5.6
11/10/99	18.9			12.2	10167.1	13.1	13.1	9371	5.6
12/11/99	18.9			9.7	10182.9	12.7	10.7	9379.2	5.1
1/25/00	18.9			5.6	10245.7	10.2	7.2	9412.2	3.4

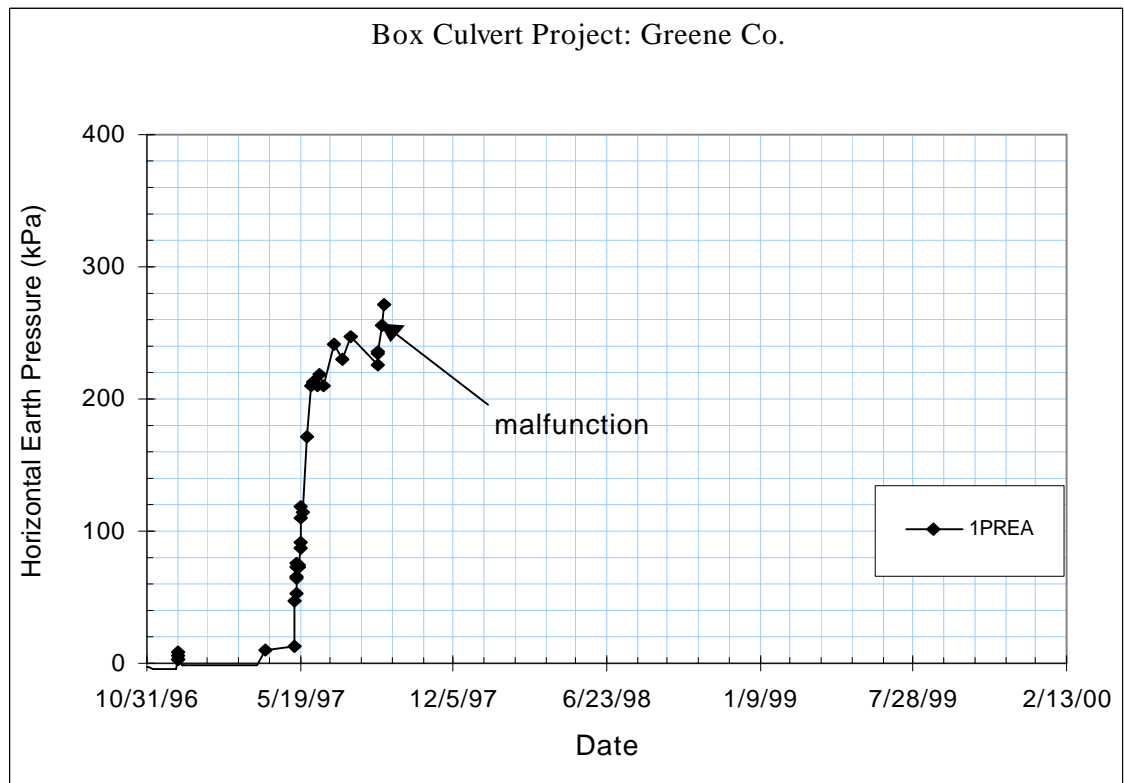
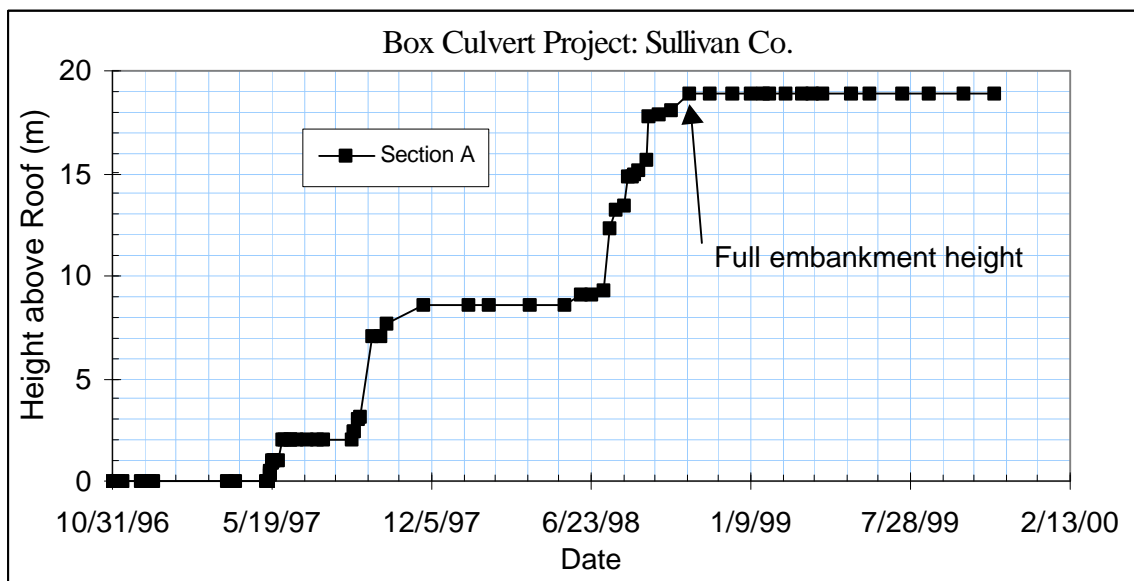


Figure B-10 Recorded Horizontal Pressure  
(Section A Cell 1PRE, Greene County, TN)



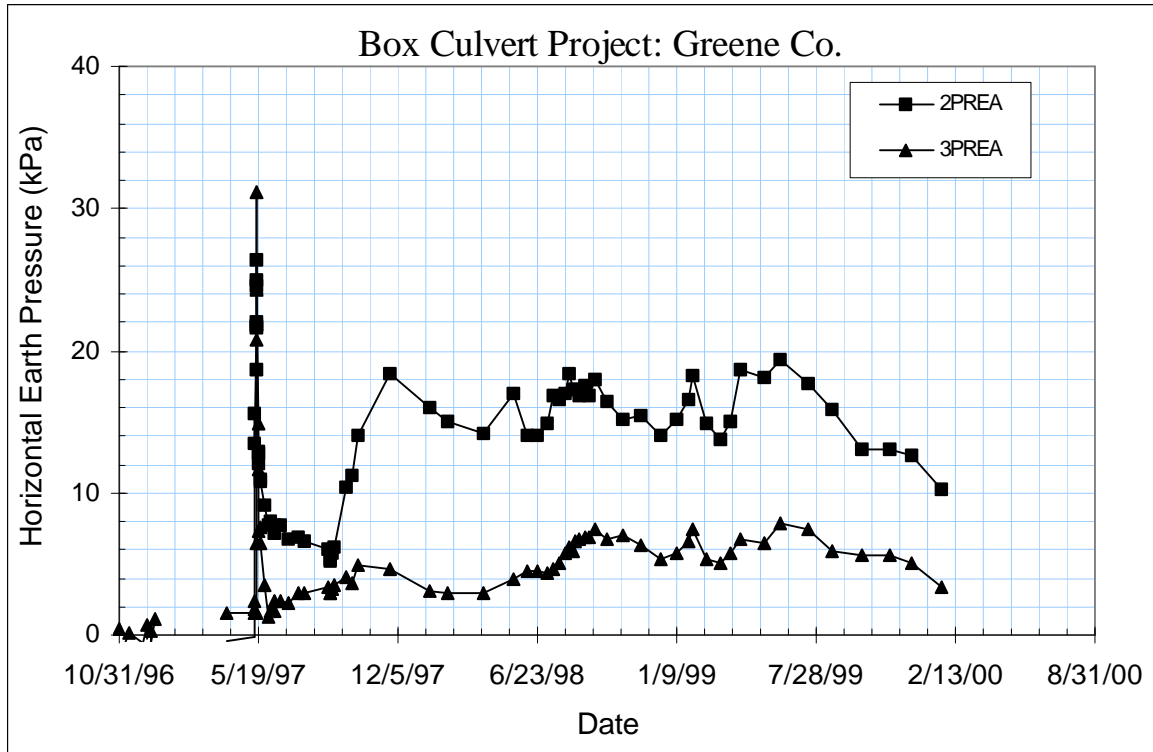


Figure B-12 Recorded Horizontal Pressures (Section A, Greene County, TN)

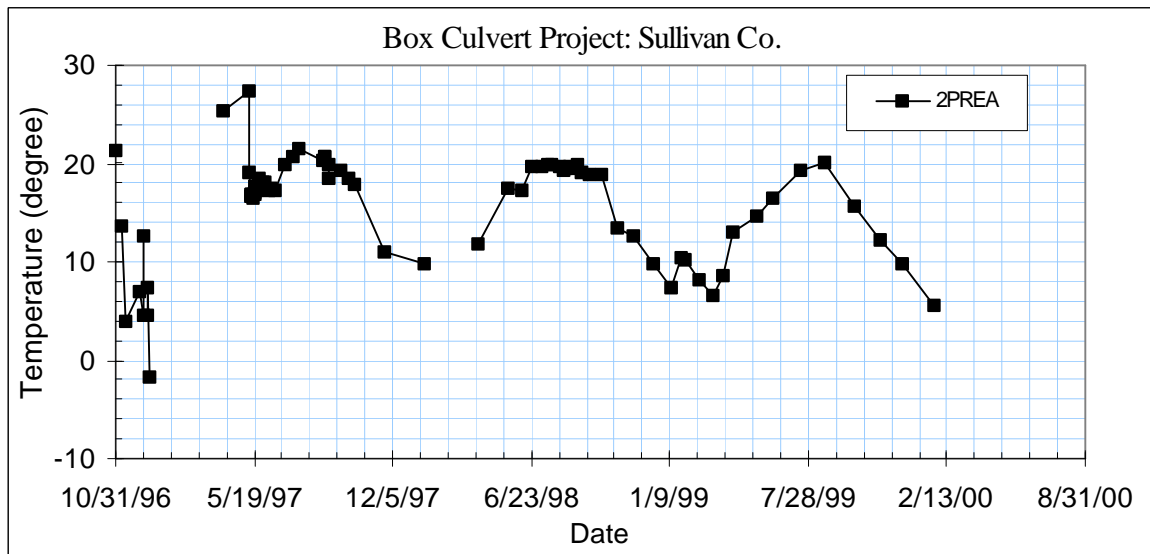


Figure B-13 Recorded Temperature at Cell 2PREA (Greene County, TN)

		4PREA 36346			5PREA 36347			6PREA 36345		
		Factor K	Factor C		Factor K	Factor C		Factor K	Factor C	
		-0.01644	0.0181		-0.02486	0.01643		-0.02017	0.01999	
		Temp	Reading	Pressure (kPa)	Temp	Reading	Pressure (kPa)	Temp	Reading	Pressure (kPa)
Initial Reading	Height above roof (m)	24.9	9129.5	NA	24.5	9330.2	NA	24.1	8494	NA
10/31/96	0	22.3	9139.1	-0.9	22.9	9338.5	0.1	22.8	8510	0.1
11/4/96	0									
11/8/96	0	11	9165.4	-0.1	12.4	9361.5	0.0	12.7	8530.3	0.0
11/13/96	0	3.7	9162.8	-0.1	8.5	9355.5	0.0	6.6	8531.3	0.0
12/5/96	0	7.2	9174.4	-0.2	8.7	9367.8	0.0	7.8	8540.9	0.0
12/9/96	0	5.6	9166.3	-0.2	5.3	9360.7	0.0	5.7	8532.9	0.0
12/11/96	0	14.9	9173.2	-0.6	16.4	9359.3	-1.8	16	8538.6	-0.1
12/11/96	0									
12/11/96	0									
12/12/96	0									
12/16/96	0	4.7	9173.6	-1.5	4.5	9368	-0.7	4.3	8539.3	-0.8
12/17/96	0	7.6	9176.1	-2.1	7.4	9368.3	-1.3	6.7	8540.5	-1.3
12/20/96	0	-4	9172.8	-0.4	-2.6	9351.4	2.4	-2.2	8516.6	3.3
3/24/97	0									
4/4/97	0	29.1	9138.1	0.2	29.6	9326.4	-0.3	29.5	8502.4	0.8
5/12/97	0	32.9	9143.7	-0.9	34.4	9334.4	-2.0	35.6	8500.5	0.2
5/13/97	0	20.5	9152.5	-0.6	18.5	9340	0.0	18.3	8519.3	0.0
5/14/97	0	15.2	9168.4	-2.0	15.3	9355.6	-1.2	15.7	8529	-0.9
5/15/97	0									
5/15/97	0									
5/15/97	0									
5/15/97	0	21.2	9114.1	4.1	20.4	9275.1	5.5	19.6	8432.3	1.6
5/16/97	0.32	15.3	9112.6	5.0	17.3	9238.5	11.7	17.1	8386.8	18.5
5/16/97	0.4	17	9070.8	10.0	17.1	9285.4	6.5			
5/16/97	0.47	17.6	9057.7	11.5	17.1	9165.7	20.0	17.1	8353.9	23.0
5/19/97	0.91	17.2	8978.2	21.5	17.4	9096.6	27.8	17	8312.9	28.7
5/19/97	0.91	17.2	8962.1	23.5	17.5	9058	32.2	17.1	8288	32.1
5/20/97	1	17.4	8954.4	24.5	17.8	9097.7	27.6	17.4	8268.9	34.7
5/21/97	1	17.7	8973.5	22.0	18.3	9068.6	30.8	17.9	8305.4	29.6
5/22/97	1	17.9	8958.5	23.9	18.5	9071.3	30.5	18.1	8283.2	32.6
5/27/97	1	18.2	8873.8	34.4	18.7	8912.7	48.4	18.4	8176.6	47.2
6/2/97	1.99	18.5	8845.4	37.9	18.9	8910.7	48.6	18.5	8174.4	47.5
6/4/97	1.99	18.6	8843.1	38.2	19	8903.8	49.4	18.6	8169.9	48.1
6/10/97	1.99	18.3	8848.9	37.5	18.5	8914.8	48.2	17.7	8175.8	47.5
6/12/97	1.99	18.3	8854.3	36.8	18.5	8924.8	47.1	18.1	8181.5	46.6
6/19/97	1.99	18.3	8849.9	37.4	18.5	8914.8	48.2	17.7	8175.8	47.5
7/1/97	1.99	20.5	8810.3	42.1	21.2	8832.2	57.1	21	8125	54.0
7/14/97	1.99	21.7	8793.1	44.1	22.3	8804.6	60.0	22.4	8105.1	56.5
7/23/97	1.99	22.6	8777.5	45.9	23.4	8777.6	62.9	23.2	8089.2	58.6
8/27/97	1.99	22.7	8798	43.4	20.8	8847.6	55.4	22.6	8131.2	52.9
8/29/97	2.46	22.7	8722.4	52.8	23	8685.1	73.5	22.6	8037.2	65.9
8/29/97	2.46	21.7	8718.1	53.5	21	8697.2	72.4	22.4	8038.2	65.8

		4PREA 36346			5PREA 36347			6PREA 36345		
		Factor K	Factor C		Factor K	Factor C		Factor K	Factor C	
		-0.01644	0.0181		-0.02486	0.01643		-0.02017	0.01999	
		Temp	Reading	Pressure (kPa)	Temp	Reading	Pressure (kPa)	Temp	Reading	Pressure (kPa)
10/1/97	7.12	19.8	7582.8	195.4	20.5	7761.4	178.5	17.6	7378.2	157.4
10/10/97	7.7	19.7	7416.7	216.1	18.1	7652.7	191.3	19	7296.7	168.4
11/24/97	8.62	14.3	7267.1	235.4	12.5	7730.7	183.4	12.1	7292.3	170.0
1/20/98	8.62	12.1	7199.2	244.1	11.3	7666.1	190.9	10.3	7245.7	176.7
2/14/98	8.62			250.0			205.0			181.0
4/8/98	8.62	12.5	7096.2	256.9	12.3	7428	217.7	11.8	7135.4	191.7
5/21/98	8.62	15.9	6901.2	280.9	16.8	7140.8	249.5	16	6910	222.2
6/9/98	9.09	17.1	6780.9	295.7	17.9	7101.5	253.7	18	6876	226.6
6/23/98	9.09	18.3	6556.4	323.6	19.3	6865.7	280.2	19.3	6739.3	245.2
7/8/98	9.31	18.4	6446.7	337.3	19.7	6813.8	286.0	19.6	6697.4	251.0
7/17/98	12.29	19	5477.2	458.2	19.9	6091.8	367.8	19.8	6086.4	335.1
7/24/98	13.25	19.7	5253.1	486.1	20	5913.6	387.9	19.9	5964.2	352.0
8/2/98	13.45	19.1	5093.9	506.1	20	5807.8	399.9	19.9	5876.2	364.1
8/8/98	14.87	18.8	5050	511.6	19.5	5418.5	444.1	19.5	5523	412.8
8/13/98	14.88	19	4510.8	578.8	19.8	5357.8	450.9	19.6	5437.2	424.7
8/17/98	14.91	19	4442	587.4	19.8	5298.9	457.6	19.7	5384.9	431.8
8/21/98	15.2	19	4288.4	606.6	19.9	5179.6	471.1	19.7	5302	443.3
8/30/98	15.68	19.2	3736.1	675.3	19.9	4783.6	516.0	19.8	4914.5	496.7
9/4/98	17.77	19	3675.4	683.1	19.7	4742.2	520.7	19.5	4866.2	503.4
9/15/98	17.83	18.3	3679.4	682.7	19	4762.7	518.5	18.6	4797.6	513.0
10/1/98	18.06	19.2	3601.9	692.2	19.2	4652	531.0	19.2	4742.3	520.5
10/24/98	18.9	16.4	3818.9	665.5	16.1	5039.9	487.6	15.4	5037.4	480.3
11/18/98	18.9	14.5	3928.6	652.0	14.2	5167.8	473.4	13.4	4964.5	490.7
12/17/98	18.9	12.7	4051.8	636.8	11.9	5361.1	451.9	11	5107.1	471.3
1/10/99	18.9	9.8	4265.1	610.5	8.7	5642.6	420.6	7.6	5274	448.8
1/25/99	18.9	11.3	3952.8	649.3	11	5101.1	481.5	10.2	4886.8	501.8
1/31/99	18.9	11.3	3929.2	652.3	10.8	5143.2	476.8	10	4863.3	505.1
2/21/99	18.9	10.6	4082.1	633.3	9.9	5330.2	455.8	9	5046.5	480.0
3/13/99	18.9	9.4	4228.2	615.2	8.4	5535.3	432.8	7.4	5199.1	459.2
3/26/99	18.9	10.4	4011.5	642.1	9.9	5196.9	470.9	9.1	4964.8	491.2
4/9/99	18.9	12.4	3663.2	685.4	12.6	4731.8	523.1	12.1	4582.9	543.4
5/14/99	18.9	14.3	3463.2	710.1	14.8	4478.1	551.5	14.4	4463.1	559.6
6/6/99	18.9	15.8	3325.3	727.1	16.4	4319.7	569.1	16.1	4360.7	573.5
7/17/99	18.9	18.5	3198.8	742.6	19.5	4188.4	583.5	19.4	4324.2	578.1
8/21/99	18.9	19.7	3215.7	740.4	20.7	4190.4	583.0	20.6	4352.3	574.0
10/3/99	18.9	17.4	3625	689.6	17.5	4570.5	540.5	17.2	4824.2	509.5
11/10/99	18.9	14.1	4043.8	637.7	13.6	5323.3	455.9	12.8	5208	457.2
12/11/99	18.9	11.8	4263.2	610.5	11.1	5635.2	421	10.1	5421.7	428.1
1/25/00	18.9	9.1	4563.4	573.4	10.1	6063.3	373.1	6.7	5669.5	394.4

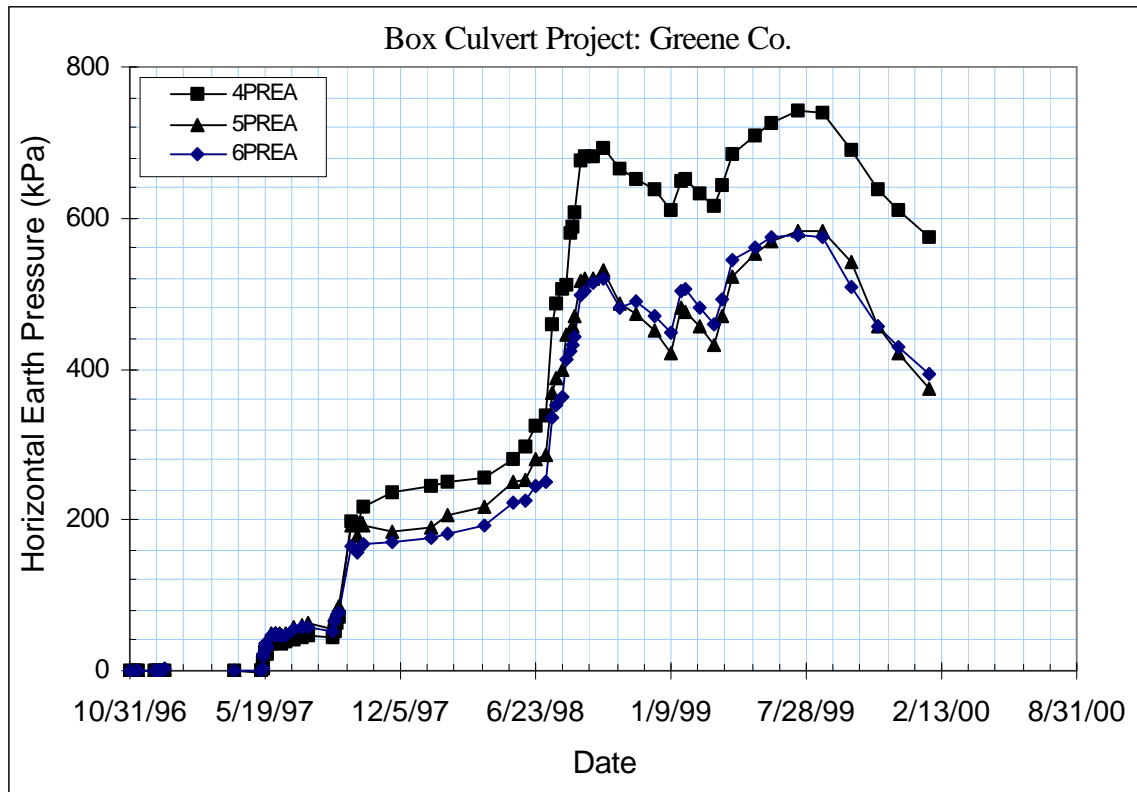


Figure B-14 Recorded Vertical Pressures (Section A, Greene County, TN)

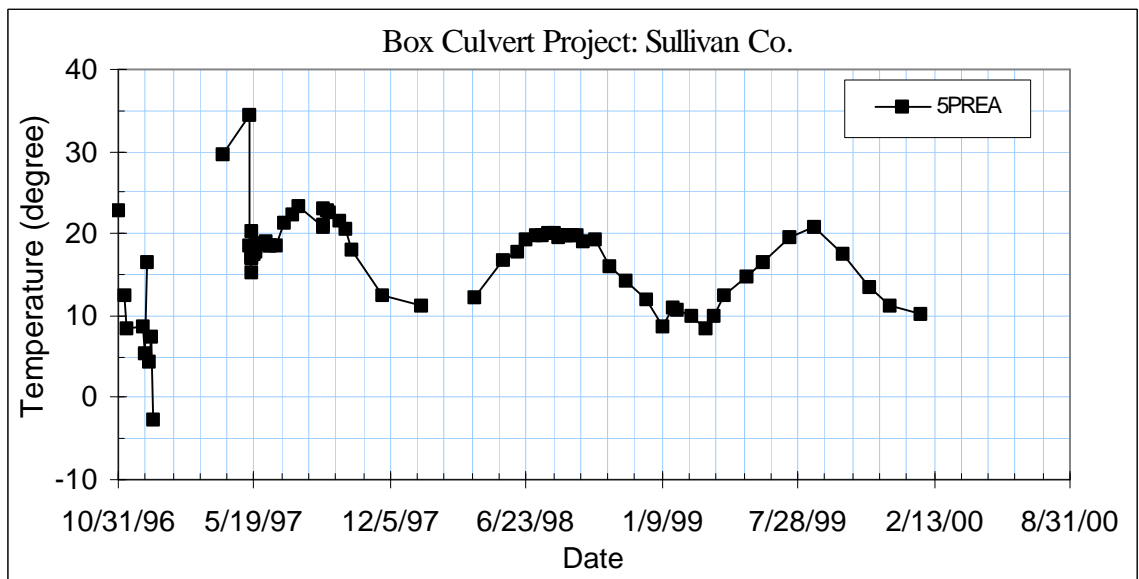
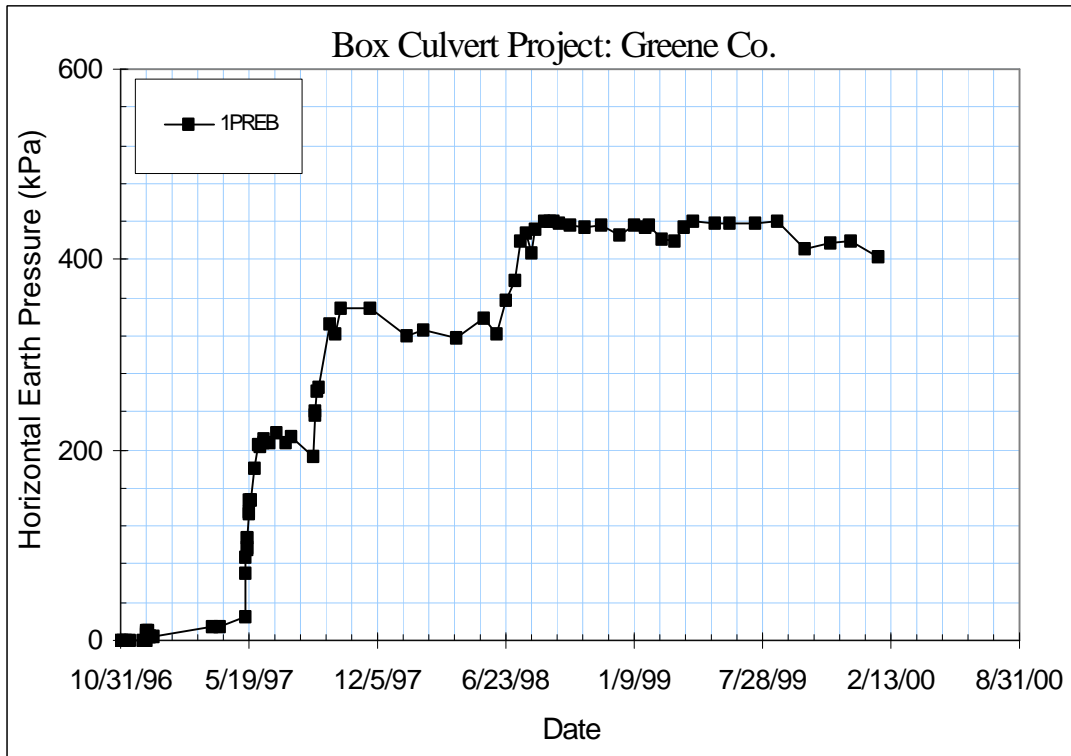


Figure B-15 Recorded Temperature at Cell 5PREA (Greene County, TN)



		1PREB 36352			2PREB 36354			3PREB 36355		
		Factor K	Factor C		Factor K	Factor C		Factor K	Factor C	
		0.001491	0.007202		0.00396	0.00765		0.001564	0.007553	
Initial Reading	Height above roof (m)	Temp	Reading	Pressure (kPa)	Temp	Reading	Pressure (kPa)	Temp	Reading	Pressure (kPa)
		24	10649.1	NA	24.3	10668.5	NA	24.3	9913.6	NA
10/31/96		21.7	10752.5	0.2	22.6	10733.6	0.0	24.5	9980.2	0.0
11/4/96		10.9	10759.5	0.1	11.9	10731.9	-3.0	13.6	9983.8	0.1
11/8/96		13.5	10778.4	0.0	12.6	10750.3	-4.0	12.3	10008	-0.3
11/13/96		3.8	10765.4	-0.1	4.5	10735.1	-3.0	4.7	9992	-0.2
12/5/96		6.6	10794.5	-0.1	7.3	10760.2	-4.4	7	10028.2	-0.5
12/9/96		3.9	10773	-0.4	4.1	10735.2	0.0	5	10004.2	-0.6
12/11/96		7.2	10626.2	6.9	17.2	10763.5	-1.2	15	10027.7	-1.7
12/11/96		6.9	10604.8	8.0						
12/11/96		6.9	10559	10.3						
12/12/96		7.3	10629.5	10.3						
12/16/96		6.6	10693.2	3.6	6	10748	-0.6	5	10014.2	-1.2
12/17/96		6.5	10697.4	3.4	7.2	10753.8	-0.9	7.3	10021.9	-1.5
12/20/96		3.7	10685.2	4.0	-2.9	10739.6	-0.4	-1.7	10007.5	-0.9
3/24/97		12.8	10479.7	14.3	28	10729.2	1.0	27.3	9975.6	1.1
4/4/97		12.9	10459.9	15.3	29	10712.1	1.9	27	9964.5	1.7
5/12/97		15.8	10273.5	24.6	33.6	10716	1.8	31.9	9770.4	11.8
5/13/97		17.4	9336.1	71.1	18.8	10306.9	23.0	21.4	9599.9	20.6
5/14/97	0.48	17.1	9005.1	87.6	18.4	10325.4	13.5	16.2	9448.4	22.0
5/15/97	0.48									
5/15/97	0.48									
5/15/97	0.48									
5/15/97	0.57	17.2	8784.3	98.5	18.2	10396.7	18.2	16.5	9397.7	31.1
5/16/97	0.57	17.1	8842	95.6	17.8	10374	19.4	16.6	9448.1	28.5
5/16/97	0.57	16.7	8578.5	108.7	17.5	10396.2	18.2	16.1	9461.4	27.8
5/16/97	0.57	16.7	8573.7	109.0	17.4	10411.5	17.4	15.9	9487.6	26.4
5/19/97	1.29	17.2	8103.2	132.3	17	10468.8	14.4	15.9	9522	24.6
5/19/97	1.29	17.2	8056.3	134.7	17	10476	14.0	16.1	9531.9	24.1
5/20/97	1.29	18	7812.9	146.8	17.7	10456	15.1	16.3	9640.9	18.4
5/21/97	1.29	17.8	7795.4	147.6	17.6	10466.2	14.5	16.6	9692.2	15.7
5/22/97	1.29	17.4	7820.2	146.4	17.2	10472.4	14.2	17.7	9663.5	17.2
5/27/97	1.29	18.8	7139.7	180.2	18.5	10501	12.7	17.4	9746	12.9
6/2/97	2.19	18.4	6619.9	206.0	18	10536.3	10.9	18	9816.8	9.3
6/4/97	2.19	18.4	6670.4	203.5	18.1	10524.7	11.5	18.3	9817.5	9.2
6/10/97	2.19	16.8	6581.7	207.9	17.2	10533.1	11.0	17.8	9817.2	9.2
6/12/97	2.19	17.1	6484.8	212.7	17.5	10534.7	10.9	17.8	9835.8	8.3
6/19/97	2.19	16.8	6587.1	207.6	17.2	10533.1	11.0	17.8	9817.2	9.2
7/1/97	2.19	19.7	6370.1	218.4	19.3	10507.9	12.4	19.8	9841.2	8.0
7/14/97	2.19	19.9	6573.8	208.3	20.5	10492.3	13.2	20.7	9823.2	8.9
7/23/97	2.19	21.3	6474	213.3	21.3	10500.6	12.8	21.5	9832.3	8.5
8/27/97	2.19	18.7	6891.5	192.5	20.1	10529	11.3	21.9	9850	7.6
8/29/97	3.02	19.4	5995.2	237.0	20.5	10505.1	12.6	21.7	9857.2	7.2
8/29/97	3.02	19.3	5900.8	241.7	20.6	10494.8	13.1	21.5	9856.3	7.2

		1PREB 36352			2PREB 36354			3PREB 36355		
		Factor K	Factor C	Pressure (kPa)	Factor K	Factor C	Pressure (kPa)	Factor K	Factor C	Pressure (kPa)
		0.001491	0.007202		0.00396	0.00765		0.001564	0.007553	
		Temp	Reading		Temp	Reading		Temp	Reading	
10/1/97	7.36	17.1	4277.3	322.3	18.5	10002.6	39.0	20.1	9771.7	11.6
10/10/97	7.8	15.6	3748	348.6	17	10040.5	37.0	19.3	9741.3	13.2
11/24/97	8.31	9.8	3727.7	349.5	10.6	9917.5	43.3	13.9	9713.6	14.6
1/20/98	8.31	8.8	4323.4	319.9	10.2	9880.8	45.2	12.1	9715.6	14.5
2/14/98	8.31	7.8	4217.9	325.2	9	9923.3	42.9	10.8	9701.6	15.2
4/8/98	8.31	11.5	4384.9	316.9	11.6	9966.5	40.7	12.3	9718	14.4
5/21/98	8.31	17	3945.8	338.8	17	9751	52.3	15.6	9678.3	16.5
6/9/98	9.37	17.6	4282	322.1	17.3	9948.7	41.8	16.7	9687.9	16.0
6/23/98	9.43	20.2	3581.5	356.9	19.4	9997.6	39.3	19.3	9677.3	16.5
7/8/98	10.58	19.4	3034.4	378.1	19.5	10108.5	33.5	18.2	9668.1	17.0
7/17/98	11.74	19.2	2223	418.4	19.5	9941.1	42.3	18.5	9640.8	18.4
7/24/98	11.74	19.2	2025.6	428.2	19.7	9857	46.7	18.8	9627.9	19.1
8/2/98	11.74	19.7	2464.6	406.4	19.5	9769.4	51.4	18.5	9614.7	19.8
8/8/98	11.74	19.9	1954.3	431.7	19.2	9712.7	54.3	18.3	9601	20.5
8/13/98	11.74									
8/17/98	11.74				19.6	9627.2	58.9	18.5	9594.6	20.8
8/21/98	11.74	19	1783.53	440.2	19.3	9627.2	58.8	18.7	9592.7	20.9
8/30/98	11.74	19	1775.83	440.6	19.5	9448.9	68.3	18.8	9596.8	20.7
9/4/98	11.74	18.4	1791	439.8	18.9	9409	70.3	19.5	9599.8	20.6
9/15/98	11.74	18	1808	439.0	18.4	9241.5	79.2	18.4	9576.9	21.8
10/1/98	11.74	18.5	1859.8	436.4	18.8	9354.6	73.2	18.8	9585.2	21.3
10/24/98	11.74	13	1929.6	432.9	13.3	9259.3	78.1	13.4	9598.7	20.6
11/18/98	11.74	11.9	1869	435.9	12.5	9107	86.1	14	9592.4	20.9
12/17/98	11.74	9	2075.2	425.6	9.7	9187.6	81.8	12.2	9620.5	19.4
1/10/99	11.74	6.7	1848.9	436.8	7.4	8983.2	92.5	9.6	9600.5	20.4
1/25/99	11.74	9.7	1893.7	434.6	10.3	8852.5	99.5	10.9	9576.3	21.7
1/31/99	11.74	9.7	1863.2	436.1	10.2	8841.3	100.1	10.9	9551	23.0
2/21/99	11.74	7.5	2166.4	421.1	8.2	8985.6	92.4	10.3	9605.5	20.2
3/13/99	11.74	5.9	2207.7	419.0	6.6	9101.3	82.6	9.1	9614.7	19.7
3/26/99	11.74	8	1916.26	433.5	8.6	8934.5	95.1	10	9586.5	21.2
4/9/99	11.74	12.3	1776	440.5	12.7	8791	102.8	11.8	9542.8	23.5
5/14/99	11.74	14.2	1829.2	437.9	14.3	8758.1	104.6	13.6	9547.4	23.2
6/6/99	11.74	15.8	1842.3	437.2	16	8776.4	103.6	16	9509.9	25.2
7/17/99	11.74	18.9	1823	438.2	18.9	8836.7	100.5	17.7	9508	25.3
8/21/99	11.74	19.3	1799.35	439.4	19.5	8869.6	98.8	18.7	9541.1	23.6
10/3/99	11.74	14.7	2379.4	410.6	15.2	9330.8	74.4	16.4	9581.8	21.5
11/10/99	11.74	11.1	2249.3	417.0	11.7	9273.6	77.3	13.1	9582.1	21.4
12/11/99	11.74	8.8	2336.1	418.6	9.2	9314.4	75.1	11	9598.9	20.5
1/25/00	11.74	4.7	2633.9	403.8	5.5	9290.2	76.3	8.4	9660.2	17.3



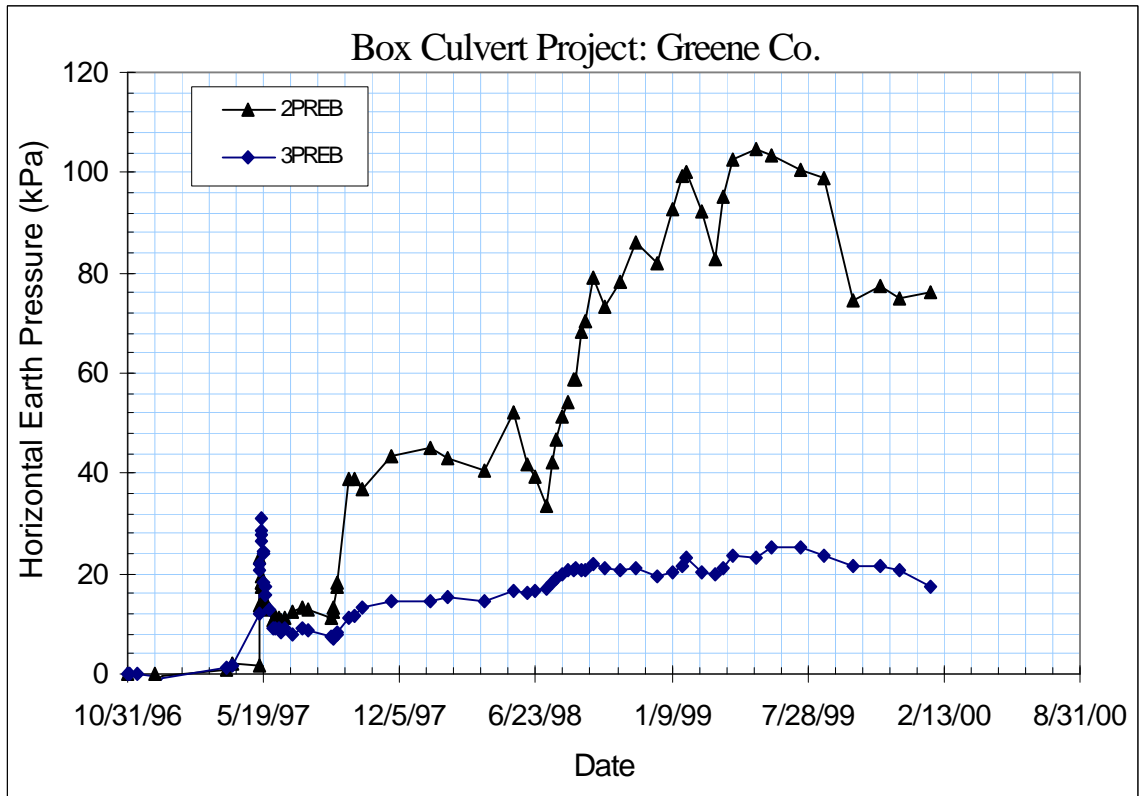


Figure B-18 Recorded Horizontal Pressures (Section B, Greene County, TN)

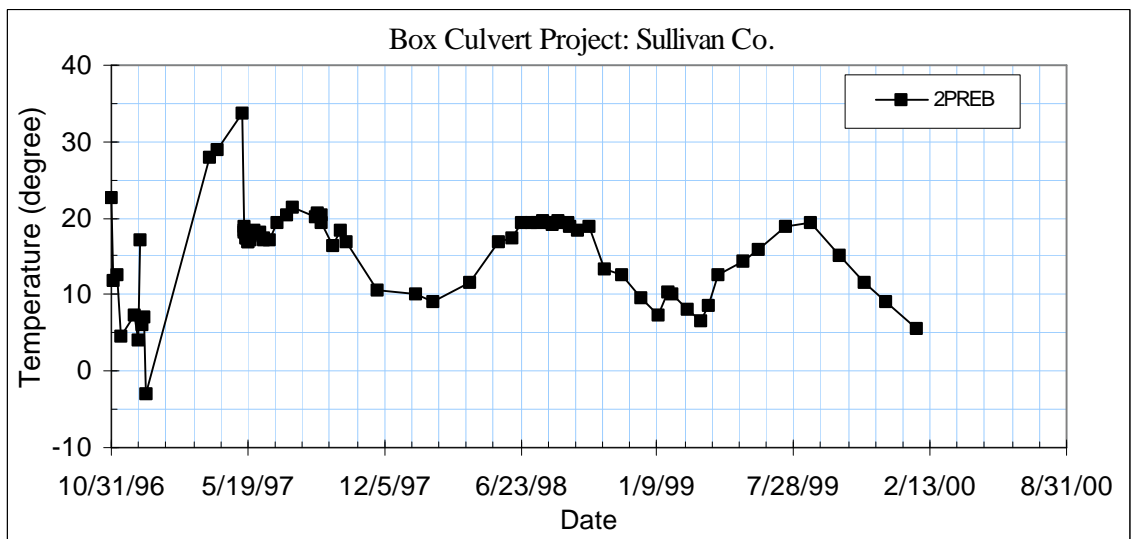


Figure B-19 Recorded Temperature at Cell 2PREB (Greene County, TN)

		4PREB 36349			5PREB 36348			6PREB 36350		
		Factor K	Factor C		Factor K	Factor C		Factor K	Factor C	
		-0.01165	0.01923		-0.03002	0.01859		-0.02828	0.02002	
Initial Reading	Height above roof (m)	Temp	Reading	Pressure (kPa)	Temp	Reading	Pressure (kPa)	Temp	Reading	Pressure (kPa)
		24.4	8097.3	NA	24.4	8859.8	NA	24.9	9045.9	NA
10/31/96		25.6	8109.1	0.0	27.7	8867.6	0.0	24.1	9064	0.0
11/4/96		12.3	8117.8	0.0	12.9	8891.7	0.0	12.2	9076.4	0.0
11/8/96		13.8	8125.6	0.0	13.3	8900.6	0.0	12.2	9086.4	-0.1
11/13/96		2.7	8130.1	-0.1	3.1	8908.6	0.1	5.8	9088.8	0.0
12/5/96		5.8	8141.4	-0.1	6	8920.5	-0.1	7.1	9099.5	0.0
12/9/96		5.2	8132.3	-0.5	7.2	8907.5	-0.7	7.4	9089.6	-0.4
12/11/96		9.6	8139.6	-1.8	10.8	8912.2	-2.1	13.3	9094.9	-2.3
12/11/96										
12/11/96										
12/12/96										
12/16/96		4.6	8141.5	-1.7	4	8922.4	-2.0	5	9101	-1.5
12/17/96		6.4	8139.5	-1.5	6	8920.2	-2.1	6.8	9099.6	-1.7
12/20/96		-4.1	8148.9	-0.9	-4.1	8933.4	-1.7	-3.6	9113.1	-1.5
3/24/97		23.6	8109.5	1.1	21.3	8880.4	-0.2	24.1	9068.7	-0.8
4/4/97		29.1	8097.56	2.2	27.7	8861.3	1.0	31.7	9051.2	0.1
5/12/97		30.2	8107.9	0.7	28.4	8871.1	-0.4	33.1	9055.6	-0.7
5/13/97		21.9	8063.8	7.2	20.6	8888.8	-1.1	22	9076.7	-1.5
5/14/97	0.48	14.4	8022.9	13.3	13.9	8816.2	9.6	13.6	9035.3	5.9
5/15/97	0.48									
5/15/97	0.48									
5/15/97	0.48									
5/15/97	0.57	16.3	8013.2	14.4	16	8822.9	8.3	15.7	9040.9	4.7
5/16/97	0.57	16	8011.8	14.6	15.6	8775.5	14.5	15.6	9007.9	9.3
5/16/97	0.57	15.2	7981.9	18.6	14.9	8757.6	16.9	15	9004.7	9.8
5/16/97	0.57	15.2	7960.3	21.5	14.8	8708.9	23.2	14.8	8986.8	12.3
5/19/97	1.29	16	7890.6	30.7	15.7	8665.7	28.5	15.6	8932.5	19.7
5/19/97	1.29	16.1	7861.2	34.6	15.7	8613	35.3	15.7	8909.3	22.8
5/20/97	1.29	16.5	7895.9	29.9	16.3	8661.3	29.0	16.2	8940.5	18.4
5/21/97	1.29	17	7863.6	34.2	16.8	8602.9	36.3	16.8	8921.9	20.9
5/22/97	1.29	17	7863.5	34.2	17	8601.5	36.5	17	8919.1	21.2
5/27/97	1.29	17.7	7783.2	44.8	17.9	8554.3	42.4	18.1	8843	31.5
6/2/97	2.19	18.2	7716	53.7	18.3	8490.1	50.5	18.5	8806.3	36.5
6/4/97	2.19	18.3	7713.6	54.0	19.5	8478.7	51.7	18.7	8801.4	37.2
6/10/97	2.19	18.2	7723.7	52.6	17.9	8496.7	49.7	18.1	8811.5	35.9
6/12/97	2.19	18.1	7730.1	51.8	17.9	8505.7	48.6	18.1	8818.5	34.9
6/19/97	2.19	18.2	7723.7	52.6	17.9	8496.7	49.7	18.1	8811.5	35.9
7/1/97	2.19	20.2	7701.3	55.4	20.5	8451.3	55.0	20.8	8775.6	40.3
7/14/97	2.19	21.3	7681.6	58.0	21.6	8416.4	59.3	22	8764.3	41.6
7/23/97	2.19	22	7675.1	58.8	22.4	8411.2	59.8	22.9	8755.1	42.7
8/27/97	2.19	21.3	7674.8	58.9	21.1	8461	53.6	22.2	8774.6	40.2
8/29/97	3.02	22.1	7489	83.4	22.1	8282.3	76.3	22.2	8572.7	68.0

		4PREB 36349			5PREB 36348			6PREB 36350		
		Factor K	Factor C		Factor K	Factor C		Factor K	Factor C	
		-0.01165	0.01923		-0.03002	0.01859		-0.02828	0.02002	
		Temp	Reading	Pressure (kPa)	Temp	Reading	Pressure (kPa)	Temp	Reading	Pressure (kPa)
9/22/97	7.18	20.9	6657.2	193.8	19.9	7673.1	154.9	20.8	8024.3	144.0
10/1/97	7.36	20.1	6706.8	187.3	19.7	7743.6	145.9	20.5	8102.3	133.0
10/10/97	7.8	19.5	6623.8	198.4	18.8	7719.2	149.2	18.7	8056.6	140.0
11/24/97	8.31	13.4	6676.5	191.9	11.9	7856.1	133.1	11.1	8162.8	126.8
1/20/98	8.31	12.1	6667	193.2	10.5	7846.7	134.6	10.2	8120.9	132.7
2/14/98	8.31	10.7	6671	192.8	9.3	7878.7	130.7	9	8164.3	127.0
4/8/98	8.31	10.6	6671	212.3	9.2	7879.2	150.6	8.8	8164.6	145.8
5/21/98	8.31	12.3	6523	240.1	11.5	7720	182.3	11.2	8025.3	175.6
6/9/98	9.37	15.9	6311.1	251.4	16.4	7464.6	187.9	16.8	7801.5	179.3
6/23/98	9.43	17	6225.7	269.6	17.5	7419.3	200.1	17.9	7772.8	191.1
7/8/98	10.58	18.2	6087.3	293.2	19.2	7321.8	212.4	19.3	7685.4	214.4
7/17/98	11.74	18.6	5908.8	321.0	19.3	7225.6	219.4	19.7	7515.7	235.5
7/24/98	11.74	18.9	5699.1	329.8	19.5	7170.4	233.0	19.9	7362.6	242.8
8/2/98	11.74	18.9	5632.9	331.2	19.6	7063.9	235.4	20.1	7309.9	245.7
8/8/98	11.74	19	5622	339.2	19.6	7045.4	240.2	19.7	7288.9	255.0
8/13/98	11.74	18.7	5562.3		19.1	7009.1		19.4	7222	
8/17/98	11.74	19	5562.3	339.2	19.5	6978.1	244.1	19	6562.7	346.1
8/21/98	11.74	19.4	5535	342.7	19.5	6947.5	248.0	20	6562.8	345.9
8/30/98	11.74	19.1	5469.5	351.5	19.6	6902.9	253.7	20	6479	357.5
9/4/98	11.74	18.9	5419.9	358.0	19.4	6868.5	258.1	19.6	6420.7	365.6
9/15/98	11.74	18.4	5410	359.4	18.5	6884.6	256.2	18.4	6373.7	372.3
10/1/98	11.74	18.8	5377.8	363.6	18.9	6845.3	261.2	19.4	6383.1	370.8
10/24/98	11.74	14.8	5717.5	318.9	15	7101.2	229.2	15.1	6664.7	332.8
11/18/98	11.74	14	5727.3	317.7	13.1	7182.7	219.2	13	6460.9	361.3
12/17/98	11.74	12.1	5847.4	301.9	10.6	7339.2	199.6	10.3	6547.7	349.9
1/10/99	11.74	9.4	5965	286.5	7.7	7438	187.5	7.3	6625.3	339.8
1/25/99	11.74	10.9	5720.5	318.8	10.2	7152.4	223.6	10	6380	373.1
1/31/99	11.74	10.9	5727.2	317.9	10	7201.4	217.4	9.8	6386	372.3
2/21/99	11.74	10.1	5895.1	295.7	8.7	7317.7	202.8	8.6	6552.2	349.6
3/13/99	11.74	8.9	5996.2	282.4	7.2	7440.1	187.4	6.9	6662.7	334.7
3/26/99	11.74	9.9	5830.5	304.3	8.9	7250.8	211.3	8.7	6488.2	358.4
4/9/99	11.74	12	5544.6	342.1	11.9	7020.1	240.2	11.9	6237.6	392.4
5/14/99	11.74	14	5401.2	360.9	14.1	6844.1	262.3	15.3	6169.3	401.1
6/6/99	11.74	15.3	5273.5	377.7	15.7	6741	275.2	16	6109.1	409.3
7/17/99	11.74	18.1	5136.5	395.7	18.8	6644.4	287.0	19.3	6083.3	412.2
8/21/99	11.74	19.2	5134	395.9	19.8	6633.9	288.1	20.3	6123.2	406.5
10/3/99	11.74	16.6	5550.1	341.0	16.2	6981.1	244.4	16.4	6467.3	359.8
11/10/99	11.74	13.1	5865.1	299.5	12	7318.6	202.0	11.8	6692.1	329.7
12/11/99	11.74	10.8	6015.9	279.7	9.5	7474.3	182.5	9.2	6811.5	313.7
1/25/00	11.74	8.1	6188.7	257	6.4	6811.5	157.8	5.9	6989.9	289.7

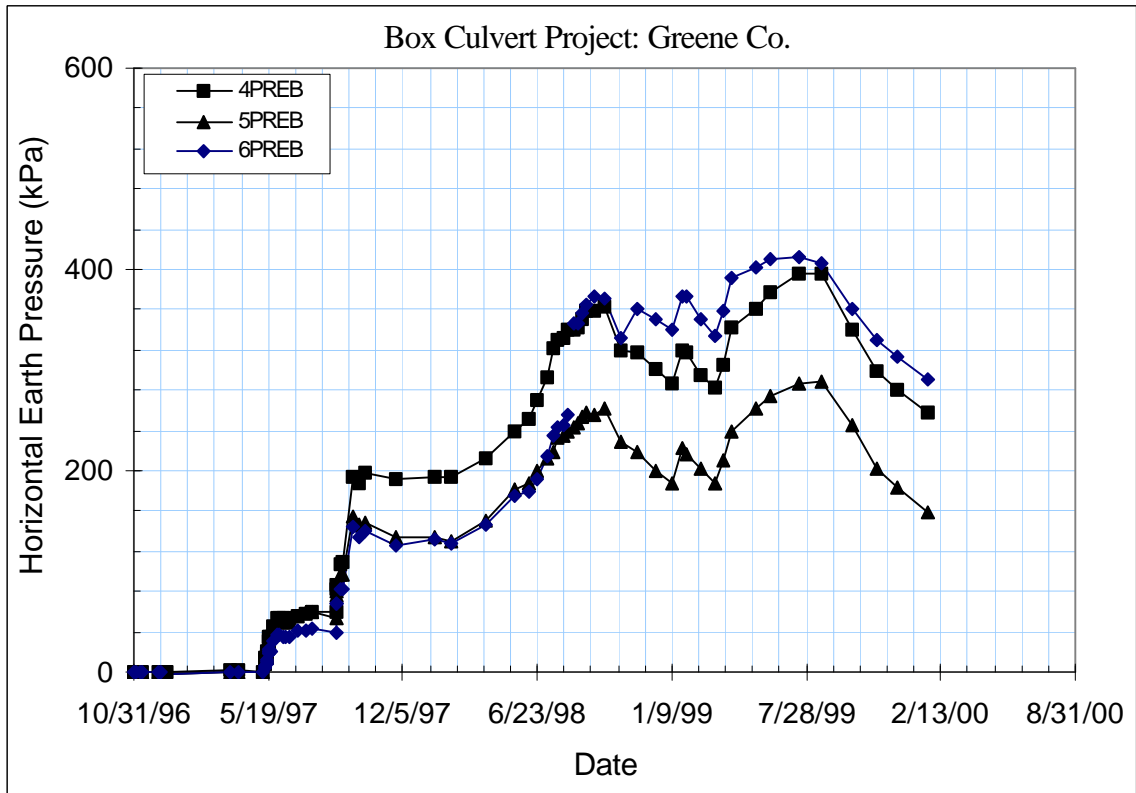


Figure B-20 Recorded Vertical Pressures (Section B, Greene County, TN)

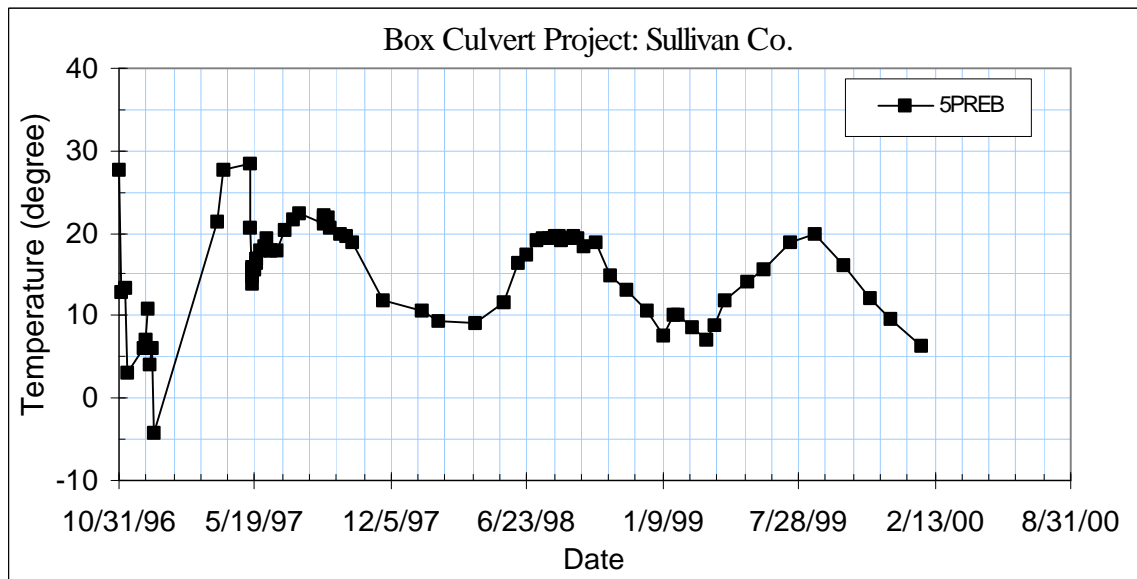


Figure B-21 Recorded Temperature at Cell 5PREB (Greene County, TN)

**Appendix B-5**

**Original Vibrating Wire Concrete Strain Gage Records**

**Greene County Culvert Site**

**(8/24/1996-1/25/2000)**



Greene County Culvert Concrete Strain Gages								
Date	1VIA		1VOUA		2VIA		2VOUA	
	Temperature	Reading	Temperature	Reading	Temperature	Reading	Temperature	Reading
8/24/96	25.5	2673.9	24.3	2541.7	24.9	2520.3	25.1	2522.4
9/23/96	25	2681.2	24.6	2542.8	25	2539.3	24.5	2517.1
9/25/96	26.2	2642.5	27.8	2539.3	28.2	2603.8	28.7	2535.5
9/30/96	16.2	2570.6	17.5	2434.7	15.7	2589.4	17.3	2534.4
10/1/96	21.4	2562.5	26.3	2403.4	20.8	2580.4	26.1	2507.2
10/4/96	21.5	2541.8	24.8	2400.3	21.4	2559.2	24.8	2498.1
10/7/96	15.3	2549.1	15.7	2414.5	15.1	2559.7	15.4	2512.2
10/9/96	15.5	2546.4	15.5	2411.7	15.4	2555.3	15.1	2506.8
10/10/96	12.1	2560.5	12.5	2405.9	11.8	2562.3	12.2	2505.7
10/15/96	16.0	2557.4	23.7	2364.5	16.0	2556.4	23.7	2468.3
10/17/96	17.8	2535.2	21.1	2376.9	17.9	2533.7	21.2	2481.6
10/21/96	10.7	2547.6	10.6	2405.6	10.4	2538.2	10.2	2505.8
10/28/96	16.9	2534.5	17.3	2386.6	16.8	2528.4	17.4	2486.7
10/31/96	18.6	2537.9	21.0	2377.6	18.8	2527.9	21.1	2479.5
11/8/96	15	2546.5	13.9	2406.6	15.7	2525.6	14.3	2506.8
12/5/96	5.7	2529.5	5.4	2426.7	5.1	2533.6	5.3	2530.1
12/9/96	3.5	2562.7	4.7	2427.7	3.2	2533.9	4.5	2530.6
12/16/96	6.1	2560.3	7.0	2434.4	5.8	2532.0	6.0	2541.5
12/17/96	7.9	2550.2	7.5	2438.9	7.5	2526.9	6.8	2539.8
12/20/96	0	2579.6	3.3	2433.9	-1.7	2542.7	0.2	2552.6
5/12/97	16	2509.9	15.7	2433.1	15.7	2467.5	16.4	2525.8
5/13/97	17	2499.4	16.7	2440	16.7	2463.8	17.4	2532.6
5/14/97	14.7	2522.6	16.2	2427.7	14.9	2468.8	16.5	2530
5/15/97	17	2499.2	16.8	2433.7	17.2	2463.7	17.2	2530.9
5/16/97	14.5	2519.3	16.6	2425.2	14.5	2470.8	16.7	2525.3
5/16/97	15.9	2479	16.2	2435.5	15.6	2460.9	16.2	2531.4
5/19/97	18.6	2488.7	17.4	2440.3	18.1	2460.4	17.1	2532.1
5/20/97	19.3	2497.5	18.7	2434.3	19	2463.5	18.4	2528.6
5/21/97	17.3	2507	18	2428.6	17.1	2468.6	17.9	2526.1
5/22/97	16.6	2506	17.5	2427.5	16.2	2468.2	17.1	2530.5
5/27/97	19.7	2499.2	19.3	2428.5	19.3	2466	18.9	2525
6/2/97	18.6	2503.7	18.5	2422.9	18.3	2470.7	18.2	2522.4
6/4/97	18.3	2505.7	18.5	2421.3	18	2471.4	18.3	2521
6/10/97	17	2501.2	16.8	2421.3	17	2520.6	17	2520.6
6/12/97	17.7	2501.4	17.2	2422.5	17.6	2520.7	17.6	2520.7
6/19/97	17	2501.2	16.8	2421.3	17	2520.6	17	2520.6
7/1/97	23.4	2500.7	21.4	2417.5	20.4	2514.7	20.4	2514.7
7/14/97	21.3	2505.6	20.4	2412.5	21.7	2473.1	20.8	2508.3
7/23/97	23.6	2520.3	22.4	2410.1	23.1	2469.8	22	2506
8/27/97	19.1	2503.7	19.1	2404.7	19.6	2473.8	19.3	2496.7
8/29/97	20.6	2496.7	19.5	2407.2	21.3	2468.1	19.3	2498
8/29/97	20.6	2494.8	19.9	2408.4	21.5	2465	20.5	2498.7
9/3/97	19.4	2494.3	18.6	2405.3	21.2	2466	20	2495.9
9/5/97	17	2500	17.7	2399	18	2468	18.4	2494.1
9/22/97	17.2	2505.6	18.3	2375.3	18.8	2459.7	17.6	2486.2
10/1/97	16.1	2517.2	17.2	2377.9	17.1	2458	17.9	2485

Date	1VIA		1VOUA		2VIA		2VOUA	
	Temperature	Reading	Temperature	Reading	Temperature	Reading	Temperature	Reading
10/10/97	17.1	2505.8	16.9	2377.8	17.4	2453.1	17	2488.1
11/24/97	8.2	2501.6	9.8	2392.7	8.3	2463	9.9	2489.1
1/20/98	7.4	2515.6	8.8	2392	7.6	2471.8	8.8	2485.1
4/8/98	12.1	2504.3	11.6	2392.9	12.2	2445.4	11.6	2478
5/21/98	20.2	2494.3	19	2390.3	19.6	2448.7	18.6	2465.8
6/9/98	18.4	2488.8	18.4	2387.3	17.9	2447.1	17.7	2463.3
6/23/98	23.9	2460.2	21.2	2393	22.6	2433.6	20.8	2467.1
7/8/98	20.8	2426.1	19.8	2383	21.1	2435	20.4	2461
7/17/98	20.6	2395.1	19.4	2418.1	21	2406.7	20.1	2467.2
7/24/98	21	2384.8	20	2426.3	21.1	2403.1	20	2470.3
8/2/98	20	2380	20.1	2429.2	20.3	2402.8	20.1	2468.4
8/8/98	20	2352.4	19.2	2441	20.5	2387.7	19.6	2477
8/13/98	20.4	2341.1	19.4	2448.2	21.1	2377.9	19.7	2480.1
8/17/98	20.8	2336.2	19.8	2451.5	21	2378.1	20.2	2479.5
8/21/98	19.1	2330.7	19.2	2455.9	20.4	2372.9	19.3	2481.1
8/30/98	20	2303.3	19.9	2465.9	20.6	2353	19.6	2486.4
9/4/98	18.7	2297.3	18.7	2468.9	19.2	2349.4	19.1	2488.5
9/15/98	18.4	2284.7	18.2	2476.6	19.1	2340.3	19.1	2491.6
10/1/98	19.9	2258.2	18.9	2485.8	20	2331.2	19	2493.4
10/24/98	10.3	2255.5	12.5	2490.6	10	2340.1	12.2	2486.7
11/18/98	10.5	2244.6	12.1	2482.8	10.5	2337.6	12	2479.6
12/17/98	7.2	2243.8	8.9	2493	7.3	2338.3	8.8	2482.4
1/10/99	4	2242.4	6.5	2500.7	4.1	2344.5	6.3	2485.4
1/25/99	8.3	2250.5	9.8	2496.5	8.4	2345.6	10	2483.2
1/31/99	9.1	2245.1	9.9	2499.4	9.4	2339.9	10.1	2485.4
2/21/99	5.3	2243.8	7.6	2503.2	5.4	2344.9	7.4	2482.6
3/13/99	4.2	2226.9	5.7	2509.2	4.3	2335.2	5.6	2485.3
3/26/99	6.5	2230.9	7.9	2507.1	6.6	2336.8	7.9	2483.3
4/9/99	15.2	2222.7	13	2513.6	15	2325.8	13.5	2490.9
5/14/99	15	2232.5	14.8	2506.6	14.1	2333.6	14.8	2483.8
6/6/99	17.4	2227	16.4	2507.3	17.7	2330.8	16.9	2485
7/17/99	20.5	2234.5	19.6	2504.6	19.8	2333	19.7	2482
8/21/99	20	2225.8	19.8	2501.7	20.3	2330	20.2	2477.7
10/3/99	14.4	2210.2	15.1	2512.3	14.2	2324.4	15.1	2475.1
11/10/99	11.4	2196.8	11.6	2529	11	2321.2	11.5	2479.4
12/11/99	7.8	2196.2	9	2538.3	7.8	2323.3	9	2482.1
1/25/00	1.7	2205.1	4.6	2560.4	1.7	2329.3	4.4	2485.7

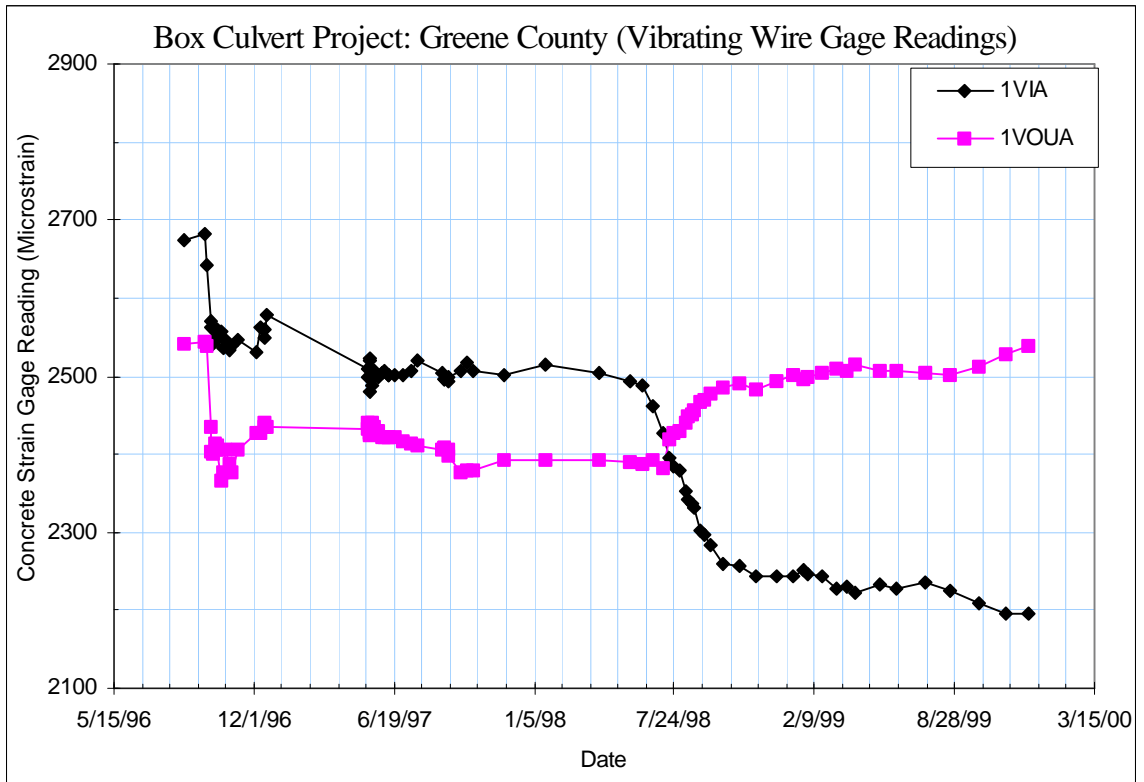


Figure B-22 Vibrating Wire Concrete Strain Gage Reading  
(1VIA, 1VOUA, Greene County, TN)

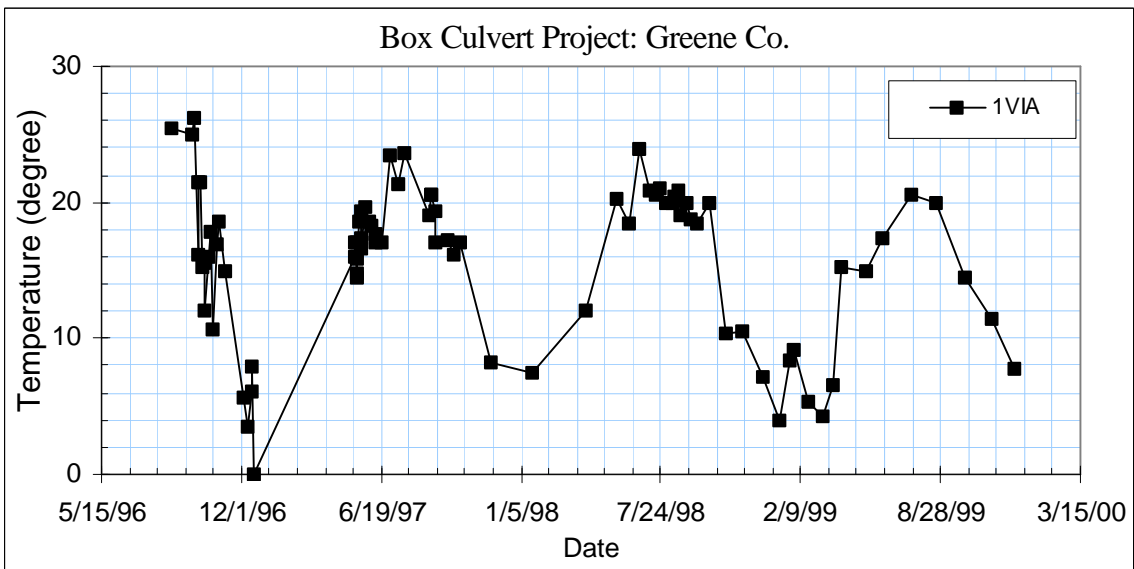


Figure B-23 Recorded Temperature at Gage 1VIA  
(Greene County, TN)

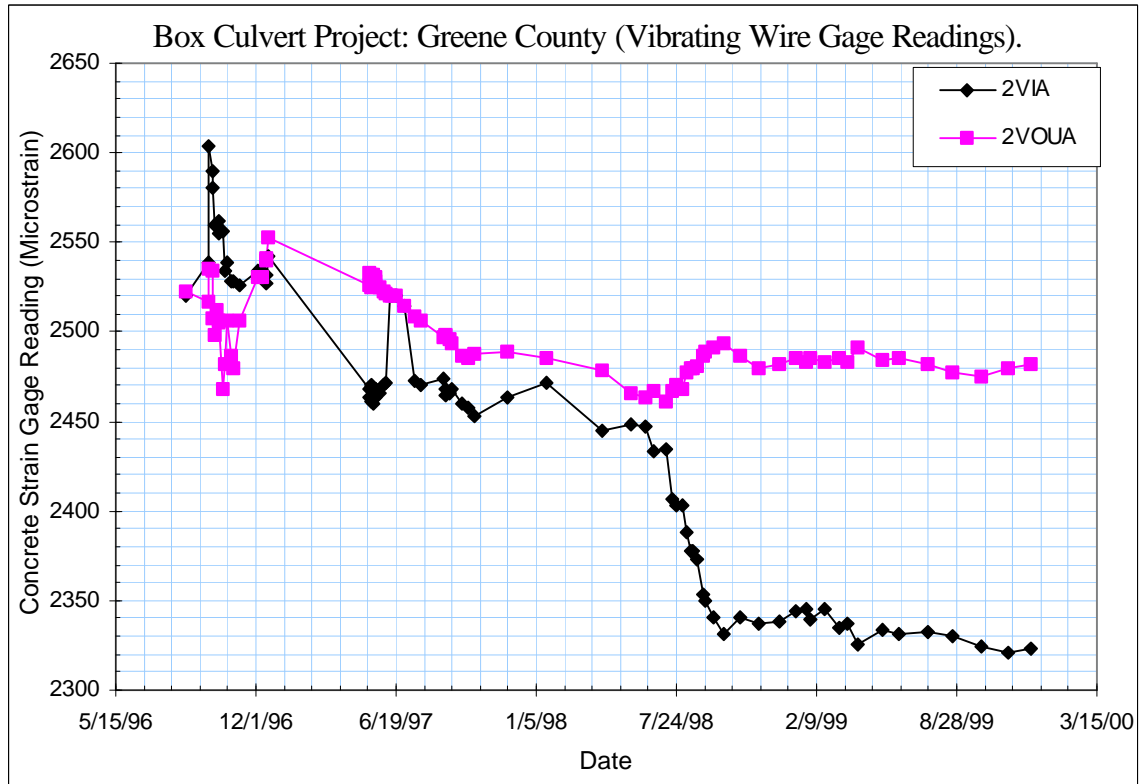


Figure B-24 Vibrating Wire Concrete Strain Gage Reading  
(2VIA, 2VOUA, Greene County, TN)

Greene County Culvert Concrete Strain Gages								
Date	3VIA		3VOUA		4VTA		4VBA	
	Temperature	Reading	Temperature	Reading	Temperature	Reading	Temperature	Reading
8/24/96	24.9	2520.3	24.8	2604.7	24.5	2558.6	23.1	2555.0
9/23/96	25	2539.3	24.6	2605.3				
9/25/96	29.7	2548.3	26.3	2613.5				
9/30/96	15	2565.5	16.4	2634.9				
10/1/96	20.2	2552.7	25.4	2609.2				
10/4/96	20.7	2530.3	24.3	2595.4				
10/7/96	15.1	2524.5	15	2609.4				
10/9/96	15.8	2519.4	14.8	2604.5	15.5	2545	16	2513.3
10/10/96	11.5	2522.5	11.3	2606.8	23.3	2554.9	18.7	2515.7
10/15/96	16.7	2519.7	23.9	2569.6	22.8	2490.1	19.7	2516.1
10/17/96	18.5	2491.3	21.3	2588.1	21.2	2505.8	20.6	2504.7
10/21/96	10.6	2486.9	10.3	2620.7	10.6	2560.7	11.7	2535.3
10/28/96	16.8	2482.6	17.1	2600.4	17.2	2532.1	15.9	2529.1
10/31/96	19.2	2483.0	21.4	2579.5	22.3	2496.9	18.5	2526.3
11/8/96	15.6	2470.4	13.7	2633.1	14.1	2555.4	15.8	2527.3
12/5/96	5.3	2477.5	5.3	2652.9	5.8	2574.5	6.1	2575.3
12/9/96	3.6	2478.8	4.5	2652.5	4.4	2576.6	3.6	2589.1
12/16/96	5.4	2474.5	4.5	2658.1	3.3	2588.8	5.3	2580.4
12/17/96	7.5	2477.5	7.2	2651.4	6.1	2576.0	6.1	2584.2
12/20/96	-3.6	2484.7	-2.8	2671.3	3.3	2609.8	-1	2601.4
5/12/97	16.5	2451.8	22.5	2575.5	20.6	2529.4	16.4	2520.7
5/13/97	17.5	2420	18.9	2592.7	21.3	2529.5	18.1	2509.6
5/14/97	15.7	2436.2	16.7	2604.7	14	2526.6	16.5	2500.5
5/15/97	17	2437.7	16.9	2600	18.4	2543.2	17	2509.8
5/16/97	15.2	2438.3	16.6	2600.4	17.4	2546.1	16.8	2505.2
5/16/97	15.7	2434.5	16.3	2602.9	16.8	2486.2	16.5	2507.2
5/19/97	18	2433.4	17	2607.7	17	2543.3	17.2	2506.9
5/20/97	18.8	2433.9	18.1	2607.9	17.4	2544.2	18.3	2502.2
5/21/97	17.2	2380.8	17.7	2606	17.8	2540.9	17.6	2504.5
5/22/97	16.4	2435.8	17	2606.5	17.9	2539	17.1	2506.2
5/27/97	19.2	2431.8	18.6	2610.3	18.3	2538.6	18.9	2502.7
6/2/97	18.3	2432	18.1	2610.1	18.4	2530	18.3	2505.1
6/4/97	18	2432.4	18.1	2610.2	18.6	2534.8	18.3	2503.4
6/10/97	17.4	2429.7	17	2610.6	18	2533.5	17.3	2505.8
6/12/97	18.1	2429.9	17.7	2611.5	18.1	2534.6	17.9	2503.8
6/19/97	17.4	2429.7	17	2610.6	18	2533.3	17.3	2505.8
7/1/97	21.3	2430.7	20.3	2615	20.7	2529.7	20.9	2498.4
7/14/97	21.8	2430.8	20.9	2612.9	21.8	2525.5	21.7	2493
7/23/97	23.1	2428.5	21.9	2614.3	22.7	2524.3	22.8	2490.2
8/27/97	19.2	2424.9	19.1	2606.4	20.3	2516.9	21.1	2481.2
8/29/97	21.5	2420.3	21.6	2608.9	22.5	2517.3	21.5	2480.5
8/29/97	21.9	2412.8	20.9	2609.9	22.4	2517.6	22.0	2479.2
9/3/97	21.5	2416.7	20.1	2607	22.2	2516.1	21.7	2477.5
9/5/97	19.3	2414.6	18.9	2605.8	21.9	2513.7	18.7	2481.1
9/22/97	19.3	2381.2	19.4	2615.6	20.7	2513.4	19.5	2468.4
10/1/97	17.5	2374.4	18.2	2617.6	19.8	2514.2	18.1	2466.2
10/10/97	17.9	2366.9	16.5	2621.5	19.2	2514.6	16.8	2466

Date	3VIA		3VOUA		4VTA		4VBA	
	Temperature	Reading	Temperature	Reading	Temperature	Reading	Temperature	Reading
11/24/97	9.1	2364.4	10.4	2610.8	12.8	2514.8	10.4	2474.6
1/20/98	8.3	2352.2	9.1	2611.8	11	2515.3	9.1	2481.5
4/8/98	12.2	2338.7	11.6	2614.2	12	2515.7	11.8	2459.8
5/21/98	19.1	2347.7	18.1	2616.7	16.5	2511.9	18.2	2497.3
6/9/98	17.7	2350.3	17.4	2606.8	17.4	2502.4	17.6	2453.3
6/23/98	20.2	2341.1	20.3	2617.8	19.6	2502.9	20.7	2499.1
7/8/98	20.9	2338.8	19.4	2611.9	19.3	2497.8	20.2	2451
7/17/98	20.8	2331.2	20	2602.5	19.5	2481.7	20.2	2463.1
7/24/98	21	2326.9	20.3	2602.8	19.6	2478.4	20.4	2463.7
8/2/98	20.2	2330.6	19.8	2599	19.6	2475.2	19.8	2467.9
8/8/98	20.4	2312.1	19.5	2611	19.7	2476.1	19.7	2467.1
8/13/98	19.4	2310.1	16.1	2613.9	19.3	2473.2	20	2469.1
8/17/98	20	2312	20	2611.8	19.4	2471.5	20.2	2470.3
8/21/98	20.4	2310.7	19.5	2608.3	19.5	2468.2	19.8	2473.4
8/30/98	20.6	2288.7	19.9	2618.3	19.4	2468.4	19.7	2470.5
9/4/98	19.3	2284.1	19	2617.7	19.2	2467.9	19.1	2471.2
9/15/98	19.1	2277.5	19	2617.3	18.6	2467.9	19	2467.1
10/1/98	20.2	2274.3	19	2617.3	18.9	2464.5	19	2467.5
10/24/98	10.7	2282.5	12.3	2587.8	15.5	2458.8	12.5	2480.6
11/18/98	10.9	2279.6	12.1	2585.3	13.8	2458.7	12	2477
12/17/98	7.9	2276.8	9.1	2581.5	11.5	2456.1	9.1	2487.9
1/10/99	4.9	2278.8	6.6	2583.2	6.5	2461.9	6.5	2496.6
1/25/99	8.7	2277.4	10.1	2589.9	10.8	2460.2	9.7	2490.9
1/31/99	9.7	2273.6	10.1	2593.2	10.7	2461.1	10	2488.9
2/21/99	6	2278.4	7.6	2581.5	9.6	2456.5	7.5	2494.8
3/13/99	4.7	2274	5.6	2579.2	8.1	2456.2	5.8	2497.2
3/26/99	7	2273.4	8.1	2581.9	9.6	2455.9	7.9	2490.7
4/9/99	15	2263.6	13.3	2605.9	12.4	2459.9	13.4	2481.1
5/14/99	15.1	2268.6	14.7	2598.8	14.1	2454.7	14.8	2478.8
6/6/99	17.6	2267.7	16.7	2603.4	160	2455.5	16.9	2474.6
7/17/99	20.3	2268.4	19.5	2608.5	19	2450	19.8	2475.2
8/21/99	20.2	2266.6	20.2	2602.8	202	2444.5	20.4	2474
10/3/99	14.6	2262.9	15.2	2583.3	16.5	2437.5	15.4	2481.7
11/10/99	11.3	2259.2	11.7	2578.8	13.3	2440.7	11.6	2482
12/11/99	8.4	2282.3	9.2	2535.4	9	2443.1	9	2481
1/25/00	2.7	2260.5	4.8	2568.5	7.5	2445.8	4.7	2488.1

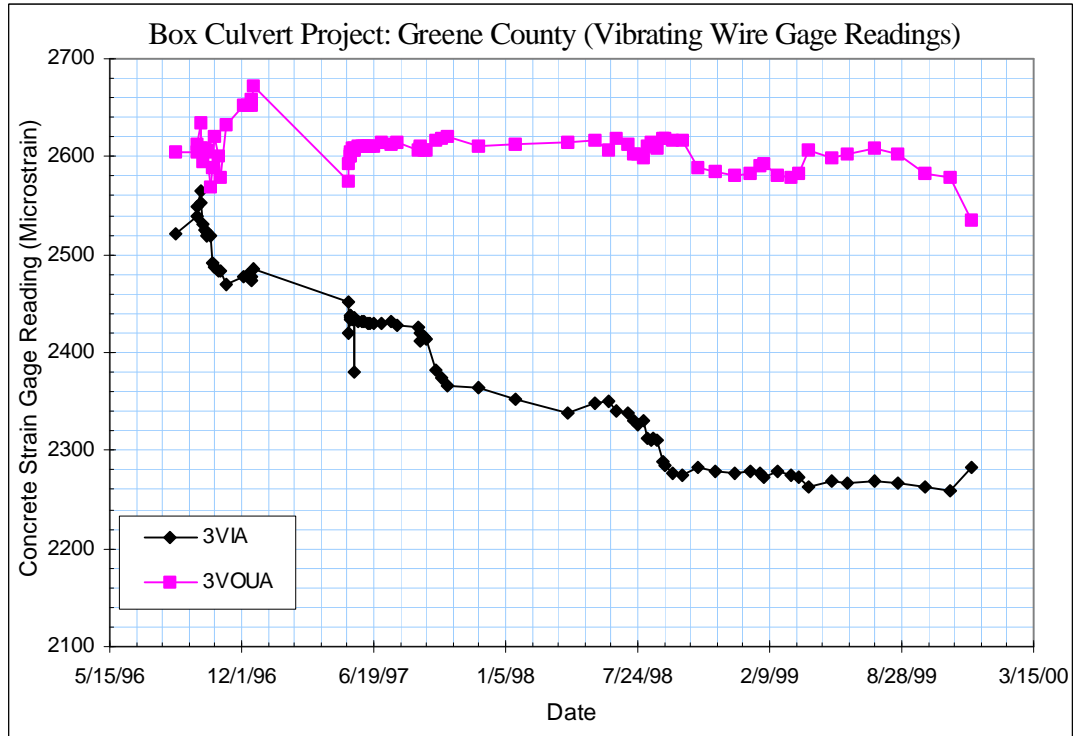


Figure B-25 Vibrating Wire Concrete Strain Gage Reading  
(3VIA, 3VOUA, Greene County, TN)

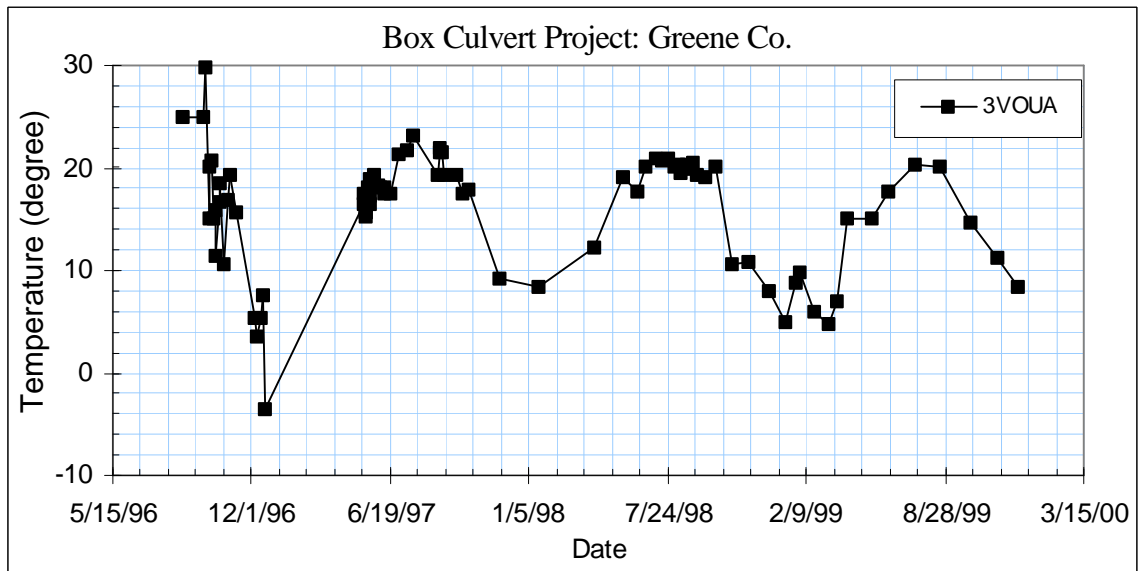


Figure B-26 Recorded Temperature at Gage 3VOUA  
(Greene County, TN)

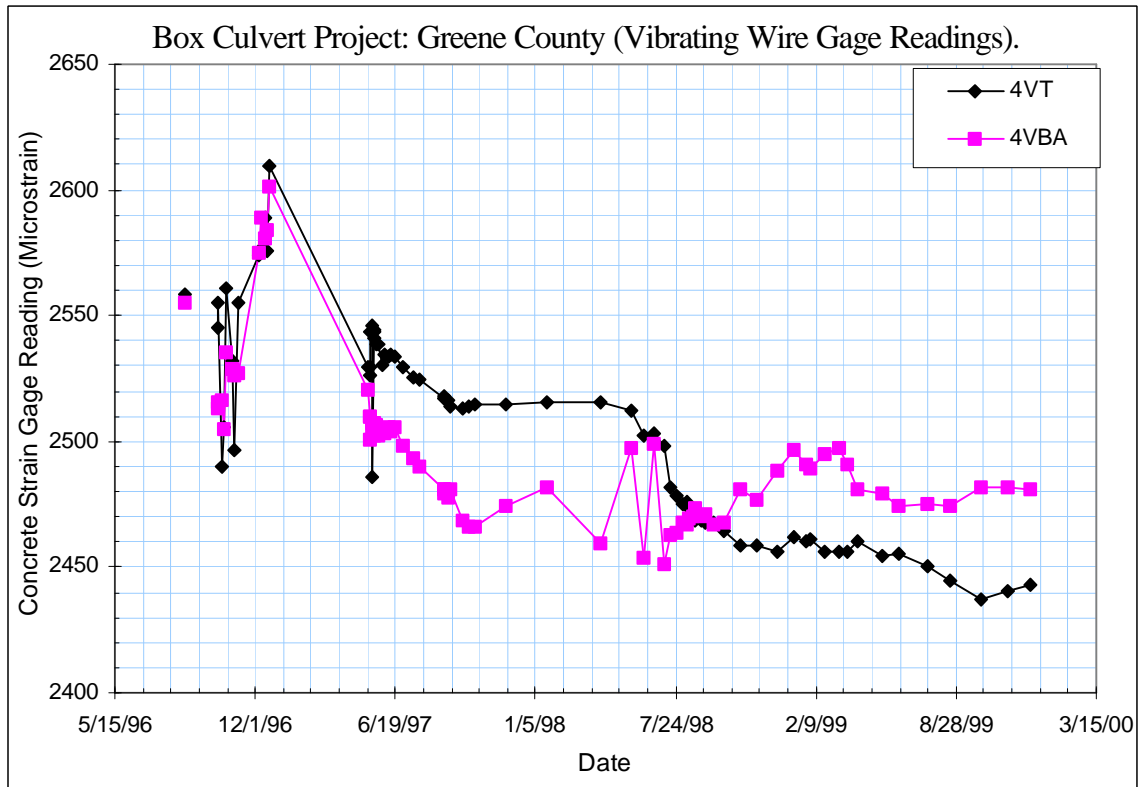


Figure B-27 Vibrating Wire Concrete Strain Gage Reading  
(4VTA, 4VBA, Greene County, TN)



Greene County Culvert Concrete Strain Gages								
Date	5VTA		5VBA		6VTA		6VBA	
	Temperature	Reading	Temperature	Reading	Temperature	Reading	Temperature	Reading
8/24/96	24.6	2555.7	25.5	2576.7	24.7	2630.6	24.6	2761.5
9/23/96								
9/25/96								
9/30/96								
10/1/96								
10/4/96								
10/7/96								
10/9/96	15.9	2505.3	16.5	2558.3	15.5	2607.6	16	2682.7
10/10/96	23.6	2515.1	18.6	2540.9	22.9	2626.4	18.6	2681.0
10/15/96	21.6	2513.7	20.7	2520.1	22.9	2632.2	20.2	2674.0
10/17/96	20.1	2532.3	20.7	2517.2	20.3	2657.4	19.9	2677.1
10/21/96	10.1	2573.2	12.0	2542.3	10.3	2700.1	11.6	2706.9
10/28/96	16.7	2546.6	16.0	2539.3	17.0	2669.8	15.8	2697.7
10/31/96	20.3	2525.4	18.4	2537.3	20.8	2642.6	18.1	2694.7
11/8/96	14.6	2561.2	15.8	2536.2	14.1	2700.3	15.3	2694.7
12/5/96	5.6	2590.0	6.3	2579.0	5.1	2735.8	5.6	2738.5
12/9/96	3.3	2601.6	3.7	2594.5	3.5	2738.7	3.3	2755.8
12/16/96	2.9	2611.7	5.3	2584.1	2.7	2766.7	5.1	2738.2
12/17/96	5.7	2600.1	6.2	2588.1	5.5	2750.7	5.8	2743.1
12/20/96	-2.8	2626.3	-0.3	2603.7	-3	2779.1	-0.1	2757.7
5/12/97	19.8	2542.4	16.6	2553	20.4	2667	18.2	2698.5
5/13/97	20.9	2536	18.2	2539.9	21.3	2675.6	17.7	2684
5/14/97	13.8	2573.4	16.7	2526.4	13.5	2731.8	16.3	2670.5
5/15/97	18.4	2552.7	17	2540.7	18.3	2701	16.7	2683
5/16/97	18	2528.4	17.2	2535.4	18.2	2700.7	17	2677
5/16/97	17.2	2552	17.1	2536.5	17.4	2711.6	16.9	2675
5/19/97	17.1	2558.4	17.9	2531.1	16.9	2729.6	17.4	2666.2
5/20/97	17.6	2560.9	19.2	2525.2	17.4	2736.5	18.4	2669.2
5/21/97	18	2552.7	18.5	2529.1	17.8	2723.5	17.9	2664.1
5/22/97	18.2	2548.5	17.9	2532.1	17.9	2715.5	17.5	2668.5
5/27/97	18.6	2553.8	19.6	2526.8	18.4	2735.6	19.2	2656.1
6/2/97	18.5	2548.9	18.8	2532.1	18.4	2729.8	18	2660.2
6/4/97	18.7	2547.4	18.9	2530.9	18.6	2727.8	18.6	2659.7
6/10/97	18	2545.4	17.5	2536.4	17.9	2723.8	17.4	2665.1
6/12/97	18	2548.5	18.1	2533.5	18.1	2729.7	17.4	2665.1
6/19/97	18	2545.4	17.5	2536.4	17.9	2723.8	17.4	2665.1
7/1/97	20.9	2543.5	21.5	2528.8	20.9	2729.4	21.3	2652
7/14/97	22.2	2536.1	22.3	2524.3	22.1	2720.7	22.1	2647.6
7/23/97	23.1	2523.6	23.5	2517	23.1	2721.1	23.3	2642.1
8/27/97	22.3	2521.3	21.3	2519.1	22.2	2702.7	21.1	2637.9
8/29/97	22	2523.4	22	2517.4	22.2	2711.3	21.7	2636
8/29/97	21.1	2524.4	22.0	2516	26.8	2712.7	21.7	2631.8
9/3/97	21.5	2522.5	22	2515.1	22.3	2712.6	21.7	2629.5
9/5/97	21.7	2515.5	21.7	2515.5	20.7	2700.4	19.1	2637.7
9/22/97	20.3	2509.6	20.1	2517.3	20.7	2716.3	19.6	2622.5
10/1/97	19.1	2510.6	18.8	2516.9	19.4	2719	18.7	2626.9
10/10/97	18.8	2512.9	18	2518.7	18.6	2727.9	16.5	2621.3
11/24/97	11.8	2519.8	10	2538.3	10.7	2747.1	9.5	2636.9
1/20/98	10.2	2517.7	8.8	2553.6	9.9	2740.1	8.5	2640.2
4/8/98	11.7	2514.6	11.9	2534.9	11.6	2743.1	11.6	2620.3
5/21/98	17.1	2509.1	19.2	2512.1	16.9	2747.3	18.9	2598.9
6/9/98	18	2497.9	18.4	2519.2	18.1	2733.5	18.3	2598.5
6/23/98	19.7	2499.3	21.8	2510.8	19.5	2748.5	21.4	2590.4
7/8/98	19.8	2492.6	21	2515.2	19.8	2741.4	20.4	2590.7

Date	5VTA		5VBA		6VTA		6VBA	
	Temperature	Reading	Temperature	Reading	Temperature	Reading	Temperature	Reading
7/17/98	20	2481.5	20.8	2526.3	19.7	2755.2	20.7	2589.2
7/24/98	20.1	2480.5	19.6	2526.3	20.4	2768.2	20.7	2584.7
8/2/98	20.1	2478.4	20.5	2529	20	2774.1	20.5	2584.6
8/8/98	19.4	2480	20.2	2530	19.4	2797.3	19.9	2579.8
8/13/98	19.7	2477.2	20.7	2533.8	19.7	2794.8	20.3	2582
8/17/98	19.8	2475.7	20.8	2535.1	18.8	2796	20.6	2581.6
8/21/98	19.8	2473.1	20.3	2538	20.3	2797.2	20.3	2581.7
8/30/98	19.9	2464.6	20.6	2539	19.9	2769.8	20.5	2578.7
9/4/98	19.4	2463.8	19.6	2540.7	19.5	2768.2	19.5	2579.8
9/15/98	18.8	2463.3	19.5	2536.3	18.3	2802.1	19.3	2596.2
10/1/98	19.3	2461.5	19.8	2536.2	19.2	2805.1	19.8	2573.4
10/24/98	15.1	2460.3	12.7	2549.6	15	2801.8	11.9	2586.8
11/18/98	13.3	2457.8	12	2545	13.1	2788	11.5	2580.5
12/17/98	10.7	2457.8	8.9	2559.2	10.5	2786.5	8.4	2590.6
1/10/99	7.5	2463.6	6.2	2562.5	7.3	2800.9	5.6	2595
1/25/99	10.5	2462.6	9.9	2557	9.1	2800	9.4	2590.5
1/31/99	10.1	2464.7	9.9	2555	9.9	2802.6	9.6	2587.5
2/21/99	8.8	2463	8.5	2560.7	8.5	2798.8	6.8	2591.9
3/13/99	6.9	2458.2	5.3	2561.8	6.9	2801	4.9	2592.9
3/26/99	9.1	2463.7	7.9	2554.4	8.8	2801.8	7.5	2586.4
4/9/99	12.4	2465.5	13.8	2543.4	12.2	2810.7	13.6	2575.6
5/14/99	14.6	2459.9	15.3	2540.3	14.5	2803.5	15.1	2552.2
6/6/99	16.4	2458.1	17.4	2535.5	16.5	2803.2	17.3	2567.2
7/17/99	19	2451.8	20.6	2534.2	18.9	2796.8	20.4	2565.5
8/21/99	20.7	2445.5	21.1	2531.9	20.7	2788.1	21	2563.3
10/3/99	16.9	2444.2	15.6	2538.7	15.6	2781.6	15.3	2566.3
11/10/99	12.7	2452.8	11.5	2539.9	12.5	2794.1	11.2	2564
12/11/99			8.9	2539.6				
1/25/00	6.4	2463.2	4.2	2550.5	6.1	2804.6	3.6	2574.0

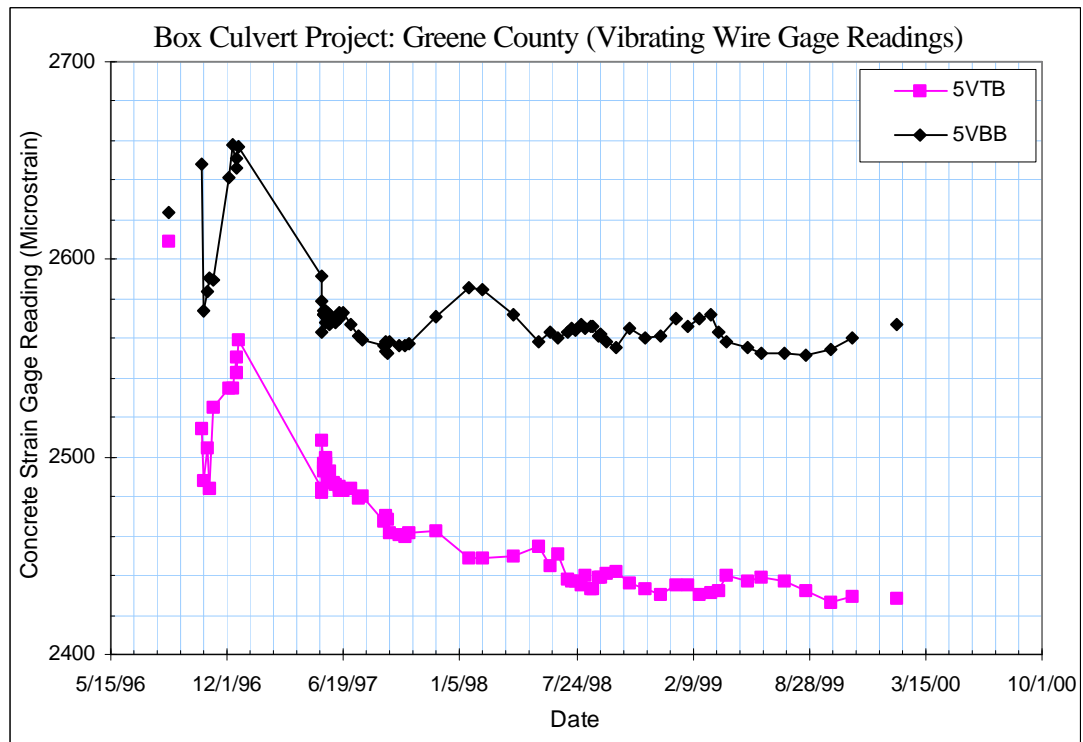


Figure B-28 Vibrating Wire Concrete Strain Gage Reading (5VTA, 5VBA, Greene County, TN)

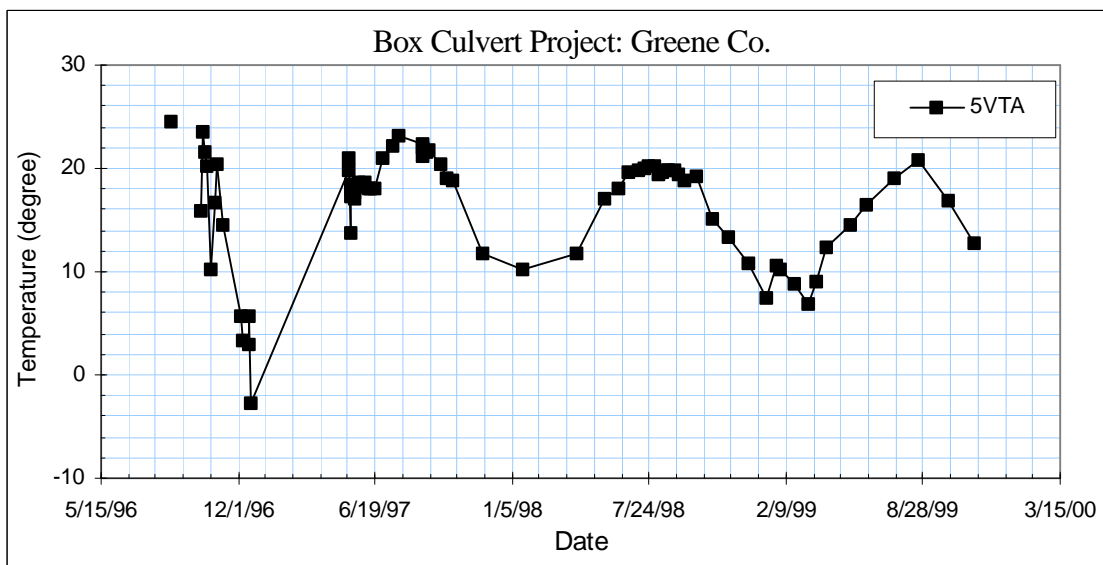


Figure B-29 Recorded Temperature at Gage 5VTA (Greene County, TN)

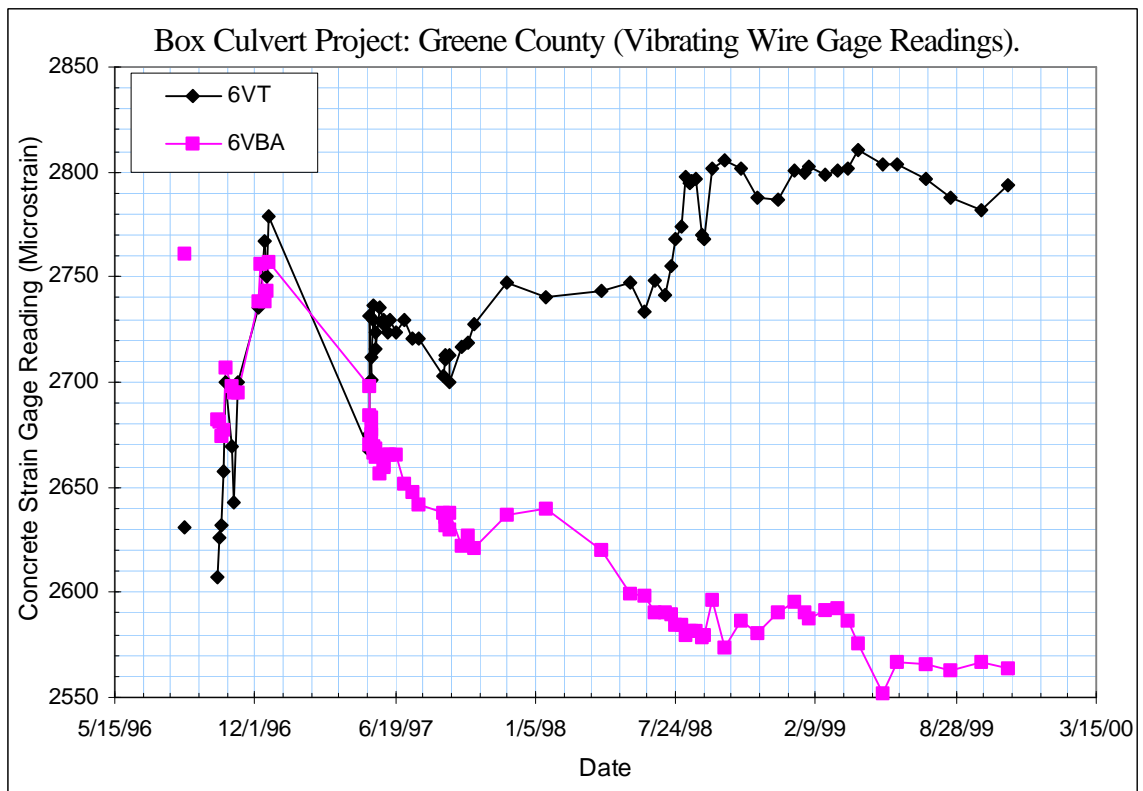


Figure B-30 Vibrating Wire Concrete Strain Gage Reading  
(6VTA, 6VBA, Greene County, TN)

Greene County Culvert Concrete Strain Gages								
Date	1VIB		1VOUB		2VIB		2VOUB	
	Temperature	Reading	Temperature	Reading	Temperature	Reading	Temperature	Reading
8/24/96	25.6	2554.2	24.6	2587.9	24.6	2619.4	25.7	2792.5
9/23/96								
9/25/96								
9/30/96								
10/1/96	26.3	2546.7	25.7	2598.4	25.9	2612.2	26.0	2776.9
10/4/96	28.1	2497.0	30.2	2592.2	31.8	2582.5	35.4	2747.6
10/7/96	16.5	2511.0	16.2	2629.2	16.4	2594.1	16.3	2773.3
10/9/96	16.6	2505.4	16.5	2613.7	16.3	2588.3	16.5	2780.3
10/10/96	12.7	2512.5	12.6	2624.6	12.3	2596.0	12.4	2791.3
10/15/96	15.4	2482.3	19.7	2619.0	15.2	2570.9	19.2	2785.4
10/17/96	17.2	2468.9	18.4	2602.8	17.5	2559.2	18.4	2768.8
10/21/96	9.6	2489.5	9.5	2601.4	9.0	2572.0	9.0	2772.1
10/28/96	17.0	2468.3	17.0	2581.3	17.0	2547.1	17.0	2752.9
10/31/96	18.8	2567.8	21.2	2568.6	18.7	2544.7	21.2	2741.3
11/8/96	15.2	2475.3	16.2	2566.4	15.7	2536.5	16.5	2743.0
12/5/96	5.7	2481.9	5.5	2601.2	5.1	2534.4	5.1	2778.8
12/9/96	3.8	2481.0	4.6	2599.1	3.5	2534.3	4.8	2773.3
12/16/96	5.8	2484.4	6.5	2604.3	5.5	2536.4	5.5	2778.0
12/17/96	7.3	2476.9	7.0	2605.5	7.1	2534.7	6.9	2779.4
12/20/96	1.4	2496.5	3.4	2604.0	-1.0	2539.0	-0.6	2784.0
5/12/97	16.0	2408.0	15.7	2575.8	16.1	2475.4	19.0	2730.6
5/13/97	17.2	2392.5	17.1	2578.4	17.1	2471.3	18.6	2725.5
5/14/97	15.1	2410.4	16.3	2574.2	15.5	2475.3	17.0	2723.5
5/15/97	17.3	2391.4	17.1	2577.6	17.4	2467.2	17.7	2725.3
5/16/97	14.8	2407.3	16.5	2571.2	15.0	2476.4	17.0	2721.2
5/16/97	16.3	2388.0	16.3	2576.5	16.0	2472.3	16.7	2726.0
5/19/97	18.6	2388.3	17.6	2576.5	18.1	2465.8	17.5	2726.8
5/20/97	19.2	2389.4	18.8	2571.5	19.0	2473.1	18.8	2722.0
5/21/97	17.7	2398.8	18.0	2570.9	17.4	2475.7	17.9	2722.3
5/22/97	16.1	2429.7	17.4	2569.8	16.3	2475.7	17.1	2722.1
5/27/97	19.8	2398.6	19.5	2568.2	19.4	2477.7	19.3	2720.4
6/2/97	19.0	2397.6	18.8	2566.3	18.1	2482.2	18.5	2717.8
6/4/97	18.4	2398.8	18.8	2564.4	18.2	2483.1	18.5	2716.5
6/10/97	17.0	2394.2	16.8	2563.9	17.2	2479.6	17.1	2716.6
6/12/97	17.4	2395.6	17.4	2563.4	17.8	2480.9	17.8	2715.8
6/19/97	17.0	2394.2	16.8	2563.9	17.2	2479.6	17.1	2716.6
7/1/97	22.3	2407.5	20.7	2563.4	21.2	2484.2	20.9	2709.6
7/14/97	21.1	2410.0	20.4	2554.5	21.4	2485.3	21.0	2707.9
7/23/97	23.4	2408.9	22.2	2555.0	22.8	2482.1	22.0	2706.9
8/27/97	19.3	2403.7	19.1	2547.8	19.5	2478.3	19.6	2697.7
8/29/97	20.0	2400.3	19.6	2547.2	20.8	2475.4	20.4	2695.9
8/29/97	19.8	2399.6	19.8	2546.8	18.9	2475.2	20.6	2695.7
9/3/97	24.0	2395.7	19.9	2543.4	19.7	2475.9	20.2	2695.0
9/5/97	17.8	2392.4	17.7	2942.6	17.5	2479.3	17.4	2690.3
9/22/97	16.8	2373.7	17.9	2534.0	18.6	2480.2	18.4	2672.2
10/1/97	16.9	2366.3	17.0	2532.8	17.1	2477.7	17.6	2669.2

Date	1VIB		1VOUB		2VIB		2VOUB	
	Temperature	Reading	Temperature	Reading	Temperature	Reading	Temperature	Reading
10/10/97	15.7	2364.6	17.8	2534.0	17.0	2476.1	16.6	2688.5
11/24/97	8.2	2345.8	8.2	2345.8	8.1	2479.7	9.3	2667.1
1/20/98	7.4	2360.0	8.3	2536.9	7.6	2496.8	8.6	2667.0
2/14/98	7.2	2356.7	7.7	2538.3	7.6	2489.8	8.1	2667.1
4/8/98	12.0	2349.9	11.3	2536.1	12.0	2473.1	11.6	2664.6
5/21/98	18.7	2369.7	18.2	2531.8	18.8	2481.1	18.3	2658.8
6/9/98	18.2	2367.5	18.0	2530.5	17.9	2479.5	17.8	2721.0
6/23/98	23.0	2363.3	21.5	2532.7	22.1	2476.4	21.1	2659.1
7/8/98	20.6	2361.7	19.7	2527.8	20.8	2483.5	20.4	2653.0
7/17/98	19.8	2359.0	19.8	2526.9	19.5	2491.7	19.0	2653.0
7/24/98	20.8	2359.4	20.0	2526.9	20.8	2495.0	20.5	2645.9
8/2/98	20.2	2355.0	19.9	2526.2	20.0	2496.0	20.0	2646.0
8/8/98	19.8	2352.7	19.3	2527.2	20.3	2492.6	19.6	2644.1
8/13/98								
8/17/98	20.7	2350.4	20.0	2527.4	20.9	2490.7	20.5	2643.0
8/21/98	19.8	2345.0	19.4	2527.7	20.3	2484.0	19.8	2643.4
8/30/98	20.0	2341.3	19.4	2527.7	20.4	2485.8	20.0	2642.0
9/4/98	18.7	2332.9	19.5	2527.6	19.0	2481.9	19.0	2640.9
9/15/98	18.7	2328.6	18.3	2327.8	19.0	2475.8	19.0	2640.0
10/1/98	19.8	2319.4	19.4	2548.8	19.4	2468.5	19.4	2641.3
10/24/98	10.3	2305.1	12.5	2529.0	9.9	2466.1	11.4	2641.9
11/18/98	10.2	2298.5	11.2	2527.3	10.1	2461.1	11.3	2639.0
12/17/98	10.6	2297.5	9.0	2528.6	10.1	2461.2	9.4	2640.1
1/10/99	4.0	2291.4	5.8	2531.6	4.1	2464.2	5.9	2642.2
1/25/99								
1/31/99	8.9	2295.0	9.6	2531.2	9.1	2461.0	9.9	2639.5
2/21/99	5.0	2290.3	6.7	2530.5	5.1	2463.4	6.8	2639.4
3/13/99	4.2	2276.4	5.1	2532.2	4.1	2452.7	5.1	2641.0
3/26/99	6.4	2279.0	7.3	2503.2	6.4	2453.1	7.5	2639.0
4/9/99	15.0	2231.1	13.0	2533.5	15.0	2446.5	13.5	2641.4
5/14/99	14.7	2297.1	14.5	2527.7	14.7	2455.4	14.8	2636.3
6/6/99	17.2	2297.6	16.4	2527.4	17.5	2442.3	16.9	2636.9
7/17/99	20.2	2327.2	19.5	2525.1	20.1	2461.2	19.8	2638.9
8/21/99	19.8	2324.4	19.4	2520.9	19.9	2458.8	20.0	2630.7
10/3/99	13.7	2314.8	14.1	2520.1	13.6	2452.6	14.1	2630.4
11/10/99			10.5	2523.5	10.2	2446.2	10.7	2633.8
12/11/99	7.3	2296.1	8.1	2522.5	7.2	2447.3	8.2	2632.5
1/25/00	1.4	2290.6	3.6	2524.1	1.4	2450.6	3.5	2633.2

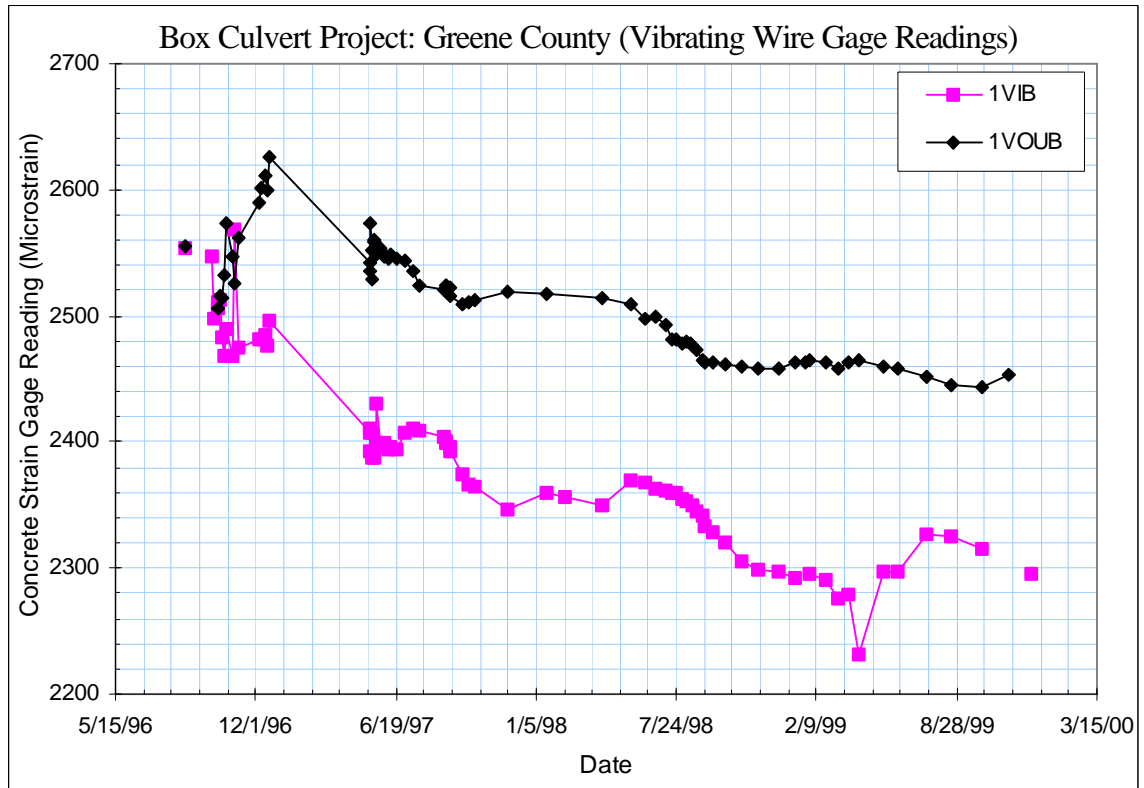


Figure B-31 Vibrating Wire Concrete Strain Gage Reading  
(1VIB, 1VOUB, Greene County, TN)

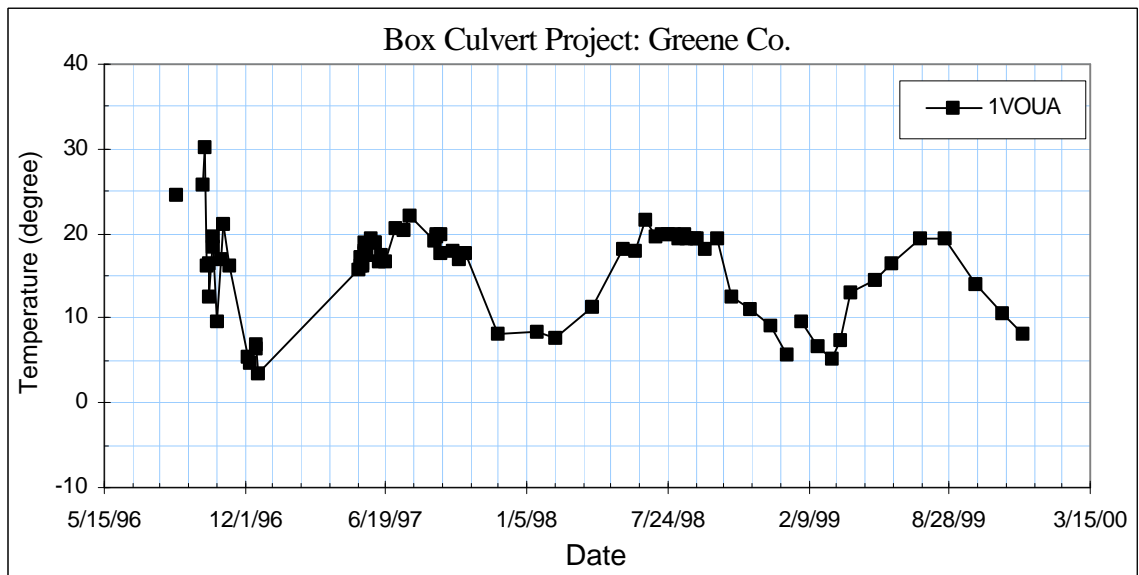


Figure B-32 Recorded Temperature at Gage 1VOUB  
(Greene County, TN)





Greene County Culvert Concrete Strain Gages								
Date	3VIB		3VOUB		4VTB		4VBB	
	Temperature	Reading	Temperature	Reading	Temperature	Reading	Temperature	Reading
8/24/96	24.6	2629.0	23.7	2511.2	24.5	2602.7	24.7	2551.4
9/23/96								
9/25/96								
9/30/96								
10/1/96	25.8	2636.9	26.1	2533.4				
10/4/96	30.6	2631.1	33.6	2510.2				
10/7/96	16.2	2645.2	16.3	2544.5				
10/9/96	16	2638.7	16	2535.7				
10/10/96	11.6	2648.0	11.4	2549.8				
10/15/96	15.2	2626.0	18.2	2545.4				
10/17/96	17.4	2614.1	17.8	2519.2	25.1	2610.8	25.2	2582
10/21/96	8.4	2623.5	8.2	2535.7	17.1	2570.7	17.6	
10/28/96	17.0	2592.2	17.1	2515.5	17.9	2563	17.3	2545
10/31/96	19.0	2590.0	21.0	2505.6	21.8	2542.3	19.0	2548.6
11/8/96	15.7	2572.6	16.4	2501.0	14.2	2585.8	16	2550.9
12/5/96	5.1	2573.0	5.1	2537.0	5.4	2600.7	5.6	2600.6
12/9/96	3.5	2573.1	4.5	2533.7	5.1	2594.3	3.5	2620.8
12/16/96	7.3	2575.5	5.3	2534.5	3.7	2608.0	5.4	2612.0
12/17/96	7.3	2575.5	7.3	2534.1	6.1	2600.9	6.2	2616.9
12/20/96	-2.3	2568.2	-2.6	2548.6	-3.1	2626	-0.2	2628.1
5/12/97	16	2535.9	18	2478	19.2	2543.4	16.2	2555.6
5/13/97	17.8	2531.2	18.5	2463.8	20.9	2538	18.8	2546.5
5/14/97	16.1	2524.2	17.3	2469.2	15	2555.9	7.2	2534.6
5/15/97	17.5	2524.5	17.9	2470.7	16.2	2548.2	16.8	2542
5/16/97	15.5	2528	16.9	2469	16.2	2548.5	16.3	2541
5/16/97	16.1	2523.2	16.6	2472.1	15.5	2549.2	16	2543.4
5/19/97	17.7	2524.3	17.1	2474.4	15.7	2545.8	16.3	2546
5/20/97	18.5	2528.2	18.4	2470.5	16.4	2546.2	17.6	2541.6
5/21/97	17	2530	17.4	2470.4	16.7	2543	16.9	2543.8
5/22/97	16.7	2470.6	16.7	2470.7	16.8	2541.8	16.6	2544.3
5/27/97	19	2531.6	18.8	2469.3	17.9	2540.7	18.6	2540.9
6/2/97	18.2	2535.9	18.2	2468.1	18.1	2536.2	18.2	2543.8
6/4/97	18	2536.4	18.2	2466.9	18.3	2535.1	18.4	2542.1
6/10/97	17.2	2533.3	17.1	2467.1	17.7	2533	17.3	2544.2
6/12/97	17.8	2534.7	17.8	2465.8	17.8	2533.5	17.8	2542.3
6/19/97	17.2	2533.3	17.1	2467.1	17.7	2533	17.3	2544.2
7/1/97	21	2540.5	20.5	2462.7	20.2	2530.6	20.6	2540.9
7/14/97	21.4	2541	21	2456.9	21.4	2526.9	21.3	2536.6
7/23/97	22.6	2540.7	22.1	2454.8	22.1	2526.8	22.5	2531.5
8/27/97	20.9	2536.9	20.0	2442.8	21.5	2518.2	20.7	2520.0
8/29/97	20.6	2534.9	20.7	2440.5	18.5	2517.1	21.3	2519.7
8/29/97	21.3	2534.3	20.4	2440.2	21.7	2517.5	21.5	2518.8
9/3/97	20.5	2534.4	19.8	2434.9	21.4	2514.4	21.4	2517.6
9/5/97	18.6	2533.5	18.7	2434.6	21	2511	19	2520.8
9/22/97	18.1	2534	17.9	2415.5	20.3	2499.1	19.6	2512.2
10/1/97	17.7	2539.2	17.7	2411.6	19.8	2459.4	18.7	2519.9

Date	3VIB		3VOUB		4VIB		4VBB	
	Temperature	Reading	Temperature	Reading	Temperature	Reading	Temperature	Reading
10/10/97	16.1	2539.8	17.1	2409.8	18.4	2457.2	17.4	2521.7
11/24/97	9	2557	9.7	2403.2	12.3	2496.8	10.6	2532.3
1/20/98	8.2	2560.9	9.3	2392.2	10.6	2495.6	9.3	2544
2/14/98	7.9	2554	8.4	2379.4	9.5	2490.2	8.5	2543.2
4/8/98	12.1	2545.3	11.7	2387.7	11.7	2489.1	11.7	2529.5
5/21/98	18.4	2553.7	18	2380.4	17.7	2487.8	16.9	2520.4
6/9/98	17.4	2556.8	17.4	2373.4	17.2	2480.5	17.6	2525.9
6/23/98	21.4	2556.3	20.9	2372.6	18.9	2482.5	20.4	2523.9
7/8/98	20.5	2568.1	20.1	2360.7	19.2	2471.8	19.9	2529.1
7/17/98	19.9	2578.5	19.8	2353	19.2	2465.1	19.5	2533.2
7/24/98	20.6	2584.9	20.3	2348	19.3	2462.3	20.1	2536.1
8/2/98	20	2587.3	19.8	2343.4	19.3	2460.4	19.7	2540.4
8/8/98	20.1	2584.8	19.7	2339.4	19.9	2461	19.2	2541.2
8/13/98								
8/17/98	20.7	2583.8	19.8	2334.5	19.3	2462.4	19.3	2538
8/21/98	19.8	2580.3	19.8	2343	19.2	2466.1	19.6	2536.8
8/30/98	19.8	2578.7	20.2	2329.6	19.3	2470.7	19.8	2533.5
9/4/98	19	2575.3	19	2327.7	19	2472.5	18.9	2532.9
9/15/98	19	2567.3	19	2322.5	18.3	2476.3	18.8	2528.8
10/1/98	19.7	2563.6	19.2	2315.9	18.7	2478.9	19.2	2526.1
10/24/98	10.5	2554.8	12	2314	15	2479.7	12.2	2529.8
11/18/98	10.5	2548.2	11.5	2310.7	13	2481.5	11.6	2523.6
12/17/98	9.7	2543.7	8.1	2311.1	9	2480.9	9.7	2527.7
1/10/99	4.9	2544.7	6.2	2312.7	7.9	2485.5	6.6	2528.7
1/25/99								
1/31/99	9.4	2542.8	9.9	2310.6	10.1	2484.7	9.8	2525.6
2/21/99	5.5	2542.9	7.1	2309.8	8.8	2483.8	7.3	2525.7
3/13/99	3.6	2534.8	5.5	2310.5	7.3	2484.3	5.7	2525.1
3/26/99	6.8	2535.1	7.7	2309.1	8.9	2484.5	7.8	2520.7
4/9/99	14.6	2533.7	13.4	2312.7	12.1	2486.4	13.1	2518.8
5/14/99	14.7	2538	14.7	2308.3	14	2483.9	14.5	2515.3
6/6/99	17.2	2539.3	16.8	2308.8	15.7	2483.7	16.5	2515.1
7/17/99	19.9	2546.3	19.5	2308	18.6	2479.9	19.4	2518.2
8/21/99	19.8	2544.2	20.1	2304.7	19.6	2475.9	19.8	2519.5
10/3/99	13.9	2532.5	14.5	2306.9	15.9	2476.3	14.7	2518.4
11/10/99	10.5	2528.1	10.9	2304.8	12.1	2478.2	10.9	2520
12/11/99	7.6	2525.3	8.4	2303.5				
1/25/00	2.3	2524.5	3.9	2303.3	6.4	2481.7	3.8	2542.7

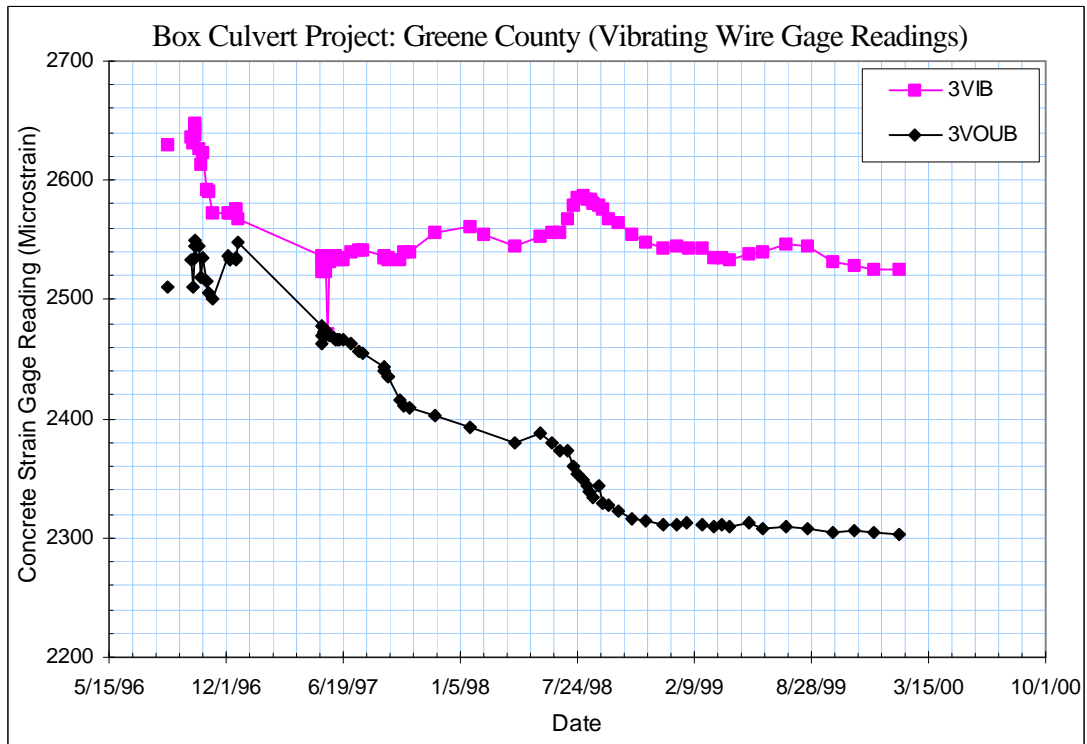


Figure B-34 Vibrating Wire Concrete Strain Gage Reading  
(3VIB, 3VOUB, Greene County, TN)

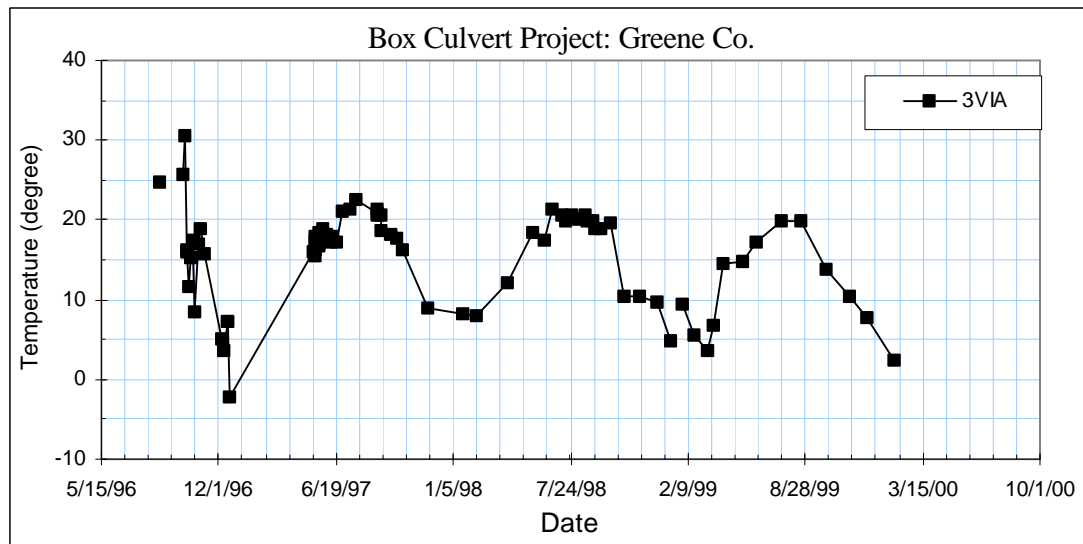


Figure B-35 Recorded Temperature at Gage 3VIB  
(Greene County, TN)

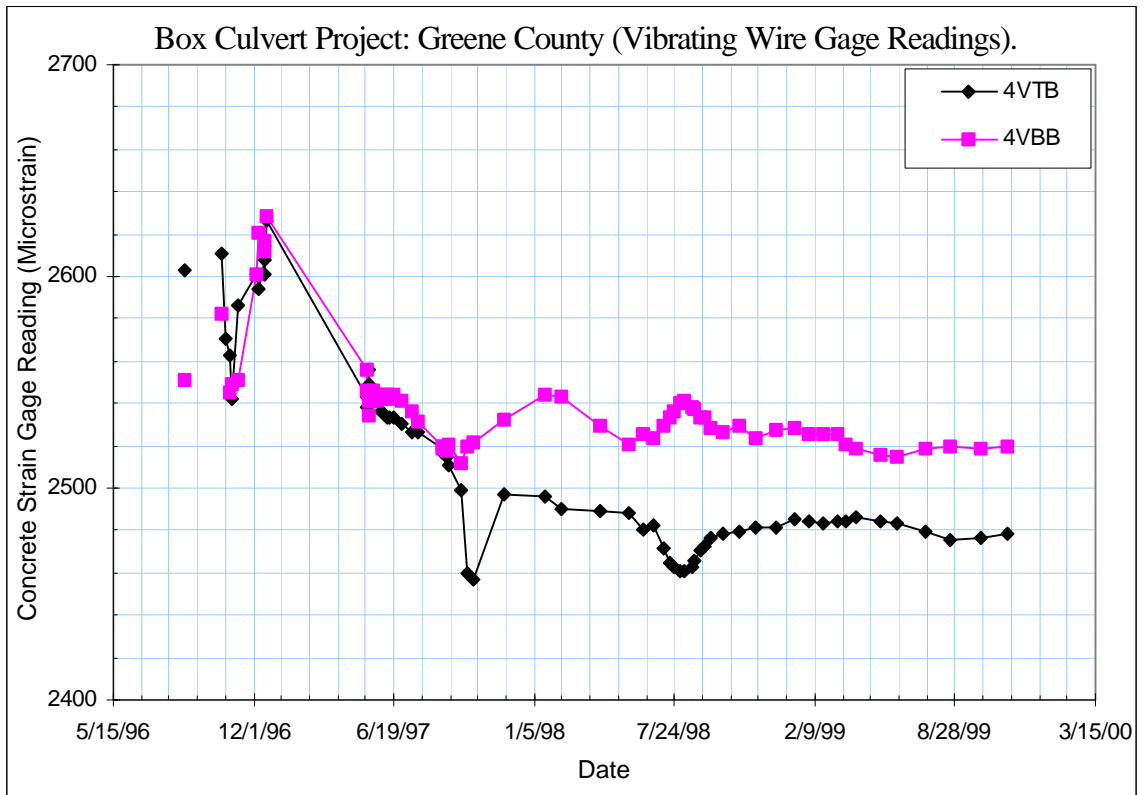


Figure B-36 Vibrating Wire Concrete Strain Gage Reading  
(4VTB, 4VBB, Greene County, TN)

Greene County Culvert Concrete Strain Gages										
Date	5VTB		5VBB		6VTB		6VBB		Reference	
	Temperature	Reading	Temperature	Reading	Temperature	Reading	Temperature	Reading	Temperature	Reading
8/24/96	24.3	2609.3	24.4	2623.9	24.9	2663.9	24.1	2674.1	21.9	2583
9/23/96										
9/25/96										
9/30/96										
10/1/96									31.5	2658.6
10/4/96									27.1	2671.3
10/7/96									16.7	2691
10/9/96									16.6	2690
10/10/96									12.6	2683.9
10/15/96									15.1	2689.0
10/17/96	25.5	2514.5	25.5	2647.9	25.2	2670.6	25.8	2697.2	17.2	2682.1
10/21/96	17.2	2487.8	17.9	2574.2	13.8	2565.9	17.7		9.9	2683.8
10/28/96	18.0	2504.6	17.3	2583.4	17.8	2620.5	17.4	2638.3	16.1	2674.8
10/31/96	22.4	2484.0	18.7	2590.3	20.2	2607.5	18.6	2645.1	18.3	2671.6
11/8/96	14.4	2525	15.9	2589.7	14.2	2645.7	15.5	2643.4	15.8	2675.7
12/5/96	5.3	2534.7	5.4	2641.7	5.0	2670.5	5.2	2685.7	6.1	2674.5
12/9/96	4.6	2534.7	3.2	2658	4.4	2667.9	3.1	2700.6	4.3	2672.9
12/16/96	3.1	2550.1	4.8	2646.3	3.1	2691.5	4.8	2685.4	6.0	2677.0
12/17/96	6.0	2542.9	5.8	2651.6	5.7	2683.5	5.7	2691.2	6.8	2678.4
12/20/96	-3.1	2558.8	0	2656.8	-3.2	2707.4	-0.1	2694.5	3.4	2674.2
5/12/97	19.6	2483.7	16.4	2591.5	19	2603.5	15.9	2631.2	15.3	2699.6
5/13/97	21.3	2482	18.2	2579.1	21.1	2607.4	17.9	2618.8	16.9	2699.5
5/14/97	14.9	2508.9	17.2	2563.2	14.2	2637.6	16.5	2542.1	15.2	2699.1
5/15/97	16	2494.6	16.4	2572.3	15.5	2632.4	16	2609.2	16.6	2699.4
5/16/97	16.1	2493.1	16.1	2572.2	15.6	2626.7	15.6	2610.6	15.7	2698.9
5/16/97	15.3	2496.5	15.8	2574.1	15	2632.2	15.4	2610.7	16.1	2699.2
5/19/97	15.7	2496.5	16.5	2574.2	15.2	2638.4	16	2608.7	17.5	2698.5
5/20/97	16.5	2499.2	17.7	2568	16	2641.8	17.3	2603.8	18.8	2699.4
5/21/97	17	2491.7	17.1	2571.5	16.4	2631.6	16.8	2607.1	17.5	2698
5/22/97	17	2488.6	16.8	2572.9	16.6	2676.9	16.4	2568	16.9	2698.4
5/27/97	18.2	2492.7	18.9	2567	17.8	2636.2	18.6	2600.6	19.5	2697.1
6/2/97	18.1	2487.4	18.4	2570.4	18.1	2631.9	18.2	2600.8	18.6	2698.3
6/4/97	18.6	2486.2	18.6	2568.4	18.2	2629.7	18.4	2599.9	18.4	2698.2
6/10/97	17.9	2482.7	17.2	2572.6	17.5	2625.6	17.2	2601	16.3	2700.4
6/12/97	17.9	2485.5	17.8	2570.5	17.9	2629	17.7	2598.4	16.8	2700.8
6/19/97	17.9	2482.7	17.2	2572.6	17.5	2625.6	17.2	2601	16.3	2700.4
7/1/97	20.7	2484.3	20.8	2567	20.6	2626.1	20.9	2593.1	20.7	2698.4
7/14/97	21.8	2478.7	21.6	2561.5	21.6	2616.7	21.6	2588.8	19.8	2695
7/23/97	22.8	2480.2	22.8	2559	22.6	2616.4	22.8	2586.9	22.3	2695.3
8/27/97	21.5	2467.3	20.7	2556.0	21.5	2593.6	20.7	2583.4	18.3	2696
8/29/97	21.9	2469.1	21.4	2558	21.6	2601.6	21.2	2579.8	19	2696.9
8/29/97	21.8	2470.2	21.4	2553.9	19.9	2603.3	21.5	2578.5	19.1	2697
9/3/97	21.9	2468.6	21.4	2552.6	21.8	2603.8	21.5	2579.6	19	2692.2
9/5/97	21.2	2461.9	19	2558.5	20.6	2595.1	19.5	2581.4	16.7	2696.1
9/22/97	19.4	2460.8	19.5	2556	19.4	2617.6	19.5	2570.3	16.4	2699
10/1/97	19.2	2459.4	18.5	2555.9	18.3	2619.4	18.4	2569.2	15.8	2699.3
10/10/97	18.3	2461.3	16.3	2557.7	18.1	2622.7	17.3	2568.1	15.9	2702.8
11/24/97	11.4	2463	8.7	2571	10.8	2633.3	9.3	2577.2	8.7	2712.6
1/20/98	10	2448.5	8.2	2586.1	10.5	2619.5	8.5	2585.6	7.6	2721.2
2/14/98	9.6	2449.2	7.9	2584.7	8.2	2620.2	7.6	2581.3	7.6	2724.9
4/8/98	11.6	2450.3	11.5	2572.2	11.2	2620.9	11.4	2570.1	10.8	2723.4
5/21/98	17.7	2454.3	17	2558.6	16.9	2623.7	18.1	2558.7	17.5	2714.9
6/9/98	17.8	2445.1	18	2562.9	17.9	2615.2	18	2561.2	18	2710.8
6/23/98	19.5	2451	19.5	2560.1	19.4	2624.2	20.8	2560.1	21.3	2706.3
7/8/98	19.7	2438.5	20.1	2563	20.8	2612.4	20.2	2560.2	19.3	2704
7/17/98	18.5	2437.2	18.9	2564.7	19.5	2617.6	19.9	2555.6	19	2703.4
7/24/98	20	2437.2	20.5	2564.2	20.1	2620.1	20.5	2552.5	19.4	2703

Date	5VTB		5VBB		6VTB		6VBB		Reference	
	Temperature	Reading	Temperature	Reading	Temperature	Reading	Temperature	Reading	Temperature	Reading
8/2/98	19.9	2435.5	20.1	2567	19.9	2618	20.2	2551.6	19.5	2701.6
8/8/98	19.7	2439.7	19.7	2565.4	19.5	2623.9	19.7	2547.8	18.7	2701
8/13/98										
8/17/98	19.8	2433.3	20.5	2566.6	22.1	2570	20.1	2557.7	19	2701.6
8/21/98	19.7	2433.6	19.7	2566	19.7	2567.3	19.9	2555.6	18.7	2699.3
8/30/98	19.8	2439.4	19.8	2561.7	19.8	2565.8	19.8	2551	18.7	2698.9
9/4/98	18.9	2438.9	19.4	2562	19.9	2561.2	19.9	2550.4	17.8	2698.1
9/15/98	18.7	2440.9	17.1	2558.1	17.1	2547.1	18	2546.3	18	2698.8
10/1/98	19.1	2442.1	19.6	2555.3	19.4	2544.9	19.3	2544.2	18.1	2698
10/24/98	14.6	2435.8	12.3	2565.2	15.1	2535.5	12.2	2553.9	10.5	2692
11/18/98	12.8	2433.1	11.7	2560.5	12.4	2540.8	11.1	2577.5	10.3	2697.8
12/17/98	12.2	2430.7	12.1	2560.9	10.6	2578.2	10.5	2581.1	7.5	2701.1
1/10/99	7.4	2434.9	6.4	2570.4	6.6	2567	5.7	2582.5	5	2707.2
1/25/99										
1/31/99	9.8	2434.7	9.9	2565.9	9.5	2608.5	9.2	2574.9	9	2708.8
2/21/99	8.4	2430.6	6.9	2570.3	7.8	2612.9	6.4	2576.8	6.1	2708.2
3/13/99	6.6	2431.2	5.2	2571.8	6.2	2619	4.6	2579	4.4	2709.4
3/26/99	8.6	2432.2	8	2563.3	8.2	2615.9	7.3	2238.3	6.6	2710.3
4/9/99	12	2439.9	13.2	2538.7	11.8	2617	12.9	2572.3	12.6	2710.6
5/14/99	14.2	2437.4	15	2555.4	14.2	2610.9	15.4	2369.8	14.1	2706.1
6/6/99	16	2439.4	16.8	2552.8	15.9	2609.6	16.7	2568.7	15.9	2703.3
7/17/99	19.2	2437	20.9	2552.6	19.3	2608.8	19.9	2569.3	19.4	2694.3
8/21/99	20.2	2432.1	21.2	2551	20.2	2598.7	20.3	2570.3	18.7	2687.2
10/3/99	16.1	2426.8	14.9	2554	16	2605.6	14.6	2575.1	13.5	2682.5
11/10/99	11.7	2429.1	11.3	2560.5	11.5	2618.4	11.3	2581.8	9.8	2687.4
12/11/99										
1/25/00	5.5	2428.7	3.7	2567.0	5.0	2636.9	3.3	2590.8	2.8	2695.2

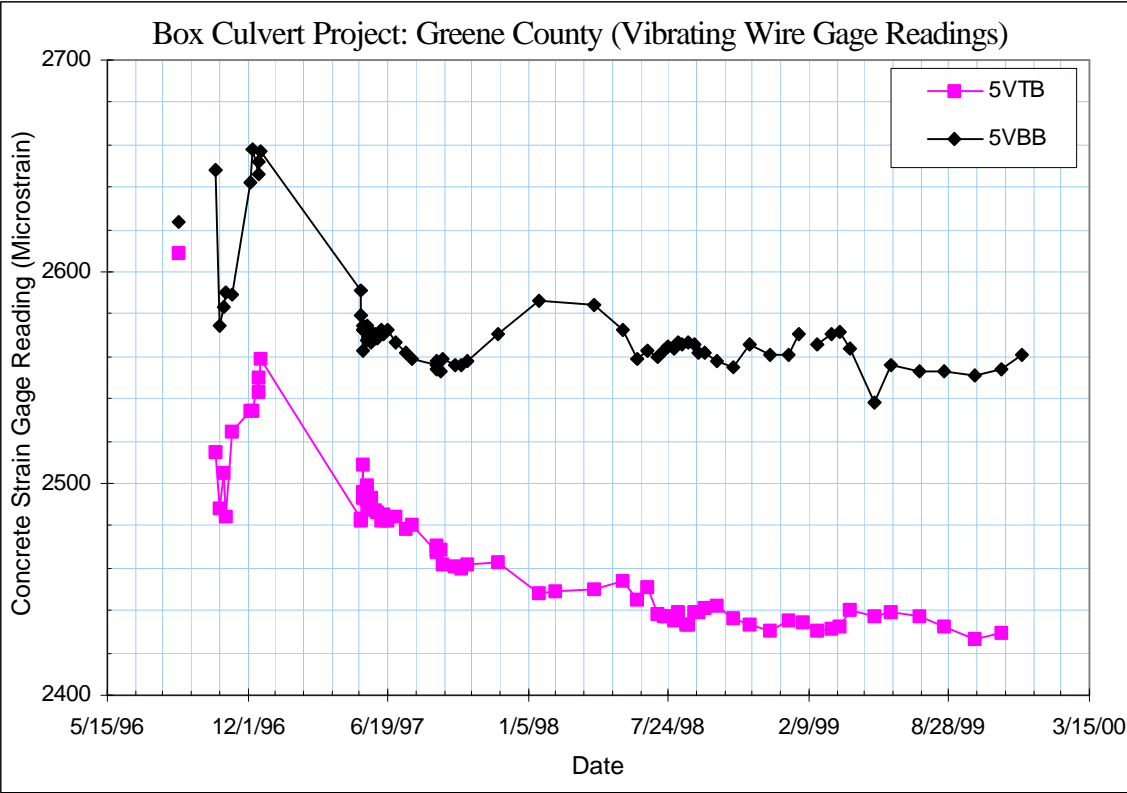


Figure B-37 Vibrating Wire Concrete Strain Gage Reading  
(5VTB, 5VBB, Greene County, TN)

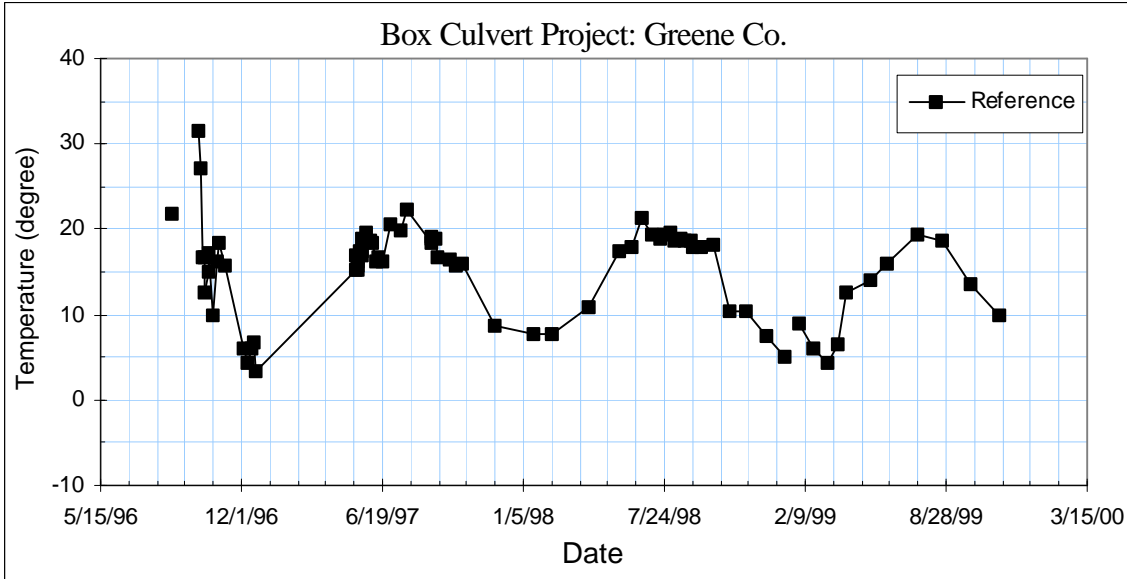


Figure B-38 Recorded Temperature at Reference Gage  
(Greene County, TN)

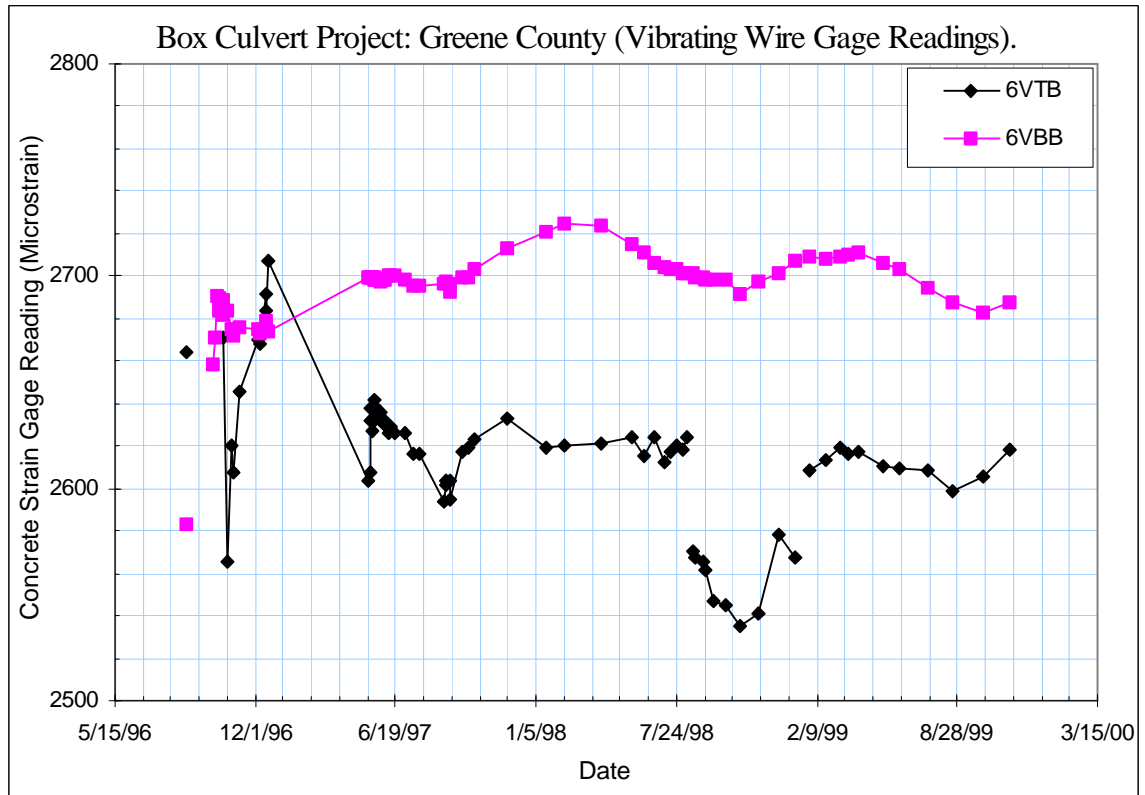


Figure B-39 Vibrating Wire Concrete Strain Gage Reading  
(6VTB, 6VBB, Greene County, TN)



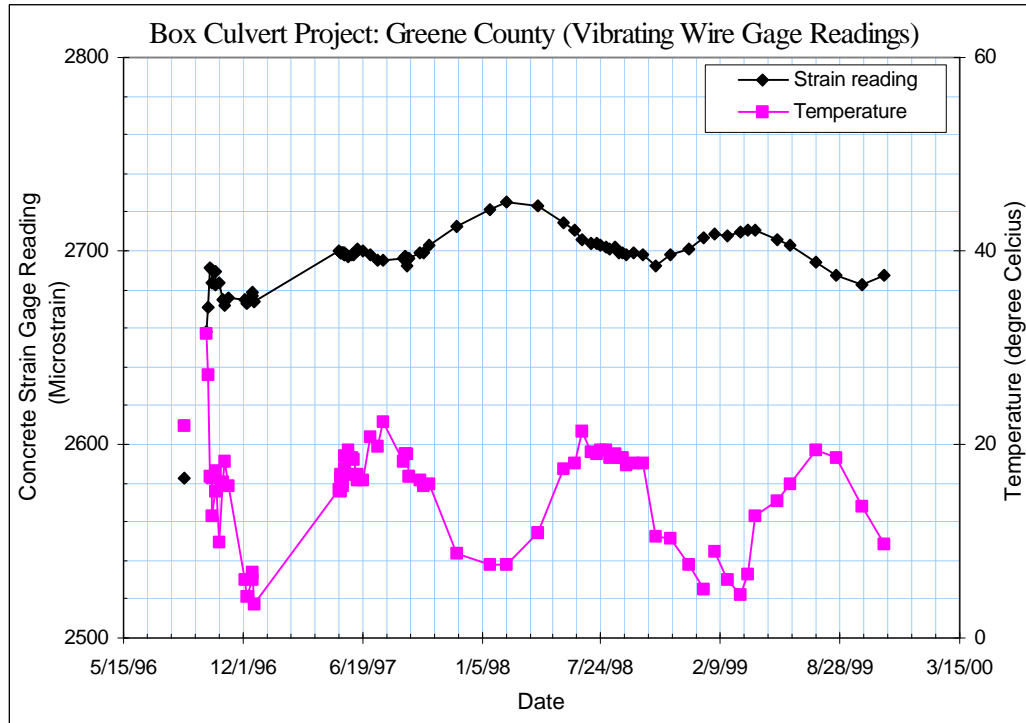


Figure B-40 Vibrating Wire Concrete Strain Gage Reading and Temperature  
(Reference Gage, Greene County, TN)

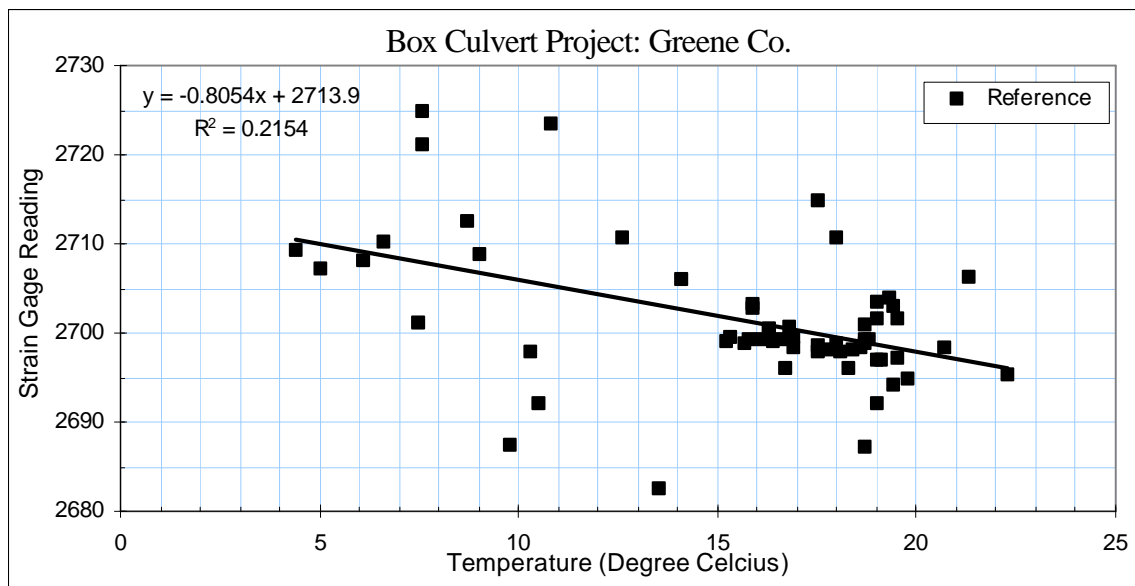


Figure B-41 Correlation between Temperature and Strain Gage Readings  
(Reference Gage, Greene County, TN)

## **Appendix C**

### **Dynamic Horizontal Earth Pressures Induced by Construction Equipment**

Note: A large amount of the dynamic horizontal earth pressures induced by the different compaction equipment were recorded during the backfill work. The following only presents the maximum pressures generated by representative machines at the closest possible distance to the culvert wall.

Table C-1 Selected Specifications of Ingersoll-Rand DD130 Double Drum Vibratory Roller

<b>Machine Weights (with ROPS/FOPS)</b>	
Operating Weight	28,430 lb. (895 kg)
Static Weight at Front Drum	14,815 lb. (6720 kg)
Static Weight at Rear Drum	13,615 lb. (6175 kg)
Shipping Weight	27,180 lb. (12330 kg)
<b>Machine Dimensions</b>	
Overall Length	227 in. (5765 mm)
Overall Width	92 in. (2435 mm)
Overall Height top of steering wheel	95 in. (2413 mm)
Overall Height (top of ROPS/FOPS)	125 in. (3175 mm)
Drum Base	135 in. (3430 mm)
Curb Clearance	21 in. (535 mm)
Outside Turning Radius	256 in. (6495 mm)
<b>Drum</b>	
Drum Width	84 in. (2135 mm)
Drum Diameter	55.1 in. (1400 mm)
Shell Thickness (nominal)	0.8 in. (20 mm)
Finish	Machined, with chamfered edges
<b>Vibration</b>	
Frequency	
Centrifugal Force maximum per drum	2500 vpm (41.7 Hz)
Centrifugal minimum per drum	36,030 lb. (160 kN)
Amplitude Settings	15,975 lb. (71.2 kN)
Nominal Amplitude maximum	Eight
Nominal Amplitude minimum	.035 in. (.89 mm)
	.016 in. (.41 mm)
<b>Propulsion</b>	
Type System	Closed-loop hydrostatic
Drum Drive (both drums)	Low speed, high torque
Speed	0-8.2 mph (0-13.2 km/hr)
Gradeability (theoretical)	32%



Figure C-1 DD-130 Vibratory Roller Compacting at Instrumented Section  
(Greene County, TN, December, 1996)

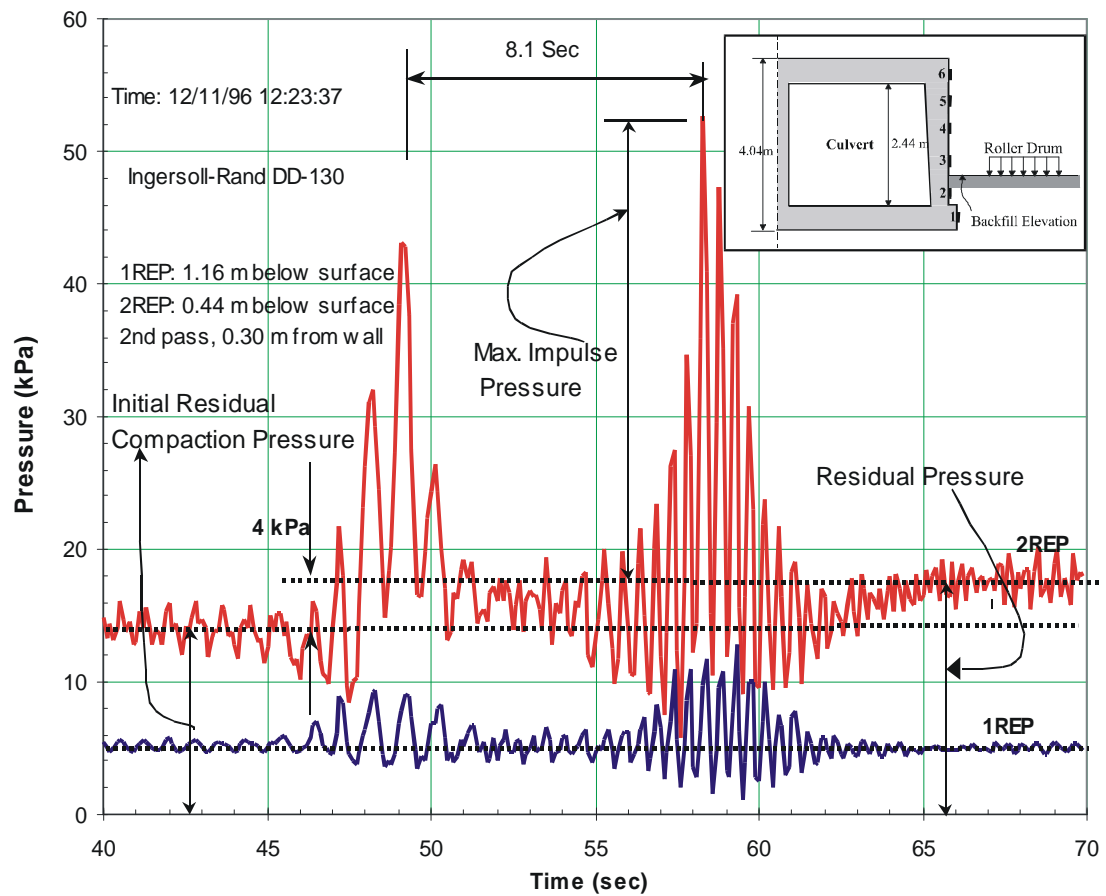


Figure C-2 Recorded Dynamic Horizontal Earth Pressures  
(Ingersoll-Rand DD130, December, 1996, Greene County TN)

Table C-2 Selected Specifications for Ingersoll-Rand SP56 Vibratory Roller

			Engine	
Dimensions			Make and Model	CAT 3804
Overall Length (L)	17'4"" (5923 mm)		Rated Power at 2300 rpm	115 hp (86 kw)
Overall Width (W)	7'7" (2311 mm)		Optional Engines	
Overall Height (H)	7'11" (2413 mm)		Propulsion System	
Wheelbase (WB)	10'7" (3226 mm)		Type	
Curb Clearance (C)	1'6" (457 mm)		Drume Drive	
Outside Turning Radius	18'5" 5613 mm)		Speed, forward & Reverse	
Drum Diameter	56" (1422 mm)		lower gear	0-3.7 mph (0.60 km/h)
Drum Width	84" (2134 mm)		high gear	0-11 mph (0.17.7 km/h)
Shell Thickness			Articulated Steering	
Weigths	lb (kg)		Articulation	40
Total Operation Weight	19650 (8913)		Oscillation	17
Tractor Module	7850 (3561)		Brake System	
Drum Module	11800 (5352)		Service Brake	
Shipping Weight	19350 (8777)		Parking Brake	
Vibration Power			Electrical System	
Frequency	0 to 1825 vpm	(30.4 Hz)	Miscellaneous	
Centralfuge Force	42000 lb	186800 N	Fuel Capacity	42 gal 1591
Norminal Amplitude	0.051"	1.3 mm	Hydraulic Oil Capacity	42 gal 1591
			Field Gradability	24%
			Tire Size	23.1*26*8 ply



Figure C-3 Side View of Ingersoll-Rand SP56 Single Drum Vibratory Roller

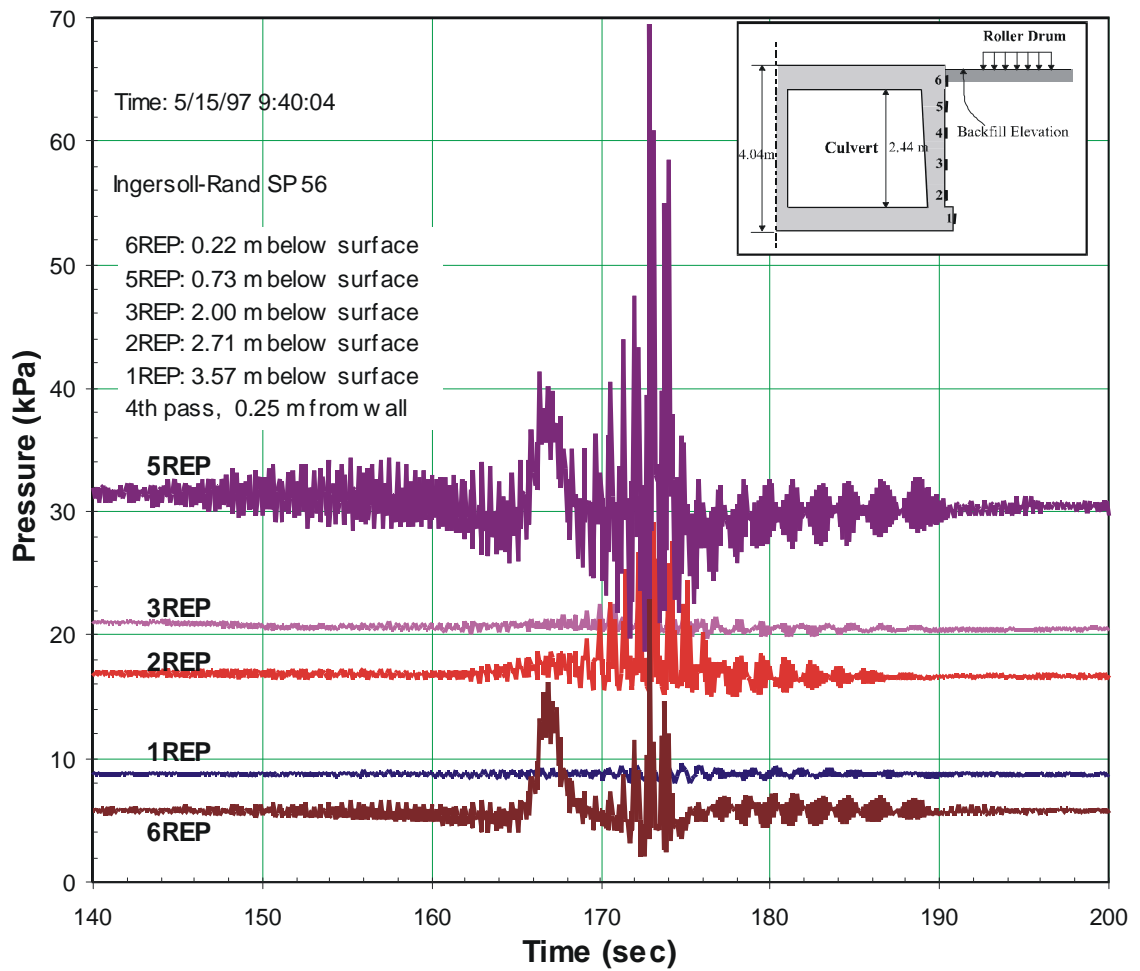


Figure C-4 Recorded Dynamic Horizontal Earth Pressures  
 (Ingersoll-Rand SP56, May, 1997, Greene County, TN)





Figure C-5 Dump Truck Spreading the Gravel

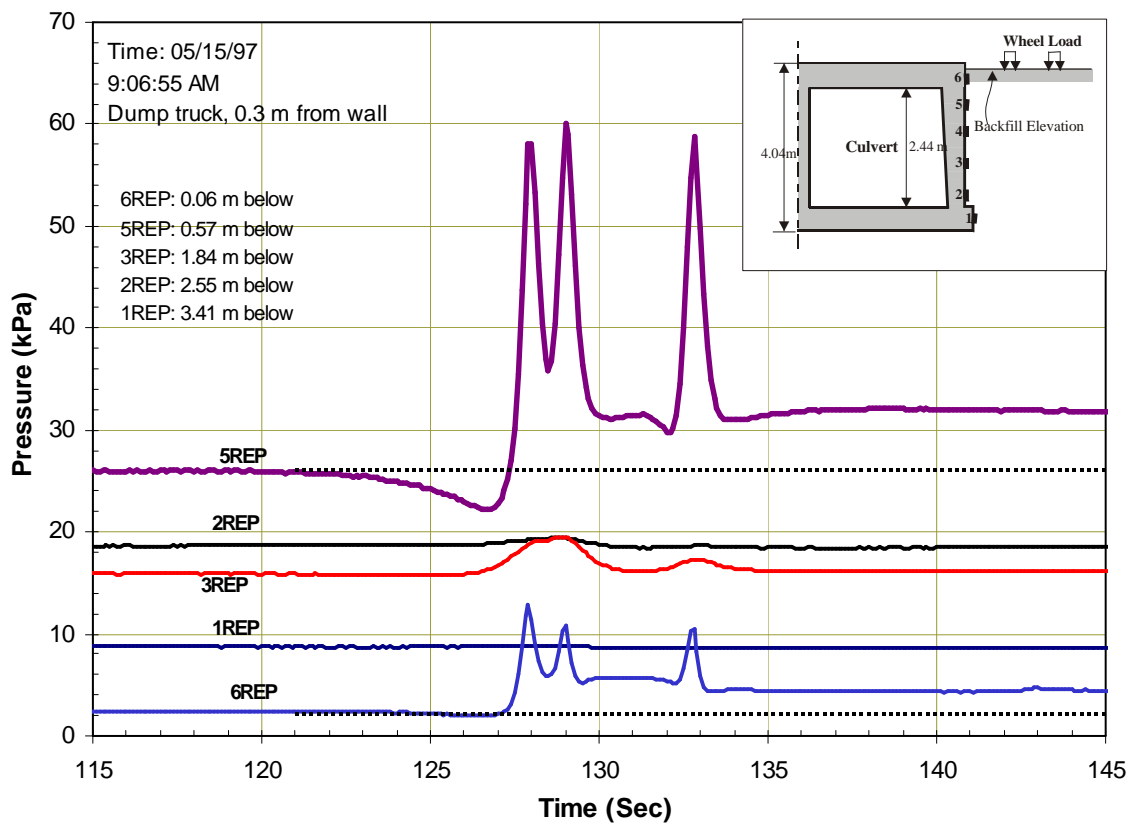


Figure C-6 Recorded Dynamic Horizontal Earth Pressures  
(Dump Truck, May, 1997, Greene County, TN)



Figure C-7 Motor Grader Leveling the Gravel

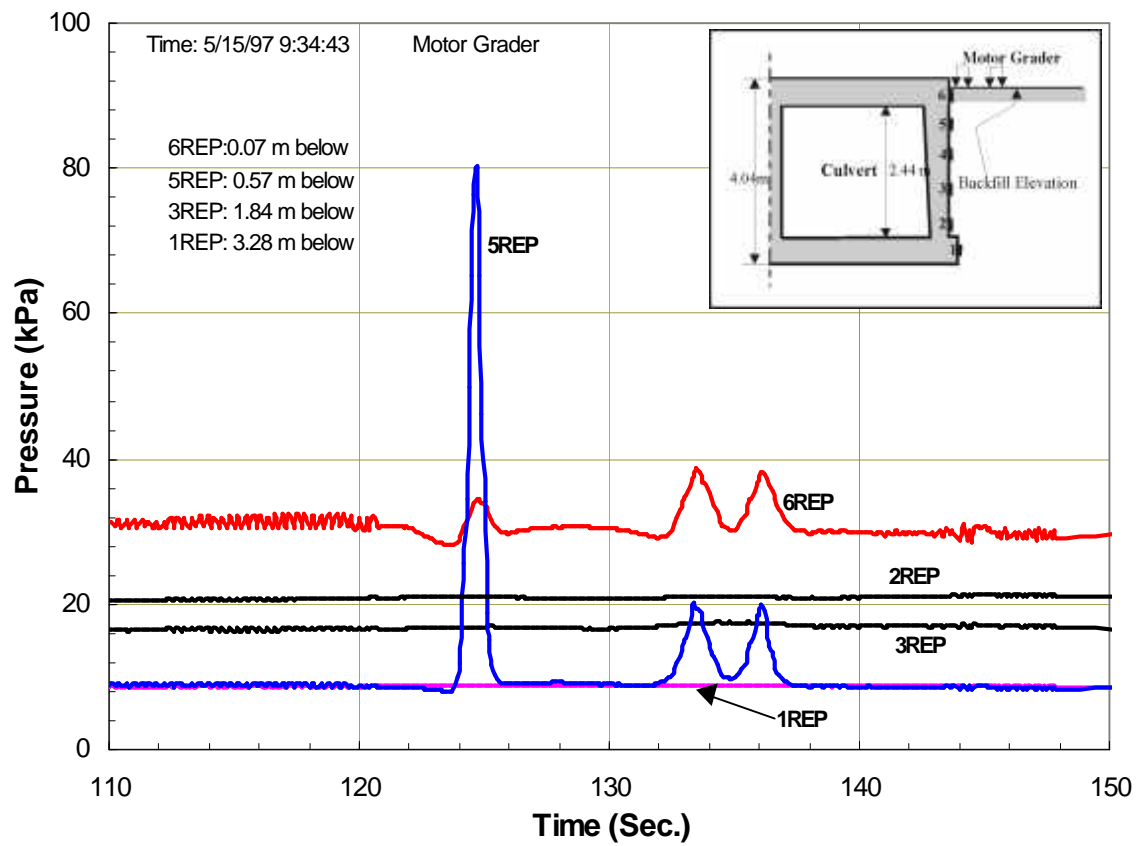


Figure C-8 Recorded Dynamic Horizontal Earth Pressures  
(Motor Grader, May, 1997, Greene County, TN)

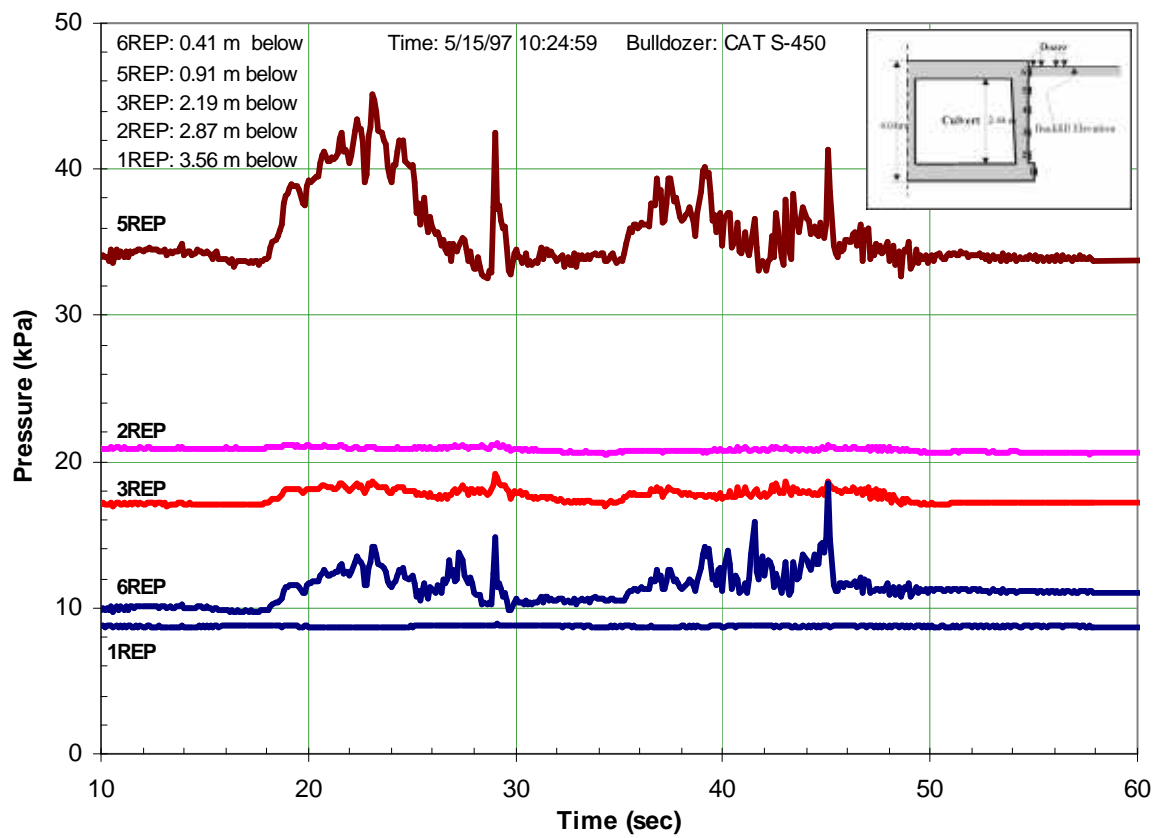


Figure C-9 Recorded Dynamic Horizontal Earth Pressures  
 (CAT S-450 Dozer, May, 1997, Greene County, TN)

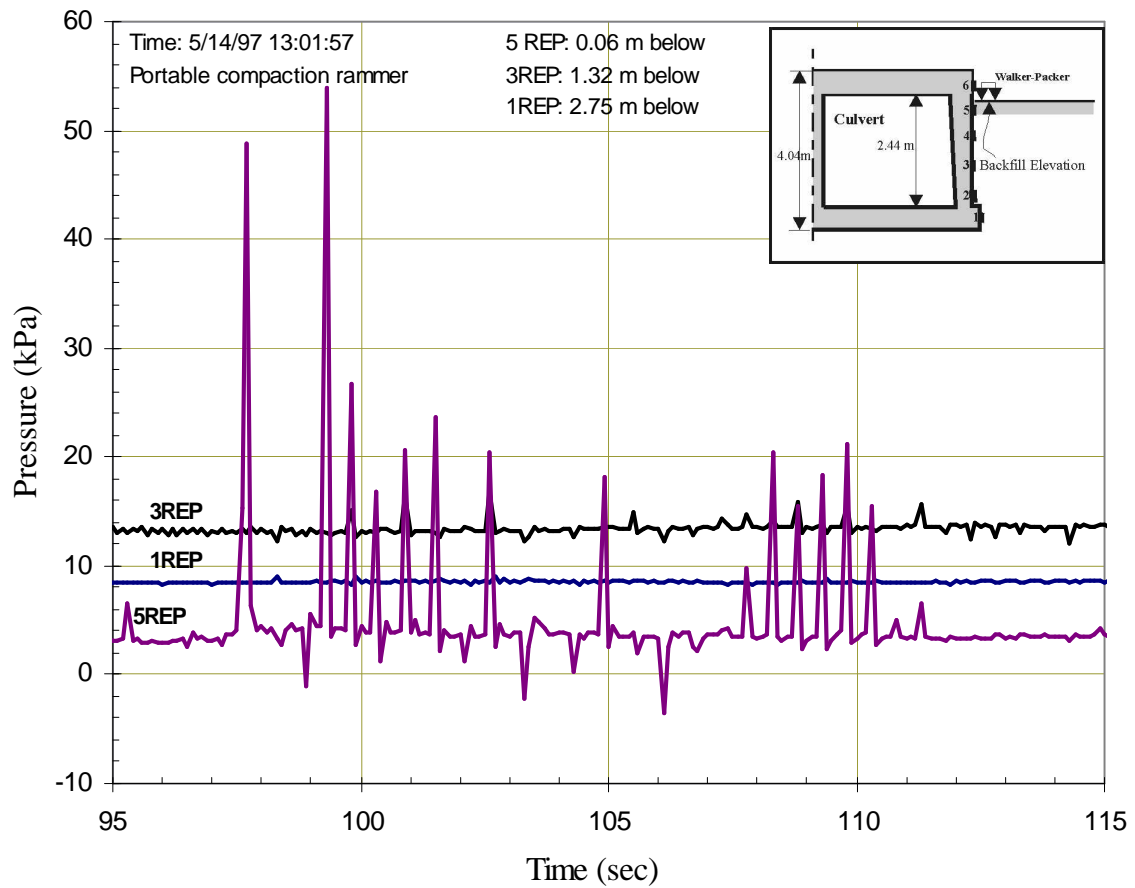


Figure C-10 Recorded Dynamic Horizontal Earth Pressures  
 (Portable Compaction Rammer, May, 1997, Greene County, TN)

**APPENDIX D**

**TRIAXIAL TEST RESULTS**

## Appendix D-1:

### Triaxial Test Results-Clayey Shale

Table D-1 Clayey Shale Test Summary:

Sample Number	Test Type	Back Pressure (kPa)	Net Confining Pressure (kPa)	Measured Density (kN/m <sup>3</sup> )	Moisture Content (%)
CD No.1	CD	137.5	193	20.19	NA
CD No. 2	CD	206.8	193	21.28	NA
CD No. 3	CD	275.8	193	21.29	NA
CU No. 1	CU	55.8	204.8	21.29	11.8
CU No. 2	CU	103	204.8	22.13	11.8

Strength at 10% Strain: Cohesion c: 2 kPa, Angle of internal friction: 22 degrees



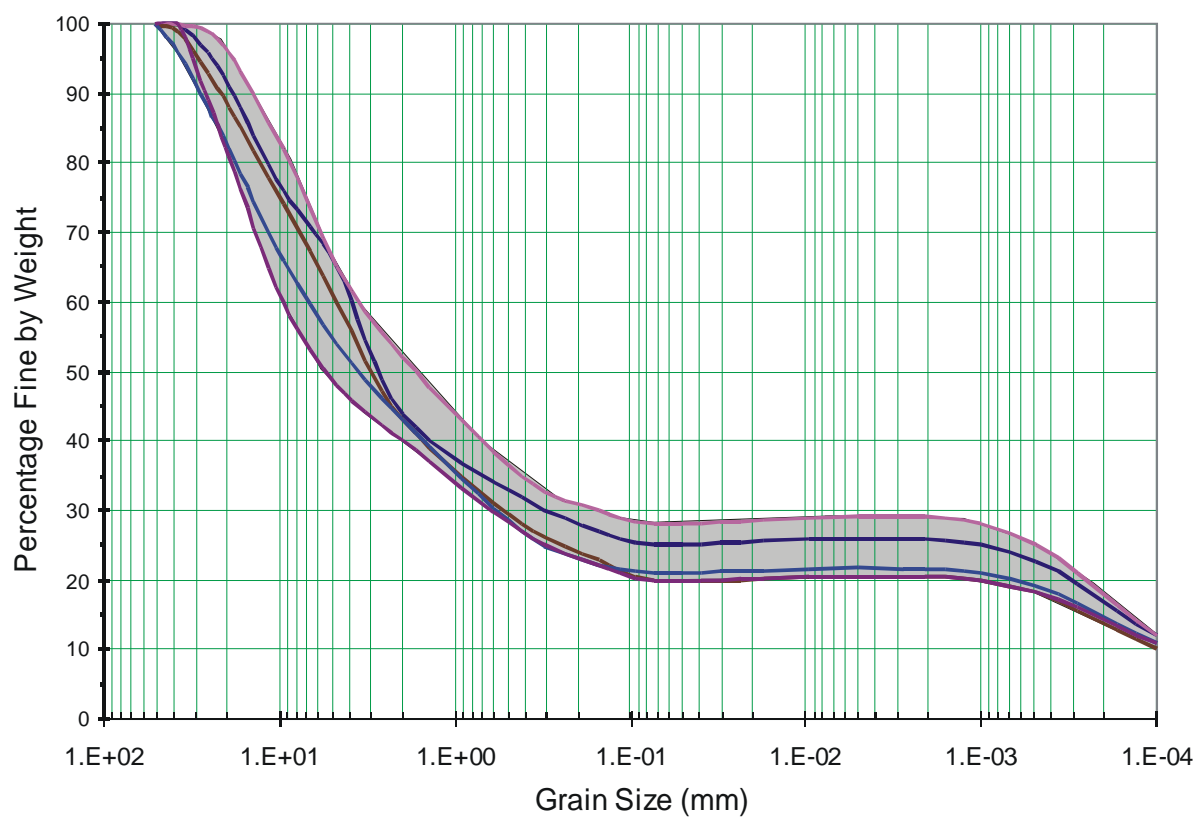


Figure D-1 Grain Size Distribution of Clayey Shale (Sullivan County, TN)

### Box Culvert Project: Triaxial Test of Clayey Shale (CD Test)

Sample: <b>Clayey Shale</b>	
Sample No.	1
Diameter:(mm)	104.1                      105.4                      102.87                      Height(mm) 205.74                      205.74                      204.5
Average Diameter.:	104.4                      Initial Area:(e-3) 8.567                      Average. Height:(mm)                      205.3
Sample Weight(g):	3621                      Ini. Volume (10E-6mm^3):                      1759.10
Moisture Content:	Moisture Content:
Aluminium Box No.:	Aluminium Box No.:
Box Weight(g):	Box Weight:
Wet Soil+ Box Weight:(g)	Wet Soil+ Box Weight:
Dry Soil+Box Weight:(g)	Dry Soil+Box Weight:
Moisture Content:(%)	Moisture Content:
Averaged Moisture Content:(%)	Initial Density (KN/M^3):                      20.19
Type of Test: CD	
Type of saturation: BP	Back Pressure For Saturation: 193 kPa
Date:1/16/98, 1998	
Confining Pressure( Net): 20 psi	137.5kPa

Displacement (1/1000 inch)	Force (lb)	Meter Reading (Volume Change)	Volume Change (Milliliter)	Volume Strain (%)	Axial Strain (%)	Corrected Area (cm^2)	Deviator Stress (Kpa)	Maximum Stress (kPa)	Stress Ratio	Normal Stress
10	67	-615	0	0.00	0.000	85.67	0.00	137.50	1.00	0.00
15	73	-613	2	0.00	0.062	85.72	3.11	140.61	1.02	0.02
20	88	-610	5	0.00	0.124	85.78	10.89	148.39	1.08	0.08
22	160	-609	6	0.01	0.148	85.80	48.23	185.73	1.35	0.35
25	112	-606	9	0.01	0.186	85.83	23.33	160.83	1.17	0.17
28	120	-604	11	0.01	0.223	85.86	27.47	164.97	1.20	0.20
30	125	-602	13	0.01	0.247	85.88	30.05	167.55	1.22	0.22
35	137	-598	17	0.01	0.309	85.93	36.25	173.75	1.26	0.26
40	145	-593	22	0.02	0.371	85.98	40.37	177.87	1.29	0.29
45	152	-590	25	0.02	0.433	86.03	43.97	181.47	1.32	0.32
50	160	-585	30	0.03	0.495	86.08	48.08	185.58	1.35	0.35
55	163	-582	33	0.03	0.557	86.13	49.60	187.10	1.36	0.36
60	168	-577	38	0.03	0.619	86.18	52.15	189.65	1.38	0.38
65	172	-574	41	0.03	0.680	86.23	54.18	191.68	1.39	0.39
70	175	-570	45	0.04	0.742	86.28	55.70	193.20	1.41	0.41
75	177	-566	49	0.04	0.804	86.33	56.70	194.20	1.41	0.41
80	178	-563	52	0.04	0.866	86.38	57.18	194.68	1.42	0.42
85	185	-559	56	0.05	0.928	86.43	60.75	198.25	1.44	0.44
90	187	-556	59	0.05	0.990	86.49	61.74	199.24	1.45	0.45
95	190	-553	62	0.05	1.051	86.54	63.25	200.75	1.46	0.46
100	193	-548	67	0.06	1.113	86.59	64.75	202.25	1.47	0.47
105	197	-545	70	0.06	1.175	86.64	66.77	204.27	1.49	0.49
110	198	-542	73	0.06	1.237	86.69	67.24	204.74	1.49	0.49
120	203	-535	80	0.07	1.361	86.80	69.72	207.22	1.51	0.51
130	210	-527	88	0.07	1.484	86.90	73.22	210.72	1.53	0.53

Displacement (1/1000 inch)	Force (lb)	Meter Reading (Volume Change)	Volume Change (Milliliter)	Volume Strain (%)	Axial Strain (%)	Corrected Area (cm <sup>2</sup> )	Deviator Stress (Kpa)	Maximum Stress (kPa)	Stress Ratio	Normal Stress
140	215	-521	94	0.08	1.608	87.00	75.69	213.19	1.55	0.55
150	218	-515	100	0.08	1.732	87.11	77.13	214.63	1.56	0.56
160	222	-509	106	0.09	1.856	87.22	79.08	216.58	1.58	0.58
170	225	-503	112	0.09	1.979	87.32	80.52	218.02	1.59	0.59
180	228	-497	118	0.10	2.103	87.43	81.95	219.45	1.60	0.60
190	233	-490	125	0.10	2.227	87.53	84.39	221.89	1.61	0.61
200	237	-484	131	0.11	2.350	87.64	86.32	223.82	1.63	0.63
225	245	-469	146	0.12	2.660	87.91	90.10	227.60	1.66	0.66
250	250	-456	159	0.13	2.969	88.18	92.35	229.85	1.67	0.67
275	258	-443	172	0.14	3.278	88.45	96.09	233.59	1.70	0.70
300	267	-430	185	0.16	3.587	88.72	100.31	237.81	1.73	0.73
325	274	-417	198	0.17	3.897	89.00	103.50	241.00	1.75	0.75
350	283	-406	209	0.18	4.206	89.28	107.66	245.16	1.78	0.78
375	289	-392	223	0.19	4.515	89.56	110.31	247.81	1.80	0.80
400	295	-378	237	0.20	4.825	89.84	112.93	250.43	1.82	0.82
425	302	-369	246	0.21	5.134	90.12	116.03	253.53	1.84	0.84
450	310	-358	257	0.22	5.443	90.41	119.60	257.10	1.87	0.87
475	318	-346	269	0.23	5.752	90.70	123.15	260.65	1.90	0.90
500	326	-334	281	0.24	6.062	90.99	126.67	264.17	1.92	0.92
525	334	-323	292	0.25	6.371	91.28	130.16	267.66	1.95	0.95
550	342	-312	303	0.25	6.680	91.57	133.63	271.13	1.97	0.97
575	347	-301	314	0.26	6.989	91.87	135.62	273.12	1.99	0.99
600	355	-291	324	0.27	7.299	92.17	139.05	276.55	2.01	1.01
625	362	-280	335	0.28	7.608	92.47	141.96	279.46	2.03	1.03
650	368	-270	345	0.29	7.917	92.77	144.38	281.88	2.05	1.05
675	377	-260	355	0.30	8.226	93.07	148.21	285.71	2.08	1.08
700	386	-250	365	0.31	8.536	93.38	152.01	289.51	2.11	1.11
725	393	-240	375	0.31	8.845	93.69	154.83	292.33	2.13	1.13
750	400	-231	384	0.32	9.154	94.00	157.63	295.13	2.15	1.15
775	405	-221	394	0.33	9.463	94.32	159.47	296.97	2.16	1.16
800	412	-212	403	0.34	9.773	94.63	162.23	299.73	2.18	1.18
825	419	-203	412	0.35	10.082	94.95	164.96	302.46	2.20	1.20
850	426	-194	421	0.35	10.391	95.27	167.68	305.18	2.22	1.22
875	435	-185	430	0.36	10.701	95.59	171.30	308.80	2.25	1.25
900	443	-176	439	0.37	11.010	95.92	174.43	311.93	2.27	1.27
925	449	-168	447	0.38	11.319	96.25	176.61	314.11	2.28	1.28
950	458	-160	455	0.38	11.628	96.58	180.16	317.66	2.31	1.31
975	465	-151	464	0.39	11.938	96.91	182.75	320.25	2.33	1.33
1000	471	-142	473	0.40	12.247	97.24	184.87	322.37	2.34	1.34
1025	478	-135	480	0.40	12.556	97.58	187.42	324.92	2.36	1.36
1050	484	-127	488	0.41	12.865	97.92	189.50	327.00	2.38	1.38
1075	491	-119	496	0.42	13.175	98.26	192.01	329.51	2.40	1.40
1100	499	-112	503	0.42	13.484	98.61	194.95	332.45	2.42	1.42
1125	507	-105	510	0.43	13.793	98.96	197.86	335.36	2.44	1.44
1150	513	-98	517	0.43	14.102	99.31	199.85	337.35	2.45	1.45
1175	519	-92	523	0.44	14.412	99.66	201.82	339.32	2.47	1.47

Displacement (1/1000 inch)	Force (lb)	Meter Reading (Volume Change)	Volume Change (Milliliter)	Volume Strain (%)	Axial Strain (%)	Corrected Area (cm <sup>2</sup> )	Deviator Stress (Kpa)	Maximum Stress (kPa)	Stress Ratio	Normal Stress
1200	524	-87	528	0.44	14.721	100.02	203.32	340.82	2.48	1.48
1225	530	-81	534	0.45	15.030	100.38	205.26	342.76	2.49	1.49
1250	537	-75	540	0.45	15.339	100.74	207.61	345.11	2.51	1.51
1275	543	-67	548	0.46	15.649	101.10	209.51	347.01	2.52	1.52
1300	548	-62	553	0.46	15.958	101.47	210.94	348.44	2.53	1.53
1325	553	-56	559	0.47	16.267	101.84	212.36	349.86	2.54	1.54
1350	560	-50	565	0.47	16.577	102.21	214.63	352.13	2.56	1.56
1375	566	-44	571	0.48	16.886	102.58	216.45	353.95	2.57	1.57
1400	571	-38	577	0.48	17.195	102.96	217.82	355.32	2.58	1.58
1425	576	-33	582	0.49	17.504	103.34	219.17	356.67	2.59	1.59
1450	583	-28	587	0.49	17.814	103.73	221.36	358.86	2.61	1.61
1475	590	-23	592	0.50	18.123	104.12	223.52	361.02	2.63	1.63
1500	596	-18	597	0.50	18.432	104.51	225.24	362.74	2.64	1.64
1525	601	-13	602	0.51	18.741	104.90	226.52	364.02	2.65	1.65
1550	610	-8	607	0.51	19.051	105.30	229.47	366.97	2.67	1.67
1575	614	-2	613	0.51	19.360	105.69	230.29	367.79	2.67	1.67

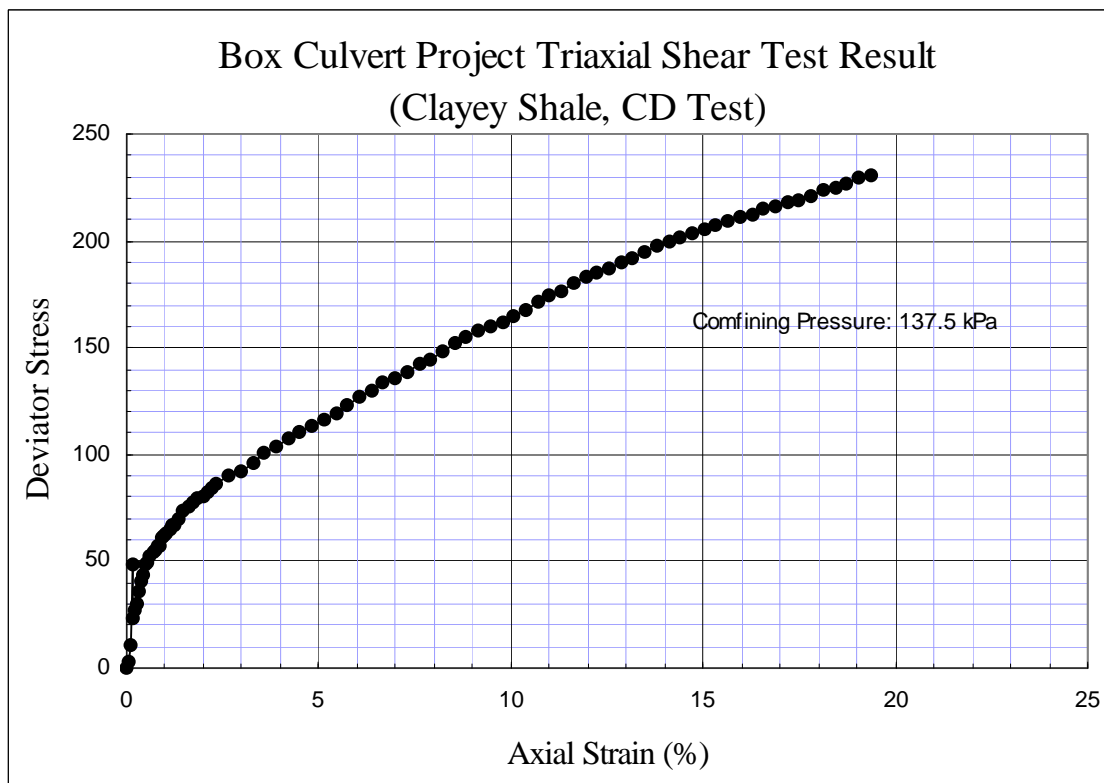


Figure D-2 Triaxial Shear Test Results- Clayey Shale  
(100 mm Sample Diameter, 137.5 kPa Confining Pressure)

## Box Culvert Project: Triaxial Test of Clayey Shale (CD Test)

Sample:		Clayey Shale						
Sample No.	2							
Diameter:(mm)	103.4	103.9	103.1		Height(mm)	205.74	203.2	205.74
Aver. Dia.:	103.6	Initial Area:(1.0e-3)		8.426	Average Height:(mm)	204.9		
Sample Weight(g):	3851				Initial Volume: (1E-6 m^3)	1726.35		
Moisture Content:					Moisture Content:			
Aluminium Box No.:					Aluminum Box No.:			
Box Weight(g):					Box Weight:			
Wet Soil+ Box Weight:(g)					Wet Soil+ Box Weight:			
Dry Soil+Box Weight:(g)					Dry Soil+Box Weight:			
Moisture Content:(%)					Moisture Content:			
Averaged Moisture Content:(%)					Initial Density (KN/M^3):	21.28		
Type of Test: CD								
Type of saturation:					Back Pressure For Saturation:	193 kPa		
Date:2/8/98, 1998								
Confining Pressure( Net): 30 psi			206.85	kPa				

Displacement (1/1000 inch)	Force (lb)	Meter Reading (Volume Change)	Volume Change (Milliliter)	Volume Strain (%)	Axial Strain (%)	Corrected Area (cm^2)	Deviator Stress (Kpa)	Maximum Stress (kPa)	Stress Ratio	Normal Stress
175	77	1793	0	0.00	0.000	84.26	0.00	206.75	1.00	0.00
180	82	1796	3	0.00	0.062	84.31	2.64	209.39	1.01	0.01
185	92	1798	5	0.00	0.124	84.36	7.91	214.66	1.04	0.04
190	102	1800	7	0.01	0.186	84.41	13.18	219.93	1.06	0.06
195	122	1799	8	0.01	0.248	84.46	23.71	230.46	1.11	0.11
200	165	1795	12	0.01	0.310	84.51	46.34	253.09	1.22	0.22
205	202	1789	18	0.02	0.372	84.56	65.78	272.53	1.32	0.32
210	227	1784	23	0.02	0.434	84.61	78.89	285.64	1.38	0.38
215	243	1779	28	0.02	0.496	84.66	87.26	294.01	1.42	0.42
220	260	1773	34	0.03	0.558	84.70	96.14	302.89	1.46	0.46
225	272	1769	38	0.03	0.620	84.75	102.38	309.13	1.50	0.50
230	283	1761	46	0.04	0.682	84.80	108.10	314.85	1.52	0.52
235	293	1754	53	0.05	0.744	84.85	113.28	320.03	1.55	0.55
240	300	1748	59	0.05	0.806	84.90	116.88	323.63	1.57	0.57
245	310	1741	66	0.06	0.868	84.95	122.06	328.81	1.59	0.59
250	317	1736	71	0.06	0.930	85.00	125.65	332.40	1.61	0.61
255	323	1728	79	0.07	0.992	85.04	128.72	335.47	1.62	0.62
260	328	1722	85	0.07	1.054	85.09	131.26	338.01	1.63	0.63
265	335	1716	91	0.08	1.116	85.14	134.84	341.59	1.65	0.65
270	342	1708	99	0.08	1.178	85.19	138.42	345.17	1.67	0.67
275	345	1702	105	0.09	1.240	85.24	139.91	346.66	1.68	0.68
280	352	1696	111	0.09	1.302	85.29	143.48	350.23	1.69	0.69
285	355	1690	117	0.10	1.364	85.34	144.96	351.71	1.70	0.70
290	362	1683	124	0.11	1.426	85.38	148.53	355.28	1.72	0.72
295	365	1677	130	0.11	1.488	85.43	150.01	356.76	1.73	0.73
300	368	1670	137	0.12	1.550	85.48	151.48	358.23	1.73	0.73
305	372	1663	144	0.12	1.612	85.53	153.48	360.23	1.74	0.74
310	376	1654	153	0.13	1.674	85.58	155.47	362.22	1.75	0.75
315	378	1648	159	0.14	1.736	85.63	156.42	363.17	1.76	0.76
320	383	1642	165	0.14	1.798	85.68	158.93	365.68	1.77	0.77
325	387	1635	172	0.15	1.860	85.73	160.91	367.66	1.78	0.78

Displacement (1/1000 inch)	Force (lb)	Meter Reading (Volume Change)	Volume Change (Milliliter)	Volume Strain (%)	Axial Strain (%)	Corrected Area (cm <sup>2</sup> )	Deviator Stress (Kpa)	Maximum Stress (kPa)	Stress Ratio	Normal Stress
330	390	1629	178	0.15	1.921	85.78	162.38	369.13	1.79	0.79
335	393	1623	184	0.16	1.983	85.83	163.84	370.59	1.79	0.79
340	397	1616	191	0.16	2.045	85.87	165.82	372.57	1.80	0.80
345	400	1609	198	0.17	2.107	85.92	167.27	374.02	1.81	0.81
350	403	1601	206	0.18	2.169	85.97	168.73	375.48	1.82	0.82
360	411	1590	217	0.19	2.293	86.07	172.67	379.42	1.84	0.84
370	418	1576	231	0.20	2.417	86.17	176.09	382.84	1.85	0.85
380	425	1564	243	0.21	2.541	86.27	179.49	386.24	1.87	0.87
390	431	1552	255	0.22	2.665	86.37	182.37	389.12	1.88	0.88
400	436	1540	267	0.23	2.789	86.48	184.73	391.48	1.89	0.89
410	441	1525	282	0.24	2.913	86.57	187.09	393.84	1.90	0.90
420	448	1514	293	0.25	3.037	86.68	190.46	397.21	1.92	0.92
430	453	1503	304	0.26	3.161	86.78	192.80	399.55	1.93	0.93
440	463	1491	316	0.27	3.285	86.88	197.70	404.45	1.96	0.96
450	468	1479	328	0.28	3.409	86.98	200.02	406.77	1.97	0.97
460	475	1468	339	0.29	3.533	87.09	203.36	410.11	1.98	0.98
470	482	1456	351	0.30	3.657	87.19	206.69	413.44	2.00	1.00
480	486	1446	361	0.31	3.781	87.30	208.48	415.23	2.01	1.01
490	493	1434	373	0.32	3.905	87.40	211.80	418.55	2.02	1.02
500	498	1422	385	0.33	4.029	87.50	214.09	420.84	2.04	1.04
510	503	1413	394	0.34	4.153	87.61	216.37	423.12	2.05	1.05
520	510	1402	405	0.35	4.277	87.72	219.66	426.41	2.06	1.06
530	516	1392	415	0.36	4.401	87.82	222.44	429.19	2.08	1.08
540	522	1382	425	0.36	4.525	87.93	225.20	431.95	2.09	1.09
550	526	1372	435	0.37	4.649	88.03	226.95	433.70	2.10	1.10
560	533	1362	445	0.38	4.773	88.14	230.21	436.96	2.11	1.11
570	538	1353	454	0.39	4.897	88.25	232.45	439.20	2.12	1.12
580	545	1343	464	0.40	5.021	88.36	235.69	442.44	2.14	1.14
590	548	1334	473	0.40	5.145	88.47	236.91	443.66	2.15	1.15
600	553	1325	482	0.41	5.269	88.58	239.13	445.88	2.16	1.16
610	560	1315	492	0.42	5.393	88.68	242.35	449.10	2.17	1.17
620	565	1305	502	0.43	5.517	88.79	244.56	451.31	2.18	1.18
630	570	1298	509	0.44	5.640	88.90	246.76	453.51	2.19	1.19
640	575	1289	518	0.44	5.764	89.01	248.95	455.70	2.20	1.20
650	578	1281	526	0.45	5.888	89.12	250.14	456.89	2.21	1.21
675	590	1260	547	0.47	6.198	89.40	255.33	462.08	2.23	1.23
700	600	1242	565	0.48	6.508	89.69	259.49	466.24	2.26	1.26
725	612	1224	583	0.50	6.818	89.97	264.60	471.35	2.28	1.28
750	622	1205	602	0.52	7.128	90.26	268.70	475.45	2.30	1.30
775	635	1184	623	0.53	7.438	90.54	274.24	480.99	2.33	1.33
800	643	1167	640	0.55	7.748	90.83	277.28	484.03	2.34	1.34
825	655	1150	657	0.56	8.058	91.13	282.25	489.00	2.37	1.37
850	665	1132	675	0.58	8.368	91.42	286.21	492.96	2.38	1.38
875	675	1116	691	0.59	8.678	91.72	290.13	496.88	2.40	1.40
900	686	1101	706	0.60	8.988	92.02	294.50	501.25	2.42	1.42
925	696	1086	721	0.62	9.298	92.32	298.36	505.11	2.44	1.44
950	706	1072	735	0.63	9.607	92.63	302.18	508.93	2.46	1.46
975	716	1058	749	0.64	9.917	92.93	305.97	512.72	2.48	1.48
1000	726	1043	764	0.65	10.227	93.24	309.73	516.48	2.50	1.50
1025	736	1030	777	0.66	10.537	93.55	313.45	520.20	2.52	1.52

Displacement (1/1000 inch)	Force (lb)	Meter Reading (Volume Change)	Volume Change (Milliliter)	Volume Strain (%)	Axial Strain (%)	Corrected Area (cm <sup>2</sup> )	Deviator Stress (Kpa)	Maximum Stress (kPa)	Stress Ratio	Normal Stress
1050	745	1017	790	0.68	10.847	93.87	316.66	523.41	2.53	1.53
1075	756	1004	803	0.69	11.157	94.19	320.80	527.55	2.55	1.55
1100	765	990	817	0.70	11.467	94.50	323.95	530.70	2.57	1.57
1125	775	977	830	0.71	11.777	94.83	327.55	534.30	2.58	1.58
1150	785	965	842	0.72	12.087	95.15	331.11	537.86	2.60	1.60
1175	790	953	854	0.73	12.397	95.48	332.30	539.05	2.61	1.61
1200	800	941	866	0.74	12.707	95.81	335.81	542.56	2.62	1.62
1225	808	929	878	0.75	13.017	96.14	338.35	545.10	2.64	1.64
1250	816	917	890	0.76	13.326	96.47	340.87	547.62	2.65	1.65
1275	826	905	902	0.77	13.636	96.81	344.29	551.04	2.67	1.67
1300	836	892	915	0.78	13.946	97.14	347.67	554.42	2.68	1.68
1325	845	881	926	0.79	14.256	97.49	350.56	557.31	2.70	1.70
1370	865	860	947	0.81	14.814	98.11	357.41	564.16	2.73	1.73

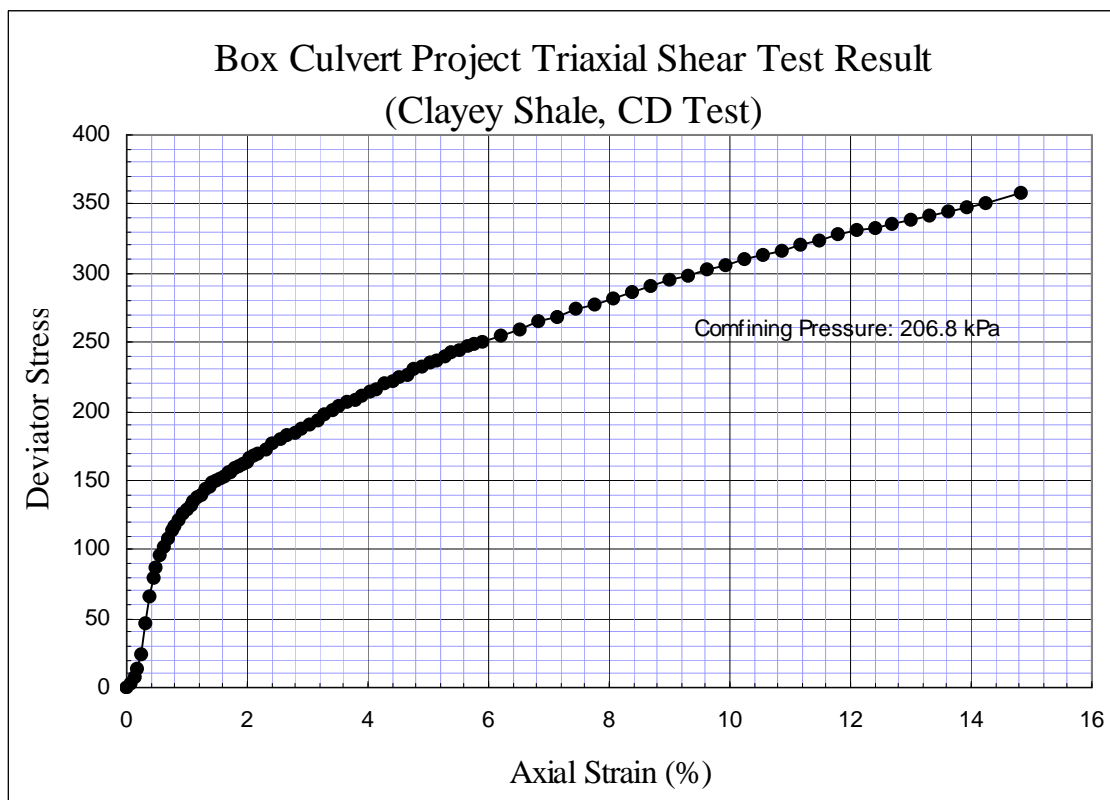


Figure D-3 Triaxial Shear Test Results- Clayey Shale  
(100 mm Sample Diameter, 206.8 kPa Confining Pressure)

### Box Culvert Project: Triaxial Test of Clayey Shale (CD Test)

Sample:	<b>Clayey Shale</b>						
Sample No.	<b>3</b>						
Diameter:(m m)	102.29	101.2	105.15	Height(mm)	177.97	200.82	177.97
Average Diameter:	102.5	Initial Area: (e-3 m^3)	8.245	Average Height:(mm)	185.6	Initial Volume (1e-6 m^3)	1530.1 9
Sample Weight(g):	3778.4						
Moisture Content:	Moisture Content:						
Aluminum Box No.:	Aluminum Box No.:						
Box Weight(g):	Box Weight:						
Wet Soil+ Box Weight:(g)	Wet Soil+ Box Weight:						
Dry Soil+Box Weight:(g)	Dry Soil+Box Weight:						
Moisture Content:(%)	Moisture Content:						
Averaged Moisture Content:(%)	Initial Density (KN/M^3): 21.29						
Type of Test: CD							
Type of saturation:	Back Pressure For Saturation: 193 kPa						
Date:1/16/98, 1998							
Confining Pressure( Net): 40 psi	275.8 kPa						

Displacement (1/1000 inch)	Force (lb)	Meter Reading (Volume Change)	Volume Change (Milliliter)	Volume Strain (%)	Axial Strain (%)	Corrected Area (cm^2)	Deviator Stress (KPa)	Maximum Stress (kPa)	Stress Ratio	Normal Stress
44	188	1913	0	0.00	0.000	82.45	0.00	0.00	0.00	0.00
48	207	1911	2	0.00	0.055	82.50	10.25	10.25	0.04	0.04
52	217	1909	4	0.00	0.096	82.53	15.64	15.64	0.06	0.06
55	257	1904	9	0.01	0.164	82.58	37.18	37.18	0.13	0.13
60	303	1898	15	0.01	0.233	82.63	61.93	61.93	0.22	0.22
65	343	1890	23	0.02	0.301	82.68	83.42	83.42	0.30	0.30
70	370	1884	29	0.03	0.383	82.75	97.87	97.87	0.35	0.35
76	388	1878	35	0.03	0.452	82.80	107.49	107.49	0.39	0.39
81	402	1873	40	0.04	0.506	82.84	114.95	114.95	0.42	0.42
85	416	1867	46	0.04	0.575	82.89	122.40	122.40	0.44	0.44
90	443	1854	59	0.06	0.739	83.02	136.68	136.68	0.50	0.50
102	463	1842	71	0.07	0.876	83.12	147.21	147.21	0.53	0.53
112	483	1829	84	0.08	1.040	83.25	157.68	157.68	0.57	0.57
124	491	1822	91	0.09	1.136	83.33	161.81	161.81	0.59	0.59
131	501	1813	100	0.10	1.259	83.42	166.96	166.96	0.61	0.61
140	520	1799	114	0.11	1.560	83.67	176.58	176.58	0.64	0.64
162	546	1790	123	0.12	1.779	83.85	190.00	190.00	0.69	0.69
178	563	1775	138	0.13	1.971	84.00	198.66	198.66	0.72	0.72
192	576	1763	150	0.14	2.176	84.16	205.14	205.14	0.74	0.74
207	586	1750	163	0.16	2.313	84.27	210.16	210.16	0.76	0.76
217	600	1742	171	0.17	2.491	84.42	217.17	217.17	0.79	0.79
230	610	1713	200	0.19	2.683	84.56	222.07	222.07	0.81	0.81
244	630	1719	194	0.19	2.956	84.80	231.92	231.92	0.84	0.84
264	638	1703	210	0.20	3.120	84.93	235.76	235.76	0.85	0.85
276	656	1693	220	0.21	3.463	85.23	244.35	244.35	0.89	0.89



Displacement (1/1000 inch)	Force (lb)	Meter Reading (Volume Change)	Volume Change (Milliliter)	Volume Strain (%)	Axial Strain (%)	Corrected Area (cm^2)	Deviator Stress (KPa)	Maximum Stress (kPa)	Stress Ratio	Normal Stress
301	663	1676	237	0.23	3.572	85.31	247.76	247.76	0.90	0.90
309	670	1668	245	0.24	3.695	85.41	251.11	251.11	0.91	0.91
318	681	1662	251	0.24	3.901	85.59	256.31	256.31	0.93	0.93
333	701	1651	262	0.25	4.325	85.96	265.56	265.56	0.96	0.96
364	721	1623	290	0.28	4.749	86.32	274.76	274.76	1.00	1.00
395	731	1609	304	0.29	4.941	86.48	279.39	279.39	1.01	1.01
409	738	1601	312	0.30	5.078	86.60	282.61	282.61	1.02	1.02
419	745	1594	319	0.31	5.256	86.76	285.69	285.69	1.04	1.04
432	755	1587	326	0.31	5.447	86.93	290.25	290.25	1.05	1.05
446	761	1578	335	0.32	5.598	87.06	292.88	292.88	1.06	1.06
457	770	1571	342	0.33	5.817	87.25	296.81	296.81	1.08	1.08
473	780	1552	361	0.35	6.049	87.45	301.22	301.22	1.09	1.09
490	791	1540	373	0.36	6.364	87.74	305.82	305.82	1.11	1.11
513	800	1530	383	0.37	6.583	87.94	309.69	309.69	1.12	1.12
529	810	1522	391	0.38	6.775	88.11	314.13	314.13	1.14	1.14
543	818	1514	399	0.39	7.021	88.34	317.35	317.35	1.15	1.15
561	830	1503	410	0.40	7.308	88.60	322.43	322.43	1.17	1.17
582	836	1497	416	0.40	7.473	88.75	324.89	324.89	1.18	1.18
594	850	1491	422	0.41	7.610	88.88	331.44	331.44	1.20	1.20
604	855	1486	427	0.41	7.829	89.09	333.16	333.16	1.21	1.21
620	863	1480	433	0.42	8.034	89.28	336.43	336.43	1.22	1.22
635	868	1477	436	0.42	8.171	89.41	338.43	338.43	1.23	1.23
645	878	1470	443	0.43	8.458	89.68	342.35	342.35	1.24	1.24
666	888	1463	450	0.43	8.732	89.95	346.30	346.30	1.26	1.26
686	893	1457	456	0.44	9.006	90.21	347.75	347.75	1.26	1.26
706	901	1452	461	0.45	9.225	90.43	350.86	350.86	1.27	1.27
722	915	1443	470	0.45	9.580	90.77	356.38	356.38	1.29	1.29
748	920	1438	475	0.46	9.827	91.02	357.87	357.87	1.30	1.30
766	930	1431	482	0.47	10.169	91.36	361.41	361.41	1.31	1.31
791	936	1426	487	0.47	10.374	91.56	363.52	363.52	1.32	1.32
806	943	1420	493	0.48	10.648	91.84	365.82	365.82	1.33	1.33
826	951	1414	499	0.48	10.922	92.12	368.58	368.58	1.34	1.34
846	981	1411	502	0.48	11.195	92.40	381.91	381.91	1.38	1.38
866	986	1408	505	0.49	11.469	92.68	383.14	383.14	1.39	1.39

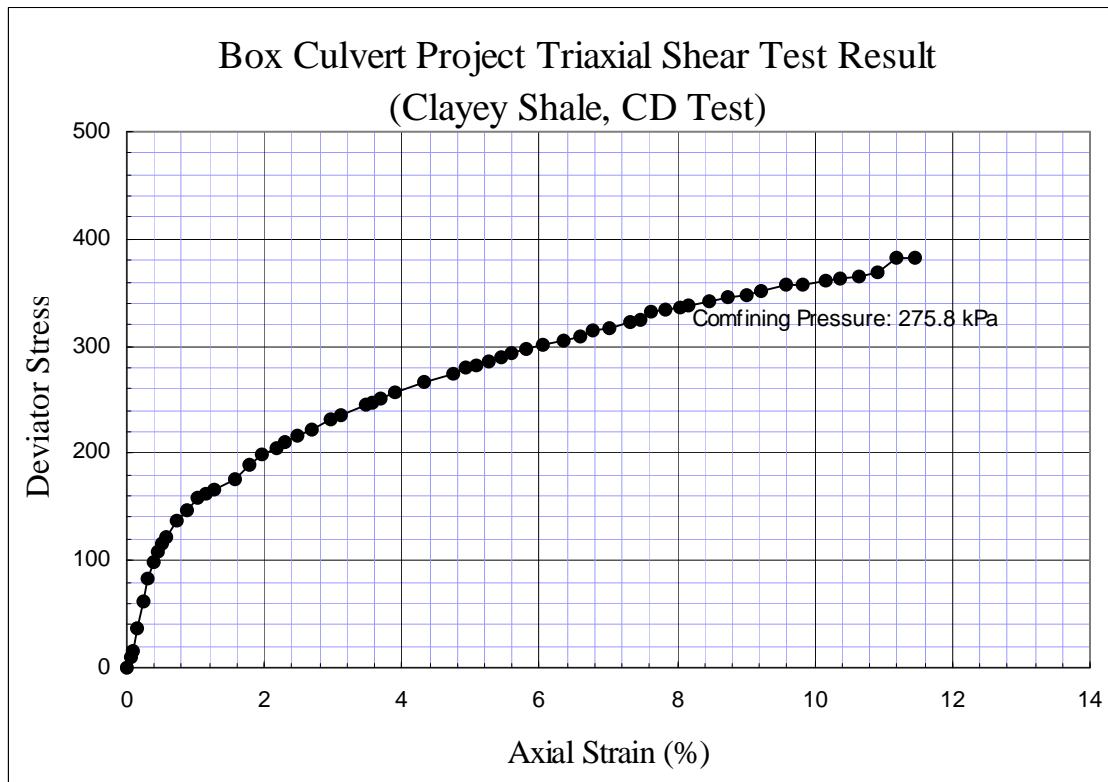


Figure D-4 Triaxial Shear Test Results- Clayey Shale  
(100 mm Sample Diameter, 275.8 kPa Confining Pressure)

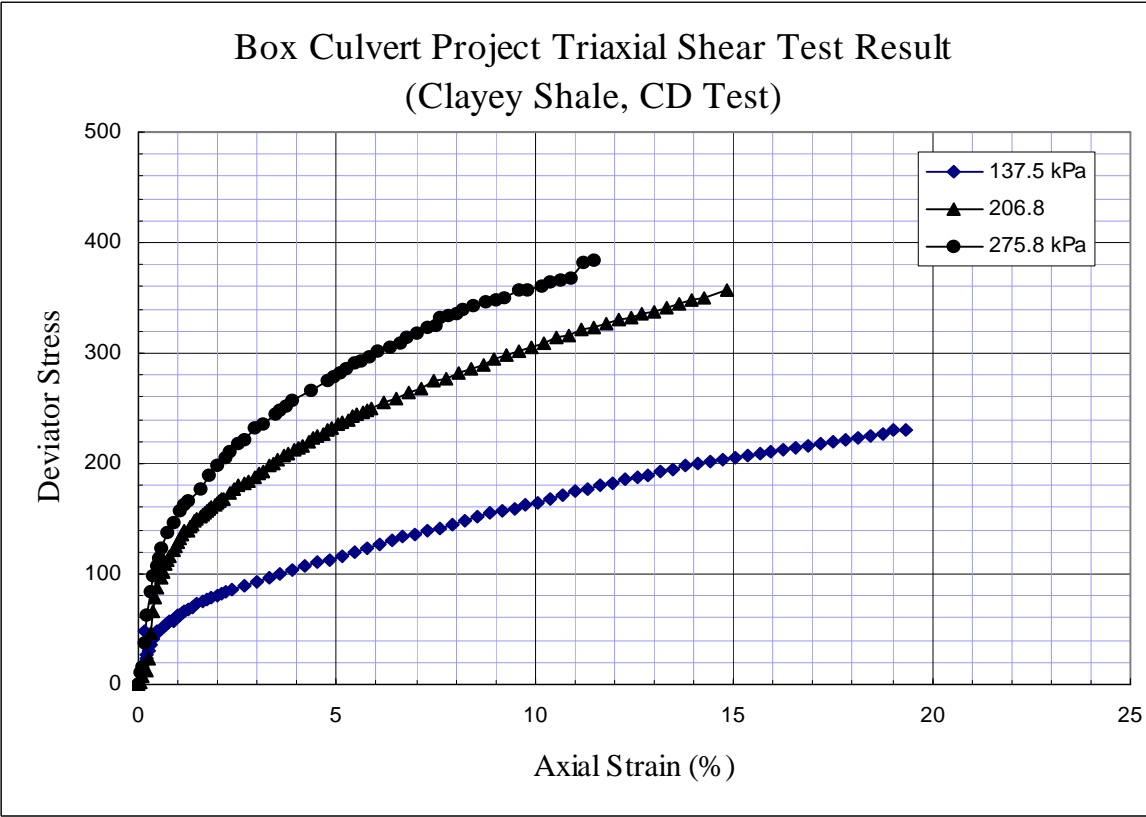


Figure D-5 Axial Strain-Deviator Stress Relationship (CD Test, Sullivan County, TN)

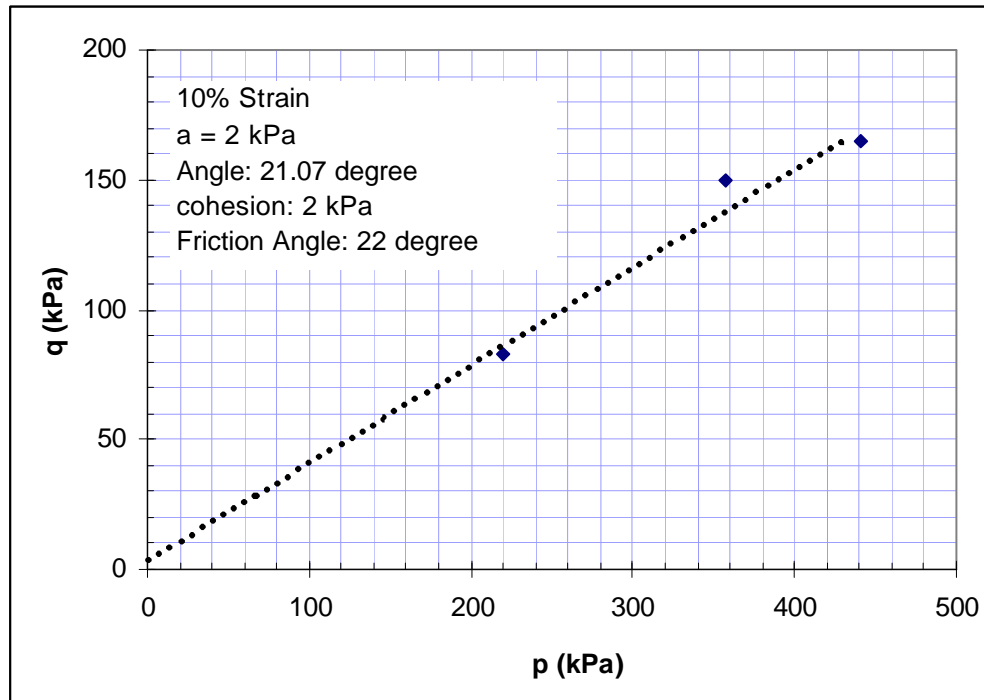


Figure D-6 Peak Strength in  $p$ - $q$  Plane

### Box Culvert Project: Triaxial Test of Clayey Shale (CU Test)

Sample:	Clayey Shale							
Sample No.	1							
Diameter:(mm)	102.2	101.24	100.84		Height(mm)	204.15	203.9	207.96
Average Diameter:		101.4	Initial Area:(1e-3 m^2)	8.072	Average Height:(mm)		205.3	
Sample Weight(g):		3597			Initial Volume (1e-6 m^3):		1657.53	
Moisture Content:					Moisture Content:			
Aluminum Box No.:		36			Aluminum Box No.:		37	
Box Weight(g):		59.4			Box Weight:		59.3	
Wet Soil+ Box Weight:(g)		230.9			Wet Soil+ Box Weight:		255.3	
Dry Soil+Box Weight:(g)		212.79			Dry Soil+Box Weight:		234.18	
Moisture Content:(%)		11.8			Moisture Content:		12.08	
Averaged Moisture Content:(%)			11.94		Initial Density (KN/M^3):		21.29	
Type of Test:	CU							
Type of saturation:					Back Pressure For Saturation:	204.8 kPa		
Date:	6/25-6/28/99							
Confining Pressure( Net):	8.1		55.8	KPa				

Displacement (1/1000 inch)	Force (lb)	Pore pressure (psi)	Axial Strain (%)	Average Area	Pore Pressure (kPa)	Deviator Stress (kPa)	Major Total Stress (kPa)	Major Stress (kPa)	Minor Stress (kPa)	Total Mean Stress	Mean Stress	Q
-27	18	26.1	0.00	80.72	0.00	0.00	55.85	55.85	55.85	55.85	55.85	0.00
-24	28	26.2	0.04	80.75	0.69	5.50	61.35	60.66	55.16	58.60	57.91	2.75
-21	36	26.2	0.07	80.78	0.69	9.90	65.75	65.06	55.16	60.80	60.11	4.95
-18	43	26.3	0.11	80.81	1.38	13.75	69.60	68.22	54.47	62.72	61.34	6.87
-15	53	26.4	0.15	80.84	2.07	19.24	75.09	73.02	53.78	65.47	63.40	9.62
-10	68	26.8	0.21	80.89	4.83	27.47	83.32	78.49	51.02	69.58	64.76	13.73
-5	81	27.2	0.27	80.94	7.58	34.59	90.44	82.85	48.27	73.14	65.56	17.29
0	93	27.6	0.33	80.99	10.34	41.15	97.00	86.66	45.51	76.43	66.08	20.58
5	103	28	0.39	81.04	13.10	46.61	102.46	89.36	42.75	79.15	66.05	23.30
10	110	28.3	0.46	81.09	15.17	50.42	106.27	91.10	40.68	81.06	65.89	25.21
15	116	28.6	0.52	81.14	17.24	53.67	109.52	92.28	38.61	82.69	65.45	26.84
25	125	29.1	0.64	81.24	20.69	58.53	114.38	93.69	35.17	85.11	64.43	29.26
35	135	30	0.76	81.34	26.89	63.92	119.77	92.88	28.96	87.81	60.92	31.96
45	140	30.3	0.89	81.45	28.96	66.57	122.42	93.46	26.89	89.13	60.17	33.28
55	146	30.6	1.01	81.55	31.03	69.75	125.60	94.58	24.82	90.73	59.70	34.88
65	156	30.8	1.13	81.65	32.41	75.11	130.96	98.55	23.44	93.41	61.00	37.56
75	158	30.9	1.26	81.75	33.10	76.10	131.95	98.86	22.75	93.90	60.81	38.05
85	163	31.1	1.38	81.85	34.48	78.72	134.57	100.10	21.38	95.21	60.74	39.36
95	166	31.2	1.50	81.95	35.16	80.25	136.10	100.94	20.69	95.98	60.81	40.13
105	168	31.3	1.63	82.06	35.85	81.23	137.08	101.23	20.00	96.47	60.61	40.62
120	173	31.3	1.81	82.21	35.85	83.78	139.63	103.78	20.00	97.74	61.89	41.89
140	178	31.4	2.06	82.42	36.54	86.27	142.12	105.58	19.31	98.99	62.44	43.14
160	180	31.5	2.30	82.63	37.23	87.13	142.98	105.75	18.62	99.41	62.18	43.56
180	183	31.5	2.55	82.84	37.23	88.52	144.37	107.14	18.62	100.11	62.88	44.26
202	186	31.5	2.82	83.07	37.23	89.88	145.73	108.49	18.62	100.79	63.56	44.94
225	190	31.5	3.10	83.31	37.23	91.75	147.60	110.37	18.62	101.72	64.49	45.87
250	193	31.5	3.41	83.58	37.23	93.05	148.90	111.67	18.62	102.38	65.14	46.53
275	196	31.5	3.72	83.84	37.23	94.35	150.20	112.96	18.62	103.02	65.79	47.17

Displacement (1/1000)	Force (lb)	Pore pressure (psi)	Axial Strain (%)	Average Area	Pore Pressure (kPa)	Deviator Stress (kPa)	Major Total Stress (kPa)	Major Stress (kPa)	Minor Stress (kPa)	Total Mean Stress	Mean Stress	Q
300	198	31.5	4.03	84.11	37.23	95.10	150.95	113.72	18.62	103.40	66.17	47.55
337	203	31.5	4.48	84.51	37.23	97.28	153.13	115.90	18.62	104.49	67.26	48.64
350	205	31.5	4.65	84.65	37.23	98.16	154.01	116.78	18.62	104.93	67.70	49.08
402	208	31.5	5.29	85.23	37.23	99.07	154.92	117.69	18.62	105.38	68.15	49.53
425	211	31.5	5.57	85.48	37.23	100.33	156.18	118.95	18.62	106.02	68.78	50.17
450	214	31.5	5.88	85.76	37.23	101.56	157.41	120.18	18.62	106.63	69.40	50.78
475	216	31.5	6.19	86.04	37.23	102.26	158.11	120.88	18.62	106.98	69.75	51.13
500	218	31.5	6.49	86.33	37.23	102.95	158.80	121.57	18.62	107.33	70.09	51.48
525	220	31.5	6.80	86.61	37.23	103.64	159.49	122.26	18.62	107.67	70.44	51.82
550	221	31.5	7.11	86.90	37.23	103.81	159.66	122.43	18.62	107.76	70.52	51.91
575	226	31.5	7.42	87.19	37.23	106.01	161.86	124.63	18.62	108.86	71.62	53.01
600	228	31.5	7.73	87.48	37.23	106.68	162.53	125.29	18.62	109.19	71.96	53.34
625	230	31.5	8.03	87.77	37.23	107.33	163.18	125.95	18.62	109.52	72.28	53.67
650	231	31.5	8.34	88.07	37.23	107.48	163.33	126.10	18.62	109.59	72.36	53.74
678	235	31.5	8.69	88.40	37.23	109.09	164.94	127.70	18.62	110.39	73.16	54.54
700	236	31.5	8.96	88.66	37.23	109.26	165.11	127.88	18.62	110.48	73.25	54.63
725	239	31.5	9.27	88.97	37.23	110.39	166.24	129.01	18.62	111.05	73.81	55.20
760	243	31.5	9.70	89.39	37.23	111.86	167.71	130.47	18.62	111.78	74.54	55.93
775	245	31.5	9.88	89.57	37.23	112.62	168.47	131.24	18.62	112.16	74.93	56.31
800	246	31.5	10.19	89.88	37.23	112.73	168.58	131.35	18.62	112.21	74.98	56.36
857	248	31.5	10.89	90.59	37.23	112.83	168.68	131.44	18.62	112.26	75.03	56.41
900	253	31.4	11.42	91.13	36.54	114.60	170.45	133.90	19.31	113.15	76.60	57.30
950	258	31.4	12.04	91.77	36.54	116.22	172.07	135.53	19.31	113.96	77.42	58.11
1000	260	31.3	12.65	92.42	35.85	116.37	172.22	136.36	20.00	114.03	78.18	58.18
1050	266	31.3	13.27	93.07	35.85	118.41	174.26	138.41	20.00	115.06	79.20	59.21
1100	268	31.3	13.89	93.74	35.85	118.52	174.37	138.51	20.00	115.11	79.26	59.26
1150	271	31.3	14.50	94.41	35.85	119.08	174.93	139.08	20.00	115.39	79.54	59.54
1200	276	31.3	15.12	95.10	35.85	120.56	176.41	140.56	20.00	116.13	80.28	60.28
1250	280	31.3	15.73	95.80	35.85	121.54	177.39	141.54	20.00	116.62	80.77	60.77
1300	281	31.2	16.35	96.50	35.16	121.11	176.96	141.80	20.69	116.41	81.24	60.56
1350	285	31.2	16.97	97.22	35.16	122.05	177.90	142.74	20.69	116.87	81.71	61.02
1400	286	31.2	17.58	97.94	35.16	121.60	177.45	142.28	20.69	116.65	81.48	60.80

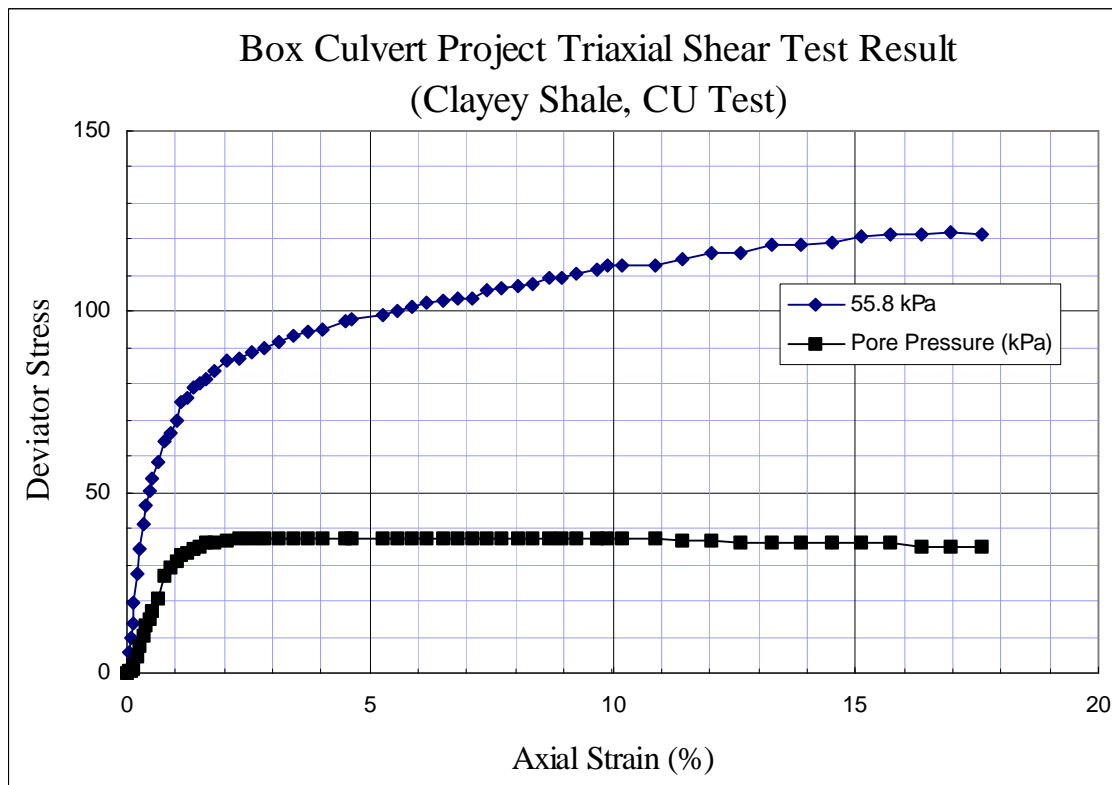


Figure D-7 Triaxial Shear Test Results- Clayey Shale  
(100 mm Sample Diameter, 55.8 kPa Confining Pressure)

### Box Culvert Project: Triaxial Test of Clayey Shale (CU Test)

Sample:	Clayey Shale						
Sample No.	2						
Diameter:(mm)	102.77	101.83	102.77	Height(mm)	208.98	211.01	212.72
Aver. Dia.:	102.3	Initial Area:(e-3 m^2)		8.219	Average Height:(mm)		210.9
Sample Weight(g):	3910		Initial Volume (1e-6 m^3):		1733.51		
Moisture Content:				Moisture Content:			
Aluminum Box No.:	36		Aluminum Box No.:		37		
Box Weight(g):	59.4		Box Weight:		59.3		
Wet Soil+ Box Weight:(g)	230.9		Wet Soil+ Box Weight:		255.3		
Dry Soil+Box Weight:(g)	212.79		Dry Soil+Box Weight:		234.18		
Moisture Content:(%)	11.8		Moisture Content:		12.08		
Average Moisture Content:(%)			11.94		Initial Density (KN/M^3):		22.13
Type of Test:	CU						
Type of saturation:	Back Pressure For Saturation: 204.8 kPa						
Date:	6/25-6/28/99						
Confining Pressure( Net):			103	Kpa			

Displacement (1/1000 inch)	Force (lb)	Pore pressure (psi)	Axial Strain (%)	Average Area	Pore Pressure (kPa)	Deviator Stress (kPa)	Major Total Stress (kPa)	Major Stress (kPa)	Minor Stress (kPa)	Total Mean Stress (kPa)	Effective Mean Stress (kPa)	Q
-203	20	26	0.00	82.19	0.00	0.00	102.74	102.74	102.74	102.74	102.74	0.00
-197	33	26.9	0.07	82.25	6.21	7.02	109.76	103.56	96.53	106.25	100.05	3.51
-174	90	28	0.35	82.48	13.79	37.71	140.45	126.66	88.95	121.60	107.81	18.86
-155	103	28.3	0.58	82.67	15.86	44.62	147.36	131.50	86.88	125.05	109.19	22.31
-150	116	28.7	0.64	82.72	18.62	51.57	154.31	135.70	84.12	128.53	109.91	25.79
-146	131	29	0.68	82.76	20.69	59.60	162.34	141.66	82.06	132.54	111.86	29.80
-141	156	30.1	0.74	82.81	28.27	72.98	175.72	147.45	74.47	139.23	110.96	36.49
-135	173	30.8	0.82	82.87	33.10	82.05	184.79	151.69	69.64	143.76	110.67	41.02
-131	185	31.1	0.86	82.91	35.16	88.44	191.18	156.01	67.58	146.96	111.79	44.22
-126	195	31.5	0.92	82.96	37.92	93.74	196.48	158.56	64.82	149.61	111.69	46.87
-121	205	31.9	0.98	83.01	40.68	99.04	201.78	161.10	62.06	152.26	111.58	49.52
-116	215	32.3	1.04	83.06	43.44	104.33	207.07	163.63	59.30	154.90	111.47	52.16
-111	221	32.6	1.10	83.11	45.51	107.47	210.21	164.71	57.23	156.48	110.97	53.74
-106	228	32.8	1.16	83.16	46.89	111.15	213.89	167.00	55.85	158.31	111.43	55.57
-101	233	33.1	1.22	83.21	48.95	113.75	216.49	167.54	53.79	159.62	110.66	56.88
-96	240	33.3	1.28	83.26	50.33	117.42	220.16	169.83	52.41	161.45	111.12	58.71
-91	245	33.6	1.34	83.31	52.40	120.01	222.75	170.35	50.34	162.75	110.35	60.01
-86	253	33.8	1.40	83.36	53.78	124.21	226.95	173.16	48.96	164.84	111.06	62.10
-81	258	34	1.46	83.42	55.16	126.79	229.53	174.37	47.58	166.14	110.98	63.40
-76	261	34.2	1.52	83.47	56.54	128.31	231.05	174.52	46.20	166.90	110.36	64.16
-71	268	34.5	1.58	83.52	58.61	131.96	234.70	176.09	44.13	168.72	110.11	65.98
-60	275	34.8	1.72	83.63	60.68	135.50	238.24	177.57	42.06	170.49	109.82	67.75
-51	285	35	1.82	83.72	62.06	140.66	243.40	181.35	40.69	173.07	111.02	70.33
-41	295	35.3	1.94	83.82	64.12	145.79	248.53	184.41	38.62	175.64	111.51	72.90
-31	303	35.6	2.06	83.93	66.19	149.85	252.59	186.40	36.55	177.67	111.47	74.93
-21	310	35.7	2.18	84.03	66.88	153.37	256.11	189.23	35.86	179.42	112.54	76.68



-10	318	35.9	2.32	84.14	68.26	157.39	260.13	191.87	34.48	181.43	113.17	78.69
Displacement (1/1000 inch)	Force (lb)	Pore pressure (psi)	Axial Strain (%)	Average Area	Pore Pressure (kPa)	Deviator Stress (kPa)	Major Total Stress (kPa)	Major Stress (kPa)	Minor Stress (kPa)	Total Mean Stress (kPa)	Effective Mean Stress (kPa)	Q
0	325	36.1	2.44	84.25	69.64	160.89	263.63	193.99	33.10	183.18	113.54	80.44
20	340	36.4	2.68	84.45	71.71	168.38	271.12	199.42	31.03	186.93	115.22	84.19
40	356	36.7	2.92	84.66	73.78	176.37	279.11	205.33	28.96	190.92	117.15	88.18
60	368	36.9	3.15	84.87	75.16	182.21	284.95	209.80	27.58	193.85	118.69	91.11
80	381	37.1	3.39	85.08	76.53	188.55	291.29	214.76	26.21	197.02	120.48	94.28
100	393	37.3	3.63	85.29	77.91	194.34	297.08	219.16	24.83	199.91	121.99	97.17
120	406	37.5	3.87	85.51	79.29	200.61	303.35	224.06	23.45	203.04	123.75	100.30
140	416	37.6	4.11	85.72	79.98	205.29	308.03	228.05	22.76	205.39	125.40	102.65
160	428	37.7	4.35	85.94	80.67	210.98	313.72	233.05	22.07	208.23	127.56	105.49
180	438	37.7	4.59	86.15	80.67	215.61	318.35	237.68	22.07	210.55	129.87	107.81
200	446	37.8	4.83	86.37	81.36	219.19	321.93	240.57	21.38	212.33	130.97	109.59
220	458	37.8	5.07	86.59	81.36	224.79	327.53	246.17	21.38	215.14	133.78	112.40
240	468	37.9	5.31	86.81	82.05	229.34	332.08	250.03	20.69	217.41	135.36	114.67
260	478	37.9	5.55	87.03	82.05	233.87	336.61	254.56	20.69	219.67	137.62	116.93
280	488	38	5.79	87.25	82.74	238.37	341.11	258.37	20.00	221.92	139.18	119.18
300	496	38	6.03	87.47	82.74	241.83	344.57	261.83	20.00	223.65	140.91	120.91
320	504	38	6.27	87.70	82.74	245.26	348.00	265.26	20.00	225.37	142.63	122.63
340	511	37.9	6.51	87.92	82.05	248.17	350.91	268.86	20.69	226.83	144.78	124.09
360	519	37.9	6.75	88.15	82.05	251.57	354.31	272.26	20.69	228.52	146.47	125.78
380	528	37.9	6.99	88.38	82.05	255.45	358.19	276.14	20.69	230.46	148.41	127.72
400	534	37.8	7.23	88.60	81.36	257.80	360.54	279.18	21.38	231.64	150.28	128.90
434	548	37.7	7.64	88.99	80.67	263.66	366.40	285.72	22.07	234.57	153.90	131.83
450	554	37.7	7.83	89.18	80.67	266.10	368.84	288.17	22.07	235.79	155.12	133.05
475	563	37.6	8.13	89.47	79.98	269.70	372.44	292.46	22.76	237.59	157.61	134.85
500	571	37.5	8.43	89.76	79.29	272.78	375.52	296.23	23.45	239.13	159.84	136.39
525	579	37.5	8.73	90.06	79.29	275.84	378.58	299.28	23.45	240.66	161.37	137.92
550	586	37.4	9.03	90.36	78.60	278.37	381.11	302.51	24.14	241.93	163.32	139.19
585	596	37.3	9.45	90.78	77.91	281.98	384.72	306.81	24.83	243.73	165.82	140.99
600	601	37.3	9.63	90.96	77.91	283.87	386.61	308.69	24.83	244.67	166.76	141.93
625	608	37.2	9.93	91.26	77.22	286.33	389.07	311.85	25.52	245.91	168.68	143.17
650	616	37.2	10.23	91.56	77.22	289.26	392.00	314.78	25.52	247.37	170.15	144.63
675	619	37.2	10.53	91.87	77.22	289.75	392.49	315.26	25.52	247.61	170.39	144.87
700	628	37.2	10.83	92.18	77.22	293.11	395.85	318.63	25.52	249.30	172.07	146.56
750	634	36.8	11.43	92.80	74.47	294.01	396.75	322.29	28.27	249.75	175.28	147.01
800	638	36.5	12.03	93.44	72.40	293.93	396.67	324.27	30.34	249.70	177.31	146.96
850	636	36.2	12.63	94.08	70.33	290.98	393.72	323.39	32.41	248.23	177.90	145.49
900	639	35.8	13.23	94.73	67.57	290.39	393.13	325.56	35.17	247.93	180.36	145.19
950	641	35.4	13.83	95.39	64.81	289.31	392.05	327.24	37.93	247.40	182.58	144.66
1000	644	35.1	14.43	96.06	62.74	288.69	391.43	328.68	40.00	247.08	184.34	144.34
1050	639	34.7	15.03	96.73	59.99	284.37	387.11	327.12	42.75	244.92	184.94	142.18
1100	634	34.3	15.63	97.42	57.23	280.08	382.82	325.59	45.51	242.78	185.55	140.04
1150	634	33.9	16.23	98.12	54.47	278.09	380.83	326.36	48.27	241.78	187.31	139.04
1200	634	33.6	16.83	98.83	52.40	276.09	378.83	326.43	50.34	240.79	188.39	138.05

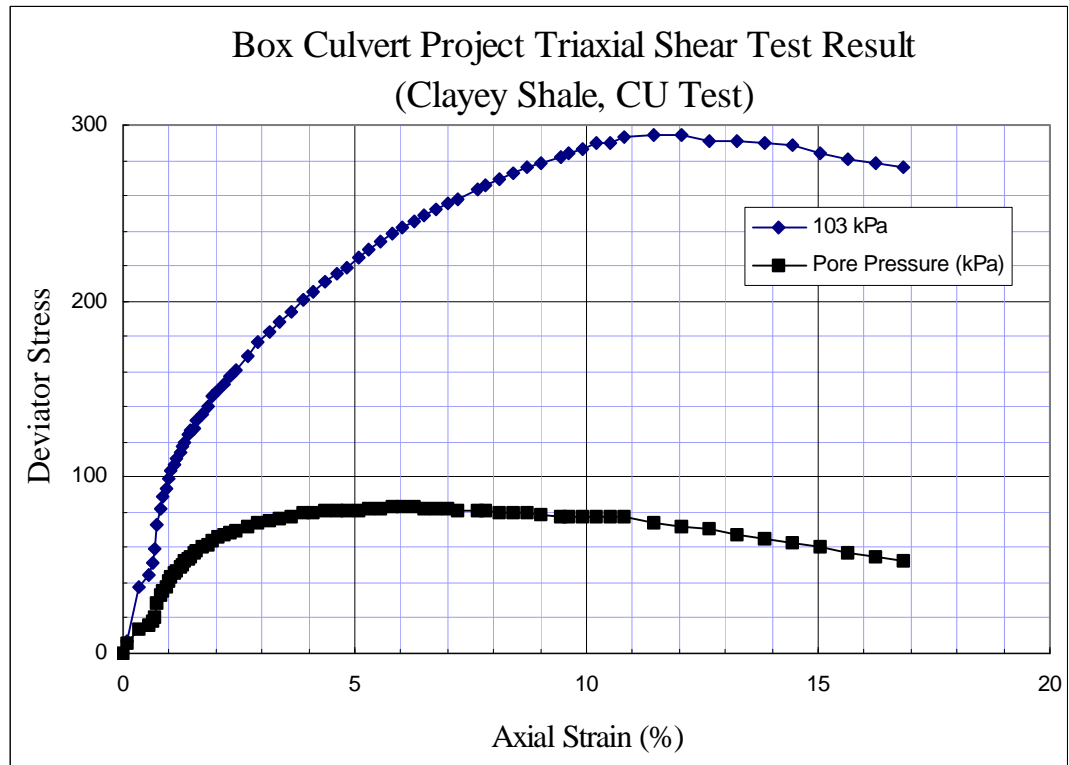


Figure D-8 Triaxial Shear Test Results- Clayey Shale  
(100 mm Sample Diameter, 103 kPa Confining Pressure)

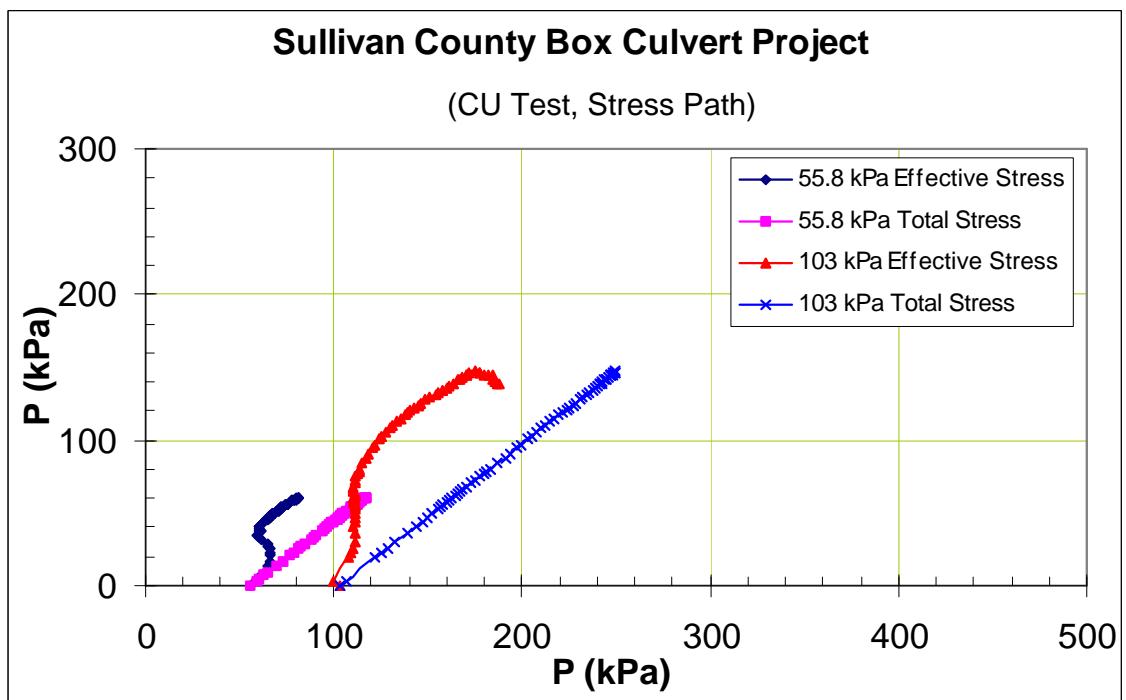


Figure D-9 Peak Strength in p-q Plane (CU Test)

## Appendix D-2

### Triaxial Shear Test Results - Gravel

Table D-2 Gravel Test Summary

Sample Number	Back Pressure (kPa)	Net Confining Pressure (kPa)	Measured Density (kN/m <sup>3</sup> )	Unloading-Reloading During Test	Maximum Axial Strain Tested (%)	Measured Initial Modulus (MPa)	Unloading Modulus (MPa)
No.1	193	69	20.98	No	10.2	56	NA
No.2	193	103.4	19.39	No	11.4	63	NA
No.3	193	137.9	21.36	No	9.5	67	NA
No.4	193	101.4	20.89	Yes	8.3	50	137
No.5	193	275	19.90	No	13.4	77	NA

Test Method: Consolidated, and Drained

Measured strength

Two sets of strength can be obtained:

**Cohesion = 0 kPa Angle of Internal Friction  $\phi = 49^\circ$**

or

**Cohesion = 54 kPa Angle of Internal Friction  $\phi = 43^\circ$**

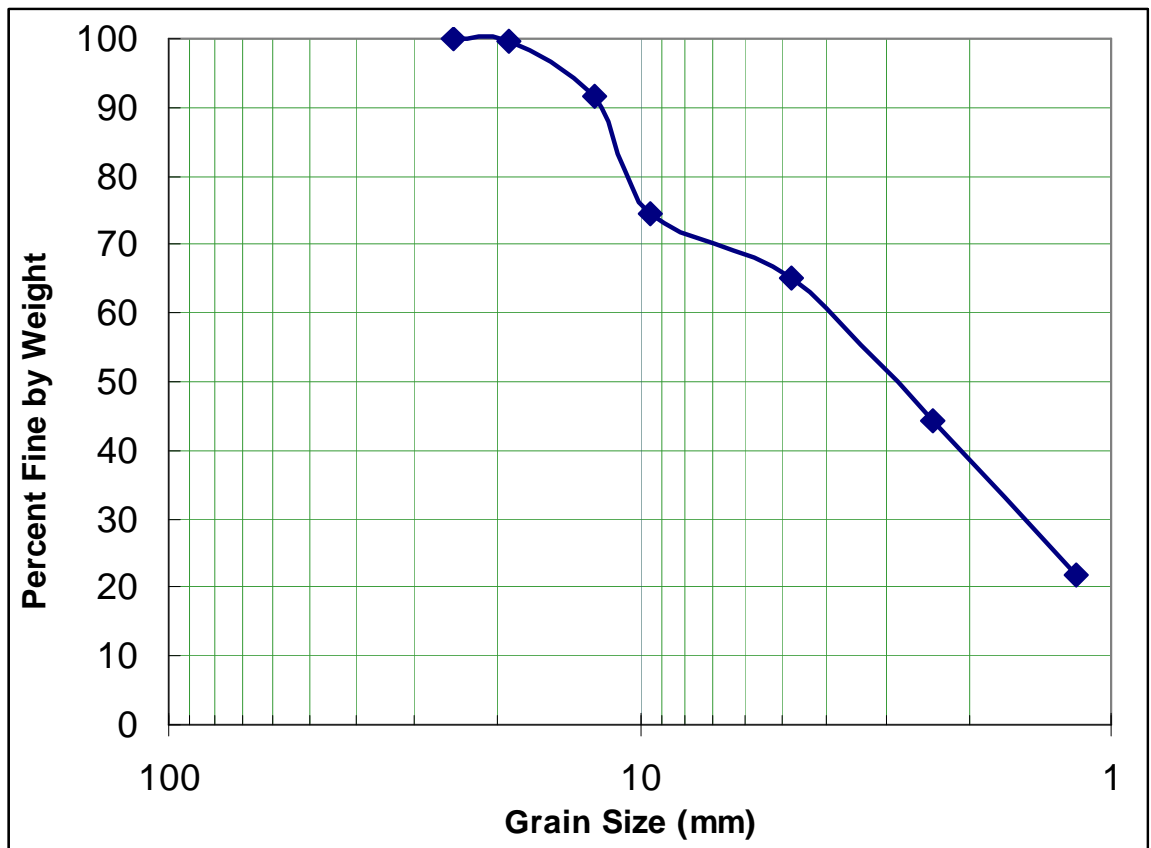


Figure D-10 Grain Size Distribution of Gravel  
(Greene County Culvert Site)

## Box Culvert Project: Triaxial Shear Test

Sample: **Gravel** Date Tested: 7/12/1997

Sample No. 1 Type of Test: Consolidated Drained

Diameter:(mm) 100.9 101.22 101.63 Average Diameter (mm): 101.2 Initial Area(mm<sup>2</sup>): 8050

Height(mm) 212.73 212.73 211.14 Average Sample Height (mm): 212.2 Initial Volume(mm<sup>3</sup>):1708.29E-3

Initial Density (kN/m<sup>3</sup>): 20.98

Net Confining Pressure: 69 kPa Back Pressure: 193.06 kPa

Displacement (1/000 inch)	Force (lb)	Meter Reading	Volume Change	Volume Strain.(%)	Axial Strain (%)	Corrected Area (cm <sup>2</sup> )	Deviator Stress(k Pa)	Maximum Stress kPa	Stress Ratio	Normalized Stress
269	27	-860	0	0.00	0.000	80.50	0.00	69.00	1.00	0.00
273	93	-841	-19	-0.02	0.048	80.56	36.46	105.46	1.53	0.53
277	150	-812	-48	-0.04	0.096	80.61	67.89	136.89	1.98	0.98
282	215	-763	-97	-0.08	0.156	80.70	103.67	172.67	2.50	1.50
286	275	-741	-119	-0.10	0.203	80.75	136.66	205.66	2.98	1.98
290	330	-722	-138	-0.12	0.251	80.80	166.86	235.86	3.42	2.42
300	441	-672	-188	-0.16	0.371	80.94	227.62	296.62	4.30	3.30
305	477	-660	-200	-0.17	0.431	80.99	247.24	316.24	4.58	3.58
315	554	-642	-218	-0.19	0.551	81.10	289.15	358.15	5.19	4.19
320	572	-636	-224	-0.19	0.610	81.16	298.83	367.83	5.33	4.33
330	639	-633	-227	-0.20	0.730	81.26	335.15	404.15	5.86	4.86
350	740	-662	-198	-0.17	0.970	81.43	389.62	458.62	6.65	5.65
370	819	-725	-135	-0.12	1.209	81.58	431.98	500.98	7.26	6.26
390	949	-925	65	0.06	1.448	81.64	502.53	571.53	8.28	7.28
425	974	-1001	141	0.12	1.867	81.94	514.30	583.30	8.45	7.45
440	1010	-1089	229	0.20	2.047	82.02	533.28	602.28	8.73	7.73
460	1030	-1020	160	0.14	2.286	82.27	542.48	611.48	8.86	7.86
480	1075	-1361	501	0.43	2.526	82.23	567.10	636.10	9.22	8.22
500	1096	-1521	661	0.57	2.765	82.32	577.85	646.85	9.37	8.37
520	1076	-1293	889	0.77	3.004	82.36	566.77	635.77	9.21	8.21
540	1089	-1109	1073	0.93	3.244	82.43	573.29	642.29	9.31	8.31
560	1117	-930	1252	1.08	3.483	82.51	587.87	656.87	9.52	8.52
580	1116	-727	1455	1.26	3.723	82.56	586.92	655.92	9.51	8.51
600	1134	-543	1639	1.42	3.962	82.64	596.09	665.09	9.64	8.64
622	1139	-332	1850	1.60	4.225	82.71	598.25	667.25	9.67	8.67
645	1139	-107	2075	1.79	4.501	82.79	597.71	666.71	9.66	8.66
670	1158	89	2271	1.96	4.800	82.90	607.07	676.07	9.80	8.80
700	1180	283	2465	2.13	5.159	83.07	617.60	686.60	9.95	8.95
730	1189	645	2827	2.44	5.518	83.12	622.05	691.05	10.02	9.02
766	1195	1021	3203	2.77	5.949	83.23	624.50	693.50	10.05	9.05
800	1192	1294	3476	3.01	6.356	83.38	621.71	690.71	10.01	9.01
840	1197	1610	3792	3.28	6.835	83.58	622.94	691.94	10.03	9.03

Displacement (1/1000 inch)	Force (lb)	Meter Reading	Volume Change	Volume Strain.(% )	Axial Strain (%)	Correcte d Area (cm^2)	Deviator Stress(k Pa)	Maximu m Stress kPa)	Stress Ratio	Normalized Stress
880	1177	1911	4093	3.54	7.314	83.78	610.78	679.78	9.85	8.85
920	1179	1657	4347	3.76	7.792	84.03	610.08	679.08	9.84	8.84
960	1161	1355	4649	4.02	8.271	84.23	599.05	668.05	9.68	8.68
1000	1168	1063	4941	4.27	8.750	84.45	601.18	670.18	9.71	8.71
1042	1161	746	5258	4.55	9.253	84.68	595.91	664.91	9.64	8.64
1080	1155	494	5510	4.76	9.708	84.91	591.13	660.13	9.57	8.57
1120	1139	200	5804	5.02	10.186	85.14	581.21	650.21	9.42	8.42

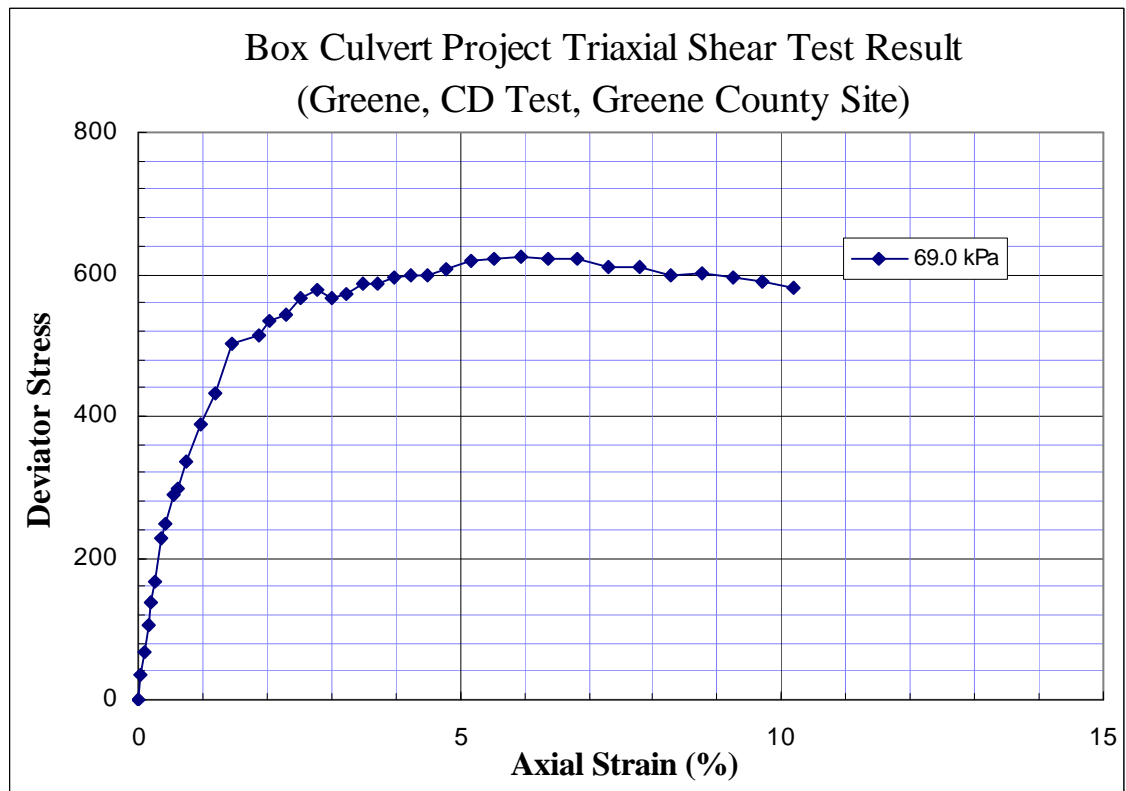


Figure D-11 Triaxial Shear Test Results- Gravel  
(100 mm Sample Diameter, 69 kPa Confining Pressure)

## Box Culvert Project: Triaxial Shear Test

Sample: <b>Gravel</b>					Date Tested:	7/24/1997
Sample No.	2				Type of Test: Consolidated Drained	
Diameter:(mm)	105	104.8	104.8	Average Diameter (mm): 104.9	Initial Area(mm^2):	8634
Height(mm):	206.4	204.8	206.4	Average Sample Height (mm): 205.9	Initial Volume(mm^3):1777.52E-3	
Initial Density (kN/m^3):			19.39			
Net Confining Pressure: 103.4 kPa			Back Pressure:		193.06 kPa	

Displacement (1/1000 inch)	Force (lb)	Meter Reading	Volume Change	Volume Strain.(%)	Axial Strain (%)	Correcte d Area (cm^2)	Deviator Stress(k Pa)	Maximu m Stress (kPa)	Stress Ratio	Normalized Stress
-40	34	-495	0	0.00	0.000	86.34	0.00	103.40	1.00	0.00
-21	234	-460	-35	-0.03	0.234	86.57	102.80	206.20	1.99	0.99
-18	263	-420	-75	-0.06	0.271	86.63	117.62	221.02	2.14	1.14
-16	294	-390	-105	-0.09	0.296	86.68	133.48	236.88	2.29	1.29
-12	337	-360	-135	-0.11	0.345	86.74	155.44	258.84	2.50	1.50
-10	368	-345	-150	-0.12	0.370	86.77	171.28	274.68	2.66	1.66
-6	407	-324	-171	-0.14	0.419	86.83	191.15	294.55	2.85	1.85
-4	539	-308	-187	-0.16	0.444	86.86	258.70	362.10	3.50	2.50
-2	550	-291	-204	-0.17	0.469	86.90	264.23	367.63	3.56	2.56
4	574	-252	-243	-0.20	0.543	86.99	276.23	379.63	3.67	2.67
8	649	-223	-272	-0.23	0.592	87.05	314.36	417.76	4.04	3.04
12	686	-203	-292	-0.24	0.642	87.11	333.05	436.45	4.22	3.22
18	728	-182	-313	-0.26	0.716	87.19	354.18	457.58	4.43	3.43
20	750	-170	-325	-0.27	0.740	87.22	365.28	468.68	4.53	3.53
25	795	-148	-347	-0.29	0.802	87.29	387.93	491.33	4.75	3.75
30	831	-131	-364	-0.30	0.864	87.36	405.97	509.37	4.93	3.93
37	872	-109	-386	-0.32	0.950	87.45	426.40	529.80	5.12	4.12
42	910	-96	-399	-0.33	1.012	87.51	445.41	548.81	5.31	4.31
50	962	-79	-416	-0.35	1.110	87.61	471.32	574.72	5.56	4.56
55	989	-70	-425	-0.35	1.172	87.68	484.69	588.09	5.69	4.69
60	1018	-64	-431	-0.36	1.234	87.73	499.07	602.47	5.83	4.83
75	1085	-50	-445	-0.37	1.419	87.91	532.00	635.40	6.15	5.15
85	1127	-47	-448	-0.37	1.542	88.02	552.55	655.95	6.34	5.34
100	1189	-52	-443	-0.37	1.727	88.18	582.82	686.22	6.64	5.64
115	1230	-63	-432	-0.36	1.912	88.34	602.43	705.83	6.83	5.83
130	1257	-71	-424	-0.35	2.097	88.50	614.90	718.30	6.95	5.95
145	1292	-99	-396	-0.33	2.283	88.65	631.45	734.85	7.11	6.11
165	1340	-152	-343	-0.29	2.529	88.84	654.18	757.58	7.33	6.33
185	1378	-211	-284	-0.24	2.776	89.02	671.84	775.24	7.50	6.50
200	1408	-263	-232	-0.19	2.961	89.15	685.82	789.22	7.63	6.63
220	1457	-340	-155	-0.13	3.208	89.32	708.92	812.32	7.86	6.86
255	1517	-511	16	0.01	3.640	89.59	736.57	839.97	8.12	7.12

Displacement (1/000 inch)	Force (lb)	Meter Reading	Volume Change	Volume Strain.(% )	Axial Strain (%)	Correcte d Area (cm^2)	Deviator Stress(k Pa)	Maximu m Stress (kPa)	Stress Ratio	Normalized Stress
260	1527	-534	39	0.03	3.701	89.63	741.20	844.60	8.17	7.17
280	1564	-636	141	0.12	3.948	89.79	758.26	861.66	8.33	7.33
305	1584	-779	284	0.24	4.257	89.97	766.62	870.02	8.41	7.41
320	1599	-871	376	0.31	4.442	90.07	773.14	876.54	8.48	7.48
340	1633	-984	489	0.41	4.688	90.22	788.64	892.04	8.63	7.63
360	1652	-1108	613	0.51	4.935	90.36	796.77	900.17	8.71	7.71
380	1653	-1232	737	0.61	5.182	90.50	796.01	899.41	8.70	7.70
400	1681	-1361	866	0.72	5.429	90.64	808.54	911.94	8.82	7.82
425	1701	-1523	1028	0.85	5.737	90.82	816.80	920.20	8.90	7.90
450	1678	-1725	1230	1.02	6.046	90.96	804.26	907.66	8.78	7.78
475	1702	-1886	1391	1.16	6.354	91.14	814.42	917.82	8.88	7.88
505	1652	-1540	1737	1.44	6.724	91.23	789.18	892.58	8.63	7.63
525	1657	-1426	1851	1.54	6.971	91.39	790.28	893.68	8.64	7.64
550	1656	-1259	2018	1.68	7.279	91.56	788.29	891.69	8.62	7.62
575	1626	-1098	2179	1.81	7.588	91.74	772.19	875.59	8.47	7.47
605	1616	-961	2316	1.92	7.958	92.00	765.15	868.55	8.40	7.40
625	1603	-864	2413	2.01	8.205	92.17	757.45	860.85	8.33	7.33
650	1585	-780	2497	2.07	8.513	92.42	746.78	850.18	8.22	7.22
685	1561	-698	2579	2.14	8.945	92.79	732.26	835.66	8.08	7.08
736	1560	-618	2659	2.21	9.574	93.38	727.22	830.62	8.03	7.03
775	1538	-653	2624	2.18	10.056	93.90	712.71	816.11	7.89	6.89
809	1475	-937	2340	1.94	10.475	94.57	678.03	781.43	7.56	6.56
860	1454	-1550	1727	1.44	11.104	95.73	660.03	763.43	7.38	6.38



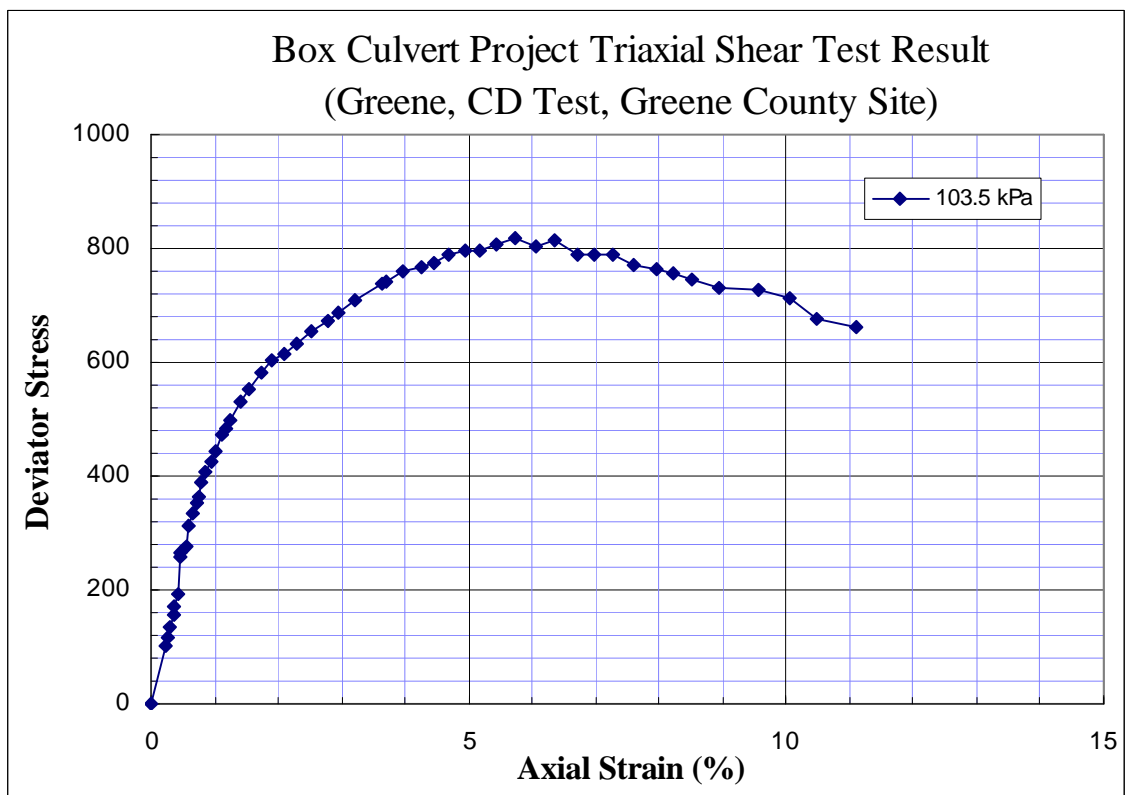


Figure D-12 Triaxial Shear Test Results- Gravel  
(100 mm Sample Diameter, 103.5 kPa Confining Pressure)

## Box Culvert Project: Triaxial Shear Test

Sample: <b>Gravel</b>	Date Tested: 9/30/1997
Sample No. 3	Type of Test: Consolidated Drained
Diameter:(mm) 100.8 101 101.5	Average Diameter (mm): 101.1 Initial Area(mm <sup>2</sup> ): 8024
Height(mm): 207.01 208.28 215.9	Average Sample Height (mm): 205.9 Initial Volume(mm <sup>3</sup> ):1688.17E-3
Initial Density (kN/m <sup>3</sup> ): 21.36	
Net Confining Pressure: 137.9 kPa	Back Pressure: 193.06 kPa

Displacement (1/000 inch)	Force (lb)	Meter Reading	Volume Change	Volume Strain (%)	Axial Strain (%)	Corrected Area (cm <sup>2</sup> )	Deviator Stress (kPa)	Maximum Stress kPa)	Stress Ratio	Normalized Stress
239	39	411	0	0.00	0.000	80.24	0.00	137.90	1.00	0.00
245	170	446	-35	-0.03	0.072	80.32	72.58	210.48	1.53	0.53
250	240	478	-67	-0.06	0.133	80.39	111.26	249.16	1.81	0.81
255	302	520	-109	-0.10	0.193	80.47	145.43	283.33	2.05	1.05
260	370	569	-158	-0.14	0.254	80.55	182.85	320.75	2.33	1.33
265	399	610	-199	-0.17	0.314	80.63	198.68	336.58	2.44	1.44
270	453	650	-239	-0.21	0.374	80.71	228.26	366.16	2.66	1.66
275	506	687	-276	-0.24	0.435	80.78	257.24	395.14	2.87	1.87
280	544	722	-311	-0.27	0.495	80.86	277.92	415.82	3.02	2.02
285	587	758	-347	-0.30	0.555	80.93	301.31	439.21	3.18	2.18
290	625	789	-378	-0.33	0.616	81.00	321.92	459.82	3.33	2.33
295	670	824	-413	-0.36	0.676	81.08	346.32	484.22	3.51	2.51
300	706	850	-439	-0.38	0.736	81.14	365.78	503.68	3.65	2.65
305	734	879	-468	-0.41	0.797	81.21	380.80	518.70	3.76	2.76
310	763	905	-494	-0.43	0.857	81.28	396.36	534.26	3.87	2.87
315	806	927	-516	-0.45	0.918	81.35	419.57	557.47	4.04	3.04
320	833	952	-541	-0.47	0.978	81.41	433.98	571.88	4.15	3.15
330	886	986	-575	-0.50	1.099	81.54	462.24	600.14	4.35	3.35
340	943	1031	-620	-0.54	1.219	81.67	492.55	630.45	4.57	3.57
350	992	1058	-647	-0.57	1.340	81.79	518.50	656.40	4.76	3.76
363	1063	1087	-676	-0.59	1.497	81.94	556.10	694.00	5.03	4.03
370	1094	1099	-688	-0.60	1.581	82.02	572.38	710.28	5.15	4.15
380	1125	1108	-697	-0.61	1.702	82.12	588.43	726.33	5.27	4.27
390	1172	1122	-711	-0.62	1.823	82.24	613.07	750.97	5.45	4.45
410	1244	1133	-722	-0.63	2.064	82.45	650.36	788.26	5.72	4.72
420	1295	1130	-719	-0.63	2.185	82.55	677.07	814.97	5.91	4.91
440	1361	1110	-699	-0.61	2.427	82.74	711.01	848.91	6.16	5.16
460	1408	1092	-681	-0.60	2.668	82.93	734.59	872.49	6.33	5.33
480	1478	1051	-640	-0.56	2.909	83.10	770.51	908.41	6.59	5.59
505	1545	989	-578	-0.51	3.211	83.32	804.31	942.21	6.83	5.83
555	1645	854	-443	-0.39	3.815	83.74	853.37	991.27	7.19	6.19
571	1674	793	-382	-0.33	4.008	83.87	867.50	1005.40	7.29	6.29

Displacement (1/1000 inch)	Force (lb)	Meter Reading	Volume Change	Volume Strain (%)	Axial Strain (%)	Corrected Area (cm <sup>2</sup> )	Deviator Stress (kPa)	Maximum Stress (kPa)	Stress Ratio	Normalized Stress
600	1732	674	-263	-0.23	4.358	84.09	895.92	1033.82	7.50	6.50
625	1780	554	-143	-0.13	4.660	84.26	919.38	1057.28	7.67	6.67
660	1802	363	48	0.04	5.082	84.50	928.42	1066.32	7.73	6.73
714	1866	98	313	0.27	5.734	84.89	957.74	1095.64	7.95	6.95
744	1877	-43	454	0.40	6.097	85.11	960.99	1098.89	7.97	6.97
758	1899	-126	537	0.47	6.266	85.20	971.45	1109.35	8.04	7.04
786	1903	-284	695	0.61	6.604	85.39	971.38	1109.28	8.04	7.04
820	1900	-486	897	0.78	7.014	85.61	967.27	1105.17	8.01	7.01
850	1920	-665	1076	0.94	7.376	85.81	975.40	1113.30	8.07	7.07
910	1918	-1050	1461	1.28	8.101	86.19	970.04	1107.94	8.03	7.03
950	1922	-1292	1703	1.49	8.584	86.46	969.08	1106.98	8.03	7.03
1000	1905	-1590	2001	1.75	9.187	86.81	956.52	1094.42	7.94	6.94
1030	1910	-1263	1674	1.46	9.549	87.41	952.48	1090.38	7.91	6.91

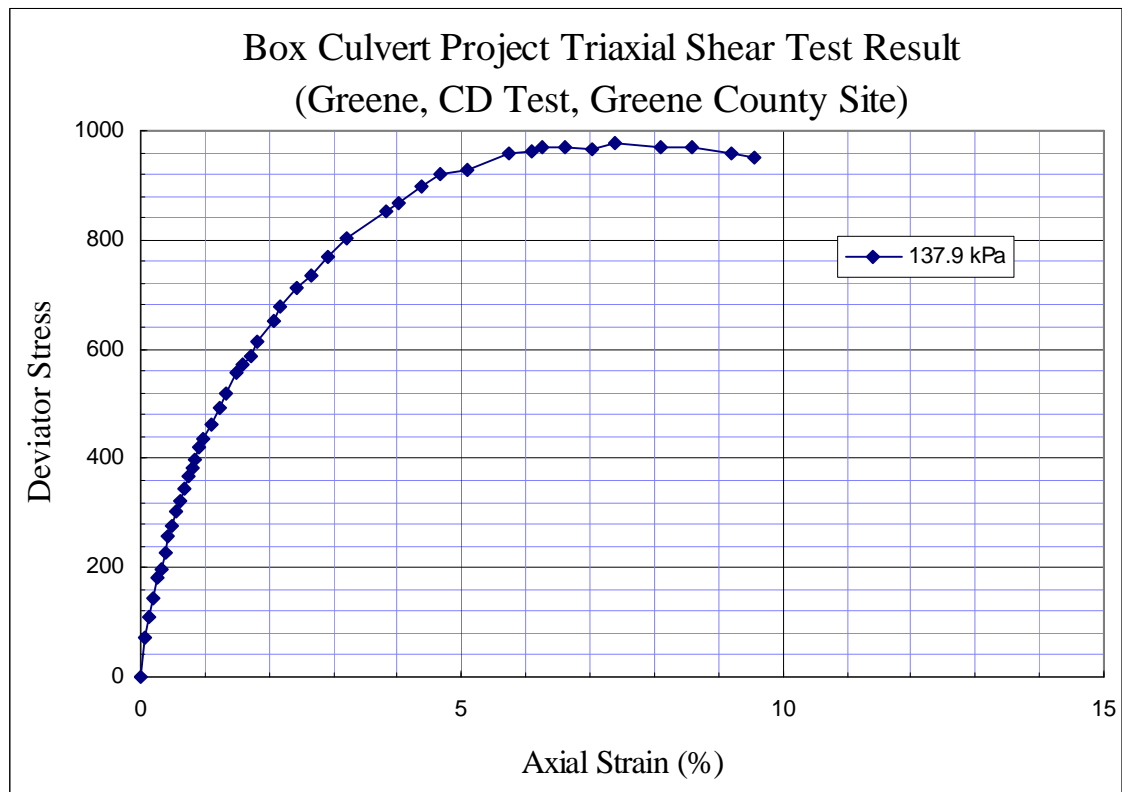


Figure D-13 Triaxial Shear Test Results- Gravel  
(100 mm Sample Diameter, 137.9 kPa Confining Pressure)

### Box Culvert Project: Triaxial Shear Test

Sample	Gravel						
Sample No.	4						
Diameter:(mm)	103.63	103.89	102.87	Height(mm)	199.39	200.66	201.93
Average Diameter:	103.5	Initial Area:(e-3 m^2)	8.413	Average Height:(mm)	200.7		
Sample Weight(g):	3595			Initial Volume: (1e-6 m^3)	1688.15		
Moisture Content:				Moisture Content:			
Aluminum Box No.:				Aluminum Box No.:			
Box Weight(g):				Box Weight:			
Wet Soil+ Box Weight(g)				Wet Soil+ Box Weight:			
Dry Soil+Box Weight(g)				Dry Soil+Box Weight:			
Moisture Content:(%)				Moisture Content:			
Averaged Moisture Content:(%)				Initial Density (KN/M^3):	20.89		
Type of Test:	Consolidated and Drained						
Type of Saturation:				Back Pressure for Saturation:	193.5 kPa		
Date:	12/31/97						
Confining Pressure (Net):	101.4 kPa						

Displacement (1/000 inch)	Force (lb)	Meter Reading	Volume Change	Volume Strain (%)	Axial Strain (%)	Corrected Area (cm^2)	Deviator Stress (kPa)	Maximum Stress (kPa)	Stress Ratio	Normalized Stress
10	148	1120	-22	-0.02	0.064	84.20	56.02	157.37	1.55	0.55
15	225	1149	-51	-0.04	0.127	84.27	96.63	197.98	1.95	0.95
20	293	1184	-86	-0.08	0.191	84.35	132.41	233.76	2.31	1.31
25	350	1218	-120	-0.10	0.255	84.43	162.32	263.67	2.60	1.60
30	400	1250	-152	-0.13	0.318	84.51	188.50	289.85	2.86	1.86
35	436	1275	-177	-0.15	0.382	84.58	207.28	308.63	3.05	2.05
40	481	1302	-204	-0.18	0.446	84.66	230.75	332.10	3.28	2.28
45	518	1325	-227	-0.20	0.510	84.73	249.99	351.34	3.47	2.47
50	551	1351	-253	-0.22	0.573	84.80	267.09	368.44	3.64	2.64
55	590	1370	-272	-0.24	0.637	84.87	287.32	388.67	3.83	2.83
60	623	1389	-291	-0.25	0.701	84.94	304.38	405.73	4.00	3.00
70	685	1418	-320	-0.28	0.828	85.07	336.34	437.69	4.32	3.32
80	741	1440	-342	-0.30	0.955	85.20	365.09	466.44	4.60	3.60
90	793	1455	-357	-0.31	1.083	85.32	391.70	493.05	4.86	3.86
95	821	1462	-364	-0.32	1.146	85.38	406.01	507.36	5.01	4.01
100	843	1466	-368	-0.32	1.210	85.43	417.20	518.55	5.12	4.12
95	483	1470	-372	-0.33	1.146	85.38	229.83	331.18	3.27	2.27
90	237	1484	-386	-0.34	1.083	85.34	101.68	203.03	2.00	1.00
85	100	1505	-407	-0.36	1.019	85.30	30.26	131.61	1.30	0.30
84	85	1511	-413	-0.36	1.006	85.29	22.43	123.78	1.22	0.22
82	52	1522	-424	-0.37	0.981	85.28	5.22	106.57	1.05	0.05
81	47	1533	-435	-0.38	0.968	85.28	2.61	103.96	1.03	0.03

Displacement (1/1000 inch)	Force (lb)	Meter Reading	Volume Change	Volume Strain (%)	Axial Strain (%)	Corrected Area (cm <sup>2</sup> )	Deviator Stress (kPa)	Maximum Stress (kPa)	Stress Ratio	Normalized Stress
80	37	1546	-448	-0.39	0.955	85.27	-2.61	98.74	0.97	-0.03
85	188	1562	-464	-0.41	1.019	85.34	76.13	177.48	1.75	0.75
87	265	1567	-469	-0.41	1.045	85.37	116.24	217.59	2.15	1.15
90	370	1577	-479	-0.42	1.083	85.41	170.89	272.24	2.69	1.69
95	565	1574	-476	-0.42	1.146	85.46	272.32	373.67	3.69	2.69
98	691	1573	-475	-0.42	1.185	85.49	337.80	439.15	4.33	3.33
100	746	1572	-474	-0.41	1.210	85.51	366.34	467.69	4.61	3.61
105	846	1571	-473	-0.41	1.274	85.57	418.11	519.46	5.13	4.13
110	895	1570	-472	-0.41	1.338	85.62	443.30	544.65	5.37	4.37
115	925	1566	-468	-0.41	1.401	85.68	458.62	559.97	5.53	4.53
125	971	1553	-455	-0.40	1.529	85.78	481.94	583.29	5.76	4.76
135	1000	1542	-444	-0.39	1.656	85.88	496.39	597.74	5.90	4.90
145	1034	1524	-426	-0.37	1.783	85.98	513.42	614.77	6.07	5.07
155	1059	1507	-409	-0.36	1.911	86.08	525.75	627.10	6.19	5.19
165	1100	1486	-388	-0.34	2.038	86.17	546.34	647.69	6.39	5.39
180	1147	1443	-345	-0.30	2.229	86.31	569.71	671.06	6.62	5.62
190	1177	1408	-310	-0.27	2.357	86.39	584.59	685.94	6.77	5.77
200	1200	1374	-276	-0.24	2.484	86.48	595.84	697.19	6.88	5.88
210	1222	1340	-242	-0.21	2.611	86.57	606.54	707.89	6.98	5.98
235	1282	1247	-149	-0.13	2.930	86.78	635.82	737.17	7.27	6.27
260	1323	1135	-37	-0.03	3.248	86.98	655.33	756.68	7.47	6.47
285	1355	1015	83	0.07	3.567	87.18	670.19	771.54	7.61	6.61
310	1380	887	211	0.18	3.885	87.37	681.46	782.81	7.72	6.72
335	1403	742	356	0.31	4.204	87.55	691.76	793.11	7.83	6.83
360	1429	580	518	0.45	4.522	87.72	703.63	804.98	7.94	6.94
385	1448	429	669	0.59	4.841	87.89	711.83	813.18	8.02	7.02
410	1446	270	828	0.72	5.159	88.06	709.43	810.78	8.00	7.00
435	1473	112	986	0.86	5.478	88.24	721.65	823.00	8.12	7.12
460	1476	-19	1117	0.98	5.796	88.43	721.56	822.91	8.12	7.12
485	1488	-120	1218	1.07	6.115	88.65	725.79	827.14	8.16	7.16
510	1488	-163	1261	1.10	6.433	88.92	723.60	824.95	8.14	7.14
535	1475	-183	1281	1.12	6.752	89.21	714.78	816.13	8.05	7.05
560	1458	-175	1273	1.11	7.070	89.52	703.84	805.19	7.94	6.94
585	1462	-110	1208	1.06	7.389	89.88	703.01	804.36	7.94	6.94
610	1433	21	1077	0.94	7.707	90.30	685.49	786.84	7.76	6.76
635	1427	287	811	0.71	8.025	90.82	678.58	779.93	7.70	6.70
660	1413	632	466	0.41	8.344	91.41	667.37	768.72	7.58	6.58

The unloading modulus of gravel can be obtained from the unloading-reloading cycle of the following figure: 137 MPa

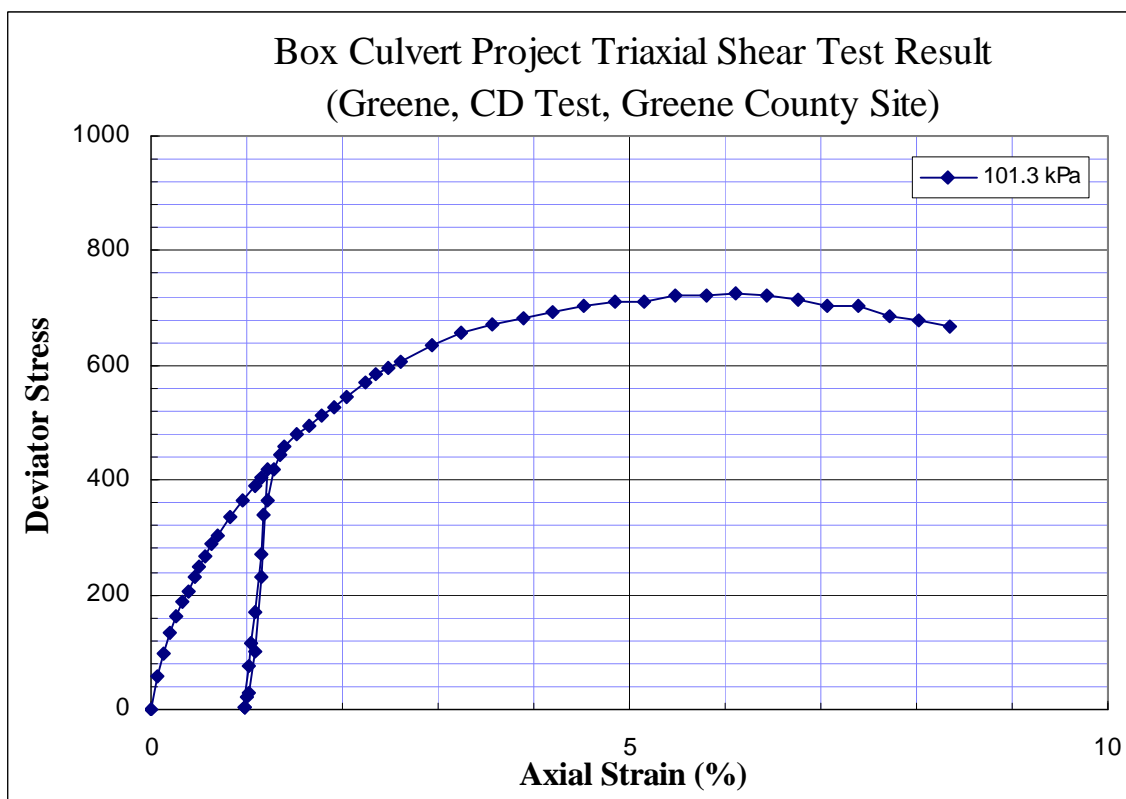


Figure D-14 Triaxial Shear Test Results- Gravel  
(100 mm Sample Diameter, 101.3 kPa Confining Pressure)

## Box Culvert Project: Triaxial Shear Test

Sample: <b>Gravel</b>	Date Tested: 1/16/1998
Sample No. 5	Type of Test: Consolidated Drained
Diameter:(mm) 101.92 101.6 102.87 Average Diameter (mm): 102.0	Initial Area(mm <sup>2</sup> ): 8171
Height(mm): 193.04 195.58 195.58 Average Sample Height (mm): 194.7	Initial Volume(mm <sup>3</sup> ): 1591.15E-3
Initial Density (kN/m <sup>3</sup> ): 19.90	
Net Confining Pressure: 275.8 kPa Back Pressure: 193.06 kPa	

Displacement (1/000 inch)	Force (lb)	Meter Reading	Volume Change	Volume Strain (%)	Axial Strain (%)	Corrected Area (cm <sup>2</sup> )	Deviator Stress (kPa)	Maximum Stress (kPa)	Stress Ratio	Normalized Stress
150	77	257	0	0.00	0.000	81.71	0.00	275.80	1.00	0.00
152	98	253	-4	0.00	0.026	81.73	11.43	287.23	1.04	0.04
154	172	234	-23	-0.02	0.052	81.77	51.70	327.50	1.19	0.19
156	222	224	-33	-0.03	0.078	81.80	78.88	354.68	1.29	0.29
158	275	208	-49	-0.05	0.104	81.83	107.67	383.47	1.39	0.39
160	303	190	-67	-0.06	0.130	81.87	122.84	398.64	1.45	0.45
162	345	175	-82	-0.08	0.157	81.90	145.61	421.41	1.53	0.53
164	377	148	-109	-0.10	0.183	81.94	162.91	438.71	1.59	0.59
166	407	127	-130	-0.12	0.209	81.98	179.12	454.92	1.65	0.65
168	436	110	-147	-0.14	0.235	82.01	194.78	470.58	1.71	0.71
170	476	192	-65	-0.06	0.261	81.97	216.60	492.40	1.79	0.79
175	555	40	-217	-0.20	0.326	82.14	258.94	534.74	1.94	0.94
180	606	4	-253	-0.23	0.391	82.22	286.29	562.09	2.04	1.04
185	670	-41	-298	-0.28	0.457	82.31	320.58	596.38	2.16	1.16
190	735	-91	-348	-0.32	0.522	82.40	355.32	631.12	2.29	1.29
195	750	-138	-395	-0.37	0.587	82.49	363.03	638.83	2.32	1.32
200	810	-189	-446	-0.41	0.652	82.59	394.95	670.75	2.43	1.43
205	865	-229	-486	-0.45	0.717	82.67	424.15	699.95	2.54	1.54
210	928	-265	-522	-0.48	0.783	82.75	457.60	733.40	2.66	1.66
215	978	-301	-558	-0.52	0.848	82.83	484.01	759.81	2.75	1.75
220	1037	-337	-594	-0.55	0.913	82.92	515.19	790.99	2.87	1.87
230	1100	-421	-678	-0.63	1.043	83.09	547.86	823.66	2.99	1.99
235	1157	-446	-703	-0.65	1.109	83.16	577.87	853.67	3.10	2.10
240	1212	-474	-731	-0.68	1.174	83.24	606.74	882.54	3.20	2.20
245	1257	-504	-761	-0.71	1.239	83.32	630.20	906.00	3.29	2.29
250	1305	-536	-793	-0.74	1.304	83.40	655.21	931.01	3.38	2.38
255	1333	-560	-817	-0.76	1.370	83.47	669.56	945.36	3.43	2.43
260	1382	-587	-844	-0.78	1.435	83.55	695.05	970.85	3.52	2.52
265	1423	-614	-871	-0.81	1.500	83.62	716.24	992.04	3.60	2.60
270	1450	-645	-902	-0.84	1.565	83.70	729.91	1005.71	3.65	2.65
275	1515	-662	-919	-0.85	1.630	83.77	763.84	1039.64	3.77	2.77
280	1537	-687	-944	-0.88	1.696	83.85	774.83	1050.63	3.81	2.81
285	1563	-711	-968	-0.90	1.761	83.92	787.93	1063.73	3.86	2.86

Displacement (1/000 inch)	Force (lb)	Meter Reading	Volume Change	Volume Strain (%)	Axial Strain (%)	Corrected Area (cm^2)	Deviator Stress (kPa)	Maximum Stress (kPa)	Stress Ratio	Normalized Stress
290	1590	-727	-984	-0.91	1.826	83.99	801.60	1077.40	3.91	2.91
295	1647	-748	-1005	-0.93	1.891	84.06	831.09	1106.89	4.01	3.01
300	1660	-765	-1022	-0.95	1.957	84.13	837.28	1113.08	4.04	3.04
316	1743	-806	-1063	-0.99	2.165	84.34	878.97	1154.77	4.19	3.19
320	1808	-832	-1089	-1.01	2.217	84.41	912.56	1188.36	4.31	3.31
330	1863	-857	-1114	-1.03	2.348	84.54	940.09	1215.89	4.41	3.41
340	1933	-880	-1137	-1.06	2.478	84.67	975.42	1251.22	4.54	3.54
350	2003	-901	-1158	-1.08	2.609	84.80	1010.66	1286.46	4.66	3.66
360	2058	-917	-1174	-1.09	2.739	84.93	1037.98	1313.78	4.76	3.76
370	2093	-934	-1191	-1.11	2.870	85.05	1054.73	1330.53	4.82	3.82
380	2146	-949	-1206	-1.12	3.000	85.18	1080.86	1356.66	4.92	3.92
390	2175	-965	-1222	-1.13	3.130	85.31	1094.37	1370.17	4.97	3.97
400	2236	-973	-1230	-1.14	3.261	85.43	1124.59	1400.39	5.08	4.08
410	2286	-980	-1237	-1.15	3.391	85.55	1149.01	1424.81	5.17	4.17
420	2310	-983	-1240	-1.15	3.522	85.67	1159.90	1435.70	5.21	4.21
430	2361	-983	-1240	-1.15	3.652	85.78	1184.78	1460.58	5.30	4.30
440	2400	-981	-1238	-1.15	3.783	85.90	1203.41	1479.21	5.36	4.36
450	2426	-978	-1235	-1.15	3.913	86.01	1215.26	1491.06	5.41	4.41
460	2466	-971	-1228	-1.14	4.043	86.12	1234.35	1510.15	5.48	4.48
470	2508	-963	-1220	-1.13	4.174	86.23	1254.44	1530.24	5.55	4.55
480	2526	-953	-1210	-1.12	4.304	86.34	1262.12	1537.92	5.58	4.58
490	2566	-943	-1200	-1.11	4.435	86.45	1281.11	1556.91	5.65	4.65
500	2598	-931	-1188	-1.10	4.565	86.56	1295.95	1571.75	5.70	4.70
510	2618	-918	-1175	-1.09	4.696	86.67	1304.60	1580.40	5.73	4.73
520	2653	-903	-1160	-1.08	4.826	86.78	1320.94	1596.74	5.79	4.79
530	2686	-882	-1139	-1.06	4.957	86.88	1336.29	1612.09	5.85	4.85
540	2713	-863	-1120	-1.04	5.087	86.98	1348.50	1624.30	5.89	4.89
550	2718	-843	-1100	-1.02	5.217	87.09	1349.45	1625.25	5.89	4.89
560	2755	-822	-1079	-1.00	5.348	87.19	1366.74	1642.54	5.96	4.96
570	2740	-796	-1053	-0.98	5.478	87.29	1357.53	1633.33	5.92	4.92
580	2770	-769	-1026	-0.95	5.609	87.39	1371.27	1647.07	5.97	4.97
590	2786	-747	-1004	-0.93	5.739	87.49	1377.79	1653.59	6.00	5.00
600	2815	-719	-976	-0.91	5.870	87.59	1390.97	1666.77	6.04	5.04
610	2833	-687	-944	-0.88	6.000	87.69	1398.59	1674.39	6.07	5.07
620	2856	-660	-917	-0.85	6.130	87.79	1408.65	1684.45	6.11	5.11
630	2843	-626	-883	-0.82	6.261	87.88	1400.55	1676.35	6.08	5.08
640	2858	-598	-855	-0.79	6.391	87.98	1406.55	1682.35	6.10	5.10
650	2881	-569	-826	-0.77	6.522	88.08	1416.59	1692.39	6.14	5.14
660	2895	-533	-790	-0.73	6.652	88.17	1422.15	1697.95	6.16	5.16
670	2900	-497	-754	-0.70	6.783	88.27	1423.15	1698.95	6.16	5.16
680	2905	-465	-722	-0.67	6.913	88.37	1424.10	1699.90	6.16	5.16
700	2921	-399	-656	-0.61	7.174	88.56	1429.01	1704.81	6.18	5.18
720	2966	-324	-581	-0.54	7.435	88.75	1448.54	1724.34	6.25	5.25
740	2978	-250	-507	-0.47	7.696	88.94	1451.45	1727.25	6.26	5.26
760	3009	-171	-428	-0.40	7.957	89.12	1463.88	1739.68	6.31	5.31



780	3023	-105	-362	-0.34	8.217	89.32	1467.60	1743.40	6.32	5.32
Displacement (1/1000 inch)	Force (lb)	Meter Reading	Volume Change	Volume Strain (%)	Axial Strain (%)	Corrected Area (cm <sup>2</sup> )	Deviator Stress (kPa)	Maximum Stress (kPa)	Stress Ratio	Normalized Stress
800	3024	-33	-290	-0.27	8.478	89.52	1464.90	1740.70	6.31	5.31
820	3029	37	-220	-0.20	8.739	89.72	1464.15	1739.95	6.31	5.31
840	3040	116	-141	-0.13	9.000	89.91	1466.48	1742.28	6.32	5.32
860	3051	183	-74	-0.07	9.261	90.11	1468.62	1744.42	6.32	5.32
880	3054	265	8	0.01	9.522	90.30	1466.99	1742.79	6.32	5.32
900	3074	334	77	0.07	9.783	90.50	1473.53	1749.33	6.34	5.34
920	3125	415	158	0.15	10.043	90.70	1495.40	1771.20	6.42	5.42
940	3100	490	233	0.22	10.304	90.90	1479.86	1755.66	6.37	5.37
960	3113	556	299	0.28	10.565	91.11	1482.82	1758.62	6.38	5.38
980	3078	622	365	0.34	10.826	91.32	1462.35	1738.15	6.30	5.30
1000	3063	700	443	0.41	11.087	91.52	1451.83	1727.63	6.26	5.26
1020	3053	770	513	0.48	11.348	91.73	1443.67	1719.47	6.23	5.23
1040	3056	856	599	0.56	11.609	91.93	1442.03	1717.83	6.23	5.23
1060	3074	921	664	0.62	11.870	92.14	1447.34	1723.14	6.25	5.25
1080	3076	981	724	0.67	12.130	92.36	1444.83	1720.63	6.24	5.24
1100	3054	1051	794	0.74	12.391	92.58	1430.91	1706.71	6.19	5.19
1120	3074	1122	865	0.80	12.652	92.79	1437.18	1712.98	6.21	5.21
1140	3064	1183	926	0.86	12.913	93.02	1428.93	1704.73	6.18	5.18
1160	3059	1238	981	0.91	13.174	93.25	1422.99	1698.79	6.16	5.16
1180	3038	1275	1018	0.95	13.435	93.50	1409.22	1685.02	6.11	5.11

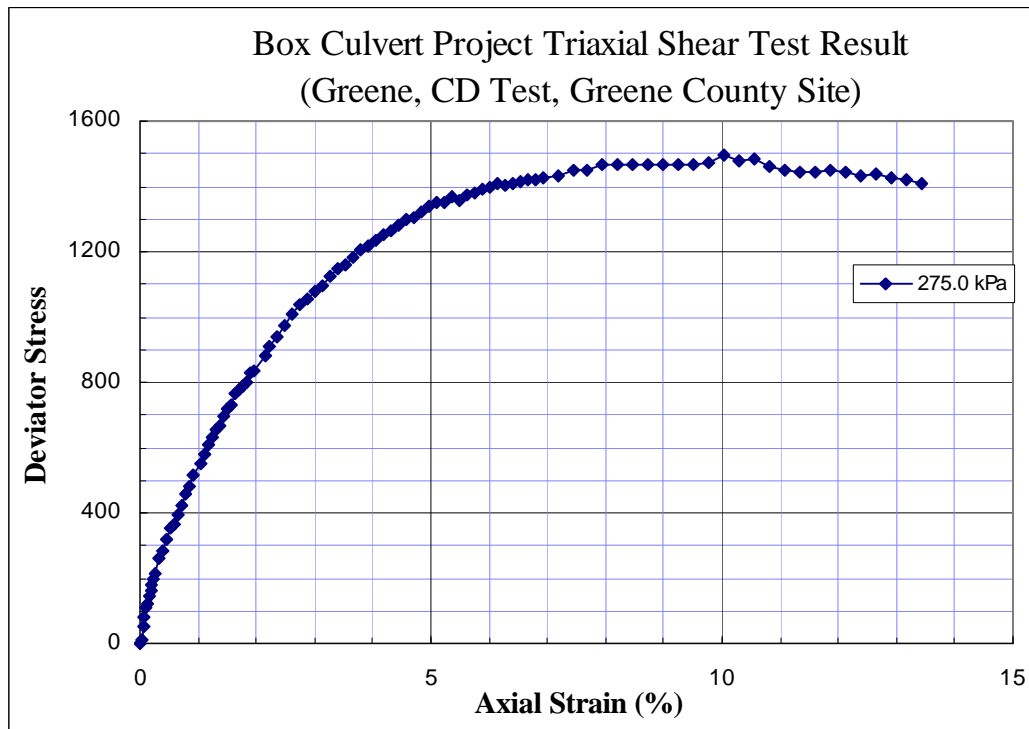


Figure D-15 Triaxial Shear Test Results- Gravel  
(100 mm Sample Diameter, 275 kPa Confining Pressure)

The secant modulus  $E_s$  is defined as the slope between the original point and the point at the half of the failure stress (Lamb and Whitman, 1979)

The secant modulus of the gravel at different condition are:

Gravel at Different Confining Pressure (kPa)	Secant Modulus at Half of Failure Stress (MPa)
69	37
103	44
137	33
275	47

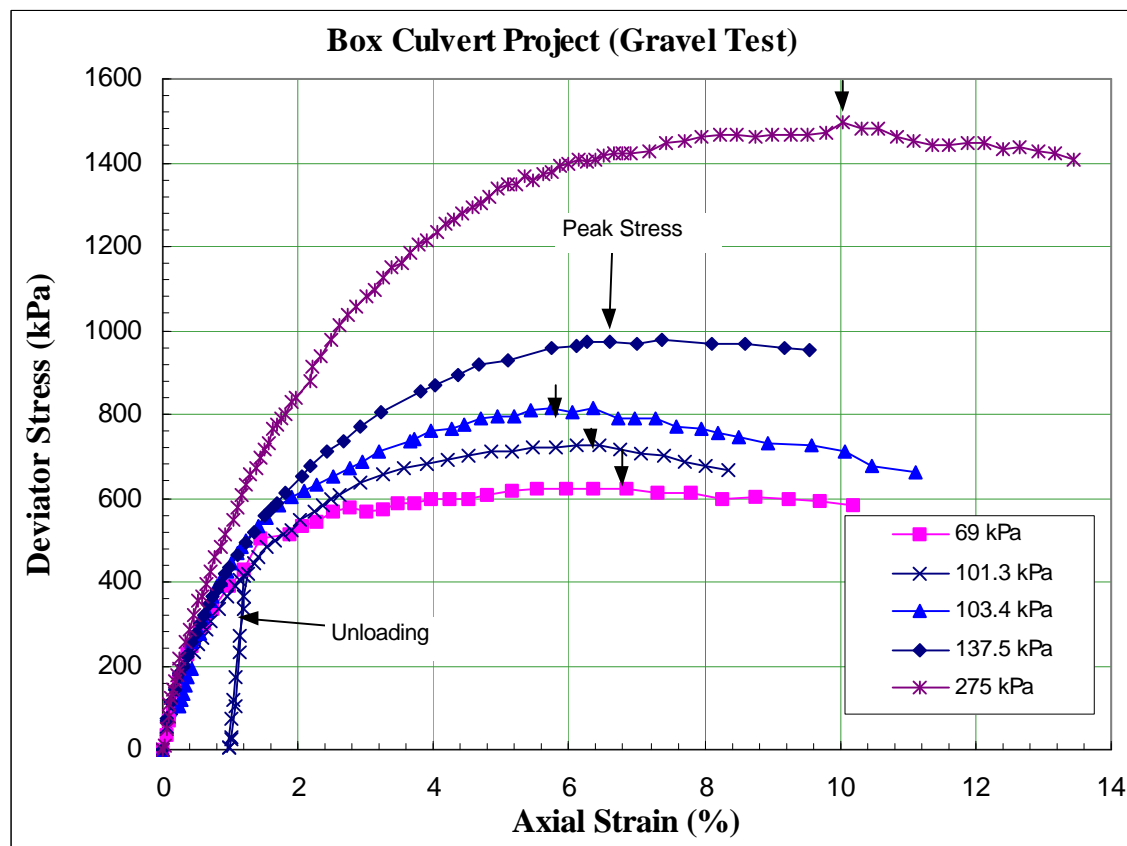


Figure D-16 Summary of Gravel Triaxial Shear Test Results: Deviator Stress (Greene County Culvert Site, 100 mm Sample Diameter)

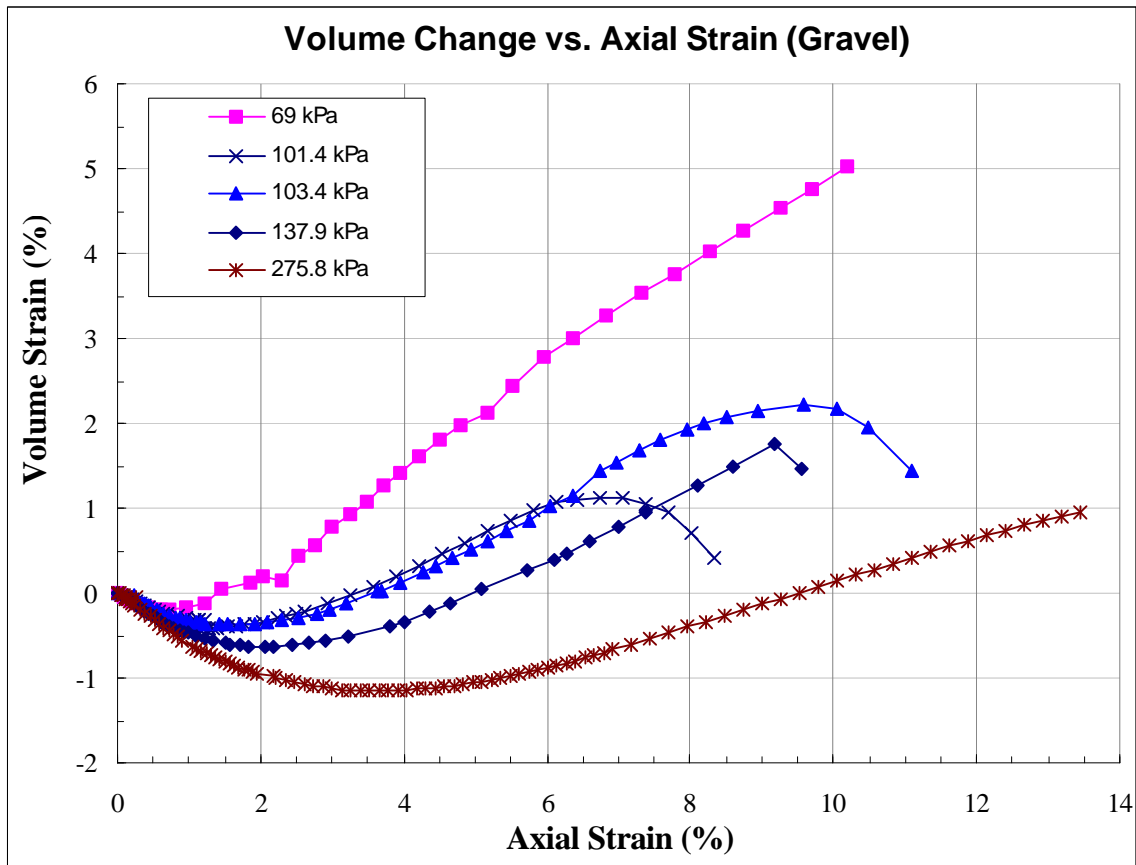


Figure D-17 Summary of Gravel Triaxial Test Results: Volume Change  
(Greene County Culvert Site: 100 mm Sample Diameter)

The strength can be obtained from the following peak stress state:

Two sets of strength can be obtained:

**Cohesion = 0 kPa Angle of Internal Friction  $\phi = 49^\circ$**

or

**Cohesion = 54 kPa Angle of Internal Friction  $\phi = 43^\circ$**

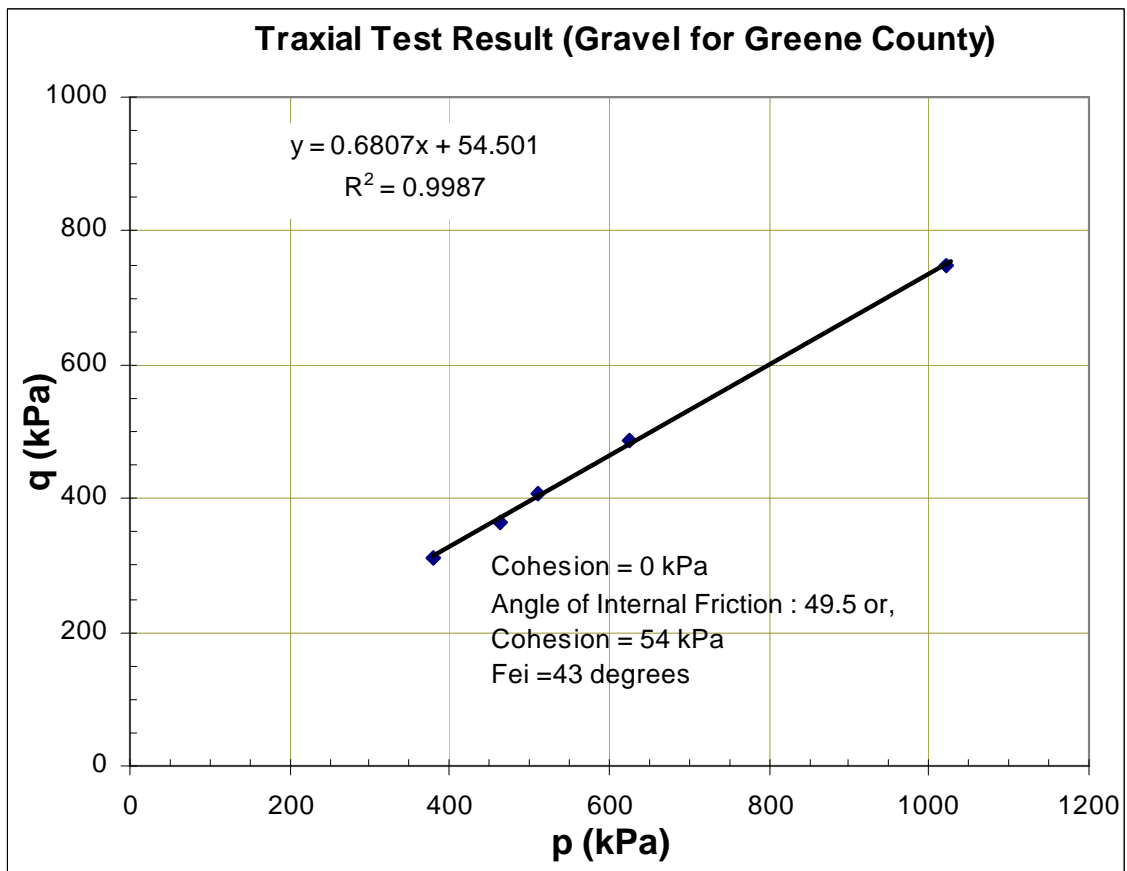


Figure D-18 Peak Strength in  $p$ - $q$  Plane

The initial modulus used in Chapter 10 can be obtained graphically from the following figure: The inverse of the interception at y axis.

Gravel at Different Confining Stress (kPa)	Initial Modulus $E_i$ Based on Hyperbolic Model (MPa)
69	56
103	63
137	67
275	77

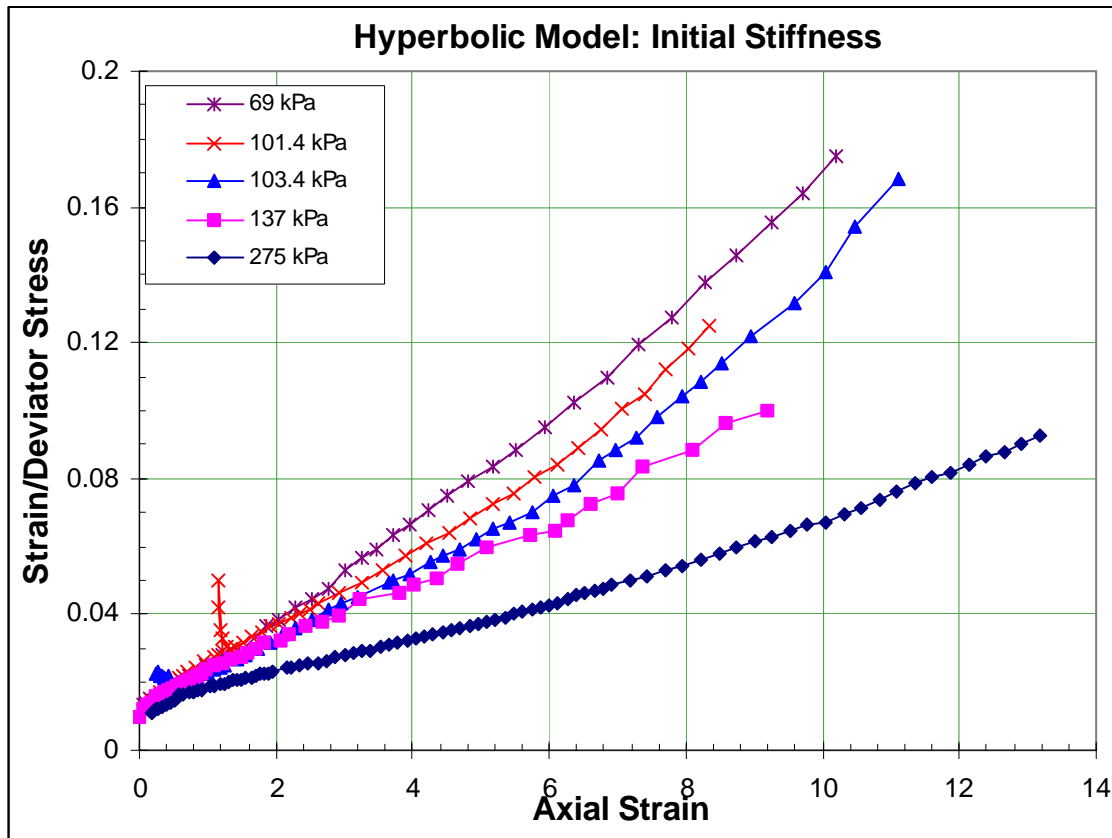


Figure D-19 Summary of Gravel Triaxial Test Results: Initial Modulus  
(Greene County Culvert Site: 100 mm Sample Diameter)

## Appendix D-3

### Triaxial Shear Test Results - Silty Clay

Table D-3 Undisturbed Silty Clay (Soil beneath the culvert bottom slab) CD Test

Sample Number	Back Pressure (kPa)	Net Confining Pressure (kPa)	Measured Density (kN/m <sup>3</sup> )	Moisture Content (%)
No. 1	205	89.6	18.38	20.48
No. 2	205	179.9	19.86	23.36
No. 3	205	301.3	20.12	23.36
No.4	205	432.6	20.16	20.48

Note: sample diameter: 50.8 mm; hydrocompression tests at 301.3 and 432.6 kPa confining pressures (Greene County culvert site).

Strength:

Cohesion  $c = 36$  kPa Angle of internal friction =  $29^\circ$

### Box Culvert Project: Triaxial Shear Test

Sample: <b>Soil Underneath Culvert</b> (Silty Clay)					Date Tested:	10/8/1996
Sample No. 1					Type of Test: Consolidated Drained	
Diameter:(mm)	50.7	50.87	50.87	Average Diameter (mm): 50.8	Initial Area(mm^2):	2029
Height(mm):	96.53	96.46	97.54	Average Sample Height (mm): 96.8	Initial Volume(cm^3):	196.50
Net Confining Pressure: 89.6 kPa			Back Pressure:	204.96 kPa		
Sample Weight(g): 368.2						
Moisture Content:(1)					Moisture Content:(2)	
Aluminum Box No.:		208			Aluminum Box No.:	5
Box Weight(g):		13.9			Box Weight:	19
Wet Soil+ Box Weight:(g)		29.1			Wet Soil+ Box Weight:	
41.2						
Dry Soil+Box Weight:(g)		26.4			Dry Soil+Box Weight:	37.6
Moisture Content:(%)		21.6			Moisture Content:	19.35
Averaged Moisture Content:(%) 20.48					Initial Density (KN/M^3):	18.38

### Triaxial Shear Results

Displacement	Force (lb)	Meter Reading	Volume Change	Volume Strain (%)	Axial Strain (%)	Corrected Area(cm^2)	Deviator Stress (kPa)	Max. Stress (kPa)	Stress Ratio	Normalized Stress
346	13	-228	0	0.00	0.000	20.014	0.00	94.46	1.00	0.00
347	16	-227	1	0.01	0.026	20.018	6.67	101.13	1.07	0.07
348	19	-227	1	0.01	0.052	20.023	13.33	107.79	1.14	0.14
349	21	-227	1	0.01	0.079	20.028	17.77	112.23	1.19	0.19
350	22	-227	1	0.01	0.105	20.034	19.99	114.45	1.21	0.21
351	28	-226	2	0.02	0.131	20.037	33.31	127.77	1.35	0.35
353	33	-224	4	0.03	0.184	20.045	44.40	138.86	1.47	0.47
355	36	-223	5	0.04	0.236	20.054	51.04	145.50	1.54	0.54
357	38	-221	7	0.05	0.289	20.061	55.45	149.91	1.59	0.59
358	41	-220	8	0.06	0.315	20.065	62.10	156.56	1.66	0.66
360	43	-218	10	0.08	0.367	20.073	66.51	160.97	1.70	0.70
362	45	-217	11	0.08	0.420	20.082	70.91	165.37	1.75	0.75
364	46	-215	13	0.10	0.472	20.089	73.10	167.56	1.77	0.77
366	48	-213	15	0.11	0.525	20.097	77.50	171.96	1.82	0.82
369	51	-211	17	0.13	0.603	20.110	84.09	178.55	1.89	0.89
372	54	-207	21	0.16	0.682	20.119	90.68	185.14	1.96	0.96
374	55	-206	22	0.17	0.734	20.128	92.85	187.31	1.98	0.98
376	56	-204	24	0.18	0.787	20.136	95.02	189.48	2.01	1.01
378	58	-203	25	0.19	0.839	20.145	99.40	193.86	2.05	1.05
380	60	-201	27	0.20	0.892	20.153	103.78	198.24	2.10	1.10
383	61	-198	30	0.23	0.970	20.164	105.93	200.39	2.12	1.12

Displacement	Force (lb)	Meter Reading	Volume Change	Volume Strain (%)	Axial Strain (%)	Corrected Area(cm^2)	Deviator Stress (kPaa)	Max. Stress (kPa)	Stress Ratio	Normalized Stress
385	63	-196	32	0.24	1.023	20.172	110.30	204.76	2.17	1.17
388	64	-194	34	0.26	1.102	20.185	112.43	206.89	2.19	1.19
390	66	-192	36	0.27	1.154	20.192	116.80	211.26	2.24	1.24
392	67	-192	36	0.27	1.206	20.203	118.94	213.40	2.26	1.26
395	69	-189	39	0.29	1.285	20.215	123.27	217.73	2.31	1.31
398	71	-186	42	0.32	1.364	20.226	127.60	222.06	2.35	1.35
400	73	-185	43	0.32	1.416	20.235	131.94	226.40	2.40	1.40
403	73	-183	45	0.34	1.495	20.248	131.86	226.32	2.40	1.40
405	75	-181	47	0.35	1.547	20.256	136.20	230.66	2.44	1.44
407	76	-180	48	0.36	1.600	20.265	138.33	232.79	2.46	1.46
410	78	-178	50	0.38	1.679	20.278	142.63	237.09	2.51	1.51
412	79	-177	51	0.38	1.731	20.288	144.76	239.22	2.53	1.53
414	80	-176	52	0.39	1.783	20.297	146.89	241.35	2.56	1.56
416	81	-174	54	0.41	1.836	20.305	149.02	243.48	2.58	1.58
418	82	-173	55	0.41	1.888	20.314	151.15	245.61	2.60	1.60
421	83	-171	57	0.43	1.967	20.327	153.24	247.70	2.62	1.62
425	85	-169	59	0.44	2.072	20.346	157.47	251.93	2.67	1.67
430	87	-166	62	0.47	2.203	20.368	161.67	256.13	2.71	1.71
438	91	-161	67	0.50	2.413	20.404	170.10	264.56	2.80	1.80
446	95	-156	72	0.54	2.623	20.441	178.51	272.97	2.89	1.89
455	98	-152	76	0.57	2.859	20.484	184.65	279.11	2.95	1.95
461	100	-150	78	0.59	3.016	20.514	188.72	283.18	3.00	2.00
465	102	-148	80	0.60	3.121	20.533	192.88	287.34	3.04	2.04
474	105	-145	83	0.62	3.357	20.578	198.94	293.40	3.11	2.11
484	109	-141	87	0.65	3.619	20.628	207.09	301.55	3.19	2.19
496	112	-136	92	0.69	3.934	20.688	212.94	307.40	3.25	2.25
506	115	-133	95	0.71	4.196	20.740	218.85	313.31	3.32	2.32
515	118	-131	97	0.73	4.433	20.788	224.76	319.22	3.38	2.38
526	121	-128	100	0.75	4.721	20.846	230.54	325.00	3.44	2.44
536	124	-126	102	0.77	4.983	20.900	236.33	330.79	3.50	2.50
545	125	-125	103	0.77	5.219	20.951	237.88	332.34	3.52	2.52
555	128	-124	104	0.78	5.482	21.007	243.60	338.06	3.58	2.58
566	129	-123	105	0.79	5.770	21.070	244.98	339.44	3.59	2.59
575	131	-122	106	0.80	6.006	21.121	248.60	343.06	3.63	2.63
585	132	-121	107	0.80	6.268	21.179	250.03	344.49	3.65	2.65
595	134	-121	107	0.80	6.531	21.238	253.52	347.98	3.68	2.68
605	136	-121	107	0.80	6.793	21.298	256.99	351.45	3.72	2.72
615	137	-121	107	0.80	7.055	21.358	258.35	352.81	3.74	2.74
625	138	-121	107	0.80	7.318	21.418	259.70	354.16	3.75	2.75
635	140	-121	107	0.80	7.580	21.479	263.11	357.57	3.79	2.79
645	141	-121	107	0.80	7.842	21.540	264.42	358.88	3.80	2.80
655	142	-122	106	0.80	8.104	21.603	265.71	360.17	3.81	2.81
665	143	-123	105	0.79	8.367	21.667	266.99	361.45	3.83	2.83
675	144	-124	104	0.78	8.629	21.731	268.25	362.71	3.84	2.84
685	145	-125	103	0.77	8.891	21.795	269.50	363.96	3.85	2.85



Displacement	Force (lb)	Meter Reading	Volume Change	Volume Strain (%)	Axial Strain (%)	Corrected Area(cm^2)	Deviator Stress (kPaa)	Max. Stress (kPa)	Stress Ratio	Normalized Stress
695	145	-126	102	0.77	9.154	21.860	268.70	363.16	3.84	2.84
705	145	-127	101	0.76	9.416	21.925	267.91	362.37	3.84	2.84
715	146	-128	100	0.75	9.678	21.990	269.14	363.60	3.85	2.85
725	146	-129	99	0.74	9.940	22.056	268.33	362.79	3.84	2.84
735	146	-130	98	0.74	10.203	22.122	267.53	361.99	3.83	2.83
745	147	-131	97	0.73	10.465	22.188	268.73	363.19	3.84	2.84
755	147	-132	96	0.72	10.727	22.255	267.93	362.39	3.84	2.84
765	147	-134	94	0.71	10.990	22.324	267.10	361.56	3.83	2.83
775	148	-135	93	0.70	11.252	22.392	268.28	362.74	3.84	2.84
785	148	-137	91	0.68	11.514	22.462	267.44	361.90	3.83	2.83
795	148	-138	90	0.68	11.776	22.530	266.63	361.09	3.82	2.82
805	149	-139	89	0.67	12.039	22.599	267.79	362.25	3.83	2.83

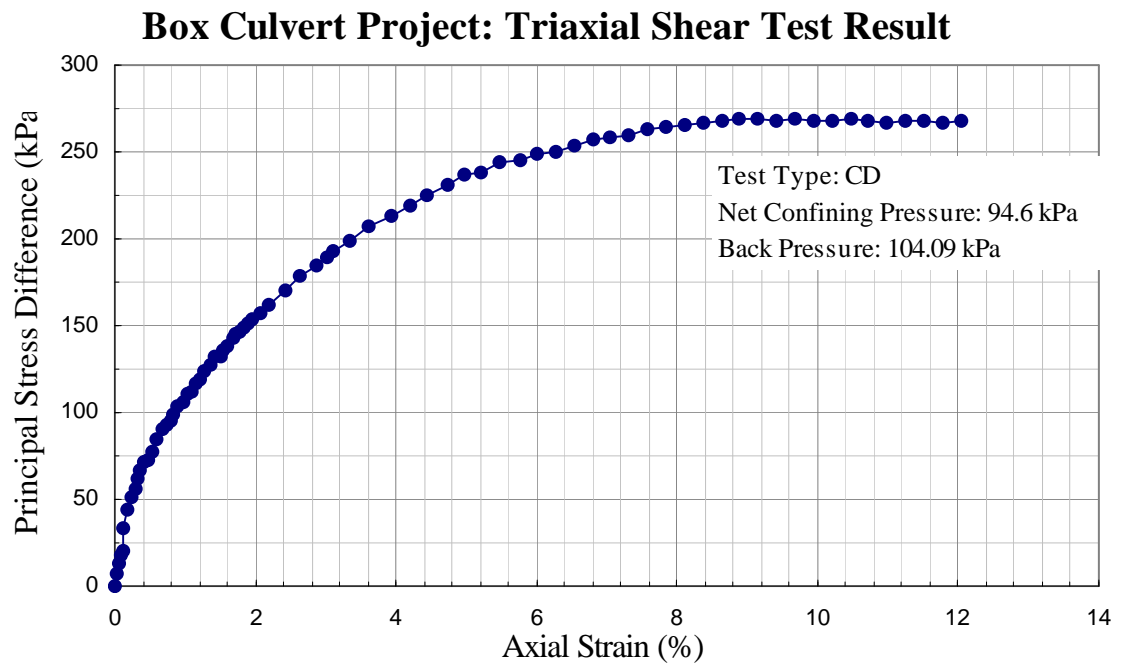


Figure D-20 Triaxial Shear Test Results- Silty Clay  
(50 mm Sample Diameter, 94.6 kPa Confining Pressure)

### Box Culvert Project: Triaxial Shear Test

Sample: <b>Soil Underneath Culvert</b> (Silty Clay)					Date Tested:	11/28/1996
Sample No. 2					Type of Test: Consolidated Drained	
Diameter:(mm)	50.52	50.72	50.33	Average Diameter (mm):	50.6	Initial Area(mm^2): 2009
Height(mm):	106.46	105.87	106.53	Average Sample Height (mm):	106.3	Initial Volume(cm^3):213.50
Net Confining Pressure: 179.9 kPa			Back Pressure:	204.96 kPa		
Sample Weight(g): 432.3						
Moisture Content:(1)					Moisture Content:(2)	
Aluminum Box No.:			10	Aluminum Box No.: 20		
Box Weight(g):			18.5	Box Weight: 15.9		
Wet Soil+ Box Weight:(g)			38.2	Wet Soil+ Box Weight: 30.3		
Dry Soil+Box Weight:(g)			32.9	Dry Soil+Box Weight: 29.0		
Moisture Content:(%)			36.8	Moisture Content: 9.92		
Averaged Moisture Content:(%)			23.36	Initial Density (KN/M^3): 19.86		

### Triaxial Shear Test

Displacement (1/1000 inch)	Force (lb)	Meter Reading	Volume Change	Volume Strain(%)	Axial Strain (%)	Corrected Area (cm^2)	Deviator Stress (kPa)	Max. Stress (KPa)	Stress Ratio	Normalized Stress
389	14	271	0	0.00	0.000	19.886	0.00	197.90	1.00	0.00
391	25	272	1	0.01	0.048	19.894	24.60	222.50	1.12	0.12
392	37	273	2	0.01	0.072	19.897	51.44	249.34	1.26	0.26
394	45	275	4	0.03	0.119	19.904	69.31	267.21	1.35	0.35
396	53	279	8	0.06	0.167	19.908	87.17	285.07	1.44	0.44
398	56	282	11	0.08	0.215	19.913	93.85	291.75	1.47	0.47
400	60	285	14	0.10	0.263	19.919	102.76	300.66	1.52	0.52
405	68	295	24	0.17	0.382	19.929	120.58	318.48	1.61	0.61
410	73	303	32	0.22	0.502	19.941	131.66	329.56	1.67	0.67
415	80	314	43	0.30	0.621	19.950	147.21	345.11	1.74	0.74
420	83	323	52	0.36	0.741	19.961	153.82	351.72	1.78	0.78
426	88	332	61	0.42	0.884	19.978	164.83	362.73	1.83	0.83
431	92	342	71	0.49	1.004	19.988	173.65	371.55	1.88	0.88
435	95	347	76	0.53	1.099	20.000	180.22	378.12	1.91	0.91
440	98	356	85	0.59	1.219	20.011	186.79	384.69	1.94	0.94
445	101	364	93	0.64	1.338	20.024	193.33	391.23	1.98	0.98
450	104	372	101	0.70	1.458	20.037	199.87	397.77	2.01	1.01
455	107	381	110	0.76	1.577	20.049	206.41	404.31	2.04	1.04
460	110	388	117	0.81	1.697	20.064	212.91	410.81	2.08	1.08
465	113	394	123	0.85	1.816	20.079	219.39	417.29	2.11	1.11
470	116	403	132	0.91	1.936	20.091	225.91	423.81	2.14	1.14
475	119	411	140	0.97	2.055	20.104	232.40	430.30	2.17	1.17

Displacement (1/1000 inch)	Force (lb)	Meter Reading	Volume Change	Volume Strain(%)	Axial Strain (%)	Corrected Area (cm^2)	Deviator Stress (kPa)	Max. Stress (KPa)	Stress Ratio	Normalized Stress
480	121	418	147	1.02	2.175	20.119	236.66	434.56	2.20	1.20
485	123	425	154	1.07	2.294	20.134	240.91	438.81	2.22	1.22
490	125	431	160	1.11	2.414	20.150	245.13	443.03	2.24	1.24
495	127	438	167	1.16	2.533	20.164	249.36	447.26	2.26	1.26
500	129	444	173	1.20	2.653	20.181	253.57	451.47	2.28	1.28
510	133	456	185	1.28	2.892	20.213	261.97	459.87	2.32	1.32
520	136	468	197	1.36	3.131	20.246	268.14	466.04	2.35	1.35
530	141	481	210	1.45	3.370	20.277	278.70	476.60	2.41	1.41
541	145	493	222	1.54	3.632	20.315	286.94	484.84	2.45	1.45
550	148	502	231	1.60	3.848	20.348	293.05	490.95	2.48	1.48
560	151	513	242	1.67	4.086	20.382	299.10	497.00	2.51	1.51
572	155	525	254	1.76	4.373	20.426	307.17	505.07	2.55	1.55
580	158	533	262	1.81	4.564	20.455	313.26	511.16	2.58	1.58
590	161	542	271	1.87	4.803	20.493	319.19	517.09	2.61	1.61
600	164	551	280	1.94	5.042	20.532	325.09	522.99	2.64	1.64
611	168	560	289	2.00	5.305	20.576	333.05	530.95	2.68	1.68
620	170	568	297	2.05	5.520	20.611	336.80	534.70	2.70	1.70
632	175	578	307	2.12	5.807	20.659	346.79	544.69	2.75	1.75
641	177	585	314	2.17	6.022	20.696	350.47	548.37	2.77	1.77
650	179	591	320	2.21	6.237	20.734	354.11	552.01	2.79	1.79
660	183	599	328	2.27	6.476	20.775	361.98	559.88	2.83	1.83
670	186	606	335	2.32	6.715	20.818	367.65	565.55	2.86	1.86
680	189	613	342	2.37	6.954	20.861	373.29	571.19	2.89	1.89
690	192	620	349	2.41	7.193	20.904	378.90	576.80	2.91	1.91
700	194	626	355	2.46	7.432	20.949	382.34	580.24	2.93	1.93
710	198	633	362	2.50	7.671	20.993	390.02	587.92	2.97	1.97
720	200	639	368	2.55	7.910	21.038	393.41	591.31	2.99	1.99
730	203	645	374	2.59	8.149	21.084	398.89	596.79	3.02	2.02
740	205	650	379	2.62	8.388	21.132	402.20	600.10	3.03	2.03
750	206	655	384	2.66	8.627	21.179	403.40	601.30	3.04	2.04
760	208	660	389	2.69	8.866	21.227	406.68	604.58	3.05	2.05
770	210	665	394	2.73	9.105	21.275	409.94	607.84	3.07	2.07
780	212	670	399	2.76	9.344	21.324	413.19	611.09	3.09	2.09
800	215	674	403	2.79	9.822	21.431	417.35	615.25	3.11	2.11
810	218	679	408	2.82	10.061	21.480	422.61	620.51	3.14	2.14
820	221	684	413	2.86	10.300	21.529	427.84	625.74	3.16	2.16
830	224	689	418	2.89	10.539	21.579	433.04	630.94	3.19	2.19
840	226	693	422	2.92	10.778	21.631	436.12	634.02	3.20	2.20
850	229	697	426	2.95	11.017	21.682	441.24	639.14	3.23	2.23
860	231	701	430	2.97	11.256	21.735	444.28	642.18	3.24	2.24
870	233	706	435	3.01	11.495	21.785	447.32	645.22	3.26	2.26
880	234	708	437	3.02	11.734	21.841	448.22	646.12	3.26	2.26
890	234	712	441	3.05	11.973	21.894	447.13	645.03	3.26	2.26
900	237	715	444	3.07	12.212	21.949	452.10	650.00	3.28	2.28
910	239	717	446	3.09	12.451	22.006	454.98	652.88	3.30	2.30
920	241	719	448	3.10	12.690	22.063	457.83	655.73	3.31	2.31
930	243	721	450	3.11	12.929	22.120	460.67	658.57	3.33	2.33
940	245	723	452	3.13	13.168	22.178	463.48	661.38	3.34	2.34

Displacement (1/1000 inch)	Force (lb)	Meter Reading	Volume Change	Volume Strain(%)	Axial Strain (%)	Corrected Area (cm^2)	Deviator Stress (kPa)	Max. Stress (KPa)	Stress Ratio	Normalized Stress
950	246	725	454	3.14	13.407	22.236	464.28	662.18	3.35	2.35
960	248	727	456	3.15	13.646	22.294	467.05	664.95	3.36	2.36
970	250	729	458	3.17	13.885	22.353	469.81	667.71	3.37	2.37
980	251	731	460	3.18	14.124	22.412	470.56	668.46	3.38	2.38
990	252	732	461	3.19	14.362	22.473	471.26	669.16	3.38	2.38
1000	254	733	462	3.20	14.601	22.534	473.93	671.83	3.39	2.39
1010	255	734	463	3.20	14.840	22.596	474.61	672.51	3.40	2.40
1020	256	735	464	3.21	15.079	22.657	475.28	673.18	3.40	2.40
1030	257	736	465	3.22	15.318	22.720	475.93	673.83	3.40	2.40
1040	258	737	466	3.22	15.557	22.782	476.58	674.48	3.41	2.41
1050	259	738	467	3.23	15.796	22.845	477.21	675.11	3.41	2.41
1060	260	739	468	3.24	16.035	22.909	477.83	675.73	3.41	2.41
1070	261	740	469	3.24	16.274	22.973	478.44	676.34	3.42	2.42
1080	262	741	470	3.25	16.513	23.037	479.04	676.94	3.42	2.42
1090	263	742	471	3.26	16.752	23.101	479.63	677.53	3.42	2.42
1100	263	743	472	3.27	16.991	23.166	478.29	676.19	3.42	2.42
1110	263	744	473	3.27	17.230	23.231	476.95	674.85	3.41	2.41
1120	265	745	474	3.28	17.469	23.297	479.43	677.33	3.42	2.42
1130	265	745	474	3.28	17.708	23.364	478.04	675.94	3.42	2.42
1140	266	746	475	3.29	17.947	23.431	478.58	676.48	3.42	2.42
1150	267	747	476	3.29	18.186	23.497	479.12	677.02	3.42	2.42
1160	269	748	477	3.30	18.425	23.565	481.53	679.43	3.43	2.43
1170	269	749	478	3.31	18.664	23.632	480.15	678.05	3.43	2.43
1180	270	749	478	3.31	18.903	23.702	480.62	678.52	3.43	2.43
1190	270	750	479	3.31	19.142	23.770	479.24	677.14	3.42	2.42

### Box Culvert Project: Triaxial Shear Test Result

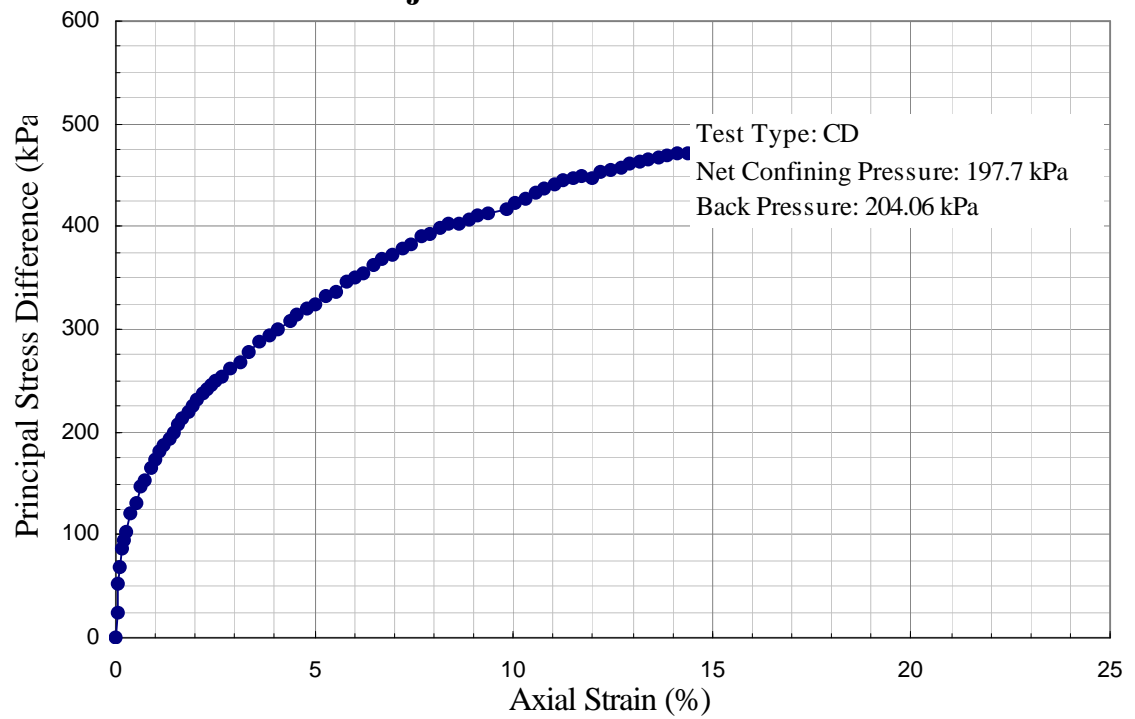


Figure D-21 Triaxial Shear Test Results- Silty Clay  
(50 mm Sample Diameter, 197.7 kPa Confining Pressure)

### Box Culvert Project: Triaxial Shear Test

Sample: <b>Soil Underneath Culvert</b> (Silty Clay)					Date Tested: 11/15/1996	
Sample No. 3					Type of Test: Consolidated Drained	
Diameter:(mm)	50.31	50.62	50.49	Average Diameter (mm):	50.5	Initial Area(mm^2): 2004
Height(mm):	105.52	104.45	105.15	Average Sample Height (mm):	105.2	Initial Volume(cm^3):210.80
Net Confining Pressure: 301.34 kPa					Back Pressure:	204.96 kPa
Sample Weight(g): 432.3						
Moisture Content:(1)					Moisture Content:(2)	
Aluminum Box No.:			10	Aluminum Box No.: 20		
Box Weight(g):			18.5	Box Weight: 15.9		
Wet Soil+ Box Weight:(g)			38.2	Wet Soil+ Box Weight: 30.3		
Dry Soil+Box Weight:(g)			32.9	Dry Soil+Box Weight: 29.0		
Moisture Content:(%)			36.8	Moisture Content: 9.92		
Averaged Moisture Content:(%)			23.36	Initial Density (KN/M^3): 20.12		

### Hydro-Static Compression Test

Date	Time	Cell Pressure (psi)	Back Pressure (psi)	Hydro-pressure (psi)	Meter Reading	Cell Pressure (kPa)	Back Pressure (psi)	Net Hydro-pressure (kPa)	Volume Change (ml)	Volume Strain (%)
7-Nov	9:30am	38.3	29.6	5	-47	264.08	204.09	34.48	0.443	0.21
8-Nov	9:30am	43.3	29.6	10	-13	298.55	204.09	68.95	0.945	0.45
9-Nov	9:30am	48.3	29.6	15	28	333.03	204.09	103.43	1.551	0.74
10-Nov	9:30am	53.3	29.6	20	72	367.50	204.09	137.90	2.201	1.04
11-Nov	9:am	43.3	29.6	10	57	298.55	204.09	68.95	1.979	0.94
11-Nov	9:pm	33.3	29.6	0	5	229.60	204.09	0.00	1.211	0.57
12-Nov	9:00am	43.3	29.6	10	53	298.55	204.09	68.95	1.920	0.91
12-Nov	9:00pm	53.3	29.6	20	85	367.50	204.09	137.90	2.393	1.14
13-Nov	9:00am	58.3	29.6	25	122	401.98	204.09	172.38	2.939	1.39
13-Nov	8:00pm	63.3	29.6	30	165	436.45	204.09	206.85	3.575	1.70
14-Nov	10:00am	68.3	29.6	35	207	470.93	204.09	241.33	4.195	1.99
15-Nov	10:00am	73.3	29.6	40	252	505.40	204.09	275.80	4.860	2.31

### Volume Strain under Hydropressure

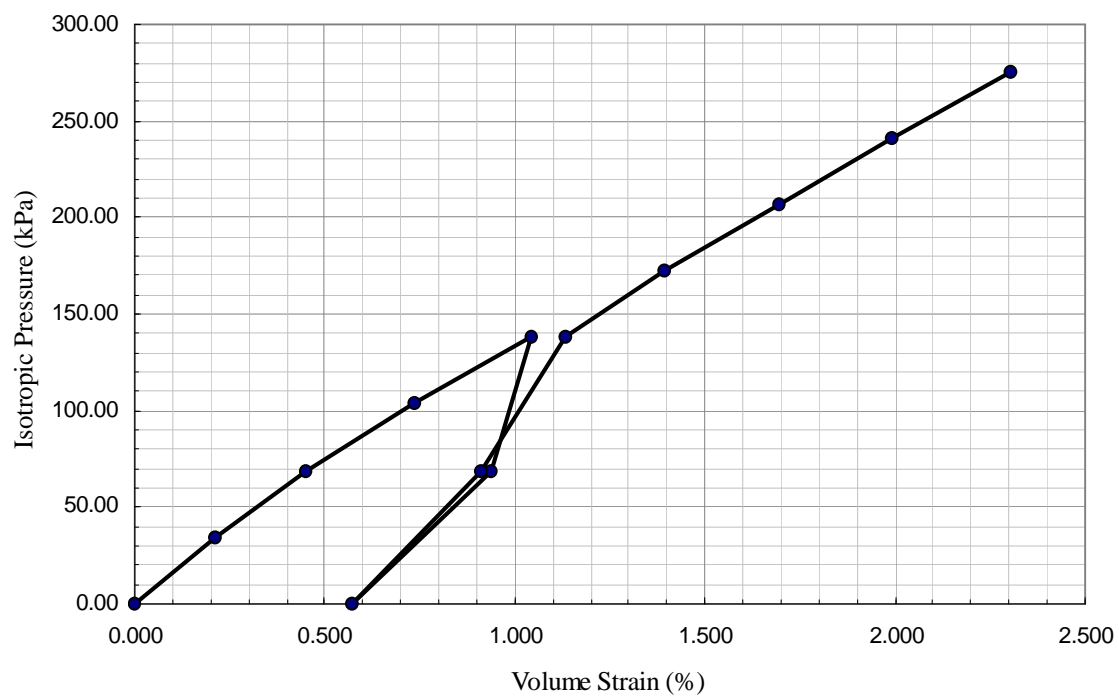


Figure D-22 Volume Strain Under Hydropressure

## Triaxial Shear Test

Displacement	Force (lb)	Meter Reading	Volume Change	Volume Strain (%)	Axial Strain (%)	Corrected Area (cm^2)	Deviator Stress (kPa)	Max. Stress (KPa)	Stress Ratio	Normalized Stress
226	19	254	0	0.00	0.000	19.573	0.00	301.31	1.00	0.00
228	22	254	0	0.00	0.048	19.582	6.82	308.13	1.02	0.02
230	44	256	2	0.01	0.097	19.589	56.79	358.10	1.19	0.19
231	48	257	3	0.02	0.121	19.592	65.87	367.18	1.22	0.22
231	52	258	4	0.03	0.121	19.591	74.96	376.27	1.25	0.25
232	58	261	7	0.05	0.145	19.591	88.58	389.89	1.29	0.29
234	63	266	12	0.08	0.193	19.594	99.93	401.24	1.33	0.33
237	69	274	20	0.14	0.266	19.597	113.53	414.84	1.38	0.38
240	73	282	28	0.20	0.338	19.600	122.60	423.91	1.41	0.41
243	77	290	36	0.25	0.410	19.603	131.66	432.97	1.44	0.44
247	83	299	45	0.32	0.507	19.609	145.23	446.54	1.48	0.48
250	86	306	52	0.36	0.579	19.613	152.01	453.32	1.50	0.50
253	89	310	56	0.39	0.652	19.622	158.74	460.05	1.53	0.53
256	91	316	62	0.43	0.724	19.628	163.23	464.54	1.54	0.54
259	95	323	69	0.48	0.797	19.632	172.26	473.57	1.57	0.57
262	99	332	78	0.55	0.869	19.634	181.31	482.62	1.60	0.60
265	102	338	84	0.59	0.942	19.640	188.05	489.36	1.62	0.62
268	104	344	90	0.63	1.014	19.646	192.53	493.84	1.64	0.64
271	109	352	98	0.69	1.087	19.649	203.82	505.13	1.68	0.68
274	112	360	106	0.74	1.159	19.652	210.58	511.89	1.70	0.70
282	115	369	115	0.81	1.352	19.677	217.09	518.40	1.72	0.72
285	118	375	121	0.85	1.425	19.683	223.81	525.12	1.74	0.74
290	121	383	129	0.90	1.545	19.696	230.44	531.75	1.76	0.76
295	126	394	140	0.98	1.666	19.705	241.63	542.94	1.80	0.80
301	131	407	153	1.07	1.811	19.715	252.79	554.10	1.84	0.84
307	134	418	164	1.15	1.956	19.728	259.39	560.70	1.86	0.86
311	137	426	172	1.21	2.052	19.736	266.05	567.36	1.88	0.88
315	141	433	179	1.25	2.149	19.746	274.93	576.24	1.91	0.91
320	144	442	188	1.32	2.270	19.757	281.53	582.84	1.93	0.93
325	147	450	196	1.37	2.390	19.770	288.10	589.41	1.96	0.96
330	150	459	205	1.44	2.511	19.782	294.68	595.99	1.98	0.98
335	153	470	216	1.51	2.632	19.790	301.30	602.61	2.00	1.00
340	157	482	228	1.60	2.752	19.798	310.18	611.49	2.03	1.03
347	163	496	242	1.70	2.921	19.812	323.43	624.74	2.07	1.07
351	165	502	248	1.74	3.018	19.823	327.74	629.05	2.09	1.09
355	168	509	255	1.79	3.115	19.833	334.31	635.62	2.11	1.11
360	171	516	262	1.84	3.235	19.847	340.79	642.10	2.13	1.13
371	179	534	280	1.96	3.501	19.876	358.21	659.52	2.19	1.19
380	184	546	292	2.05	3.718	19.903	368.90	670.21	2.22	1.22
390	189	559	305	2.14	3.960	19.934	379.49	680.80	2.26	1.26
402	195	575	321	2.25	4.249	19.971	392.16	693.47	2.30	1.30
411	201	587	333	2.33	4.467	19.999	404.96	706.27	2.34	1.34
422	206	601	347	2.43	4.732	20.034	415.36	716.67	2.38	1.38
432	211	612	358	2.51	4.974	20.068	425.73	727.04	2.41	1.41



Displacement	Force (lb)	Meter Reading	Volume Change	Volume Strain (%)	Axial Strain (%)	Corrected Area (cm^2)	Deviator Stress (kPa)	Max. Stress (KPa)	Stress Ratio	Normalized Stress
440	214	622	368	2.58	5.167	20.094	431.82	733.13	2.43	1.43
450	219	632	378	2.65	5.408	20.131	442.09	743.40	2.47	1.47
460	224	642	388	2.72	5.650	20.167	452.32	753.63	2.50	1.50
470	228	653	399	2.80	5.891	20.203	460.34	761.65	2.53	1.53
481	233	665	411	2.88	6.157	20.242	470.44	771.75	2.56	1.56
490	238	675	421	2.95	6.374	20.274	480.67	781.98	2.60	1.60
500	243	684	430	3.01	6.616	20.313	490.70	792.01	2.63	1.63
510	247	693	439	3.08	6.857	20.352	498.51	799.82	2.65	1.65
520	251	702	448	3.14	7.098	20.391	506.27	807.58	2.68	1.68
532	255	711	457	3.20	7.388	20.441	513.74	815.05	2.71	1.71
544	259	720	466	3.27	7.678	20.492	521.16	822.47	2.73	1.73
552	263	726	472	3.31	7.871	20.526	528.97	830.28	2.76	1.76
560	265	731	477	3.34	8.064	20.561	532.39	833.70	2.77	1.77
570	269	739	485	3.40	8.306	20.603	539.95	841.26	2.79	1.79
580	273	746	492	3.45	8.547	20.647	547.42	848.73	2.82	1.82
594	279	755	501	3.51	8.885	20.709	558.66	859.97	2.85	1.85
602	282	760	506	3.55	9.078	20.746	564.12	865.43	2.87	1.87
610	285	765	511	3.58	9.271	20.782	569.55	870.86	2.89	1.89
621	289	772	518	3.63	9.537	20.832	576.72	878.03	2.91	1.91
630	293	777	523	3.66	9.754	20.875	584.08	885.39	2.94	1.94
640	296	783	529	3.71	9.996	20.921	589.16	890.47	2.96	1.96
650	300	789	535	3.75	10.237	20.968	596.33	897.64	2.98	1.98
660	304	795	541	3.79	10.479	21.015	603.46	904.77	3.00	2.00
671	307	800	546	3.83	10.744	21.070	608.23	909.54	3.02	2.02
681	310	806	552	3.87	10.986	21.118	613.18	914.49	3.04	2.04
690	312	809	555	3.89	11.203	21.165	616.03	917.34	3.04	2.04
702	317	815	561	3.93	11.493	21.224	624.77	926.08	3.07	2.07
710	319	818	564	3.95	11.686	21.266	627.73	929.04	3.08	2.08
722	323	824	570	3.99	11.976	21.327	634.30	935.61	3.11	2.11
730	325	826	572	4.01	12.169	21.370	637.17	938.48	3.11	2.11
743	329	831	577	4.04	12.483	21.439	643.43	944.74	3.14	2.14
753	332	835	581	4.07	12.724	21.492	648.06	949.37	3.15	2.15
764	335	839	585	4.10	12.990	21.551	652.48	953.79	3.17	2.17
774	337	842	588	4.12	13.231	21.606	654.93	956.24	3.17	2.17
780	339	844	590	4.13	13.376	21.639	658.05	959.36	3.18	2.18
791	342	848	594	4.16	13.642	21.699	662.38	963.69	3.20	2.20
800	345	851	597	4.18	13.859	21.749	667.00	968.31	3.21	2.21
810	348	854	600	4.20	14.100	21.805	671.40	972.71	3.23	2.23
820	350	858	604	4.23	14.342	21.860	673.79	975.10	3.24	2.24
830	352	861	607	4.25	14.583	21.917	676.10	977.41	3.24	2.24
840	354	863	609	4.27	14.825	21.976	678.34	979.65	3.25	2.25
851	356	865	611	4.28	15.090	22.041	680.36	981.67	3.26	2.26
860	358	868	614	4.30	15.308	22.093	682.80	984.11	3.27	2.27
880	362	872	618	4.33	15.790	22.213	687.13	988.44	3.28	2.28
891	365	875	621	4.35	16.056	22.278	691.11	992.42	3.29	2.29

Displacement	Force (lb)	Meter Reading	Volume Change	Volume Strain (%)	Axial Strain (%)	Corrected Area (cm <sup>2</sup> )	Deviator Stress (kPa)	Max. Stress (KPa)	Stress Ratio	Normalized Stress
900	368	877	623	4.37	16.273	22.332	695.40	996.71	3.31	2.31
910	370	879	625	4.38	16.515	22.394	697.47	998.78	3.31	2.31
920	372	881	627	4.39	16.756	22.455	699.52	1000.83	3.32	2.32
930	374	883	629	4.41	16.998	22.517	701.55	1002.86	3.33	2.33
940	376	885	631	4.42	17.239	22.579	703.56	1004.87	3.33	2.33
950	378	887	633	4.44	17.481	22.642	705.54	1006.85	3.34	2.34
960	380	889	635	4.45	17.722	22.705	707.50	1008.81	3.35	2.35
970	382	890	636	4.46	17.963	22.770	709.39	1010.70	3.35	2.35
980	383	891	637	4.46	18.205	22.836	709.30	1010.61	3.35	2.35
990	384	892	638	4.47	18.446	22.902	709.20	1010.51	3.35	2.35
1000	385	893	639	4.48	18.688	22.968	709.09	1010.40	3.35	2.35
1010	387	894	640	4.48	18.929	23.034	710.90	1012.21	3.36	2.36
1020	389	896	642	4.50	19.171	23.100	712.75	1014.06	3.37	2.37
1030	390	897	643	4.51	19.412	23.167	712.59	1013.90	3.36	2.36
1040	392	898	644	4.51	19.654	23.235	714.34	1015.65	3.37	2.37
1050	393	899	645	4.52	19.895	23.303	714.16	1015.47	3.37	2.37
1060	394	901	647	4.53	20.137	23.370	714.02	1015.33	3.37	2.37
1070	394	902	648	4.54	20.378	23.439	711.91	1013.22	3.36	2.36
1080	395	902	648	4.54	20.619	23.511	711.64	1012.95	3.36	2.36
1090	396	903	649	4.55	20.861	23.581	711.42	1012.73	3.36	2.36

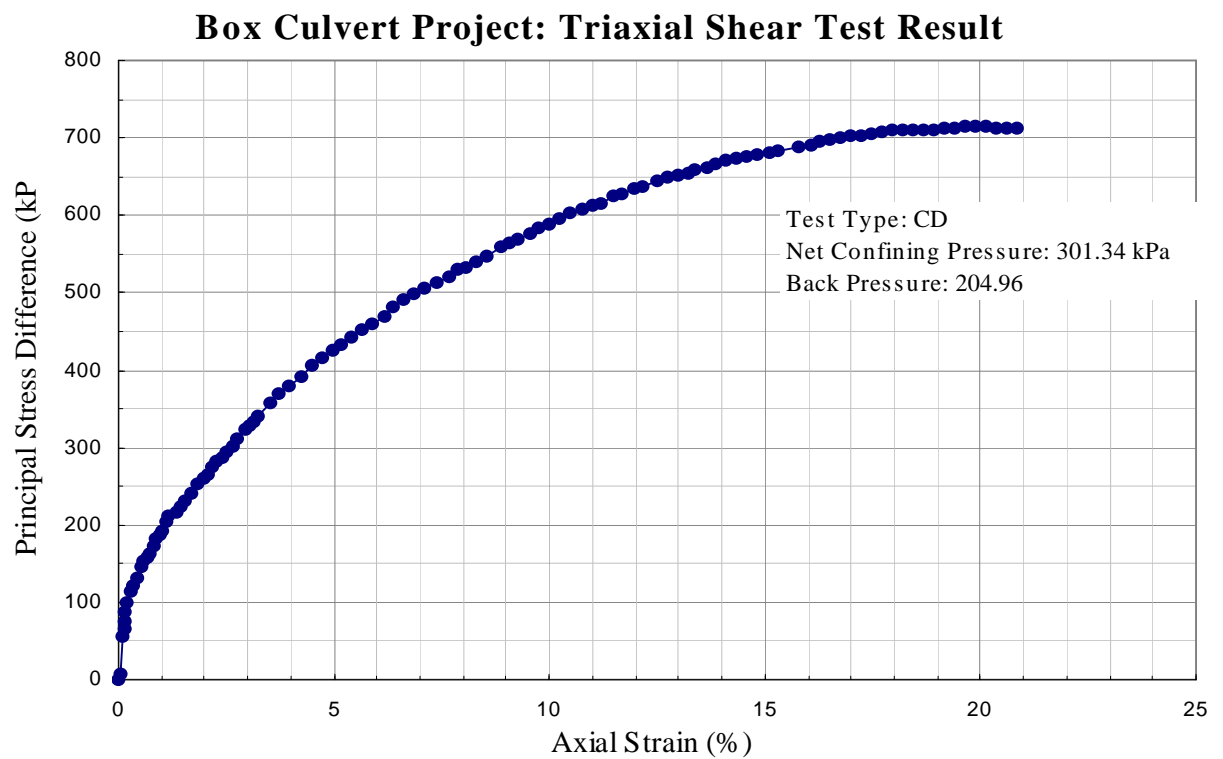


Figure D-23 Triaxial Shear Test Results- Silty Clay  
(50 mm Sample Diameter, 301.4 kPa Confining Pressure)

### Box Culvert Project: Triaxial Shear Test

Sample: <b>Soil Underneath Culvert</b> (Silty Clay)					Date Tested: 10/28/1996	
Sample No. 4				Type of Test: Consolidated Drained		
Diameter:(mm)	50.03	50.63	50.6	Average Diameter (mm): 50.5	Initial Area(mm^2):	2001
Height(mm):	104.72	105.16	105.72	Average Sample Height (mm):105.2	Initial Volume(cm^3):	210.48
Net Confining Pressure: 439.2 kPa			Back Pressure: 204.96 kPa			
Sample Weight(g): 432.60						
Moisture Content:(1)				Moisture Content:(2)		
Aluminum Box No.:			208	Aluminum Box No.: 5		
Box Weight(g):			13.9	Box Weight: 19		
Wet Soil+ Box Weight:(g)			29.1	Wet Soil+ Box Weight: 41.2		
Dry Soil+Box Weight:(g)			26.4	Dry Soil+Box Weight: 37.6		
Moisture Content:(%)			21.6	Moisture Content: 19.35		
Averaged Moisture Content:(%)		20.48	Initial Density (KN/M^3): 20.16			

### Hydro-Static Compression Test

Date	Time	Cell Pressure (psi)	Back Pressure (psi)	Hydro-pressure (psi)	Meter Reading	Cell Pressure (kPa)	Back Pressure (psi)	Net Hydro-pressure (kPa)	Volume Change (ml)	Volume Strain (%)
14-Oct	7:40 PM	38.3	29.6	5	789	264.08	204.09	34.48	0.399	0.19
15-Oct	10:00 PM	43.3	29.6	10	829	298.55	204.09	68.95	0.990	0.47
16-Oct	10:00 AM	48.3	29.6	15	873	333.03	204.09	103.43	1.640	0.78
17-Oct	9:30 AM	53.3	29.6	20	930	367.50	204.09	137.90	2.482	1.18
17-Oct	11:00 PM	43.3	29.6	10	908	298.55	204.09	68.95	2.157	1.02
18-Oct	8:30 AM	33.3	29.6	0	856	229.60	204.09	0.00	1.388	0.66
18-Oct	8:30 PM	43.3	29.6	10	899	298.55	204.09	68.95	2.024	0.96
19-Oct	8:40 AM	53.3	29.6	20	935	367.50	204.09	137.90	2.555	1.21
	8:00 PM	58.3	29.6	25	962	401.98	204.09	172.38	2.954	1.40
20-Oct	11:30am	63.3	29.6	30	1002	436.45	204.09	206.85	3.545	1.68
	10.15 pm	68.3	29.6	35	1035	470.93	204.09	241.33	4.032	1.92
21-Oct	10:00 AM	73.3	29.6	40	1075	505.40	204.09	275.80	4.623	2.20
	10:00 PM	63.3	29.6	30	1062	436.45	204.09	206.85	4.431	2.11
22-Oct	10:00 AM	53.3	29.6	20	1047	367.50	204.09	137.90	4.210	2.00
	9:00 PM	43.3	29.6	10	1019	298.55	204.09	68.95	3.796	1.80
23-Oct	10:00 AM	33.3	29.6	0	954	229.60	204.09	0.00	2.836	1.35
	9:00 PM	43.3	29.6	10	999	298.55	204.09	68.95	3.501	1.66
24-Oct	10:00 AM	53.3	29.6	20	1027	367.50	204.09	137.90	3.914	1.86
	10:00 PM	63.3	29.6	30	1049	436.45	204.09	206.85	4.239	2.01
25-Oct	10:00 AM	73.3	29.6	40	1077	505.40	204.09	275.80	4.653	2.21
	10:00 PM	78.3	29.6	45	1092	539.88	204.09	310.28	4.874	2.32

Date	Time	Cell Pressure (psi)	Back Pressure (psi)	Hydropressure (psi)	Meter Reading	Cell Pressure (kPa)	Back Pressure (psi)	Net Hydropressure (kPa)	Volume Change (ml)	Volume Strain (%)
26-Oct	11:00 AM	83.3	29.6	50	1123	574.35	204.09	344.75	5.332	2.53
	10:30 PM	88.3	29.6	55	1146	608.83	204.09	379.23	5.672	2.69
27-Oct	12:00 AM	93.3	29.6	60	1177	643.30	204.09	413.70	6.130	2.91

### Volume Strain under Hydropressure

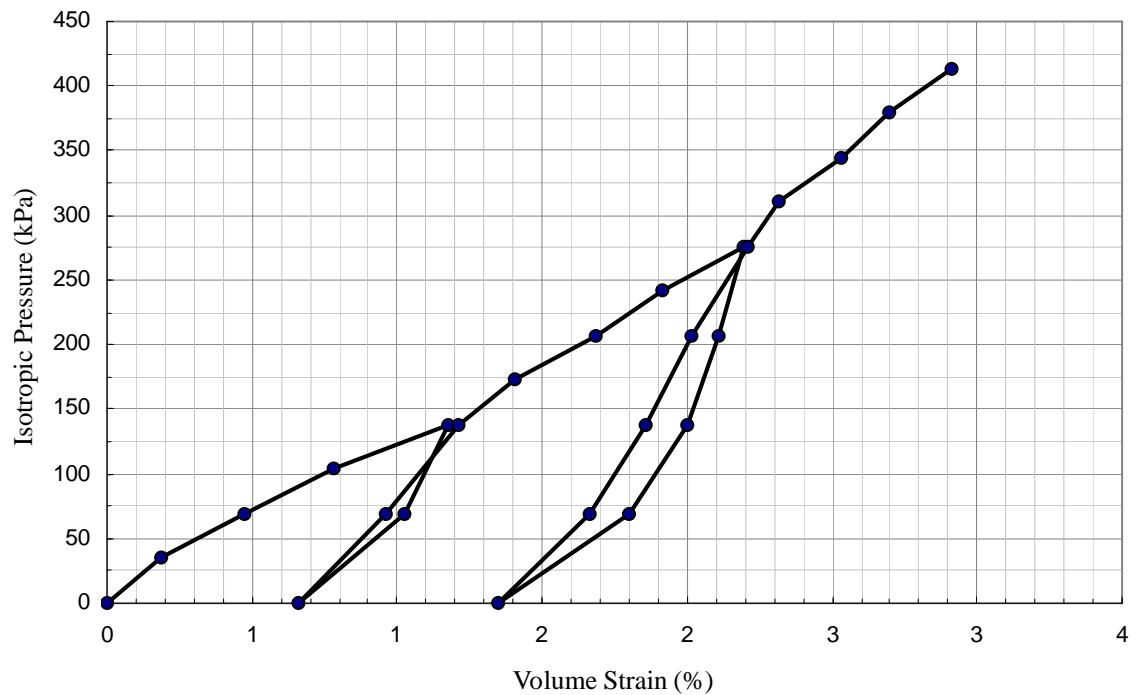


Figure D-24 Volume Strain Under Hydropressure (II)

Displacement (1/1000 inch)	Force (lb)	Meter Reading	Volume Change	Volume Strain(%)	Axial Strain (%)	Corrected Area (cm <sup>2</sup> )	Deviator Stress (Kpa)	Max. Stress (KPa)	Stress Ratio	Normalized Stress
309	25	1185	0	0.00	0.000	19.414	0.00	439.21	1.00	0.00
311	31	1185	0	0.00	0.048	19.423	13.75	452.96	1.03	0.03
313	57	1186	1	0.01	0.097	19.431	73.28	512.49	1.17	0.17
314	69	1188	3	0.02	0.121	19.433	100.75	539.96	1.23	0.23
315	76	1190	5	0.04	0.145	19.435	116.77	555.98	1.27	0.27
317	83	1194	9	0.06	0.193	19.439	132.77	571.98	1.30	0.30
318	86	1194	9	0.06	0.217	19.444	139.60	578.81	1.32	0.32
319	90	1198	13	0.09	0.241	19.443	148.76	587.97	1.34	0.34
320	93	1200	15	0.11	0.266	19.445	155.62	594.83	1.35	0.35
321	94	1202	17	0.12	0.290	19.446	157.89	597.10	1.36	0.36
322	96	1203	18	0.13	0.314	19.450	162.44	601.65	1.37	0.37
323	98	1205	20	0.14	0.338	19.452	167.00	606.21	1.38	0.38
324	99	1205	20	0.14	0.362	19.456	169.24	608.45	1.39	0.39
325	102	1209	24	0.17	0.386	19.455	176.11	615.32	1.40	0.40
327	105	1212	27	0.19	0.435	19.461	182.93	622.14	1.42	0.42
331	110	1220	35	0.25	0.531	19.468	194.28	633.49	1.44	0.44
333	115	1225	40	0.28	0.579	19.471	205.69	644.90	1.47	0.47
336	118	1230	45	0.32	0.652	19.478	212.46	651.67	1.48	0.48
338	121	1235	50	0.35	0.700	19.480	219.29	658.50	1.50	0.50
340	125	1239	54	0.38	0.748	19.484	228.38	667.59	1.52	0.52
343	129	1245	60	0.42	0.821	19.490	237.45	676.66	1.54	0.54
345	131	1248	63	0.44	0.869	19.495	241.95	681.16	1.55	0.55
348	135	1254	69	0.48	0.942	19.501	251.01	690.22	1.57	0.57
350	137	1258	73	0.51	0.990	19.505	255.52	694.73	1.58	0.58
353	141	1264	79	0.55	1.062	19.510	264.57	703.78	1.60	0.60
355	144	1268	83	0.58	1.111	19.514	271.36	710.57	1.62	0.62
358	147	1274	89	0.62	1.183	19.520	278.11	717.32	1.63	0.63
360	150	1277	92	0.65	1.231	19.525	284.88	724.09	1.65	0.65
363	153	1283	98	0.69	1.304	19.531	291.63	730.84	1.66	0.66
366	157	1288	103	0.72	1.376	19.538	300.63	739.84	1.68	0.68
370	160	1295	110	0.77	1.473	19.547	307.32	746.53	1.70	0.70
375	166	1303	118	0.83	1.594	19.560	320.77	759.98	1.73	0.73
380	171	1313	128	0.90	1.714	19.570	331.98	771.19	1.76	0.76
385	175	1321	136	0.95	1.835	19.582	340.85	780.06	1.78	0.78
390	179	1330	145	1.02	1.956	19.594	349.74	788.95	1.80	0.80
395	182	1338	153	1.07	2.076	19.606	356.33	795.54	1.81	0.81
400	186	1345	160	1.12	2.197	19.620	365.14	804.35	1.83	0.83
405	191	1353	168	1.18	2.318	19.633	376.24	815.45	1.86	0.86
413	198	1366	181	1.27	2.511	19.653	391.70	830.91	1.89	0.89
415	200	1369	184	1.29	2.559	19.659	396.12	835.33	1.90	0.90
421	204	1377	192	1.35	2.704	19.676	404.81	844.02	1.92	0.92
426	209	1386	201	1.41	2.825	19.688	415.87	855.08	1.95	0.95
430	211	1391	206	1.45	2.921	19.700	420.13	859.34	1.96	0.96
435	216	1398	213	1.49	3.042	19.715	431.11	870.32	1.98	0.98
441	221	1407	222	1.56	3.187	19.731	442.03	881.24	2.01	1.01

Displacement (1/1000 inch)	Force (lb)	Meter Reading	Volume Change	Volume Strain(%)	Axial Strain (%)	Corrected Area (cm^2)	Deviator Stress (Kpa)	Max. Stress (KPa)	Stress Ratio	Normalized Stress
446	225	1414	229	1.61	3.308	19.746	450.72	889.93	2.03	1.03
451	228	1421	236	1.66	3.429	19.760	457.14	896.35	2.04	1.04
455	232	1428	243	1.71	3.525	19.770	465.92	905.13	2.06	1.06
460	236	1434	249	1.75	3.646	19.786	474.54	913.75	2.08	1.08
465	239	1440	255	1.79	3.767	19.802	480.90	920.11	2.09	1.09
471	244	1449	264	1.85	3.911	19.818	491.72	930.93	2.12	1.12
477	248	1456	271	1.90	4.056	19.838	500.20	939.41	2.14	1.14
482	252	1463	278	1.95	4.177	19.853	508.80	948.01	2.16	1.16
485	254	1467	282	1.98	4.249	19.862	513.04	952.25	2.17	1.17
490	258	1474	289	2.03	4.370	19.877	521.62	960.83	2.19	1.19
495	262	1481	296	2.08	4.491	19.892	530.18	969.39	2.21	1.21
501	265	1487	302	2.12	4.636	19.913	536.31	975.52	2.22	1.22
505	269	1493	308	2.16	4.732	19.924	544.94	984.15	2.24	1.24
510	272	1497	312	2.19	4.853	19.944	551.10	990.31	2.25	1.25
515	274	1502	317	2.22	4.974	19.962	555.07	994.28	2.26	1.26
520	278	1508	323	2.27	5.094	19.978	563.52	1002.73	2.28	1.28
525	281	1513	328	2.30	5.215	19.996	569.68	1008.89	2.30	1.30
530	285	1520	335	2.35	5.336	20.011	578.15	1017.36	2.32	1.32
535	287	1524	339	2.38	5.457	20.031	582.03	1021.24	2.33	1.33
541	291	1531	346	2.43	5.602	20.051	590.31	1029.52	2.34	1.34
545	293	1535	350	2.46	5.698	20.066	594.32	1033.53	2.35	1.35
550	296	1539	354	2.48	5.819	20.086	600.38	1039.59	2.37	1.37
555	299	1544	359	2.52	5.940	20.104	606.47	1045.68	2.38	1.38
560	302	1548	363	2.55	6.060	20.124	612.51	1051.72	2.39	1.39
565	305	1552	367	2.58	6.181	20.144	618.53	1057.74	2.41	1.41
570	310	1560	375	2.63	6.302	20.158	629.14	1068.35	2.43	1.43
580	314	1568	383	2.69	6.543	20.198	636.70	1075.91	2.45	1.45
593	319	1577	392	2.75	6.857	20.252	645.98	1085.19	2.47	1.47
600	323	1583	398	2.79	7.026	20.280	653.87	1093.08	2.49	1.49
610	328	1592	407	2.86	7.267	20.319	663.56	1102.77	2.51	1.51
620	334	1599	414	2.91	7.509	20.362	675.29	1114.50	2.54	1.54
631	340	1608	423	2.97	7.775	20.407	686.89	1126.10	2.56	1.56
643	347	1618	433	3.04	8.064	20.456	700.47	1139.68	2.59	1.59
654	352	1626	441	3.09	8.330	20.503	709.71	1148.92	2.62	1.62
670	361	1636	451	3.16	8.716	20.574	726.71	1165.92	2.65	1.65
680	367	1643	458	3.21	8.958	20.618	738.12	1177.33	2.68	1.68
694	375	1653	468	3.28	9.296	20.679	753.15	1192.36	2.71	1.71
700	377	1656	471	3.31	9.440	20.707	756.41	1195.62	2.72	1.72
710	382	1662	477	3.35	9.682	20.754	765.45	1204.66	2.74	1.74
720	387	1668	483	3.39	9.923	20.800	774.45	1213.66	2.76	1.76
730	392	1673	488	3.42	10.165	20.848	783.33	1222.54	2.78	1.78
740	397	1678	493	3.46	10.406	20.896	792.17	1231.38	2.80	1.80
750	402	1682	497	3.49	10.648	20.946	800.89	1240.10	2.82	1.82
760	405	1689	504	3.54	10.889	20.992	805.51	1244.72	2.83	1.83
774	411	1695	510	3.58	11.227	21.063	815.49	1254.70	2.86	1.86

Displacement (1/1000 inch)	Force (lb)	Meter Reading	Volume Change	Volume Strain(%)	Axial Strain (%)	Corrected Area (cm^2)	Deviator Stress (Kpa)	Max. Stress (KPa)	Stress Ratio	Normalized Stress
780	415	1699	514	3.61	11.372	21.091	822.84	1262.05	2.87	1.87
790	418	1703	518	3.64	11.613	21.142	827.16	1266.37	2.88	1.88
800	421	1706	521	3.66	11.855	21.195	831.39	1270.60	2.89	1.89
811	427	1711	526	3.69	12.121	21.251	841.76	1280.97	2.92	1.92
820	430	1715	530	3.72	12.338	21.297	846.20	1285.41	2.93	1.93
830	435	1718	533	3.74	12.579	21.351	854.48	1293.69	2.95	1.95
844	441	1723	538	3.78	12.917	21.426	863.95	1303.16	2.97	1.97
852	445	1728	543	3.81	13.110	21.466	870.65	1309.86	2.98	1.98
860	448	1730	545	3.82	13.304	21.510	875.05	1314.26	2.99	1.99
870	452	1734	549	3.85	13.545	21.564	881.13	1320.34	3.01	2.01
880	455	1737	552	3.87	13.787	21.619	885.05	1324.26	3.02	2.02
890	458	1739	554	3.89	14.028	21.677	888.86	1328.07	3.02	2.02
900	462	1743	558	3.92	14.269	21.731	894.82	1334.03	3.04	2.04
910	466	1747	562	3.94	14.511	21.786	900.74	1339.95	3.05	2.05
920	469	1748	563	3.95	14.752	21.846	904.37	1343.58	3.06	2.06
930	472	1749	564	3.96	14.994	21.907	907.97	1347.18	3.07	2.07
940	475	1750	565	3.97	15.235	21.967	911.54	1350.75	3.08	2.08
950	477	1750	565	3.97	15.477	22.030	912.98	1352.19	3.08	2.08
960	480	1751	566	3.97	15.718	22.092	916.49	1355.70	3.09	2.09
970	482	1752	567	3.98	15.960	22.153	917.95	1357.16	3.09	2.09
980	482	1753	568	3.99	16.201	22.216	915.38	1354.59	3.08	2.08
990	482	1754	569	3.99	16.442	22.278	912.81	1352.02	3.08	2.08
1000	482	1756	571	4.01	16.684	22.339	910.31	1349.52	3.07	2.07
1010	482	1758	573	4.02	16.925	22.401	907.81	1347.02	3.07	2.07
1020	483	1760	575	4.04	17.167	22.463	907.29	1346.50	3.07	2.07
1030	483	1762	577	4.05	17.408	22.525	904.78	1343.99	3.06	2.06
1040	483	1763	578	4.06	17.650	22.589	902.20	1341.41	3.05	2.05
1050	484	1763	578	4.06	17.891	22.656	901.52	1340.73	3.05	2.05
1060	484	1763	578	4.06	18.133	22.723	898.87	1338.08	3.05	2.05
1070	483	1763	578	4.06	18.374	22.790	894.27	1333.48	3.04	2.04



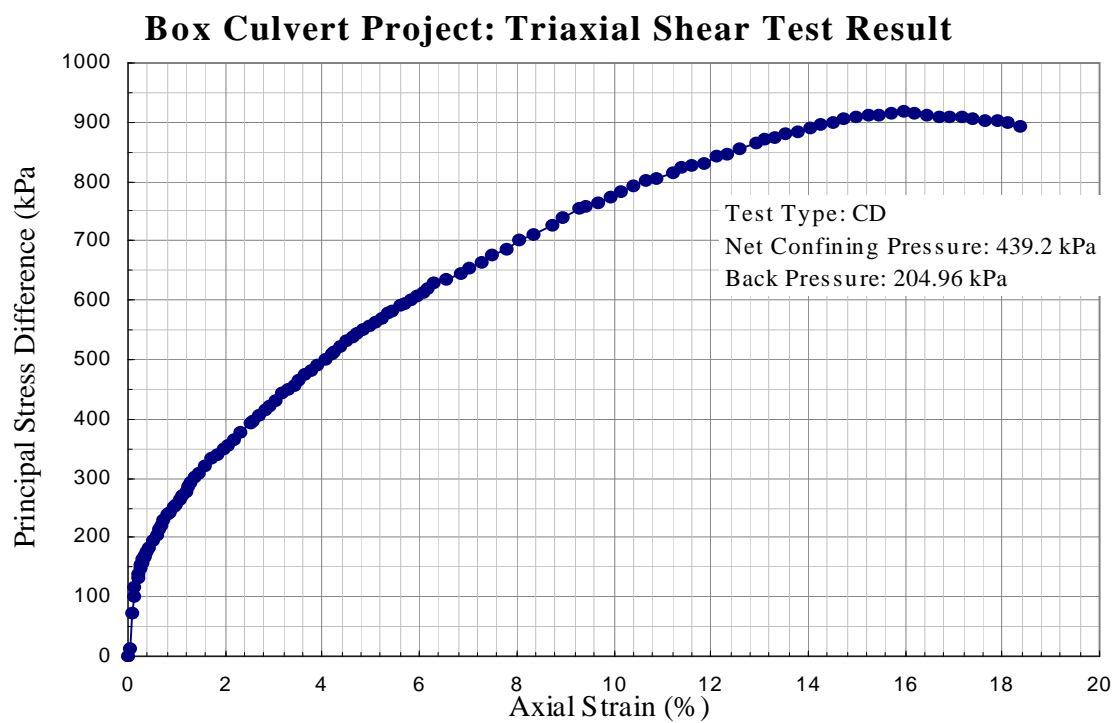


Figure D-25 Triaxial Shear Test Results- Silty Clay  
(50 mm Sample Diameter, 439.2 kPa Confining Pressure)

### Finding of Cohesion and Internal Friction Angle (Stress Path)

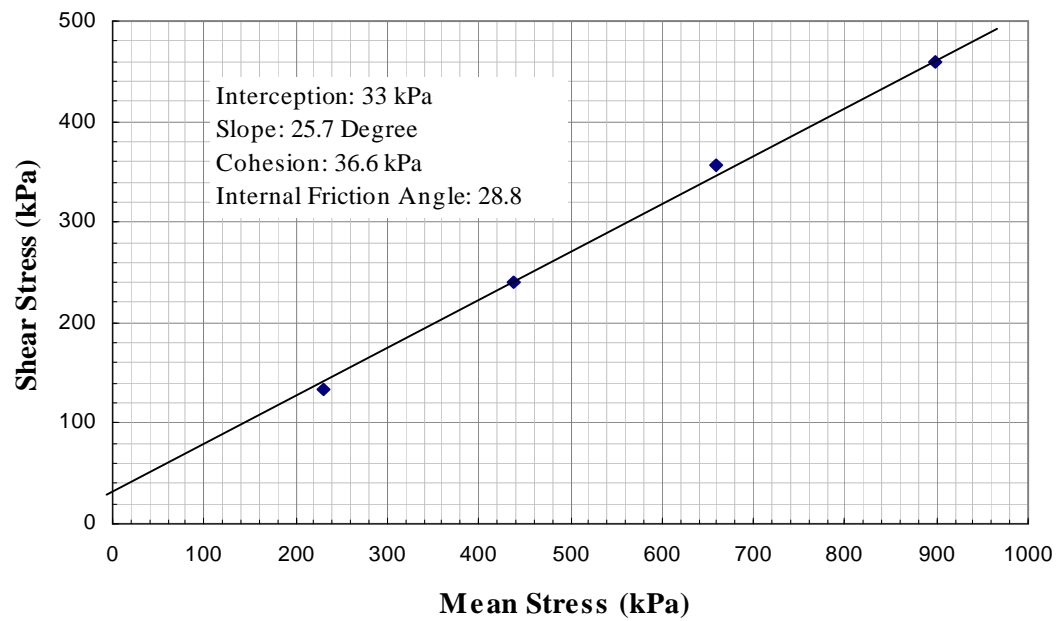


Figure D-26 Peak Strength in p-q Plane

### Mohr Circles of Silty Soil

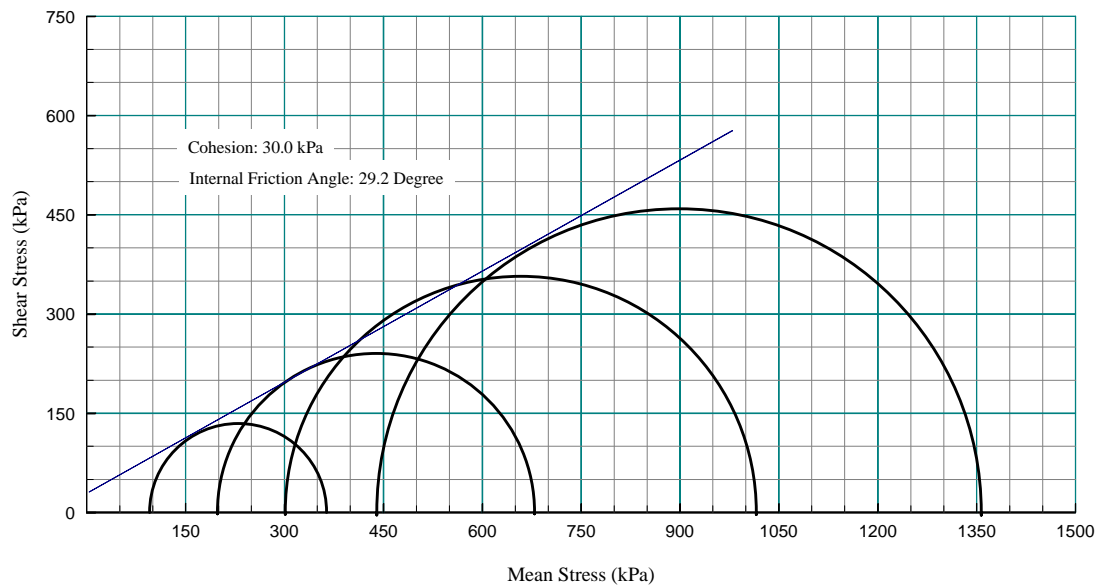


Figure D-27 Mohr Circles for Silty Clay

## Appendix D-4

### Triaxial Shear Test Results- Backfill Clay

Table D-4 Clay (undisturbed sample of compacted backfill material) CU Test

Sample Number	Back Pressure (kPa)	Net Confining Pressure (kPa)	Measured Density (kN/m <sup>3</sup> )	Moisture Content (%)
No.1	204	172.4	20.15	16.9
No.2	171	387.5	NA	16.7
No.3	172.4	112.4	19.86	16.81
No.4	172	49.6	NA	16.80

Note : Sample diameter: 50.8 mm; samples from Greene County culvert site.

Strength:

Effective Strength:

Cohesion  $c = 22$  kPa and Angle of internal friction  $\phi = 27^\circ$

Total Strength:

Cohesion  $c = 32$  kPa and Angle of internal friction  $\phi = 22^\circ$

## Box Culvert Project: Triaxial Shear Test

Sample **Backfill Material (Clay, Greene County Culvert)**

Sample No.1

Diameter:(mm )	50.35	50.09	52.37	Height(mm)	107.52	105.94	107.52
Aver. Dia.:	50.7	Initial Area:(1e-3 m^2)	2.02	Average Height:(mm)	107.0		
Sample Weight(g):	444.1	Initial Volume (1e-6 m^3):	216.22				
Moisture Content:		Moisture Content:					
Aluminum Box No.:	D12	Aluminum Box No.:	D6				
Box Weight(g):	19.4	Box Weight:	19.5				
Wet Soil+ Box Weight:(g)	29	Wet Soil+ Box Weight:	29.3				
Dry Soil+ Box Weight:(g)	27.6	Dry Soil+Box Weight:	27.9				
Moisture Content:(%)	17.1	Moisture Content:	16.67				
Averaged Moisture Content:(%)	16.87	Initial Density (KN/M^3):	20.15				
Type of Test: CU							
Type of saturation:	CU with pore pressure measurement	Back Pressure For Saturation:	29.6 psi				
Date:5/20-5/28, 1999							
Confining Pressure ( Net): 25 psi (172.4KPa)							

Displacement (1/1000 inch)	Force (lb)	Pore pressure (psi)	Axial Strain (%)	Average Area	Pore Pressure (kPa)	Deviator Stress (kPa)	Major Total Stress (kPa)	Major Stress (kPa)	Minor Stress (kPa)	Total Mean Stress	Mean Stress	Q
32	8	21.3	0	20.21	0	0	172.4	172.37	172.4	172.37	172.37	0.00
34	13	22.2	0.05	20.22	6.21	10.99	183.36	177.15	166.16	177.87	171.66	5.50
36	16	22.3	0.09	20.23	6.90	17.58	189.95	183.05	165.48	181.16	174.26	8.79
37	23	23.4	0.12	20.23	14.48	32.95	205.32	190.84	157.89	188.84	174.36	16.47
39	33	24.7	0.17	20.24	23.44	54.89	227.26	203.81	148.93	199.81	176.37	27.44
41	40	26.1	0.21	20.25	33.10	70.22	242.59	209.49	139.27	207.48	174.38	35.11
44	48	27.7	0.28	20.27	44.13	87.71	260.08	215.95	128.24	216.23	172.10	43.86
46	55	28.6	0.33	20.28	50.33	103.01	275.38	225.05	122.04	223.88	173.54	51.51
48	60	29.3	0.38	20.29	55.16	113.92	286.29	231.13	117.21	229.33	174.17	56.96
50	65	30.1	0.43	20.29	60.68	124.81	297.18	236.51	111.69	234.78	174.10	62.41
55	78	31.5	0.54	20.32	70.33	153.10	325.47	255.14	102.04	248.92	178.59	76.55
60	85	32.5	0.66	20.34	77.22	168.21	340.58	263.35	95.15	256.47	179.25	84.10
66	93	33.2	0.80	20.37	82.05	185.42	357.79	275.74	90.32	265.08	183.03	92.71
70	98	33.5	0.90	20.39	84.12	196.14	368.51	284.39	88.25	270.44	186.32	98.07

Displacement (1/1000 inch)	Force (lb)	Pore pressure (psi)	Axial Strain (%)	Average Area	Pore Pressure (kPa)	Deviator Stress (kPa)	Major Total Stress (kPa)	Major Stress (kPa)	Minor Stress (kPa)	Total Mean Stress	Mean Stress	Q
80	108	34	1.13	20.44	87.57	217.41	389.78	302.21	84.80	281.07	193.51	108.70
90	115	34.1	1.37	20.49	88.26	232.07	404.44	316.18	84.11	288.41	200.15	116.04
101	121	33.9	1.63	20.54	86.88	244.44	416.81	329.93	85.49	294.59	207.71	122.22
115	128	33.6	1.96	20.61	84.81	258.71	431.08	346.27	87.56	301.72	216.91	129.35
120	130	33.4	2.08	20.64	83.43	262.70	435.07	351.64	88.94	303.72	220.29	131.35
130	133	33.1	2.32	20.69	81.36	268.51	440.88	359.52	91.01	306.63	225.26	134.26
141	135	32.7	2.58	20.74	78.60	272.08	444.45	365.85	93.77	308.41	229.81	136.04
153	138	32.4	2.86	20.80	76.53	277.70	450.07	373.53	95.84	311.22	234.68	138.85
160	138	32.1	3.03	20.84	74.47	277.22	449.59	375.13	97.90	310.98	236.52	138.61
171	140	31.8	3.29	20.90	72.40	280.73	453.10	380.71	99.97	312.74	240.34	140.37
188	143	31.3	3.69	20.98	68.95	285.92	458.29	389.34	103.42	315.33	246.38	142.96
193	143	31.2	3.81	21.01	68.26	285.57	457.94	389.68	104.11	315.15	246.89	142.78
202	143	30.9	4.02	21.05	66.19	284.94	457.31	391.12	106.18	314.84	248.65	142.47
210	143	30.6	4.21	21.10	64.12	284.38	456.75	392.62	108.25	314.56	250.43	142.19
220	145	30.4	4.45	21.15	62.74	287.88	460.25	397.50	109.63	316.31	253.56	143.94
234	145	30	4.78	21.22	59.99	286.88	459.25	399.26	112.38	315.81	255.82	143.44
240	146	29.9	4.92	21.25	59.30	288.54	460.91	401.62	113.07	316.64	257.34	144.27
250	149	29.7	5.15	21.31	57.92	294.08	466.45	408.53	114.45	319.41	261.49	147.04
273	151	29.2	5.70	21.43	54.47	296.54	468.91	414.44	117.90	320.64	266.17	148.27
280	153	29.1	5.86	21.47	53.78	300.16	472.53	418.75	118.59	322.45	268.67	150.08
290	155	28.9	6.10	21.52	52.40	303.54	475.91	423.51	119.97	324.14	271.74	151.77
302	156	28.7	6.38	21.59	51.02	304.68	477.05	426.03	121.35	324.71	273.69	152.34
325	160	28.5	6.93	21.71	49.64	311.10	483.47	433.82	122.73	327.92	278.27	155.55
340	160	28	7.28	21.80	46.20	309.91	482.28	436.09	126.17	327.33	281.13	154.96
361	161	27.7	7.78	21.91	44.13	310.28	482.65	438.52	128.24	327.51	283.38	155.14
382	165	27.3	8.28	22.03	41.37	316.68	489.05	447.68	131.00	330.71	289.34	158.34
406	165	26.9	8.84	22.17	38.61	314.72	487.09	448.48	133.76	329.73	291.12	157.36
420	165	26.7	9.17	22.25	37.23	313.58	485.95	448.71	135.14	329.16	291.92	156.79
440	170	26.4	9.65	22.37	35.16	321.88	494.25	459.08	137.21	333.31	298.14	160.94
460	171	26.1	10.12	22.48	33.10	322.17	494.54	461.44	139.27	333.45	300.36	161.08
480	173	25.9	10.59	22.60	31.72	324.41	496.78	465.06	140.65	334.57	302.86	162.20
500	180	25.4	11.07	22.72	28.27	336.38	508.75	480.48	144.10	340.56	312.29	168.19
550	182	25	12.25	23.03	25.51	335.77	508.14	482.63	146.86	340.25	314.74	167.88
591	184	24.6	13.22	23.29	22.75	335.88	508.25	485.49	149.62	340.31	317.55	167.94
622	185	24.3	13.95	23.48	20.69	334.93	507.30	486.62	151.69	339.84	319.15	167.47
662	188	23.9	14.90	23.75	17.93	336.86	509.23	491.31	154.44	340.80	322.87	168.43
689	191	23.6	15.53	23.93	15.86	339.91	512.28	496.42	156.51	342.32	326.47	169.95
724	195	23.5	16.36	24.16	15.17	343.94	516.31	501.14	157.20	344.34	329.17	171.97
752	196	23	17.02	24.35	11.72	343.04	515.41	503.69	160.65	343.89	332.17	171.52
785	200	22.7	17.80	24.59	9.65	347.04	519.41	509.76	162.72	345.89	336.24	173.52
817	200	22.4	18.56	24.81	7.58	343.85	516.22	508.63	164.79	344.29	336.71	171.92

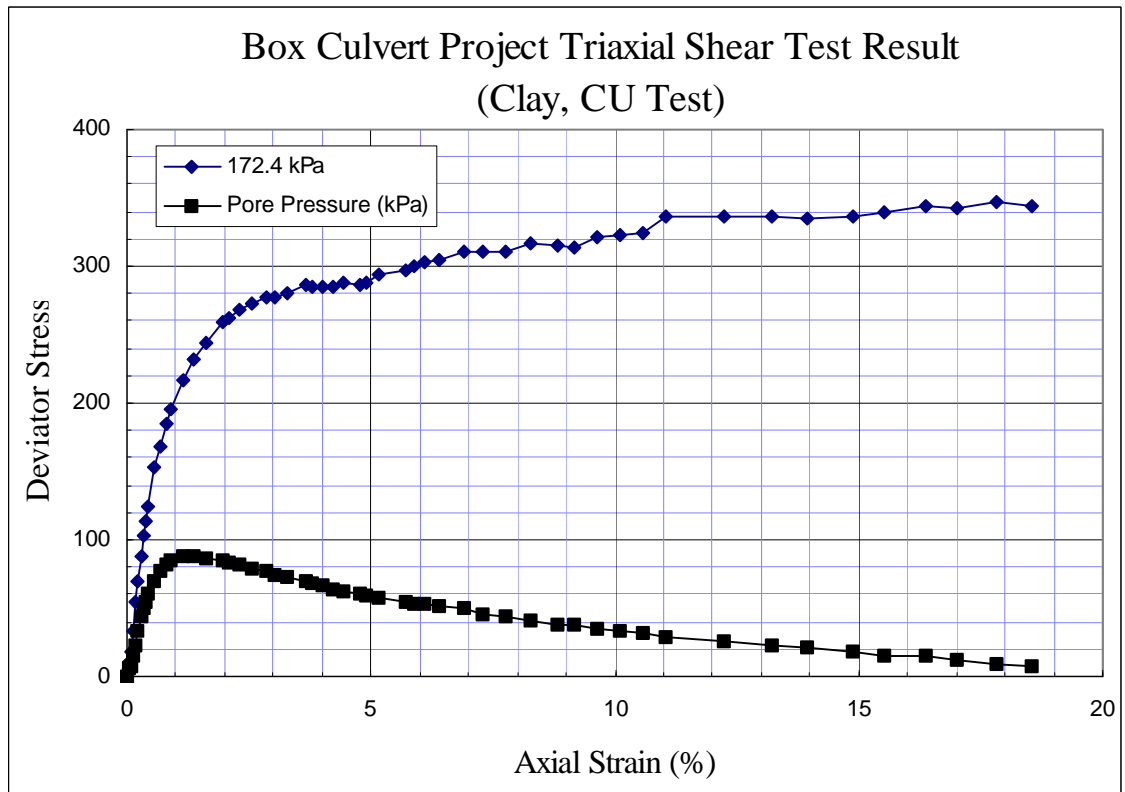


Figure D-28 Triaxial Shear Test Results- Backfill Clay  
(50 mm Sample Diameter, 172.4 kPa Confining Pressure)

## Box Culvert Project: Triaxial Shear Test

Sample	Backfill Material (Clay, Greene County Culvert)						
Sample No.2							
Diameter:(mm)	50.95	51.3	50.85	Height(mm)	101.5	102.45	101.5
Average Diameter	51.1	Initial Area: (e-3) 2.0488		Average Height (mm)	101.8		
Sample Weight(g):				Initial Volume (1e-6 m^3):	208.61		
Moisture Content:				Moisture Content:			
Aluminum Box No.:	D6			Aluminum Box No.:	D12		
Box Weight(g):	19.5			Box Weight:	19.4		
Wet Soil+ Box Weight:(g)	25.4			Wet Soil+ Box Weight:	25.4		
Dry Soil+Box Weight:(g)	24.6			Dry Soil+Box Weight:	24.5		
Moisture Content:(%)	15.7			Moisture Content:	17.65		
Averaged Moisture Content:(%)			16.67	Initial Density (KN/M^3):	0.00		
Type of Test: CU							
Type of saturation:				Back Pressure For Saturation: 24.8 psi	171 kPa		
Date:5/31-6/6, 1999							
Confining Pressure( Net): 56.2 psi (387.5KPa)							

Displacement (1/1000 inch)	Force (lb)	Pore pressure (psi)	Axial Strain (%)	Average Area	Pore Pressure (kPa)	Deviator Stress (kPa)	Major Total Stress (kPa)	Major Stress (kPa)	Minor Stress (kPa)	Total Mean Stress	Mean Stress	Q
13	11	21.4	0.00	20.49	0	0	387.5	387.5	387.5	387.50	388	0.00
15	16	21.4	0.05	20.5	0.0	10.8	398.3	398.3	387.5	392.9	392.9	5.4
16	26	21.4	0.07	20.5	0.0	32.5	420.0	420.0	387.5	403.8	403.8	16.3
17	28	21.4	0.09	20.5	0.0	36.8	424.3	424.3	387.5	405.9	405.9	18.4
18	35	21.5	0.12	20.5	0.7	52.0	439.5	438.8	386.8	413.5	412.8	26.0
19	43	21.5	0.14	20.5	0.7	69.3	456.8	456.1	386.8	422.2	421.5	34.7
20	56	21.6	0.17	20.5	1.4	97.4	484.9	483.6	386.1	436.2	434.8	48.7
22	68	21.7	0.21	20.5	2.1	123.4	510.9	508.8	385.4	449.2	447.1	61.7
24	81	21.9	0.26	20.5	3.4	151.4	538.9	535.5	384.1	463.2	459.8	75.7
26	90	22.1	0.31	20.6	4.8	170.8	558.3	553.5	382.7	472.9	468.1	85.4
28	98	22.3	0.35	20.6	6.2	188.0	575.5	569.3	381.3	481.5	475.3	94.0
30	110	22.5	0.40	20.6	7.6	213.9	601.4	593.8	379.9	494.4	486.9	106.9
32	115	22.6	0.45	20.6	8.3	224.6	612.1	603.8	379.2	499.8	491.5	112.3
34	123	22.8	0.50	20.6	9.7	241.7	629.2	619.6	377.8	508.4	498.7	120.9
38	128	23.2	0.59	20.6	12.4	252.3	639.8	627.4	375.1	513.6	501.2	126.1
42	146	23.5	0.69	20.6	14.5	290.8	678.3	663.8	373.0	532.9	518.4	145.4

Displacement (1/1000 inch)	Force (lb)	Pore pressure (psi)	Axial Strain (%)	Average Area	Pore Pressure (kPa)	Deviator Stress (kPa)	Major Total Stress (kPa)	Major Stress (kPa)	Minor Stress (kPa)	Total Mean Stress	Mean Stress	Q
46	158	23.9	0.78	20.6	17.2	316.4	703.9	686.6	370.3	545.7	528.4	158.2
50	168	24.2	0.87	20.7	19.3	337.6	725.1	705.8	368.2	556.3	537.0	168.8
60	191	25.1	1.11	20.7	25.5	386.1	773.6	748.1	362.0	580.5	555.0	193.0
70	206	25.8	1.35	20.8	30.3	417.3	804.8	774.4	357.2	596.1	565.8	208.6
80	216	26.5	1.58	20.8	35.2	437.6	825.1	789.9	352.3	606.3	571.1	218.8
90	226	27.2	1.82	20.9	40.0	457.9	845.4	805.4	347.5	616.4	576.4	228.9
101	233	27.9	2.08	20.9	44.8	471.5	859.0	814.2	342.7	623.3	578.4	235.8
111	238	28.4	2.32	21.0	48.3	481.0	868.5	820.2	339.2	628.0	579.7	240.5
122	243	29	2.58	21.0	52.4	490.2	877.7	825.3	335.1	632.6	580.2	245.1
131	250	29.5	2.79	21.1	55.8	503.9	891.4	835.6	331.7	639.5	583.6	252.0
140	251	29.9	3.00	21.1	58.6	504.9	892.4	833.8	328.9	640.0	581.4	252.5
152	256	30.5	3.29	21.2	62.7	513.9	901.4	838.7	324.8	644.5	581.7	257.0
160	258	30.6	3.48	21.2	63.4	517.1	904.6	841.2	324.1	646.1	582.6	258.6
180	265	31.7	3.95	21.3	71.0	529.2	916.7	845.7	316.5	652.1	581.1	264.6
200	271	32.3	4.42	21.4	75.2	539.0	926.5	851.4	312.3	657.0	581.9	269.5
220	276	32.6	4.89	21.5	77.2	546.7	934.2	856.9	310.3	660.8	583.6	273.3
240	281	33.4	5.37	21.7	82.7	554.2	941.7	859.0	304.8	664.6	581.9	277.1
266	286	33.6	5.98	21.8	84.1	560.8	948.3	864.2	303.4	667.9	583.8	280.4
280	288	34	6.31	21.9	86.9	562.9	950.4	863.5	300.6	668.9	582.1	281.4
300	291	34.2	6.79	22.0	88.3	566.1	953.6	865.4	299.2	670.6	582.3	283.1
320	295	34.5	7.26	22.1	90.3	571.3	958.8	868.5	297.2	673.1	582.8	285.6
352	300	34.7	8.02	22.3	91.7	576.6	964.1	872.4	295.8	675.8	584.1	288.3
360	301	34.7	8.20	22.3	91.7	577.4	964.9	873.2	295.8	676.2	584.5	288.7
380	305	34.8	8.68	22.4	92.4	582.4	969.9	877.5	295.1	678.7	586.3	291.2
400	305	34.8	9.15	22.6	92.4	579.3	966.8	874.5	295.1	677.2	584.8	289.7
420	310	34.9	9.62	22.7	93.1	586.1	973.6	880.5	294.4	680.6	587.5	293.1
440	311	34.6	10.10	22.8	91.0	585.0	972.5	881.5	296.5	680.0	589.0	292.5
500	313	34.6	11.52	23.2	91.0	579.6	967.1	876.1	296.5	677.3	586.3	289.8
533	311	34.5	12.30	23.4	90.3	570.7	958.2	867.9	297.2	672.9	582.5	285.4
566	311	34.3	13.08	23.6	88.9	565.6	953.1	864.2	298.6	670.3	581.4	282.8
598	311	34.2	13.83	23.8	88.3	560.7	948.2	859.9	299.2	667.9	579.6	280.4
630	310	34.1	14.59	24.0	87.6	553.9	941.4	853.9	299.9	664.5	576.9	277.0
662	310	34	15.35	24.2	86.9	549.0	936.5	849.6	300.6	662.0	575.1	274.5
703	308	33.9	16.31	24.5	86.2	539.1	926.6	840.4	301.3	657.1	570.9	269.6
730	308	33.8	16.95	24.7	85.5	535.0	922.5	837.0	302.0	655.0	569.5	267.5
766	308	33.7	17.80	24.9	84.8	529.5	917.0	832.2	302.7	652.3	567.4	264.8
790	308	33.7	18.37	25.1	84.8	525.9	913.4	828.5	302.7	650.4	565.6	262.9
803	310	33.7	18.68	25.2	84.8	527.4	914.9	830.1	302.7	651.2	566.4	263.7
848	310	33.6	19.74	25.5	84.1	520.5	908.0	823.9	303.4	647.7	563.6	260.2



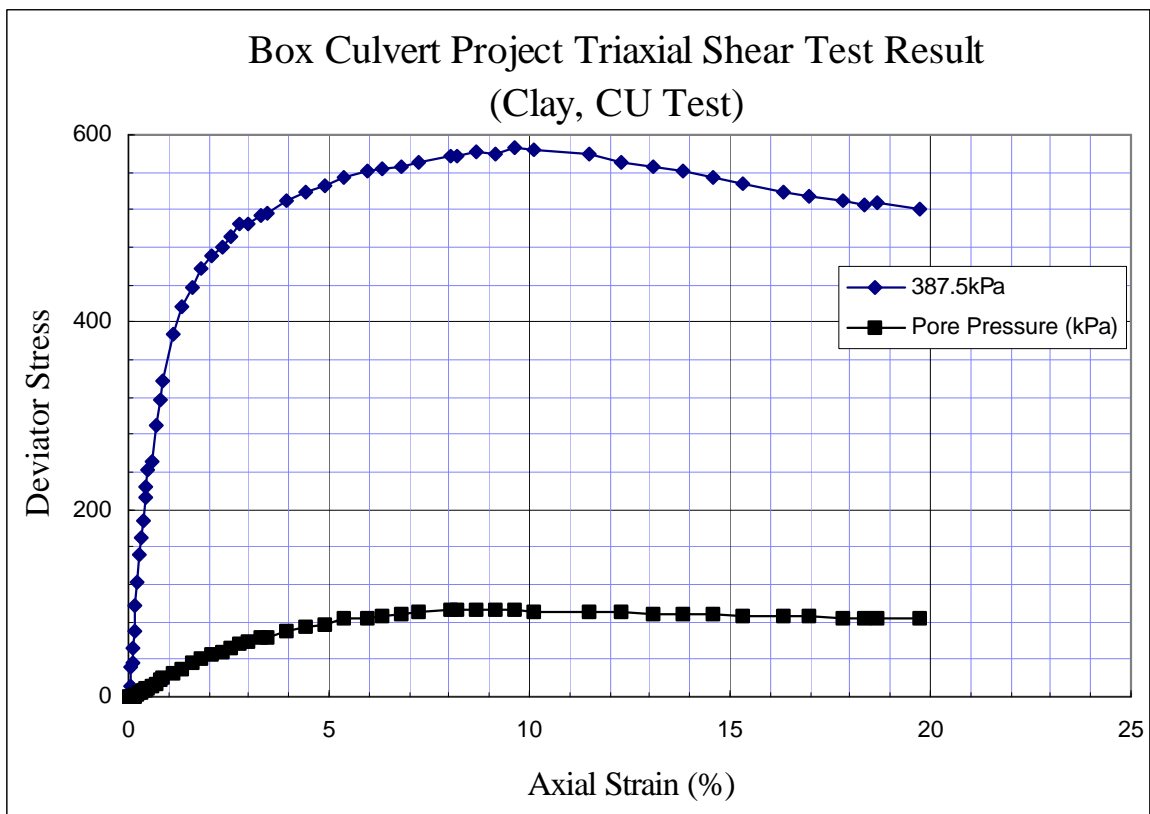


Figure D-29 Triaxial Shear Test Results- Backfill Clay  
(50 mm Sample Diameter, 387.5 kPa Confining Pressure)

### Box Culvert Project: Triaxial Shear Test

Sample: **Clay**

Sample No.3

Diameter:(mm)	51	50.8	51	Height(m m)	111	111.3	110.75
Average Diameter.:	50.9	Initial Area:(e-3 m^2)	2.03	Average Height:(mm)	111.0		
Sample Weight(g):	457.2			Initial Volume (1e-6 m^3):	225.90		
Moisture Content:				Moisture Content:			
Aluminum Box No.:	B7			Aluminum Box No.:	B3		
Box Weight(g):	19.69			Box Weight:	19.68		
Wet Soil+ Box Weight:(g)	30.82			Wet Soil+ Box Weight:	25.7		
Dry Soil+Box Weight:(g)	29.17			Dry Soil+Box Weight:	24.86		
Moisture Content:(%)	17.4			Moisture Content:	16.22		
Averaged Moisture Content:(%)		16.81		Initial Density (KN/M^3):	19.86		
Type of Test: CU							
Type of saturation:				Back Pressure For Saturation: 25.0 psi		172.4 kPa	
Date:6/8-6/10, 1999							
Confining Pressure( Net): 16.3 psi (112.4KPa)							

Displace ment (1/1000 inch)	Force (lb)	Pore pressure (psi)	Axial Strain (%)	Average Area	Pore Pressure (kPa)	Deviator Stress (kPa)	Major Total Stress (kPa)	Major Stress (kPa)	Minor Stress (kPa)	Total Mean Stress	Mean Stress	Q
-175	8.3	21.1	0.00	20.348	0.0	0.0	112.40	112.40	112.40	112.40	112.40	0.00
-173	23	22.4	0.05	20.4	9.0	32.1	144.49	135.53	103.44	128.44	119.48	16.04
-171	32.9	23.9	0.09	20.4	19.3	53.7	166.08	146.77	93.09	139.24	119.93	26.84
-169	38.8	24.6	0.14	20.4	24.1	66.5	178.92	154.79	88.27	145.66	121.53	33.26
-167	42.6	25.2	0.18	20.4	28.3	74.8	187.17	158.90	84.13	149.79	121.52	37.39
-165	47.6	26	0.23	20.4	33.8	85.6	198.03	164.25	78.61	155.22	121.43	42.82
-163	51.7	26.7	0.27	20.4	38.6	94.5	206.92	168.31	73.79	159.66	121.05	47.26
-160	57.3	27.5	0.34	20.4	44.1	106.6	219.05	174.92	68.27	165.72	121.60	53.32
-155	62.2	28.1	0.46	20.4	48.3	117.2	229.58	181.31	64.14	170.99	122.72	58.59
-150	68	28.8	0.57	20.5	53.1	129.6	242.04	188.95	59.31	177.22	124.13	64.82
-145	72.7	29.3	0.68	20.5	56.5	139.7	252.09	195.55	55.86	182.24	125.70	69.84
-140	77.2	29.6	0.80	20.5	58.6	149.3	261.67	203.07	53.79	187.04	128.43	74.64
-130	84	29.9	1.03	20.6	60.7	163.6	276.03	215.35	51.72	194.22	133.54	81.82
-120	89.3	29.9	1.25	20.6	60.7	174.7	287.08	226.41	51.72	199.74	139.07	87.34
-110	92.8	29.8	1.48	20.7	60.0	181.8	294.21	234.22	52.41	203.31	143.32	90.91
-100	95.6	29.6	1.71	20.7	58.6	187.4	299.80	241.19	53.79	206.10	147.49	93.70

Displacement (1/1000 inch)	Force (lb)	Pore pressure (psi)	Axial Strain (%)	Average Area	Pore Pressure (kPa)	Deviator Stress (kPa)	Major Total Stress (kPa)	Major Stress (kPa)	Minor Stress (kPa)	Total Mean Stress	Mean Stress	Q
-85	99.3	29.3	2.05	20.8	56.5	194.7	307.06	250.52	55.86	209.73	153.19	97.33
-70	103	29	2.39	20.8	54.5	201.7	314.06	259.59	57.93	213.23	158.76	100.83
-55	105	28.5	2.74	20.9	51.0	206.1	318.45	267.43	61.38	215.43	164.40	103.03
-40	108	28.2	3.08	21.0	49.0	210.0	322.38	273.43	63.45	217.39	168.44	104.99
-25	109	27.9	3.42	21.1	46.9	212.6	325.02	278.13	65.51	218.71	171.82	106.31
-10	111	27.4	3.76	21.1	43.4	215.4	327.84	284.40	68.96	220.12	176.68	107.72
10	112	26.9	4.22	21.2	40.0	217.1	329.54	289.55	72.41	220.97	180.98	108.57
30	116	26.5	4.67	21.3	37.2	224.0	336.41	299.18	75.17	224.41	187.17	112.01
50	118	26.2	5.13	21.4	35.2	227.7	340.11	304.94	77.24	226.25	191.09	113.85
70	120	25.9	5.58	21.6	33.1	230.3	342.73	309.63	79.30	227.56	194.47	115.16
93	122	25.5	6.11	21.7	30.3	233.6	345.96	315.62	82.06	229.18	198.84	116.78
120	124	25	6.72	21.8	26.9	236.1	348.50	321.61	85.51	230.45	203.56	118.05
150	127	24.7	7.41	22.0	24.8	240.2	352.64	327.81	87.58	232.52	207.70	120.12
180	129	24.2	8.09	22.1	21.4	242.3	354.68	333.30	91.03	233.54	212.16	121.14
215	133	23.9	8.89	22.3	19.3	247.1	359.54	340.23	93.09	235.97	216.66	123.57
245	134	23.4	9.57	22.5	15.9	248.6	361.04	345.18	96.54	236.72	220.86	124.32
270	137	23.3	10.14	22.6	15.2	252.0	364.38	349.21	97.23	238.39	223.22	125.99
300	139	22.8	10.83	22.8	11.7	254.0	366.36	354.63	100.68	239.38	227.66	126.98
346	142	22.4	11.88	23.1	9.0	257.5	369.91	360.95	103.44	241.16	232.19	128.76
380	144	22	12.65	23.3	6.2	258.5	370.89	364.69	106.19	241.65	235.44	129.25
420	146	21.7	13.56	23.5	4.1	260.5	372.91	368.78	108.26	242.66	238.52	130.26
460	149	21.4	14.47	23.8	2.1	263.0	375.40	373.33	110.33	243.90	241.83	131.50
500	152	21	15.39	24.0	-0.7	266.1	378.51	379.20	113.09	245.45	246.14	133.05
540	154	20.7	16.30	24.3	-2.8	266.7	379.11	381.87	115.16	245.76	248.51	133.36
580	156	20.5	17.21	24.6	-4.1	267.6	380.00	384.14	116.54	246.20	250.34	133.80
620	159	20.2	18.12	24.9	-6.2	268.8	381.17	387.38	118.61	246.79	252.99	134.39
660	161	19.9	19.03	25.1	-8.3	270.2	382.60	390.87	120.67	247.50	255.77	135.10
700	164	19.7	19.94	25.4	-9.7	271.5	383.93	393.58	122.05	248.16	257.82	135.76
740	165	19.5	20.86	25.7	-11.0	270.0	382.39	393.42	123.43	247.40	258.43	135.00

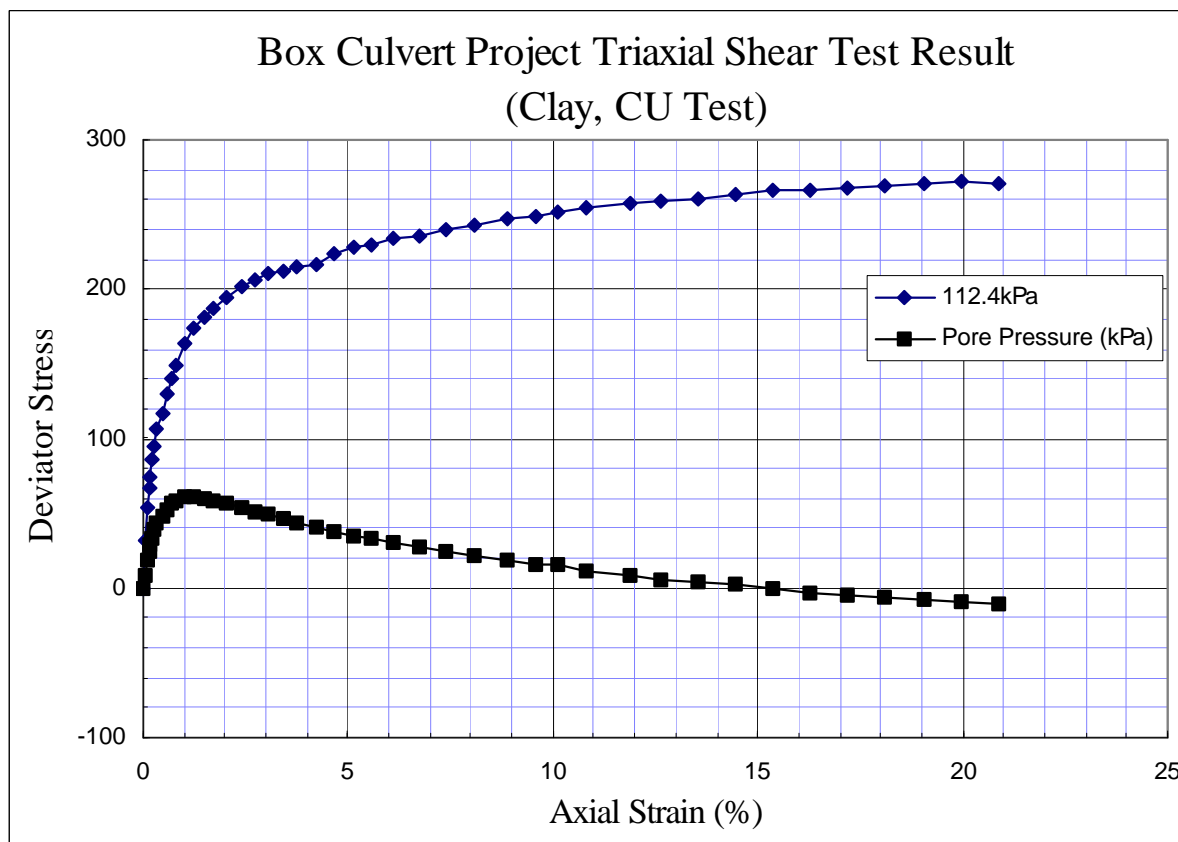


Figure D-30 Triaxial Shear Test Results- Backfill Clay  
(50 mm Sample Diameter, 112.4 kPa Confining Pressure)

Box Culvert Project: Triaxial Shear Test							
Sample: <b>Clay</b>							
Sample No.4							
Diameter:(mm)	50	50	49.9	Height(mm)	102.4	102.5	102.4
Average Diameter:	50.0	Initial Area:(e-3 m^2)	1.96	Aver. H.:(mm)	102.4		
Sample Weight(g):				Initial Volume (1e-6 m^3):	200.93		
Moisture Content:				Moisture Content:			
Aluminum Box No.:	B7			Aluminum Box No.:	B3		
Box Weight(g):	19.69			Box Weight:	19.68		
Wet Soil+ Box Weight:(g)	30.82			Wet Soil+ Box Weight:	25.7		
Dry Soil+ Box Weight:(g)	29.17			Dry Soil+Box Weight:	24.86		
Moisture Content:(%)	17.4			Moisture Content:	16.22		
Averaged Moisture Content:(%)		16.81		Initial Density (KN/M^3):	0.00		
Type of Test: CU							
Type of saturation: CU				Back Pressure For Saturation: 25.0 psi	172 kPa		
Date:6/8-6/10, 1999							
Confining Pressure( Net): 7.2 psi (49.6 kPa)							

Displacement (1/1000 inch)	Force (lb)	Pore pressure (psi)	Axial Strain (%)	Average Area	Pore Pressure (kPa)	Deviator Stress (kPa)	Major Total Stress (kPa)	Major Stress (kPa)	Minor Stress (kPa)	Total Mean Stress	Mean Stress	Q
245	5.8	26.3	0.00	18.1	0.0	0.0	49.60	49.60	49.60	49.60	49.60	0.00
247	13.3	26.7	0.05	18.1	2.8	18.4	68.00	65.25	46.84	58.80	56.04	9.20
249	20.5	27.2	0.10	18.1	6.2	36.1	85.66	79.45	43.39	67.63	61.42	18.03
251	24.4	27.6	0.15	18.1	9.0	45.6	95.20	86.24	40.64	72.40	63.44	22.80
253	26.6	27.9	0.20	18.1	11.0	51.0	100.57	89.54	38.57	75.08	64.05	25.48
256	30	28.2	0.27	18.1	13.1	59.3	108.85	95.75	36.50	79.23	66.13	29.63
259	32	28.4	0.35	18.2	14.5	64.1	113.70	99.22	35.12	81.65	67.17	32.05
261	33.8	28.6	0.40	18.2	15.9	68.5	118.07	102.22	33.74	83.84	67.98	34.24
265	36.7	28.8	0.49	18.2	17.2	75.5	125.09	107.85	32.36	87.35	70.11	37.75
270	39.7	29.1	0.62	18.2	19.3	82.7	132.32	113.01	30.29	90.96	71.65	41.36
275	41.5	29.2	0.74	18.2	20.0	87.0	136.60	116.61	29.60	93.10	73.11	43.50
280	43.1	29.3	0.86	18.3	20.7	90.8	140.39	119.70	28.92	94.99	74.31	45.39
290	45.4	29.9	1.11	18.3	24.8	96.1	145.75	120.92	24.78	97.67	72.85	48.07
300	46.9	29.9	1.36	18.3	24.8	99.5	149.14	124.32	24.78	99.37	74.55	49.77
315	48.3	29.9	1.73	18.4	24.8	102.5	152.14	127.32	24.78	100.87	76.05	51.27
330	49.7	29.8	2.10	18.5	24.1	105.5	155.12	130.99	25.47	102.36	78.23	52.76
345	51.1	29.4	2.47	18.6	21.4	108.5	158.07	136.70	28.23	103.84	82.46	54.24

Displacement (1/1000 inch)	Force (lb)	Pore pressure (psi)	Axial Strain (%)	Average Area	Pore Pressure (kPa)	Deviator Stress (kPa)	Major Total Stress (kPa)	Major Stress (kPa)	Minor Stress (kPa)	Total Mean Stress	Mean Stress	Q
360	52.8	29.3	2.84	18.6	20.7	112.1	161.72	141.03	28.92	105.66	84.97	56.06
375	53.7	29.1	3.21	18.7	19.3	113.8	163.43	144.12	30.29	106.51	87.21	56.91
390	54.8	29	3.58	18.8	18.6	116.0	165.60	146.98	30.98	107.60	88.98	58.00
410	56.5	28.9	4.08	18.9	17.9	119.4	169.00	151.08	31.67	109.30	91.38	59.70
430	57.8	28.7	4.57	19.0	16.5	121.8	171.44	154.89	33.05	110.52	93.97	60.92
450	59.6	28.5	5.06	19.1	15.2	125.4	175.00	159.83	34.43	112.30	97.13	62.70
470	60.7	28.4	5.56	19.2	14.5	127.3	176.90	162.42	35.12	113.25	98.77	63.65
490	61.9	28.3	6.05	19.3	13.8	129.4	179.00	165.21	35.81	114.30	100.51	64.70
510	63.2	28.1	6.55	19.4	12.4	131.7	181.30	168.89	37.19	115.45	103.04	65.85
530	64.2	27.9	7.04	19.5	11.0	133.3	182.89	171.86	38.57	116.24	105.21	66.64
553	65.6	27.7	7.61	19.6	9.7	135.6	185.25	175.60	39.95	117.42	107.77	67.82
575	67	27.5	8.15	19.7	8.3	138.0	187.61	179.33	41.33	118.60	110.33	69.00
600	69	27.3	8.77	19.8	6.9	141.6	191.16	184.26	42.71	120.38	113.48	70.78
640	71.5	26.6	9.76	20.1	2.1	145.6	195.16	193.10	47.53	122.38	120.31	72.78
680	73.5	26.5	10.75	20.3	1.4	148.4	197.95	196.57	48.22	123.78	122.40	74.18
722	75.8	26.1	11.79	20.5	-1.4	151.6	201.21	202.59	50.98	125.41	126.78	75.81
760	78	25.9	12.72	20.7	-2.8	154.7	204.31	207.07	52.36	126.96	129.71	77.36
802	80.2	25.5	13.76	21.0	-5.5	157.5	207.13	212.65	55.12	128.36	133.88	78.76
840	82.6	25.3	14.70	21.2	-6.9	160.8	210.44	217.34	56.50	130.02	136.92	80.42
890	85	25	15.94	21.5	-9.0	163.5	213.06	222.03	58.56	131.33	140.30	81.73
920	86.2	24.8	16.68	21.7	-10.3	164.5	214.08	224.42	59.94	131.84	142.18	82.24
960	88.5	24.5	17.67	22.0	-12.4	167.2	216.78	229.19	62.01	133.19	145.60	83.59
1000	90.7	24.3	18.65	22.3	-13.8	169.6	219.16	232.95	63.39	134.38	148.17	84.78
1040	92.5	24.1	19.64	22.5	-15.2	171.1	220.66	235.82	64.77	135.13	150.30	85.53
1104	95.5	23.7	21.22	23.0	-17.9	173.5	223.09	241.02	67.53	136.35	154.27	86.75
1120	95.9	23.6	21.62	23.1	-18.6	173.4	222.99	241.61	68.22	136.30	154.91	86.70
1160	98.2	23.4	22.61	23.4	-20.0	175.6	225.17	245.17	69.60	137.39	157.38	87.79
1200	101	23.2	23.60	23.7	-21.4	177.8	227.44	248.81	70.97	138.52	159.89	88.92

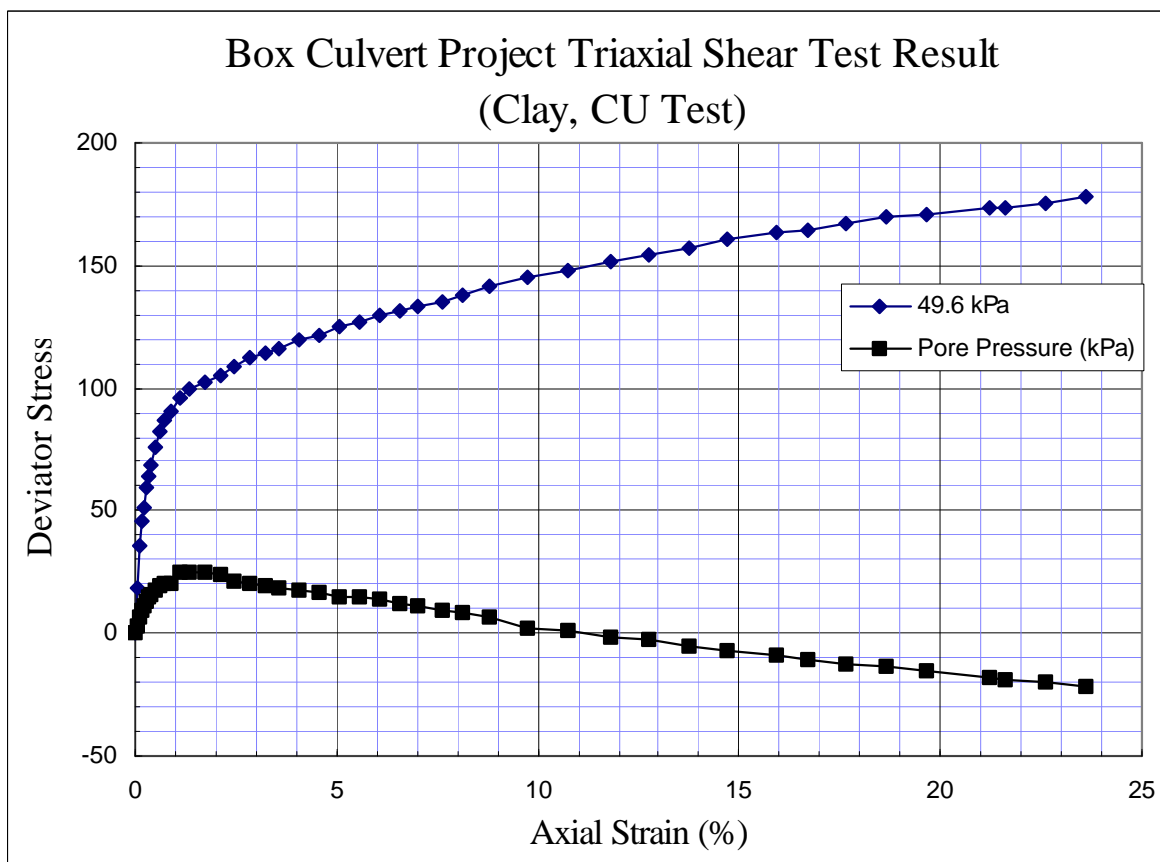


Figure D-31 Triaxial Shear Test Results- Backfill Clay  
(50 mm Sample Diameter, 49.6 kPa Confining Pressure)

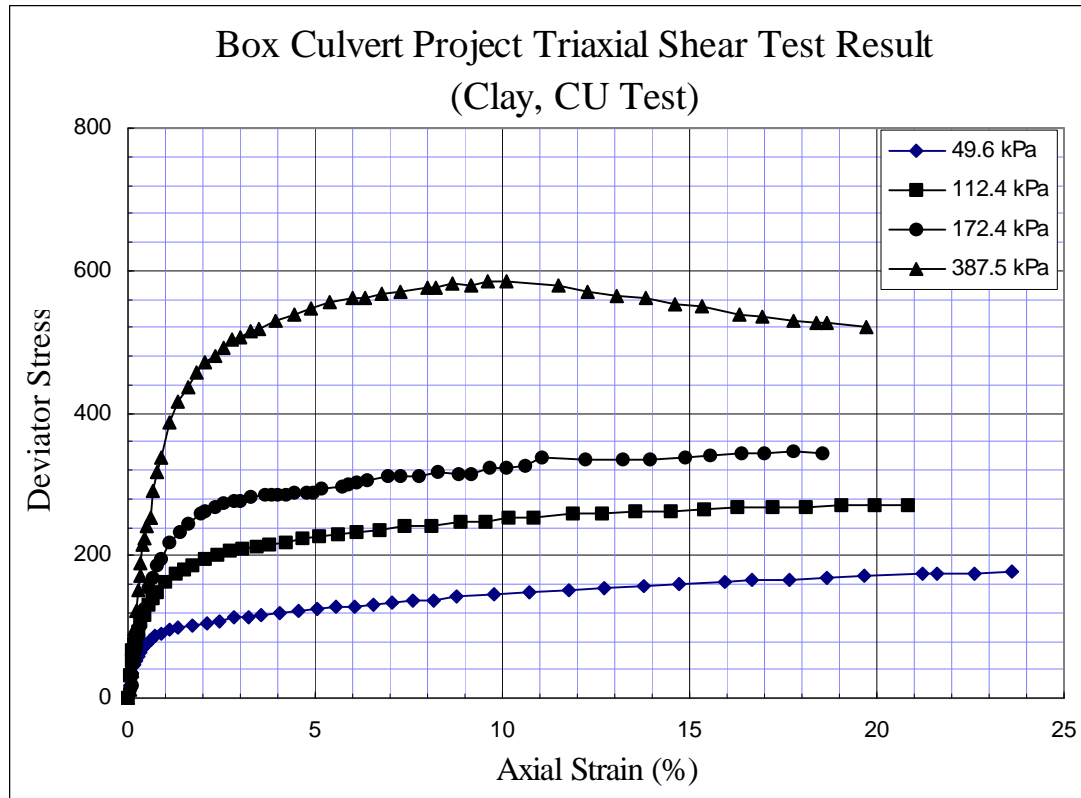


Figure D-32 Deviator Stress of Clay Under Different Confining Pressures



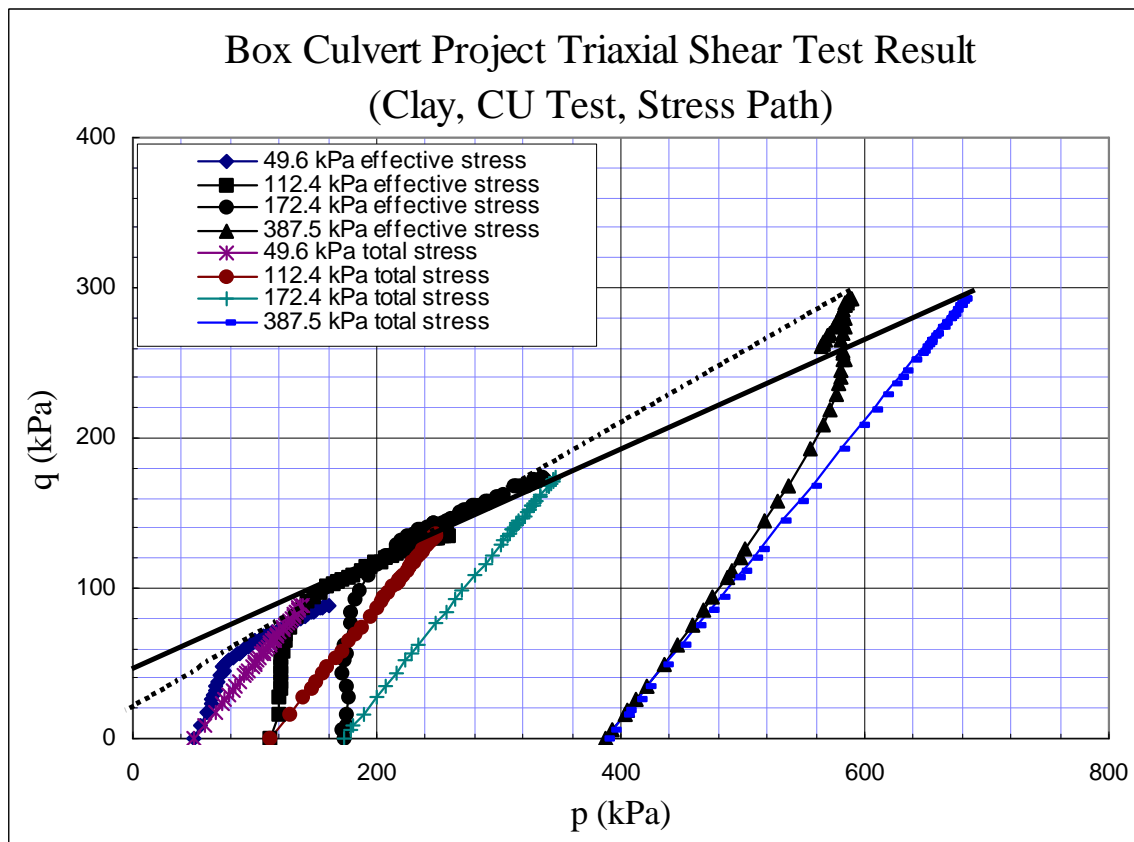


Figure D-33 Stress Path of Clay under Different Confining Pressures

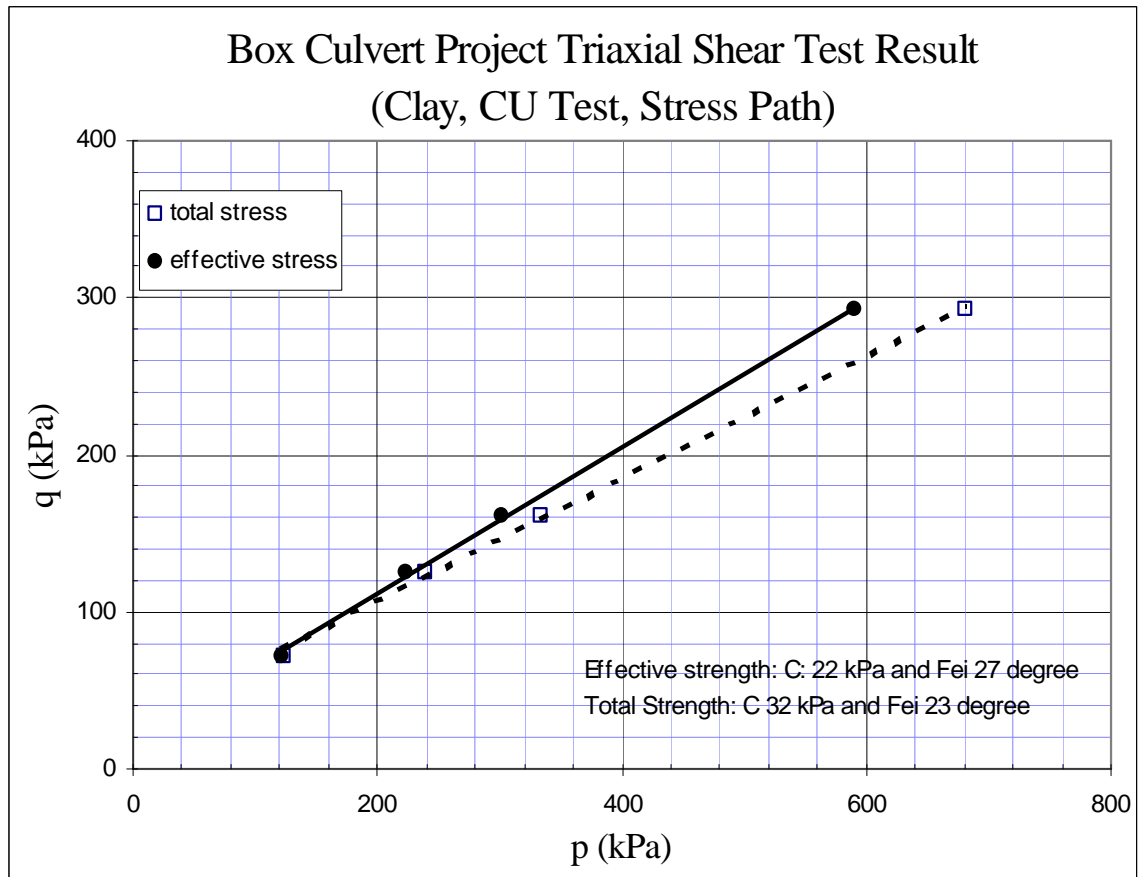


Figure D-34 Effective and Total Strength at 10% Strain

## **APPENDIX E**

### **Concrete Cylinder Data**

The compressive strength of the concrete cylinders was determined using ASTM C39.

The modulus of elasticity was determined using ASTM C469. The modulus of elasticity reported is the 40% chord modulus. Specimens were stored in a moist room until the time of testing.

#### **Summary of Results**

Culvert	Average Compressive Strength (MPa)	Average Modulus of Elasticity (GPa)
Sullivan	31.6	37.8
Greene	33.1	37.2

### Sullivan County Concrete Test Cylinders

Cylinder	Date Cast	Test Date	Stress at $S = 50 \times 10^{-6}$ (KPa)	Ultimate Stress (KPa)	Stress at 40% of Ultimate (KPa)	Strain at 40% of Ultimate (mm/mm)	Modulus of Elasticity (KPa)
UT21			2,069	30,690	12,280	0.0003050	40,040,000
UT22			7,930	36,830	14,730	0.0002276	38,290,000
UT12			8,593	31,790	12,720	0.0001694	34,570,000
UT31			7,268	28,950	11,580	0.0001624	38,360,000
UT32			3,683	27,000	10,800	0.0002330	38,890,000
UT13			10,343	31,670	12,670	0.0001128	37,050,000
UT23			2,439	35,120	14,050	0.0003580	37,700,000
UT33				30,730			-

S = 252,780

S = 264909680.5

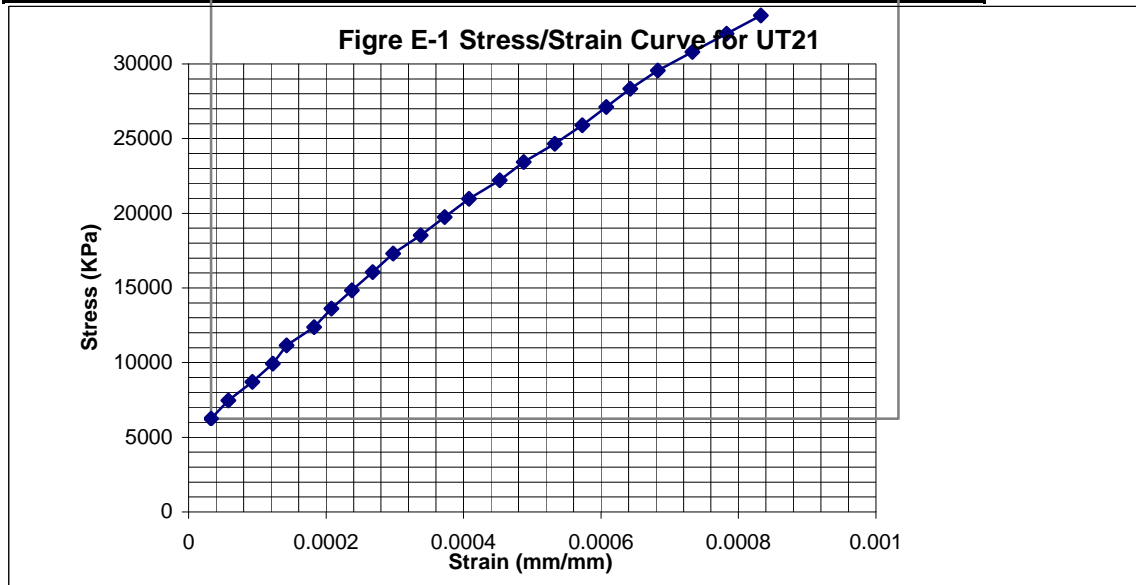
**Ave. Compressive Strength(KPa): 31,600**

**Ave. Modulus(KPa) : 37,840,000**

## SULLIVAN CO. CULVERT CONCRETE TEST CYLINDERS

Cylinder **UT21** Date Cast  Date Tested  Dia. (in.) **5.98**

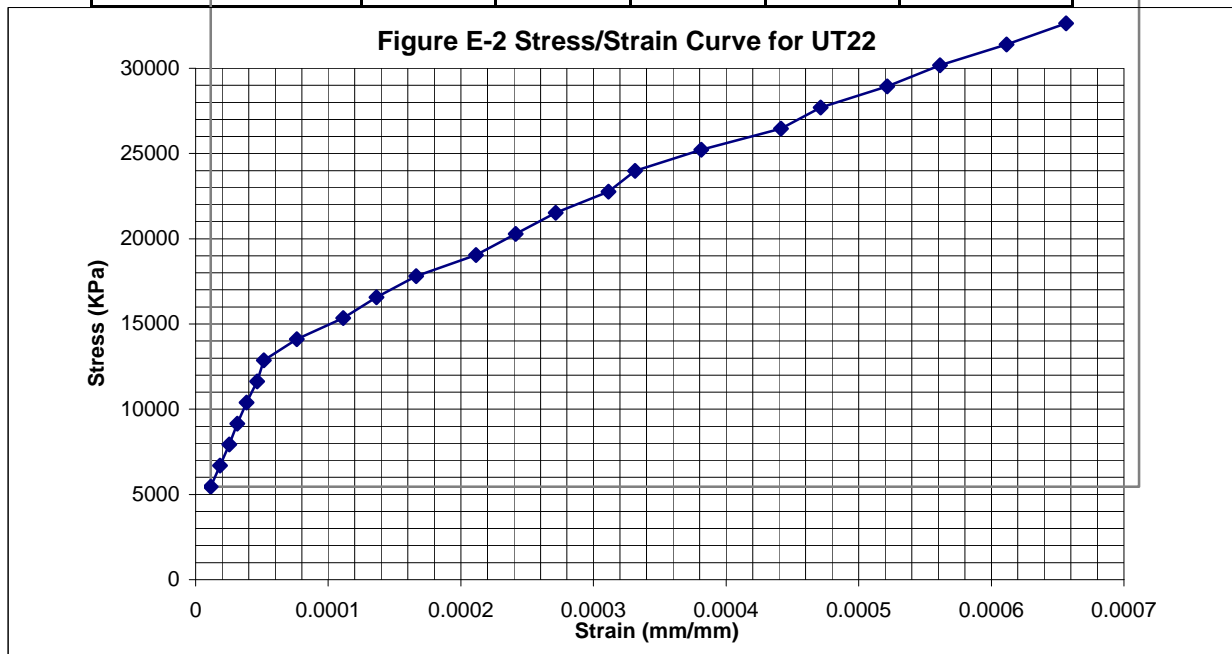
$\Delta$ (in.*0.001)	Load(lbs*10 <sup>3</sup> )	Stress(KPa)	Strain(mm/mm)
0	0	0	0
0.25	5	1227.543	0.000025
0.6	10	2455.086	0.00006
0.9	15	3682.628	0.00009
1.1	20	4910.171	0.00011
1.5	25	6137.714	0.00015
1.75	30	7365.257	0.000175
2.05	35	8592.8	0.000205
2.35	40	9820.343	0.000235
2.65	45	11047.89	0.000265
3.05	50	12275.43	0.000305
3.4	55	13502.97	0.00034
3.75	60	14730.51	0.000375
4.2	65	15958.06	0.00042
4.55	70	17185.6	0.000455
5	75	18413.14	0.0005
5.4	80	19640.69	0.00054
5.75	85	20868.23	0.000575
6.1	90	22095.77	0.00061
6.5	95	23323.31	0.00065
7	100	24550.86	0.0007
7.5	105	25778.4	0.00075
8	110	27005.94	0.0008
<b>Maximum Load=</b>	125	30688.57	



## SULLIVAN CO. CULVERT CONCRETE TEST CYLINDERS

Cylinder **UT22** Date Cast  Date Tested  Dia. (in.) **5.96**

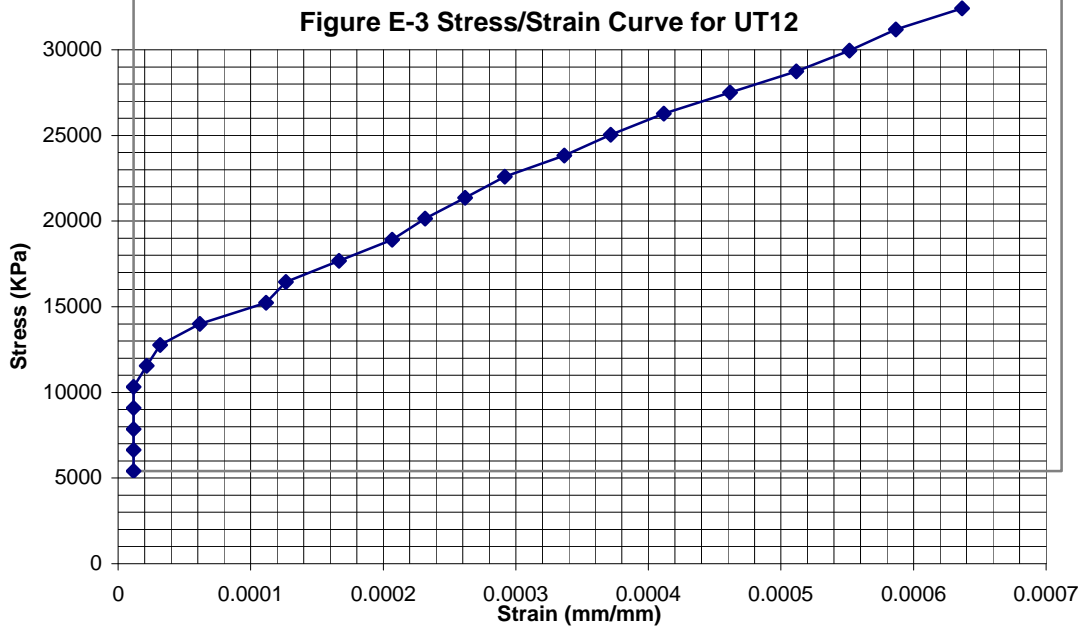
$\Delta$ (in.*0.001)	Load(lbs*10 <sup>3</sup> )	Stress(KPa)	Strain(mm/mm)
0	0	0	0
0.07	5	1235.795	0.000007
0.14	10	2471.59	0.000014
0.2	15	3707.386	0.00002
0.27	20	4943.181	0.000027
0.35	25	6178.976	0.000035
0.4	30	7414.771	0.00004
0.65	35	8650.566	0.000065
1	40	9886.362	0.0001
1.25	45	11122.16	0.000125
1.55	50	12357.95	0.000155
2	55	13593.75	0.0002
2.3	60	14829.54	0.00023
2.6	65	16065.34	0.00026
3	70	17301.13	0.0003
3.2	75	18536.93	0.00032
3.7	80	19772.72	0.00037
4.3	85	21008.52	0.00043
4.6	90	22244.31	0.00046
5.1	95	23480.11	0.00051
5.5	100	24715.9	0.00055
6	105	25951.7	0.0006
6.45	110	27187.49	0.000645
<b>Maximum Load=</b>	149	36826.7	



## SULLIVAN CO. CULVERT CONCRETE TEST CYLINDERS

Cylinder **UT12** Date Cast  Date Tested  Dia. (in.) **5.98**

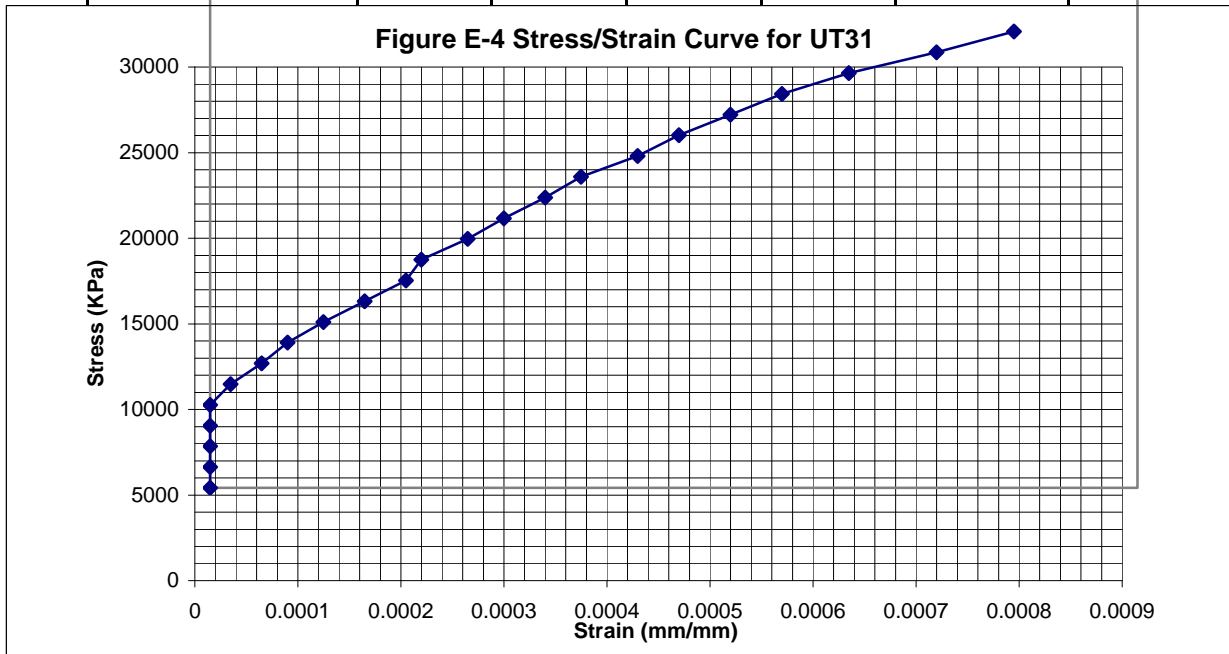
$\Delta$ (in.*0.001)	Load(lbs*10 <sup>-3</sup> )	Stress(KPa)	Strain(mm/mm)
0	0	0	0
	5	1227.543	0
	10	2455.086	0
	15	3682.628	0
	20	4910.171	0
0.1	25	6137.714	0.00001
0.2	30	7365.257	0.00002
0.5	35	8592.8	0.00005
1	40	9820.343	0.0001
1.15	45	11047.89	0.000115
1.55	50	12275.43	0.000155
1.95	55	13502.97	0.000195
2.2	60	14730.51	0.00022
2.5	65	15958.06	0.00025
2.8	70	17185.6	0.00028
3.25	75	18413.14	0.000325
3.6	80	19640.69	0.00036
4	85	20868.23	0.0004
4.5	90	22095.77	0.00045
5	95	23323.31	0.0005
5.4	100	24550.86	0.00054
5.75	105	25778.4	0.000575
6.25	110	27005.94	0.000625
<b>Maximum Load=</b>	129.5	31793.36	



## SULLIVAN CO. CULVERT CONCRETE TEST CYLINDERS

Cylinder **UT31** Date Cast  Date Tested  Dia. (in.) **6.02**

$\Delta$ (in.*0.001)	Load(lbs*10 <sup>3</sup> )	Stress(KPa)	Strain(mm/mm)
0	0	0	0
	5	1211.284	0
	10	2422.568	0
	15	3633.852	0
	20	4845.137	0
0.2	25	6056.421	0.00002
0.5	30	7267.705	0.00005
0.75	35	8478.989	0.000075
1.1	40	9690.273	0.00011
1.5	45	10901.56	0.00015
1.9	50	12112.84	0.00019
2.05	55	13324.13	0.000205
2.5	60	14535.41	0.00025
2.85	65	15746.69	0.000285
3.25	70	16957.98	0.000325
3.6	75	18169.26	0.00036
4.15	80	19380.55	0.000415
4.55	85	20591.83	0.000455
5.05	90	21803.11	0.000505
5.55	95	23014.4	0.000555
6.2	100	24225.68	0.00062
7.05	105	25436.97	0.000705
7.8	110	26648.25	0.00078
<b>Maximum Load=</b>	119.5	28949.69	

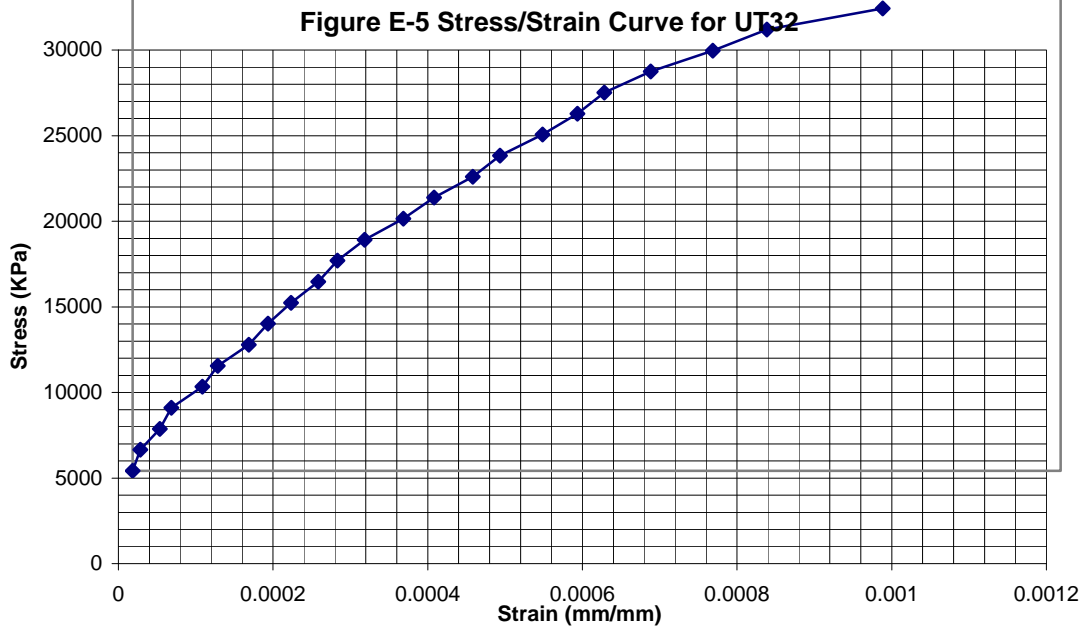




## SULLIVAN CO. CULVERT CONCRETE TEST CYLINDERS

Cylinder **UT32** Date Cast  Date Tested  Dia. (in.) **5.98**

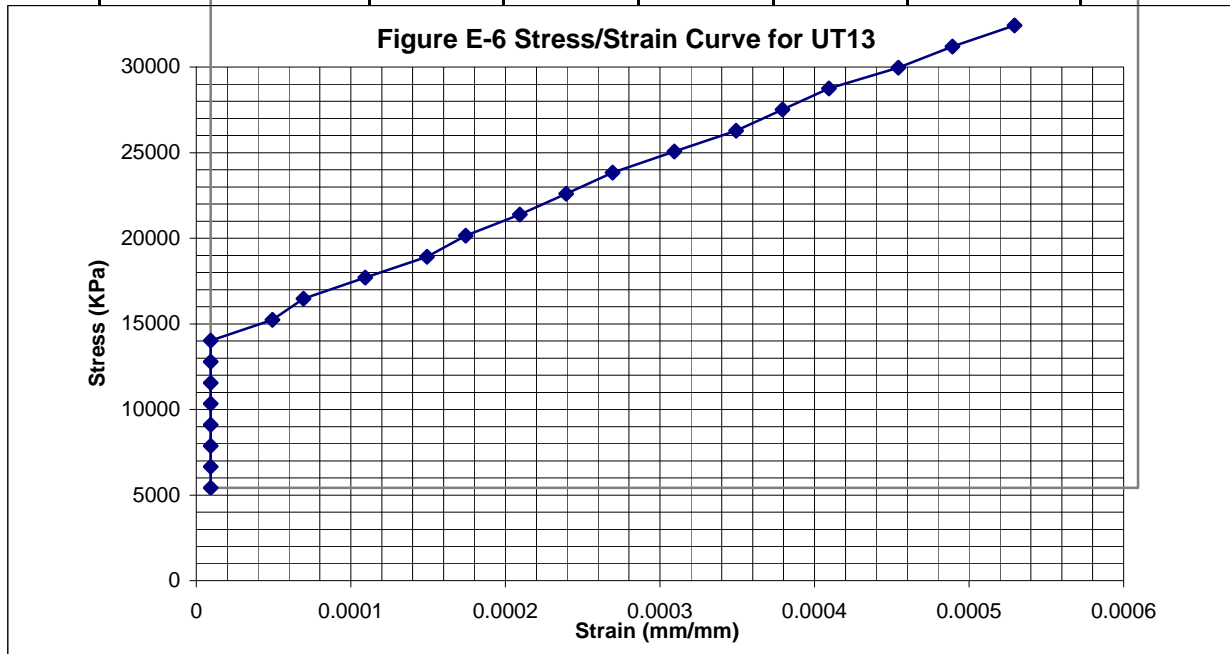
$\Delta$ (in.*0.001)	Load(lbs*10 <sup>3</sup> )	Stress(KPa)	Strain(mm/mm)
0	0	0	0
0.1	5	1227.543	0.00001
0.35	10	2455.086	0.000035
0.5	15	3682.628	0.00005
0.9	20	4910.171	0.00009
1.1	25	6137.714	0.00011
1.5	30	7365.257	0.00015
1.75	35	8592.8	0.000175
2.05	40	9820.343	0.000205
2.4	45	11047.89	0.00024
2.65	50	12275.43	0.000265
3	55	13502.97	0.0003
3.5	60	14730.51	0.00035
3.9	65	15958.06	0.00039
4.4	70	17185.6	0.00044
4.75	75	18413.14	0.000475
5.3	80	19640.69	0.00053
5.75	85	20868.23	0.000575
6.1	90	22095.77	0.00061
6.7	95	23323.31	0.00067
7.5	100	24550.86	0.00075
8.2	105	25778.4	0.00082
9.7	110	27005.94	0.00097
<b>Maximum Load=</b>	110	27005.94	



## SULLIVAN CO. CULVERT CONCRETE TEST CYLINDERS

Cylinder **UT13** Date Cast  Date Tested  Dia. (in.) **5.98**

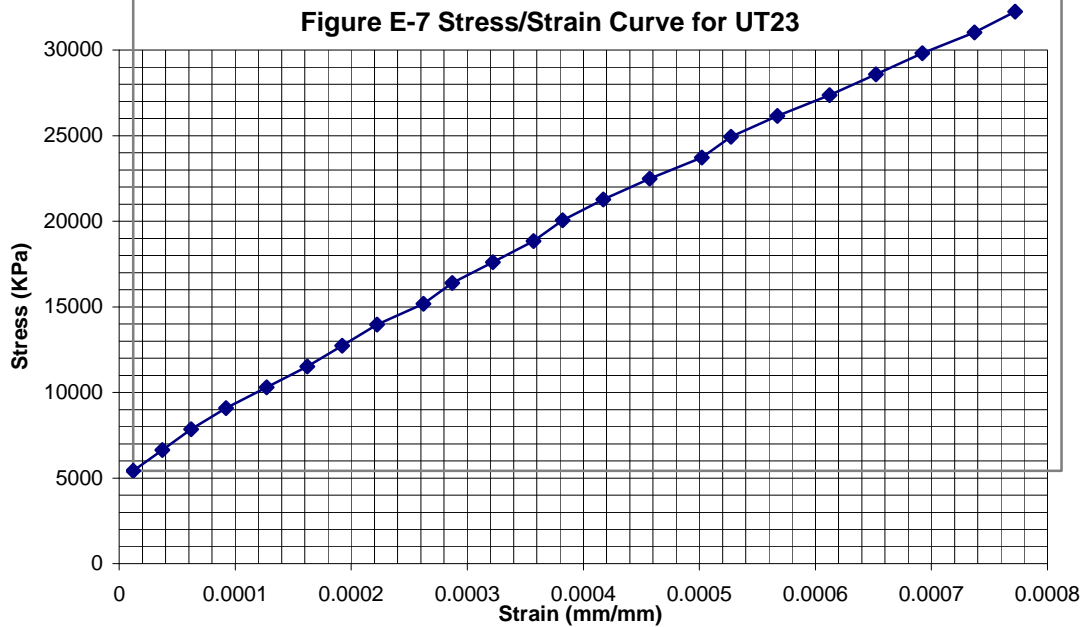
$\Delta$ (in.*0.001)	Load(lbs*10 <sup>3</sup> )	Stress(KPa)	Strain(mm/mm)
0	0	0	0
	5	1227.543	0
	10	2455.086	0
	15	3682.628	0
	20	4910.171	0
	25	6137.714	0
	30	7365.257	0
	35	8592.8	0
0.4	40	9820.343	0.00004
0.6	45	11047.89	0.00006
1	50	12275.43	0.0001
1.4	55	13502.97	0.00014
1.65	60	14730.51	0.000165
2	65	15958.06	0.0002
2.3	70	17185.6	0.00023
2.6	75	18413.14	0.00026
3	80	19640.69	0.0003
3.4	85	20868.23	0.00034
3.7	90	22095.77	0.00037
4	95	23323.31	0.0004
4.45	100	24550.86	0.000445
4.8	105	25778.4	0.00048
5.2	110	27005.94	0.00052
<b>Maximum Load=</b>	129	31670.6	



## SULLIVAN CO. CULVERT CONCRETE TEST CYLINDERS

Cylinder **UT23** Date Cast  Date Tested  Dia. (in.) **6**

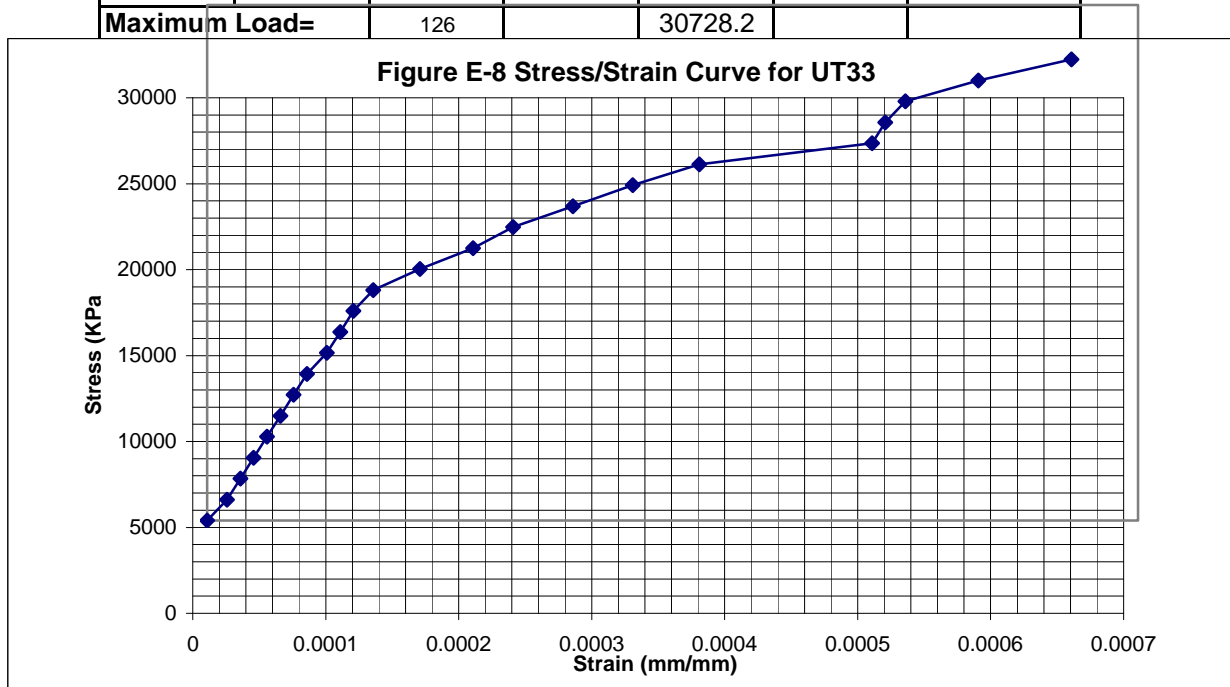
$\Delta$ (in.*0.001)	Load(lbs*10 <sup>3</sup> )	Stress(KPa)	Strain(mm/mm)
0	0	0	0
0.25	5	1219.373	0.000025
0.5	10	2438.746	0.00005
0.8	15	3658.119	0.00008
1.15	20	4877.491	0.000115
1.5	25	6096.864	0.00015
1.8	30	7316.237	0.00018
2.1	35	8535.61	0.00021
2.5	40	9754.983	0.00025
2.75	45	10974.36	0.000275
3.1	50	12193.73	0.00031
3.45	55	13413.1	0.000345
3.7	60	14632.47	0.00037
4.05	65	15851.85	0.000405
4.45	70	17071.22	0.000445
4.9	75	18290.59	0.00049
5.15	80	19509.97	0.000515
5.55	85	20729.34	0.000555
6	90	21948.71	0.0006
6.4	95	23168.08	0.00064
6.8	100	24387.46	0.00068
7.25	105	25606.83	0.000725
7.6	110	26826.2	0.00076
<b>Maximum Load=</b>	144	35117.94	



## SULLIVAN CO. CULVERT CONCRETE TEST CYLINDERS

Cylinder **UT33** Date Cast  Date Tested  Dia. (in.) **6**

$\Delta$ (in.*0.001)	Load(lbs*10 <sup>3</sup> )	Stress(KPa)	Strain(mm/mm)
0	0	0	0
0.15	5	1219.373	0.000015
0.25	10	2438.746	0.000025
0.35	15	3658.119	0.000035
0.45	20	4877.491	0.000045
0.55	25	6096.864	0.000055
0.65	30	7316.237	0.000065
0.75	35	8535.61	0.000075
0.9	40	9754.983	0.00009
1	45	10974.36	0.0001
1.1	50	12193.73	0.00011
1.25	55	13413.1	0.000125
1.6	60	14632.47	0.00016
2	65	15851.85	0.0002
2.3	70	17071.22	0.00023
2.75	75	18290.59	0.000275
3.2	80	19509.97	0.00032
3.7	85	20729.34	0.00037
5	90	21948.71	0.0005
5.1	95	23168.08	0.00051
5.25	100	24387.46	0.000525
5.8	105	25606.83	0.00058
6.5	110	26826.2	0.00065
<b>Maximum Load=</b>	126	30728.2	



### Greene County Concrete Test Cylinders

Cylinder	Date Cast	Location	Test Date	Stress at Strain of 50*10 <sup>-6</sup> (KPa)	Ultimate Stress (KPa)	Stress at 40% of Ultimate(KPa)	Strain at 40% of Ultimate (mm/mm)	Modulus of Elasticity (KPa)
1	9/25/96	Sidewall section A	6/26/97	2,443	31,370	12,550	0.0003010	40,220,000
2	10/21/96	Top section B	6/26/97	2,068	36,860	14,740	0.0004030	35,920,000
3	10/3/96	Sidewall section B	6/26/97	2,148	31,070	12,430	0.0003380	35,730,000
4	10/3/96	Sidewall section B	6/26/97	2,107	30,760	12,310	0.0003400	35,170,000
5	9/25/96	Sidewall section A	6/26/97	2,383	35,490	14,200	0.0003513	39,220,000
6	10/21/96	Top section B	6/26/97	-	33,170	-	-	-

S = 198,720

S = 186,250,117

**Ave.Compressive Strength(KPa) = 33,120**

**Ave.Modulus(KPa) = 37,250,000**



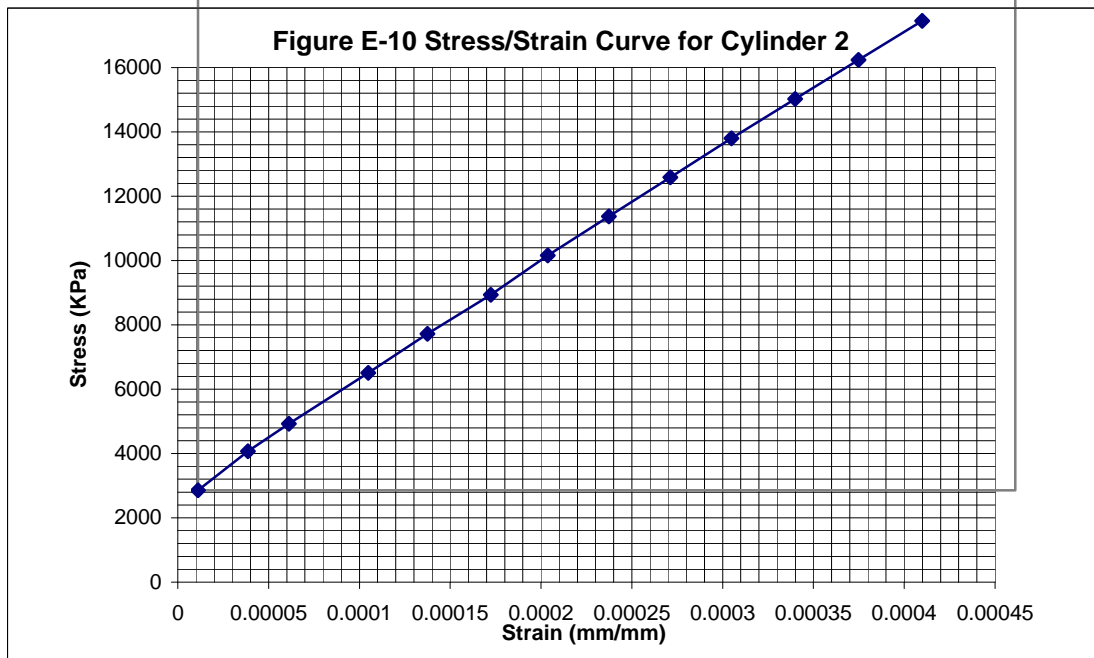
## GREENE CO. CULVERT CONCRETE TEST CYLINDERS

Cylinder **2**Date Cast **10/21/96**Test Date **6/26/97**

Dia.1 (in.)      5.904

Dia.2(in.) 6.11

Ave.Dia.	<b>6.007</b>
----------	--------------

[illegible]

## GREENE CO. CULVERT CONCRETE TEST CYLINDERS

Cylinder	3
----------	---

Date Cast **10/3/96**Test Date **6/26/97**

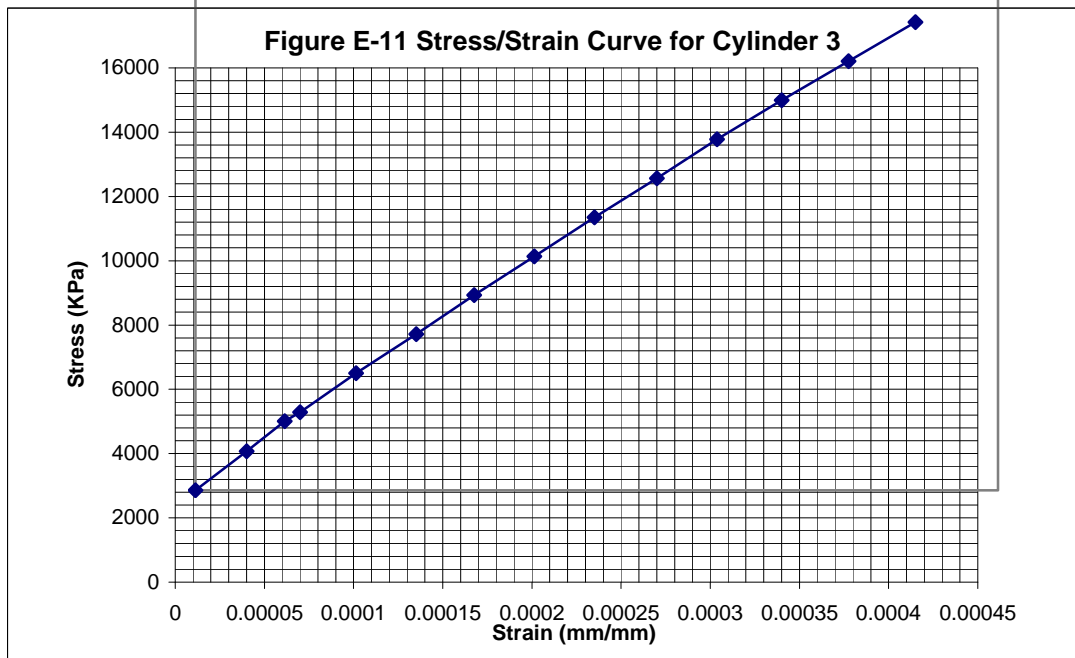
6.051

5.977

6.014

Ave.Dia.

6.014

[illegible]



## GREENE CO. CULVERT CONCRETE TEST CYLINDERS

Cylinder 

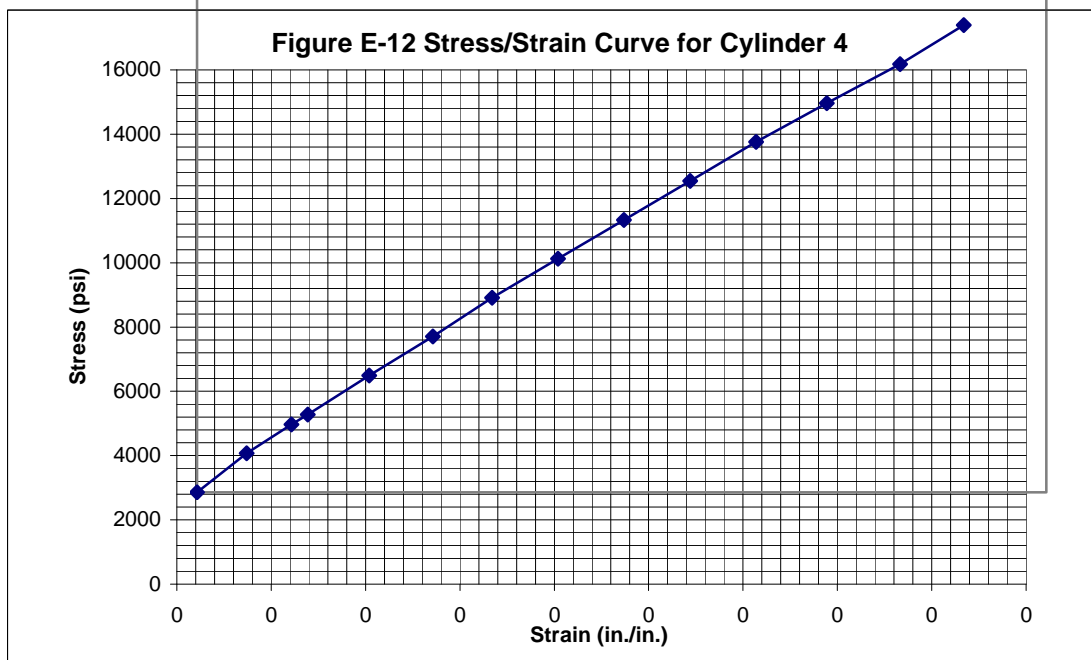
4
---

Date Cast **10/3/96**Test Date **6/26/97**

Dia.1 (in.)	5.99
-------------	------

Dia.2(in.) 6.051

Ave.Dia.	6.0205
----------	--------

[illegible]

## GREENE CO. CULVERT CONCRETE TEST CYLINDERS

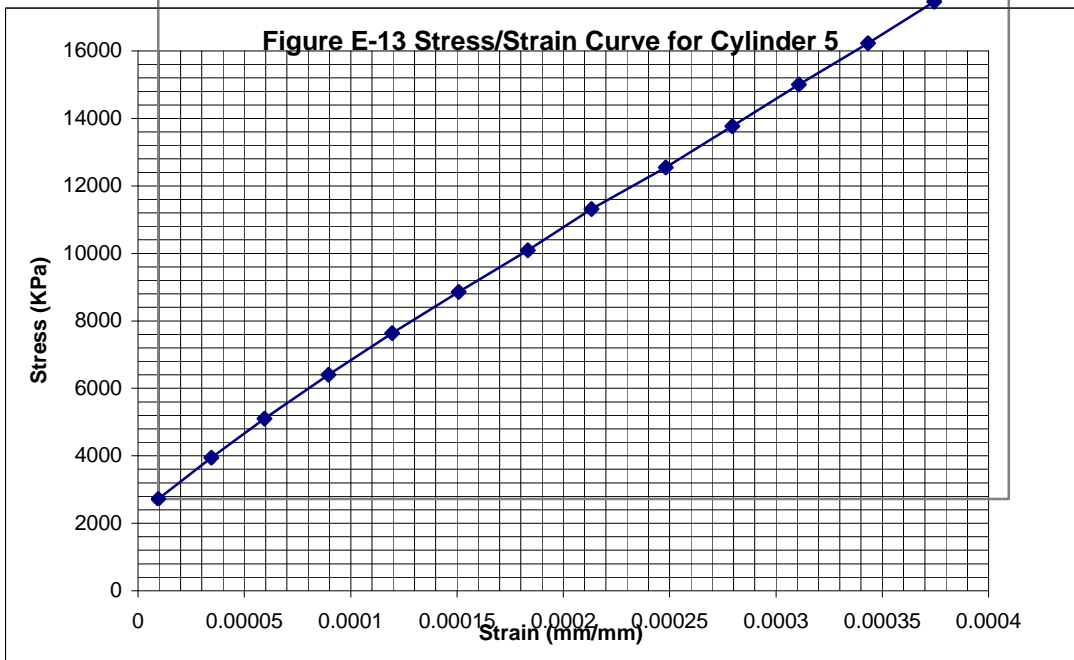
Date Cast **9/25/96**

Dia.1 (in.)

Dia.2(in.)

Ave.Dia.

Deformation(in.\*0.00005)

[illegible]

## Appendix F

### Selected Input Files for Finite Element Analysis Using ABAQUS Code

#### Input File for Original Sullivan County, TN

(ABAQUS 5-7, 1998)

**Row  
No.**

```
1. *HEADING
2. ** this is the input file of Sullivan county original culvert analysis under normal
3. ** compaction effort, this is also used for parametric study with the minor
4. ** change of the parameters. The basic scheme of Greene County culvert is
5. ** also based on this mesh.
6. BOX CULVERT ANALYSIS (CULVERT ELEMENT: CPE4I, ORIGINAL, NORMAL
   CONDITION)
7. *PREPRINT, CONTACT=YES, HISTORY=NO, ECHO=NO, MODEL=NO
8. ** generate the nodes and the elements of box culvert
9. *RESTART, WRITE, FREQUENCY=10
10. *NODE
11. 11, 0., -2.774
12. 12, 0.125, -2.774
13. 22, 4.695, -2.774
14. 24, 4.945, -2.774
15. 51, 0., -2.454
16. 52, 0.125, -2.454
17. 62, 4.695, -2.454
18. 64, 4.945, -2.454
19. 211, 0., -.32
20. 212, 0.125, -.32
21. 222, 4.695, -.32
22. 224, 4.945, -.32
23. 251, 0.,
24. 252, 0.125,,
25. 262, 4.695,,
26. 264, 4.945,,
27. *NGEN
28. 11,51,20
29. 12,52,20
30. 211,251,20
31. 212,252,20
32. 22,62,20
```

```

33. 24,64,20
34. 222,262,20
35. 224,264,20
36. 51,211,20
37. 52,212,20
38. 62,222,20
39. 64,224,20
40. 52,62
41. 12,22
42. 252,262
43. 212,222
44. 22,24
45. 62,64
46. 262,264
47. 222,224
48. *NSET, NSET=TOP, GENERATE
49. 251,264
50. *NSET, NSET=L1,GENERATE
51. 211,224
52. *NFILL
53. L1, TOP, 2, 20
54. *NSET, NSET=L2, GENERATE
55. 51,64
56. *NSET, NSET=BOTTOM, GENERATE
57. 11,24
58. *NSET, NSET=L3,GENERATE
59. 62,222,20
60. *NSET, NSET=L4,GENERATE
61. 64,224,20
62. *NFILL
63. L1, TOP, 2, 20
64. BOTTOM, L2, 2, 20
65. L3, L4, 2, 1
66. *ELEMENT, TYPE=CPE4I, ELSET=BOX
67. 1, 11, 12, 32, 31
68. 41, 51, 52, 72, 71
69. 52, 62, 63, 83, 82
70. 201, 211, 212, 232, 231
71. *ELGEN, ELSET=BOX
72. 1, 13, 1, 1, 2, 20, 20, 1
73. 41, 1, 0, 0, 8, 20, 20, 1
74. 52, 2, 1, 1, 8, 20, 20, 1
75. 201, 13, 1, 1, 2, 20, 20, 1
76. **end of nodes and meshes generation
77. **check mesh, O.K.
78. *NODE, NSET=ALLNODES
79. **generate the nodes and meshes of surrounding soil mass
80. **starts from 1001(for the first loading step)
81. 1001, 0., -9.0
82. 1101, 0., -8.194
83. 1201, 0., -7.494
84. 1301, 0., -6.794

```

85. 1401, 0., -6.094  
86. 1014, 4.945, -9.  
87. 1114, 4.945, -8.194  
88. 1214, 4.945, -7.494  
89. 1314, 4.945, -6.794  
90. 1414, 4.945, -6.094  
91. 1901, 0., -3.594  
92. 1914, 4.945, -3.594  
93. 2001, 0., -3.094  
94. 2002, 0.18, -3.094  
95. 2012, 4.425, -3.094  
96. 2014, 4.945, -3.094  
97. 2101, 0., -2.774  
98. 2114, 4.945, -2.774  
99. 2102, 0.125, -2.774  
100. 2112, 4.695, -2.774  
101. \*NGEN, NSET=ALLNODES  
102. 2112,2114  
103. 2102,2112  
104. 1001,1014  
105. 1101,1114  
106. 1201,1214  
107. 1301,1314  
108. 1401,1414  
109. 1401,1901,100  
110. 1414,1914,100  
111. 2012,2014  
112. 2002,2012  
113. \*NSET,NSET=MIDL1, GENERATE  
114. 1401,1901,100  
115. \*NSET, NSET=MIDL2, GENERATE  
116. 1414,1914,100  
117. \*NFILL, NSET=ALLNODES  
118. MIDL1,MIDL2,13,1  
119. \*NODE, NSET=ALLNODES  
120. \*\*right hand side of first loading step  
121. 1029, 20., -9.0  
122. 1129, 20., -8.194  
123. 1229, 20., -7.494  
124. 1329, 20., -6.794  
125. 1429, 20., -6.094  
126. 2029, 20., -3.094  
127. 2129, 20., -2.774  
128. \*NGEN, NSET=ALLNODES  
129. 1429,2129,100  
130. \*NSET, NSET=MIDL3, GENERATE  
131. 1014,2114,100  
132. \*NSET, NSET=MIDL4, GENERATE  
133. 1029,2129,100  
134. \*NFILL, BIAS=0.9, NSET=ALLNODES  
135. MIDL3,MIDL4,15,1  
136. \*ELEMENT, ELSET=SOIL, TYPE=CPE4

```

137. 1001,1001,1002,1102,1101
138. *ELGEN,ELSET=SOIL
139. 1001,28,1,1,11,100,100,1,0,0
140. **end of bottom slab contact pair definition
141. **mesh checked, O.K.
142. **mesh generation for layer1 and side soil
143. *NODE
144. 2314, 4.945, -2.454
145. 3114, 4.945, -0.32
146. 3314, 4.945, 0.00
147. 3514, 4.945, 0.60
148. 2329, 20., -2.454
149. 3129, 20., -0.32
150. 3329, 20., 0.
151. 3529, 20., 0.60
152. 3301, 0., 0.
153. 3314, 4.945, 0.
154. 3302, 0.125, 0.
155. 3312, 4.695, 0.
156. 3501, 0., 0.6
157. 3514, 4.945, 0.6
158. *NGEN
159. 2114,2314,100
160. 2314,3114,100
161. 3114,3314,100
162. 3314,3514,100
163. 2129,2329,100
164. 2329,3129,100
165. 3129,3329,100
166. 3329,3529,100
167. 3302,3312
168. 3312,3314
169. 3501,3514
170. 3301,3501,100
171. 3302,3502,100
172. 3312,3512,100
173. 3314,3514,100
174. 3402,3412
175. 3412,3414
176. *NSET,NSET=RIT1, GENERATE
177. 2114,3514,100
178. *NSET, NSET=LET1,GENERATE
179. 2129,3529,100
180. *NFILL, BIAS=0.9
181. RIT1,LET1,15,1
182. *ELEMENT, TYPE=CPE4, ELSET=SOIL
183. 2114,2114,2115,2215,2214
184. 2316,2316,2317,2417,2416
185. 2315,2315,2316,2416,2415
186. 2116,2116,2117,2317,2316
187. 3116,3116,3117,3317,3316
188. 2122,2122,2123,2423,2422

```

189. 2322,2422,2423,2623,2622  
190. 2922,3022,3023,3323,3322  
191. \*\* This is for elements above culvert  
192. 3301,3301,3302,3402,3401  
193. 3322,3322,3323,3523,3522  
194. \*ELEMENT, TYPE=CPE3, ELSET=SOIL  
195. 2115,2115,2116,2215  
196. 2175,2215,2316,2315  
197. 2145,2215,2116,2316  
198. 3115,3115,3116,3215  
199. 3175,3215,3316,3315  
200. 3145,3215,3116,3316  
201. 2121,2121,2122,2321  
202. 2181,2321,2422,2421  
203. 2151,2321,2122,2422  
204. 2921,3021,3022,3121  
205. 2981,3121,3322,3321  
206. 2951,3121,3022,3322  
207. 2321,2421,2422,2521  
208. 2381,2521,2622,2621  
209. 2351,2521,2422,2622  
210. 3321,3321,3322,3421  
211. 3351,3421,3522,3521  
212. 3381,3421,3322,3522  
213. \*ELGEN, ELSET=SOIL  
214. 2114,1, 1,1,12,100,100  
215. 2316,5,1,1,8 ,100,100  
216. 2315,1, 1,1,8 ,100,100  
217. 2116,5,1,1,1, 100,100  
218. 3116,5,1,1,1, 100,100  
219. 2321,1,1,1,3, 200,200  
220. 2381,1,1,1,3,200,200  
221. 2351,1,1,1,3,200,200  
222. 2122,7,1,1,1,200,200  
223. 2922,7,1,1,1,200,200  
224. 2322,7,1,1,3,200,200  
225. 3301,20,1,1,2,100,100  
226. 3322,7,1,1,1,100,100  
227. \*\* Preparing the nodes and elements above the gravels  
228. \*NODE  
229. 4801, 0, 13.00  
230. 4814, 4.945, 13.00  
231. 4815, 5.3787, 13.00  
232. 4816, 5.8606, 13.00  
233. 4817, 6.3960, 13.00  
234. 4818, 6.9910, 13.00  
235. 4819, 7.6520, 13.00  
236. 4820, 8.3865, 13.00  
237. 4821, 9.2026, 13.00  
238. 4822, 10.1090, 13.00  
239. 4823, 11.1170, 13.00  
240. 4824, 12.2360, 13.00

241. 4825, 13.4800, 13.00  
 242. 4826, 14.8620, 13.00  
 243. 4827, 16.3980, 13.00  
 244. 4828, 18.1400, 13.00  
 245. 4829, 20.0000, 13.00  
 246. \*NGEN  
 247. 4801,4814  
 248. \*NSET, NSET=TOPGEN, GENERATE  
 249. 4801,4829  
 250. \*NSET, NSET=BOTGEN, GENERATE  
 251. 3501,3529  
 252. \*NFILL, BIAS=0.9  
 253. BOTGEN, TOPGEN, 13,100  
 254. \*ELEMENT, TYPE=CPE4, ELSET=SOIL  
 255. 3501, 3501, 3502,3602,3601  
 256. 3801, 3801,3803, 3903,3901  
 257. 3715, 3715,3716,3816,3815  
 258. \*ELEMENT, TYPE=CPE3, ELSET=SOIL  
 259. 3701, 3701, 3702, 3801  
 260. 3702, 3702, 3703, 3803  
 261. 3751, 3702, 3803, 3801  
 262. \*ELGEN, ELSET=SOIL  
 263. 3501, 28,1,1,2,100,100  
 264. 3701, 7,2,2,1,100,100  
 265. 3702, 7,2,2,1,100,100  
 266. 3751, 7,2,2,1,100,100  
 267. 3801, 7, 2,2,10,100,100  
 268. 3715, 14,1,1,11,100,100  
 269. \*\* End of Mesh Generation, nset for boundary conditions  
 270. \*NSET, NSET=SOILSYMM, GENERATE  
 271. 1001, 2101,100  
 272. 3301, 4801,100  
 273. 11, 251, 20  
 274. \*NSET, NSET=BOTT, GENERATE  
 275. 1001, 1029, 1  
 276. \*NSET, NSET=RIGHT, GENERATE  
 277. 1029, 2129, 100  
 278. 2429, 3029, 200  
 279. 3329, 3329  
 280. 3529, 4829, 100  
 281. \*\*End of Boundary nset definition  
 282. \*NSET, NSET=HORI1, GENERATE  
 283. 3501, 3529  
 284. \*\*Elset definition for soil layers  
 285. \*ELSET, ELSET = GRAVEL, GENERATE  
 286. 2001, 2014  
 287. 2014, 3214, 100  
 288. 3301, 3315  
 289. 3401, 3415  
 290. 2315, 3115,100  
 291. 2116, 3116,100  
 292. 2117, 3017, 100



293. 2118, 2818,100  
 294. 2119, 2619,100  
 295. 2120, 2520, 100  
 296. \*ELSET, ELSET=GRAVEL  
 297. 3145, 3175, 2115, 2145, 2175, 2121, 2151, 2181  
 298. 2321, 2122  
 299. \*ELSET, ELSET =UGRAVEL, GENERATE  
 300. 2114, 3214, 100  
 301. 3301, 3315  
 302. 3401, 3415  
 303. 2315, 3115,100  
 304. 2116, 3116,100  
 305. 2117, 3017, 100  
 306. 2118, 2818,100  
 307. 2119, 2619,100  
 308. 2120, 2520, 100  
 309. \*ELSET, ELSET=UGRAVEL  
 310. 3145, 3175, 2115, 2145, 2175, 2121, 2151, 2181  
 311. 2321, 2122  
 312. \*ELSET, ELSET=CLAY,GENERATE  
 313. 2015, 2028  
 314. 1901, 1928  
 315. 1401,1428  
 316. 1501,1528  
 317. 1601,1628  
 318. 1701,1728  
 319. 1801,1828  
 320. \*ELSET, ELSET=WSHALE, GENERATE  
 321. 1101,1128  
 322. 1201,1228  
 323. 1301,1328  
 324. \*ELSET, ELSET=FSHALE, GENERATE  
 325. 1001,1028  
 326. \*ELSET, ELSET=LEVEL  
 327. CLAY, WSHALE, FSHALE  
 328. \*ELSET, ELSET=LEVEL, GENERATE  
 329. 2001, 2014  
 330. \*\* definition of other backfill materials  
 331. \*ELSET, ELSET=LAYER1, GENERATE  
 332. 2123, 2128  
 333. 2322, 2328  
 334. 2522, 2528  
 335. 2722, 2728  
 336. 2922, 2928  
 337. 3322, 3328  
 338. 3416, 3420  
 339. 3316, 3320  
 340. 3117, 3120  
 341. 3018, 3020  
 342. 2918, 2920  
 343. 2719, 2819, 100  
 344. 2620, 2820, 100

345. 3321, 3381, 30  
 346. 2351, 2951, 200  
 347. 2521, 2921, 200  
 348. 2381, 2981, 200  
 349. \*ELSET, ELSET=LAYER2, GENERATE  
 350. 3501, 3528  
 351. 3601, 3628  
 352. \*ELSET, ELSET=LAYER3, GENERATE  
 353. 3751, 3763, 2  
 354. 3701, 3728  
 355. 3801, 3813, 2  
 356. 3815, 3828  
 357. \*ELSET, ELSET=LAYER4, GENERATE  
 358. 3901,3913,2  
 359. 3915,3928  
 360. 4001, 4013,2  
 361. 4015, 4028  
 362. \*ELSET, ELSET=LAYER5, GENERATE  
 363. 4101, 4113,2  
 364. 4115, 4128  
 365. 4201, 4213,2  
 366. 4215, 4228  
 367. \*ELSET, ELSET=LAYER6, GENERATE  
 368. 4301, 4313,2  
 369. 4315, 4328  
 370. 4401, 4413,2  
 371. 4415, 4428  
 372. \*ELSET, ELSET=LAYER7, GENERATE  
 373. 4501, 4513,2  
 374. 4515, 4528  
 375. 4601, 4613,2  
 376. 4615, 4628  
 377. 4701, 4713,2  
 378. 4715, 4728  
 379. \*ELSET, ELSET=FILLS  
 380. UGRAVEL, LAYER1, LAYER2, LAYER3, LAYER4, LAYER5  
 381. LAYER6, LAYER7  
 382. \*INITIAL CONDITIONS, TYPE=STRESS, GEOSTATIC  
 383. LEVEL, 0., -2.774, -140.46, -9., 0.47  
 384. \*\*Contact surface definition  
 385. \*ELSET, ELSET=BOXCON, GENERATE  
 386. 1, 13  
 387. 33, 213, 20  
 388. 221, 233  
 389. \*ELSET, ELSET=SOILCON, GENERATE  
 390. 2001, 2014  
 391. 2114, 3314, 100  
 392. 3301, 3313  
 393. \*SURFACE DEFINITION, NAME=CONSLA, TRIM=YES  
 394. SOILCON  
 395. \*SURFACE DEFINITION, NAME=CONMAS  
 396. BOXCON

397. \*CONTACT PAIR, INTERACTION=FRIC  
398. CONSLA, CONMAS  
399. \*SURFACE INTERACTION, NAME=FRIC  
400. 1.0  
401. \*FRICTION  
402. 0.5303  
403. \*\*end of contact pair definition  
404. \*SOLID SECTION, ELSET=BOX, MATERIAL =CONCRETE  
405. \*MATERIAL, NAME=CONCRETE  
406. \*ELASTIC, TYPE=ISOTROPIC  
407. 4.0645E7, 0.18  
408. \*SOLID SECTION, ELSET=GRAVEL, MATERIAL=STONE  
409. \*MATERIAL, NAME=STONE  
410. \*ELASTIC, TYPE=ISOTROPIC  
411. 3.2E4, 0.27  
412. \*DRUCKER PRAGER HARDENING  
413. 66.09, 0.  
414. \*DRUCKER PRAGER, SHEAR CRITERION=LINEAR  
415. 46.14, 1., 20.  
416. \*SOLID SECTION, ELSET=CLAY, MATERIAL=SHALEA  
417. \*MATERIAL, NAME=SHALEA  
418. \*ELASTIC, TYPE=ISOTROPIC  
419. 6.5E4, 0.30  
420. \*SOLID SECTION, ELSET=WSHALE, MATERIAL=SHALEW  
421. \*MATERIAL, NAME=SHALEW  
422. \*ELASTIC, TYPE=ISOTROPIC  
423. 6.5E4, 0.30  
424. \*SOLID SECTION, ELSET=FSHALE, MATERIAL=SHALEF  
425. \*MATERIAL, NAME=SHALEF  
426. \*ELASTIC, TYPE=ISOTROPIC  
427. 1.12E6,0.25  
428. \*SOLID SECTION, ELSET=LAYER1, MATERIAL=FILL1  
429. \*MATERIAL, NAME=FILL1  
430. \*ELASTIC, TYPE=ISOTROPIC  
431. 1.58E4,0.32  
432. \*DRUCKER PRAGER HARDENING  
433. 40.95,0.  
434. \*DRUCKER PRAGER, SHEAR CRITERION=LINEAR  
435. 41.89,1.,15.  
436. \*SOLID SECTION, ELSET=LAYER2, MATERIAL=FILL2  
437. \*MATERIAL, NAME=FILL2  
438. \*ELASTIC, TYPE=ISOTROPIC  
439. 1.58E4,0.32  
440. \*DRUCKER PRAGER HARDENING  
441. 40.95,0.  
442. \*DRUCKER PRAGER, SHEAR CRITERION=LINEAR  
443. 41.89,1.,15.  
444. \*SOLID SECTION, ELSET=LAYER3, MATERIAL=FILL3  
445. \*MATERIAL, NAME=FILL3  
446. \*ELASTIC, TYPE=ISOTROPIC  
447. 1.58E4,0.32  
448. \*DRUCKER PRAGER HARDENING

449. 40.95,0.  
 450. \*DRUCKER PRAGER, SHEAR CRITERION=LINEAR  
 451. 41.89,1.,15.  
 452. \*SOLID SECTION, ELSET=LAYER4, MATERIAL=FILL4  
 453. \*MATERIAL, NAME=FILL4  
 454. \*ELASTIC, TYPE=ISOTROPIC  
 455. 1.58E4,0.32  
 456. \*DRUCKER PRAGER HARDENING  
 457. 40.95,0.  
 458. \*DRUCKER PRAGER, SHEAR CRITERION=LINEAR  
 459. 41.89,1.,15.  
 460. \*SOLID SECTION, ELSET=LAYER5, MATERIAL=FILL5  
 461. \*MATERIAL, NAME=FILL5  
 462. \*ELASTIC, TYPE=ISOTROPIC  
 463. 1.58E4,0.32  
 464. \*DRUCKER PRAGER HARDENING  
 465. 40.95,0.  
 466. \*DRUCKER PRAGER, SHEAR CRITERION=LINEAR  
 467. 41.89,1.,15.  
 468. \*SOLID SECTION, ELSET=LAYER6, MATERIAL=FILL6  
 469. \*MATERIAL, NAME=FILL6  
 470. \*ELASTIC, TYPE=ISOTROPIC  
 471. 1.58E4,0.32  
 472. \*DRUCKER PRAGER HARDENING  
 473. 40.95,0.  
 474. \*DRUCKER PRAGER, SHEAR CRITERION=LINEAR  
 475. 41.89,1.,15.  
 476. \*SOLID SECTION, ELSET=LAYER7, MATERIAL=FILL7  
 477. \*MATERIAL, NAME=FILL7  
 478. \*ELASTIC, TYPE=ISOTROPIC  
 479. 1.58E4,0.32  
 480. \*DRUCKER PRAGER HARDENING  
 481. 40.95,0.  
 482. \*DRUCKER PRAGER, SHEAR CRITERION=LINEAR  
 483. 41.89,1.,15.  
 484. \*EQUATION  
 485. 2  
 486. 3301,2,1.,251, 2,-1.  
 487. 2  
 488. 2101,2,1.,11,2,-1.  
 489. \*STEP  
 490. \*\* add initial stress, step 1  
 491. GEOSTATIC INITIAL STRESS STATE  
 492. \*GEOSTATIC  
 493. \*DLOAD  
 494. LEVEL, BY, -22.56  
 495. \*MODEL CHANGE, REMOVE  
 496. FILLS,  
 497. BOX,  
 498. \*MODEL CHANGE, TYPE=CONTACT PAIR, REMOVE  
 499. CONSLA, CONMAS  
 500. \*NODEPRINT, NSET=HORI1, FREQUENCY=100

```

501. U
502. *ELPRINT, ELSET=BOX, FREQUENCY=0, POSITION=AVERAGED AT NODES
503. S
504. E
505. *ELPRINT, ELSET=SOILCON, POSITION=AVERAGED AT NODES, FREQUENCY=100
506. S
507. *CONTACT PRINT, FREQUENCY=30
508. *BOUNDARY
509. ALLNODES, 1,2
510. *END STEP
511. *STEP, INC=100
512. **Step2, initial stress condition
513. *STATIC
514. 0.01, 1., 0.001, .1
515. *BOUNDARY, OP=NEW
516. BOTT, 2
517. SOILSYMM, 1
518. RIGHT, 1
519. *END STEP
520. *STEP
521. **step 3 , add UGRAVEL, BOX, stress free
522. *STATIC
523. *MODEL CHANGE, ADD = STRAIN FREE
524. UGRAVEL,
525. BOX,
526. *MODEL CHANGE, ADD = STRAIN FREE, TYPE = CONTACT PAIR
527. CONSLA, CONMAS
528. *END STEP
529. *STEP, INC=100
530. ** step 4, apply UGRAVEL body force
531. *STATIC
532. 0.00725, 1., 0.0007, 0.1
533. *DLOAD
534. UGRAVEL, BY, -19.42
535. BOX, BY, -24.53
536. *END STEP
537. *STEP
538. **step 5 , add LAYER1, stress free
539. *STATIC
540. *MODEL CHANGE, ADD = STRAIN FREE
541. LAYER1,
542. *END STEP
543. *STEP, INC=100
544. ** step 6, apply LAYRE1 body force
545. *STATIC
546. 0.00725, 1., 0.0007, 0.1
547. *DLOAD
548. LAYER1, BY, -21.09
549. *END STEP
550. *STEP
551. **step 7 , add LAYER2, stress free
552. *STATIC

```

```

553. *MODEL CHANGE, ADD = STRAIN FREE
554. LAYER2,
555. *END STEP
556. *STEP, INC=100
557. ** step 8, apply LAYRE2 body force
558. *STATIC
559. 0.00725, 1., 0.0007, 0.1
560. *DLOAD
561. LAYER2, BY, -21.09
562. *END STEP
563. *STEP
564. **step 9 , add LAYER1, stress free
565. *STATIC
566. *MODEL CHANGE, ADD = STRAIN FREE
567. LAYER3,
568. *END STEP
569. *STEP, INC=100
570. ** step 10, apply LAYRE3 body force
571. *STATIC
572. 0.00725, 1., 0.0007, 0.1
573. *DLOAD
574. LAYER3, BY, -21.09
575. *END STEP
576. *STEP
577. **step 11 , add LAYER4, stress free
578. *STATIC
579. *MODEL CHANGE, ADD = STRAIN FREE
580. LAYER4,
581. *END STEP
582. *STEP, INC=100
583. ** step 12, apply LAYRE4 body force
584. *STATIC
585. 0.00725, 1., 0.0007, 0.1
586. *DLOAD
587. LAYER4, BY, -21.09
588. *END STEP
589. *STEP
590. **step 13 , add LAYER5, stress free
591. *STATIC
592. *MODEL CHANGE, ADD = STRAIN FREE
593. LAYER5,
594. *END STEP
595. *STEP, INC=100
596. ** step 14, apply LAYRE5 body force
597. *STATIC
598. 0.00725, 1., 0.0007, 0.1
599. *DLOAD
600. LAYER5, BY, -21.09
601. *END STEP
602. *STEP
603. **step 15 , add LAYER6, stress free
604. *STATIC

```

605. \*MODEL CHANGE, ADD = STRAIN FREE  
606. LAYER6,  
607. \*END STEP  
608. \*STEP, INC=100  
609. \*\* step 16, apply LAYRE6 body force  
610. \*STATIC  
611. 0.00725, 1., 0.0007, 0.1  
612. \*DLOAD  
613. LAYER6, BY, -21.09  
614. \*END STEP  
615. \*STEP  
616. \*\*step 17 , add LAYER7, stress free  
617. \*STATIC  
618. \*MODEL CHANGE, ADD = STRAIN FREE  
619. LAYER7,  
620. \*END STEP  
621. \*STEP, INC=100  
622. \*\* step 18, apply LAYRE7 body force  
623. \*STATIC  
624. 0.00725, 1., 0.0007, 0.1  
625. \*DLOAD  
626. LAYER7, BY, -21.09  
627. \*END STEP

**Input File for Original Sullivan County, TN**  
(ABAQUS 5-6, 1997)

```

1  *HEADING
2  ** this input file using basic data of 29soft.inp, remove and add contact pair
3  ** between concrete and the gravel. the contact pair is added between the gravel
4  ** on the wall and the roof to reduce the bending effect of the gravel model.
5  BOX CULVERT ANALYSIS ( CULVERT ELEMENT: CPE4I,MATCHED MESHES FOR
   CONATCT)
6  *PREPRINT,CONTACT=YES, HISTORY=NO, ECHO=NO, MODEL=NO
7  ** generate the nodes and the elements of box culvert
8  *RESTART, WRITE,FREQUENCY=10
9  *NODE
10 11, 0., -3.7
11 12, 0.23, -3.7
12 22, 4.38, -3.7
13 24, 5., -3.7
14 51, 0., -2.93
15 52, 0.23, -2.93
16 62, 4.38, -2.93
17 64, 5., -2.93
18 211, 0., -.77
19 212, 0.23, -0.77
20 222, 4.38, -0.77
21 224, 5.00, -0.77
22 251, 0.,
23 252, 0.23,,
24 262, 4.38,,
25 264, 5.00,,
26 *NGEN
27 11,51,20
28 12,52,20
29 211,251,20
30 212,252,20
31 22,62,20
32 24,64,20
33 222,262,20
34 224,264,20
35 51,211,20
36 52,212,20
37 62,222,20
38 64,224,20
39 52,62
40 12,22
41 252,262
42 212,222

```



```

43 22,24
44 62,64
45 262,264
46 222,224
47 *NSET, NSET=TOP, GENERATE
48 251,264
49 *NSET, NSET=L1,GENERATE
50 211,224
51 *NFILL
52 L1, TOP, 2, 20
53 *NSET, NSET=L2, GENERATE
54 51,64
55 *NSET, NSET=BOTTOM, GENERATE
56 11,24
57 *NSET, NSET=L3,GENERATE
58 62,222,20
59 *NSET, NSET=L4,GENERATE
60 64,224,20
61 *NFILL
62 L1, TOP, 2, 20
63 BOTTOM, L2, 2, 20
64 L3, L4, 2, 1
65 *ELEMENT, TYPE=CPE4I, ELSET=BOX
66 1, 11, 12, 32, 31
67 41, 51, 52, 72, 71
68 52, 62, 63, 83, 82
69 201, 211, 212, 232, 231
70 *ELGEN, ELSET=BOX
71 1, 13, 1, 1, 2, 20, 20, 1
72 41, 1, 0, 0, 8, 20, 20, 1
73 52, 2, 1, 1, 8, 20, 20, 1
74 201, 13, 1, 1, 2, 20, 20, 1
75 **end of nodes and meshes generation
76 **check mesh, O.K.
77 *NODE
78 **generate the nodes and meshes of surrounding soil mass. the node numbers,
79 **starts from 1001 (for the first loading step)
80 1001, 0., -18.7
81 2601, 0., -3.7
82 2602, 0.23, -3.7
83 2612, 4.38, -3.7
84 2614, 5., -3.7
85 2616, 6., -3.7
86 2619, 8.1, -3.7
87 2621, 10.3, -3.7
88 2623, 13.5, -3.7
89 1014, 5., -18.7
90 1016, 6., -18.7
91 1019, 8.1, -18.7
92 1021, 10.3, -18.7

```

```

93      1023, 13.5, -18.7
94      *NGEN
95      **generate the soil nodes underneath the culvert
96      10,011,014
97      10,141,016
98      10,161,019
99      10,191,021
100     10,211,023
101     26,022,612
102     26,122,614
103     26,142,616
104     26,162,619
105     26,192,621
106     26,212,623
107     *NSET, NSET=BOTTOM1, GENERATE
108     10,011,023
109     *NSET, NSET=LL1, GENERATE
110     26,012,623
111     *NFILL, BIAS=1.25, TWO STEP
112     BOTTOM1, LL1, 16, 100
113     *NODE
114     **generate nodes on the right hand side of culvert
115     2814, 5., -2.93
116     3614, 5., -.77
117     3814, 5., 0.
118     4014, 5., 0.62
119     3816, 6., 0.
120     4016, 6., 0.62
121     3828, 9.70, 0.
122     4030, 10.32, 0.62
123     4037, 13.5, 0.62
124     *NGEN
125     26,234,037,101
126     38,284,030,101
127     26,164,030,101
128     4030,4037,1
129     26,164,030,101
130     26,234,037,101
131     4030,4037,1
132     *NSET, NSET=LL2, GENERATE
133     2616,2623,1
134     *NSET, NSET=LL3, GENERATE
135     4030,4037,1
136     *NFILL
137     LL2, LL3, 14, 101
138     **the following is the node in wedge area.
139     *NODE
140     3801, 0., 0.
141     3802, 0.23, 0.
142     3812, 4.38, 0.

```

```

143 4001, 0., 0.62
144 *NGEN
145 38,014,001,100
146 38,144,014,100
147 38,164,016,100
148 26,142,814,100
149 28,143,614,100
150 36,143,814,100
151 2614,2616,1
152 3814,3816,1
153 26,153,815,100
154 26,163,816,100
155 2816,2818,1
156 2916,2919,1
157 3016,3020,1
158 3116,3121,1
159 3216,3222,1
160 3316,3323,1
161 3416,3424,1
162 3516,3525,1
163 3616,3626,1
164 3716,3727,1
165 3802,3812,1
166 3812,3814,1
167 3816,3828,1
168 3901,3914,1
169 3914,3916,1
170 3916,3929,1
171 4001,4014,1
172 4014,4016,1
173 4016,4030,1
174 **generate additional surface between the gravel for construction step
175 *NODE
176 92515, 5.5, -4.0780
177 92514, 5., -4.0780
178 92516, 6.0, -4.0780
179 94030, 10.32,0.62
180 92616, 6., -3.7
181 92614, 5., -3.7
182 93814, 5., 0.
183 93914, 5., 0.31
184 94014, 5., 0.62
185 *NGEN
186 9,261,694,030,202
187 *ELEMENT, TYPE=CPE4,ELSET=GRAVEL
188 26,149,251,492,515,200,000,000
189 27,142,614,261,527,100,000
190 39,013,801,380,239,000,000
191 *ELEMENT, TYPE=CPE4,ELSET=GRAVEL
192 26,159,251,592,516,900,000,000

```

```

193 271,526,159,261,628,000,000
194 29,152,815,281,630,100,000
195 291,628,169,281,830,000,000
196 31,163,016,301,832,100,000
197 381,437,143,715,381,000,000
198 3,914,938,143,815,390,000,000
199 4,014,939,143,915,400,000,000
200 *ELEMENT, TYPE=CPE3, ELSET=GRAVEL
201 271,692,616,928,182,000
202 2,815,271,528,162,810
203 *ELGEN,ELSET=GRAVEL
204 2714,1,0,0,11,100,100
205 2716,1,0,0,7,202,202
206 2815,1,0,0,7,200,200
207 2915,1,0,0,6,200,200
208 2916,1,0,0,6,202,202
209 3116,1,0,0,5,200,200
210 3316,2,2,2,1,0,0
211 3516,3,2,2,1,0,0
212 3716,4,2,2,1,0,0
213 3916,5,2,2,1,0,0
214 3901,13,1,1,2,100,100
215 **right side slope area node generation
216 *NODE
217 **slope surface
218 4038, 14.9, 1.32
219 4039, 16.3, 2.02
220 4040, 18.9, 3.32
221 4041, 21.5, 4.62
222 4042, 25.1, 6.42
223 4043, 28.7, 8.22
224 4044, 33.3, 10.52
225 4045, 37.9, 12.82
226 2624, 14.9, -3.7
227 2625, 16.3, -3.7
228 2626, 18.9, -3.7
229 2627, 21.5, -3.7
230 2628, 25.1, -3.7
231 2629, 28.7, -3.7
232 2630, 33.3, -3.7
233 2631, 37.9, -3.7
234 1024, 14.9, -18.7
235 1025, 16.3, -18.7
236 1026, 18.9, -18.7
237 1027, 21.5, -18.7
238 1028, 25.1, -18.7
239 1029, 28.7, -18.7
240 1030, 33.3, -18.7
241 1031, 37.9, -18.7
242 **end of control nodes input

```

```

243 *NSET, NSET=SLOPN, GENERATE
244 4037,4045,1
245 *NSET, NSET=KK, GENERATE
246 2623,2631,1
247 *NSET, NSET=KK2, GENERATE
248 1023,1031,1
249 *NFILL
250 KK,SLOPN,7,202
251 *NFILL,BIAS=1.25,TWO STEP
252 KK2,KK,16,100
253 **end of node generation
254 ** boundary node set definitions
255 *NSET, NSET=LHS, GENERATE
256 10,012,001,200
257 20,012,601,100
258 *NSET, NSET=BOTTOM2, GENERATE
259 1001, 1019,2
260 10,191,031
261 **elset SLOPN has been defined
262 *NSET, NSET=SLOPE, GENERATE
263 4037,4044,1
264 *NSET, NSET=RHS1, GENERATE
265 10,312,031,200
266 20,312,631,100
267 *NSET, NSET=RHS2, GENERATE
268 28,334,045,202
269 *NSET,NSET=TOP1, GENERATE
270 **this is for the original soil top boundary
271 4030,4037,1
272 *NSET, NSET=TOP2, GENERATE
273 ** for gravel boundary
274 40,024,016
275 4016,4030,2
276 *NSET, NSET=LHSGR
277 380,139,014,001
278 *NSET, NSET=MIDN, GENERATE
279 11,251,20
280 *NSET,NSET=ROOFN,GENERATE
281 212,222,1
282 *NSET, NSET=SLABN,GENERATE
283 52,62,1
284 *NSET, NSET=WALLN, GENERATE
285 82,202,20
286 *NSET, NSET=CONGRAV,GENERATE,UNSORTED
287 25,142,516
288 26,164,030,202
289 *NSET, NSET=GRAVB,GENERATE,UNSORTED
290 92514,92516,1
291 9,261,694,030,202
292 ** the following is the element generation for both soil and gravel

```

```

293 *ELEMENT, TYPE=CPE4,ELSET=BEDROCK1
294 10,011,001,100,312,000,000
295 10,191,019,102,012,200,000
296 *ELEMENT, TYPE=CPE4,ELSET=RSOIL
297 27,172,616,261,728,100,000
298 *ELEMENT, TYPE=CPE4, ELSET=USOIL
299 21,192,019,202,021,200,000
300 21,012,001,200,321,000,000
301 26,162,516,251,726,100,000
302 22,012,101,210,222,000,000
303 *ELEMENT,TYPE=CPE3, ELSET=USOIL
304 2,102,210,220,032,100
305 *ELEMENT, TYPE=CPE4, ELSET=UNDER2
306 26,012,501,250,226,000,000
307 *ELGEN, ELSET=BEDROCK1
308 1001,9,2,2,5,200,200
309 1019,4,1,1,5,200,200
310 *ELGEN,ELSET=USOIL
311 2119,4,1,1,1,0,0
312 2201,22,1,1,4,100,100
313 2616,7,1,1,1,0,0
314 2101,9,2,2,1,0,0
315 2102,9,2,2,1,0,0
316 *ELGEN, ELSET=RSOIL
317 2717,7,1,1,7,202,202
318 *ELGEN,ELSET=UNDER2
319 2601,13,1,1,1,0,0
320 ** mesh checked, O.K.
321 **mesh generation for slope surface
322 *ELEMENT,TYPE=CPE4,ELSET=BEDROCK2
323 10,231,023,102,412,200,000
324 *ELEMENT,TYPE=CPE4,ELSET=MIDDLE
325 22,242,123,202,422,200,000
326 22,252,024,202,522,200,000
327 *ELEMENT,TYPE=CPE4,ELSET=SSOIL
328 27,242,623,262,428,200,000
329 *ELEMENT,TYPE=CPE3,ELSET=MIDDLE
330 2,123,202,320,242,120
331 *ELGEN,ELSET=BEDROCK2
332 1023,8,1,1,5,200,200
333 *ELGEN,ELSET=MIDDLE
334 2123,1,0,0,3,200,200
335 2224,1,0,0,3,200,200
336 2225,7,1,1,3,200,200
337 *ELGEN,ELSET=SSOIL
338 2724,8,1,1,7,202,202
339 **define the element set for the first loading step)
340 *ELSET, ELSET=BOXB1,GENERATE
341 221,232,1
342 *ELSET, ELSET=BOXB2,GENERATE

```

343 13,233,20  
344 \*ELSET,ELSET=SOILB1,GENERATE  
345 2601,2613,1  
346 \*ELSET,ELSET=SOILB2,GENERATE  
347 27,143,814,100  
348 \*ELSET,ELSET=SOILB3,GENERATE  
349 3901,3913,1  
350 \*ELSET,ELSET=SOILB4  
351 381,439,144,014  
352 \*ELSET,ELSET=SOILB5  
353 39,134,013  
354 \*ELSET,ELSET=SOILB  
355 SOILB2,SOILB3  
356 \*ELSET, ELSET=ROOF, GENERATE  
357 221,233,1  
358 \*ELSET, ELSET=WALL,GENERATE  
359 13,233,20  
360 \*ELSET, ELSET=BSLAB, GENERATE  
361 1,13,1  
362 \*ELSET, ELSET=SIDESO, GENERATE  
363 27,144,014,100  
364 27,154,015,100  
365 \*ELSET, ELSET=TOPSO, GENERATE  
366 3901,3913,1  
367 4001, 4013,1  
368 \*\*elset definition for material properties  
369 \*\*elset RSOIL, BEDROCK1 has been defined  
370 \*ELSET, ELSET=BEDSLAB, GENERATE  
371 2601, 2613,1  
372 \*ELSET, ELSET=SOIL1  
373 USOIL, RSOIL  
374 \*ELSET, ELSET=SOIL2  
375 SOIL1,GRAVEL,BEDSLAB  
376 \*ELSET, ELSET=SSOIL2,GENERATE  
377 21,232,523,200  
378 22,242,624,200  
379 22,252,625,200  
380 22,262,626,200  
381 \*ELSET,ELSET=BEDRO2,GENERATE  
382 2227,2231,1  
383 2427,2431,1  
384 2627,2631,1  
385 \*ELSET, ELSET=RUSOIL  
386 SSOIL2, BEDRO2  
387 \*ELSET, ELSET=ROCK  
388 BEDROCK1, BEDROCK2  
389 \*ELSET, ELSET=SOIL  
390 RSOIL,USOIL,SSOIL,RUSOIL  
391 \*ELSET, ELSET=ALLSOIL  
392 USOIL,RSOIL,GRAVEL,BEDROCK1,BEDROCK2,SSOIL,RUSOIL

```

393 *ELSET, ELSET=SOIL3
394 SOIL1, SSOIL, ROCK, RUSOIL
395 **elset definition for initial stress
396 *ELSET, ELSET=INISOIL1, GENERATE
397 27,244,138,202
398 *ELSET, ELSET=INISOIL2, GENERATE
399 27,254,139,202
400 *ELSET, ELSET=INISOIL3, GENERATE
401 27,264,140,202
402 *ELSET, ELSET=INISOIL4, GENERATE
403 27,274,141,202
404 *ELSET, ELSET=INISOIL5, GENERATE
405 27,284,142,202
406 *ELSET, ELSET=INISOIL6, GENERATE
407 27,294,143,202
408 *ELSET, ELSET=INISOIL7, GENERATE
409 27,304,144,202
410 *ELSET, ELSET=INISOIL8, GENERATE
411 27,314,145,202
412 **end of elset definition
413 **node and element definition for LAYER1
414 *NODE
415 10001,0.,0.62
416 10014,5.,0.62
417 10016,6.,0.62
418 10023,10.32,0.62
419 10030,13.5,0.62
420 10114,5.,0.97
421 10116,6.,0.97
422 10123,10.35,0.97
423 10130,13.5,0.97
424 10201,0.,1.32
425 10214,5.,1.32
426 10216,6.,1.32
427 10223,10.32,1.32
428 10230,13.5,1.32
429 10232,14.9,1.32
430 *NGEN
431 10001,10014,1
432 10014,10016,1
433 10016,10023,1
434 10023,10030,1
435 1,000,110,201,100
436 10201,10214,1
437 10214,10216,1
438 10216,10223,1
439 10223,10230,1
440 10230,10232,1
441 10101,10114,1
442 10114,10116,1

```



```

443 10116,10123,1
444 10123,10130,1
445 *ELEMENT, TYPE=CPE3,ELSET=LAYER1
446 10,001,100,011,000,200,000
447 10,023,100,231,002,400,000
448 10,129,101,291,023,000,000
449 10,130,100,301,023,200,000
450 *ELEMENT, TYPE=CPE4,ELSET=LAYER1
451 1,000,210,002,100,030,000,000,000
452 1,010,210,101,101,030,000,000,000
453 1,001,510,015,100,160,000,000,000
454 1,002,410,024,100,250,000,000,000
455 1,012,310,123,101,250,000,000,000
456 1,002,910,029,100,300,000,000,000
457 *ELGEN,ELSET=LAYER1
458 10001,7,2,2,1,0,0
459 10002,7,2,2,1,0,0
460 10102,7,2,2,1,0,0
461 10015,8,1,1,2,100,100
462 10023,3,2,2,1,0,0
463 10024,3,2,2,1,0,0
464 10123,3,2,2,1,0,0
465 **end of definition of meshes to be added(LAYER1)
466 **nset and elset definition
467 *NSET, NSET=GRAVEL, GENERATE,UNSORTED
468 40,024,015
469 4016,4028,2
470 9,403,094,030
471 40,314,038
472 *NSET,NSET=LAYER1B, GENERATE,UNSORTED
473 1,000,210,030
474 1,023,210,232
475 *NSET,NSET=LAYER1T,GENERATE,UNSORTED
476 10203,10215,2
477 1,021,610,222
478 10223,10229,2
479 1,023,010,230
480 1,023,210,232
481 40,394,039
482 *NSET, NSET=LEFTL1
483 100,011,010,110,201
484 **end of nset elset definition in LAYER1
485 **meshes for LAYER2
486 *NODE
487 20001,0.,1.32
488 20014,5.,1.32
489 20016,6.,1.32
490 20023,10.32,1.32
491 20030,13.5,1.32
492 20032,14.9,1.32

```

```

493 20101,0.,2.02
494 20112,16.3,2.02
495 *NGEN
496 2,000,120,014
497 2,001,420,016
498 2,001,620,023
499 2,002,320,030
500 2,010,120,112
501 *ELEMENT, TYPE=CPE3, ELSET=LAYER2
502 20,001,200,012,000,300,000
503 20,002,201,012,000,300,000
504 20,003,200,032,000,500,000
505 20,004,200,052,000,700,000
506 20,005,201,022,000,700,000
507 20,006,200,072,000,900,000
508 20,007,200,092,001,100,000
509 20,008,201,032,001,100,000
510 20,009,200,112,001,300,000
511 20,010,200,132,001,500,000
512 20,011,201,042,001,500,000
513 20,012,200,152,001,600,000
514 20,013,200,162,001,700,000
515 20,014,201,052,001,700,000
516 20,015,200,172,001,800,000
517 20,016,200,182,001,900,000
518 20,017,201,062,001,900,000
519 20,018,200,192,002,000,000
520 20,019,200,202,002,100,000
521 20,020,201,072,002,100,000
522 20,021,200,212,002,200,000
523 20,022,200,222,002,300,000
524 20,023,201,082,002,300,000
525 20,024,200,232,002,500,000
526 20,025,200,252,002,700,000
527 20,026,201,092,002,700,000
528 20,027,200,272,002,900,000
529 20,028,200,292,003,000,000
530 20,029,201,102,003,000,000
531 20,030,200,302,003,200,000
532 20,031,201,112,003,200,000
533 **nset, elset definition
534 *NSET, NSET=LAYER2B, GENERATE, UNSORTED
535 20003,20015,2
536 2,001,620,022
537 20023,20029,2
538 2,003,020,030
539 2,003,220,032
540 2,011,220,112
541 *NSET, NSET=LAYER2T, GENERATE, UNSORTED
542 2,010,220,112

```

```

543 40,404,040
544 *NSET,NSET=LEFTL2
545 2,000,120,101
546 **end of LAYER2 definition,and start LAYER3 definition
547 *NODE
548 30001, 0., 2.02
549 30012, 16.3, 2.02
550 30101, 0., 3.32
551 30113, 18.9, 3.32
552 *NGEN
553 3,000,130,012
554 3,010,130,113
555 *ELEMENT,TYPE=CPE4,ELSET=LAYER3
556 3,000,130,001,300,020,000,000,000
557 *ELEMENT,TYPE=CPE3,ELSET=LAYER3
558 30,012,300,123,011,300,000
559 *ELGEN,ELSET=LAYER3
560 30001,11,1,1,1,0,0
561 *NSET,NSET=LAYER3B, GENERATE, UNSORTED
562 3,000,230,012
563 3,011,330,113
564 *NSET, NSET=LAYER3T, GENERATE, UNSORTED
565 3,010,230,113
566 40,414,041
567 *NSET, NSET=LEFTL3
568 3,000,130,101
569 **end of LAYER3 and start of LAYER4 definition
570 *NODE
571 40001, 0., 3.32
572 40013, 18.9, 3.32
573 40101, 0., 4.62
574 40114, 21.5, 4.62
575 *NGEN
576 4,000,140,013
577 4,010,140,114
578 *ELEMENT, TYPE=CPE4,ELSET=LAYER4
579 4,000,140,001,400,020,000,000,000
580 *ELEMENT,TYPE=CPE3, ELSET=LAYER4
581 40,013,400,134,011,400,000
582 *ELGEN,ELSET=LAYER4
583 40001,12,1,1,1,0,0
584 *NSET,NSET=LAYER4B, GENERATE, UNSORTED
585 4,000,240,013
586 4,011,440,114
587 *NSET, NSET=LAYER4T, GENERATE, UNSORTED
588 40102, 40114
589 40,424,042
590 *NSET, NSET=LEFTL4
591 4,000,140,101
592 **end of LAYER4 and start of LAYER5 definition

```

```

593 *NODE
594 50115, 25.1, 6.42
595 50101, 0., 6.42
596 50001, 0., 4.62
597 50014, 21.5, 4.62
598 *NGEN
599 5,000,150,014
600 5,010,150,115
601 *ELEMENT, TYPE=CPE4,ELSET=LAYER5
602 5,000,150,001,500,020,000,000,000
603 *ELEMENT,TYPE=CPE3, ELSET=LAYER5
604 50,014,500,145,011,500,000
605 *ELGEN,ELSET=LAYER5
606 50001,13,1,1,1,0,0
607 *NSET,NSET=LAYER5B, GENERATE, UNSORTED
608 5,000,250,014
609 5,011,550,115
610 *NSET, NSET=LAYER5T, GENERATE, UNSORTED
611 5,010,250,115
612 40,434,043
613 *NSET, NSET=LEFTL5
614 5,000,150,101
615 **end of LAYER5 and start of LAYER6 definition
616 *NODE
617 60001, 0., 6.42
618 60015, 25.1, 6.42
619 60101, 0., 8.22
620 60116, 28.7, 8.22
621 *NGEN
622 6,000,160,015
623 6,010,160,116
624 *ELEMENT, TYPE=CPE4,ELSET=LAYER6
625 6,000,160,001,600,020,000,000,000
626 *ELEMENT,TYPE=CPE3, ELSET=LAYER6
627 60,015,600,156,011,600,000
628 *ELGEN,ELSET=LAYER6
629 60001,14,1,1,1,0,0
630 *NSET,NSET=LAYER6B, GENERATE, UNSORTED
631 6,000,260,015
632 6,011,660,116
633 *NSET, NSET=LAYER6T, GENERATE, UNSORTED
634 60102, 60116
635 40,444,044
636 *NSET, NSET=LEFTL6
637 6,000,160,101
638 **end of LAYER6 and start of LAYER7 definition
639 *NODE
640 70101, 0., 10.52
641 70116, 28.7, 10.52
642 70117, 33.3, 10.52

```

[illegible]

```

693 NEW1,LAYER2
694 *ELSET, ELSET=ALLSOIL3
695 ALLSOIL2,LAYER3
696 *ELSET,ELSET=NEW3
697 NEW2,LAYER3
698 *ELSET,ELSET=ALLSOIL4
699 ALLSOIL3,LAYER4
700 *ELSET,ELSET=NEW4
701 NEW3,LAYER4
702 *ELSET, ELSET=ALLSOIL5
703 ALLSOIL4,LAYER5
704 *ELSET,ELSET=NEW5
705 NEW4,LAYER5
706 *ELSET, ELSET=ALLSOIL6
707 ALLSOIL5,LAYER6
708 *ELSET,ELSET=NEW6
709 NEW5,LAYER6
710 *ELSET, ELSET=ALLSOIL7
711 ALLSOIL6,LAYER7
712 *ELSET, ELSET=ALLSOIL8
713 ALLSOIL7, LAYER8
714 **contact surface definition
715 *SURFACE DEFINITION, NAME=SLAVE1,TRIM=YES
716 SOILB3,S1
717 *SURFACE DEFINITION, NAME=MASTER1
718 BOXB1
719 *CONTACT PAIR, INTERACTION=FRIC1
720 SLAVE1, MASTER1
721 *SURFACE INTERACTION, NAME=FRIC1
722 1
723 *FRICTION
724 0.5303
725 *SURFACE DEFINITION, NAME=SLAVE2,TRIM=YES
726 SOILB2,S4
727 *SURFACE DEFINITION, NAME=MASTER2
728 BOXB2
729 *CONTACT PAIR, INTERACTION=FRIC2
730 SLAVE2, MASTER2
731 *SURFACE INTERACTION, NAME=FRIC2
732 1
733 *FRICTION
734 0.5303
735 *SURFACE DEFINITION, NAME=SLAVE3,TRIM=YES
736 SOILB4
737 *SURFACE DEFINITION, NAME=MASTER3
738 SOILB5
739 *CONTACT PAIR, INTERACTION=FRIC3
740 SLAVE3, MASTER3
741 *SURFACE INTERACTION, NAME=FRIC3
742 1

```

743 \*FRICTION  
744 0.758  
745 \*SURFACE DEFINITION, NAME=SLAVE4,TRIM=YES  
746 SOILB1,S3  
747 \*SURFACE DEFINITION, NAME=MASTER4  
748 BSLAB  
749 \*CONTACT PAIR, INTERACTION=FRIC4  
750 SLAVE4, MASTER4  
751 \*SURFACE INTERACTION, NAME=FRIC4  
752 1  
753 \*FRICTION  
754 0.5303  
755 \*\*end of contact definition  
756 \*\*material definition  
757 \*SOLID SECTION, ELSET=USOIL, MATERIAL=SHALE1  
758 \*MATERIAL, NAME=SHALE1  
759 \*ELASTIC,TYPE=ISOTROPIC  
760 6.5E4,0.30  
761 \*SOLID SECTION, ELSET=RUSOIL, MATERIAL=SHALE4  
762 \*MATERIAL, NAME=SHALE4  
763 \*ELASTIC,TYPE=ISOTROPIC  
764 6.5E4,.30  
765 \*SOLID SECTION, ELSET=RSOIL, MATERIAL=SHALE2  
766 \*MATERIAL, NAME=SHALE2  
767 \*ELASTIC, TYPE=ISOTROPIC  
768 1.58E4,0.32  
769 \*DRUCKER PRAGER HARDENING  
770 40.95,0.  
771 \*DRUCKER PRAGER, SHEAR CRITERION=LINEAR  
772 41.89,1.,15.  
773 \*SOLID SECTION, ELSET=SSOIL,MATERIAL=SHALE3  
774 \*MATERIAL, NAME=SHALE3  
775 \*ELASTIC, TYPE=ISOTROPIC  
776 1.58E4, 0.32  
777 \*DRUCKER PRAGER HARDENING  
778 40.95,0.  
779 \*DRUCKER PRAGER, SHEAR CRITERION=LINEAR  
780 41.89,1.,15.  
781 \*SOLID SECTION, ELSET=GRAVEL, MATERIAL=STONE  
782 \*MATERIAL, NAME=STONE  
783 \*ELASTIC, TYPE=ISOTROPIC  
784 1.6E4, 0.27  
785 \*DRUCKER PRAGER HARDENING  
786 66.09,0.  
787 \*DRUCKER PRAGER, SHEAR CRITERION=LINEAR  
788 46.14,1.,20.  
789 \*SOLID SECTION, ELSET=BOX, MATERIAL=CON1  
790 \*MATERIAL, NAME=CON1  
791 \*ELASTIC, TYPE=ISOTROPIC  
792 4.0645E7,0.18

793 \*SOLID SECTION, ELSET=BEDSLAB, MATERIAL=CON2  
 794 \*MATERIAL,NAME=CON2  
 795 \*ELASTIC,TYPE=ISOTROPIC  
 796 2.E7, 0.18  
 797 \*SOLID SECTION, ELSET=BEDROCK1,MATERIAL=ROCK11  
 798 \*MATERIAL,NAME=ROCK11  
 799 \*ELASTIC, TYPE=ISOTROPIC  
 800 1.12E6, 0.25  
 801 \*SOLID SECTION, ELSET=BEDROCK2,MATERIAL=ROCK11  
 802 \*\*material definition of to be added layer  
 803 \*SOLID SECTION, ELSET=LAYER1, MATERIAL=FILL1  
 804 \*MATERIAL, NAME=FILL1  
 805 \*ELASTIC, TYPE=ISOTROPIC  
 806 6.5E3,.366  
 807 \*DRUCKER PRAGER HARDENING  
 808 35.30,0.  
 809 \*DRUCKER PRAGER, SHEAR CRITERION=LINEAR  
 810 36.2,1.,0.  
 811 \*SOLID SECTION, ELSET=LAYER2, MATERIAL=FILL2  
 812 \*MATERIAL, NAME=FILL2  
 813 \*ELASTIC, TYPE=ISOTROPIC  
 814 6.5E3,.366  
 815 \*DRUCKER PRAGER HARDENING  
 816 35.30,0.  
 817 \*DRUCKER PRAGER, SHEAR CRITERION=LINEAR  
 818 36.2,1.,0.  
 819 \*SOLID SECTION, ELSET=LAYER3, MATERIAL=FILL3  
 820 \*MATERIAL, NAME=FILL3  
 821 \*ELASTIC, TYPE=ISOTROPIC  
 822 1.58E4,0.32  
 823 \*DRUCKER PRAGER HARDENING  
 824 40.95,0.  
 825 \*DRUCKER PRAGER, SHEAR CRITERION=LINEAR  
 826 41.89,1.,15.  
 827 \*SOLID SECTION, ELSET=LAYER4, MATERIAL=FILL4  
 828 \*MATERIAL, NAME=FILL4  
 829 \*ELASTIC, TYPE=ISOTROPIC  
 830 1.58E4,0.32  
 831 \*DRUCKER PRAGER HARDENING  
 832 40.95,0.  
 833 \*DRUCKER PRAGER, SHEAR CRITERION=LINEAR  
 834 41.89,1.,15.  
 835 \*SOLID SECTION, ELSET=LAYER5, MATERIAL=FILL5  
 836 \*MATERIAL, NAME=FILL5  
 837 \*ELASTIC, TYPE=ISOTROPIC  
 838 1.58E4,0.32  
 839 \*DRUCKER PRAGER HARDENING  
 840 40.95,0.  
 841 \*DRUCKER PRAGER, SHEAR CRITERION=LINEAR  
 842 41.89,1.,15.



843 \*SOLID SECTION, ELSET=LAYER6, MATERIAL=FILL6  
844 \*MATERIAL, NAME=FILL6  
845 \*ELASTIC, TYPE=ISOTROPIC  
846 1.58E4,0.32  
847 \*DRUCKER PRAGER HARDENING  
848 40.95,0.  
849 \*DRUCKER PRAGER, SHEAR CRITERION=LINEAR  
850 41.89,1.,15.  
851 \*SOLID SECTION, ELSET=LAYER7, MATERIAL=FILL7  
852 \*MATERIAL, NAME=FILL7  
853 \*ELASTIC, TYPE=ISOTROPIC  
854 1.58E4,0.32  
855 \*DRUCKER PRAGER HARDENING  
856 40.95,0.  
857 \*DRUCKER PRAGER, SHEAR CRITERION=LINEAR  
858 41.89,1.,15.  
859 \*SOLID SECTION, ELSET=LAYER8, MATERIAL=FILL8  
860 \*MATERIAL, NAME=FILL8  
861 \*ELASTIC, TYPE=ISOTROPIC  
862 1.58E4,0.32  
863 \*DRUCKER PRAGER HARDENING  
864 40.95,0.  
865 \*DRUCKER PRAGER, SHEAR CRITERION=LINEAR  
866 41.89,1.,15.  
867 \*\*  
868 \*MPC  
869 TIE,LAYER7T,LAYER8B  
870 TIE,LAYER6T,LAYER7B  
871 TIE,LAYER5T,LAYER6B  
872 TIE,LAYER4T,LAYER5B  
873 TIE,LAYER3T,LAYER4B  
874 TIE,LAYER2T,LAYER3B  
875 TIE,LAYER1T,LAYER2B  
876 TIE,GRAVEL,LAYER1B  
877 TIE,CONGRAV,GRAVB  
878 \*EQUATION  
879 2  
880 70101,2,1.,80001,2,-1.  
881 2  
882 4045,2,1.,80118,2,-1.  
883 2  
884 60101,2,1.,70001,2,-1.  
885 2  
886 50101,2,1.,60001,2,-1.  
887 2  
888 40101,2,1.,50001,2,-1.  
889 2  
890 30101,2,1.,40001,2,-1.  
891 2  
892 20101,2,1.,30001,2,-1.

```

893 2
894 10201,2,1.,20001,2,-1.
895 2
896 4001,2,1.,10001,2,-1.
897 2
898 3801,2,1.,251,2,-1.
899 **end of material definition
900 *INITIAL CONDITIONS, TYPE=STRESS, GEOSTATIC
901 INISOIL1,0.,0.97,-105.36,-3.7,0.47
902 INISOIL2,0.,1.67,-120.02,-3.7,0.47
903 INISOIL3,0.,2.67,-143.70,-3.7,0.47
904 INISOIL4,0.,3.97,-173.64,-3.7,0.47
905 INISOIL5,0.,5.52,-208., -3.7,0.47
906 INISOIL6,0.,7.32,-248.61,-3.7,0.47
907 INISOIL7,0.,9.37,-274.86,-3.7,0.47
908 INISOIL8,0.,11.67,-341.25,-3.7,0.47
909 RSOIL,0.,0.62,-91.08,-3.7,0.4
910 *STEP
911 **add initial stress, step 1
912 GEOSTATIC INITIAL STRESS STATE
913 *GEOSTATIC
914 *DLOAD
915 RSOIL,BY,-21.09
916 USOIL,BY,-22.56
917 RUSOIL,BY,-22.56
918 SSOIL,BY,-22.56
919 BOX, BY,-24.53
920 BEDSLAB,BY,-24.53
921 ROCK,BY,-24.53
922 *MODEL CHANGE,REMOVE
923 LAYER8,
924 LAYER7,
925 LAYER6,
926 LAYER5,
927 LAYER4,
928 LAYER3,
929 LAYER2,
930 LAYER1,
931 GRAVEL,
932 *MODEL CHANGE,TYPE=CONTACT PAIR,REMOVE
933 SLAVE1, MASTER1
934 SLAVE2, MASTER2
935 SLAVE3, MASTER3
936 *ELPRINT, ELSET=BOX, FREQUENCY=0, POSITION=AVERAGED AT NODES
937 S
938 E
939 *ELPRINT, ELSET=GRAVEL, POSITION=AVERAGED AT NODES, FREQUENCY=0
940 S
941 *ELPRINT, ELSET=SOILB, POSITION=AVERAGED AT NODES, FREQUENCY=0
942 S

```

```

943 *NODEPRINT, NSET=ROOFN, FREQUENCY=0
944 U
945 *NODEPRINT, NSET=WALLN, FREQUENCY=0
946 U
947 *BOUNDARY
948 MIDN,1
949 LHSGR,1
950 LHS,1
951 RHS1,1
952 RHS2,1
953 BOTTOM2,2
954 *CONTACT PRINT,FREQUENCY=20
955 **CONTACT FILE
956 *END STEP
957 *STEP, INC=100
958 *STATIC
959 .01,1,.,.001,.,1
960 *ENDSTEP
961 *STEP
962 step 3 add GRAVEL2 stress free
963 *STATIC
964 *MODEL CHANGE,ADD
965 GRAVEL,
966 *MODEL CHANGE, TYPE=CONTACT PAIR, ADD
967 SLAVE1,MASTER1
968 SLAVE2,MASTER2
969 SLAVE3,MASTER3
970 *END STEP
971 *STEP,INC=100
972 **apply GRAVEL2 body force
973 *STATIC
974 0.00725,1,.,0.0007,0.1
975 *DLOAD
976 GRAVEL,BY,-19.42
977 *BOUNDARY,OP=NEW
978 MIDN,1
979 LHSGR,1
980 LHS,1
981 RHS1,1
982 RHS2,1
983 BOTTOM2,2
984 *END STEP
985 *STEP
986 step 5 add LAYER1 and LAYER2 stress free
987 *STATIC
988 *MODEL CHANGE,ADD
989 LAYER1,
990 LAYER2,
991 *END STEP
992 *STEP,INC=100

```

```

993    **apply LAYER2 body force,step 6
994    *STATIC
995    0.002,1.,0.001,0.1
996    *DLOAD
997    LAYER1,BY,-21.09
998    LAYER2,BY,-21.09
999    *BOUNDARY,OP=NEW
1000   MIDN,1
1001   LHSGR,1
1002   LHS,1
1003   RHS1,1
1004   RHS2,1
1005   LEFTL1,1
1006   LEFTL2,1
1007   BOTTOM2,2
1008   *END STEP
1009   *STEP
1010   step 7 add LAYER3 stress free
1011   *STATIC
1012   *MODEL CHANGE,ADD
1013   LAYER3,
1014   *END STEP
1015   *STEP,INC=150
1016   **apply LAYER3 body force,step 8
1017   *STATIC
1018   0.002,1.,0.001,0.1
1019   *DLOAD
1020   LAYER3,BY,-21.09
1021   *BOUNDARY,OP=NEW
1022   MIDN,1
1023   LHSGR,1
1024   LHS,1
1025   RHS1,1
1026   RHS2,1
1027   LEFTL1,1
1028   LEFTL2,1
1029   LEFTL3,1
1030   BOTTOM2,2
1031   *END STEP
1032   *STEP
1033   step 9 add LAYER4 stress free
1034   *STATIC
1035   *MODEL CHANGE,ADD
1036   LAYER4,
1037   *END STEP
1038   *STEP,INC=150
1039   **apply LAYER4 body force,step10
1040   *STATIC
1041   0.002,1.,0.001,0.1
1042   *DLOAD

```

```

1043 LAYER4,BY,-21.09
1044 *BOUNDARY,OP=NEW
1045 MIDN,1
1046 LHSGR,1
1047 LHS,1
1048 RHS1,1
1049 RHS2,1
1050 LEFTL1,1
1051 LEFTL2,1
1052 LEFTL3,1
1053 LEFTL4,1
1054 BOTTOM2,2
1055 *END STEP
1056 *STEP
1057 step 11 add LAYER5 stress free
1058 *STATIC
1059 *MODEL CHANGE,ADD
1060 LAYER5,
1061 *END STEP
1062 *STEP,INC=200
1063 **apply LAYER5 body force,step12
1064 *STATIC
1065 0.002,1.,0.001,0.1
1066 *DLOAD
1067 **LAYER5,BY,-17.34
1068 LAYER5,BY,-21.09
1069 *BOUNDARY,OP=NEW
1070 MIDN,1
1071 LHSGR,1
1072 LHS,1
1073 RHS1,1
1074 RHS2,1
1075 LEFTL1,1
1076 LEFTL2,1
1077 LEFTL3,1
1078 LEFTL4,1
1079 LEFTL5,1
1080 BOTTOM2,2
1081 *END STEP
1082 *STEP
1083 step 13 add LAYER6 stress free
1084 *STATIC
1085 *MODEL CHANGE,ADD
1086 LAYER6,
1087 *END STEP
1088 *STEP,INC=200
1089 **apply LAYER6 body force,step 14
1090 *STATIC
1091 0.002,1.,0.001,0.1
1092 *DLOAD

```

```

1093  **LAYER6,BY,-29.52
1094  LAYER6,BY,-21.09
1095  *BOUNDARY,OP=NEW
1096  MIDN,1
1097  LHSGR,1
1098  LHS,1
1099  RHS1,1
1100  RHS2,1
1101  LEFTL1,1
1102  LEFTL2,1
1103  LEFTL3,1
1104  LEFTL4,1
1105  LEFTL5,1
1106  LEFTL6,1
1107  BOTTOM2,2
1108  *END STEP
1109  *STEP
1110  step 15 add LAYER7 stress free
1111  *STATIC
1112  *MODEL CHANGE,ADD
1113  LAYER7,
1114  *END STEP
1115  *STEP,INC=200
1116  **apply LAYER7 body force,step 16
1117  *STATIC
1118  0.002,1.,0.001,0.1
1119  *DLOAD
1120  **LAYER7,BY,-9.54
1121  LAYER7,BY,-21.09
1122  *BOUNDARY,OP=NEW
1123  MIDN,1
1124  LHSGR,1
1125  LHS,1
1126  RHS1,1
1127  RHS2,1
1128  LEFTL1,1
1129  LEFTL2,1
1130  LEFTL3,1
1131  LEFTL4,1
1132  LEFTL5,1
1133  LEFTL6,1
1134  LEFTL7,1
1135  BOTTOM2,2
1136  *END STEP
1137  *STEP
1138  step 17 add LAYER8 stress free
1139  *STATIC
1140  *MODEL CHANGE,ADD
1141  LAYER8,
1142  *END STEP

```

```

1143 *STEP,INC=200
1144 **apply LAYER8 body force,step 18
1145 *STATIC
1146 0.002,1.,0.001,0.1
1147 *DLOAD
1148 **LAYER8,BY,-14.183
1149 LAYER8,BY,-11.71
1150 *BOUNDARY,OP=NEW
1151 MIDN,1
1152 LHSGR,1
1153 LHS,1
1154 RHS1,1
1155 RHS2,1
1156 LEFTL1,1
1157 LEFTL2,1
1158 LEFTL3,1
1159 LEFTL4,1
1160 LEFTL5,1
1161 LEFTL6,1
1162 LEFTL7,1
1163 LEFTL8,1
1164 BOTTOM2,2
1165 *NODE PRINT,FREQUENCY=0,NSET=SECT1
1166 U
1167 *ELPRINT, ELSET=GRAVEL, POSITION=AVERAGED AT NODES, FREQUENCY=100
1168 S
1169 *ELPRINT, ELSET=SOILB, POSITION=AVERAGED AT NODES, FREQUENCY=100
1170 S
1171 *NODEPRINT, NSET=ROOFN, FREQUENCY=100
1172 U
1173 *NODEPRINT, NSET=WALLN, FREQUENCY=100
1174 U
1175 *ELPRINT, ELSET=BOX, FREQUENCY=20, POSITION=AVERAGED AT NODES
1176 S
1177 E
1178 *END STEP

```

## **Appendix G**

### **Calibration Sheet for Instrumentation Gages**



Sullivan County Culvert Site: Vibrating Wire Pressure Cell

Section A	Serial Number	Calibration Factor C (psi/digit)	Thermal Factor K (psi/EC up)	Section B	Serial Number	Calibration Factor C (psi/digit)	Thermal Factor K (psi/EC up)
1PRE	34647	0.006531	-0.00067	1PRE	34671	0.006462	-0.01643
2PRE	34668	0.006546	-0.00808	2PRE	34672	0.006837	-0.01899
3PRE	34670	0.006683	-0.01856	3PRE	34675	0.006929	-0.01711
4PRE	34678	0.006607	-0.01427	4PRE	34676	0.006588	-0.01830
5PRE	34679	0.006752	-0.00695	5PRE	34669	0.006456	-0.02391
6PRE	34673	0.006514	-0.01675	6PRE	34677	0.006739	-0.00139

Greene County Culvert Site: Vibrating Wire Pressure Cell

Section A	Serial Number	Calibration Factor C (psi/digit)	Thermal Factor K (psi/EC up)	Section B	Serial Number	Calibration Factor C (psi/digit)	Thermal Factor K (psi/EC up)
1PRE	36353	0.007210	0.008956	1PRE	36352	0.007202	0.001491
2PRE	37156	0.006652	-0.01648	2PRE	36354	0.007651	0.003960
3PRE	36356	0.007194	0.003724	3PRE	36355	0.007553	0.001564
4PRE	36346	0.01810	-0.01644	4PRE	36349	0.01923	-0.01165
5PRE	36347	0.01643	-0.02486	5PRE	36348	0.01859	-0.03002
6PRE	36345	0.01999	-0.02017	6PRE	36350	0.02002	-0.02828
7PRE	20326	0.00516	-0.00619				

Greene County Culvert Site: Resistance Strain Pressure Cell

Cell	Serial Number	Gage Factor	Cell	Serial Number	Gage Factor
1REP	719	5.508	4REP	698	7.607
2REP	718	5.540	5REP	721	5.532
3REP	699	9.078	6REP	720	2.751



## Vibrating Wire Pressure Transducer Calibration

Model Number: 4810-1-25 Pressure Range: 25 psi  
Serial Number: 34674 Mfg. Number: 5-4443  
Customer: Univ. of Tenn. *Sullivan* Temp: 21 °C  
Cust. I.D. Number: n/a *1 PREA* Baro: 996 mbar.  
Job No.: 8774-A Date: 10/12/95  
Test Gage: 336 Technician: *Shawn P. Edson*  
32

	Applied Pressure	Reading	Change
First Cycle	0.0156	10717	
	5.0017	9962	755
	10.0040	9200	762
	15.0130	8433	767
	20.0070	7664	769
	25.0090	6891	773
Second Cycle	0.0157	10718	
	5.0101	9961	757
	10.0160	9199	762
	15.0080	8435	764
	20.0060	7666	769
	25.0070	6891	775

Calibration Factor (C): 0.006531 (PSI/Digit)

Thermal Factor (K): -0.00067 (PSI/°C Rise)

Calculated Pressure =  $C(R0-R1) + K(T1-T0)$

GK-401 Reading at Shipment:

Date: 3/28/96

Position "B":\* 10422

Temperature: 25.0 °C

or

Position "F":\*

Baro: 1013 mbar\*\*

\* Users are advised to establish their own zero conditions.

\*\* Factory elevation 580 ft. above sea level.

Wiring Code:

Red and Black: Gage

White and Green: Thermistor



## Vibrating Wire Pressure Transducer Calibration

Model Number: 4810-1-25 Pressure Range: 25 psi  
Serial Number: 34668 Mfg. Number: 5-4435  
Customer: Univ. of Tenn. *Sullivan* Temp: 21 °C  
Cust. I.D. Number: n/a *2 PREA* Baro: 996 mbar.  
Job No.: 8774-A Date: 10/12/95  
Test Gage: 336 Technician: *Shuan P. Edson*  
26

	Applied Pressure	Reading	Change
First Cycle	0.0155	10889	
	4.9978	10133	756
	10.0040	9372	761
	15.0110	8608	764
	20.0080	7841	767
	25.0090	7069	772
Second Cycle	0.0160	10888	
	5.0057	10131	757
	10.0150	9371	760
	15.0080	8608	763
	20.0050	7841	767
	25.0090	7070	771

Calibration Factor (C): 0.006546 (PSI/Digit)

Thermal Factor (K): -0.00808 (PSI/°C Rise)

Calculated Pressure =  $\frac{C(R0-R1)}{T1-T0}$

GK-401 Reading at Shipment:

Date: 3/28/96

Position "B":\* 10718

Temperature: 25.0 °C

or

Position "F":\* \_\_\_\_\_

Baro: 1013 mbar\*\*

\* Users are advised to establish their own zero conditions.

\*\* Factory elevation 580 ft. above sea level.

Wiring Code:

Red and Black: Gage

White and Green: Thermistor



## Vibrating Wire Pressure Transducer Calibration

Model Number: 4810-1-25 Pressure Range: 25 psi  
Serial Number: 34670 Mfg. Number: 5-4439  
Customer: Univ. of Tenn. Temp: 21 °C  
Cust. I.D. Number: n/a *Sullivan* Baro: 996 mbar.  
Job No.: 8774-A *3/PREA* Date: 10/12/95  
Test Gage: 336 Technician: *Shuan P. Edson*  
24

	Applied Pressure	Reading	Change
First Cycle	0.0155	9942	
	4.9997	9202	740
	10.0070	8456	746
	15.0120	7707	749
	20.0080	6957	750
	25.0100	6201	756
Second Cycle	0.0160	9942	
	5.0075	9200	742
	10.0130	8455	745
	15.0080	7707	748
	20.0060	6957	750
	25.0080	6202	755

Calibration Factor (C): 0.006683 (PSI/Digit)

Thermal Factor (K): -0.01856 (PSI/°C Rise)

Calculated Pressure =  $C(R0-R1) + K(T1-T0)$

GK-401 Reading at Shipment:

Date: 3/28/96

Position "B":\* 9501

Temperature: 25.2 °C

or

Position "F":\* \_\_\_\_\_

Baro: 1013 mbar\*\*

\* Users are advised to establish their own zero conditions.

\*\* Factory elevation 580 ft. above sea level.

Wiring Code:

Red and Black: Gage

White and Green: Thermistor



## Vibrating Wire Pressure Transducer Calibration

Model Number: 4810-1-25 Pressure Range: 25 psi  
Serial Number: 34678 Mfg. Number: 5-4448  
Customer: Univ. of Tenn. *Sullivan* Temp: 21 °C  
Cust. I.D. Number: n/a *4 PREA* Baro: 996 mbar.  
Job No.: 8774-A Date: 10/12/95  
Test Gage: 336 Technician: *Sullivan P. Edison*  
28

	Applied Pressure	Reading	Change
First Cycle	0.0144	9987	
	5.0065	9239	748
	10.0060	8486	753
	15.0060	7729	757
	20.0030	6971	758
	25.0040	6205	766
Second Cycle	0.0163	9990	
	5.0088	9239	751
	10.0170	8485	754
	15.0020	7730	755
	20.0140	6970	760
	25.0020	6206	764

Calibration Factor (C): 0.006607 (PSI/Digit)

Thermal Factor (K): -0.01427 (PSI/°C Rise)

Calculated Pressure =  $C(R0-R1) + K(T1-T0)$

GK-401 Reading at Shipment:

Date: 3/28/96

Position "B":\* 9726

Temperature: 24.7 °C

or

Position "F":\* \_\_\_\_\_

Baro: 1013 mbar\*\*

\* Users are advised to establish their own zero conditions.

\*\* Factory elevation 580 ft.above sea level.

Wiring Code:

Red and Black: Gage

White and Green: Thermistor



## Vibrating Wire Pressure Transducer Calibration

Model Number: 4810-1-25 Pressure Range: 25 psi  
Serial Number: 34679 Mfg. Number: 5-4452  
Customer: Univ. of Tenn. *Sullivan* Temp: 21 °C  
Cust. I.D. Number: n/a *5 PREA* Baro: 996 mbar.  
Job No.: 8774-A Date: 10/12/95  
Test Gage: 336 Technician: *Shuan P. Edison*  
25

	Applied Pressure	Reading	Change
First Cycle	0.0144	10669	
	5.0051	9935	734
	10.0030	9199	736
	15.0050	8459	740
	20.0020	7716	743
	25.0040	6968	748
Second Cycle	0.0160	10671	
	5.0087	9937	734
	10.0180	9198	739
	15.0000	8460	738
	20.0130	7715	745
	25.0010	6969	746

Calibration Factor (C): 0.006752 (PSI/Digit)

Thermal Factor (K): -0.00695 (PSI/°C Rise)

Calculated Pressure =  $C(R0-R1) + K(T1-T0)$

GK-401 Reading at Shipment:

Date: 3/28/96

Position "B":\* 10355

Temperature: 24.9 °C

or

Position "F":\* \_\_\_\_\_

Baro: 1013 mbar\*\*

\* Users are advised to establish their own zero conditions.

\*\* Factory elevation 580 ft. above sea level.

Wiring Code:

Red and Black: Gage

White and Green: Thermistor



## Vibrating Wire Pressure Transducer Calibration

Model Number: 4810-1-25 Pressure Range: 25 psi  
Serial Number: 34673 Mfg. Number: 5-4442  
Customer: Univ. of Tenn. *Sullivan* Temp: 21 °C  
Cust. I.D. Number: n/a *6 PREA* Baro: 996 mbar.  
Job No.: 8774-A Date: 10/12/95  
Test Gage: 336 Technician: *Shuan P. Edson*  
25

	Applied Pressure	Reading	Change
First Cycle	0.0158	10777	
	5.0009	10017	760
	10.0060	9253	764
	15.0120	8485	768
	20.0080	7716	769
	25.0090	6939	777
Second Cycle	0.0161	10777	
	5.0093	10016	761
	10.0140	9252	764
	15.0060	8485	767
	20.0050	7716	769
	25.0080	6939	777

Calibration Factor (C): 0.006514 (PSI/Digit)

Thermal Factor (K): -0.01675 (PSI/°C Rise)

Calculated Pressure =  $C(R0-R1) + K(T1-T0)$

GK-401 Reading at Shipment:

Date: 3/28/96

Position "B":\* 10606

Temperature: 25.1 °C

or

Position "F":\* \_\_\_\_\_

Baro: 1013 mbar\*\*

\* Users are advised to establish their own zero conditions.

\*\* Factory elevation 580 ft.above sea level.

Wiring Code:

Red and Black: Gage

White and Green: Thermistor



### Vibrating Wire Pressure Transducer Calibration

Model Number: 4810-1-25 Pressure Range: 25 psi  
Serial Number: 34671 Mfg. Number: 5-4440  
Customer: Univ. of Tenn. *Sullivan* Temp: 21 °C  
Cust. I.D. Number: n/a *1 PR 12-13* Baro: 996 mbar.  
Job No.: 8774-A Date: 10/12/95  
Test Gage: 336 Technician: *Shuan P. Edson*  
28

	Applied Pressure	Reading	Change
First Cycle	0.0154	10630	
	4.9979	9866	764
	10.0050	9095	771
	15.0120	8319	776
	20.0080	7544	775
	25.0090	6762	782
Second Cycle	0.0158	10630	
	5.0061	9865	765
	10.0160	9092	773
	15.0070	8320	772
	20.0060	7544	776
	25.0070	6763	781

Calibration Factor (C): 0.006462 (PSI/Digit)

Thermal Factor (K): -0.01463 (PSI/°C Rise)

Calculated Pressure =  $C(R0-R1) + K(T1-T0)$

GK-401 Reading at Shipment:

Date: 3/28/96

Position "B":\* 10412

Temperature: 25.1 °C

or

Position "F":\* \_\_\_\_\_

Baro: 1013 mbar\*\*

\* Users are advised to establish their own zero conditions.

\*\* Factory elevation 580 ft. above sea level.

Wiring Code:

Red and Black: Gage

White and Green: Thermistor





## Vibrating Wire Pressure Transducer Calibration

Model Number: 4810-1-25 Pressure Range: 25 psi  
Serial Number: 34672 Mfg. Number: 5-4441  
Customer: Univ. of Tenn. *Sullivan* Temp: 21 °C  
Cust. I.D. Number: n/a *2 PREB* Baro: 996 mbar.  
Job No.: 8774-A Date: 10/12/95  
Test Gage: 336 Technician: *Shuan P. Edison*  
32

	Applied Pressure	Reading	Change
First Cycle	0.0155	10641	
	5.0000	9919	722
	10.0040	9192	727
	15.0130	8459	733
	20.0090	7724	735
	25.0100	6985	739
Second Cycle	0.0158	10642	
	5.0080	9917	725
	10.0130	9190	727
	15.0080	8459	731
	20.0070	7724	735
	25.0080	6986	738

Calibration Factor (C): 0.006837 (PSI/Digit)

Thermal Factor (K): -0.01899 (PSI/°C Rise)

Calculated Pressure =  $C(R0-R1) + K(T1-T0)$

GK-401 Reading at Shipment:

Date: 3/28/96

Position "B":\* 10474

Temperature: 25.1 °C

or

Position "F":\* \_\_\_\_\_

Baro: 1013 mbar\*\*

\* Users are advised to establish their own zero conditions.

\*\* Factory elevation 580 ft. above sea level.

Wiring Code:

Red and Black: Gage

White and Green: Thermistor



## Vibrating Wire Pressure Transducer Calibration

Model Number: 4810-1-25 Pressure Range: 25 psi  
Serial Number: 34675 Mfg. Number: 5-4445  
Customer: Univ. of Tenn. *Sullivan* Temp: 21 °C  
Cust. I.D. Number: n/a *34675* Baro: 996 mbar.  
Job No.: 8774-A *3/PREB* Date: 10/12/95  
Test Gage: 336 Technician: *Shuan P. Edson*  
27

	Applied Pressure	Reading	Change
First Cycle	0.0155	10904	
	4.9987	10190	714
	10.0060	9471	719
	15.0130	8749	722
	20.0080	8025	724
	25.0090	7296	729
Second Cycle	0.0158	10904	
	5.0070	10190	714
	10.0140	9470	720
	15.0080	8750	720
	20.0050	8025	725
	25.0080	7297	728

Calibration Factor (C): 0.006929 (PSI/Digit)

Thermal Factor (K): -0.01711 (PSI/°C Rise)

Calculated Pressure =  $C(R0-R1) + K(T1-T0)$

GK-401 Reading at Shipment:

Date: 3/28/96

Position "B":\* 10627

Temperature: 25.5 °C

or

Position "F":\* \_\_\_\_\_

Baro: 1013 mbar\*\*

\* Users are advised to establish their own zero conditions.

\*\* Factory elevation 580 ft.above sea level.

Wiring Code:

Red and Black: Gage

White and Green: Thermistor



## Vibrating Wire Pressure Transducer Calibration

Model Number: 4810-1-25 Pressure Range: 25 psi  
Serial Number: 34676 Mfg. Number: 5-4446  
Customer: Univ. of Tenn. Temp: 21 °C  
Cust. I.D. Number: n/a *Sullivan* Baro: 996 mbar.  
Job No.: 8774-A *4PREB* Date: 10/12/95  
Test Gage: 336 Technician: *Shuan P. Edson*  
27

	Applied Pressure	Reading	Change
First Cycle	0.0143	10974	
	5.0076	10223	751
	10.0040	9467	756
	15.0060	8709	758
	20.0030	7947	762
	25.0050	7181	766
Second Cycle	0.0165	10976	
	5.0095	10223	753
	10.0160	9466	757
	15.0030	8710	756
	20.0140	7946	764
	25.0010	7183	763

Calibration Factor (C): 0.006588 (PSI/Digit)

Thermal Factor (K): -0.01830 (PSI/°C Rise)

Calculated Pressure =  $C(R0-R1) + K(T1-T0)$

GK-401 Reading at Shipment:

Date: 3/28/96

Position "B":\* 10716

Temperature: 24.8 °C

or

Position "F":\* \_\_\_\_\_

Baro: 1013 mbar\*\*

\* Users are advised to establish their own zero conditions.

\*\* Factory elevation 580 ft. above sea level.

Wiring Code:

Red and Black: Gage

White and Green: Thermistor



## Vibrating Wire Pressure Transducer Calibration

Model Number: 4810-1-25 Pressure Range: 25 psi  
Serial Number: 34669 Mfg. Number: 5-4438  
Customer: Univ. of Tenn. Temp: 21 °C  
Cust. I.D. Number: n/a Baro: 996 mbar.  
Job No.: 8774-A Date: 10/12/95  
Test Gage: 336 Technician: 29 *Sullivan*  
*5PREB* *P. Edison*

### First Cycle

Applied Pressure	Reading	Change
0.0157	10934	
5.0013	10169	765
10.0040	9396	773
15.0130	8620	776
20.0080	7843	777
25.0100	7063	780

### Second Cycle

0.0160	10933	
5.0097	10167	766
10.0140	9396	771
15.0060	8621	775
20.0070	7844	777
25.0080	7063	781

Calibration Factor (C): 0.006456 (PSI/Digit)

Thermal Factor (K): -0.02391 (PSI/°C Rise)

Calculated Pressure =  $C(R0-R1) + K(T1-T0)$

GK-401 Reading at Shipment:

Date: 3/28/96

Position "B":\* 10571

Temperature: 24.6 °C

or

Position "I":\* \_\_\_\_\_

Baro: 1013 mbar\*\*

\* Users are advised to establish their own zero conditions.

\*\* Factory elevation 580 ft. above sea level.

Wiring Code:

Red and Black: Gage

White and Green: Thermistor



## Vibrating Wire Pressure Transducer Calibration

Model Number: 4810-1-25 Pressure Range: 25 psi  
Serial Number: 34677 Mfg. Number: 5-4447  
Customer: Univ. of Tenn. Temp: 21 °C  
Cust. I.D. Number: n/a Baro: 996 mbar.  
Job No.: 8774-A Date: 10/12/95  
Test Gage: 336 Technician: 31 Sullivan PREB P. Edison

	Applied Pressure	Reading	Change
First Cycle	0.0144	10319	
	5.0053	9586	733
	10.0080	8848	738
	15.0050	8106	742
	20.0020	7362	744
	25.0040	6611	751
Second Cycle	0.0163	10321	
	5.0092	9587	734
	10.0160	8847	740
	15.0010	8107	740
	20.0120	7361	746
	25.0020	6612	749

Calibration Factor (C): 0.006739 (PSI/Digit)

Thermal Factor (K): -0.00139 (PSI/°C Rise)

Calculated Pressure =  $C(R0-R1) + K(T1-T0)$

GK-401 Reading at Shipment:

Date: 3/28/96

Position "B":\* 10177

Temperature: 24.5 °C

or

Position "F":\* \_\_\_\_\_

Baro: 1013 mbar\*\*

\* Users are advised to establish their own zero conditions.

\*\* Factory elevation 580 ft. above sea level.

Wiring Code:

Red and Black: Gage

White and Green: Thermistor



## Vibrating Wire Pressure Transducer Calibration

Model Number: 4810-2-25 Pressure Range: 25 psi  
Serial Number: 37156 Mfg. Number: 5-1152  
Customer: U. of Tenn. GREENE Temp: 23 °C  
Cust. I.D. Number: 3 PRE 2 PRE A Baro: 996.7 mbar.  
Job No.: 9419R Date: 9/4/96  
Test Gage: 336 Technician: 25 *Shawn P. Edison*

	Applied Pressure	Reading	Change
First Cycle	0.0180	10683	
	5.0085	9939	744
	10.0160	9190	749
	15.0070	8440	750
	20.0060	7686	754
	25.0080	6927	759
Second Cycle	0.0165	10685	
	5.0048	9940	745
	10.0060	9192	748
	15.0080	8440	752
	20.0100	7685	755
	25.0030	6927	758

Calibration Factor (C): 0.006652 (PSI/Digit)

Thermal Factor (K): -0.01648 (PSI/°C Rise)

Calculated Pressure =  $C(R0-R1) + K(T1-T0)$

GK-401 Reading at Shipment:

Date: 9/20/96

Position "B":\* 10333

Temperature: 22.1 °C

or

Position "F":\*

Baro: 992.6 mbar\*\*

\* Users are advised to establish their own zero conditions.

\*\* Factory elevation 580 ft. above sea level.

Wiring Code:

Red and Black: Gage

White and Green: Thermistor



## Vibrating Wire Pressure Transducer Calibration

Model Number: 4810-2-25 Pressure Range: 25 psi  
Serial Number: 36353 GREENE Mfg. Number: 6-2524  
Customer: U. of Tennessee PREA Temp: 23 °C  
Cust. I.D. Number: n/a Baro: 982 mbar.  
Job No.: 9419 Date: 7/9/96  
Test Gage: 336 Technician: 30 *Shawn P. Edison*

	Applied Pressure	Reading	Change
First Cycle	0.0136	10934	
	5.0000	10250	684
	9.9976	9559	691
	15.0150	8864	695
	20.0020	8170	694
	25.0010	7468	702
Second Cycle	0.0143	10935	
	4.9950	10251	684
	10.0020	9559	692
	15.0010	8866	693
	20.0020	8170	696
	25.0040	7468	702

Calibration Factor (C): 0.007210 (PSI/Digit)

Thermal Factor (K): 0.008956 (PSI/°C Rise)

Calculated Pressure =  $C(R0-R1) + K(T1-T0)$

GK-401 Reading at Shipment:

Date: 8/19/96

Position "B":\* 10479

Temperature: 24.6 °C

or

Position "F":\*

Baro: 1007.1 mbar\*\*

\* Users are advised to establish their own zero conditions.

\*\* Factory elevation 580 ft. above sea level.

Wiring Code:

Red and Black: Gage

White and Green: Thermistor



## Vibrating Wire Pressure Transducer Calibration

Model Number: 4810-2-25 Pressure Range: 25 psi  
Serial Number: 36356 Mfg. Number: 6-2527  
Customer: U. of Tennessee **GREENE** Temp: 23 °C  
Cust. I.D. Number: n/a **3PRA** Baro: 982 mbar.  
Job No.: 9419 Date: 7/9/96  
Test Gage: 336 Technician: 31 **Shawn P. Edson**

	Applied Pressure	Reading	Change
First Cycle	0.0133	9972	
	5.0015	9286	686
	9.9970	8595	691
	15.0150	7898	697
	20.0030	7201	697
	25.0010	6499	702
Second Cycle	0.0140	9973	
	4.9979	9287	686
	10.0020	8594	693
	15.0000	7900	694
	20.0010	7202	698
	25.0020	6499	703

Calibration Factor (C): 0.007194 (PSI/Digit)

Thermal Factor (K): 0.003724 (PSI/°C Rise)

Calculated Pressure =  $C(R0-R1) + K(T1-T0)$

GK-401 Reading at Shipment:

Date: 8/19/96

Position "B":\* 9464

Temperature: 24.6 °C

or  
Position "F":\*

Baro: 1007.1 mbar\*\*

\* Users are advised to establish their own zero conditions.

\*\* Factory elevation 580 ft. above sea level.

Wiring Code:

Red and Black: Gage

White and Green: Thermistor





### Vibrating Wire Pressure Transducer Calibration

Model Number: 4810-1-50 Pressure Range: 50 psi  
Serial Number: 36346 Mfg. Number: 6-2418  
Customer: U. of Tennessee Temp: 23 °C  
Cust. I.D. #: n/a GREENE  
Job No.: 9419 4PREA Baro: 1005 mbar.  
Test Gage: 182 Technician: Shawn P. Edson  
18

Applied Pressure (psi)	Reading First Cycle	Reading Second Cycle	Average Reading	Change
0	9265	9269	9267	
10	8719	8720	8720	548
20	8167	8167	8167	553
30	7613	7615	7614	553
40	7059	7059	7059	555
50	6506	6506	6506	553

Calibration Factor (C): 0.01810 (PSI/Digit)

Thermal Factor (K): -0.01644 (PSI/°C. Rise)

Calculated Pressure =  $C(R0-R1) + K(T1-T0)$

GK-401 Reading at Shipment:

Position "B":\* 9108 Date: 8/19/96  
or  
Position "F":\* \_\_\_\_\_ Temperature: 24.3 °C

\* Users are advised to establish their own zero conditions. Baro: 1007.1 mbar\*\*

\*\* Factory elevation 580 ft. above sea level.

Wiring Code: Red and Black: Gage White and Green: Thermister

The above named instrument has been calibrated by comparison with standards traceable to the NIST, in compliance with MIL-STD-45662A.



### Vibrating Wire Pressure Transducer Calibration

Model Number: 4810-1-50 Pressure Range: 50 psi  
Serial Number: 36347 Mfg. Number: 6-2420  
Customer: U. of Tennessee 5 PREA Temp: 23 °C  
Cust. I.D. #: n/a GREENE Baro: 1005 mbar.  
Job No.: 9419 Date: 7/29/96  
Test Gage: 182 Technician: Shawn P. Edson  
14

Applied Pressure (psi)	Reading First Cycle	Reading Second Cycle	Average Reading	Change
0	9369	9373	9371	
10	8766	8767	8767	605
20	8158	8158	8158	609
30	7546	7549	7548	611
40	6938	6938	6938	610
50	6329	6328	6329	610

Calibration Factor (C): 0.01643 (PSI/Digit)

Thermal Factor (K): -0.02486 (PSI/°C. Rise)

Calculated Pressure =  $C(R0-R1) + K(T1-T0)$

GK-401 Reading at Shipment:

Position "B": \* 9323 Date: 8/19/96  
or  
Position "F": \* \_\_\_\_\_ Temperature: 24.3 °C

\* Users are advised to establish their own zero conditions. Baro: 1007.1 mbar\*\*

\*\* Factory elevation 580 ft. above sea level.

Wiring Code: Red and Black: Gage White and Green: Thermister

The above named instrument has been calibrated by comparison with standards traceable to the NIST, in compliance with MIL-STD-45662A.



### Vibrating Wire Pressure Transducer Calibration

Model Number: 4810-1-50

Pressure Range: 50 psi

Serial Number: 36345

Mfg. Number: 6-2417

Customer: U. of Tennessee GREENE

Temp: 23 °C

Cust. I.D. #: n/a GREY

Baro: 1005 mbar.

Job No.: 9419

Date: 7/29/96

Test Gage: 182

Technician:  
23

Shawn P. Edson

Applied Pressure (psi)	Reading First Cycle	Reading Second Cycle	Average Reading	Change
0	8596	8600	8598	
10	8103	8104	8104	495
20	7603	7603	7603	501
30	7101	7103	7102	501
40	6600	6600	6600	502
50	6099	6098	6099	502

Calibration Factor (C): 0.01999 (PSI/Digit)

Thermal Factor (K): -0.02017 (PSI/°C. Rise)

Calculated Pressure =  $C(R0-R1) + K(T1-T0)$

GK-401 Reading at Shipment:

Position "B":\* 8485

Date: 8/19/96

or

Position "F":\* \_\_\_\_\_

Temperature: 23.8 °C

\* Users are advised to establish their own zero conditions.

Baro: 1007.1 mbar\*\*

\*\* Factory elevation 580 ft. above sea level.

Wiring Code:

Red and Black: Gage

White and Green: Thermister

The above named instrument has been calibrated by comparison with standards traceable to the NIST, in compliance with MIL-STD-45662A.

**geo** kon**Vibrating Wire Pressure Transducer Calibration**Model Number: 4800E-25Pressure Range: 25 psiSerial Number: 20326Mfg. Number: 2-3077Customer: U. of Tenn.Temp: 22 °CJob No.: 4724Baro: 1029 mbar.Test Gage: 1132668By: SPE 8Date: 9/14/92**GREENE TP RE A :**

Applied Pressure	First Cycle	Second Cycle	Average	Change
0	15326	15329	15328	
5	14352	14358	14355	973
10	13385	13389	13387	968
15	12420	12425	12423	965
20	11452	11454	11453	970
25	10482	10481	10482	972

Calibration Factor (C): 0.00516 (PSI/Digit)Thermal Factor (K): -0.00619 (PSI/°C. Rise)Calculated Pressure =  $C(R0-R1) + K(T1-T0)$ 

GK-401 Reading at Shipment:

Date: 10/19/92Position "B":\*                     Temperature: 20 °C

or

Position "F":\* 15167Baro: 1018 mbar\*\*

\* Users are advised to establish their own zero conditions.

\*\* Barometric pressure is corrected for 580 ft. above sea level.

Wiring Code:

Red and Black: Gage

White and Green: Thermistor

TOTAL P.03



## Vibrating Wire Pressure Transducer Calibration

Model Number: 4810-2-25 Pressure Range: 25 psi  
Serial Number: 36352 Mfg. Number: 6-2523  
Customer: U. of Tennessee **GREENE** Temp: 23 °C  
Cust. I.D. Number: n/a **IPREB** Baro: 982 mbar.  
Job No.: 9419 Date: 7/9/96  
Test Gage: 336 Technician: 27 *P. Edson*

	Applied Pressure	Reading	Change
First Cycle	0.0135	11166	
	5.0035	10479	687
	10.0010	9789	690
	15.0150	9092	697
	20.0030	8396	696
	25.0030	7697	699
Second Cycle	0.0144	11168	
	4.9951	10480	688
	10.0060	9788	692
	15.0030	9094	694
	20.0010	8397	697
	25.0030	7697	700

Calibration Factor (C): 0.007202 (PSI/Digit)

Thermal Factor (K): 0.001491 (PSI/°C Rise)

Calculated Pressure =  $C(R0-R1) + K(T1-T0)$

GK-401 Reading at Shipment:

Date: 8/19/96

Position "B":\* 10862

Temperature: 24.6 °C

or

Position "F":\* \_\_\_\_\_

Baro: 1007.1 mbar\*\*

\* Users are advised to establish their own zero conditions.

\*\* Factory elevation 580 ft. above sea level.

Wiring Code:

Red and Black: Gage

White and Green: Thermistor



## Vibrating Wire Pressure Transducer Calibration

Model Number: 4810-2-25 Pressure Range: 25 psi  
Serial Number: 36354 Mfg. Number: 6-2525  
Customer: U. of Tennessee Temp: 23 °C  
Cust. I.D. Number: n/a **GREENE** Baro: 982 mbar.  
**2-PREB.** Date: 7/9/96  
Job No.: 9419  
Test Gage: 336 Technician: Shawn P. Edson  
26

	Applied Pressure	Reading	Change
First Cycle	0.0134	10995	
	4.9996	10348	647
	9.9980	9699	649
	15.0150	9043	656
	20.0030	8389	654
	25.0010	7729	660
Second Cycle	0.0142	10997	
	4.9959	10349	648
	10.0040	9698	651
	15.0020	9045	653
	20.0010	8389	656
	25.0030	7729	660

Calibration Factor (C): 0.007651 (PSI/Digit)

Thermal Factor (K): 0.003960 (PSI/°C Rise)

Calculated Pressure =  $C(R0-R1) + K(T1-T0)$

GK-401 Reading at Shipment:

Date: 8/19/96

Position "B":\* 10648

Temperature: 24.9 °C

or

Position "F":\* \_\_\_\_\_

Baro: 1007.1 mbar\*\*

\* Users are advised to establish their own zero conditions.

\*\* Factory elevation 580 ft. above sea level.

Wiring Code:

Red and Black: Gage

White and Green: Thermistor



## Vibrating Wire Pressure Transducer Calibration

Model Number: 4810-2-25 Pressure Range: 25 psi  
Serial Number: 36355 Mfg. Number: 6-2526  
Customer: U. of Tennessee Temp: 23 °C  
Cust. I.D. Number: n/a Baro: 982 mbar.  
Job No.: 9419 Date: 7/9/96  
Test Gage: 336 Technician: 28 *Shuan P. Edison*

	Applied Pressure	Reading	Change
First Cycle	0.0134	10304	
	5.0008	9649	655
	9.9990	8991	658
	15.0160	8327	664
	20.0020	7664	663
	25.0020	6996	668
Second Cycle	0.0142	10305	
	4.9969	9651	654
	10.0050	8990	661
	14.9990	8330	660
	20.0020	7665	665
	25.0020	6995	670

Calibration Factor (C): 0.007553 (PSI/Digit)

Thermal Factor (K): 0.001564 (PSI/°C Rise)

Calculated Pressure =  $C(R0-R1) + K(T1-T0)$

GK-401 Reading at Shipment:

Date: 8/19/96

Position "B":\* 9870

Temperature: 24.9 °C

or

Position "F":\*

Baro: 1007.1 mbar\*\*

\* Users are advised to establish their own zero conditions.

\*\* Factory elevation 580 ft. above sea level.

Wiring Code:

Red and Black: Gage

\* White and Green: Thermistor



## Vibrating Wire Pressure Transducer Calibration

Model Number: 4810-1-50

Pressure Range: 50 psi

Serial Number: 36349

Mfg. Number: 6-2422

Customer: U. of Tennessee

Temp: 23 °C

Cust. I.D. #: n/a

Baro: 1005 mbar.

Job No.: 9419

Date: 7/29/96

Test Gage: 182

Technician:  
18

*Shawn P. Edison*

Applied Pressure (psi)	Reading First Cycle	Reading Second Cycle	Average Reading	Change
0	8265	8269	8267	
10	7751	7753	7752	515
20	7232	7232	7232	520
30	6710	6712	6711	521
40	6190	6190	6190	521
50	5669	5669	5669	521

Calibration Factor (C): 0.01923 (PSI/Digit)

Thermal Factor (K): -0.01165 (PSI/°C. Rise)

Calculated Pressure =  $C(R0-R1)+K(T1-T0)$

GK-401 Reading at Shipment:

Position "B":\* 8128

Date: 8/19/96

or

Position "F":\*

Temperature: 24.6 °C

\* Users are advised to establish their own zero conditions.

Baro: 1007.1 mbar\*\*

\*\* Factory elevation 580 ft. above sea level.

Wiring Code:

Red and Black: Gage

White and Green: Thermister

The above named instrument has been calibrated by comparison with standards traceable to the NIST, in compliance with MIL-STD-45662A.





## Vibrating Wire Pressure Transducer Calibration

Model Number: 4810-1-50

Pressure Range: 50 psi

Serial Number: 36348

Mfg. Number: 6-2421

Customer: U. of Tennessee

GREENE  
5 PRE B

Temp: 23 °C

Cust. I.D. #: n/a

Baro: 1005 mbar.

Job No.: 9419

Date: 7/29/96

Test Gage: 182

Technician:  
19

*Shawn P. Edison*

Applied Pressure (psi)	Reading First Cycle	Reading Second Cycle	Average Reading	Change
0	9020	9024	9022	
10	8489	8490	8490	533
20	7952	7952	7952	538
30	7412	7414	7413	539
40	6874	6874	6874	539
50	6334	6334	6334	540

Calibration Factor (C): 0.01859 (PSI/Digit)

Thermal Factor (K): -0.03002 (PSI/°C. Rise)

Calculated Pressure =  $C(R0-R1) + K(T1-T0)$

GK-401 Reading at Shipment:

Position "B":\* 8850

Date: 8/19/96

or

Position "F":\* \_\_\_\_\_

Temperature: 24.1 °C

444

\* Users are advised to establish their own zero conditions.

Baro: 1007.1 mbar\*\*

\*\* Factory elevation 580 ft. above sea level.

Wiring Code:

Red and Black: Gage

White and Green: Thermister

The above named instrument has been calibrated by comparison with standards traceable to the NIST, in compliance with MIL-STD-45662A.



## Vibrating Wire Pressure Transducer Calibration

Model Number: 4810-1-50

Pressure Range: 50 psi

Serial Number: 36350

Mfg. Number: 6-2423

Customer: U. of Tennessee

Temp: 23 °C

Cust. I.D. #: n/a

Baro: 1005 mbar.

Job No.: 9419

Date: 7/29/96

Test Gage: 182

Technician:  
24

*Shawn P. Edson*

Applied Pressure (psi)	Reading First Cycle	Reading Second Cycle	Average Reading	Change
0	9254	9258	9256	
10	8761	8764	8763	494
20	8263	8262	8263	500
30	7762	7763	7763	500
40	7261	7262	7262	501
50	6760	6760	6760	502

Calibration Factor (C): 0.02002 (PSI/Digit)

Thermal Factor (K): -0.02828 (PSI/°C. Rise)

Calculated Pressure =  $C(R0-R1) + K(T1-T0)$

GK-401 Reading at Shipment:

Position "B":\* 9093

Date: 8/19/96

or

Position "F":\* \_\_\_\_\_

Temperature: 24.9 °C

\* Users are advised to establish their own zero conditions.

Baro: 1007.1 mbar\*\*

\*\* Factory elevation 580 ft. above sea level.

Wiring Code:

Red and Black: Gage

White and Green: Thermister

The above named instrument has been calibrated by comparison with standards traceable to the NIST, in compliance with MIL-STD-45662A.

# SENSOTEC

1200 CHESAPEAKE AVE. COLUMBUS, OHIO 43212 (614) 486 - 7723

## CERTIFICATE OF CALIBRATION

MODEL: LM/2345-23

SERIAL NUMBER: ~~1111000~~ 698

DATE: 09/17/94

CAPACITY: 30.000 PSIG  
PRESSURE

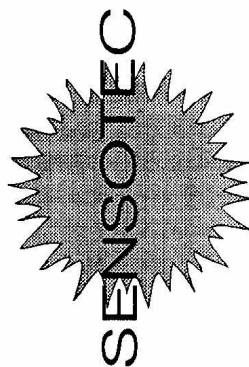
EXCITATION: 10.0 VOLTS

CALIBRATION FACTOR: 8.2146 MV/V

INPUT RESISTANCE: 8437 $\Omega$

OUTPUT RESISTANCE: 5712 $\Omega$

LEAKAGE:  $\infty$



Accepted and Certified by:

*Michael A. Stanley*

# SENSOTEC

1200 CHESAPEAKE AVE. COLUMBUS, OHIO 43212 (614) 486 - 7723

## CERTIFICATE OF CALIBRATION

MODEL: LM/2345-23

SERIAL NUMBER: ~~464058~~ - 699

DATE: 5/29/1996

CAPACITY: 30.0 PSIG

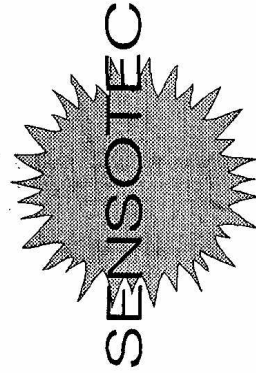
PRESSURE

EXCITATION: 10.0 VOLTS

CALIBRATION FACTOR: 9.8035 MV/V

OUTPUT RESISTANCE: 4724 $\Omega$

LEAKAGE:  $\infty$



Accepted and Certified by: *Michael A. Stanley*

Calibration Date: 05/29/96 @ 10:48

# SENSOTEC

1200 CHESAPEAKE AVE. COLUMBUS, OHIO 43212 (614) 486 - 7723

## CERTIFICATE OF CALIBRATION

MODEL: LM/2345-01

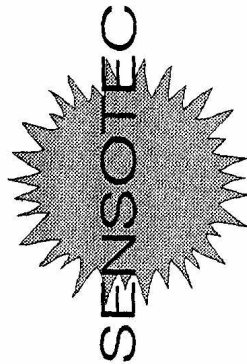
SERIAL NUMBER: ~~3456789~~ 718

DATE: 9/20/1996

CAPACITY: 50.0 PSIG  
PRESSURE  
EXCITATION: 10.0 VOLTS  
CALIBRATION FACTOR: 9.7919 MV/V

OUTPUT RESISTANCE: 4735 $\Omega$

LEAKAGE:  $\infty$



Accepted and Certified by: *Michael A. Stanley*  
Calibration Date: 09/20/96 @ 09:32

# SENSOTEC

1200 CHESAPEAKE AVE. COLUMBUS, OHIO 43212 (614) 486 - 7723

## CERTIFICATE OF CALIBRATION

MODEL: LM/2345-01

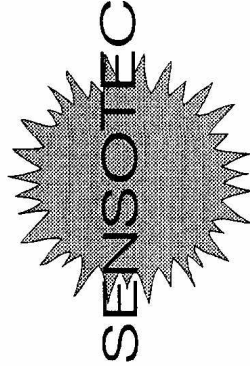
SERIAL NUMBER: ~~540113~~ 719

DATE: 9/20/1996

CAPACITY: 50.0 PSIG  
PRESSURE  
EXCITATION: 10.0 VOLTS  
CALIBRATION FACTOR: 9.9143 MV/V

OUTPUT RESISTANCE: 4680 $\Omega$

LEAKAGE:  $\infty$



Accepted and Certified by: Michael A. Stanley

Calibration Date: 09/20/96 @ 09:32



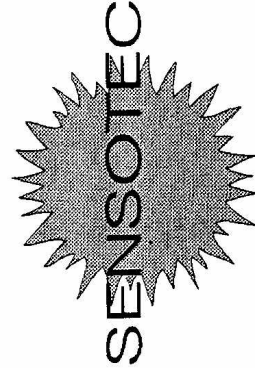
1200 CHESAPEAKE AVE. COLUMBUS, OHIO 43212 (614) 486 - 7723

## CERTIFICATE OF CALIBRATION

MODEL: LM/2345-01  
SERIAL NUMBER: ~~510757~~ 720  
DATE: 10/14/1996

CAPACITY: 50.0 PSIG  
PRESSURE  
EXCITATION: 10.0 VOLTS  
CALIBRATION FACTOR: 4.9533 MV/V

OUTPUT RESISTANCE: 5084 $\Omega$   
LEAKAGE:  $\infty$



Accepted and Certified by: *Michael A. Stanley*  
Calibration Date: 10/14/96 @ 09:04

# SENSOTEC

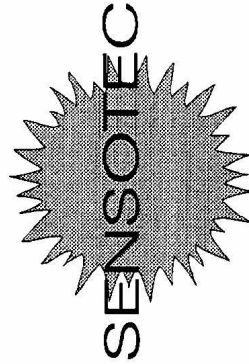
1200 CHESAPEAKE AVE. COLUMBUS, OHIO 43212 (614) 486 - 7723

## CERTIFICATE OF CALIBRATION

MODEL: LM/2345-01  
SERIAL NUMBER: ~~540116~~ 721  
DATE: 9/20/1996

CAPACITY: 50.0 PSIG  
PRESSURE  
EXCITATION: 10.0 VOLTS  
CALIBRATION FACTOR: 9.9579 MV/V

OUTPUT RESISTANCE: 4689 $\Omega$   
LEAKAGE:  $\infty$



Accepted and Certified by: Michael A. Stanley  
Calibration Date: 09/20/96 @ 09:32



## **Appendix H**

### **Earth Pressure Variations under Constant Embankment Height**

#### **H.1 Abstract**

The hydraulic type vibrating wire earth pressure cell is one of the best instrumentation tools for long-term earth pressure observation, especially when it can be mounted directly on an underground structure. Factors affecting the earth pressures are reviewed in this paper, and most of them have significant effect immediately after the construction work. Field earth pressure instrumentation on box culverts suggested that temperature and seasonal moisture change due to precipitation are major factors resulting in the earth pressure fluctuations.

Recorded earth pressures from instrumented culverts exhibited distinct fluctuations even through the embankment heights were constant. Resulting from the long term pressure observation on two different instrumented culverts under full embankment height as well as very small loads, the pressure readings were observed to be highly related to the temperature in the pressure cell. The results from long term observation data suggest that the temperature effect can be divided as cell part and transducer part. Under field condition, cell temperature coefficient was much greater than the transducer temperature coefficient.

The temperature corrected earth pressures were also found having a direct relationship with regional streamflow data, which is an indication of soil moisture in the

embankment material. Higher moisture content resulted in a high earth pressure acting on the box culverts.

**Keywords:** earth pressure, temperature effects, box culvert, field instrumentation, vibrating wire, long term observation, soil-structure interaction

## **H.2 Introduction**

The earth pressures on buried structures such as culverts are reported (Selig et al., 1982; Spangler, 1982; Yang et al, 1997) to have a great variety of magnitudes due to the different culvert stiffness and subsoil conditions. An inappropriate approximation of these earth pressures may lead to a structure failure (Selig et al, 1982). To confirm the design load and to understand the soil-structure interaction mechanisms in the buried or retaining structures, it is critical to measure the actual earth pressures acting on the structural surface under a long term service load. The earth pressures recorded by contact pressure cells are often better than those of pressure cells entirely embedded in the soil mass (Dunnicliff, 1988). Since these cells on the structure are often near to the atmosphere, the temperature at cells is subject to change during the long term instrumentation. Observed seasonal pressure change of cells mounted on structures have reported previously (Coyle and Bartoskwtz, 1976; Smoltczyk, 1977; Felio and Bauer, 1980; Symons and Murray 1988).

In the current research, the long term earth pressure observation results from two different instrumented box culvert sites are collected to demonstrate the temperature effects on the pressure readings. Empirical method obtained from the regression analysis is proposed to relate the field earth pressures to a constant temperature datum.

## **H.3 Examples of Earth Pressures Variation during the Long-term Observation**

### H.3.1 Previous Case Studies

A full-scale lateral pressure instrumentation reported by Coyle and Bartoskewitz (1976) was applied to a precast panel retaining wall about 3.5 m high. The instrumentation included 9 hydraulic type pneumatic earth pressure cells installed on one panel surface. The retaining wall was backfilled with the medium sand. Before the field installation, the pressure cells were calibrated in the laboratory. The expected operating temperature in the field was 10 -32 °C, and the cells were calibrated in the lab under the field temperature fluctuation. There was no temperature related pressure variation found. About 400 days of filed earth pressures on the wall under service condition were reported. The total force recorded by the pressure cells indicated a seasonal fluctuation as shown in Figure 1. The normalized pressure variation with time, where the normalized pressure is the ratio of the recorded pressure over average pressure during the entire measurement, is presented in the figure. The difference between the highest and the lowest readings was 60% of the average pressure.

Long term earth pressures were also recorded on a bridge abutment in England (Symons and Murray, 1988). The retaining wall was a reinforced concrete inverted T structure with an approximate height of 7 meters. The backfill material was a well-graded sand-gravel mixture with a maximum grain size of 50 mm. Pneumatic pressure cells were embedded both in the soil and at the soil-structure interface. During 5 years of earth pressure observation, the magnitude of earth pressure was strongly related to the temperature. Figure 2 demonstrates the relationship between the recorded horizontal earth pressure and temperature variation. The temperature in the figure was the daily average air temperature, and no temperature inside each cell was recorded. The measured average earth pressure was

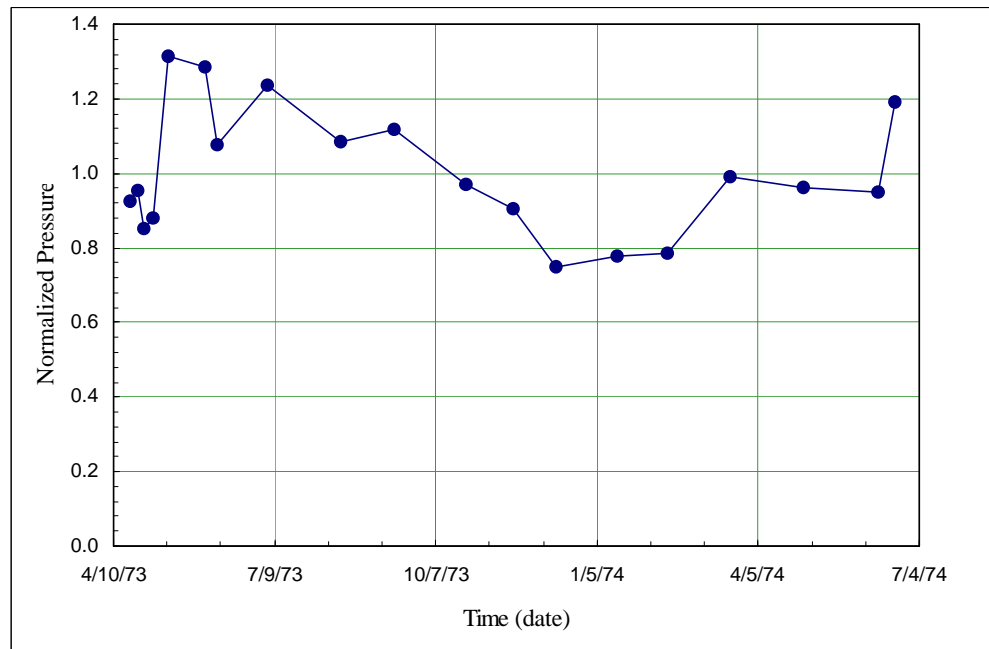


Figure 1 Recorded Normalized Pressure over Time  
(After Coyle and Bartoskwtz, 1976)

34.9 kPa, with the minimum pressure reading was 25 kPa at  $-5.5^{\circ}\text{C}$  and maximum reading 46.2 kPa at  $28.3^{\circ}\text{C}$ . The range of earth pressure readings was more than 60% of the average recorded pressure.

Similar temperature affected pressure fluctuation in an instrumentation on a bridge abutment was reported by Felio (1980). The hydraulic type pneumatic pressure cell was used in the instrumentation. A five years long term earth pressure in instrumentation on a ship lock (Smolczyk et al., 1977) indicated that the earth pressures were also closely related to temperature.

### H.3.2 Earth Pressures on A Box Culvert under the Constant Embankment Height

The long term earth pressures were measured on a double cell cast-in-place reinforced concrete box culvert site in east Tennessee. The culverts were 150 m in length, respectively. The maximum embankment height in Site I was 11.74 m. The hydraulic type vibrating wire

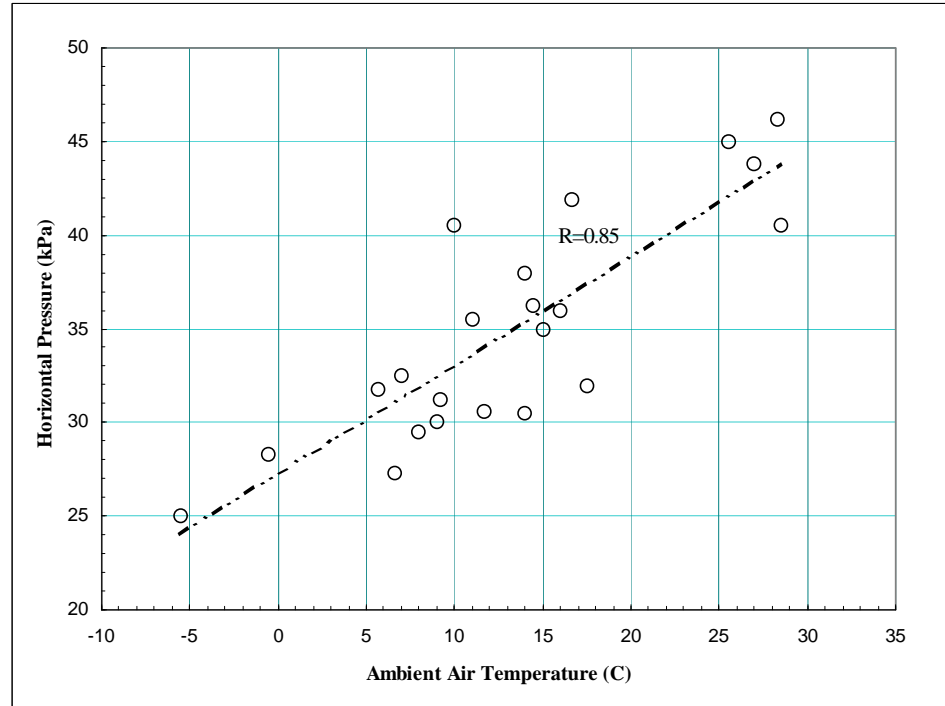


Figure 2 Relation Between the Measured Horizontal Pressure and Ambient Air Temperature (After Symons and Murray, 1988)

pressure cell was used in the instrumentation work. The earth pressure data in Site I under a full embankment height (11.7 m) was monitored continuously for more than three years.

The location of pressure cells is shown in Figure 3. Both vertical and lateral pressure exhibited a great fluctuation against their measured average. The maximum vertical difference at same location was 105 kPa, which is 34% of average measured pressure at the same cell. A 71 kPa of maximum lateral pressure variation, which was 64% of measured mean value, was found.

#### H.4 Factors Influence the Earth Pressure Reading with Time

The earth pressure measurements are often erratic and difficult to interpret. Both the erratic variations in readings from cell to cell (scatter) and the progressive changes in readings with time have been reported (Coyle and Bartoskewitz, 1976; Roth et al., 1979;

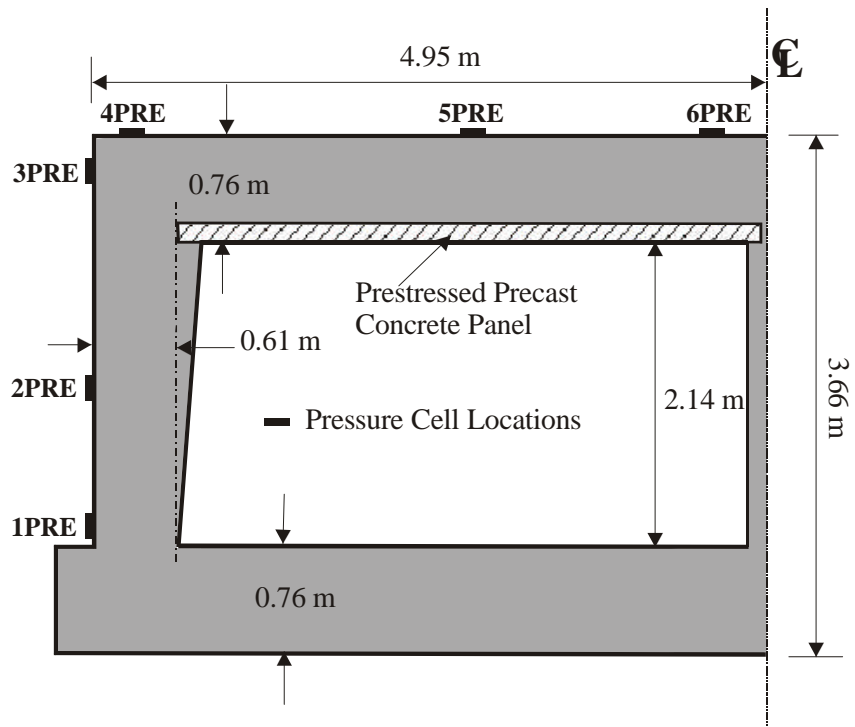


Figure 3 Illustration of Instrumented Culvert Dimensions and Pressure Cell Locations (Site I)

Smolczyk et al., 1979, James et al., 1986; Tadros, 1986; Dunnicliff, 1988; Symons and Murray, 1988; Clayton and Symons, 1991). The scattered data in the field measurement can be attributed to the different sources. Some of them are the difference in cell construction, cell installation procedure, and soil grain size near the cells (Weller and Kulhawy, 1982; Dunnicliff, 1988). The measurements might be also affected by the pressure cell construction factors, such as the cell size, the aspect ratio (cell diameter to cell thickness), the pressure sensing configuration, the cell stiffness, and the lead wire length, etc. The variation in local soil conditions around the pressure cell could also influence the earth pressure registration. The time variation of the recorded earth pressure could be significant and several interpretations have been reported. They factors are summarized as follow:

- Development of soil cohesion at the soil-structure interface. This could lead to an increase of the vertical pressure above the circular culverts and a decrease of horizontal pressures on the field instrumentations (Spangler, 1982). Carder and Krawczyk (1975) reported that the shear stresses at the pressure cell appeared to affect the normal pressure. Usually, the soil-structure induced earth pressure changes are most significant immediately after the construction.
- Relaxation of the compaction induced pressures. This could lead to a decrease of the horizontal earth pressure acting on the earth retaining structures (Roth et al., 1979). The stress relaxation is likely to maintain shortly after the removal of compaction equipment and shortly after the construction work.
- Structural movement. Large scale laboratory instrumentation tests (Carder et al., 1977, Duncan and Seed, 1986) suggested that even a very small wall translation or

rotations could lead to a significant horizontal pressure state changed from at rest ( $K_0$ ) state to active ( $K_a$ ) state. Lateral earth pressures could be significantly decreased as results of the displacement in the structure.

- Moisture content changes inside the soil mass. The clay fill might exist with positive or negative pore pressures, which is controlled by the plasticity and placement moisture content of the fill. For high plasticity soil (Clayton and Symons, 1991), when it absorbs moisture, it will produce a horizontal swelling pressure against the retaining structure. Therefore, the significant earth pressure fluctuation in the field condition is likely to be limited to the potentially expansive soil within a range of shallow subsurface, which the moisture content in the soil has the largest potential to be significantly influenced by the ambient environment.
- Moisture migration at the soil-structure interface. If the pressure cells were flush-mounted, it might be the source of the pressure fluctuations (Filz and Duncan, 1993). When the moisture in the backfill soil moves into a dry, well-cured concrete structure surface, it will cause a slight expansion of the concrete around the embedded cell. Concrete expansion around the cell might result in the distortion of the cell. The registered pressure is therefore reduced.
- Temperature effect (Smoltczyk, et al., 1977; Felio, 1980; James et al., 1986; Dunnicliff, 1988; Symons and Murray, 1988; McRae and Simmons, 1991; Filz and Duncan, 1993). Temperature variation in a pressure cell can cause the thermal expansion of the fluid in the cell, the metal cell body, and the surrounding material. The influence of temperature can be more prominent when the cells are firmly



mounted on the structure surface and confined by soil than when it is only confined in media such as air or water, which is usually used in the manufacture calibration. To minimize this effect, measures are taken during the cell manufacture, such as using a thin fluid layer in the cell (Dunnicliff, 1988), and evacuating the interior of the cell to eliminate the effects of pressures that are caused by changing the temperature of air with in the confined fixed volume of cell interior (McRae and Simmons, 1991). In spite of these improvements, significant pressure changes still occurred due to the temperature variation in the field conditions.

## **H.5 Contact Pressure Cells Configurations**

There are two basic types of contact earth pressure cells: diaphragm cell and hydraulic cell (Dunnicliff, 1988). In the diaphragm type, the external earth pressure is sensed by a deformable stiff circular membrane, which is fully supported by an integral stiff edge ring. The deformation transducer is bounded on the interior face. The hydraulic type of cell consists two circular or rectangular steel plates, welded together around their periphery, with liquid filling the intervening opening and high pressure steel tubing connecting the opening to a nearby pressure transducer. From the published data, the hydraulic type pressure cell had wider applications.

To have a better performance of the contact earth pressure cell, Dunnicliff (1988) summarized the long term pressure cell instrumentation results, and recommend that the hydraulic cells should have an inner inactive face and the layer of liquid within the two plates should as thin as possible. Further, the active face should also be thick and grooved. This cell

configuration is also reported (Dunnicliff, 1988) to have a better performance under temperature variation.

There are different ways to reflect the deformation at the soil contact pressure cell: pneumatic, electric resistance and vibrating wire gage, etc. Regardless the pressure sensing configuration in the pressure cell constructions, it is generally accepted that the vibrating wire readout system is a reliable way for the long-term monitoring in the field condition (Bordes and Debreuille, 1984; McRae and Simmons 1991). Different types of vibrating wire gages are used in the geotechnical instrumentation practice (Hannon and Jackura, 1984; Dunnicliff, 1988; Tadros, et al., 1989; Filz and Duncan, 1993; Benmokrane, et al., 1995; Yang, et al., 1997).

## **H.6 Instrumentation on Box Culvert Sites**

Two similar reinforced box culverts under deep embankment in East Tennessee were instrumented to measure the earth pressures under the construction and service load. The maximum embankment height in Site I and II are 11.7 and 18.9 m, respectively. The instrumentation on each site included two instrumented sections. In one section, six hydraulic type vibrating wire pressure cells (Geokon 4810) with different capacity were placed around one cell of the structure, three on the top and three on the side. The dimension of the culvert and the location of pressure cells are illustrated in Figure 4. All 12 cells in Site I and 6 cells on culvert wall in Site II have a capacity of 173 kPa, and 6 cells on the culvert roof in Site II (on the culvert roof) have 345 kPa of rated capacity. According to the manufacturer (Flynn, 1999), the cells are capable of operating at up to twice the rated capacity. Transducer is designed such that as pressure increases, wire tension decreases. At some point, wire will

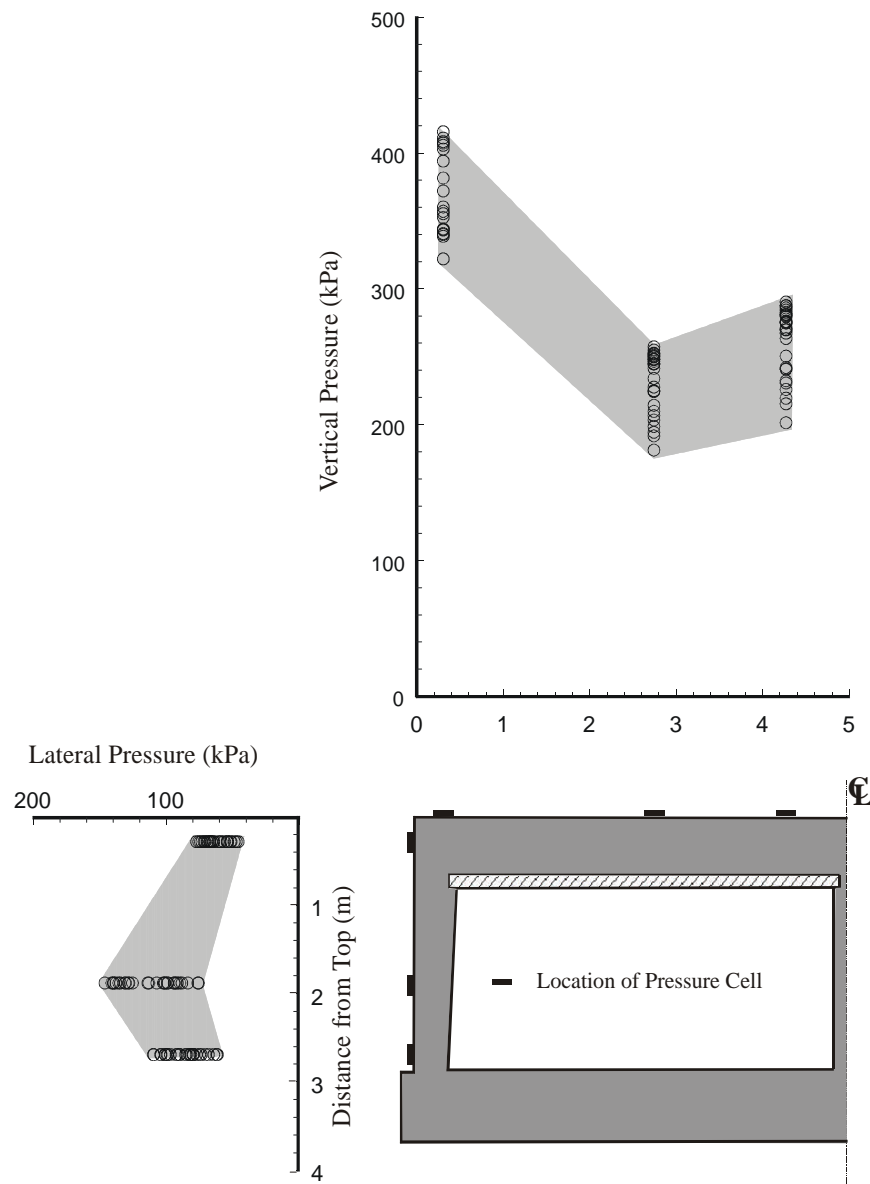


Figure 4 Observed Earth Pressures on Box Culvert under Constant Embankment Height

"go slack" and therefore it will not respond to excitation or "plucking." If load is decreased, tension will be restored and function will return. So that in the transducer responding range, linear relationship between the recorded and applied pressure can be assumed.

The pressure cells consist of two 230-mm diameter circular plates. One of the plates is thicker (inactive plate) and designed to bear against the external surface the structure in a way that will prevent flexure of the cell, and the other is thinner and more sensitive to react to the soil pressure. The aspect ratio (cell diameter over plate total thickness) for these cells is 38, which is considered as an "intermediate" size cell appropriate for the measurement of soil pressure (Weller and Kulhawy, 1982). The pressure cell configuration is illustrated in Figure 5. The cell was first fixed to the culvert wall and roof with concrete anchors through 4 mounting lugs around the edge of the plate, and a quick setting high strength grout pad was used to assure uniform contact between the plate and concrete. Medium sand was used to cover the cell and transducer housing to protect the cell from possible point loads or other

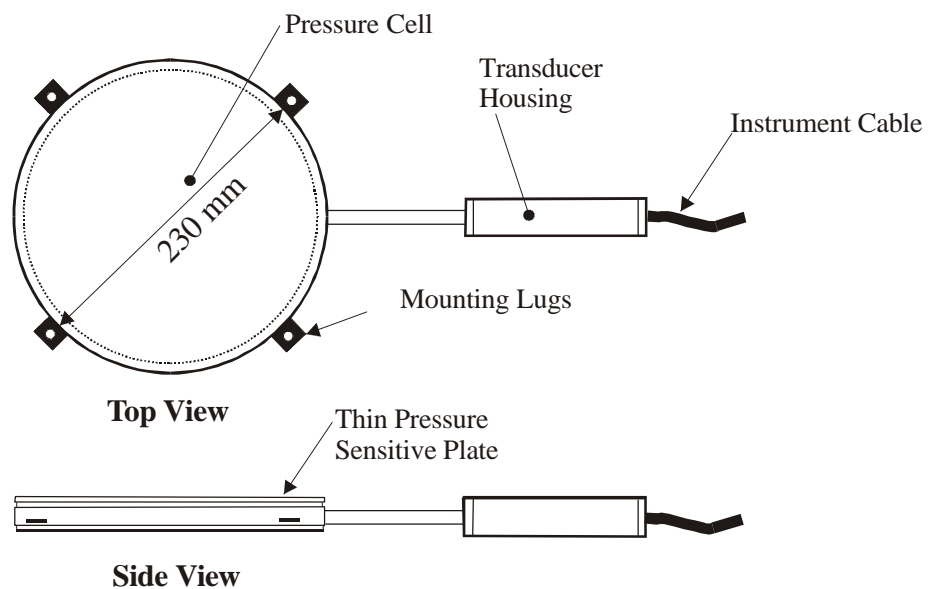


Figure 5 Illustration of Pressure Cell Used in the Instrumentation

stress distortions induced by the large size particles in the crushed gravel. A geosynthetic cover was attached to the concrete with adhesive to separate the gravel and the sand. The installation of pressure cell is illustrated in Figure 6.

### H.7 Observed Temperature Effects at Different Conditions

For a commercial hydraulic type vibrating pressure cell, the temperature correction coefficient is usually provided by the manufacturer together with a pressure calibration factor. Usually, both the calibration and temperature correction work are conducted under the laboratory condition, with the cell free from constraint. The calibration of temperature effect for the pressure transducer can be expressed by (Geokon, 1995):

$$p_k = p + k_1 \times (T_0 - T_1) \quad (1)$$

where:  $p_k$  is temperature corrected pressure using thermal coefficient provided by manufacturer;

$p$  is uncorrected pressure reading;

$k_1$  is thermal coefficient of the vibrating wire transducer;

$T_1$  is the current temperature;

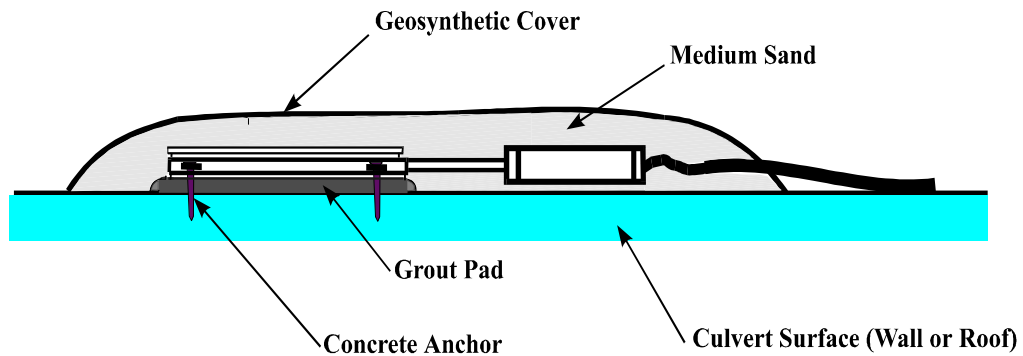


Figure 6 Installation of Contact Pressure Cell on the Culvert (Site II)

$T_0$  is the initial temperature;

Usually, the thermal coefficient of the transducers is designed with thermal insensitive materials to minimize the temperature effect on the reading (McRae and Simmons, 1991).

At the field condition, the pressure cell is likely to be fixed on the structure with anchors and cements, and constraint on the cell is greatly different from the lab calibration condition. When a contact pressure cell is fixed on the structure surface, the temperature variation is expected to be significant, so that it is important to have “close to in-situ” condition calibration under different temperature environment, in order to obtain a reliable earth pressure result. But the calibration work like this would be very complex and time consuming in practice. So that, for most of the field instrumentation projects, the only available calibration chart provided by the manufacturer is the temperature correction of the pressure transducer. The temperature related pressure variation under different loading conditions are discussed in detail below.

### **H7.1 Earth Pressure Changes at Zero Load**

The pressure cells at Site II were not loaded for approximately 7 months after the initial installation. The pressure cells were under a very small load of sand in the geosynthetic packs. The temperature recorded by thermistor varied from  $-4$  to  $30$  °C during this period. The uncorrected pressure drifted from  $-3.5$  kPa to  $5$  kPa, as shown in Figure 7. The high correlation coefficients indicate that the pressure cell reading was dependent on the temperature. After the temperature coefficient for the pressure transducer was applied on each cell, the “corrected” pressure reading is still strongly related to the temperature change (Figure 8). The pressure reading variation range in Figure 8 decreased to about  $4$  kPa. The

### Temperature Effect on Pressure Cell (Site II, Section B)

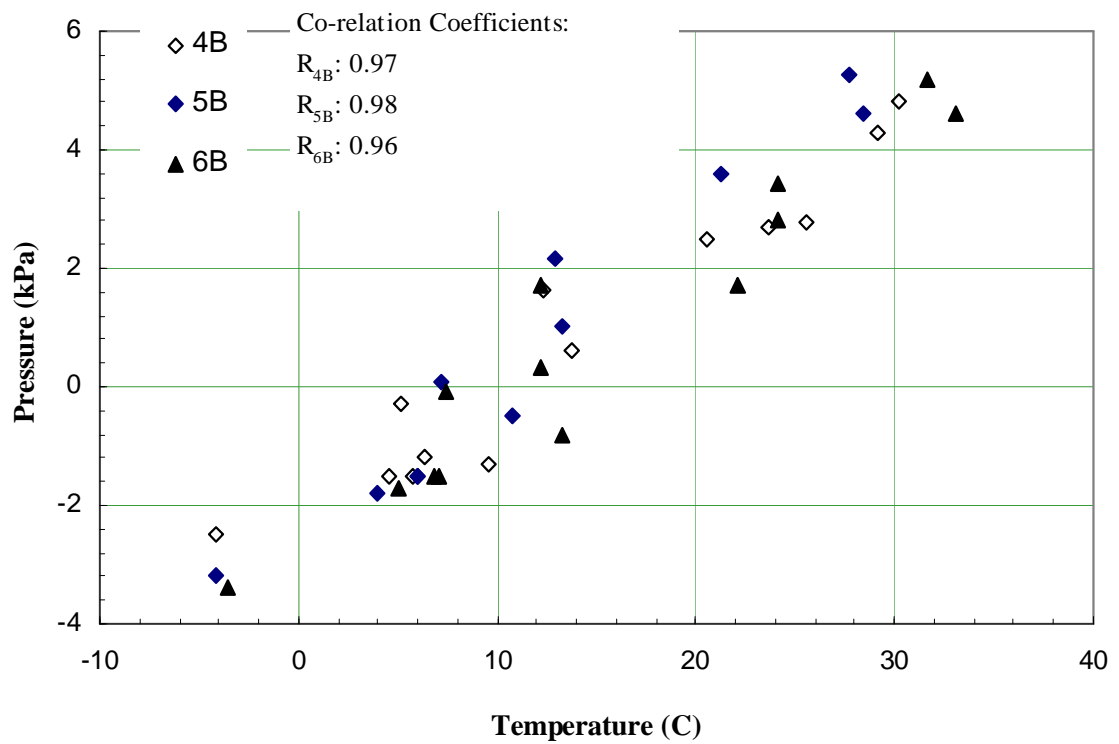


Figure 7 Relationship Between Uncorrected Pressure Readings and Temperature

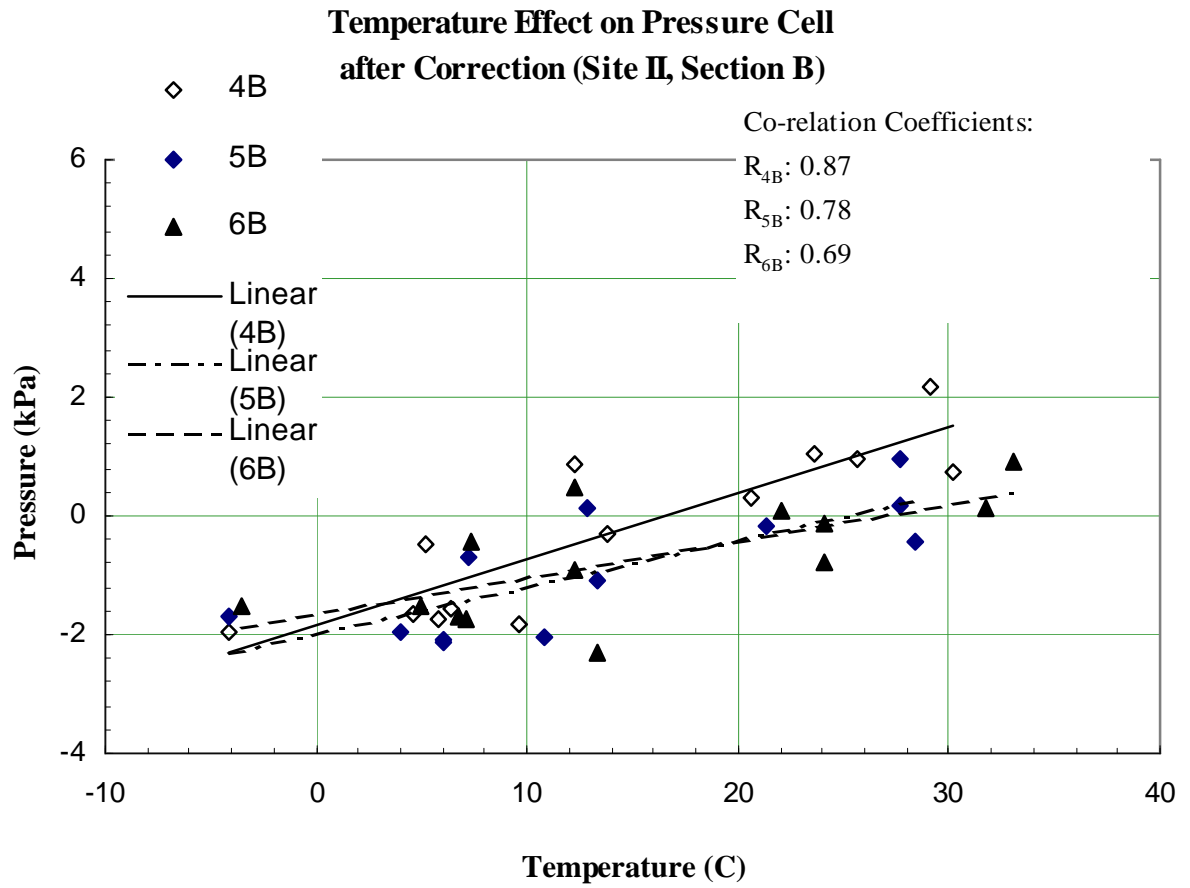


Figure 8 Temperature Relationship using Transducer Correction Coefficient



“total corrected” pressure  $p_{ck}$ , which is corrected for both the fluid fill cell and pressure transducer can be obtained:

$$p_{ck} = p_k + k_1 \times (T_{01} - T_1) + k_2 \times (T_{02} - T_1) \quad (2)$$

where:

$p_k$  is the transducer corrected reading defined in (1).

$k_2$  is the temperature coefficient of cell fluid sensing part which can be obtained statistically from Figure 7.

$T_{01}$ , and  $T_{02}$  are initial temperatures for transducer and cell.

The equation (2) suggests that the completed temperature correction for the pressure cell consists of the contribution of transducer and the cell. For zero load condition,  $T_{01}$  and  $T_{02}$  are the same, and both the temperature effect of transducer and cell are linear functions of temperature, we can combine these effects into one temperature coefficient  $k$ . They are listed in Table 1.

It is clear from Table 1 that the zero temperature drift cannot be neglected. From the 34 EC temperature variation recorded over the 7 months small load period, this corresponds

Table 1. Different Temperature Coefficients of Site II, Section B.

Cell Number	Capacity (kPa)	Transducer Coefficient $k_1$ from Manufacturer (kPa/EC)	Cell Coefficient $k_2$ from Figure 8 (kPa/EC)	“Total” Temperature Coefficient $k$ (kPa/EC)
4PREB	345	0.0803	0.1114	0.1917
5PREB	345	0.2070	0.0785	0.2855
6PREB	345	0.1950	0.0615	0.1555

to about -3.6 kPa to 5.2 kPa of stress. The contribution of pressure readings drifts of each coefficient is about 1% at the zero load condition.

## H7.2 Earth Pressure Variation under Constant Embankment Height

Great pressure changes under constant embankment heights (11.74 m for Section A, and 10.8 m for Section B) recorded in Site I. Figure pressure results. The average temperature recorded by the thermistor in the transducers was also shown in each figure.

The data were recorded more than three years for each cell. A strong relationship between the earth pressure reading and the temperature recorded at each cell.

The recorded pressure readings were corrected for temperature using the manufacturer transducer thermal coefficients. For the pressure readings on the culvert roof, the recorded maximum variation of reading was about 40 % of the measured average. At the culvert wall, the maximum earth pressure fluctuation was about 78 % of the measured average.

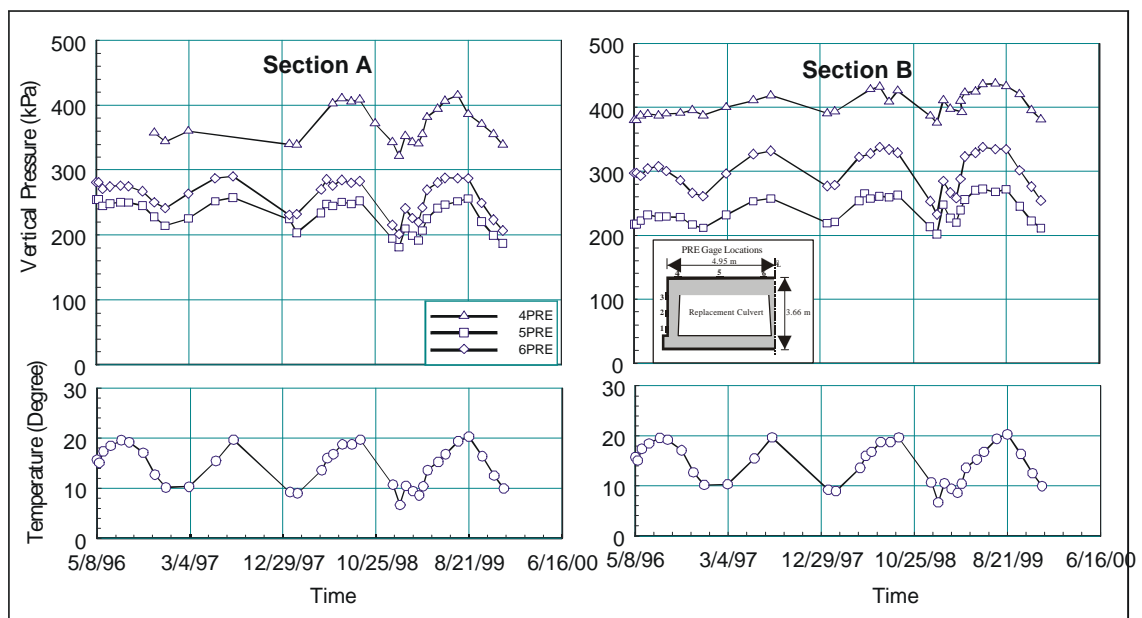


Figure 9 Observed Vertical Pressures on the Culvert Roof (Site I)

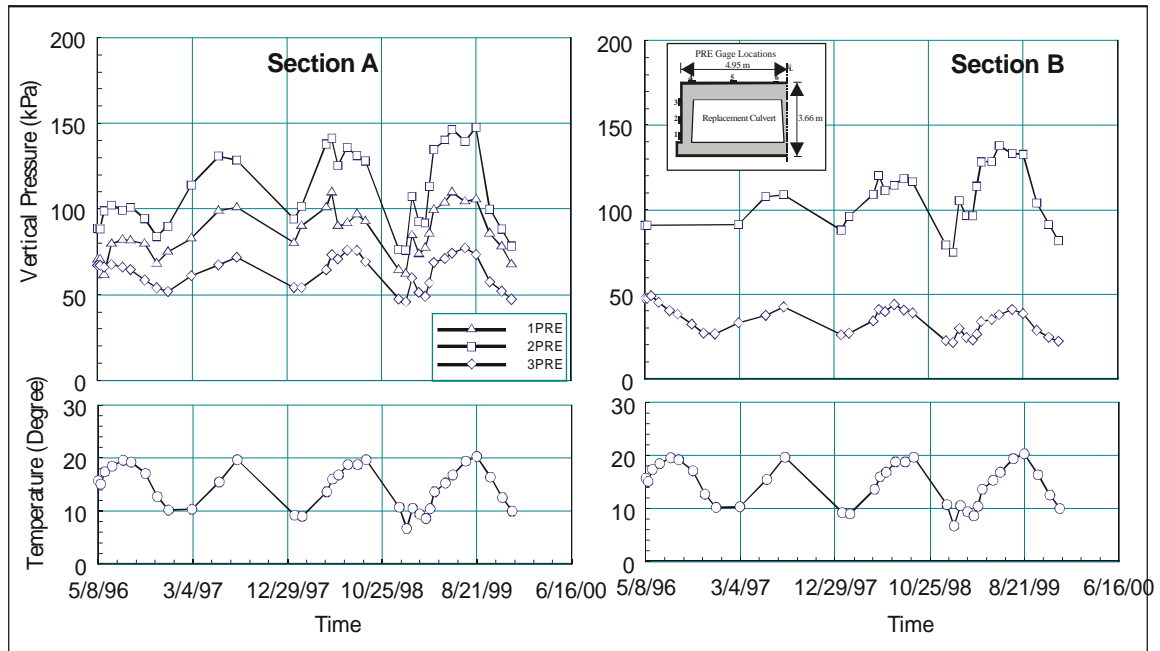


Figure 10 Observed Lateral Pressures on the Culvert Wall (Site I)

The effect of temperature on the earth pressure readings under constant embankment height can be evaluated statistically, as indicated in figures 11 and 12. A better linear relationship between the earth pressure reading and recorded temperature can be obtained using data approximately 9 months after the construction work. The slope of linear regression line of each cell represents the effect of temperature on the fluid filled part of pressure cells ( $k_2$ ). Steeper slope suggests a stronger temperature effect in the pressure cell. Two temperature coefficients  $k_1$  and  $k_2$  at each pressure cell in Site I are summarized in Table 2. All the cells have a capacity of 173 kPa. Vertical pressures on the culvert root yield a better temperature relationship than those pressures recorded at culvert wall.

The maximum  $k_1$  was about 0.17 kPa/°C, whereas the maximum  $k_2$  was 7.09 kPa/°C. For all the pressure cells, the minimum  $k_2/k_1$  ratio was about 25. Compared with the temperature coefficients of cell less than zero or very small load, the cell coefficient  $k_2$

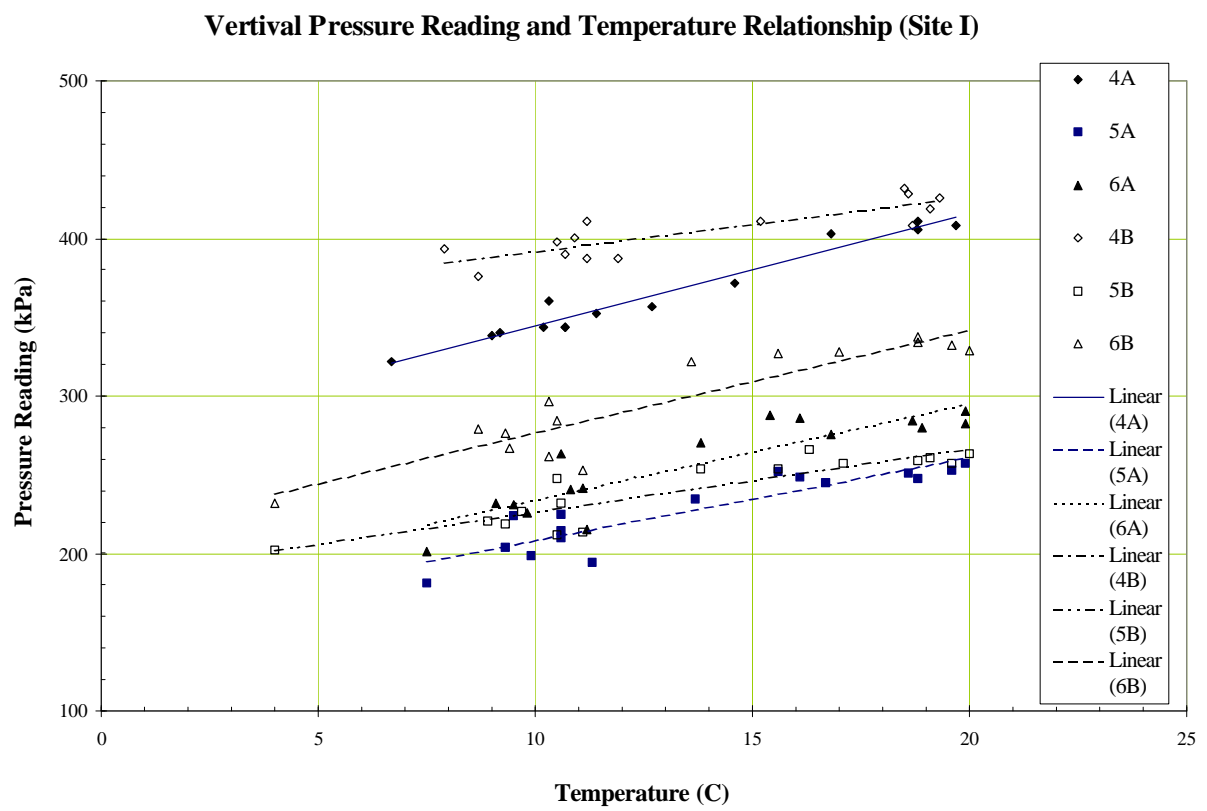


Figure 11 Vertical Pressure Reading and Temperature Correlation

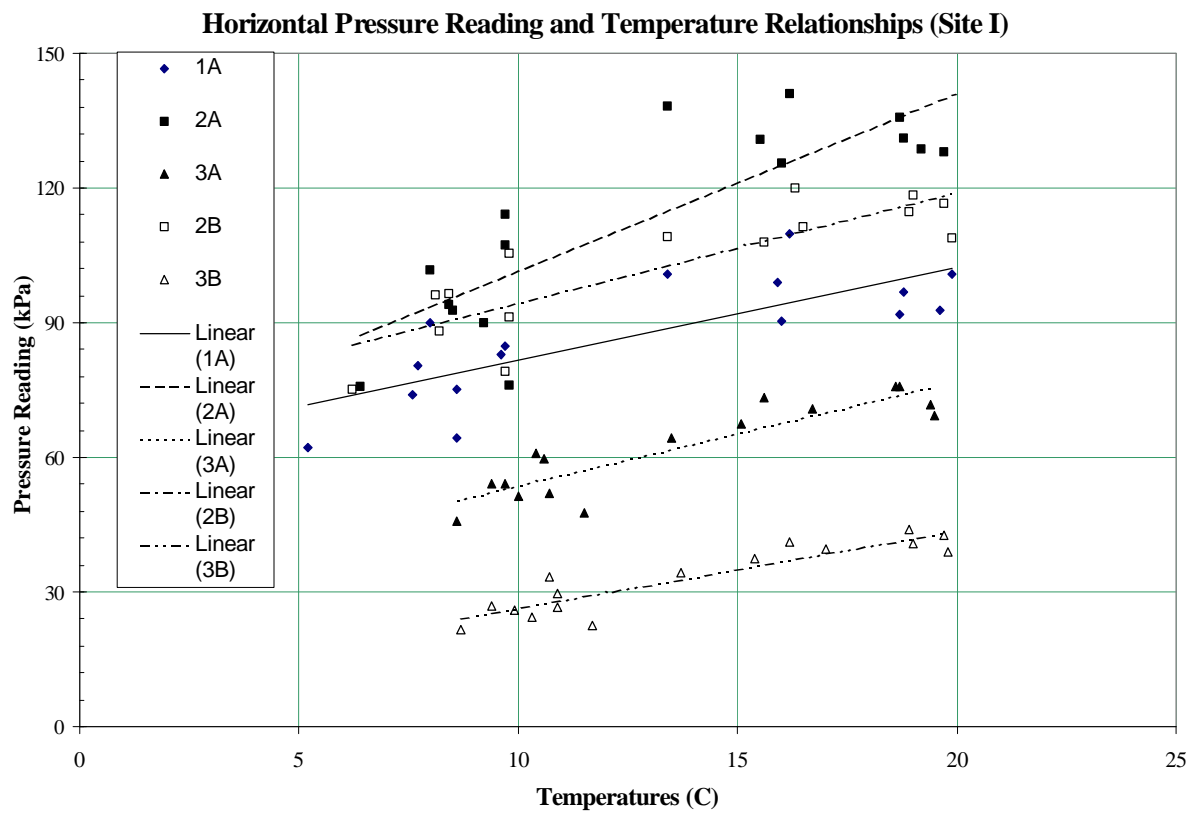


Figure 12 Lateral Pressure Reading and Temperature Correlation

Table 2 Comparison between the Temperature Coefficient of Transducer  $k_1$  and Cell  $k_2$

Cell Number	Recorded Average Normal Pressure (kPa)	$k_1$ (kPa/EC)	$k_2$ (kPa/EC)	Correlation Coefficient	Cell Number	Recorded Average Normal Pressure (kPa)	$k_1$ (kPa/EC)	$k_2$ (kPa/EC)	Correlation Coefficient
1APRE	85.5	0.0046	2.4740	0.78	1BPRE		0.1009	N/A	N/A
2APRE	110.2	0.0577	4.1288	0.84	2BPRE	106.2	0.1309	2.4616	0.85
3APRE	62.7	0.1280	2.4275	0.89	3BPRE	34.4	0.1180	1.7437	0.91
4APRE	368.6	0.0984	7.4779	0.98	4BPRE	403.7	0.1262	3.7437	0.85
5APRE	230.7	0.0479	5.4202	0.90	5BPRE	238.6	0.1649	4.2820	0.89
6APRE	260.0	0.1155	6.3031	0.89	6BPRE	298.4	0.0096	6.7630	0.92

increased significantly. Cells on the culvert roof demonstrated a stronger temperature effect compared with those on the culvert wall.

In Site II, two kinds of cell capacity were used: 345 kPa and 173 kPa. Cells with larger capacity were installed on the roof while lower capacity cells were on the wall. Small lateral earth pressures (from 5 to 90 kPa) recorded at culvert wall. Large and wide variety of earth pressures (from 180 to 610 kPa) were registered on the roof correspond to different embankment height and cell locations. Similar temperature related variations were also recorded in the 14-month earth pressure observation under the constant embankment heights in Site II. The cell temperature coefficient  $k_2$  for each pressure cell can also be obtained statistically.

The relationship between the cell temperature coefficient  $k_2$  and the recorded average normal pressure of all cells in Site I and Site II are summarized in Figure 13. It is suggested from this figure that the cell temperature coefficient increase with the normal pressure acting on the cell surface. Higher normal pressure yielded higher correction coefficient. The cell

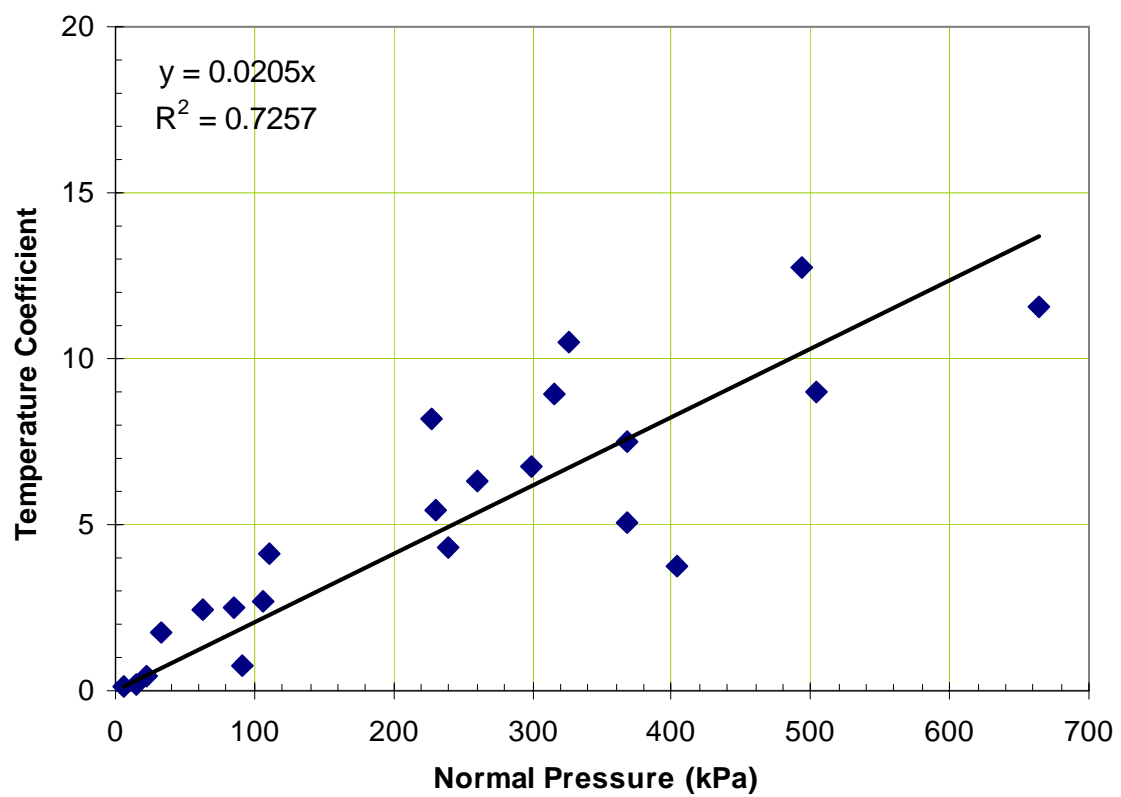


Figure 13 Relationship Between the Temperature Coefficient and the Normal Pressure

temperature coefficient is likely independent from the cell capacity. A linear relationship between  $k_2$  and normal pressure  $p$  can be obtained with a high co-relation coefficient of 0.85:

$$k_2 = 0.0205p \quad (3)$$

where:

$k_2$  is in  $\text{kPa}/^\circ\text{C}$ , and  $p$  is in  $\text{kPa}$ .

The pressure sensing part for hydraulic pressure cell mounted on the external structure is consisted of at least three materials: stainless steel cell plates, de-aired fluid (oil) in the thin slot between the plates, and the high strength mortar. A temperature change will result in a different thermal response. The normal pressure related cell temperature correction coefficient behavior might be interpreted from the different constraint in the system. Different frictional constraint between the cell base plate and mortar due to certain temperature change resulted in a different thermal deformation of the cell. This additional thermal deformation in the cell could not be distinguished from the stress-induced deformation by the cell transducer. So that the output signal from the transducer was a total deformation coupled with two different mechanisms.

## **H.8 Earth Pressures acting on the Culvert after Temperature Correction**

Temperature corrected earth pressures can be obtained by applying equation (2). The initial temperature  $T_0$  used in the equation was taken as the first reading after the construction work. These “initial” temperature values were also close to a approximate ground temperature of 15 EC. Therefore, the corrected earth pressures reflected the earth pressure changes under constant embankment height without the temperature effect. The results are



shown in Figures 14 and 15. Although the recorded earth pressures after temperature correction exhibited less variation than uncorrected pressures, periodical pressure variations still exist. The results indicate that the cells on the wall have a greater pressure fluctuation than those on the roof, and cell at bottom of wall have a larger pressure variation than those at higher places of wall.

To interpret this non-temperature related periodical pressure change, the relationship between the earth pressure and the streamflow data from a USGS gaging station (Beaver Creek at Bristol, Va. Station No. 03478400, about 20 km from Site I) was analyzed. The streamflow is a part of stream discharge from ground water seeping into the stream. The ground water is recharged by freshly infiltrated precipitation. Higher streamflow value indicated more groundwater entered into the soil, and the subsurface soil is likely to have a higher moisture content. Therefore, the streamflow data is an indication of moisture content in the subsurface soil in the nearby area. To summarize the recorded earth pressure, normalized pressure is introduced into the comparison. The normalized pressure is the ratio of the temperature corrected earth pressure and the average temperature corrected earth pressure. Typically, all pressure cells demonstrated similar pressure variation pattern, and the cells on the culvert wall have larger normalized pressure value than those cells on the culvert roof. Figures 16 and 17 illustrated the comparison between the normalized earth pressure and the daily average streamflow. The comparison of streamflow data collected from three gaging stations near the site indicated a similar general trend of streamflow pattern. The discharge data used in figures was collected from a nearest USGS gaging station about 20 km north of Site I. Currently, historical data before Oct. 1, 1998 are available.

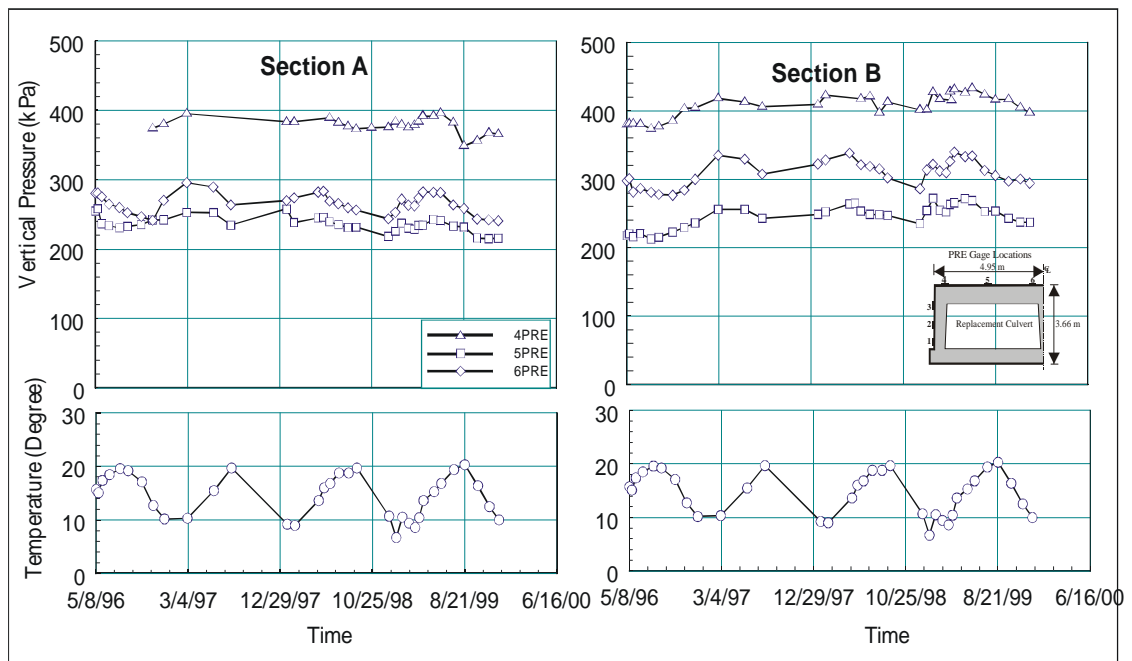


Figure 14 Temperature Corrected Vertical Pressures (Site I)

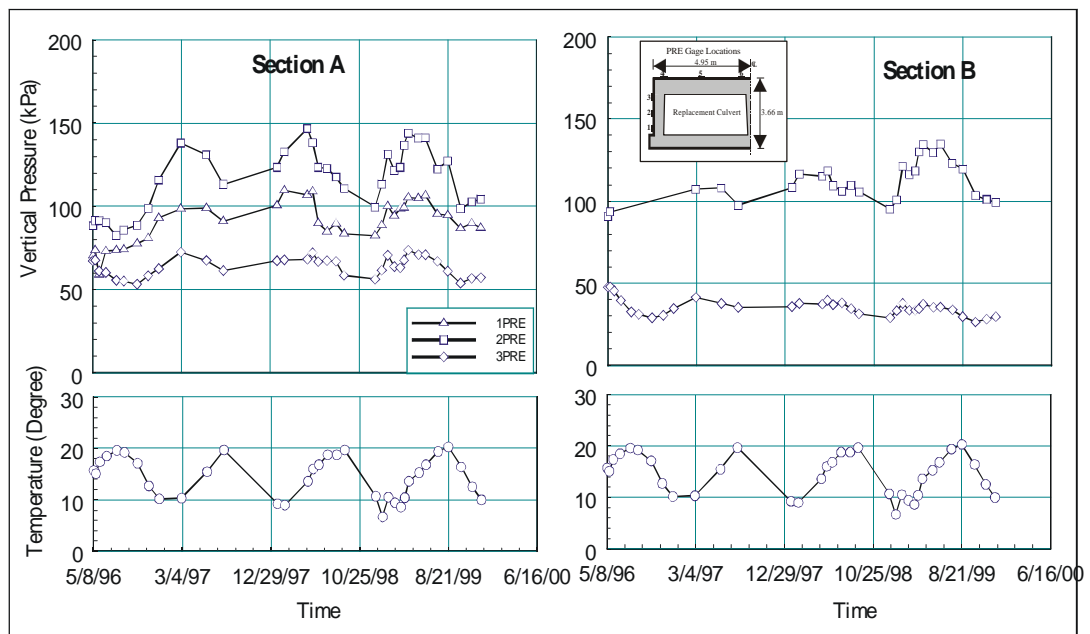


Figure 15 Temperature Corrected Lateral Pressures (Site I)

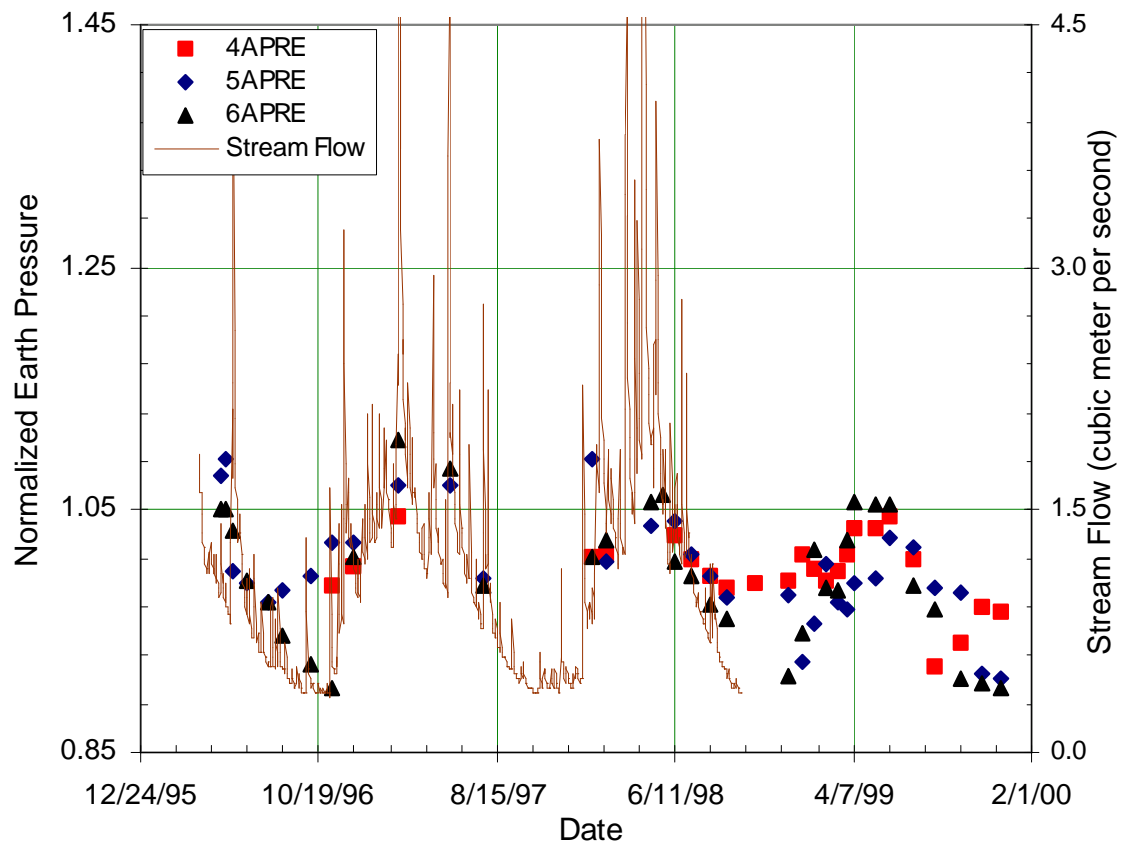


Figure 16 Relationship Between Normalized Vertical Earth Pressures and Streamflow (Section A, Site I)

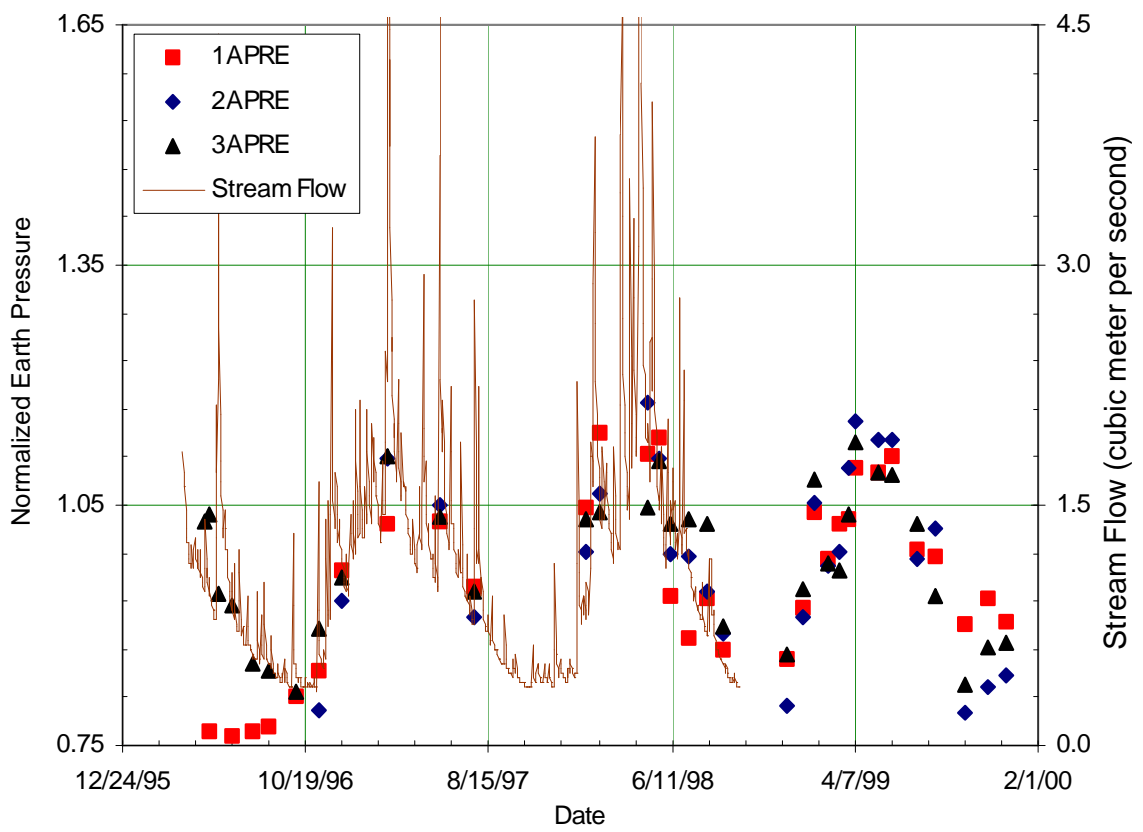


Figure 17 Relationship Between Normalized Horizontal Earth Pressures and Streamflow (Section A, Site I)

Although there is a slight discrepancy immediately after the construction, figures 16 and 17 demonstrate a direct correlation between the temperature corrected earth pressures and the streamflow, which suggests that the temperature corrected earth pressure is related to the moisture content of embankment material. Higher normalized earth pressure correspondent to a higher moisture content of embankment backfill material.

## **H.9 Summary and Conclusions**

The long term earth pressure instrumentation on large size box culverts suggests that the magnitude of earth pressure under a constant embankment height varies with time. Many factors can results in a fluctuated earth pressure acting on the retaining or buried structures. Previously investigated factors such as the development of soil cohesion at the soil-structure interface, relaxation of compaction induced pressures and structural movement is likely to have most significant affecting immediately after the construction work. For hydraulic type contact pressure cells, the periodical earth pressure reading variation on a long term was mainly contributed by temperature effect in cell and the seasonal variation of the moisture content in the backfill material of embankment.

The temperature behavior of pressure cell between the field condition was significantly different from the laboratory calibration. Different temperature coefficients between the concrete surface, grouting pad, and pressure cell resulted in a normal pressure related cell temperature coefficient. Cell under higher earth pressure, which was perpendicular to the cell surface, had a larger constraint. Therefore, it exhibited a larger cell temperature coefficient  $k_2$ . The cell temperature effect consisted of a large portion of the periodical variation of measured earth pressures. Since the temperature related pressure fluctuation is only the

variation of earth pressure registration system, the actual earth pressure does not change. So that it should be eliminated in the earth pressure measurement.

The character of the cell temperature related behavior makes the calibration of cell for contact pressure measurement to be extremely complicated. It requires not only the cell to be embedded in the similar material with similar installation of the cell to be place in the field condition, but also the calibration at various temperature and normal pressure. The long term earth pressure observation provided an appropriate way to eliminate the influence of temperature.

The streamflow is an approximate indication of moisture content in the backfill material of embankment. After the construction, higher moisture content results in a larger unite weight, and a higher earth pressure was therefore recorded. The embankment backfill material was mainly consisted of clayey shale, which had a fairly good drainage condition. The groundwater runoff can easily infiltrate into the embankment. The temperature corrected earth pressure suggests a direct relationship with moisture. Calculation indicates that one percent of average moisture content change in embankment material can result in a 15 kPa of vertical earth pressure acting on the culvert roof.

The groundwater condition around the culvert may also explain the larger fluctuation of later earth pressure at the bottom of culvert wall. Since the pressure cell recorded the total pressure, higher pore water pressure was likely to build up at the bottom, but the bottom cells had a shorter drainage path compared with other cells on the culvert wall. A larger lateral pressure fluctuation was consequently found at cells at the bottom. Other cells on the wall had similarly amount of pressure variation with those cells on the culvert roof.

As a summary from the field instrumentation, a great earth pressure variation with time can be found. Largest earth pressure reading took place in summer and after a heavy precipitation. Temperature and precipitation related moisture change inside the embankment are two major factors resulting in the fluctuation of earth pressures for the certain period of time after the construction.

## **9 Acknowledgments**

This investigation was supported by the Tennessee Department of Transportation, contract #CUT123RES1085. This support, and the input from William D. Trolinger, Division of Materials and Tests, and Billy R. Burke, Structures Division, are appreciated.

## **10 References:**

- Benmokrane, B., Chekired, M. and Xu, H., (1995), "Monitoring behavior of grouted anchors using vibrating -wire gauges," *J. of Geotech. Engrg. Div.*, ASCE, 121(6), 466-475.
- Carder, D. R. and Krawczyk, J. V., (1975), "Performance of cells design to measure soil pressure on earth retaining structures," *Transport and Road Research Laboratory Report No. LR689*, Crowthorne, Berkshire, UK.
- Carder, D. R., Pocock, R. G., and Murray, R. T. (1977), "Experimental retaining wall facility - Lateral stress measurement with sand backfill," *Transport and Road Research Laboratory Report No. LR766*, Crowthorne, England.
- Clayton, C. R. I, Symons, I. F., and Hiedra-Cobo, J. C. (1991). "The pressure of clay backfill against structures" *Can. Geotech. J.* 28 (1), 282-297.
- Coyle, H. M and Bartoskwtz, R. E., (1976), "Earth pressure on precast panel retaining wall," *J. of Geotech. Engrg. Div.*, ASCE, 102(5), 441-456.
- Duncan, J. M. and Seed, R. B. (1986). "Compaction-induced earth pressures under  $K_0$ -conditions" *J. Geotech. Engrg. Div. ASCE*, 112(1), 1-22.
- Dunnicliff, J. (1988). *Geotechnical instrumentation for monitoring field performance*. John Wiley and Sons, New York.

- Felio, G. Y., (1980). *Monitoring of a bridge abutment founded on a granular compacted fill*, Thesis for Master of Engineering, Carleton University, Ottawa, Canada.
- Filz, G. M. and Duncan, J. M., (1993), "Drift of flush – mounted pressure cell readings," *Geotechnical Test Journal*, GTJODJ, 16(4), 432-441.
- Geokon Inc., (1995). *Instruction Manual for Models 4800/4810/4820 VW Earth Pressure Cells*.
- Flynn, J. (1999) "Response of vibrating wire earth pressure cells at pressures exceeding stated capacity" Geokon Incorporated, Personal Communication by E.C.Drumm, 7-26-99.
- Hannon, J. B. and Jackura, K. A., (1984), "Measurement of earth pressure," *Trans. Res. Record 1004*, 6-13.
- James, R. W., Brown, D. E., Bartoskewitz, R. E. and Cole, H. M., (1986), "Earth pressures on reinforced concrete box culvert," *Research Report 294-2F*, Texas Trans. Ins., The Texas A&M Univ. Sys. College Station.
- McRae, J. B. and Simmonds, T. (1991). "Long-term stability of vibrating wire instruments: one manufacturer's perspective," *Field Measurements in Geomechanics*, Balkema, Rotterdam. 283-293.
- Roth, W. H., Lee, K. L., and Crandall, L., (1979), "Calculate and measured earth pressures on a deep basement wall," *Proceedings*, Third International Conference on Numerical Methods in Geomechanics, Vol. 3, 1179-1191.
- Selig, E. T., McVay, M. C. and C. S. Chang. (1982) "Finite element modeling of buried concrete pipe installations." *Trans. Res. Record 878*, 17-23.
- Spangler, M. G. and Handy, R. L. (1982). *Soil Engineering*. 4th edition, Harper & Row, New York.
- Smoltczk, U., Vogt, N. and Hilmer, K., (1979), "Lateral earth pressure due to surcharge loads," *Proceedings, Seventh European Conference on Soil Mechanics and Foundation Engineering*, Brighton, England, Vol. 2, 131-139.



- Smolczyk, U. Hilmer, K., and Schuppener, B. (1977). "Earth pressure variations due to temperature change," *Proceedings of the Ninth International Conference on Soil Mechanics and Foundation Engineering*. Vol. 2, 725-733.
- Symons, I. F. and Murray, R. T. (1988). "Conventional retaining walls: pilot and full-scale studies," *Proc. Instn. Civ. Engrs*, Part I, 84(6), 519-538.
- Weller, K. A., Jr., and Kulhawy, F. H. (1982). "Factors affecting stress cell measurements." *J. of Geotech. Engrg. Div.*, ASCE, 118(12) 442-449.
- Yang, M. Z., Drumm, E. C., Bennett, R. M. and Mauldon, M. (1997), "Influence of compactive effort on earth pressure around a box culvert," *Proceedings, 9<sup>th</sup> International Conference of the Association for Computer Methods and Advances in Geomechanics (IACMAG 97)*, Wuhan, China, pp2021-2026